Developing Small Molecule Inhibitors of Bromodomain-Histone Interactions

Brian G. Wilson

Balliol College, University of Oxford

DPhil Dissertation

Organic Chemistry

November 2015

Supervisors: Professor Stuart Conway and

Mr James Reuberson

Abstract

Developing Small Molecule Inhibitors of Bromodomain-Histone Interactions

Brian G. Wilson Balliol College Michaelmas 2015 University of Oxford

Bromodomains, protein modules found in 46 human chromatin-associated proteins, bind to acetylated lysine residues (KAc), and modulate the formation of complex protein scaffolds, which are often involved in transcription. The work in this dissertation focuses on the development of small molecule inhibitors for the BRD9 bromodomain, which is a component of nucleosome remodelling complexes, and has been linked to lung and cervical cancers.

The lead molecule was based on the triazole KAc mimic, which is a promiscuous bromodomain ligand. Using a rational approach involving evaluation at the four positions shown on scaffold **1**, this work led to compound **2**, which has nanomolar affinity for the BRD9 bromodomain, and some selectivity over BRD4(1). Compound **2** was shown to have a high lipophilic ligand efficiency, high aqueous solubility, and moderate metabolic stability in an *in vitro* mouse model, making it suitable for further studies in a biological setting.

Microscale Thermophoresis has been used as a new technique to measure interactions between small molecule ligands and their bromodomain binding partners. This work has provided useful structure-activity relationships for a subset of bromodomains, which will be useful in future ligand development programmes of this emerging therapeutic target class.

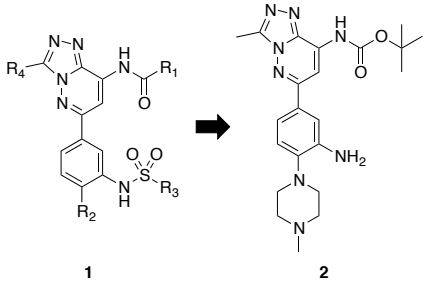

1 2

BRD9	BRD4(1)	
MST K_D/nM	**MST K_D/nM**	**Fold Selectivity BRD9/BRD4(1)**
164	4060	24.8
ITC K_D/nM	**ITC K_D/nM**	**Fold Selectivity BRD9/BRD4(1)**
65.8	3910	59.4
BROMO*scan*™ K_D/nM	**BROMO*scan*™ K_D/nM**	**Fold Selectivity BRD9/BRD4(1)**
54	150	2.8

Contents

Chapter 2. Bicyclic triazoles as BRD9 inhibitors

Chapter 4. Probing the acetyl lysine binding pocket of the BRD9 bromodomain

Chapter 5. Conclusion and future work

Chapter 6. Experimental

References

Appendix

Acknowledgements

Thank you to Prof Stuart Conway for accepting me to work on this exciting project. I am grateful to my industrial supervisors at UCB, initially Dr Rikki Alexander and then James Reuberson, who have both provided valuable insights and advice throughout my DPhil. I especially appreciate James' time and patience during my placement in Slough, where I learned a great deal about life in the pharmaceutical industry.

I have been privileged to work in the Chemistry department at Oxford. Like all researchers in the department, I have relied heavily on the NMR facilities. I especially appreciate the hard work and reliability of Tina Jackson, who has always been exceptionally helpful throughout my time at Oxford.

A considerable amount of the biophysical data was recorded by workers at the SGC. I particularly appreciate the patience of Oleg Fedorov, who has had to cope with many emails from me over the past few years. Cynthia Tallant was incredibly helpful in teaching me how to run ITC experiments, and I appreciate her time and input. My efforts in the strange, isolating, but often insightful world of computational chemistry were assisted greatly by the time and effort of Angelina Measures, Wilian Cortopassi, and Gregory Ross.

During my brief placement in UCB Slough, Nicolas Basse was extremely helpful during the MST assay optimisation process, and Harry MacKenzie did an amazing job with my NMR experiments.

An interest in postgraduate Chemistry research was ignited by my experience of working in the laboratory of Prof Ed Tate, during my final year project at Imperial College London. Ed's positivity and encouragement was amazing.

The input from all of the members of the SJC group has been amazing over the past few years- I couldn't have done this work without the members of G11 and G12. Slim Tim Rooney (TR) has been especially helpful during the writing process. David 'Dizzy' Hewings provided a great deal of valuable advice during my DPhil, for which I am very grateful. Each of the PostDocs within the group often displayed the patience of a saint during my time in the lab. Jess, Lingbing, Dr J, Sonia, and Megan all deserve recognition for their unwavering support and direction. I enjoyed the unpredictable but priceless humour of Sam 'no antiques' Grayer, to whom I wish good luck in his forthcoming academic career. Di was a source of lighthearted relief and perspective, with a little help from KP. To all my fellow Bromodominators, I feel privileged to have been part of such a special team. LJ was there from start to finish and KK deserves a mention for her distinctive presence in G11. Michael 'Machine' Brand was especially helpful in assisting me during the final hurdles of the DPhil racecourse. Coco- enjoy my desk!

The Seal was a Bass, and the squash court sessions helped to focus the mind. Noli Timere. Thank you to Maya Graffy, a joyous Part II student whom I had the fortunate opportunity to supervise. You taught me a lot (of yoga poses). Namaste.

Professor Rob Adlington and Professor Nick Green were very important sources of advice during the final stages of my DPhil, as was the ever-dependable Nicola Trott. Thank you all for your support during this challenging period.

Oxford University Golf Club added an incredible dimension to my time in Oxford. My scientific endeavours were often fuelled by the anticipation of an early morning weekend wake-up call to play on some of the best courses in the world, with a great group of people. Dr Jim Mercurio and Alex Gems have become especially strong friends during my time on the links. I am honored (#kth) to have been part of the six-year Varsity winning streak- keep the run going Oxford! JR, I will see you in the fairway. Reyn, it is perfect. Rob Mays, 2&1 off top says it all. And yes, I did just hole that putt!

Speaking of strong teams, we have one at number 71. My parents have been a source of dependable support and love during my DPhil. Our journey will never stop. My sister Carol has provided many useful nuggets of wisdom on life as a PhD student, helping me to persevere when Chemistry seemed like an uphill battle. My brother Joseph's pragmatism and positive mental attitude (PMA) often helped me along the way, and reminded me to see the bigger picture. His words are true, "The greatest pressure comes from within."

Abbreviations

AlphaScreen™	amplified luminescent proximity homogeneous assay
AML	acute myeloid leukaemia
ApoA1	apolipoprotein A1
ATAD2	ATPase family, AAA domain containing protein 2
BAF	BRG-1 or HRBM-associated factors
BAZ2A/B	bromodomain adjacent to zinc finger domain protein 2A/B
BCP	bromodomain-containing protein
BET	bromodomain and extra terminal domain
BLI	bio-layer interferometry
Boc	*tert*-butoxycarbonyl
Bpin	4,4,5,5-tetramethyl-1,3,2-dioxaborolyl
BRD2/3/4/7/9	bromodomain-containing protein 2/3/4/9
BRPF1	bromodomain and PHD Finger-Containing Protein 1
BRDT	bromodomain testis-specific protein
BSA	Bovine Serum Albumin
CECR2	Cat Eye Syndrome Chromosome Region, Candidate 2
CREBBP	cAMP-response element binding protein (CREB)-binding protein
CTD	C-terminal domain
DTT	dithiothreitol
4-DMAP	4-dimethylaminopyridine
DMF	*N*,*N*-dimethylformamide
DMI	dimethylisoxazole
DMSO	dimethyl sulfoxide
dppf	1,1'-bis(diphenylphosphino)ferrocene
DSF	differential scanning fluorimetry
e.e.	enantiomeric excess
ELISA	enzyme-linked immunosorbent assay
eq	equivalents
ES	electrospray
ET	extra terminal
Et	ethyl
FI	field ionisation
FRAP	fluorescence recovery after photobleaching
FRET	Förster resonance energy transfer
GCN5	general control of amino acid synthesis protein 5 (alternative name: histone acetyltransferase KAT2A)
GFP	green fluorecent protein
GSK	GlaxoSmithKline
HAT	histone acetyltransferase
HAT1	histone acetyltransferase 1
HBTU	*O*-(benzotriazol-1-yl)-*N*,*N*,*N*′,*N*′-tetramethyluronium hexafluorophosphate
HDAC	histone deacetylase

HIV	human immunodeficiency virus
HPLC	high-performance liquid chromatography
HRMS	high-resolution mass spectrometry
HTRF	homogeneous time resolved fluorescence
HTS	high-throughput screening
IL-6	interleukin-6
IC_{50}	half maximal inhibitory concentration
ITC	isothermal titration calorimetry
KAc	*N*-ε-acetyl-L-lysine
K_D	dissociation constant
LC	liquid chromatography
LE	ligand efficiency
LLE	ligand-lipophilic efficiency
MD	molecular dynamics
MLL	mixed lineage leukaemia
MEG	monoethylene glycol
MM	Multiple myeloma
MORF	MOZ-related factor
MOZ	Monocytic leukaemia zinc-finger protein
MS	mass spectrometry
MST	microscale thermophoresis
Me	methyl
MW	microwave
P-TEFb	positive transcription elongation factor
PB1	polybromo-1
PBAF	polybromo-associated BAF
PCAF	p300-CREBBP associated factor
PBS	phosphate-buffered saline
PDB	protein data bank
PEG	polyethylene glycol
PHD	plant homeodomain
PID	P-TEFb interaction domain
PK	pharmacokinetics
Pol II	RNA polymerase II
Propyl	propyl
PTM	post-translational modification
RBP1	retinol binding protein 1
RT	room temperature
SAHA	suberoylanilide hydroxamic acid
SAR	structure-activity relationship
SGC	Structural Genomics Consortium
SMARCA2	probable global transcription activator SNF2L2 (alternative name: SWI/SNF-related matrix-associated actin-dependent regulator of chromatin subfamily A member 2)
SMARCA4	transcription activator BRG1 (alternative name: SWI/SNF-related matrix-

	associated actin-dependent regulator of chromatin subfamily A member 4)
SPR	surface plasmon resonance
STD	saturation transfer difference
SWI/SNF	switch/sucrose non-fermentable
TFA	trifluoroacetic acid
THF	tetrahydrofuran
TLC	thin later chromatography
TRIM24	tripartite motif-containing protein 24
TRIM33	tripartite motif-containing protein 33
UCB	Union chimique belge

Chapter 1: Introduction

1.1. Post-translational modifications and histone modification

1.1.1. Protein post-translational modification

Genes encode proteins and proteins play a fundamental role in cell function, therefore the approximate 21,000 genes in a particular cell determine cellular phenotype.[1] Since the human genome was decoded in 2001, it has become clear that as the total number of proteins in the human proteome is estimated at over 1 million, the flow of information from DNA to RNA to protein is vastly more complex than initially anticipated.[2] Scientists have increasingly gravitated towards RNA to explain the much greater array of biological functions that occur within us. Efforts to explain how multiple protein functions can be generated from individual genes have led to the identification of a series of relevant mechanisms including RNA editing, differential transcription termination and alternative splicing.[3,4]

The increase in complexity from the level of the genome to the proteome is further facilitated by protein post-translational modifications (PTMs). PTMs refer to chemical changes to a protein made by enzymes to affect its function and can occur at any stage in a protein's life cycle. These changes are accepted as an essential mechanism used by eukaryotic cells to diversify their protein functions.[5] The chemical changes are diverse, but most commonly involve additions to the protein. These additions range from other proteins, amino acids, sugars or lipids, but the addition of small functional groups have been the most intensely studied.[6,7]

Reversible protein phosphorylation, principally on serine, threonine or tyrosine residues, is one of the most important and well-studied PTMs. Phosphorylation plays critical roles in the regulation of many cellular processes including cell cycle, apoptosis and signal transduction pathways. The phosphorylation level of proteins is mediated by two classes of enzymes, kinases and phosphatases, which phosphorylate and dephosphorylate substrates, respectively. It is estimated that one-third of the proteins in the human proteome are substrates for phosphorylation at some point, driving the emergence of 'phosphoproteomics' as a branch of proteomics that focuses solely on the identification and characterization of phosphorylated proteins.[8] Kinases have become one of the most intensively pursued classes of drug target, and many of the drugs that will be developed over the next century are likely to be compounds that target this enzyme class.[9]

1.1.2. Histone lysine acetylation and the 'histone code'

In the nucleus of eukaryotes DNA is packaged into chromatin by wrapping around histone proteins to form a nucleosome. Histones are very basic, positively charged proteins (on average, 23% of the total residues are lysine or arginine), facilitating their interaction with the negatively charged DNA backbone. The histone core consists of two copies of four conserved histone proteins, namely H2A, H2B, H3 and H4, which form an octamer around which a portion of DNA (~146 base pairs) is wound (Figure 1). The N- and C-terminal histone tails can be covalently modified, and although many PTMs have been identified, acetylation is the most widely studied.[10,11]

A key PTM is the addition of an acetyl group to the terminal nitrogen of lysine. First identified in 1964 by Vincent Allfrey, lysine acetylation of histones was proposed to "affect the capacity of the histones to inhibit ribonucleic acid synthesis *in vivo*".[12] The same laboratory later identified that the acetylation occurred on the *ε*–nitrogen of lysine.[13] Soon after, enzymes possessing histone acetyltransferase (HAT)[14] or histone deacetylase (HDAC)[15,16] activity were isolated. However, it was not until 1995 that the first gene encoding histone acetyltransferase activity, histone acetyltransferase 1, (*HAT1*) was successfully identified and cloned in yeast. The following year, Schreiber *et al*.[17] used an irreversible covalent inhibitor of histone deacetylation activity to isolate and clone the first histone deacetylase gene, histone deacetylase 1 (*HDAC1*), from human cells. These results confirmed that lysine acetylation was a dynamic, reversible modification, with corresponding 'writer' and 'eraser' proteins, which act in a reversible manner to create a particular combinatorial pattern or 'code' which is closely linked to a biological event.

A growing awareness of the remarkable diversity and biological specificity associated with distinct patterns of covalent histone marks led Strahl[18] and others[10,19] to "support the view that a histone 'language' may be encoded on these tail domains that is read by other proteins or protein modules."[18] This language is referred to as the 'histone code' (Figure 1). The histone modifications occur at specific residues and the particular pattern of marks (the 'histone code') is thought to result in a given phenotype.

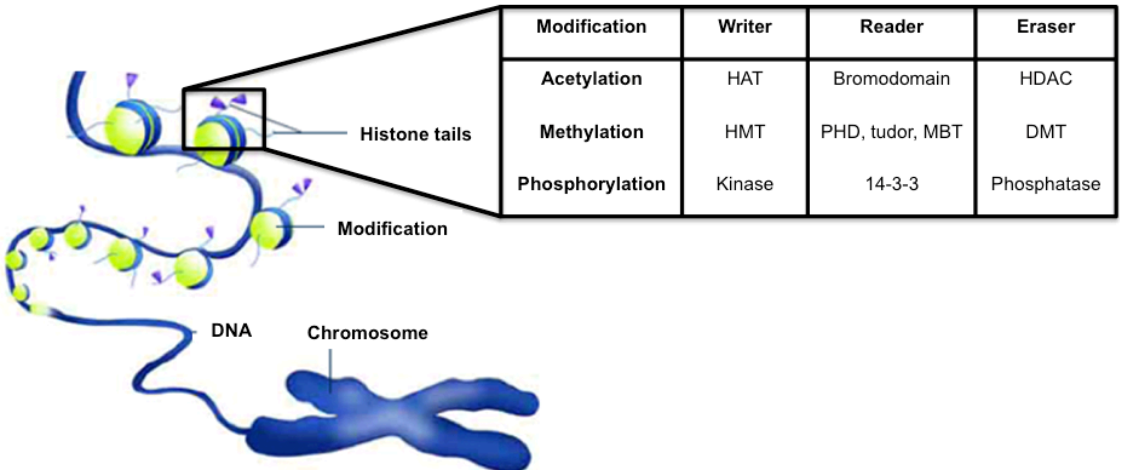

Modification	Writer	Reader	Eraser
Acetylation	HAT	Bromodomain	HDAC
Methylation	HMT	PHD, tudor, MBT	DMT
Phosphorylation	Kinase	14-3-3	Phosphatase

Figure 1: **Chromosome structure, histone post-translational modifications and the 'histone code'.** (Adapted with permission from the National Institue of General Medical Sciences, NIH Publication No. 10-662*)*.[20] Chromatin structure has been descibed as resemmbling "beads on a string". The "tails" of histone proteins (purple triangles) are subjected to post-translational modifications, including acetylation, methylation and phosphorylation. These chemical modifactions impact whether a gene will be transcribed by RNA polymerase.[20]

The acetylation state of histones is dynamically controlled by two key regulators, HATs ('writers') and HDACs ('erasers'). The actions of these enzymes on histones serve as an important mechanism for the regulation of gene expression.[21] Stable alterations like these are said to be 'epigenetic' literally meaning 'outside conventional genetics'. Bird has used this term to describe "the study of stable alterations in gene expression potential that arise during development."[22] These alterations are vital for proper cellular growth and proliferation, and their misregulation has become associated with disease.[23] Bromodomains (Section 1.2.) are responsible for 'reading' the acetylation state, which leads to a range of downstream biological outcomes.

Acetylation of histone lysine residues is associated with increased gene transcription and this phenomenon has become well established in the literature.[11,24,25] This modification neutralises the positively charged lysine *ε*-amino group, reducing the electrostatic force of attraction with the negatively

charged DNA phosphate backbone, giving a more relaxed chromatin structure (euchromatin) that is associated with transcriptionally active genes.[26]

Large-scale genome-wide mapping of histone modifications has enabled certain histone modifications to be associated with particular chromosomal regions and with particular transcriptional states.[27] For example, hyperacetylation of histones correlates with active expression of the associated genes. In contrast, lysine methylation at histone 3 lysine 36 ($H3K_{36}$) is associated with actively transcribed genes, whereas lysine methylation at histone 3 lysine 9 ($H3K_9$) is associated with silenced genes.[28]

The 'histone code' is undoubtedly very complex and a huge challenge remains in understanding how multiple PTM patterns lead to different biological outcomes. Local impacts of histone modifications on individual nucleosome structure as well as their global effects on chromosome structure, must be taken into account.

1.1.3. Non-histone lysine acetylation

Lysine acetylation is not limited to the histone proteins in which this modification was first identified. Numerous examples exist in the literature demonstrating that the acetylation state of proteins is highly relevant to their stability and activity in cells. Indeed, an important conclusion from a range of recent proteomic studies is that the majority of acetylation events take place on non-nuclear proteins.[25,29-31] It took more than 20 years from the discovery of histone acetylation until the first non-histone acetylation target, tubulin,[32]

was discovered. It was another 10 years before the tumour suppressor p53,[33] and the HIV transcriptional regulator Tat,[34] were identified as lysine acetylation targets.

Lysine acetylation can influence protein modification at nearby sites or result in the recruitment of other PTM-regulating enzymes, in addition to competing with other lysine PTMs, such as ubiquitinylation. The competitive cross-talk between these modifications has been found to be responsible for regulating protein stability.[35] Lysine acetylation also engages in non-competitive cross-talk between PTMs. In the case of the transcription factor p53 which is mutated in over 50% of human cancers, there is considerable cross-talk between lysine acetylation and methylation which is thought to be crucial for p53 activation in response to DNA damage.[36]

Recent advances in high-resolution mass spectrometry-based proteomics have enabled both the identification and relative quantification of thousands of acetylation sites in a single experiment. Acetylation has been found to be one of the most common PTMs in the mitochondrial proteome, consistent with the endosymbiotic theory of a prokaryotic origin for mitochondrion.[37] Additionally, acetylation is more prevalent than phosphorylation in bacteria.[37-39] A recent global analysis of this PTM in three human cell lines using an antibody specific for acetyl-lysine identified 3,600 lysine acetylation sites on 1,750 proteins.[25] This demonstrates that the abundance of this modification is almost as high as protein phosphorylation, which is estimated to occur on >2,000 proteins.[40] The results showed that lysine acetylation preferentially

targets large macromolecular complexes involved in diverse cellular processes, such as chromatin remodeling, DNA repair and the cell cycle. Furthermore, due to its prevalence, lysine acetylation is likely to have broad regulatory functions in addition to the few that are actively studied. These striking results have been highlighted as a "…glimpse of the acetylome which will be a valuable resource for researchers in many fields and will surely stimulate further analysis of the functional relevance of the acetylated sites in regulatory pathways."[41]

1.2. Bromodomain structure, classification and biological relevance

1.2.1. Bromodomain structure

Named after the *Drosophila* gene *brahma* from which they were first identified by Tamkun *et al.* in 1992, bromodomains are ~110 amino acid modules that exist as sub-units of larger protein architectures.[42] The bromodomain motif can be found at the C- or N-terminus, as a single copy in the middle of the protein sequence or repeated up to five times in a single polypeptide chain.[43] These modules recognise ('read') acetylated lysine residues, which in turn leads to a range of important biological outcomes. For example, BRD2 (Figure 2, BRD2(1)) has been shown to bind to acetylated chromatin[44,45] such as transcription factors,[46] chromatin remodeling proteins,[47] and many vital components of the transcriptional machinery.[45] BRD2 was shown to be an essential component of RNA polymerase II catalysed transcription through nucleosomes, possessing histone chaperone activity.[48] Despite having large

sequence variations, bromodomain modules share a conserved fold that comprises a left-handed bundle of four α-helices (named αZ, αA, αB and αC) linked by two diverse loop regions of variable charge and length (known as ZA and BC loops) (Figure 2).

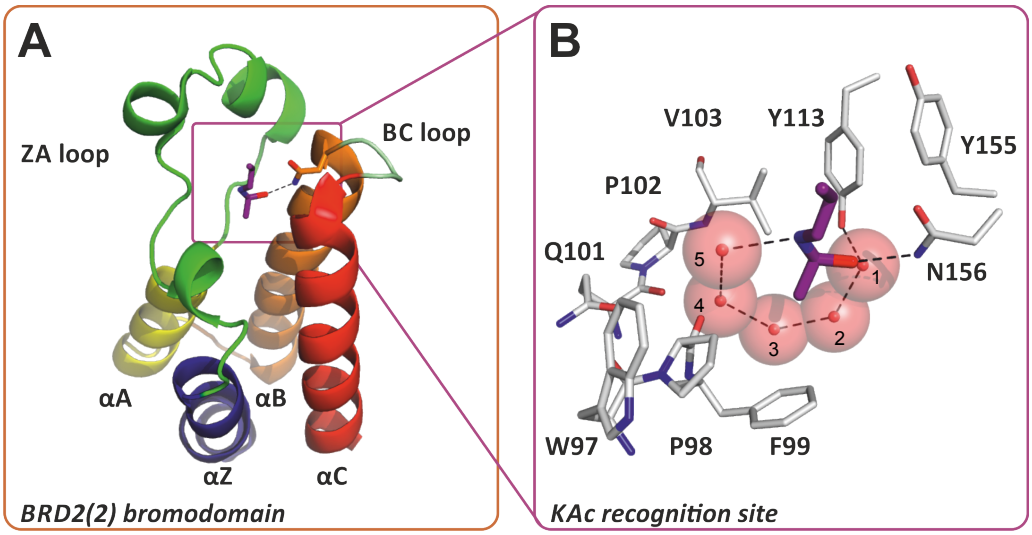

Figure 2: **Bromodomain structure**.[49] (**A**) An X-ray crystal structure of the second bromodomain of BRD2 in complex with KAc, modified with permission from Jennings *et al*. 2014 (PDB ID: 2DVQ). Copyright 2012 Future Science.[49] The bromodomain structure is composed of four helices and two loop regions known as the ZA loop and the BC loop. **(B)** The KAc residue binds in a well-defined hydrophobic pocket, forming interactions with a highly conserved asparagine residue (N156 in BRD2(2)) and several tightly bound water molecules (red spheres, numbered for clarity).

The KAc residue binds in a well-defined pocket at one end of the helical bundle. The amino acid residues engaged in KAc recognition are among the most highly conserved residues in the bromodomain family.[50] Although this pocket is primarily hydrophobic in nature, it typically contains four crystallographically conserved water molecules that form the base of the KAc binding site. The KAc residue interacts with the bromodomain *via* a direct hydrogen bond between the acetyl carbonyl oxygen atom and the NH_2 group of the asparagine amide. A second interaction occurs between the acetate carbonyl oxygen atom and a conserved tyrosine residue *via* water molecule 1. Despite the conserved three-dimensional structure, the sequence similarity of

the bromodomain family is relatively low (approximately 30% homology, on average). It is the sequence diversity in the ZA and BC loop regions which enables the bromodomains to distinguish between different protein binding partners.

1.2.2. Classification of bromodomains

A wealth of structural information has enabled the comprehensive structural analysis of bromodomains, establishing the sequence and structural conservation of these modules.[51] Structure-based alignments have arranged the 61 human bromodomains found within 46 separate proteins into eight distinct families (Figure 3).[52]

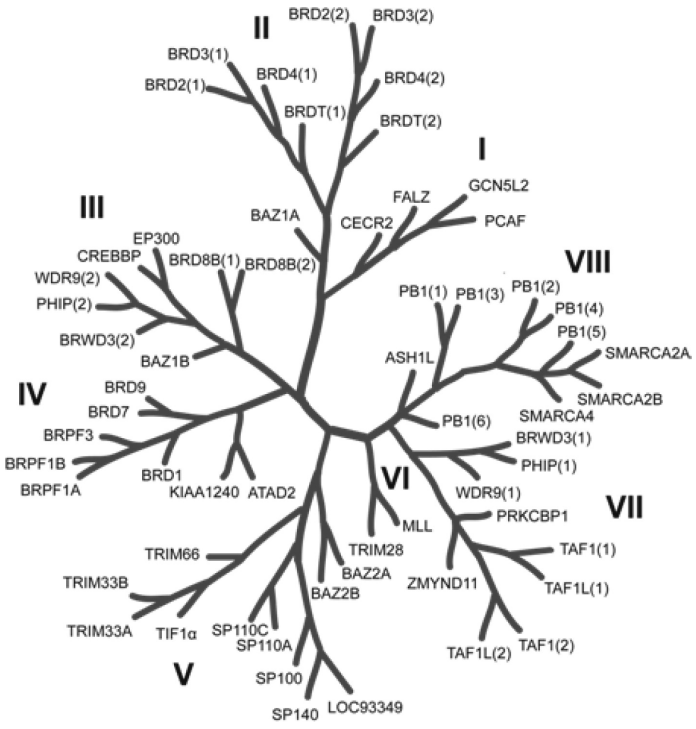

Figure 3: Phylogenetic tree of the human bromodomain family constructed on a structure-based alignment. The eight bromodomain families are highlighted with Roman numerals. Where more than one bromodomain exists in a single protein, bromodomains are numbered according to their position from the N-terminus. (Reprinted with permission from Hewings *et. al*.[52] Copyright 2012 American Chemical Society.)

1.2.3. Biological relevance of bromodomains

Bromodomains exclusively recognise acetylation motifs and are present in diverse proteins including HATs (GCN5, PCAF), ATP-dependent chromatin-remodeling complexes (BAZ1B), helicases (SMARCA), methyltransferases (MLL, ASH1L), transcriptional coactivators (TRIM/TIF1, TAFs) transcriptional mediators (TAF1) and nuclear-scaffolding proteins (PB1).[51] Of the bromodomains that have been studied in depth to date, their biological roles are clearly crucial.[53-56] The bromodomain containing protein BRD4 has arguably been the most rigorously studied. It is involved in mitosis and as a transcriptional co-activator it recruits a variety of transcription factors to acetylated chromatin.[57-59] Altered levels of BRD4 expression have been observed in a variety of cancers.[60,61] Given its biological prevalence, it is unsurprising that knockout of BRD4 in mice is lethal,[62] and knockdown of BRD4 in cultured human cells significantly reduces cell growth.[63]

Small organic molecules have become invaluable tools for investigating biological systems. Unlike gene knockout experiments that eliminate specific proteins completely, chemical probes can be used to perturb individual domains of a protein, resulting in a more accurate understanding of protein function.[64] The following section will examine the progress made to date in developing bromodomain inhibitors and their application in biological environments.

1.3. Discovery of bromodomain inhibitors

1.3.1. BET bromodomain inhibitors

1.3.1.1. BET-bromodomain inhibitor development and progress into the clinic

The bromodomain and extra C-terminal domain (BET) family (Figure 3, family II) has been the focus of the majority of small molecule bromodomain inhibitor development. The BET family comprises BRD2-4 and the testis-specific BCP, BRDT. A key feature of the BET proteins is their ability to associate with mitotic chromosomes, unlike other bromodomain-containing proteins which are displaced from condensed chromosomes during mitosis.[65] BRD4 has been found to have a general role in transcription,[54] and has been associated with a wide range of diseases and conditions.[66] BRDT has also been found to have an important role in transcriptional elongation,[67] whereas the biology of BRD2 and BRD3 is less well understood.

The interest in identifying potent and selective bromodomain ligands was catalysed in 2010 and 2011, by the publication of two methyltriazolodiazepine-based ligands (**3** and **4**, Figure 4) for the bromodomain and extra C-terminal domain (BET) family of BCPs.[68,69] (+)-JQ1 (**3**, Figure **4**) was reported by the Structural Genomics Consortium (SGC; Oxford, UK) and the Bradner laboratory at Harvard (MA, USA) as a high-affinity BET bromodomain ligand with an IC_{50} value of 77 nM for BRD4(1).[39] This compound has been vital in unravelling the biological role of the BET family of bromodomains, linking inhibition of this protein class as a therapeutic strategy to target a variety of

diseases including leukemia[53] and multiple myeloma.[70] A phenotypic screen at GSK to identify small molecule up-regulators of apolipoprotein A1 (ApoA1), which is involved in protection from atherosclerosis progression, led to the development of the BET bromodomain probe I-BET762 (**4**).[40,71,72] This compound has IC_{50} values of 32.5-42.5 nM for the BET bromodomains and is currently in phase I clinical trials for nuclear protein in testes (NUT) midline carcinoma (NMC), a rare but lethal form of cancer.[73] These publications provided a wealth of structural and biological information, igniting a rapid effort to extensively probe the BET family of bromodomains using both phenotypic and fragment-based approaches, leading to a wide range of inhibitors, some of which are shown in Figure 4.

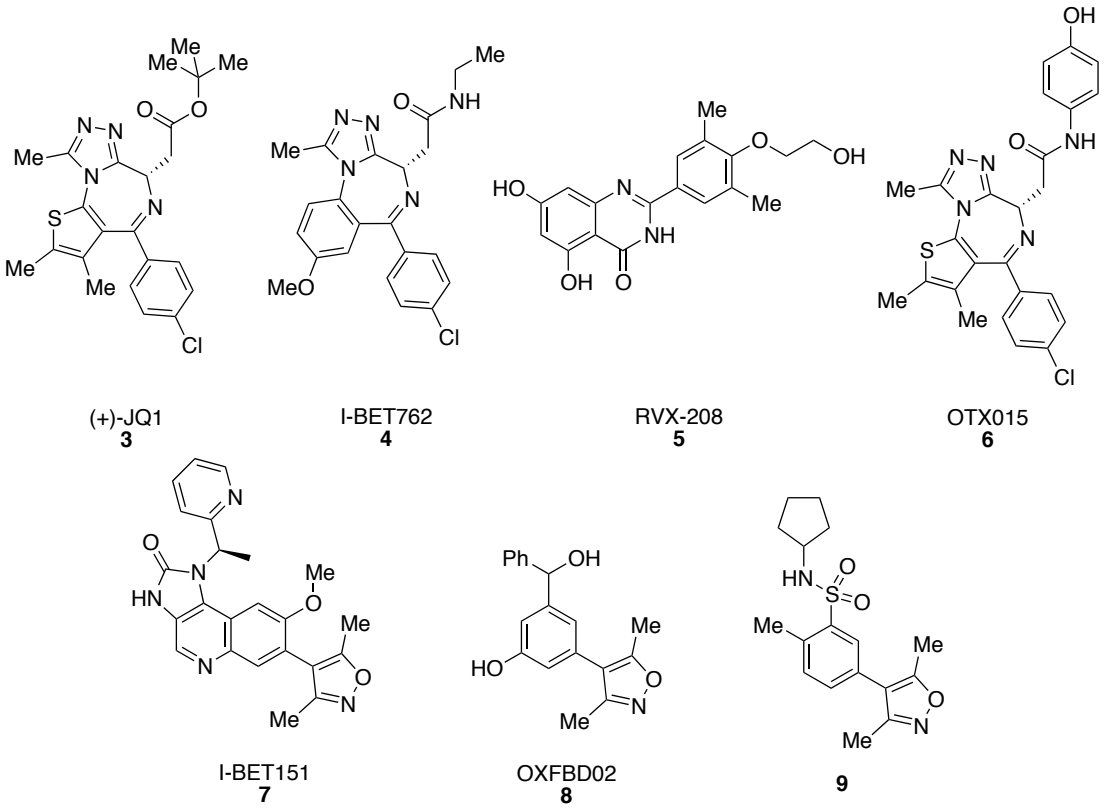

Figure 4: **Structures of key BET bromodomain inhibitors**.[69,70,74-79]

The rapid progress in the understanding of BET-bromodomain biology has been underpinned by the development of these tool compounds, and has led

to the entry of five compounds into clinical trials for a variety of indications (Table 1). In 2010 RVX-208 (**5**) was the first BET-bromodomain inhibitor to enter clinical trials for atherosclerosis treatment after a phenotypic screen to identify upregulators of ApoA1 expression by workers at Resverlogix identified the quinolinone-based compound.[44,77,80] This compound was not initially known to be a BET ligand, but subsequent studies showed that **5** binds to BET bromodomains with modest selectivity demonstrated for BRD4(2) (K_D = 140 nM) over BRD4(1) (K_D = 1.1 μM) in ITC measurements.[81,82] OncoEthix later developed OTX015 (**6**, Figure 4) as a BET-bromodomain inhibitor which is structurally very similar to (+)-JQ1.[79,83,84]

Compound	Company	Phase	Disease area	Status
RVX-208 (**5**)	Resverlogix	II	Coronary artery disease	Completed[85]
		II	Type 2 diabetes	Active[86]
I-BET762 (**4**)	GlaxoSmithKline	I	NMC and other cancers	Recruiting[73]
OTX015 (**6**)	OncoEthix	I	Glioblastoma multiforme (GBM)	Active[87]
		I	Advanced solid tumors	Recruiting[88]
		I	Hematological malignancies	Recruiting[89]
CPI-0610	Constellation Pharmaceuticals	I	Aggressive lymphoma	Recruiting[90]
		I	Acute leukemias or myelodysplastic syndrome	Recruiting[91]
		I	Previously treated multiple myeloma	Recruiting[92]
TEN-010	Tensha Therapeutics	I	NMC	Recruiting[93]
		I	Advanced solid tumors	Recruiting[94]

Table 1: Summary of BET-bromodomain inhibitors currently undergoing clinical evaluation.

Constellation Pharmaceuticals has been progressing a compound (CPI-0610) in a Phase 1 clinical trial in patients with lymphoma since September 2013.[95]

In August 2014 it announced the initiation of two additional Phase 1 clinical trials involving this compound. The first trial will evaluate CPI-0610 in patients with multiple myeloma, while the second trial will focus on patients with acute leukemias or myelodysplastic syndrome.[96] Tensha Pharmaceuticals is also evaluating a compound known as TEN-010 in an initial Phase 1 clinical trial with patients having advanced solid tumors that have proved intolerant to standard therapies.[97] These studies will hopefully lead to the development of new approaches to treat a variety of disease areas.

1.3.1.2. Other BET-bromodomain inhibitors

The 3,5-dimethylisoxazole moiety was independently discovered by a number of groups as a highly effective KAc mimic. Work by researchers at GSK led to the 3,5-dimethylisoxazole containing compound **9** which showed nanomolar potency for the BET-bromodomain family.[75] This chemotype was also identified in a phenotypic screen by GSK, leading to the BET-bromodomain inhibitor I-BET151 (**7**) which had a BRD4(1) K_D value by ITC of 100 nM and displayed improved pharmacokinetic properties compared to triazolobenzodiazepine scaffolds.[70,98] This scaffold was then used in several structure-based approaches to develop ligands against the BET bromodomains. Work by Hewings *et al.* led to **8**, a potent inhibitor of BRD4(1) with an IC_{50} value of 382 nM which showed strong antiproliferative effects on MV4;11 acute myeloid leukemia cells.[76] A remarkable collection of BET bromodomain inhibitors has been developed, which is discussed at length in a selection of recently published reviews.[52,99-101]

1.3.2. Non-BET bromodomain inhibitors

The functions of BCPs other than the BET bromodomains are much less well understood, although there has recently been a surge in publications involving these proteins, which should help to unravel their biological role. Table 2 lists non-oncology diseases or therapeutic areas where non-BET BCPs have been implicated.

	Bromodomain containing protein	Biochemical pathway or disease implication	Reference
Cell maintenance	FALZ / FAC1	Neurodegenerative (Alzheimer's, amyotrophic lateral sclerosis)	[102]
	PB1 / BAF180 & BRD7	Cellular senescence	[103]
	PCAF	Coronary heart disease (CHD) and mortality	[104]
	BAZ2B	Sudden cardiac death	[105]
Development	BAZ1B	Cardiac and craniofacial defects	[106]
	CECR2	Chromosome abnormality (Schmid-Fraccaro syndrome)	[107]
		Neurogenesis	[108]
		Inner ear development	[109]
	CREBBP / CBP	Growth disorders (Rubinstein-Taybi syndrome)	[110]
	SMARCA4 / BRG1	Mental retardation (Coffin-Siris syndrome)	[111]
Immunology	PCAF	HIV-1 viral replication	[31]
	TRIM28	HIV-1 integration	[112]
		Autoinflammatory T cell development	[113]
	TRIM33	Myositis-specific autoantibodies (dermatomyositis)	[114]
Psychiatric	CREBBP / CBP	Cocaine addiction	[115]
	BRPF2	Bipolar disorder and schizophrenia	[116]
	PBRM1	Schizophrenia and bipolar disorder	[117]
	SMARCA2	Schizophrenia	[118]

Table 2: A list of non-oncology diseases or therapeutic areas where non-BET BCPs have been implicated. It is important to note that although the BCP is involved, the importance of the bromodomain in mediating actions relating to the relevant disease(s) is unknown.

The range of disease areas in Table 2 indicate that there is great potential to develop a variety of bromodomain inhibitors with therapeutic relevance for a wide range of pathologies.The progress made to date in the development of non-BET bromodomain ligands is outlined in the following section. This research has led to a collection of small-molecule inhibitors that should greatly enhance our ability to unravel the biological role of each bromodomain in normal human development and human disease.

1.3.2.1. Early work on the PCAF bromodomain

In 1999 Zhou and colleagues were the first to report a solution structure of a bromodomain (PCAF: p300-CREBBP associated factor) using NMR-based methods.[119] Their pioneering work into the development of new HIV therapeutics led to the first non-peptidic ligand for a bromodomain.[120] Initial studies confirmed that a key stage in HIV replication involved recruitment of the Tat transcriptional coactivator *via* KAc50 (Tat-K50Ac) to the bromodomain of the coactivator PCAF.[31] This finding suggested that Tat/PCAF recruitment *via* a bromodomain-KAc interaction is essential for HIV transcription, providing a new therapeutic target for disrupting the HIV replication pathway. An NMR-based screen of small-molecules was then conducted with an emphasis placed on gaining selectivity by identifying molecules that bound in the peptide-binding groove rather than within the KAc-binding pocket. Lead optimisation and subsequent SAR studies led to **10**, which had a PCAF IC_{50} value of 1.6 μM (Figure 5).

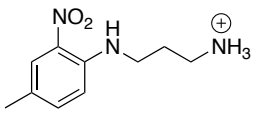

10

Figure 5: **Structure of PCAF ligand 10, the first non-peptidic bromodomain ligand.**[120]

An NMR structure of **10** in complex to PCAF was solved which showed the ligand located in the peptide binding groove. This early study provided a valuable platform to deliver more potent and selective inihibitors of the non-BET bromodomains.

1.3.2.2. CREBBP bromodomain inhibitors

1.3.2.2.1. Early work by the Zhou group

Some of the earliest structural information on the CREBBP (cAMP-response element binding protein (CREB)-binding protein) bromodomain was obtained by the Zhou group during their investigation into its interaction with the transcription factor p53.[121] Using their previous results as a valuable platform, in 2007 the same group were the first to screen for small molecule inhibitors of the CREBBP bromodomain, leading to the identification of 14 bromodomain ligands.[122] Two of these, **11** (MS2126) and **12** (MS7972), (Figure 6), were shown to block the interaction between p53 and CREBBP in a concentration-dependent manner.

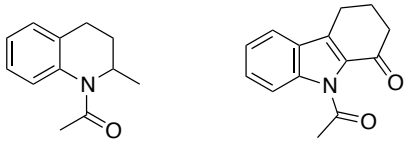

MS2126 **11**

MS7972 **12**

Figure 6: **CREBBP bromodomain ligands 11 and 12, identified by the Zhou group**.[122]

In a fluorescence-based assay **12** (MS7179) was found to bind to CREBBP with a K_D value of approximately 20 μM. The NMR structure of **12** bound to CREBBP showed that, although the compound occupies the KAc binding site, it forms no specific interactions with the conserved asparagine residue. These fragments have not been further optimised against CREBBP, although the tetrahydroquinoline moiety of **11** is contained in highly potent and selective BET-inhibitor I-BET726.[123]

In a subsequent NMR screen conducted by the Zhou group on a larger set of 3000 compounds, a range of hits containing an azobenzene scaffold were identified.[124] Further SAR studies using a p53 dependent cell-based assay led to compound **13** which had an IC_{50} value of 5 μM and up to four-fold selectivity over BRD4(1), PCAF and BAZ2B, (Figure 7).

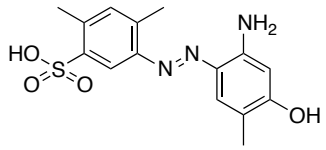

Ischemin
13

Figure 7: **The CREBBP ligand 13 (Ischemin), developed by the Zhou group**.[124]

The NMR-structure of **13** bound to CREBBP revealed that the ligand binds at the entrance to the KAc binding pocket, sandwiched through hydrophobic and aromatic interactions. It was shown that **13** inhibits doxorubicin-induced apoptosis in living cells, demonstrating that this compound is cell-permeable and functions as a cellular protective agent against myocardial ischemic stress, giving it the name Ischemin.

1.3.2.2.2. Potent and selective inhibitors of the CREBBP bromodomain

The ability of solvent molecules to disrupt bromodomain-peptide binding has been demonstrated by workers at the SGC, who found that several solvents, including DMSO and NMP, inhibited the binding of acetylated peptides to bromodomains, with NMR and X-ray crystallography confirming that these compounds acted as KAc mimics.[125] Further screening of NMP analogues revealed that 3,4-dihydro-3-methyl-2(1*H*)-quinazolinone (DHQ) also binds to the CREBBP bromodomain, and this fragment has since been used to develop a number of BET bromodomain ligands.[99] A key limitation of this fragment was its susceptibility to oxidation at the benzylic position.[126] Work by Rooney *et al*. sought to address this problem by replacement of the DHQ with a dihydroquinoxalinone core (Figure 8).[127] Extensive synthetic and computational work led to the development of **14**, which binds to CREBBP with an IC_{50} value of 323 nM.

A **B**

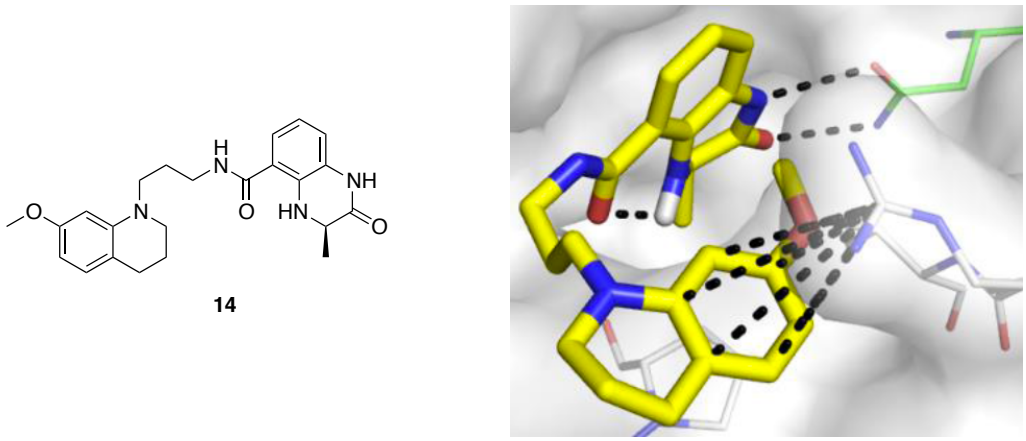

Figure 8: **CREBBP ligand 14, developed by Rooney and co-workers**. (**A**) The CREBBP dihydroquinoxalinone-based inhibitor **14**. (**B**) Crystal structure of **14** bound to CREBBP (PDB ID: 4NTX) with key interactions shown (adapted with permission from Rooney *et al*.).[127]

The X-ray crystal structure of **14** bound to CREBBP revealed that the ligand binds in an induced-fit pocket, with the electron rich tetrahydroquinoline moiety forming a cation-π interaction with R1173 of CREBBP.

Using a fluorescence recovery after photobleaching (FRAP) assay,[128] **14** was shown to displace the CREBBP bromodomain from chromatin in living cells, demonstrating its utility for future studies *in vivo*. This work would prove vital in the development of subsequent inhibitors of the CREBBP bromodomain.

Benzimidazole containing dimethylisoxazoles (DMIs) were initially found to be promiscuous BET and CREBBP bromodomain inhibitors[129] but have recently been optimised in the development of SGC-CBP030 **15**, (Figure 9), which has a K_D value of 21 nM for CREBBP and 40-fold selectivity over BRD4(1).[130] The crystal structure of **15** bound to CREBBP indicates that as expected, the DMI core binds in the KAc binding site, while the aryl substituent forms a cation-π interaction with R1173 of CREBBP, consistent with Rooney's findings. A FRAP assay was used to show that **15** can displace the CREBBP bromodomain from chromatin in living cells. This compound, also referred to as CBP030, was subsequently shown to suppress human Th17 responses in human cells.[131] In unbiased cellular testing across a panel of cultured primary human cells, CBP30 reduced immune cell production of IL-17A and other proinflammatory cytokines. It was also shown that treatment of human T cells with CBP30 led to a much more restricted effect on gene expression than that observed with the pan-BET (bromo and extra-terminal domain protein family) bromodomain inhibitor JQ1. These promising results suggest that CBP30

could lead to fewer side effects than the broadly acting epigenetic inhibitors currently undergoing clinical development.

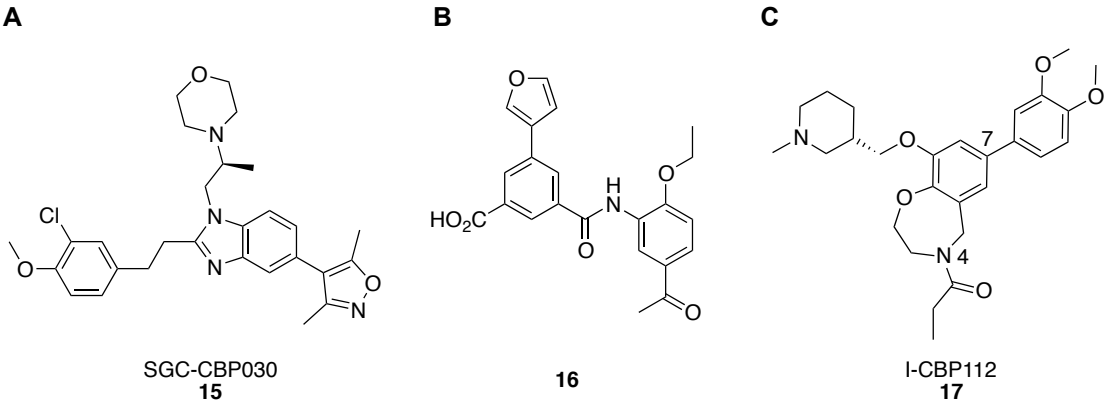

Figure 9: Nanomolar ligands for the CREBBP bromodomain. (**A**) 3,5-DMI probe developed by the SGC.[130] (**B**) CREBBP acetyl benzene probe.[132,133] (**C**) Benzoxazepine probe developed by collaborations between the SGC and GSK.[134]

Unzue *et al*. recently combined high-throughput docking and structure-based optimisation to develop the potent and selective CREBBP inhibitor **16** (Figure 9).[133] During their work, X-ray crystallography studies identified the acetyl-benzene moiety as an attractive KAc-mimetic and revealed the carboxylic acid group of **16** engaged in an electrostatic interaction with R1173 of CREBBP. Further binding studies showed that **16** has a K_D value of 170 nM by ITC and is approximately 60-fold selective over BRD4(1). Derivatives of **16** including its methyl ester analogue were screened across a panel of cancer cell lines and showed growth inhibition for a selection of leukaemia cell lines, suggesting a potential involvement of CREBBP in this pathology.

The SGC and GSK have recently collaborated to develop a benzoxazepine based inhibitor, I-CBP112 (**17**) (Figure 9) which binds to the bromodomains of CREBBP and EP300 with K_D values by ITC of 151 nM and 625 nM respectively.[134] The development of **17** is yet to be disclosed but a structure is

available in the PDB. Interestingly, the acyl group attached to N(4) acts as the KAc mimic and the aryl group at C(7) forms a cation-π interaction with R1173 of CREBBP. This compound was active in a FRAP assay, demonstrating an on-target effect in a cellular environment.

1.3.2.3. BAZ2A and BAZ2B bromodomain inhibitors

The BAZ2B (bromodomain adjacent to zinc finger domain protein 2B) bromodomain was initially categorised as one of the least druggable bromodomains due to an unusually small KAc-binding pocket compared to the other 41 bromodomains for which structural information is available (92-105 $Å^3$ volume compared to 131-221 $Å^3$ in BRD4(1)).[135] Despite this, progress has recently been made to develop inhibitors of this bromodomain. Ferguson *et al.* adopted a fragment-based approach leading to **18**, which although was a relatively weak binder with an IC_{50} value of 9 μM, demonstrated that this family may be tractable to small molecule modulation.[136] Interestingly, synthetic efforts to optimise interactions in and around the KAc binding pocket proved more productive than explorations in its wider peripheries.

Collaborations between the SGC and the Institute of Cancer Research (ICR) have recently led to the BAZ2-ICR (**20**, Figure 10), a chemical probe of the BAZ2A and BAZ2B bromodomains.[137] A series of putative bromodomain inhibitors previously reported during a virtual screening campaign were used to identify a chemical starting point.[138] Compound **19** was identified as a weak inhibitor of BAZ2A (IC_{50} = 51 μM) and BAZ2B (IC_{50} = 26 μM).

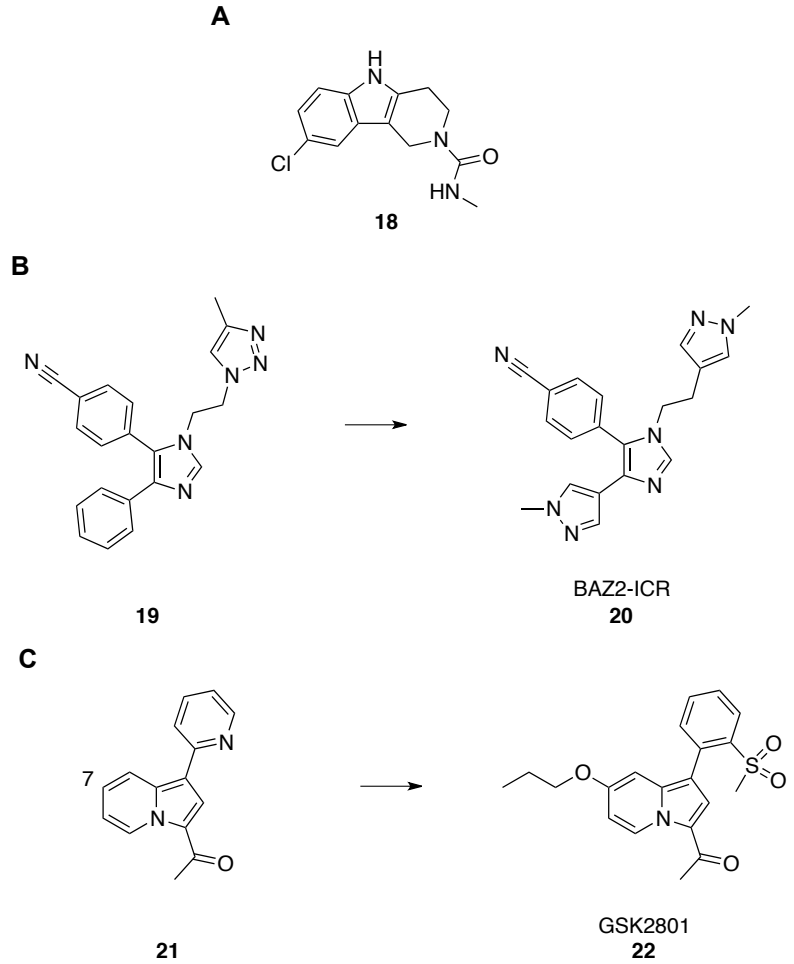

Figure 10: Ligands for the BAZ2A and BAZ2B bromodomains. (**A**) The first small molecule ligand of BAZ2B, **18**.[136] (**B**) Development of BAZ2-ICR (**20**).[137] (**C**) Development of GSK2801 (**22**).[139]

A crystal structure of **19** bound to BAZ2B was solved, and surprisingly the structure revealed that the hydrophobic phenyl ring of **19** occupied the KAc binding pocket, instead of the expected methyl-triazolo group. A large gain in potency was achieved by replacing this phenyl ring with a pyrazole group, capable of acting as the KAc mimetic. It was also found that **19** engaged in an intramolecular, face-to-face π-π-stacking interaction in the bound state, between the nitrile substituted phenyl ring and the triazole ring. ^{1}H NMR spectroscopy revealed that **19** did not adopt this π-stacked conformation in solution, therefore attention turned to stabilising the bioactive conformation. This approach led to BAZ2-ICR (**20**), the most potent compound of the series,

which had K_D values by ITC of 109 nM and 170 nM to BAZ2A and BAZ2B, respectively. The selectivity of **20** was assessed against 47 bromodomains using thermal shift and the compound showed no significant stabilisation of all other bromodomains, except for CECR2 (Cat Eye syndrome Chromosome Region, candidate 2), where a small stabilisation was observed (ΔT_m: 2.0 °C). The CECR2 K_D of **20** was determined by ITC to be 1.55 μM, representing 15-fold selectivity when compared to BAZ2A and a 10-fold window to BAZ2B. No binding to BRD4(1) could be detected up to a compound concentration of 50 μM in an AlphaScreen assay, translating to a greater than 100-fold window. Using a fluorescence recovery after photobleaching (FRAP) assay, **20** was shown to displace BAZ2 bromodomains from chromatin in living cells. Physicochemical and mouse pharmacokinetic measurements showed that **20** has high solubility (25 mM in (D_2O)), moderate clearance (~50% of mouse liver blood flow) and 70% bioavailability. These results suggest that **20** is suitable for modulating BAZ2A and BAZ2B *in vivo* and experiments to investigate the biological role of BAZ2A and BAZ2B are underway.[137]

GSK and the SGC have reported GSK2801 (**22**, Figure 10) as a chemical probe of the BAZ2A and BAZ2B bromodomains that can be used in addition to **22** as an orthogonal inhibitor of this target.[139] To identify a lead BAZ2A ligand, a set of KAc-mimetic ligands were screened against the BAZ2A bromodomain. This led to indolizine containing compound **21** as a ligand efficient BAZ2A inhibitor with an IC_{50} value of 1.5 μM, and similar activity against the BET bromodomains. This hit was optimised in two positions, the indolizine 7-position and the pendant aryl substituent, leading to GSK2801

(**22**), which had K_D values by ITC of 136 nM and 257 nM for BAZ2B and BAZ2A, respectively. The selectivity of **22** against a panel of 46 bromodomains was measured using a thermal shift assay. Significant thermal stabilisation was observed for the second bromodomain in TAF1L(2) (3.4 °C) and BRD9 (2.3 °C). The off-target interactions were quantified by ITC which showed that **22** bound to TAF1L(2) and BRD9 with K_D values of 3.2 μM and 1.1 μM, respectively. Using a FRAP assay, **22** was shown to displace full length BAZ2A from chromatin in living cells. Pharmacokinetic studies in mice showed that **22** is suitable for further biological studies into the physiological role of these bromodomains.[139]

1.3.2.4. BRPF1 and TRIM24 bromodomain inhibitors

GSK have developed a potent inhibitor of the BRPF1 (Bromodomain and PHD Finger-Containing Protein 1) bromodomain.[140] Their starting fragment **23** (Figure 11) was derived from an STD-NMR screen against BRD4(1). An X-ray crystal structure of BRD4(1) in complex with **23** showed the carbonyl oxygen of the benzimidazolone making interactions mimicking those of the KAc side chain. This compound had good BRPF1 potency (pIC_{50} value 5.0) but low selectivity over BRD4(1) (pIC_{50} value 4.1) as determined by TR-FRET competition experiments. A set of compounds derived from BET-binding fragments, such as **23**, were then screened against BRPF1 and BRD4(1) which led to a collection of 1,3-dimethyl benzimidazolone-containing molecules. The hits were verified in an NMR-based assay, and structure-guided modifications to the amide and piperidine were explored. Compound **24** (Figure 11) was found to have the highest selectivity window over BRD4(1)

and was therefore evaluated in the BROMO*scan* panel of 35 bromodomains. In this assay, **24** showed a high potency for BRPF1 (pK_D = 8.0) and 500-fold selectivity over the BET family, as well as 80-fold and 300-fold selectivity over BRPF2(1) and BRPF3, respectively. Compound **24** displaced the BRPF1 bromodomain from chromatin in a cellular protein interaction assay, demonstrating its potential utility for future experiments *in vivo*.

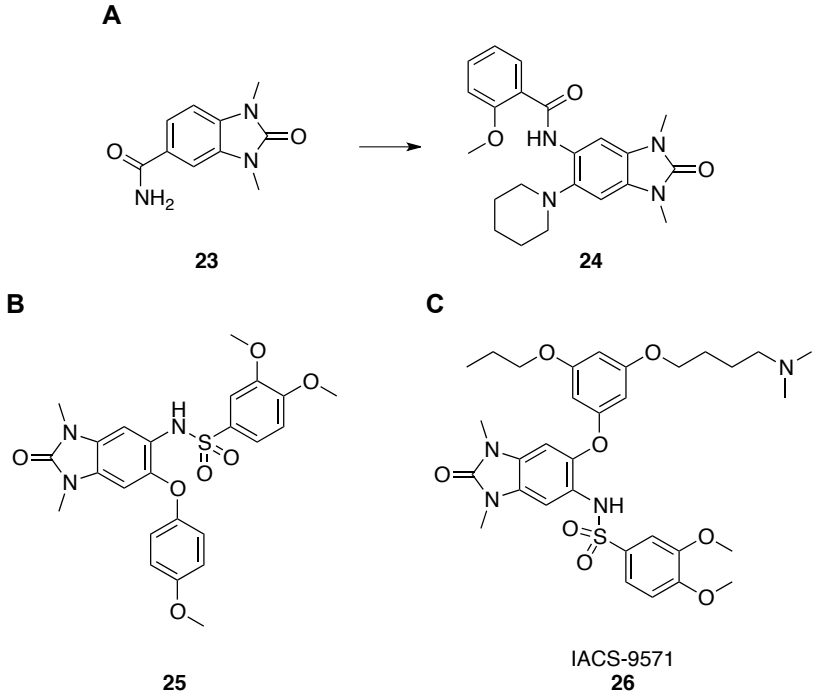

23 **24** **25** **26**

Figure 11: Ligands for the BRPF1 and TRIM24 bromodomains. (**A**) Development of the BRPF1 probe **24**.[140] (**B**) Structure of the TRIM24 bromodomain probe **25**.[141] (**C**) The TRIM24-BRPF1 bromodomain inhibitor **26**.[142]

Tripartite motif 24 protein (TRIM24), also known as TIF1α, contains a plant homeodomain (PHD) and a bromodomain. This dual protein recognises unmodified H3K4 with its PHD zinc finger domain and H3K23Ac with its bromodomain.[141] The SGC has developed a potent inhibitor of this bromodomain to examine its potential role in human cancers.[143] Based on the previous identification of the 1,3-benzimidazolone scaffold as a KAc competitive inhibitor of bromodomains of the BRPF family, a selection of 5-

position substituted sulfonamides were screened against the TRIM24 bromodomain using an AlphaScreen assay. This led to a compound that had a TRIM24 IC_{50} value of 3.5 μM. Structure-activity relationship studies resulted in compound **25**, which showed good activity for TRIM24 (IC_{50} = 430 nM), although selectivity over BRPF bromodomains was not achieved (BRPF1 IC_{50} = 340 nM, BRPF2 IC_{50} = 1.75 μM). Compound **25** displayed excellent selectivity for these three bromodomains in a panel of 45 bromodomains. Using a FRAP assay, **25** was shown to displace the full length GFP-TRIM24 from chromatin in living cells. As overexpression of TRIM24 has been linked to cancer, the impact of **25** on a small panel of diverse cancer cell lines was examined. However, **25** showed no significant cytotoxicity in the cell lines tested, with only modest sensitivity shown in the myeloma MM1S model (GI_{50} >10 μM).

Research carried out at the University of Texas by Palmer *et al*. led to a selective high-affinity dual TRIM24-BRPF1 bromodomain inhibitor.[142] At the start of their work there were no known small molecule TRIM-24 bromodomain inhibitors, therefore three different hit identification approaches for finding novel scaffolds were employed: virtual in silico high-throughput screening (HTS), construction of a focused KAc mimetic library and a traditional small-molecule library HTS. This approach led to five chemotypes, including the 1,3-dimethyl benzimidazolone scaffold that was found to be the most potent and synthetically attractive for further optimisation. Rigorous structure-activity relationship studies led to **26** (IACS-9571), which had an IC_{50} value of 7.6 nM in a TRIM24 AlphaScreen™ assay. The selectivity of **26** was

confirmed in a BROMO*scan* panel of 32 bromodomains, which also revealed low nanomolar affinity for the BRPF family of bromodomains and greater than 7,700-fold selectivity versus BRD4(1,2) relative to TRIM24. Cellular target engagement was confirmed using an AlphaLisa assay[144] in which **26** displaced TRIM24 from chromatin in HeLa cells, and studies in mice revealed attractive pharmacokinetic features, making this compound useful for future studies *in vivo*.

1.3.2.5. A SMARCA2, SMARCA4 and PB1(5) bromodomain inhibitor

Pfizer and the SGC have collaborated to develop PFI-3 (**27**, Figure 12), a potent and selective inhibitor of the bromodomains of SMARCA2/4 and PB1(5).[145] A detailed description of this compound's development has not yet been disclosed, although it has been reported to bind to the bromodomains of SMARCA4 and PB1(5) with K_D values by ITC of 89 nM and 48 nM, respectively. It also showed good selectivity against a panel of diverse bromodomains in a thermal shift assay. Using a FRAP assay, **27** was shown to displace the SMARCA-2 from chromatin in living cells.[125]

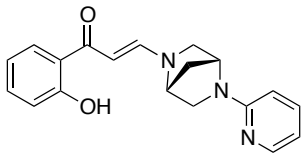

PFI-3
27

Figure 12: Structure of PFI-3, a SMARCA2/4 and PB1(5) bromodomain probe.[145]

A recent genetic and pharmacological study showed that PFI-3 is capable of displacing the SMARCA2-bromodomain from chromatin in tumor cells.[146] However, this inhibitor failed to display an antiproliferative phenotype,

explained by its inability to displace endogenous, full-length SMARCA2 from chromatin. Interestingly, the authors "…identify the ATPase domain, and not the bromodomain of SMARCA2, as the relevant therapeutic target."[146]

1.3.2.6. ATAD2 bromodomain ligands

The bromodomain of ATAD2 has a very polar and shallow binding pocket, suggesting that this poorly understood bromodomain is unlikely to be ligandable.[135] Yet three recent publications of KAc-mimetic fragments of this bromodomain have provided useful chemical starting points for more potent inhibitors of this bromodomain (Figure 13). Chaikuad *et al*. hypothesised that the ATAD2 binding pocket, which is highly negatively-charged, may favour hydrophilic ligands.[147] Further work by this group led to identification of thymine **28**, which contains a putative KAc mimetic moiety, as the most potent compound reported with an ATAD2 K_D value of 10 mM determined by NMR.

Harner *et al.* independently identified twelve micromolar fragments of the ATAD2 bromodomain using a diverse chemical library in combination with NMR spectroscopy and X-ray crystallography studies.[148] Of these, **29** was the tightest binder with a K_D value of 350 μM and **30** had the highest ligand efficiency value (0.38). The tricyclic compound **30** was successfully crystallised with ATAD2 (Figure 13).

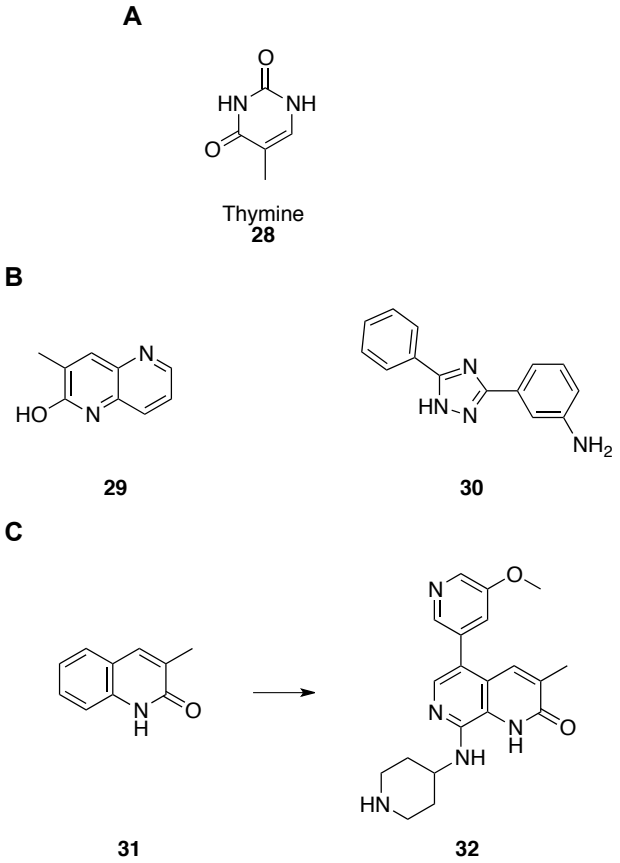

Figure 13: Starting points for selective probes of the ATAD2 bromodomains. (**A**) The structure of thymine (**28**).[147] (**B**) The first micromolar ATAD2 ligands.[148] (**C**) The most potent ATAD2 ligands published to date.[149]

Interestingly, the structure revealed that the KAc mimetic triazole unit appears to displace a conserved water molecule in the binding site, helping to explain its relatively high affinity. It is also clear from the X-ray crystal structure that the 3-aminophenyl substituent sits deep within the KAc binding pocket, displacing three additional water molecules. Strikingly, compound **30** displaced a total of four water molecules from the ATAD2 bromodomain, by far the largest number observed to date in the bromodomain literature.

Workers at GSK have developed the most potent ATAD2 ligands to date using a fragment-based approach.[149] A focused set of compounds containing known and hypothetical KAc mimics were screened using time-resolved

fluorescence resonance energy transfer (TR-FRET)-labeled peptide displacement assay. This led to the quinolinone hit **31** (Figure 13), which was inspired by the dihydroquinazolinone fragment, known to bind to the BET bromodomains. Subsequent optimisation of this compound led to **32**, which has an ATAD2 IC_{50} value of 1.3 μM, with no selectivity reported over the BET bromodomain family. The X-ray crystal structure of **32** bound to ATAD2 confirms the expected binding mode; the amide moiety sits in the KAc binding pocket and forms hydrogen bonds to the conserved asparagine resdidue. The authors comment that this compound has been developed into "the first potent and cell-permeable ATAD2 chemical probe with selectivity over the BET family and other bromodomains," which will be the subject of their next publication.

1.3.3. BRD9

1.3.3.1. BRD9 in human disease

The precise biological function of BRD9 (bromodomain-containing protein 9) remains elusive, although several studies have linked it to a variety of human diseases. The *BRD9* gene is located on chromosome 5p, in a region that has been found to be frequently altered in cervical cancer. Scotto *et al*. have found that gain at this region resulted in up-regulation of BRD9.[150] The same alteration is one of the most consistent mutations in the early stages of non-small cell lung cancer and up-regulation of BRD9 has also been linked to this disease.[151] In addition, BRD9 has been reported as a component of the chromatin remodeling SWI/SNF BAF complex.[152,153] SWI/SNF subunits are

mutated in 20% of all human tumors reported in 44 studies and have been implicated as tumor suppressors in a variety of human malignancies.[152]

The studies above relate disease phenotype to levels of expression of the BRD9 protein as a whole and the specific role of the bromodomain remains unknown. Small molecule inhibitors enable protein activity to be profiled in a rapid, reversible and highly selective manner.[154] A potent and selective inhibitor of the BRD9 bromodomain would provide a useful tool to investigate its biological role and to determine whether it is an attractive therapeutic target. In the past two years great progress has been made to develop potent and selective inhibitors of BRD9, a summary of which is described in the following section

1.3.3.2 BRD9 inhibitors

1.3.3.2.1 Triazoles

The triazolopyridazine scaffold was reported as a BRD9 inhibitor in a patent by Constellation Pharmaceuticals[155] and the closely related triazolophthalizine scaffold was subsequently developed by the SGC into the first nanomolar inhibitor of BRD9.[156] Their studies began by screening a of commercially available triazole-containing compounds in a thermal shift assay against 17 bromodomains. Sulfonamides at the R1 position of scaffold **33** (Figure 14) were found to have greater potency than amides, and the potency of N- and S-linked sulfonamides were found to be similar.

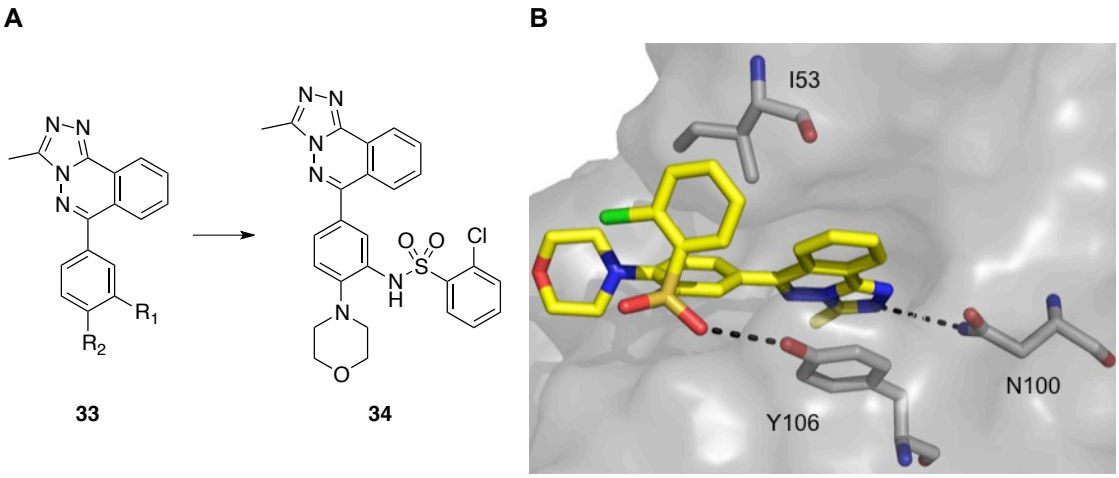

Figure 14: Tricyclic triazole ligands of BRD9. (**A**) Scaffold development. (**B**) X-ray crystal structure of **34** bound to BRD9 (PDB ID: 4NQN).[156]

All of the purchased compounds contained an R2 methyl group and a des-methyl analogue was also synthesised and shown to be inactive across all bromodomains. Extensive SAR was challenging due to the poor solubility of this compound series, although a substantial improvement in solubility was gained by introducing a morpholine moiety at the R2 position. A series of alkyl and aryl sulfonamides were found to be well tolerated across a range of bromodomains, leading to **34** which had BRD9, BRD4(1) and CREBBP IC_{50} values of 200 nM, 158 nM and 158 nM respectively. Co-crystal structures of **34** bound to BRD9 and BRD4(1) were obtained, which showed the triazole moiety forming hydrogen bonds to the conserved asparagine N100 in BRD9 and N140 in BRD4(1). In BRD9 the sulfonamide is rotated to allow a hydrophobic interaction between the 2-chlorophenyl group and I53 in BRD4(1), leaving the sulfonamide in a position to accept a hydrogen bond from the phenol of Y106. Using a fluorescence recovery after photobleaching (FRAP) assay, **34** was shown to displace the CREBBP bromodomain from chromatin in living cells.

Work done by the SGC led to bromosporine (**35**), a pan-bromodomain inhibitor which displayed a thermal shift value of 3.9 °C against BRD9.[157] This compound was evaluated against 19 bromodomains in a thermal shift assay and showed a $\Delta T_m \geq 3.0$ °C for 12 of these targets. The highest stabilisation was observed for CECR2, BRDT(1) and BRD4(1), which had ΔT_m values of 8.3 °C, 7.3 °C and 6.9 °C respectively.

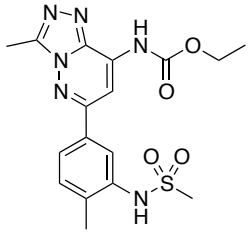

Bromosporine
35

Figure 15: Structure of the pan-bromodomain inhibitor, bromosporine (35).[157]

Cellular potency against BRD4 and CREBBP was confirmed in a FRAP assay, and **35** showed moderate cytotoxicity in HeLa cells at 18 μM. This non-selective inhibitor should be useful in studying other bromodomains for which small molecules have yet to be developed.

1.3.3.2.2. The 9*H*-purine scaffold

Picaud and co-workers at the SGC recently developed the 9*H*-purine scaffold as a useful chemical starting point for the discovery of selective BRD9 ligands.[158] As a "privileged" chemical template,[159,160] purine is an attractive scaffold, leading this group to complete a computational and *in vitro* evaluation of purine-based fragments including compound **36**. Structural optimisation of a 6-aryl substituent led to identification of **37**, which had a BRD9 K_D value of 397 nM by ITC.

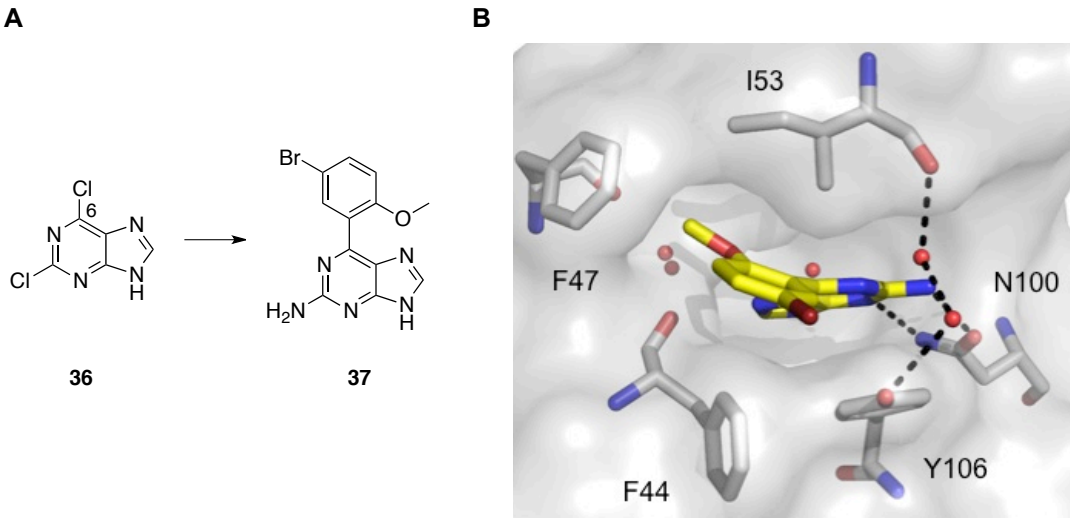

Figure 16: Development of the 9*H*-purine scaffold as a BRD9 inhibitor class. (**A**) Scaffold development. (**B**) X-Ray crystal structure of **37** (ligand carbon framework shown in yellow) bound to BRD9 (PDB ID: 4XY8).[158]

The X-ray crystal structure of **37** (Figure 16) bound to BRD9 revealed that the primary amine forms a hydrogen bonding interaction with the conserved asparagine residue (N100). Interestingly, **37** has an induced-fit binding mode which results in substantial rotations of the side chains of F47 and F44 while the top of the ZA loop collapses toward the ligand (Figure 16). The high potency of **37** is also explained by its ability to bind *via* a network of water-mediated hydrogen bonds within the KAc binding cavity, extending to the top of the ZA-loop to the carbonyl of I53. Disappointingly, **37** showed only approximately five-fold selectivity over the BET family member BRD3(1) by ITC, although it was capable of displacing the BRD9 bromodomain from chromatin in living cells, while failing to displace full length human BRD4 at the same concentration. This scaffold offers a simple template that can be further optimised to produce selective biological tools of the BRD9 bromodomain.

1.3.3.2.3. I-BRD9

Theodoulou and co-workers at GSK recently reported I-BRD9 (**39**) as a selective chemical probe for BRD9.[161] An initial cross-screening strategy of GSK internal compounds identified thienopyridone **38** as a potent inhibitor of BRD9 (TR-FRET assay), displaying pIC_{50} values of 6.7 and 4.7 against BRD9 and BRD4(1), respectively (Figure 17).

The X-ray crystal structure of **38** bound to BRD9 confirmed the *N*-methyl pyridone moiety as the key KAc mimetic and this group sits in a small cavity surrounded by four conserved water molecules. Optimisation of **38** began with analysis of the X-ray crystal structure of **38** in complex with the bromodomain of BRD9, which indicated a clash between the amide carbonyl and the backbone carbonyl of I53. Replacement of the amide carbonyl with a hydrogen-bond donating amidine linkage gave a substantial increase in BRD9 selectivity. Changing the methyl sulfonamide to a cyclic sulfone resulted in a 10-fold improvement in BRD9 potency, as the sulfone is able to form a hydrogen bond to the backbone NH atoms of R101. Attention then turned to optimisation of the 7-position substituent of the thienopyridone core. Late-stage Suzuki-coupling of a variety of both electron-donating and electron-withdrawing substituents led to the conclusion that a 3-trifluoromethyl phenyl ring was optimal, leading to a 160-fold selectivity window over BRD4.

The final element of SAR focused on increasing the KAc mimetic alkyl chain from *N*-methyl to *N*-ethyl leading to I-BRD9 (**39**) which displayed a superior selectivity profile in a selection of TR-FRET assays and was therefore profiled

a broader selectivity screen in the BROMO*scan* assay against 34 bromodomains. The results indicated that **39** had a K_D value of 1.9 nM for BRD9, which translates to 700-fold selectivity over the BET family, 200-fold selectivity over the closely related BRD7 bromodomain and 70-fold selectivity over the next-strongest interacting partner CECR2.

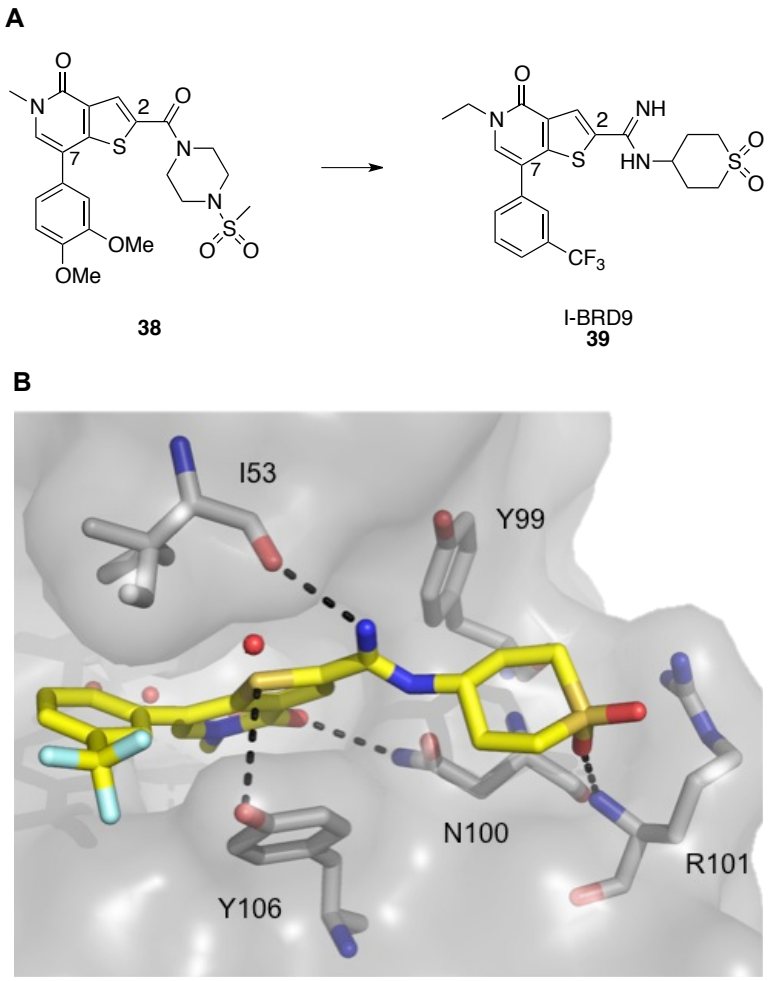

Figure 17: Development of I-BRD9 (39). (A) Lead **38** and I-BRD9 (**39**). **(B)** X-ray crystal structure of **39** (ligand carbon framework shwon in yellow) bound to BRD9 (PDB ID: 4UIV).[161]

Cellular target engagement of BRD9 was demonstrated as I-BRD9 was shown to displace the BRD9 bromodomain from chromatin in a dose-dependent manner in living cells. Further screening across a broad range of pharmacological targets including ion channels and kinases showed that **39** had no activity at less than 5 μM against a panel of targets. The specific

genes which are regulated by BRD9 bromodomain inhibition were then investigated. To achieve this, Kasumi-1 cells were treated with the BET-inhibitor I-BET151 and I-BRD9 for 6 h. Four representative genes (CLEC1, DUSP6, FES and SAMSN1) were found to be selectively down-regulated, each of which have been implicated in cancer and inflammatory indications.

1.3.3.2.4. LP99

Clark *et al*. recently reported the development of a potent BRD9 inhibitor.[162] Their studies began with the fragment 1-methylquinolone (**40**), which was found to bind to BRD9 with a K_D value of 5.0 μM by ITC (Figure 18). An X-ray crystal structure of **40** in complex with BRD9 confirmed the *N*-methyl amide moiety as the KAc mimic, forming similar hydrogen bonds to the conserved asparagine residue. Further analysis of this X-ray crystal structure led to the hypothesis that gains in potency could be made by introducing a C4 methyl group on the quinolone core, which would be projected into a small hydrophobic pocket in BRD9. It was also observed that the ZA loop in BRD9 was much larger than that of other bromodomains. The C7 position of **40** (Figure 18) was identified as an attractive location to attach a large heterocyclic component capable of exploiting this hydrophobic region, in order to increase selectivity for BRD9. A structure-activity relationship was quickly established at this position through the use of an asymmetric cascade reaction process, which led to LP99 (**41**). LP99 has BRD9 K_D value of 99 nM by ITC. The X-ray crystal structure of **41** in complex with BRD9 shows the extensive hydrogen bonding (G43) and hydrophobic (F47) interactions between the protein and pendant lactam portion of the ligand.

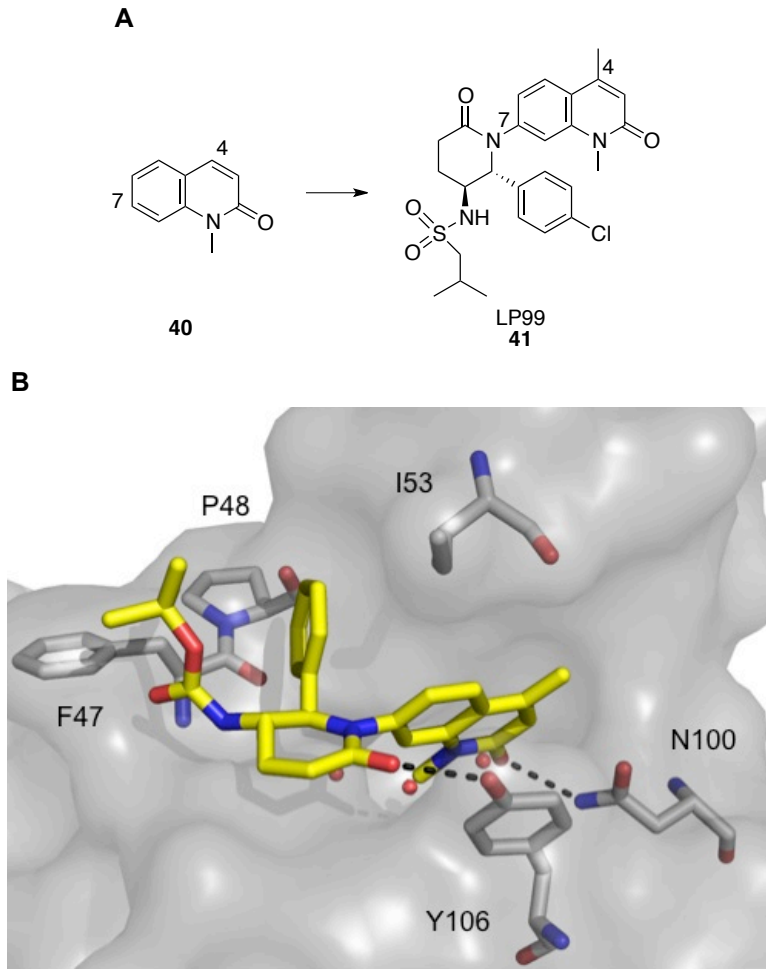

Figure 18: Development of LP99 (41). (**A**) Progress from hit **40** to **LP99**. (**B**) X-ray crystal structure of **41** bound to BRD9 (PDB ID: 4Z6I).[162]

In a broad DSF assay, compound **41** was found to have similar affinity for the closely related bromodomain of BRD7. For the 46 other bromodomains examined in this assay, a stabilisation of <1 °C for all proteins was observed. Using a FRAP assay, **41** was shown to displace BRD9 and BRD7 bromodomains from chromatin in living cells. Further biological studies demonstrated that **41** inhibited secretion of the pro-inflammatory cytokine interleukin 6 (IL-6) in a dose-dependent manner. This interesting result demonstrates that BRD7 and BRD9 play a role in the regulation of inflammatory cytokines and are potential novel targets for anti-inflammatory treatment.

1.3.3.2.5. Keto-indolizines

Hay *et al*. recently reported the keto-indolizine **43** (Figure 19), as a potent and selective inhibitor of the BRD7 and BRD9 bromodomains.[163] During the development of the BAZ2A/B chemical probe **22** (GSK2801), it was observed that pyridine-containing analogues of this compound such as **42** (Figure 19) exhibited nanomolar potency for the BRD9 bromodomain. Subsequent SAR studies led to compound **43**, which had BRD9 and BRD7 K_D values by ITC of 68 nM and 368 nM respectively, in addition to modest affinity for BRPF1B, CREBBP and FALZ.

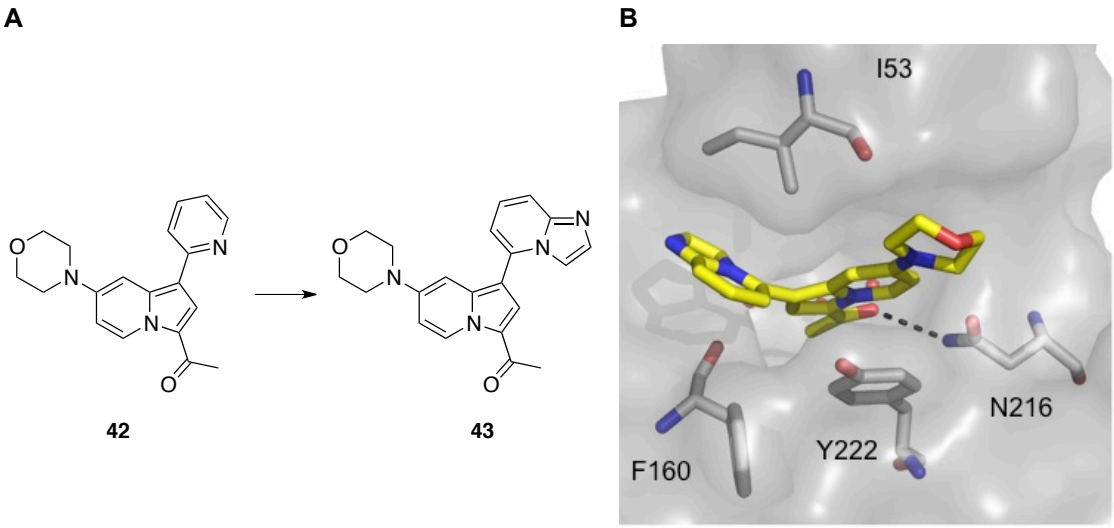

Figure 19: Keto-indolizines as BRD9 inhibitors. (**A**) Scaffold development. (**B**) X-ray crystal structure of **43** bound to BRD9 (PDB file requested from journal authors).[163]

The X-ray structure of **43** bound to BRD9 was determined (Figure 19) which showed the ketone of **43** engaged in the expected KAc mimicking interactions with N216 and the indolizine ring involved in a π-π interaction with Y222. Using a FRAP assay, **43** was shown to displace the BRD9 bromodomain from chromatin in living cells.

1.4. Summary

The research which led to the publication in 2010 of the first two nanomolar bromodomain ligands (+)-JQ1 and IBET-762 ignited a period of significant interest in this field. Five BET-bromodomain ligands are currently undergoing clinical evaluation and the results should guide us as to whether human diseases can be treated using this approach. More recently, the early success in developing small-molecule inhibitors of the BET family of bromodomains has been extended into non-BET bromodomains. Several potent CREBBP and BRD9 ligands have been developed, and particular encouragement can be taken from the progress made in developing small molecule ligands for bromodomains which were once considered difficult to drug, such as BAZ2B and ATAD2. The biological functions of the non-BET BCPs are relatively poorly understood and there remains a high demand to expand the availability of small molecule probes for this protein class, to enhance our ability to dissect their biological roles and therapeutic relevance.

1.5. Project Aims

At the start of this project, the BET bromodomain inhibitors (+)-JQ1 and IBET-762 had recently been developed by co-workers at the SGC, and their biological utility was beginning to become appreciated. There was a great incentive to expand the rapid success made in probing the BET-bromodomain sub-family, to develop potent and selective inhibitors of the non-BET bromodomains in order to understand their biological importance and therapeutic potential.

BRD9 was chosen as the primary target of this project due to the interesting biology, previously outlined, in combination with the availability of structural and ligand binding information. By completing a detailed structure-activity relationship against this target, we aim to develop a compound possessing nanomolar affinity *in vitro* with attractive physicochemical properties for further studies in a biological setting. Selectivity over other bromodomains, especially the BET family member BRD4(1) is also desired. We hope to generate unique insights into this exciting epigenetic target class, which could be used in other ligand discovery efforts to deliver new chemical tools for other bromodomains.

The number of reliable, high-throughput assays available to measure the interaction between bromodomains and their ligands remains relatively low. We aim to investigate new ways of quantifying these interactions in order to extend the range of techniques available to rapidly and reliably generate structure-activity relationships.

Chapter 2: Bicyclic triazoles as BRD9 inhibitors

2.1 Introduction and aims

2.1.1 The need for new bromodomain ligands

The development of several open-access chemical probes, notably (+)-JQ1, has led to a period of rapid progress in this research area, assisting the entry of five compounds into clinical trials,[73,85-94] as outlined in Chapter 1. The availability of a diverse set of well-characterised small molecules has greatly assisted in understanding the biological role and therapeutic relevance of the BET family of bromodomains. At the start of this work, however, there were no published potent and selective bromodomain inhibitors outside the BET-family, and it was unknown whether they could be successfully targeted with small molecules in a similar manner. Since then, three potent and selective inhibitors of BRD9 have been developed and used to identify this epigenetic modulator as a potential therapeutic target in both cancer and the inflammatory response pathway.[158,161,162]

Despite the success of these compounds, the demand for new inhibitors remains. In particular, by having access to a range of chemically distinct small molecules with the same molecular target, greater confidence can be placed in conclusions made from responses observed in a biological system.

2.1.2 Tricyclic triazole starting point

In order to identify new chemical starting points of the non-BET bromodomains, a high throughput screen was carried out at the SGC, which identified the tricyclic triazole scaffold as an interesting chemotype for further development. The results were followed by a structure-activity study, which led to **34**, a potent inhibitor of BRD9 (Table 3).[156]

Structure	Parameters	Value
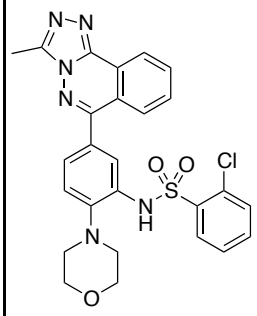 **34**	**IC_{50} *vs* BRD9 / nM**	200
	IC_{50} *vs* BRD4(1) / nM	158
	Fold selectiivty over BRD4(1)	0.8
	c log $D_{pH7.4}$	3.4
	SFI (c log D + # aryl rings)	8.4

Table 3: Parameters for the tricyclic triazole 34.[156] c Log D was calculated using ACD/Labs algorithm (version 5.0.0.184).

This compound was found to be a non-selective bromodomain inhibitor, and the development of this tricyclic scaffold is discussed in more detail in Chapter 1.

2.1.3. Aims

The crystallographic and binding data for **34** gave rise to some interesting questions:

- Can the BRD9 potency and selectivity of **34** be increased?
- Would substituents other than morpholine be tolerated by BRD9?
- Can the sulfonamide substituent be optimised with respect to affinity, selectivity and physiochemical characteristics?

- Is it possible to dramatically improve the aqueous solubility and physicochemical properties of this scaffold?

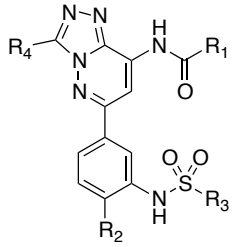

1

Figure 20: Four positions to optimise in the triazole scaffold 1.

We aimed to address these questions by exploring SAR in four locations on scaffold **1** (Figure 20) in combination with a frequent analysis of physical properties of the biologically evaluated compounds.

2.2. Alternative scaffold design

2.2.1. Docking and retrosynthetic analysis

A key shortcoming of compound **34** and this compound series in general was its low aqueous solubility. This solubility problem is widely reported in drug discovery and is consistent with the calculated log $D_{pH7.4}$ of 3.4, which is a contributor to poor aqueous solubility. The distribution coefficient (log D) is the ratio of the sum of the concentrations of all forms of the compound (ionised plus un-ionised at pH 7.4) in the aqueous and organic phases.

A high aromatic ring count has been found to have a large negative impact on compound solubility, even when the *c* log $D_{pH7.4}$ is relatively constant.[164] This characteristic has been found to correlate directly with a compound's flatness and the degree of π-π stacking in the solid phase. Given that **34** contains five aryl rings, the compound's low solubility is unsurprising. In 2010 Hill and

Young at GSK developed the 'Solubility Forecast Index' (SFI), which provides an enhanced guide to predicting solubility, relative to *c* log $D_{pH7.4}$ values alone.[165] (SFI = *c* log $D_{pH7.4}$ + number of aryl rings) An SFI value <5 is recommended for compound design in drug discovery, which gives a high probability of securing good physical properties. As compound **34** has an SFI value of 8.4, this was a major drawback we sought to improve, firstly by reducing the tricyclic triazole to a bicyclic scaffold. We also hypothesised that in doing so, an additional hydrogen bonding interaction could be exploited with the conserved asparagine residue, if an NH-containing carbamate was introduced onto the bicyclic core, as shown in Figure 21.

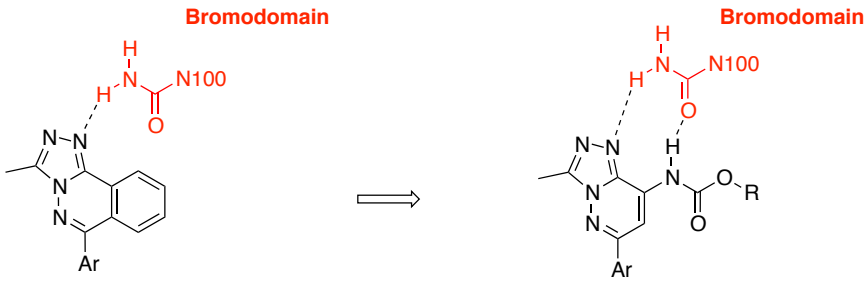

Figure 21: Introduction of a bicyclic triazole to improve potency and solubility.

The docking result of the bicyclic triazole **47** was consistent with our hypothesis that an additional hydrogen bond could be formed with the conserved asparagine residue in BRD9 (Figure 22). Crystallographic data reported by Fedorov *et al*. indicated that gains in BRD9 potency and selectivity could also be *via* introduction of a sulfonamide group in the 3-position of the phenyl ring.[156]

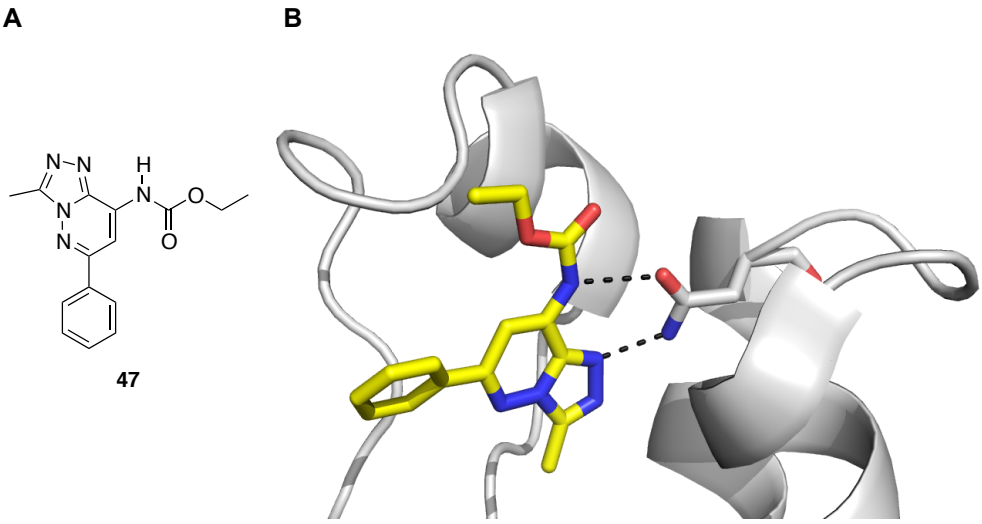

Figure 22: Docking of bicyclic compound 47 to BRD9. (**A**) Structure of bicyclic compound **47**. (**B**) Predicted binding mode of compound **47** to BRD9. The receptor was prepared from chain A of *apo*-BRD9 (PDB ID: 3HME) and water molecules numbered 2 and 165 were removed. Docking of **47** was carried out using ICM-Pro 3.6-1 (Molsoft LLC). A volume of 5 Å near the KAc binding pocket was used as a guide. The hydrogen bonding interaction between the ligand and the conserved asparagine residue is indicated.

With these results in mind, a synthetic route to the bicyclic triazole scaffold **1** was designed, which would enable SAR to be established at four positions on this template (Scheme 1).

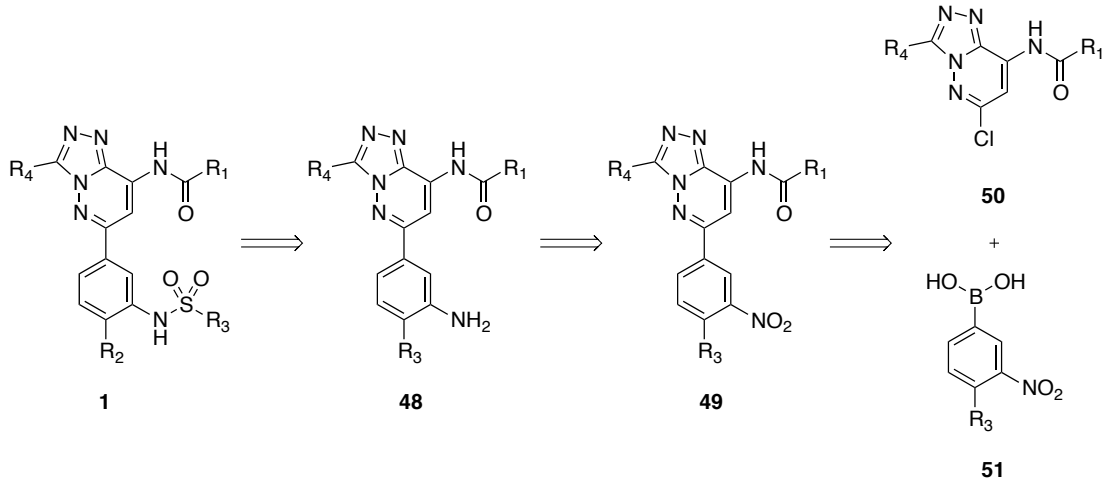

Scheme 1: Retrosynthetic route involving Suzuki coupling as the key step.

Suzuki coupling of the heteroaryl chloride **55** with the commercially available boronic acid **56** was identified as the key step (Scheme 2).

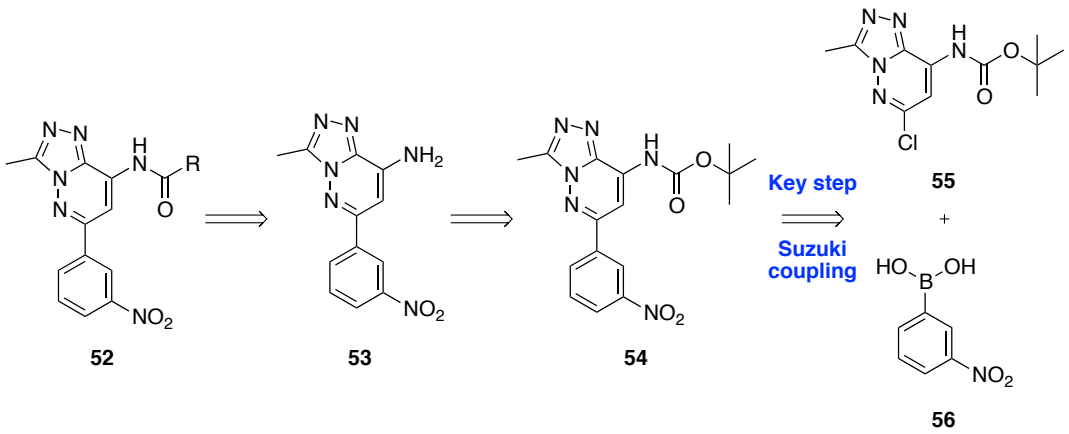

Scheme 2: Retrosynthetic route involving the heteroaryl chloride 55 as the key intermediate.

Docking studies with compound **47** and analysis of the crystal structure of tricyclic triazole **34** bound to BRD9 revealed that the R1 substituent was likely to be located in a predominantly hydrophobic region of the BRD9 bromodomain, formed by residues A54, P55 and Y99 (Figure 23). There is a putative π-π stacking interaction between the **34** and Y106, which may be an important in the high affinity of this ligand for BRD9. We envisaged simplifying the large tricyclic scaffold to a more ligand efficient framework. The three compounds **54**, **57** and **58**, all of which contain small, hydrophobic R1 substituents capable of interacting favourably with residues in BRD9, were identified as our initial targets. Each of these compounds had Solubility Forecast Index (SFI) values between 4.0-5.2, representing a significant improvement compared to the starting triazole, which had an SFI value of 8.4.

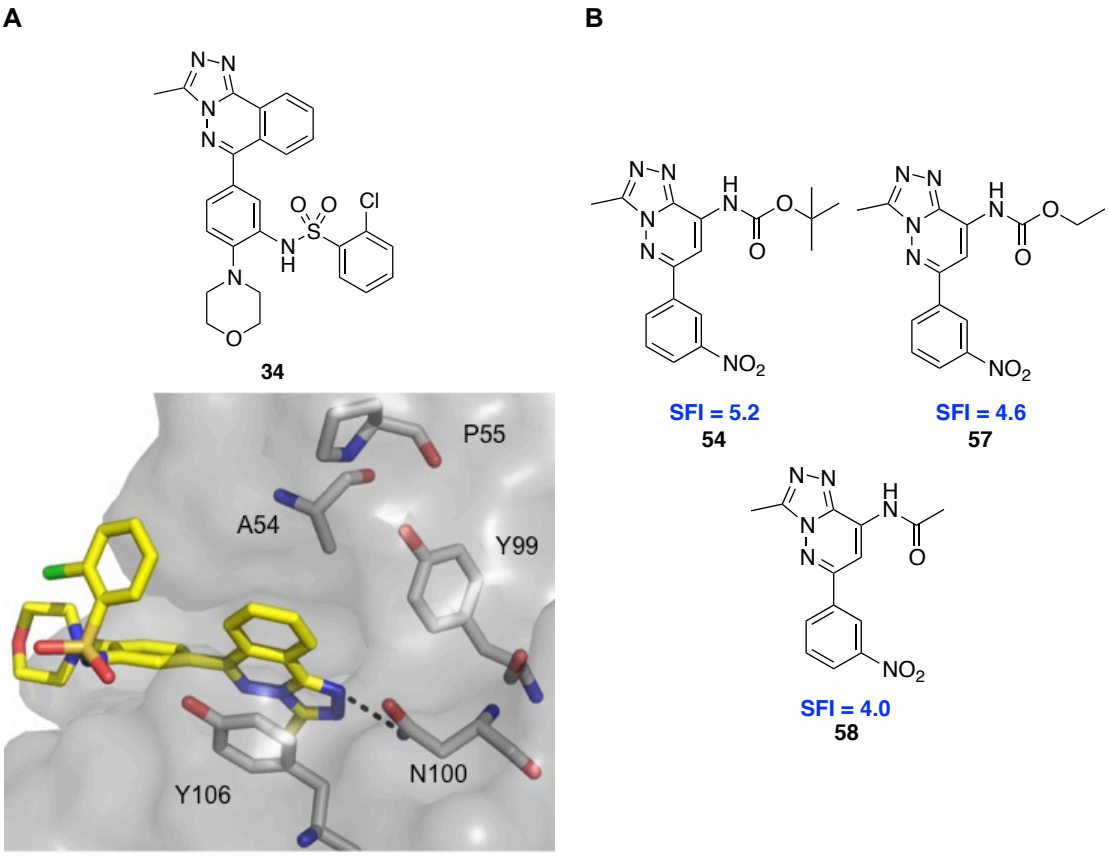

Figure 23: **Crystal structure analysis and target compound identification.** (**A**) Crystal structure of tricyclic triazole **34** bound to BRD9 (PDB ID: 4NQN), reported by Fedorov *et al*.[156] The R1 substituent of scaffold **1** is hypothesised to project into a predominantly hydrophobic region containing residues P55, Y99 and Y106. (**B**) Initial target compounds **54**, **57** and **58.** SFI = *c* log $D_{pH7.4}$ + number of aryl rings. *c* log $D_{pH7.4}$ was calculated using ACD/Labs algorithm (version 5.0.0.184)

2.2.2. Synthesis of heteroaryl chloride 55

In order to complete an extensive structural assessment of this scaffold, a large quantity of the heteroaryl chloride **55** was targeted. A robust and scalable synthetic procedure was required (Scheme 3). This was achieved starting from commercially available bromomaleic anhydride **59**, and furnished **61** in a 64% yield over two steps using a modification of the procedure reported by Townsend.[22] Considerable optimisation of the amination reaction to form compound **62** was completed (Table 4).

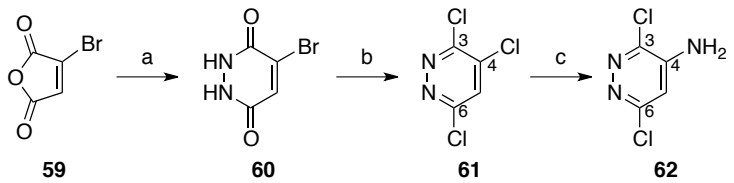

59 **60** **61** **62**

Scheme 3: *Reagents and conditions*: (a) $NH_2NH_2{\cdot}H_2O$, H_2SO_4, H_2O, reflux, 99%; (b) $POCl_3$, reflux, 65% (2 steps); (c) 2 M NH_3 in ^{i}PrOH, 130 °C (microwave), 63%.

Reagents	Conditions	Result
1.5 eq NH_3 in MeOH	120 °C, MW, 1 h	1:1:1 ratio of **62**:**61**:methoxy analogue by NMR.
1.5 eq NH_3 in ^{i}PrOH	120 °C, MW, 1 h	1:1 ratio of **62**:**61** by NMR.
1.5 eq NH_3 in ^{i}PrOH	130 °C, MW, 1 h	3:1 ratio of **62**:**61** by NMR.
2.0 eq NH_3 in ^{i}PrOH	130 °C, MW, 1 h	4:1 ratio of **62**:**61** by NMR.
3.0. eq NH_3 in ^{i}PrOH	130 °C, MW, 1 h	Complete consumption of **61**. 63% isolated yield.

Table 4: Optimisation of amination reaction (step c in Scheme 3).

Without microwave irradiation, complete conversion of **61** to **62** could not be achieved, as excessive temperatures, or prolonged heating, resulted in starting material decomposition. By using 3 equivalents of ammonia in isopropanol at 130 °C under microwave irradiation, **62** was furnished in 63% yield, after crystallisation from water. The choice of the more sterically hindered isopropanol as a solvent in this reaction was found to be important, as when the more commonly used reagent of ammonia in methanol was employed, substitution of the chlorine by a methoxy group was observed.

The rate determining step of this nucleophilic aromatic substitution reaction is most likely to be the nucleophilic attack by ammonia (Figure 24). The lone pairs of electrons on the nitrogens of the pyridazine are situated in a region close to C(3) and C(6). Therefore the proposed attack on C(4) is expected to be the most kinetically favourable, resulting in the high regiospecificity of this reaction.

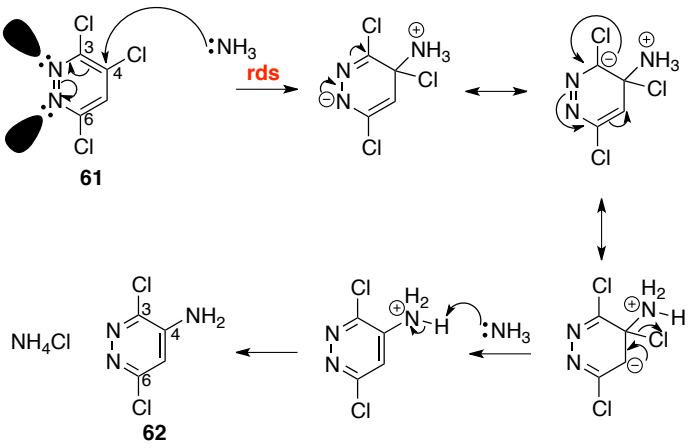

Figure 24: Proposed mechanism for the formation of 62.

Analysis of the HSQC spectrum of **62**, in combination with ^{13}C NMR predictions using ChemBioDraw Ultra (version 12.0.3.1216), confirmed formation of the desired product. The hydrazination reaction was found to be sensitive to the purity of the starting amine, which often required repeated crystallisation from water, to ensure that **63** could be isolated.

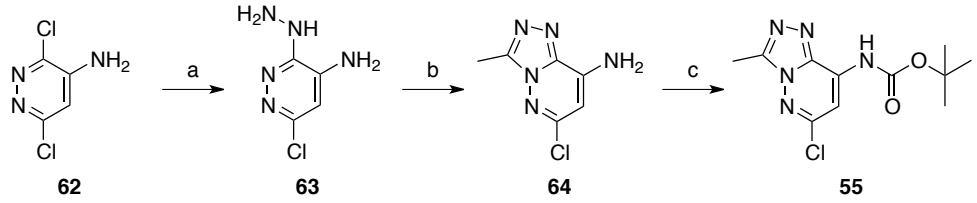

Scheme 4: *Reagents and conditions*: (a) $NH_2NH_2{\cdot}H_2O$, reflux, 43%; (b) AcOH, reflux, 68%; (c) (i) Boc_2O, DMAP, THF, RT (ii) 2 M NaOH/MeOH, RT, 72%.

It was hypothesised that nucleophilic attack by hydrazine at the C(3) position would be preferred over attack at C(6) (Figure 25). This is due to the possibility of exploiting a hydrogen bonding interaction with the C(4) amine substituent during the rate-determining nucleophilic attack step, which is expected to lower the activation energy. As with **62**, analysis of the HSQC spectrum of **63**, in combination with ^{13}C NMR predictions using ChemBioDraw Ultra (version 12.0.3.1216), confirmed formation of the desired product.

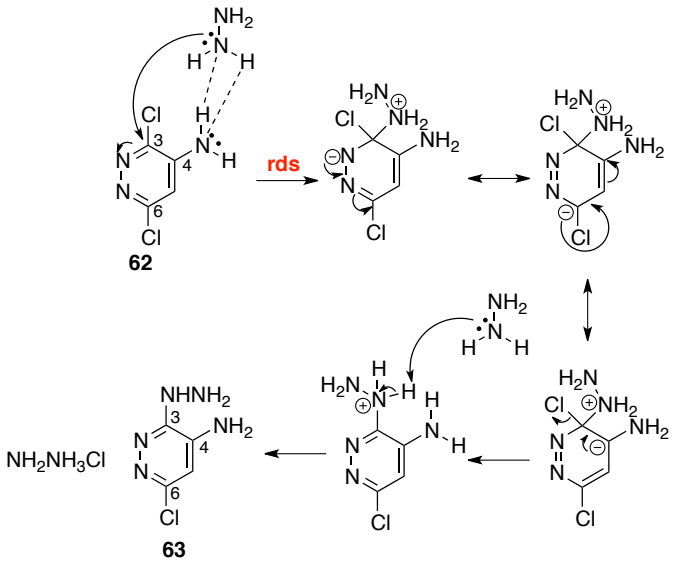

Figure 25: Proposed mechanism for the formation of 63.

Ring closure with acetic acid proceeded well, and the product was crystallised from methanol. Boc protection of the amine was achieved in 72% yield, enabling the key heteroaryl chloride **55** to be synthesised in six steps, without the need for column chromatography.

2.2.3. Suzuki coupling and amine derivatisation

The Suzuki coupling of **55** and **56** was first attempted using $Pd(PPh_3)_4$ as the catalyst, however, separation of the product from triphenylphosphine oxide generated in the reaction proved problematic (Scheme 5, Table 5). An alternative approach using ferrocene-based $Pd(dppf)Cl_2{\cdot}CH_2Cl_2$ which has been reported to be a successful catalyst for the coupling of aryl chlorides, was explored.[166]

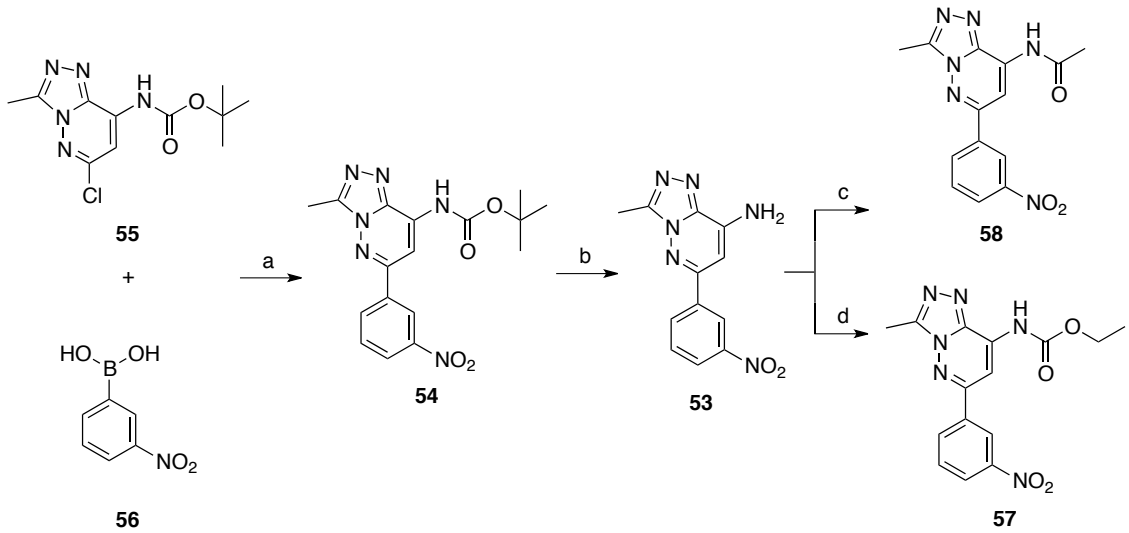

Scheme 5: *Reagents and conditions*: (a) K_2CO_3, Pd(dppf)Cl_2·CH_2Cl_2, 1,4-dioxane/H_2O (10:1), 80 °C, 65%; (b) TFA/CH_2Cl_2 (1:1), RT, 76%; (c) Ac_2O, Pyridine, DMAP, RT, 53%; (d) $ClCO_2Et$, NaH, DMF, 0 °C, 10%.

Reagents	Conditions	Result
55, 1.5 eq **56**, K_2CO_3, 0.1 eq $Pd(PPh_3)_4$, 1,4-dioxane/H_2O (10:1)	120 °C, 24 h	60% Boc deprotection, by NMR. 20% product detected by NMR. Product detected by MS.
55, 1.5 eq **56**, K_2CO_3, 0.1 eq Pd(dppf)Cl_2·CH_2Cl_2, 1,4-dioxane/H_2O (10:1)	120 °C, 24 h	80% Boc deprotection, by NMR. Product detected by MS.
55, 1.5 eq **56**, K_2CO_3, 0.1 eq Pd(dppf)Cl_2·CH_2Cl_2, 1,4-dioxane/H_2O (10:1)	100 °C, 24 h	20% Boc deprotection, by NMR. Product detected by MS.
55, 1.5 eq **56**, K_2CO_3, 0.1 eq Pd(dppf)Cl_2·CH_2Cl_2, 1,4-dioxane/H_2O (10:1)	80 °C, 24 h	No Boc deprotection observed. 70% conversion to product. 30% starting material remaining.
55, 2.5 eq **56**, K_2CO_3, 0.1 eq Pd(dppf)Cl_2·CH_2Cl_2, 1,4-dioxane/H_2O (10:1)	80 °C, 24 h	No Boc deprotection observed. >90% conversion to product. 65% isolated yield.

Table 5: Optimisation of amination reaction (step a in Scheme 5).

The Suzuki coupling reaction was found to be temperature sensitive due to the lability of the Boc group, but controlling the temperature at 80 °C for 24 hours was eventually found to enable optimal recovery of desired product (Table 5). Deprotection under acidic conditions gave the amine **53** (Scheme 5), which was found to be insoluble in organic solvents. This amine was derivatised to give the methyl amide and ethyl carbamate, **58** and **57**, respectively.

2.2.4. *In vitro* evaluation of R1 derivatives 54, 57, and 58

With the final compounds **54**, **57** and **58** in hand, their relative affinity for BRD9 and BRD4(1) was measured in a Differential Scanning Fluorimetry (DSF) assay, also known as a thermal shift assay (Table 6).[167] This is a rapid and relatively inexpensive technique used to determine the strength with which low-molecular-weight ligands bind to and stabilise proteins. In this assay the change in melting temperature (ΔT_m) of the unbound protein to that of the ligand-bound protein is measured. The melting temperature of the protein is detected by monitoring the change in fluorescence of a fluorescent dye, such as SYPRO® Orange. In the native, folded state, fluorescence of the dye is quenched by nearby water molecules. As the protein is heated, it unfolds, exposing hydrophobic regions, which the dye binds to, resulting in an increase in fluorescence. A stability curve can then be plotted and its transition mid-point, defined as the melting temperature (T_m), is compared in the presence and absence of ligand, enabling the change in melting temperature (ΔT_m) upon ligand binding to be quoted. In general terms, a larger ΔT_m correlates with a higher binding affinity for the protein. It is important to bear in mind that lipophilic compounds tend to give large ΔT_m values compared to their protein affinity.

Scaffold			
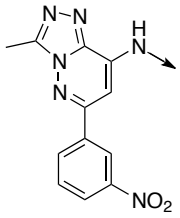			
Compound Number	**Compound**	**ΔT_m/°C (at 10 μM)**	
		BRD9	**BRD4(1)**
54	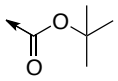	1 (4)	1 (5)
57	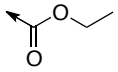	4 (3)	3 (1)
58		1 (5)	1 (5)

Table 6: **DSF data obtained by the SGC for the three bicyclic triazole derivatives 54, 57, and 58, against BRD9 and BRD4(1).** ΔT_m values are reported to the nearest 1 °C, with the number of measurements shown in parentheses. Compound concentration was 10 μM, and protein concentration was 2 μM.

The DSF results in Table 6 indicate that **54**, **57**, and **58** showed binding to both BRD9 and BRD4(1). Compound **57** had the highest ΔT_m value against BRD9 and BRD4(1), but because **54** was considerably more soluble in organic solvents, and more synthetically tractable, an R1 *tert*-butoxycarbonyl group was deemed optimal.

2.2.5. Investigating the importance of the aryl linkage

To examine whether an alternative linkage other than an sp^2 hybridised carbon-carbon bond would be tolerated by BRD9, the aniline derivative **44** was synthesised. It was hypothesised that the new NH linkage could engage in a hydrogen bonding interaction with Y106 in BRD9 (Figure 26).

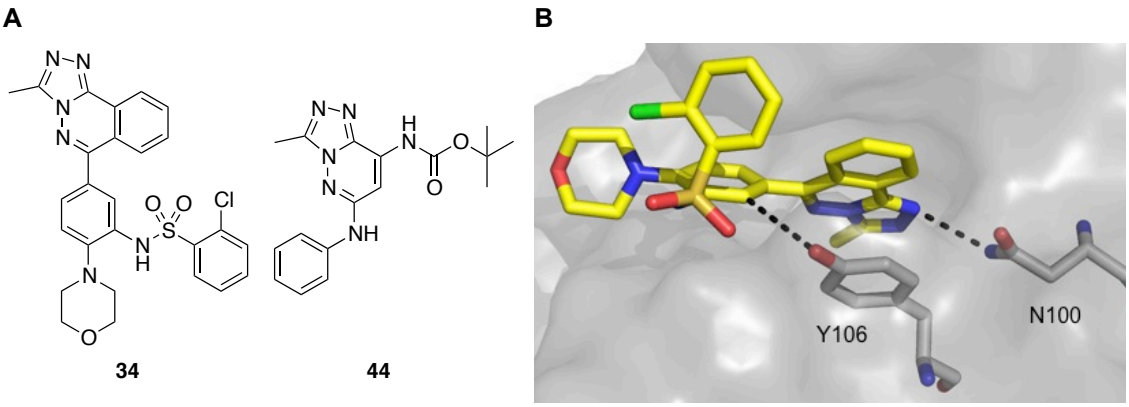

Figure 26: **Crystal structure analysis and target compound identification.** (**A**) Compound **34** developed by Fedorov *et al*. and target compound **44**.[156] (**B**) Crystal structure of tricyclic triazole **34** bound to BRD9 (PDB ID: 4NQN), reported by Fedorov *et al*.[156] The possible hydrogen bonding interaction with Y106 is highlighted.

Attempts to synthesise this target by direct chloride displacement *via* nucleophilic aromatic substitution at elevated temperatures were found to be unsuccessful, with only starting material or the deprotected triazole observed. The desired product was instead synthesised using a Buchwald-Hartwig coupling between **55** and **65** (Scheme 6). Deprotection under acidic conditions furnished the free amine **66** in 93% yield.

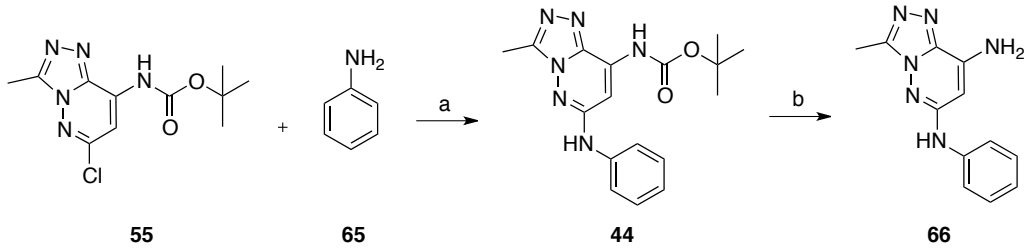

Scheme 6: **Buchwald-Hartwig coupling followed by deprotection to give 66**. *Reagents and conditions*: i. $Pd_2(dba)_3$ J-Phos, NaO^tBu, toluene, 80 °C, 66%; ii. TFA/CH_2Cl_2 (1:1), RT, 93%.

The aniline derivative **44** was evaluated against BRD9 and BRD4(1) in a DSF assay, the results of which are shown in Table 7.

Scaffold			
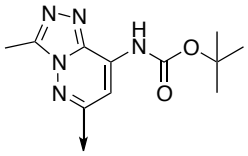			
Compound Number	**Compound**	**ΔT_m/°C (at 10 μM)**	
		BRD9	**BRD4(1)**
54	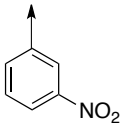	1 (4)	1 (5)
44	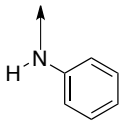	1 (4)	2 (4)

Table 7: **DSF data obtained by the SGC for compounds 54 and 44 against BRD9 and BRD4(1).** Compound concentration was 10 μM, and protein concentration was 2 μM. ΔT_m values are reported to the nearest 1 °C, with the number of measurements shown in parentheses.

Disappointingly, the aniline derivative was found to be slightly more selective for BRD4(1) than BRD9. This result could arise from new vector of the CNC linkage in **44**, which could enable the lipophilic phenyl ring to twist towards a hydrophobic region in BRD4(1), which is defined by residues W97, P98 and F99 [BRD4(1) numbering], known as the WPF shelf. A carbon-carbon linkage was maintained in this position in all future compounds.

2.2.6 Synthesis and evaluation of fused biaryl compounds

The 5,6-fused ring of the BRD9/7 inhibitor **43** (Figure 27) is thought to contribute to its selectivity, and this motif was thought to overlay well with the bicyclic component highlighted in compounds **67**-**69**. To examine the possibility of improving the BRD9 selectivity, these compounds were synthesised *via* Suzuki coupling of the commercially available boronic derivatives and the heteroaryl chloride **55** generated in-house.

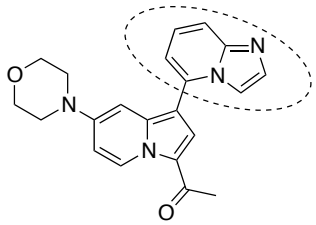

43

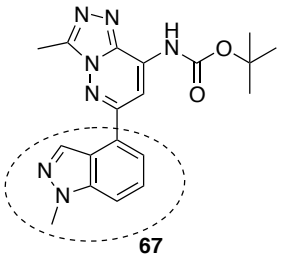

67

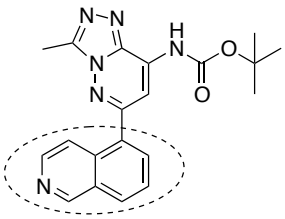

68

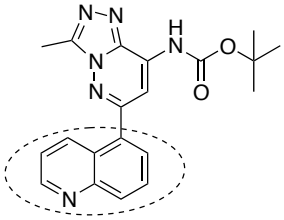

69

Compound Numer	Compound	ΔT_m/°C (at 10 μM)			
		BRD9	CECR2	BRPF1B	PB1(5)
68	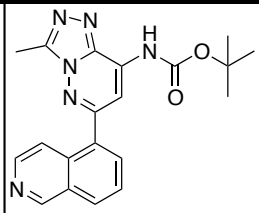	3 (3)	1 (3)	0 (3)	0 (3)
69	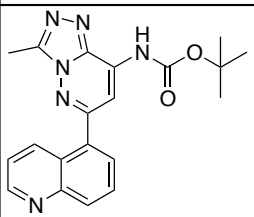	3 (3)	1 (3)	0 (3)	-1 (3)

Figure 27: The BRD9/7 inhibitor 43, and 5,6- and 6,6-fused triazole targets 67-69. DSF results obtained by the SGC. Compound concentration was 10 μM, and protein concentration was 2 μM. ΔT_m values are reported to the nearest 1 °C, with the number of measurements shown in parentheses.

Compounds **68** and **69** were screened in a DSF assay at the SGC against the bromodomains shown in the table above. Both compounds displayed relatively low BRD9 affinity, although some selectivity over CECR2 was demonstrated, often a key off-target of other BRD9 inhibitors.[161] The low solubility of these analogues was their primary drawback, however, and they were not progressed further.

2.3. Introduction of piperazine core

The overall solubility of **54** and related analogues was found to be particularly low. We hypothesised that the solubility, and potentially the selectivity of compound **54** could be improved by introducing a 1-methylpiperazine core at the 4-position of the aryl ring. Solubility predictions on both **54** and **70** were consistent with our hypothesis that the 1-methylpiperazine would be protonated at physiological pH, and therefore have higher aqueous solubility (Figure 28).

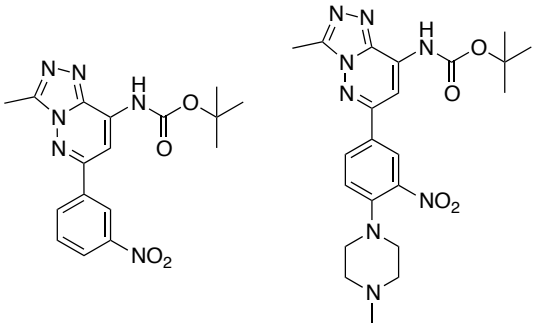

	54	**70**
c log $D_{pH7.4}$	2.2	1.9
SFI (c log D + # aryl rings)	5.2	4.9

Figure 28: **Predicted solubility parameters for piperazine and unsubstituted analogues.** (*c* Log D was calculated using ACD/Labs algorithm (version 5.0.0.184).)

Docking studies performed with compound **71** suggested the piperazine group was predicted to engage in a hydrophobic interaction with F47 (Figure 29).

A

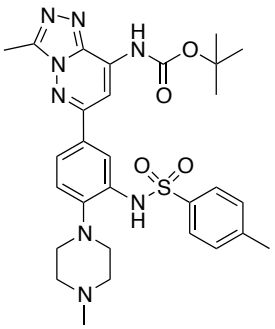

71

B

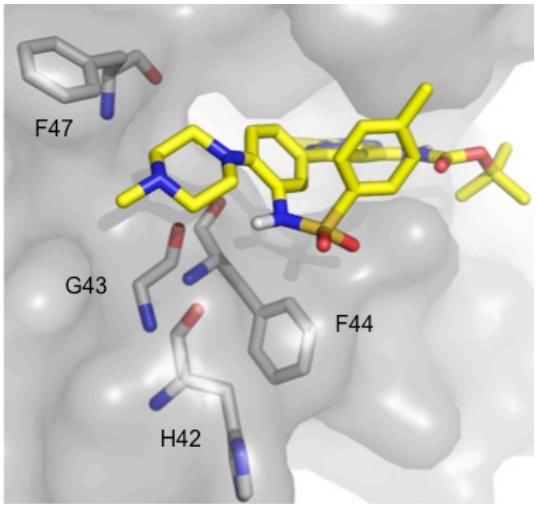

Figure 29: **Docking of 4-substituted sulfonamide 71.** (**A**) Structure of docked compound **71**. (**B**) Predicted binding mode of **71**, carried out by Angelina Sekernik. The receptor was prepared from chain A of *apo*-BRD9 (PDB ID: 3HME) with a hydration state used from an analysis of the crystal structure of **34** bound to BRD9 (PDB ID: 4NQM),[156] i.e. water molecules numbered 2 and 165 were removed. Docking of **71** was carried out using Vina. A volume of 10 Å near the KAc binding pocket was used as a guide, with the number of accessible modes and the exhaustiveness both set to 20.

The 1-methylpiperazine group was also predicted to be located in a region close to the two backbone carbonyls of H42 and G43. Given that the nitrogen at the *N*-methyl position of **71** is expected to be protonated at pH 7.4, it was hypothesised that this group could also improve BRD9 potency, by engaging in an ionic interaction with these backbone carbonyls.

2.3.1. Synthesis and *in vitro* evaluation of piperazine analogue 70

To synthesise the compounds designed above, a reliable route to the boronpinacol ester **74** was required. The first step nucleophilic substitution was straightforward, affording **73** in 97% yield (Scheme 7). Significant optimisation of the subsequent borylation step to form **74** was required. The main hurdle was the observation that **74** was unstable on silica, with

significant protodeboronation observed by ^{1}H-NMR, and mass spectrometry analysis.

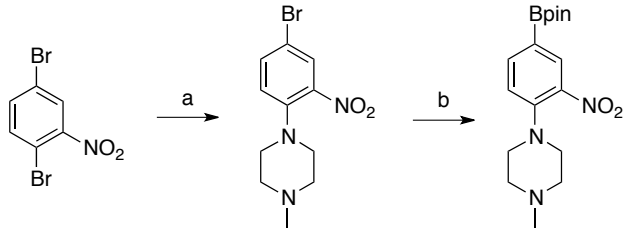

72 **73** **74**

Scheme 7: *Reagents and conditions*: (a) 1-Methylpiperazine, Et_3N, ^{i}PrOH, reflux, 97%; (b) $(BOpin)_2$, KOAc, $Pd(dppf)Cl_2{\cdot}CH_2Cl_2$, 1,4-dioxane/DMSO (30:1), 109 °C, 45%.

The challenge of how to purify successfully compound **74** was overcome by switching to a neutral alumina plug, affording the desired product in 45% yield.

In the process of optimising formation of **74**, two alternative routes were explored (Scheme 8). The first involved the formation of organotin derivative **75** followed by Stille coupling with the heteroaryl chloride **55**. However, although the organotin **75** could be successfully isolated, the Stille coupling gave no consumption of the heteroaryl chloride. Efforts were also made to synthesise the trifluoroborate **76**, which was hypothesised to couple favourably using a procedure reported by Buchwald on similar systems.[168] However, it was not possible to isolate **76** to an acceptable level of purity.

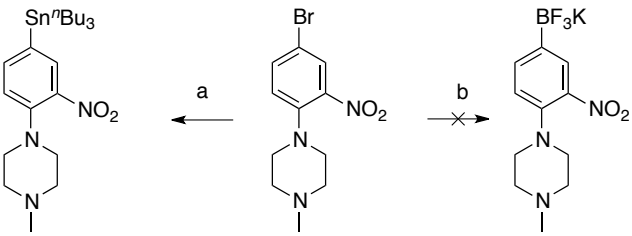

75 **73** **76**

Scheme 8: *Reagents and conditions*: (a) $Pd(PPh_3)_4$, $Bu_3SnSnBu_3$, toluene, reflux, 25%; (b) i. $(BOpin)_2$, $Pd(dppf)Cl_2{\cdot}CH_2Cl_2$, KOAc, 1,4-dioxane/DMSO (40:1), reflux, ii. KHF_2, MeOH/H_2O (1:1), RT.

With the boronpinacol ester **74** in hand, the Suzuki coupling proceeded smoothly at 80 °C to give **70** in 65% yield.

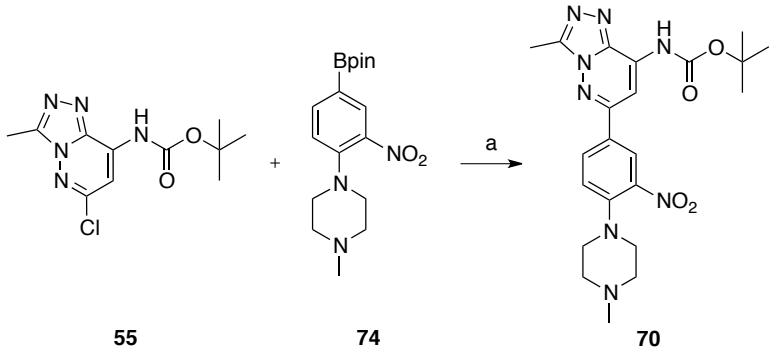

Scheme 9: *Reagents and conditions*: (a) K_2CO_3, $Pd(dppf)Cl_2 \cdot CH_2Cl_2$, 1,4-dioxane/$H_2O$ (10:1), 80 °C, 86%.

Compound **70** was evaluated in a broad thermal shift assay against 16 bromodomains, the results of which are shown in Figures 30 and 31. This ligand shows a high ΔT_m value for BRD9, the closely related BRD7, and the bromodomain of CECR2, which is a member of bromodomain subfamily I.

A

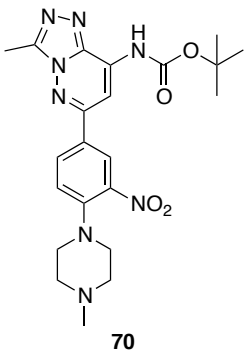

B

ΔT_m/°C (at 10 µM)			
BRD9	**BRD7**	**CREBBP**	**CECR2**
8 (5)	9 (2)	0 (2)	10 (2)
BRD4(1)	**BRD2(1)**	**BRDT(1)**	**BRD1**
3 (4)	2 (2)	0 (2)	1 (2)
TIF1α	**BAZ2A**	**BAZ2B**	**PB1(1)**
0 (2)	0 (2)	0 (2)	0 (2)
FALZ	**BRPF1A**	**BRPF3**	**PCAF**
2 (2)	4 (2)	2 (2)	0 (2)

Figure 30: DSF screening results of compound 70. (**A**) Structure of compound **70**. (**B**) DSF data obtained by the SGC for compound **70**. Compound concentration was 10 µM, and protein concentration was 2 µM. ΔT_m values are reported to the nearest 1 °C, with the number of measurements shown in parentheses.

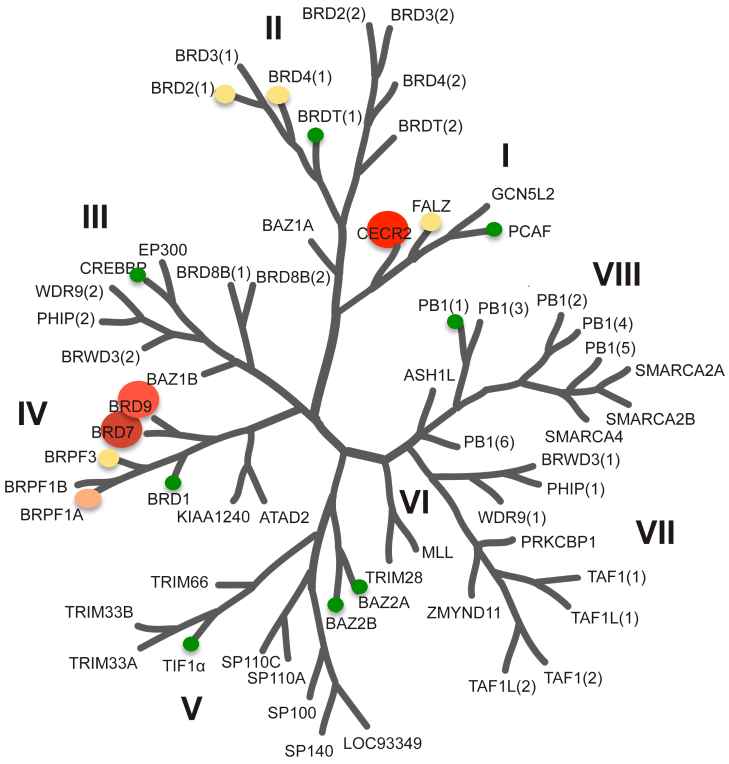

Figure 31: DSF screening results of compound 70. (**C**) DSF results displayed on the bromodomain phylogenetic tree. Circle size and colour are representative of the ΔT_m of each protein tested. (Edited with permission from Hewings *et. al.*[52] Copyright 2012 American Chemical Society.)

The higher BRD9 potency of **70** compared to **54** in this assay is predicted to arise from a combination of interactions between the piperazine core with the backbone carbonyls of H42 and G43. As **70** was significantly more water soluble than **54**, it is likely that a much greater proportion of **70** is in solution, capable of binding to BRD9.

Initially, the high CECR2 ΔT_m value of compound **70** was surprising. In order to assess the degree of sequence similarity between these two bromodomains, a sequence alignment was carried out using PyMol (Figure 32).[169] Despite the fact that the bromodomains of BRD9 and CECR2 have low sequence homology (28% for BRD9 vs CECR2), there is a very high

homology of residues in the peptide loops which make up the receptor binding pocket.

A

BRD9: F44F47P48V49 I53 Y99N100Y106

CECR2: P44C47P48V49Y53Y99N100Y106 **63% homology**

B

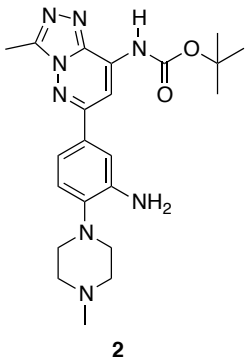

2

C

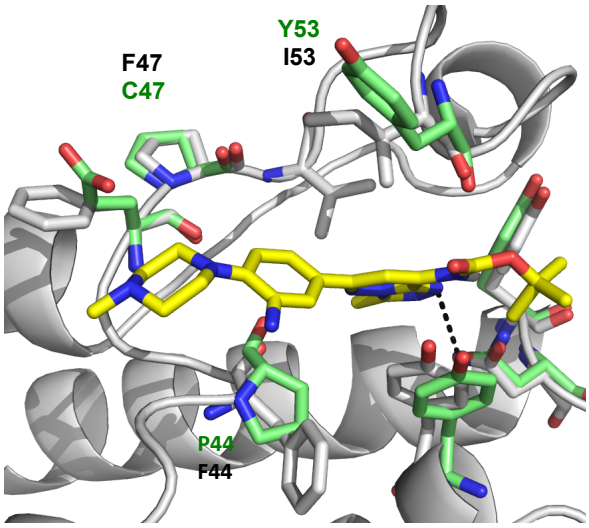

Figure 32: Comparison of the binding pocket of BRD9 and CECR2. (**A**) Sequence alignment of CECR2 and BRD9. Residues close to docked compound **2** to BRD9 are shown. (**B**) Overlay of BRD9 and CECR2. CECR2 carbon atoms shown in green. Differing residues are labelled.

Of the eight residues that were identified to be in close proximity to the amine ligand **2**, which is structurally very similar to **70**, five of these (63%) were identical. Each of the three differing residues had a similar size and occupied a relatively similar position in space. This sequence similarity presents a challenge when trying to design a selective chemical probe using this scaffold. It also helps to explain the observation that the primary bromodomain off-target of I-BRD9 was CECR2.[161]

2.3.2. Aryl bromide alternative and *in vitro* evaluation of corresponding compound

To develop a complementary route towards similar compounds in this series, the aryl bromide **82** was synthesised in five steps starting from 2,5-dibromo-3-nitropyridine **77** (Scheme 9). The initial nucleophilic aromatic substitution reaction with **77** was straightforward, although a one-step ring closure with acetic acid to go from **78** to **80** could not be achieved. Instead, **78** was acetylated to give the intermediate acetohydrazide **79** in 64% yield, which could then be reacted with acetic acid under microwave irradiation to give the triazole in 95% yield. Reduction of the nitro group with iron (0) under acidic conditions proved particularly reliable.

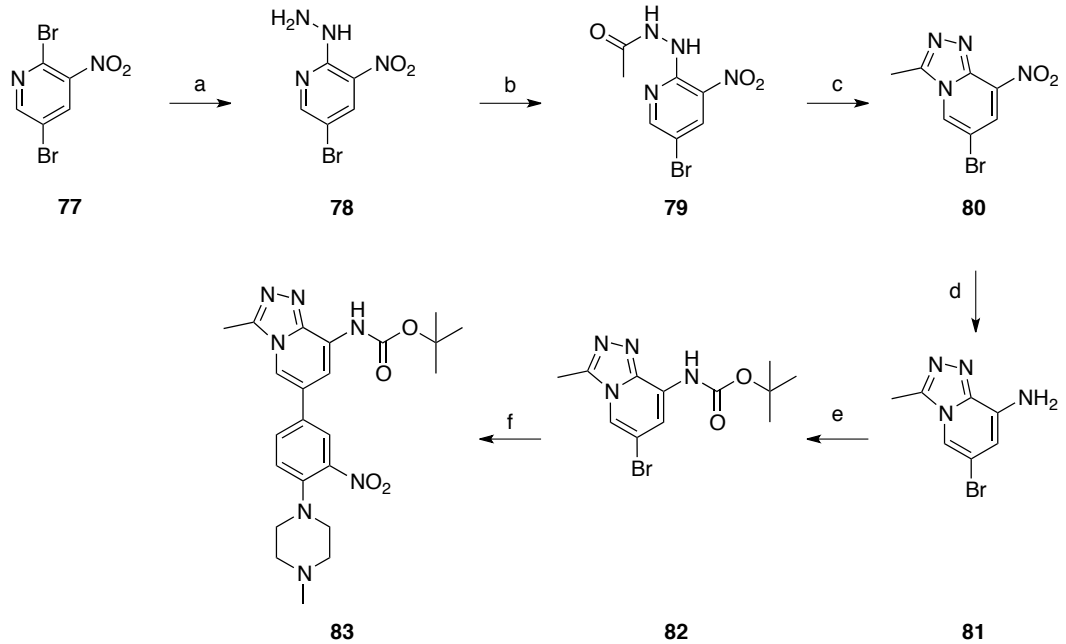

Scheme 9: *Reagents and conditions*: (a) $NH_2NH_2 \cdot H_2O$, EtOH, RT, 88%; (b) Ac_2O, CH_2Cl_2, Et_3N, 0 °C, 64%; (c) AcOH, 180 °C (microwave), 95%; (d) $Fe^{(0)}$, AcOH/H_2O (4:1), 80 °C, 82%; (e) Boc_2O, DMF, DMAP, RT; (f) ArBpin **74**, K_2CO_3, $Pd(dppf)Cl_2 \cdot CH_2Cl_2$, 1,4-dioxane/$H_2O$ (10:1), 80 °C, 39% (over 2 steps).

The final two steps proceeded in low yield, most likely due to the low solubility of each intermediate. Compound **83** was evaluated against a panel of nine bromodomains in a DSF assay (Figure 30).

A

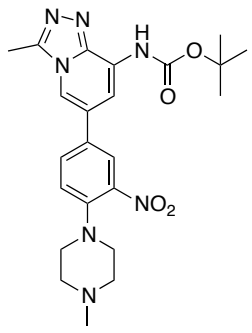

83

B

ΔT_m/°C (at 10 μM)		
BRD9	**BRD4**	**CREBBP**
0 (3)	-1 (1)	-1 (2)
CECR2	**BRPF1**	**BRPF3**
-1 (2)	0 (2)	0 (1)
FALZ	**BRD1**	**BAZ2A**
0 (2)	-1 (2)	-1 (2)

Figure 33: DSF screening results of compound 83. (**A)** Structure of **83.** (**B**) Table showing the DSF results for **83** against a panel of bromodomains. Compound concentration was 10 μM, and protein concentration was 2 μM. ΔT_m values are reported to the nearest 1 °C, with the number of measurements shown in parentheses.

Interestingly, this compound was inactive across all bromodomains tested. It is likely that removal of the 5-position nitrogen has had a detrimental impact on the aqueous compound solubility. This is consistent with its slightly higher *c* log $D_{pH7.4}$ and SFI values, of 2.1 and 5.1, respectively, compared to the nitrogen-containing analogue which had corresponding values of 1.9 and 4.9. The organic solubility of this compound was also found to be particularly low. The carbon replacement could also disrupt the binding mode, contributing to the large drop in potency observed.

2.3.3. Piperazine derivatisation

In order to further improve the solubility of this compound series, the three derivatives **84**-**86** were targeted (Figure 34). The amido piperazine **84** was synthsised to explore the impact of introducing an additional oxygen atom, which could act as a hydrogen bond acceptor. The two chiral piperazines **85**

and **86** were expected to improve solubility by reducing the overall symmetry of the compounds and thereby disrupting the π-π stacking in the solid phase, leading to higher solubility.[170]

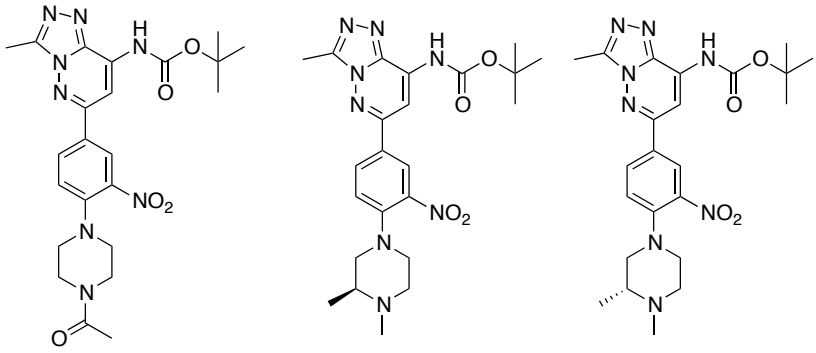

84 **85** **86**

Figure 34: Piperazine analogue targets 84-86.

Compounds **84**-**86** all have SFI values which are in the same range as the unsubstituted piperazine **70** (SFI = 4.9), but still substantially lower than that of the tricyclic triazole **34**. The amido derivative **84** was synthesised in three steps from 2,5-dibromonitrobenzene **72** (Scheme 10). Complete removal of pinacol could not be achieved, so crude **89** was coupled with the heteroaryl chloride **55** under previously optimised conditions.

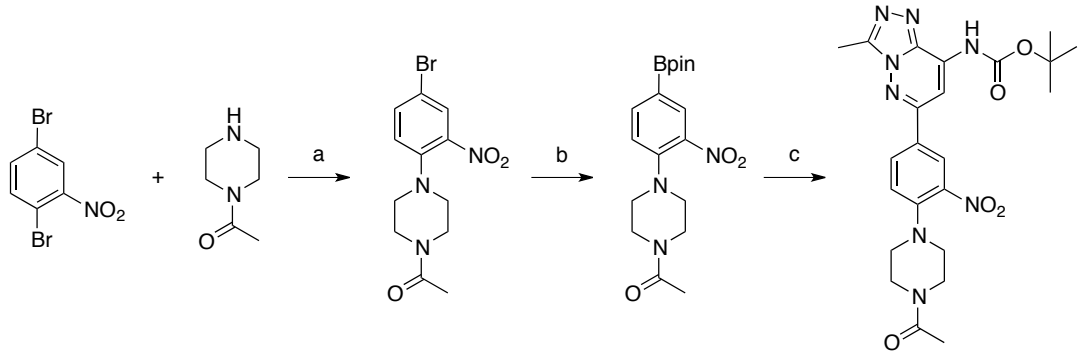

72 **87** **88** **89** **84**

Scheme 10: *Reagents and conditions*: (a) ^{i}PrOH, Et_3N, reflux; (b) $(BOpin)_2$, KOAc, $Pd(dppf)Cl_2{\cdot}CH_2Cl_2$, 1,4-dioxane/DMSO (30:1), 109 °C, 32%; (c) **55**, K_2CO_3, $Pd(dppf)Cl_2{\cdot}CH_2Cl_2$, 1,4-dioxane/$H_2O$ (10:1), 80 °C, 44%.

During the synthesis of the two chiral piperazines, the (*S*)-enantiomer **85** was made starting from the 1-position Boc-protected amine **90**, which was first reacted with 2,5-dibromonitrobenzene (**72**) (Scheme 11). Deprotection under acidic conditions proceeded smoothly, and the Eschweiler-Clarke methylation reaction, under microwave irradiation, proved particularly reliable in this synthesis. Borylation followed by final step Suzuki coupling gave the desired compound **85**.

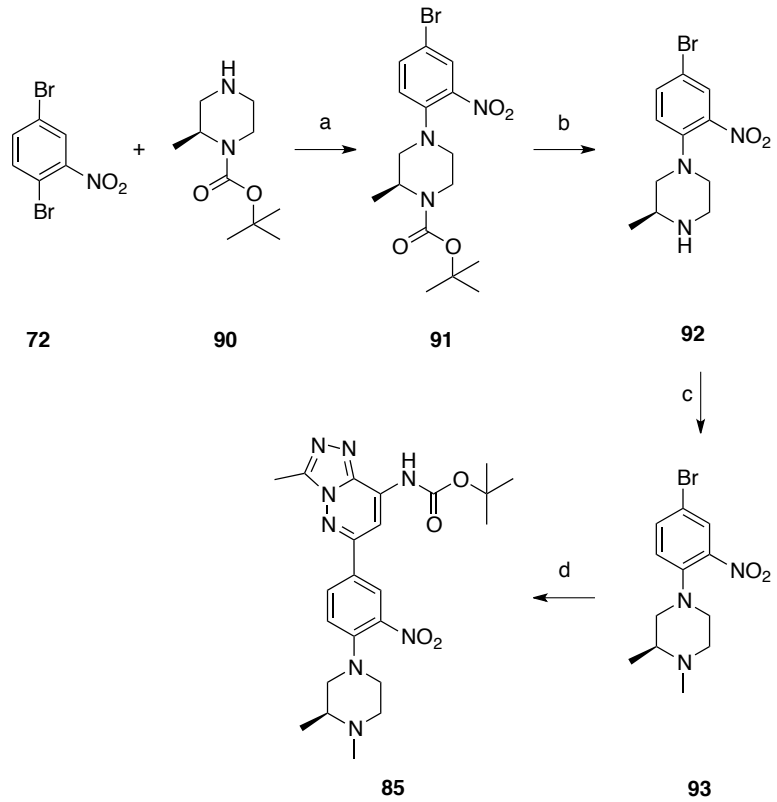

Scheme 11: *Reagents and conditions*: (a) ^{i}PrOH, Et_3N, reflux, 99%; (b) TFA/CH_2Cl_2, (1:1), RT, 76%; (c) CH_2O, HCOOH, 150 °C (MW), 99% (d) (i) $(BOpin)_2$, KOAc, Pd(dppf)Cl_2·CH_2Cl_2, 1,4-dioxane/DMSO, (30:1), 109 °C; (ii) ArBocCl (**55**), K_2CO_3, Pd(dppf)Cl_2·CH_2Cl_2, 1,4-dioxane/H_2O (10:1), 80 °C, 10% (over 2 steps).

The (*R*)-enantiomer **86** was synthesised starting from the 1-methylated piperazine **94** (Scheme 12). Purification of **86** was particularly challenging due to the large number of by-products observed, therefore preparative HPLC performed by Justin Staniforth at UCB was used to give the product in high purity.

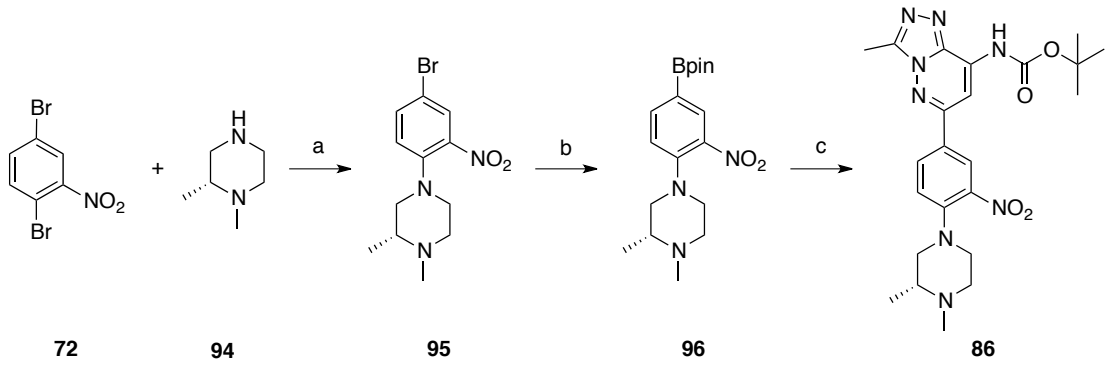

72 94 95 96 86

Scheme 12: *Reagents and conditions*: (a) ^{i}PrOH, Et_3N, reflux, 99%; (b) $(BOpin)_2$, KOAc, $Pd(dppf)Cl_2{\cdot}CH_2Cl_2$, 1,4-dioxane/DMSO, (30:1), 109 °C; (c) **55**, K_2CO_3, $Pd(dppf)Cl_2{\cdot}CH_2Cl_2$, 1,4-dioxane/$H_2O$ (10:1), 80 °C, 1 % (over 3 steps).

The four piperazine derivatives were screened against BRD9 and CECR2 in a DSF assay (Table 8). The results indicate that each modification to the piperazine core was well tolerated, with each compound showing a ΔT_m value >8.0 °C, suggesting strong binding to each of these bromodomains.

Scaffold					
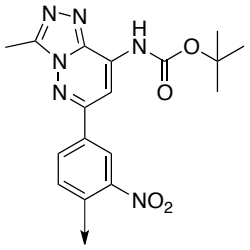					
	ΔT_m/°C (at 10 µM)			**ΔT_m/°C (at 10 µM)**	
Compound	**BRD9**	**CECR2**	**Compound**	**BRD9**	**CECR2**
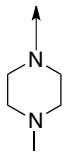	8 (5)	10 (2)	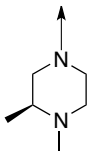	9 (4)	11 (2)
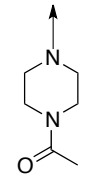	9 (4)	11 (2)	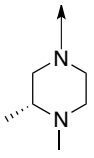	9 (2)	10 (2)

Table 8: **DSF data obtained by the SGC for piperazine derivatives screened against BRD9 and CECR2.** Compound concentration was 10 µM, and protein concentration was 2 µM. ΔT_m values are reported to the nearest 1 °C, with the number of measurements shown in parentheses.

The aqueous solubility of these compounds was then evaluated in the "SnapSol" assay developed at UCB, which gives a direct measure of compound solubility at a particular pH (Figure 35). The procedure used in the "SnapSol" assay is shown in Figure 35.A. Compounds are defined to have low, moderate, or high aqueous solubility according to the bands 0-30 μM, 30-100 μM, and >100 μM, respectively.

The unsubstituted piperazine **70** was found to be the most soluble derivative, with a high solubility of 92 μM. The amido derivative **84** had the lowest aqueous solubility of the four compounds examined in this assay, presumably due to the inability of the amide nitrogen to become protonated at pH 7.4. Both chiral piperazines were found to have lower aqueous solubilities, possibly due to the increased lipophilic property imparted by the additional methyl group outweighing the expected disruption of solid phase stacking.

A

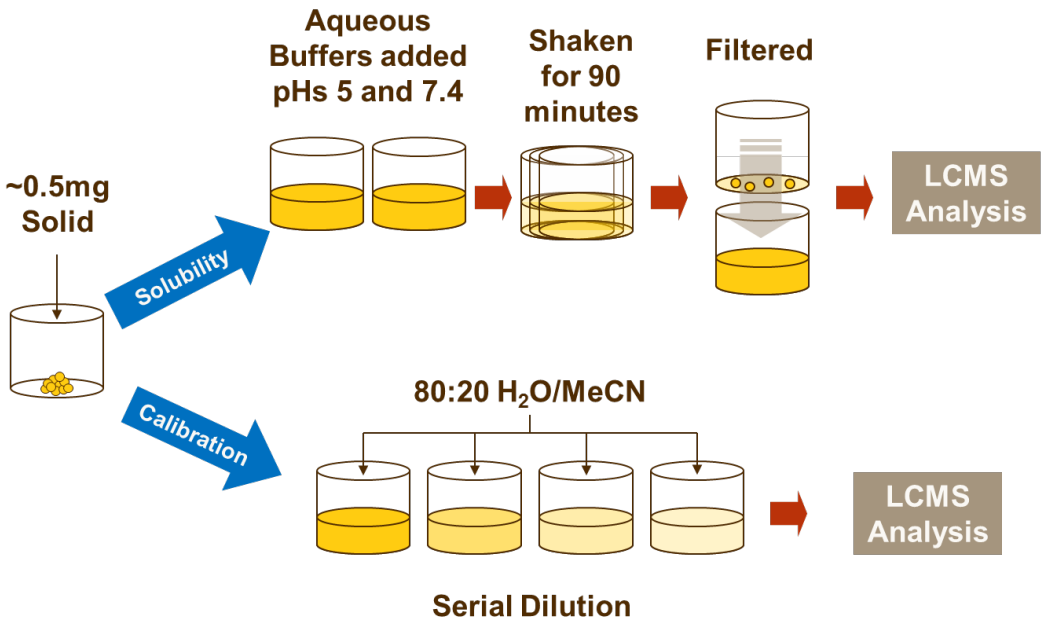

B

Compound Number	Structure	SnapSol at pH 7.4/μM	Compound Number	Structure	SnapSol at pH 7.4/μM
70	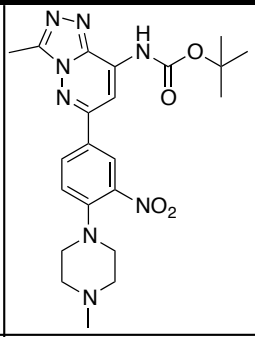	92	**85**	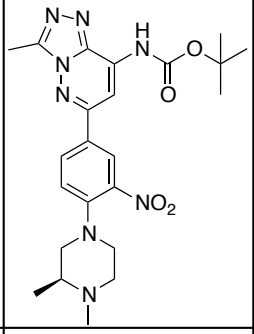	52
84	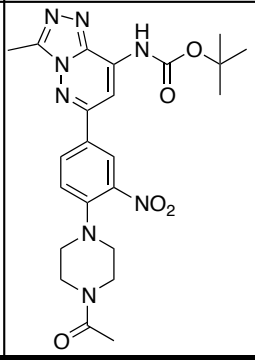	25	**86**	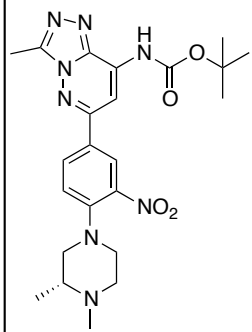	51

Figure 35: SnapSol aqueous solubility method and results. (**A**) SnapSol solubility assay method developed by UCB (Figure provided by Christine Prosser). A calibration measurement is completed in which the compound is dissolved in DMSO and analysed by LCMS. Buffer is then added to a solid sample which is shaken for 90 minutes, filtered and the concentration of compound in solution is measured by LCMS. Compounds with SnapSol values of >80 μM are considered to be highly soluble. (**B**) SnapSol results for piperazine derivatives.

2.4. Initial round of sulfonamide optimisation

2.4.1. BRD9 and BRD4 ligand binding pocket analysis

With the aim of improving BRD9 affinity and selectivity, a detailed analysis of the BRD9 KAc binding pocket was undertaken. By examining the crystal structure of **34** bound to BRD9, we noticed that the phenyl ring of the pendant sulfonamide is projected towards a region containing two backbone carbonyl groups (Figure 36).

A **B**

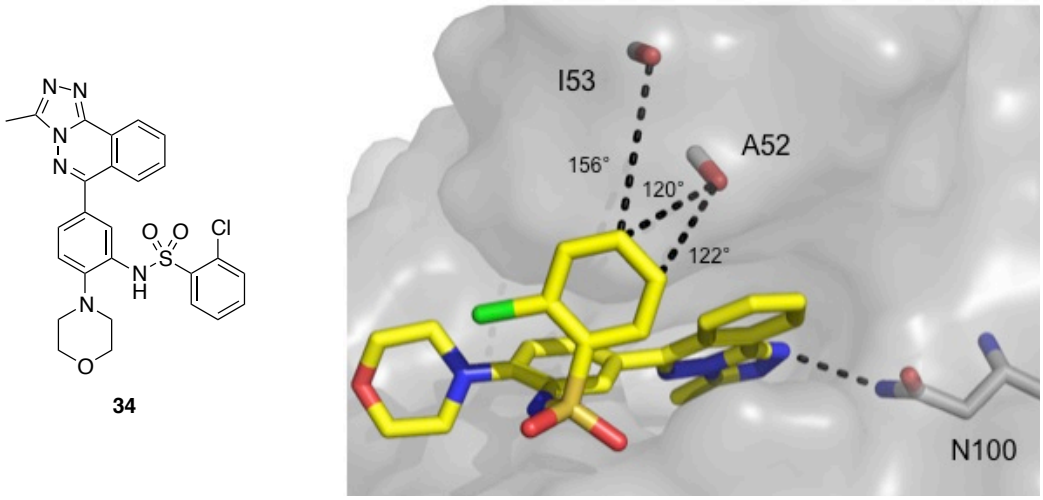

Figure 36: **Halogen bonding as a possible route to improve BRD9 selectivity**. (**A**) Tricyclic triazole **34**. (**B**) Crystal structure of **34** bound to BRD9 (PDB ID: 4NQN), reported by Fedorov *et al*.[156]

Halogens are widely used substituents in medicinal chemistry, and had historically been accepted as merely hydrophobic moieties and Lewis bases in accordance with their electronegativities. This perception altered in 1978, when compounds containing chlorine, bromine or iodine, were also found to engage in a directional interaction with hydrogen bond donating groups.[171] The interaction, of the type R-X---Y-R, where the halogen X acts as a Lewis acid, and Y is an electron donor moiety, is referred to as “halogen bonding”. It

is ‘driven by the σ-hole, a positively charged region on the hind side of X along the R-X bond axis that is caused by anisotropy of electron density on the halogen’ (Figure 37).[172,173] The strength of this interaction can be tuned in a variety of ways, though a C-X---O angle close to 180° is accepted to be crucial.

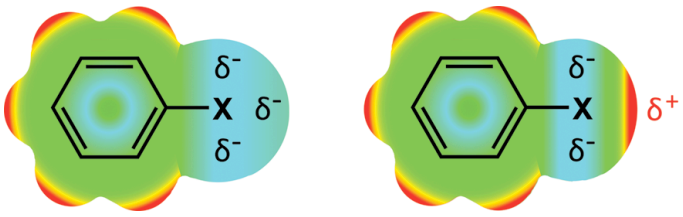

Figure 37: Schematic overview of the changing perception of halogen moieties in organic compounds. (Reprinted with permission from Wilcken *et. al*.[172] Copyright 2012 American Chemical Society.) The color gradient from cyan to red represents the electrostatic potential mapped onto the electron mdensity surface. (Left) Traditional view of the halogen as a Lewis base (electron donor) with an isotropic electron distribution on the cap. (Right) Real description, highlighting the anisotropy of the electron density on the halogen (for fluorine, a positive potential appears only in special cases). The most positive surface potential is coloured in red, the most negative surface potential is coloured in cyan.

We hypothesied that an improvement in BRD9 selectivity could be achieved *via* a halogen-bonding interaction in this region. Due to the high directionality of this interaction, the C-X---O angle was estimated using the crystal structure of **34** bound to BRD9.[156] A 4-position substituted halogen was estimated to have C-X---O angles of 156° and 120°, to the carbonyls of I53 and A52, respectively. A C-X---O angle of 122° was estimated between a 5-position substituted halogen and the carbonyl of A52 (Figure 38.B). As these values were reasonably close to those for which halogen bonding has been reported in the literature,[172] and taking into the flexibility of both the protein and ligand, this interaction was deemed worthy of further investigation.

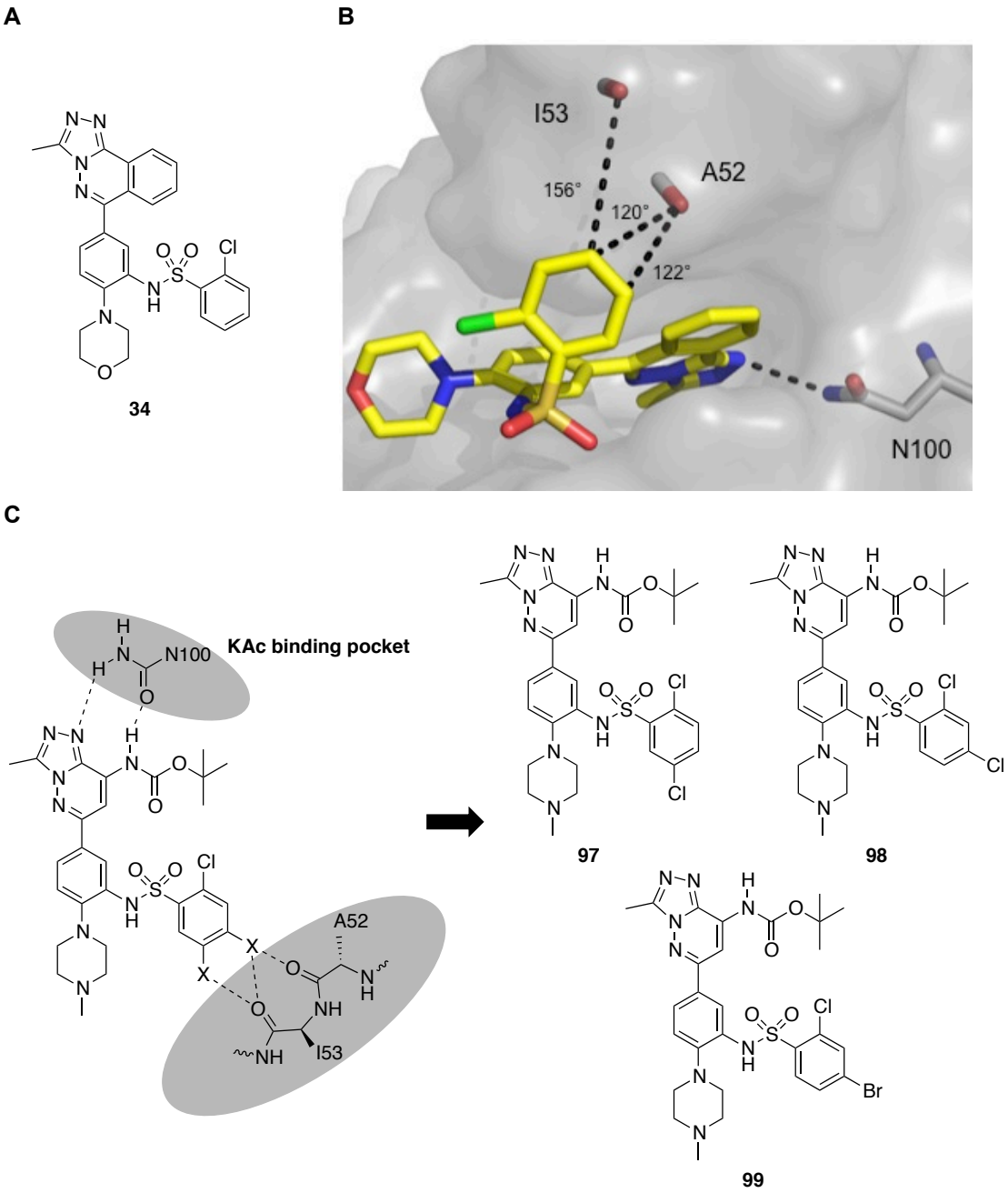

Figure 38: Halogen bonding as a possible route to improve BRD9 selectivity. (**A**) Tricyclic triazole **34**. (**B**) Crystal structure of **34** bound to BRD9 (PDB ID: 4NQN), reported by Fedorov *et al*.[156] (**C**) Hypothesised binding mode of bicyclic scaffold. The proposed halogen bonding interaction is indicated and the three targets **97**-**99** are shown.

With the aim of improving the selectivity over BRD4(1), the crystal structure of **34** bound to this bromodomain was then examined. The affinity of **34** for BRD4(1) is partly explained by the 2-chlorophenyl sulfonamide group which sits in the WPF shelf (Figure 39). The lipophilic region is conserved in the BET

family of bromodomains, and occupancy of this site is thought to be an important contributor to BET-bromodomain activity.[69,71,174]

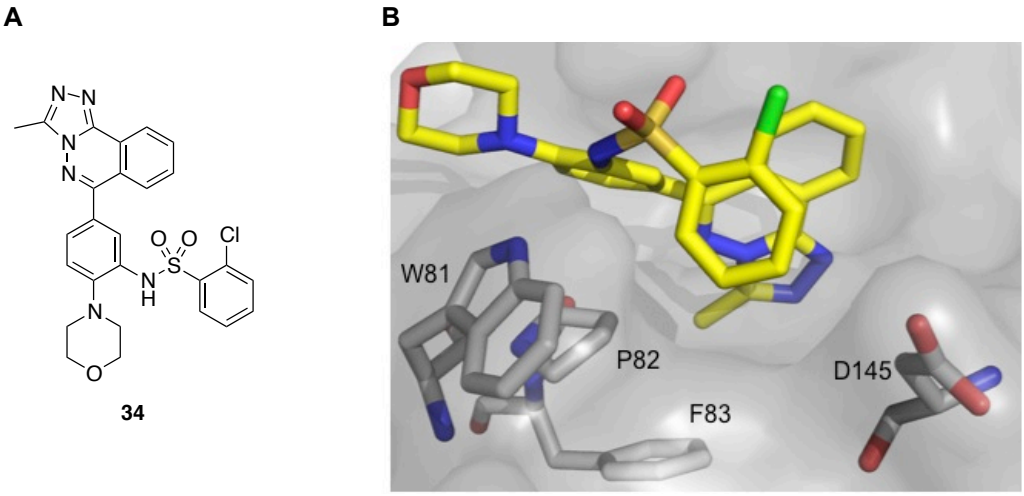

Figure 39: **The aryl ring of sulfonamide 34 is directed towards the WPF shelf**. (**A**) Structure of tricyclic triazole. (**B**) Crystal structure of **34** bound to BRD4(1) (PDB ID: 4NQM).[156] The 2-chlorophenyl substituent sits in the site formed between the WPF shelf and D145.

In order to improve the selectivity over BRD4(1), we hypothesised that 4-substitution of the phenyl ring could result in a steric clash with the large WPF shelf, and thereby reduce the affinity for BRD4(1). With this hypothesis in mind, the two 4-substituted aryl sulfonamides **71** and **100** were designed as putative ligands. Docking studies were then carried out with **71** on the *apo*-structure of BRD9 (PDB ID: 3HME). These studies revealed that the sulfonamide could twist into an orientation such that a hydrophobic interaction between the 4-methyl group and I53 is possible, while the hydrogen bonding interaction between Y106 and a sulfonamide oxygen is maintained (Figure 40).

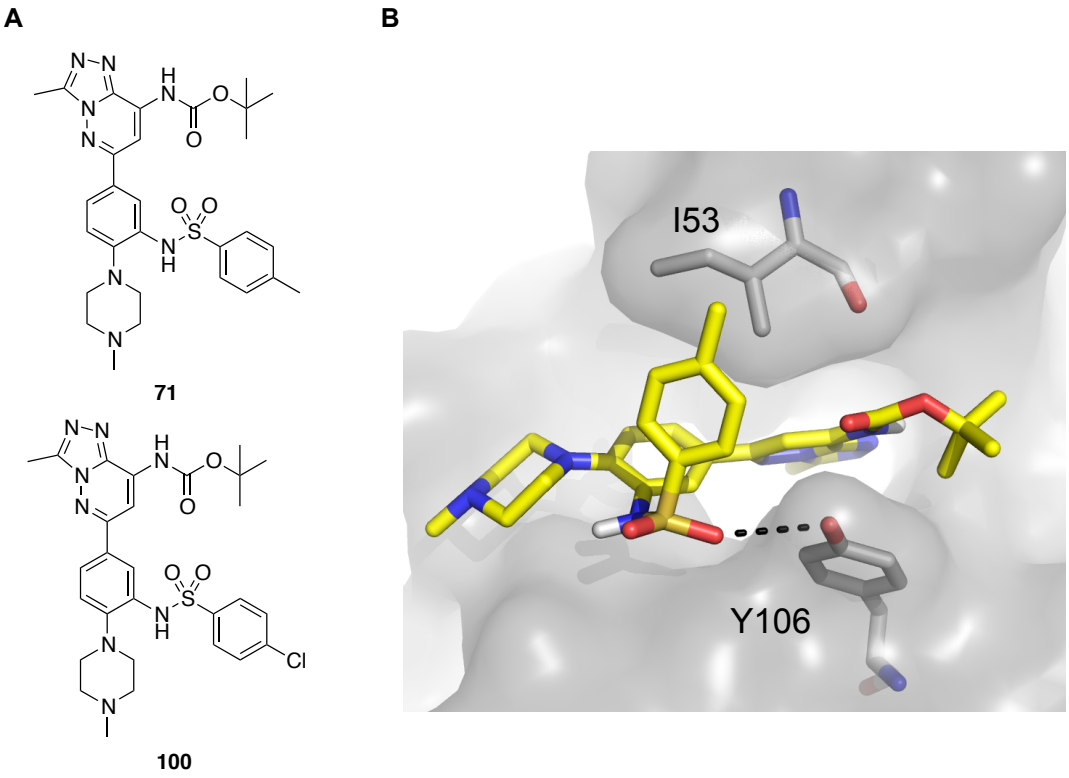

Figure 40: Docking of 4-substituted sulfonamide. (**A**) Structure of 4-substituted aryl sulfonamide targets. (**B**) Predicted binding mode of compound **71** to BRD9. Docking was performed using Molsoft ICM browser software into the KAc binding pocket of BRD9 using the *apo* structure (PDB ID: 3HME).

Having identified five target sulfonamides, we also aimed to synthesise the unsubstituted phenyl sulfonamide **101** for SAR purposes. The impact of substituent size was also examined with a sterically demanding quinoline derivative **102**, along with the smaller cyclopropyl derivative **103**.

2.4.2. Sulfonamide synthesis and *in vitro* evaluation by DSF and AlphaScreen™

The eight desired sulfonamides were synthesised from the corresponding sulfonyl chlorides (Table 9). In most cases the aniline was found to be very unreactive, and an excess of five equivalents sulfonyl chloride was required for any substantial consumption of **2** to be achieved. The purification of each

compound was often challenging, however crystallisation from ethanol proved successful in many cases.

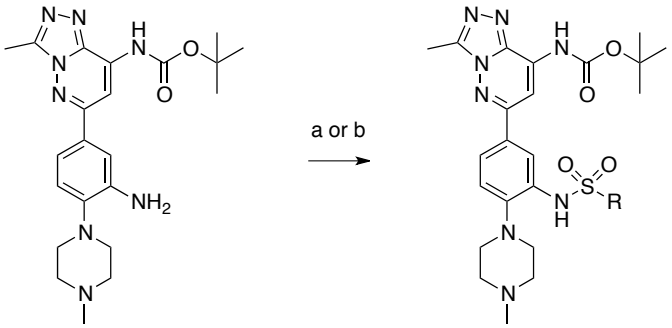

2 **95**

Compound Number	Compound	%Yield	Compound Number	Compound	%Yield
101		66	**99**	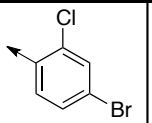	50
102	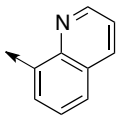	33	**100**	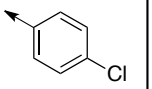	66
97	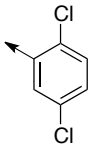	11	**71**	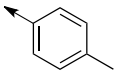	44
98	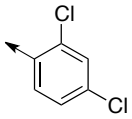	12	**103**		44

Scheme 13 and Table 9: *Reagents and conditions*: (a) RSO_2Cl, Et_3N, CH_2Cl_2, DMAP, 0 °C to RT (**103**); or (b) RSO_2Cl, pyridine, DMAP, 0 °C to RT (all other sulfonamides above).

The sulfonamides were screened against BRD9 and BRD4(1) in a DSF assay, the results of which are shown in Table 13. The unsubstituted phenyl sulfonamide **101** was well tolerated by BRD9, although its selectivity over BRD4(1) in this assay was poor. The quinoline derivative **102** was found to have the lowest ΔT_m of all sulfonamides tested, possibly due to its size and relatively poor solubility. The three di-halogenated sulfonamides **97**-**99** all had lower potency than the simple phenyl derivative **101**. Interestingly, in

agreement with our hypothesis, a gain in BRD9 selectivity is achieved with the 4-substituted analogues, notably the 4-methyl derivative **71** which had a considerably lower BRD4(1) ΔT_m value in relation to the unsubstituted phenyl derivative. A key observation was also made with the cyclopropyl compound **103**, which displayed a very high BRD9 ΔT_m value of 10 °C and showed a good improvement in selectivity over BRD4(1). This BRD9 ΔT_m value is considerably higher than that reported for LP99 (6 °C), which binds to BRD9 with a K_D value of 99 nM by ITC. The cyclopropyl derivative **103** was a very interesting compound to examine in greater depth.

Some caution should be taken when ranking compounds based on their ΔT_m values, as these values often do not accurately reflect the relative affinities of each molecule. This is because the results depend upon the relative contributions of enthalpy and entropy of binding; larger ΔT_m shifts are often observed for more entropically driven (for example hydrophobic) binding interactions, which is magnified at elevated temperatures.[167] As this compound set is quite hydrophobic, a detailed interpretation of the results is difficult.[175] The 4-methyl sulfonamide **71** was evaluated in a BRD9 AlphaScreen™ assay and its measured IC_{50} value of 315 nM confirmed its high BRD9 affinity.

Scaffold					
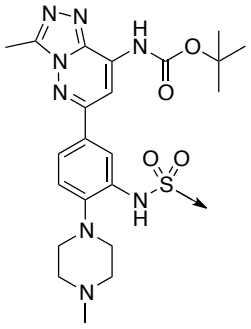					
Compound Number	**Compound**	**ΔT_m/°C (at 10 μM)**		**Ratio ΔT_m**	**AlphaScreen IC_{50}/μM**
		BRD9	**BRD4(1)**	**BRD9/BRD4(1)**	**BRD9**
101		9 (1)	6 (1)	1.5	4.7
102	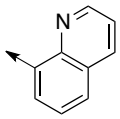	5 (1)	1 (1)	5.0	
97	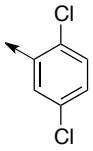	6 (1)	4 (1)	1.5	
98	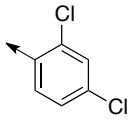	5 (1)	3 (1)	1.7	
99	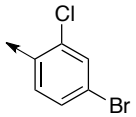	5 (1)	3 (1)	1.7	
100	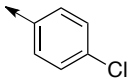	9 (1)	5 (1)	1.8	
71	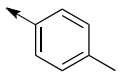	11 (1)	2 (1)	5.5	0.315
103		10 (4)	3 (1)	3.3	

Table 10: **DSF and AlphaScreen™ data obtained by the SGC for the eight sulfonamide derivatives against BRD9 and BRD4(1).** In the DSF assay, compound concentration was 10 μM, and protein concentration was 2 μM. ΔT_m values are reported to the nearest 1 °C, with the number of measurements shown in parentheses.

2.4.3. Analysis of potency, aqueous solubility and metabolic stability of key compounds

The aqueous solubility of three compounds (**70**, **71**, and **103**) was determined using a SnapSol solubility assay (Table 11). The aryl sulfonamide **71** was found to have the lowest aqueous solubility of these three compounds, consistent with its SFI value (6.9), which was the highest of this subset. The impact of the additional lipophilic aryl ring is clearly detrimental to this compound's solubility. Both the nitro (**70**) and cyclopropyl (**103**) sulfonamides showed improved aqueous solubility, in line with their lower SFI values (4.9 and 4.6, respectively). Compounds **70** and **103** were then evaluated in a Homogeneous Time Resolved Fluorescence (HTRF) assay at the SGC. This assay combines fluorescence resonance energy transfer technology (FRET) with time resolved measurement (TR). In this platform, a signal is generated through fluorescent resonance energy transfer between a donor and an acceptor molecule when in close proximity to each other.[176] Compounds **70** and **103** were found to have BRD9 IC_{50} values of 128 ± 41 nM, and 104 ± 13 nM, respectively (Table 11, bottom).

Human *In vitro* Cl_{int} (µL/min/mg protein)		
<8.0	8.0 - 43.0	>43.0

Scaffold
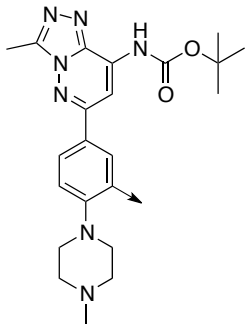

Compound Number	Compound	SFI	SnapSol at pH 7.4/µM	Human *In vitro* Cl_{int} (µL/min/mg protein)
70		4.9	92	15
71	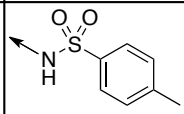	6.9	11	36
103	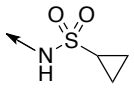	4.6	>100	26

Compound Number	Compound	ΔT_m/°C (at 10 µM)		Ratio ΔT_m	BRD9 IC_{50}/nM
		BRD9	BRD4(1)	BRD9/BRD4(1)	
70		8 (5)	3 (4)	2.7	128*
71	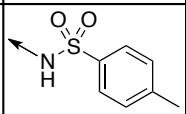	11 (1)	2 (1)	5.5	315**
103	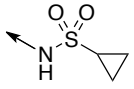	10 (4)	3 (1)	3.3	104*

Table 11: **Key binding information and physical parameters of compounds 70, 71, and 103.** SFI values were calculated from corresponding c log D results, which were found using ACD/Labs algorithm (version 5.0.0.184). BRD9 IC_{50} measurements were performed by the SGC (*HTRF assay, **AlphaScreen™ assay). For clearances, the compound was incubated with liver microsomes and the required cofactors (detailed method provided in Experimental section). To determine clearance, the depletion of substrate over time should follow an exponential decline i.e. linear disappearance on a Natural Log (l_n) – plot. Results obtained by Hayley Roy, UCB.

The *in vitro* clearance of **70**, **71**, and **103,** in the presence of human hepatic microsomes was then assessed, in order to gain an insight into their metabolic stability (Table 10, top). This was performed by UCB, using a protocol developed in-house, similar to that reported by Obach.[177] The

Intrinsic Clearance (Cl_{int}) is defined as the maximal rate of clearance that can occur in the absence of any limiting factors. Since clearance can only operate on unbound drug delivered by the blood, the limiting factors are protein binding and blood flow. Cl_{int} is categorised as low, medium or high, depending on the loss of compound detected over time (Table 10). All compounds were found to have moderate Cl_{int}, with the aryl sulfonamide **71** having the highest rate of *in vitro* clearance. The slightly lower *in vitro* metabolic stability of **71** is consistent with its higher lipophilicity and larger molecular weight, leading to a higher metabolic instability.[178] The additional aryl ring of compound **71** resulted in an improvement in BRD9 selectivity over BRD4(1), however this was offset by the detrimental impact on compound solubility, and *in vitro* metabolic stability. Promisingly, the cyclopropyl (**103**) and nitro (**70**) derivatives both had moderate *in vitro* metabolic stability.

2.5. Ligand efficiency comparison

It is well known that highly lipophilic compounds have an increased risk of developmental attrition in ligand optimisation programmes.[179] Ligand efficiency (LE) has been developed as a tool to provide an accurate measure of the efficiency of a binding interaction with respect to a physiochemical property, most notably molecular weight.[179] The LE, which quantifies affinity per heavy atom, and lipophilic-ligand efficiency (LLE), which takes into account lipophilicity, are useful objectives for compound optimisation studies and are shown for compounds **34**, **70**, **71**, and **103** in Table 12.[180]

Compound	BRD9 IC_{50}/nM	pIC_{50}	LE	c log P	LLE
34 (tricyclic lead)	200**	6.7	0.25	3.02	3.7
70 (nitro piperazine)	128*	6.9	0.28	3.03	3.9
71 (4-Me sulfonamide)	315**	6.5	0.22	3.12	3.4
103 (cyclopropyl sulfonamide)	104*	7.0	0.26	1.40	5.6

Table 12: Ligand efficiency (LE) and ligand-lipophilic efficiency (LEE) for 34, 70, 71, and 103. c Log P was calculated using ACD/Labs algorithm (version 5.0.0.184). BRD9 IC_{50} assay: *HTRF, **AlphaScreen™.

$$pIC_{50} = -\log_{10} IC_{50}\ ;\ LE = \frac{pIC_{50} \times 1.4\ (\text{kcal/mol})}{\text{Heavy atom count}}\ ;\ LLE = pIC_{50} - c\log P$$

All compounds were found to have similar LE values, whereas a key trend becomes clear when assessing the LLE results. From our starting point **34**, to **70**, and **71**, LLE remained relatively constant, in contrast to the cyclopropyl derivative **103**, which was found to have a considerably lower calculated log P value, and consequently the highest LLE of 5.6, which is within the accepted target range of approximately 5-7. These data indicate that **103** has a respectable potency with in relation to compound size and lipophilicity, representing an attractive ligand for further optimisation. The moderate Cl_{int} value for **103** was another promising result, which gave us further momentum to further investigate alternative analogues of this scaffold.

2.6. Summary

We have developed a robust eleven-step synthesis of novel bicyclic triazole sulfonamides, which have nanomolar potency for the BRD9 bromodomain. Starting from a tricyclic triazole lead, we have used computational molecular docking and ligand design to generate a new set of BRD9 ligands with improved physiochemical properties. Most notably, the cyclopropyl derivative **103** has good ligand efficiency and lipophilic ligand efficiency, nanomolar

BRD9 potency, evidence of selectivity over the off target BRD4(1), excellent solubility and attractive *in vitro* metabolic stability. Further studies to assess and optimise the potency and selectivity of derivatives of **103** will be discussed in Chapter 3.

Chapter 3: Optimisation of triazole sulfonamides and the use of Microscale Thermophoresis to profile ligand binding to bromodomains

3.1. Introduction and aims

The work outlined in Chapter 2 led to the development of **94**, a potent ligand of the BRD9 bromodomain, with good aqueous solubility, and attractive *in vitro* metabolic stability (Figure 41). The aim of the work described in this chapter was to extend the sulfonamide SAR study by further exploring scaffold **104**.

A

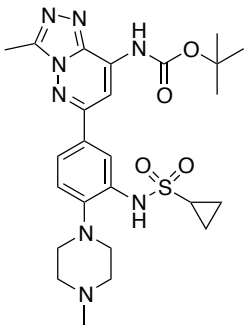

103

B

ΔT_m/°C (at 10 μM)	**BRD9**	10 (3)
	BRD4(1)	3 (1)
	BRD9 IC_{50}/nM HTRF	104
	SnapSol at pH 7.4/μM	>100
	Human *In vitro* Cl_{int} (μL/min/mg protein)	26

C

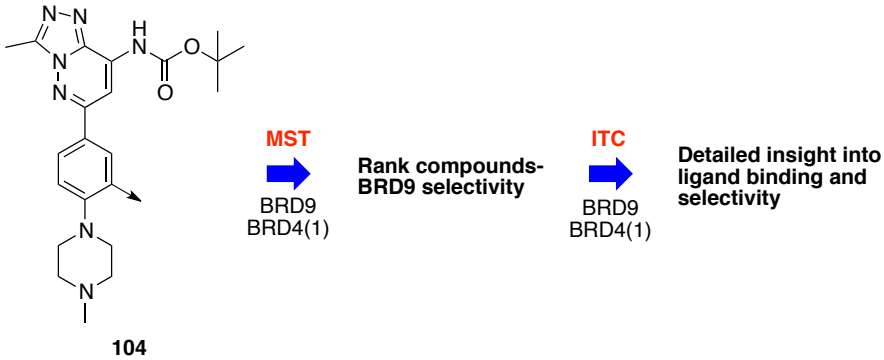

104

Figure 41: **Starting point for the work described in Chapter 3**. (**A**) Structure of cyclopropyl sulfonamide **103**. (**B**) Important parameters for compound **103**. (**C**) Target plan for this chapter, involving scaffold **104**.

In order to make useful structural and physicochemical conclusions that will be useful in future bromodomain and wider medicinal chemistry programmes, we aimed to:

- Identify and synthesise a range of compounds based on **104**, which maintain high BRD9 potency, and selectivity over BRD4(1).
- Complete a detailed assessment of each compound's selectivity for BRD9 over the important bromodomain off-target BRD4(1).
- Develop a new small-molecule binding assay for each bromodomain, using the highly sensitive technique of Microscale Thermophoresis.
- Rank each compound in terms of its selectivity over BRD4(1). The most interesting compounds will be further evaluated by ITC.
- Interpret and explain the structure-activity relationship obtained using crystallographic analysis and docking studies.

3.2. A comparative structural analysis of the bromodomains of BRD9 and BRD4(1)

In order to identify the most attractive sulfonamide targets, we first examined the X-ray crystal structures of **34** bound to BRD4(1) and BRD9 (Figure 42).[156] As noted in Chapter 2, the 2-chlorophenyl substituent sits in the lipophilic WPF shelf region in BRD4(1). Hydrophobic interactions in this region have been identified as a significant contributor to the affinity of a wide range of BET-bromodomain ligands.[69,70,75,126] We therefore hypothesised that a polar, hydrophilic substituent in this position could result in a reduction in BRD4(1) affinity, and provide an improvement in selectivity.

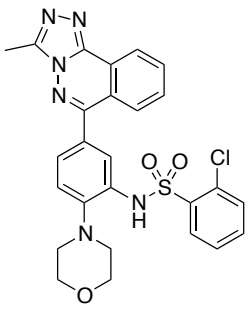

34

BRD4(1) **BRD9**

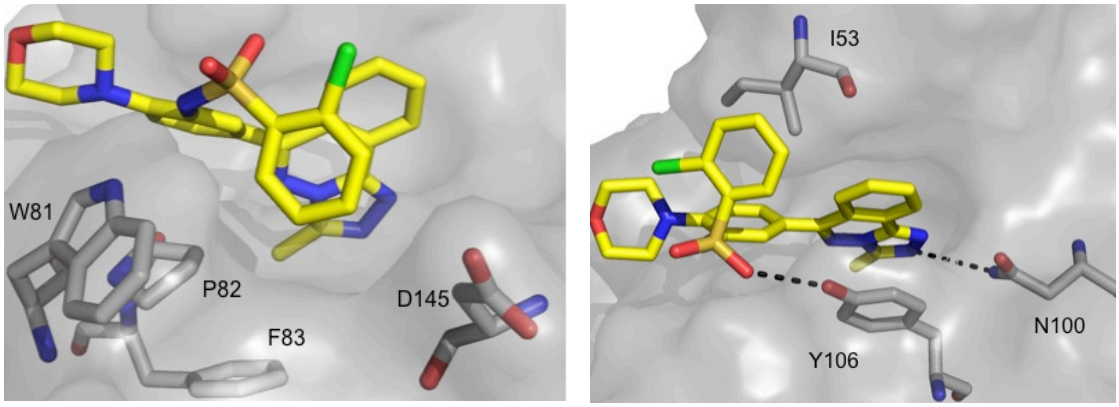

Figure 42: **Comparison of sulfonamide orientation of 34 when bound to BRD4(1) and BRD9.** Top: Structure of tricyclic triazole. Left: Crystal structure of **34** bound to BRD4(1) (PDB ID: 4NQM).[156] The 2-chlorophenyl substituent sits in the site formed between the WPF shelf and N145. Right: X-Ray crystal structure of **34** bound to BRD9 (PDB ID: 4NQN).[156]

When **34** is bound to the BRD9, the sulfonamide adopts an alternative conformation, enabling its oxygen to engage in a hydrogen bonding interaction with Y106. This conformation results in the pendant aryl ring residing in a relatively exposed region of BRD9, close to I53.

The sulfonamide **71** was docked into the BRD9 bromodomain and the most commonly observed binding mode of the six resulting lowest energy modes was very similar to that of **34**, with the aryl ring of the sulfonamide residing in a location in close proximity to I53 (Figure 43). With this result in mind, it provided us with greater confidence in the proposed binding mode of this compound series to BRD9.

A

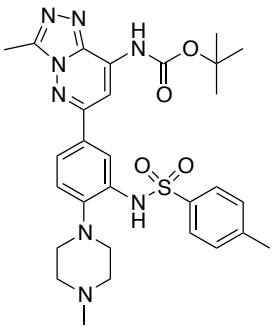

71

B

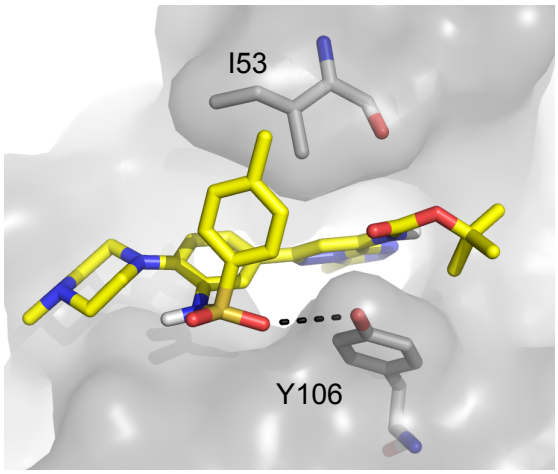

Figure 43: **Docking of 4-substituted sulfonamide 71 with BRD9**. (**A**) Structure of 4-substituted aryl sulfonamide **71**. (**B**) Predicted binding mode of compound **71** to BRD9. Docking was performed using Molsoft ICM browser software into the KAc binding pocket of BRD9 (PDB ID: 3HME).

In the course of docking studies into BRD9, it was noticed that I53 changed position slightly, in relation to other residues, suggesting that there might be some plasticity in this part of the protein. This was also observed during work by Picaud *et al*.,[158] which led to identification of the 9*H*-purine scaffold as a BRD9 inhibitor chemotype. As both the docking studies and X-ray crystal structure analysis suggested that the sulfonamide would reside in a primarily open region of BRD9, we decided to focus our attention on reducing the affinity of this compound set for the important off-target BRD4(1). In order to assess the affinities of compounds for BRD9 and BRD4(1), we required a robust and reliable assay. We also wanted a technique capable of ranking compounds in order to make the most informed judgment as to which compound should be progressed for further evaluation.

3.3. Identification and synthesis of sulfonamide targets

In order to identify the most physicochemically attractive sulfonamides, we first re-examined the predicted and measured solubilities of the sulfonamides **71** and **103**, to ensure that any synthesised compounds would have sufficiently high aqueous solubility (Table 13).

Compound Number	Structure	c log D at pH 7.4/μM	SnapSol at pH 7.4/μM
71	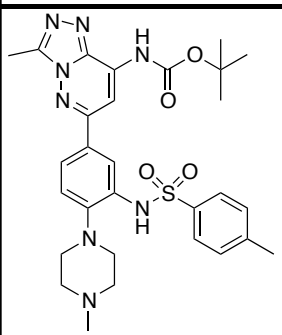	2.9	13
103	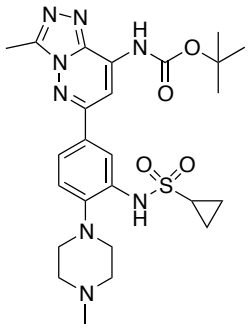	1.6	>100

Table 13: **Predicted and measured solubilities of sulfonamides 62 and 94.** c Log $D_{pH7.4}$ was calculated using ACD/Labs algorithm (version 5.0.0.184).

As there is a substantial increase in aqueous solubility upon modification from tosyl to a cyclopropyl group, we decided to target sulfonamides having calculated log D values <1.6. With this in mind, a search of commercially available sulfonyl chlorides was completed. Those compounds which were readily available and chemically diverse were then evaluated in terms of predicted aqueous solubility of the resulting sulfonamides. Six of these compounds had calculated log D values <1.6, and were synthesised from the corresponding aniline in one step (Table 14).

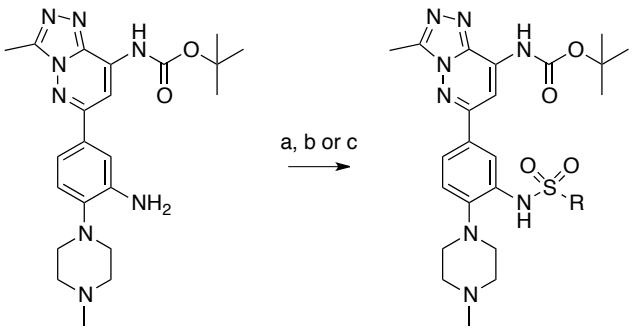

2 95

Compound Number	R	Reaction Conditions	Yield/%	Compound Number	R	Reaction Conditions	Yield/%
105		a	14	**108**	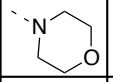	b	12
106		a	25	**109**	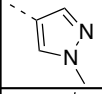	c	12
107		b	14	**110**		c	15

Scheme 14 and Table 14, *Reagents and conditions*: (a) RSO_2Cl, Et_3N, CH_2Cl_2, 0 °C-RT; (b) RSO_2Cl, Hünig's base, 4-DMAP, 1,4-dioxane, 70 °C; (c) RSO_2Cl, 4-DMAP, pyridine, 70 °C.

The mesyl and oxetane derivatives, **105** and **106**, respectively, were synthesised using previously optimised conditions with Et_3N and CH_2Cl_2. Reactions involving the pyrrolidine- and morpholine- sulfonyl chlorides were particularly sluggish, requiring heating to 70 °C with five equivalents of sulfonyl chloride, for substantial conversion of **2** to be achieved. For the pyrazole and imidazole analogues **100** and **101**, respectively, changing the solvent from 1,4-dioxane to pyridine was found to be optimal. The aqueous solubility of these sulfonamides was assessed in the SnapSol assay, and compared to the results previously obtained for a selection of closely-related compounds (Table 15).

Scaffold									
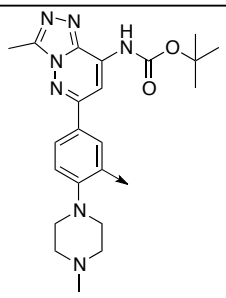									
Compound Number	**Compound**	***c* log D pH 7.4**	**SFI**	**SnapSol pH 7.4/μM**	**Compound Number**	**Compound**	***c* log D pH 7.4**	**SFI**	**SnapSol pH 7.4/μM**
70		1.9	4.9	92	**107**	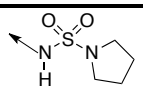	1.5	4.5	>100
2		1.0	3.0	>100	**108**	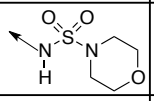	1.3	4.3	90
105	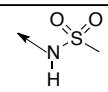	1.1	4.1	>100	**109**	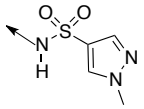	1.3	5.3	59
103	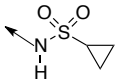	1.6	4.6	>100					
106	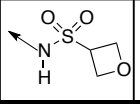	0.7	3.7	>100	**110**	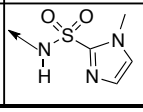	1.1	5.1	87

Table 15: Predicted and measured aqueous solubilities of triazole derivatives. SFI = Solubility Forecast Index = c log $D_{pH7.4}$ + #Aryl rings.[165] c Log $D_{pH7.4}$ was calculated using ACD/Labs algorithm (version 5.0.0.184).

The SnapSol assay defines 'moderately soluble' compounds as those having SnapSol values between 30-100 μM, and 'highly soluble' compounds as those with values >100 μM. All of the compounds in Table 15 displayed moderate or high solubility in the SnapSol assay. The aryl sulfonamide derivatives **109** and **110** were found to have a marginally lower solubility in relation to all other compounds, presumably due to the impact of an additional aryl ring. This is consistent with their Solubility Forecast Index (SFI) values (SFI = *c* log $D_{pH7.4}$ + number of aryl rings), which were approximately one unit higher than those of all other sulfonamides in Table 14. As outlined in Chapter 2, and in line with log D, the higher the SFI, the lower the predicted solubility. For this set of compounds and this scaffold in general, the SFI seems to

provide a more accurate prediction of aqueous solubility than calculated log D values, consistent with the proposition made by Hill and Young at GSK, who developed this enhanced solubility prediction tool.[165] The presence of an additional aryl ring overrides the heteroatoms in the pendant aryl sulfonamide, resulting in a lower measured aqueous solubility.

With these nine compounds in hand, we aimed to evaluate their affinity for both BRD9 and BRD4(1). This required access to a robust and reliable assay, capable of determining which compounds should be taken forward for further evaluation.

3.4. Microscale Thermophoresis (MST) as a new technique to measure ligand binding to bromodomains

3.4.1. Current assays available to identify bromodomain ligands

Robust and reliable tools to measure biomolecular interactions provide a fundamental insight into the molecular biology of the cell, and give us a platform for the treatment of disease. As protein interactions in the human body are expected to differ from the situation *in vitro*, it is important that the assay conditions used are as close as possible to the native environment. This is crucial when investigating protein functions, stressing value of new techniques to investigate target-ligand interactions.

As a reader domain, a bromodomain lacks any form of catalytic activity, which presents a challenge during assay development. Procedures must therefore

detect the compound-ligand interaction directly ('label-free' techniques), or measure displacement of a known binding partner. The bromodomain-KAc interaction is also relatively weak (typically 3-20 μM), presenting an additional problem.

3.4.1.1. Label-free techniques

Label-free biochemical techniques have been extensively used to detect bromodomain ligands, particularly in earlier studies, and are especially useful in many circumstances where a cognate peptide sequence for a bromodomain has yet to be developed. NMR-based techniques were pioneered by Zhou and colleagues during the development of small molecule ligands of the PCAF[31] and CREBBP[124] bromodomains. This method can provide a detailed insight into the location of the ligand, but requires substantial amounts of protein and is therefore unsuitable for extensive screening programmes. Nevertheless, the wide range of NMR experiments which have been developed to measure protein-ligand binding, such as CPMG, STD, and waterLOGSY, enable an array of information to be gathered using this technique. Fluorescence spectroscopy was also used by Zhou and colleagues to measure dissociation constants for the CREBBP ligands, relying on ligand-induced variation in the fluorescence spectrum of tryptophan residues near the KAc binding site.[122,124]

Surface plasmon resonance (SPR) is attractive in comparison to NMR or fluorescence spectroscopy methods as it provides kinetic data on compound binding, in addition to consuming a lower amount of protein. This technique

has been used as a secondary assay in bromodomain ligand development.[70,71,75,181,182] Bio-layer interferometry (BLI), which like SPR, also involves surface immobilisation of a protein, has been used by the SGC to measure affinity for the CREBBP bromodomain. The immobilisation process on to a surface can result in issues such as steric hindrance and mass transport effects.[183,184]

Differential scanning fluorimetry (DSF) or thermal shift has been used to evaluate compound selectivity over multiple bromodomains.[69-71,81,82,136,156,174,185-187] Isothermal titration calorimetry (ITC) provides a direct measurement of the thermodynamics of binding, differentiating between enthalpic and entropic binders in a single experiment. This method remains the "gold standard" method for evaluating small-molecule–bromodomain interactions.[69,71,81,82,162,174,188-190] The main drawbacks of ITC are its low throughput and exceptionally high rate of protein consumption.

A comparison of label-free K_D values of small-molecule protein interactions found that surface-based methods tend to overestimate affinity, compared to ITC and NMR methods, bringing the accuracy of the binding data produced into question.[191] Myszka has shown that SPR-based equilibrium constants often disagree with those obtained from solution-based methods for a variety of reasons.[192] The main source of error is thought to arise from the immobilsation step, which restricts the protein's rotational freedom and diffusional properties, thereby altering the thermodynamics of the reaction and the binding kinetics.

Given the differences in these assays, it is therefore preferable to assess bromodomain binding using as many techniques as possible, enabling greater confidence to be placed in the data obtained.

3.4.1.2. Competition assays

A competition assay to identify small molecule bromodomain ligands was first developed by Zhou and co-workers.[120] They used an ELISA in which a GST-tagged KAc-containing peptide and immobilised PCAF bromodomain were employed, to measure IC_{50} values of compounds derived from a 2D ^{15}N-HSQC NMR screen. As the affinity of bromodomains for histone-mimicking acetylated peptides is low, the highly sensitive AlphaScreen™ technique has become especially useful. It has been used to characterise inhibitors from several bromodomain famiies.[81,136,138,156,174,182,186,189] TR-FRET assays also have high sensitivity and consume relatively low amounts of protein. This method has been successfully used to validate hits against the BET bromodomains.[69,71,75,82,193] It has also be used in ligand optimisation studies during the development of inhibitors for the bromodomains of BRPF1[140], ATAD2[149] and BRD9.[161]

DiscoveRX have commercialised a polymerase chain-reaction (PCR)-based displacement assay. This assay, known as BROMO*scan*, employs immobilised ligands and DNA-tagged bromodomains.[194] Compounds that bind the bromodomain reduce the amount of protein captured on a solid support. The amount of captured bromodomain is quantified by quantitative PCR (qPCR) and is proportional to the compound's affinity. A detailed assessment

of compound selectivity can now be made on over thirty bromodomains, representing approximately 50% coverage of the human bromodomain family.

Displacement assays are clearly advantageous in comparison to many of the label-free methods, in terms of sensitivity and throughput. The requirement of cognate peptides is an important drawback to consider, however, in addition to the lack of comprehensive thermodynamic binding information which can be gained from label-free methods. Each of these assays varies in attractiveness depending on what specific information is desired, as well as other considerations such as time requirements, protein stability and size of compound set under examination. The general complications of making measurements in biological liquids is still a significant challenge in modern bioanalytics. By developing a wider selection of assays to measure the interactions between bromodomains and their binding partners, we are more likely to be able to overcome these challenges and have greater confidence in the data produced.

3.4.2. Microscale Thermophoresis as a technique for protein-ligand binding affinity measurement

Microscale Thermophoresis (MST) is a powerful technique to quantify biomolecular interactions. This method is based on thermophoresis, defined as “the directed movement of molecules in a temperature gradient”.[195] Since the discovery of this phenomenon by Ludwig in 1856[196] it has mostly been used to study inorganic molecules or polymer blends.[197,198] Most fluorescence-based assay techniques have a rather limited scope, since they

depend on parameters such as molecule size and size-change upon binding, and the relative position of fluorophores.[195,199] They also frequently require large sample volumes, complex experimental setups, and intensive data analysis.[200,201] In addition to relying on changes in particle size and charge upon binding, MST is also dependent upon variation of the hydration shell, making it an extremely sensitive measurement technique.[195,200]

The scope of this technique is exceptional, as interactions between two proteins of approximately equal molecular weight can be analysed with the same sensitivity as interactions with small molecules or even ions (Figure 44).

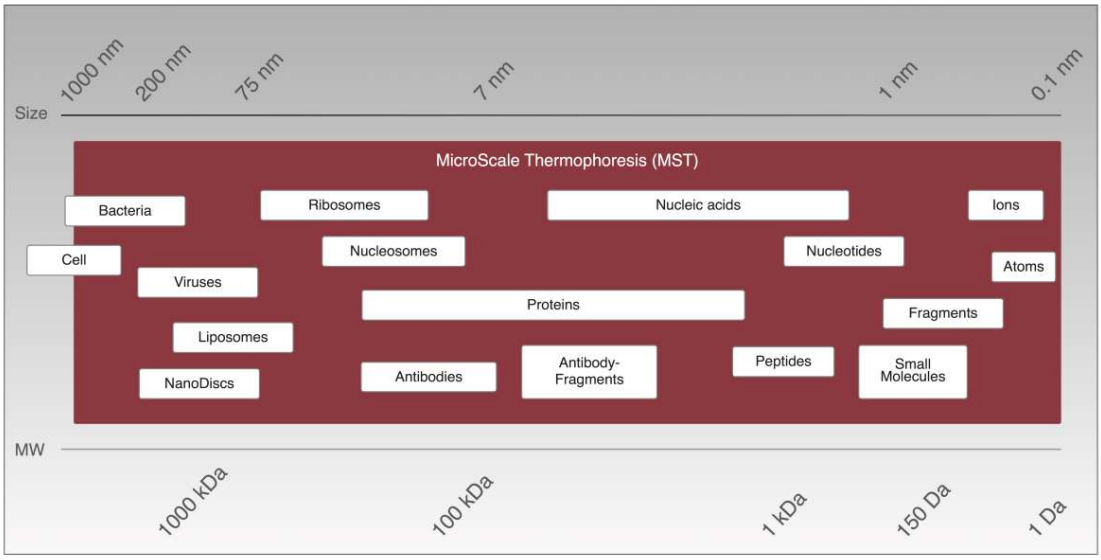

Figure 44: **A summary of the scope of interactions accessible with MST.** Figure created by Astrid Sitte, Nano Temper Technologies (reprinted with permission).

The analysis of small molecule-protein interactions is often complicated by the fact that low-molecular weight binders frequently fail to change significantly the charge or size of a biomolecule.[200,202-207] It has been demonstrated, however, that MST is highly suitable for the analysis of this kind of interaction, possibly due to changes in the hydration shell of molecules upon

binding.[195,200] In addition to its broad scope, MST has numerous additional advantages, allowing the user to:

- Measure affinities (K_D values) directly in solutions of choice such as standard buffers, to bioliquids such as cell serum and cell lysate
- Study the binding energetics ΔG (free energy), ΔH (enthalpy) and ΔS (entropy)
- Explore biochemical activity under close to native conditions without the need for target immobilisation, and at a temperature of choice
- Measure IC_{50} values directly or in a competition experiment
- Investigate the stoichiometry and determine the number of binding sites within biomolecules
- Discriminate between different binding modes of a set of ligands
- Distinguish aggregation and other artifacts from true binding events
- Study membrane bound proteins directly in liposomes and vesicles
- Become highly efficient. K_D values can be measured in minutes, using 3-5 µL of sample per capillary, at labeled biomolecule concentrations as low as 1 nM

MST is gradually becoming appreciated as a valuable additional technique to monitor a wide range of interactions, as evidenced by its use in a diverse set of recent studies.[202-208]

3.4.3. Experiment implementation

MST is an all-optical approach in which visible light is used for fluorescence excitation. In the particular instrument used during this study (Monolith

NT.115), three types of LED-filter combinations are available: blue (excitation 460-480 nm, emission 515-530 nm), green (excitation 515-525 nm, emission 560-580 nm) and red (excitation 605-645 nm, emission 680-685 nm). As shown in Figure 45, the sample solution inside a glass capillary is heated with an IR-laser. The path of fluorescence light and the heating IR-laser are focused with the same objective used for fluorescence detection, resulting in the IR-radiation being focused on exactly the same location where fluorescence intensity is measured.

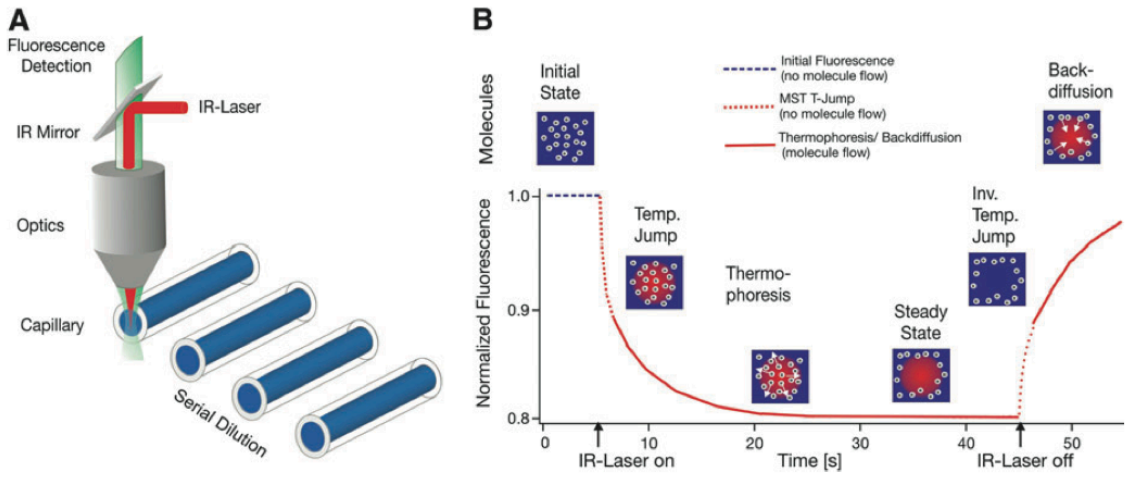

Figure 45: **Experimental setup and MST signal.** (Figure modified from Jerabek-Willemsen *et al.*[195,209] 2014, permission granted.) (**A**) MST is measured from a capillary with a total volume of 4 µL. In most cases, the concentration of the fluorophore-biomolecule is kept constant, while a 10-16 fold serial dilution of the ligand is made. Fluorescence excitation and measurement are made through the same optical element. An IR-Laser heats the sample volume that is subsequently observed by fluorescence. The T-Jump and thermophoresis are directly observed as a change in fluorescence at different time scales. (**B**) A typical MST signal for a single capillary. Initially, the molecules are homogeneously distributed and a constant ‘‘initial fluorescence’’ is measured. Upon switching on the IR-Laser, a fast temperature jump (T-Jump) is observed, followed by thermophoretic molecule motion. The fluorescence decrease is often measured for 30 s. When the IR-Laser is turned off, an inverse T-Jump is observed, followed by the ‘‘backdiffusion’’ of molecules, driven by mass diffusion.

The IR-radiation is absorbed by the water molecules of the sample buffer to create a temperature gradient. As the laser-beam is easily focused, the temperature gradient is localised whilst the overall temperature remains low. Typically, a total sample volume of 2 nL is heated by 1-6 K, depending on IR-

laser power and sample capillary type.[195,208] The IR-laser allows heating a solution with very high precision and reproducibility in the mK range. This is very important, as a typical interaction analysis involves a serial dilution that results in 10-16 different samples to be analysed.[200,209] By restricting the temperature distribution to the µm scale, changes in thermophoretic properties can be quantified in <30 s, enabling K_D measurement in minutes. Observation of fluorescence is made in thin glass capillaries. Before each MST experiment, a "capillary scan" is completed which precisely defines the position of each capillary, guaranteeing highly reproducible temperature gradients during each measurement. Each capillary has a constant inner and outer diameter, made from highly pure glass, ensuring that a constant amount of laser power is absorbed.[195,208]

3.4.4. MST signal analysis

The fluorescence time trace represented in Figure 43 displays a series of thermophoretic processes, each of which can provide detailed information on the binding event. The normalised fluorescence (F_{norm}) is used to quantify binding *via* MST, according to Equation 1.

$$F_{norm} = \frac{F_1}{F_0}$$

Equation 1: The normalised fluorescence (F_{norm}) is measured as the concentration of a binding partner changes. F_0 is the initial fluorescence intensity, typically measured 1 s after the laser is turned on. F_1 is the fluorescence intensity measured several seconds after this, when the traces of unbound and bound states can be discriminated.

It is noteworthy that the steady state does not have to be reached within the time peiod of the experiment, only that there is a detectable difference in the normalised fluorescence in the bound and unbound states.[200]

3.4.5. Design and optimisation of an MST assay to measure binding to BRD9

MST assays can be performed without biomolecule labelling if the target of interest is intrinsically fluorescent due to the presence of tryptophan residues. As BRD9 lacks any tryptophan residues, the protein was labelled with an NT.115 amine-reactive dye (structure not disclosed). This dye is reported to contain an *N*-hydroxysuccinimide (NHS) ester functional group, capable of reacting with primary amines of lysine side chains or at the protein's N-terminus.[125,208] Typically one primary amine is labelled per protein, therefore the position of the dye is statistically distributed.[200,209] As BRD9 has a high composition of lysine residues (14, 10% of the total amino acids), the distribution of labelled residues is likely to be large. Analysis of the *apo* X-ray crystal structure of BRD9 (PDB ID: 3HME) indicated that all of the lysine residues are located in regions far away from the KAc-binding site, minimising the chance that the label could interfere with binding. The labelling procedure was straightforward, involving incubation of a mixture of the protein and dye in a HEPES buffer for 30 min, followed by a gel-filtration step to remove any unreacted dye.

Attention then turned to finding the optimal conditions to run a series of MST experiments while the compound concentration was varied. Firstly, the optimal capillaries had to be determined. The initial capillary scan in standard capillaries showed broad peaks, indicative of non-specific binding of labeled BRD9 to the capillary walls. However, when hydrophilic capillaries were used, slightly sharper peaks were observed. As low volumes are used in this

technique, adhesion of protein to both the capillaries, and the micro reaction tubes, is often a problem. Pluronic® F127 detergent prevented this issue, and led to an increase in fluorescence to approximately 500 units (optimal value between 80-1500 units). The optimal conditions were achieved with a combination of hydrophobic capillaries and 0.005% Pluronic® F127 detergent, leading to sharp signals (Figure 46).

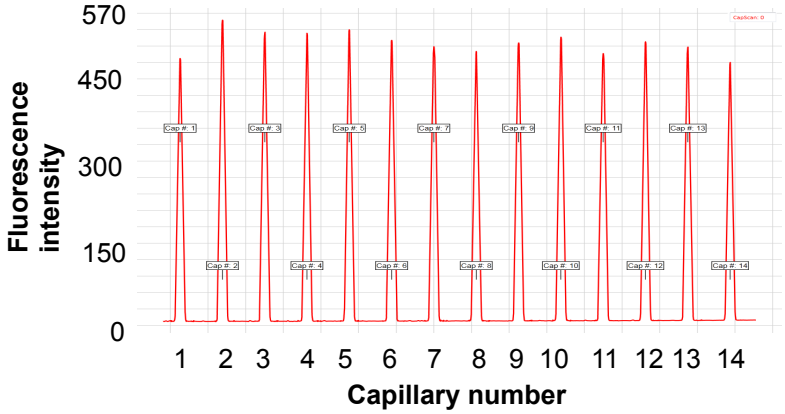

Figure 46: **Capillary scan in hydrophilic caplillaries with 0.005% detergent.** This is the initial fluorescence intensity before the IR-laser is turned on. The sharpness of the peaks indicates that the fluorescent molecule is free in solution and does not stick to the capillary surface. (20 nM BRD9; LED power; 100%)

As the compounds to be tested are in a DMSO stock solution, and given that DMSO has been found to bind to bromodomains, the effect of DMSO concentration on the MST curves was examined.[125,209] A 13-fold serial dilution of DMSO from 0.5% to 0.0006% (volume/volume (*v/v*)) was performed (Figure 47).

A

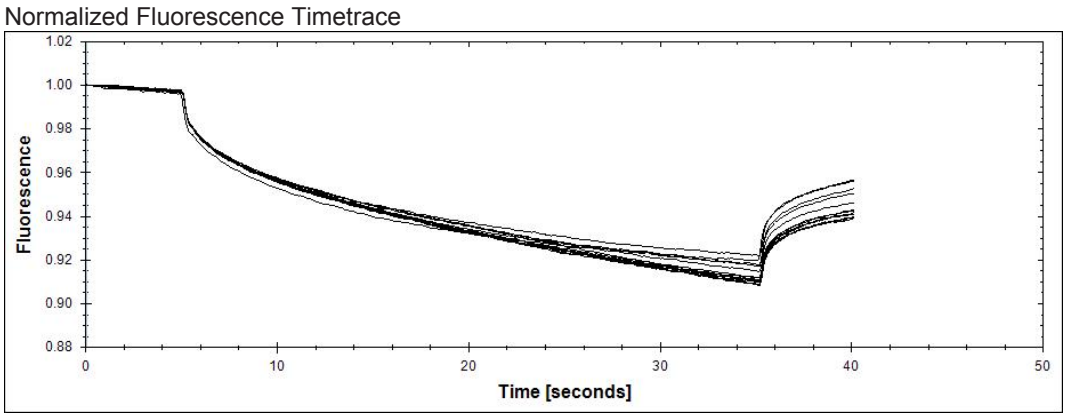

B

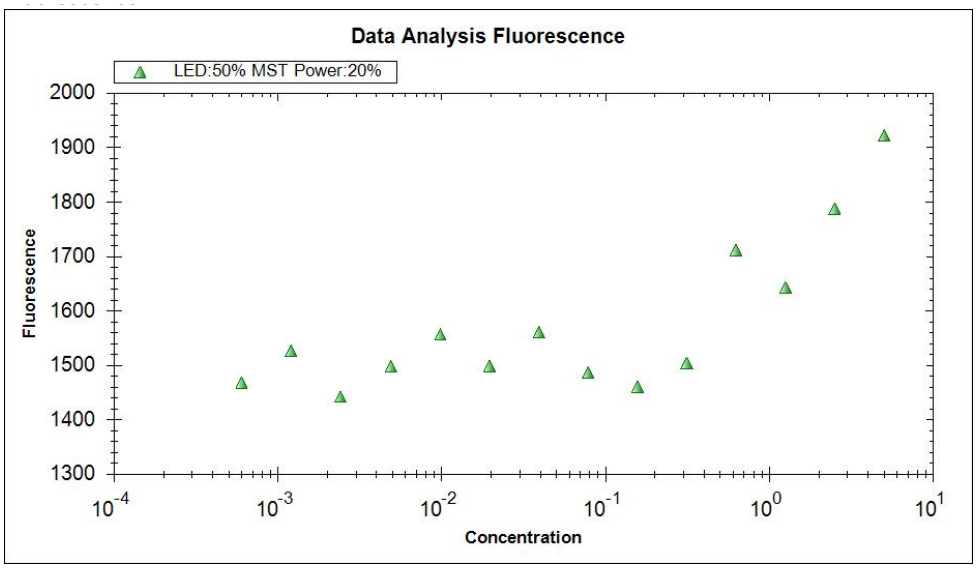

Figure 47: MST DMSO study on BRD9. (**A**) MST curves of BRD9 incubated with DMSO from 5%-0.0006% (*v/v*) DMSO. (**B**) Normalised fluorescence as the concentration of DMSO is varied. (20 nM BRD9; 100% LED power; 20% MST power; laser-on time was 30 s, laser-off time was 5 s, delay was 25 s, fluorescence before was 5 s.)

The results of this study confirmed that DMSO does bind to BRD9 at high concentrations, causing a change in normalised fluorescence during the MST experiment. For concentrations of DMSO from 5%-1.25%, there is a large change in fluorescence, indicating binding to BRD9. For DMSO concentrations <1.25% (*v/v*), no change in fluorescence was detected. Therefore, in order to make sure that no buffer effects are observed a final DMSO concentration of 0.8% (*v/v*) was used throughout. This enabled a 160 µM compound stock to be made from a 10 mM solution in DMSO. A

serial dilution giving final compound concentrations from 40 µM - 2.4 nM was then completed. The experiments were performed in triplicate, from compound dilution to laser irradiation. The normalised fluorescence intensities at concentrations of 80 µM and 40 µM **103** are shown in Figure 46. There was significant variation of the normalised fluorescence values when binding of **103** to BRD9 was measured at these concentrations. Additionally, there was a lack of MST curve smoothness, indicative of some form of interference between the compound and the fluorescently labeled BRD9 under these conditions. For example, at concentrations of **103** of 80 µM and 40 µM, the noise level is approximately 29 units, and 14 units, respectively (Figure 48).

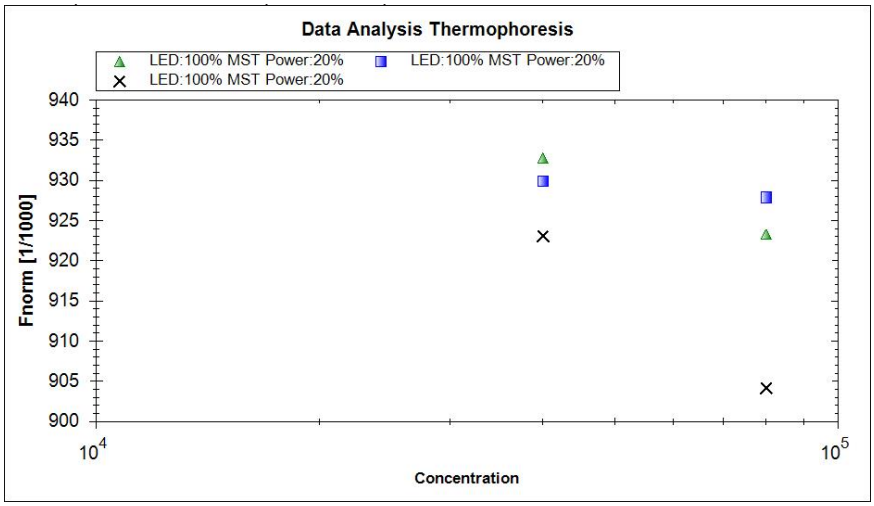

Figure 48: Indication of large noise at high ligand concentrations (right- 80 µM, left- 40 µM).

The problem of high noise is often observed at high ligand concentrations, though communications with several expert users of this technique have failed to identify a conclusive reason for this observation. As these ligand concentrations represent a large excess in relation to the concentration of fluorescent molecule (BRD9 concentration = 20 nM), some interference is therefore unsurprising.

The binding of **103** to BRD9 was then measured, starting from a compound concentration of 20 µM (Figure 49). This gave MST curves that overlaid extremely well during each of the three runs, with a considerably lower deviation in normalised fluorescence (2 units) at the highest compound concentration of 20 µM.

A

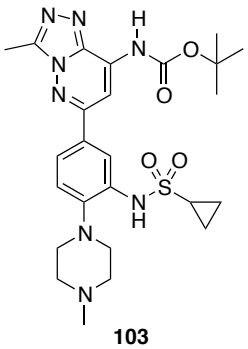

103

B

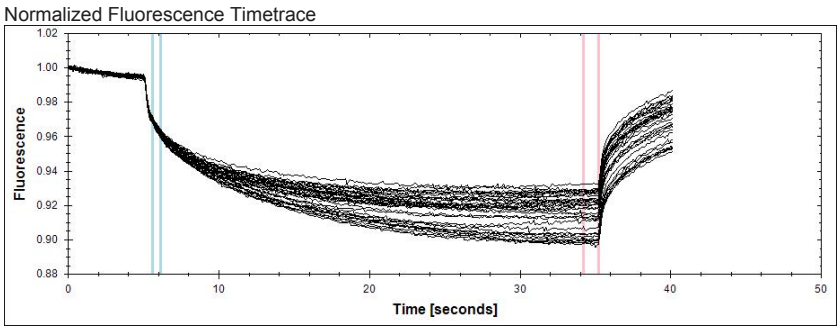

C

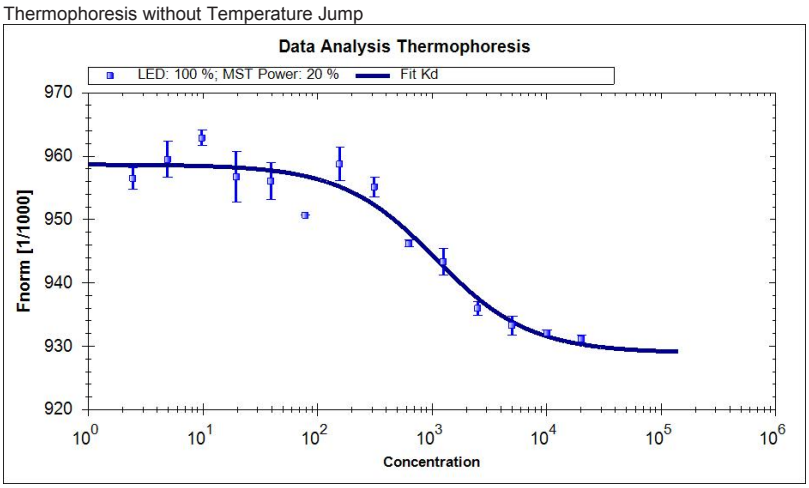

Figure 49: Binding of 103 to BRD9, measured by MST (K_D = 951 ± 88 nM). (20 nM BRD9; 100% LED power; 20% MST power; laser-on time 30 s; laser-off time 5 s; delay 25 s; fluorescence before 5 s).

Further analysis of the shape of individual MST curves indicated an uneven architecture, consistent with a degree of aggregation of the fluorescent molecule. During the initial optimisation, the BRD9 protein was labeled with the fluorescent dye, then aliquoted and frozen, before being thawed and diluted. One reason for the evidence of aggregation was therefore identified

as the freezing step. Many attempts were made to overcome this aggregation, including centrifugation, increasing detergent concentration, or addition of Bovine Serum Albumin (BSA), though none resulted in a detectable improvement. Protein labeling on the same day as MST measurements were to be carried out resulted in substantially smoother MST curves, as shown in Figure 50.

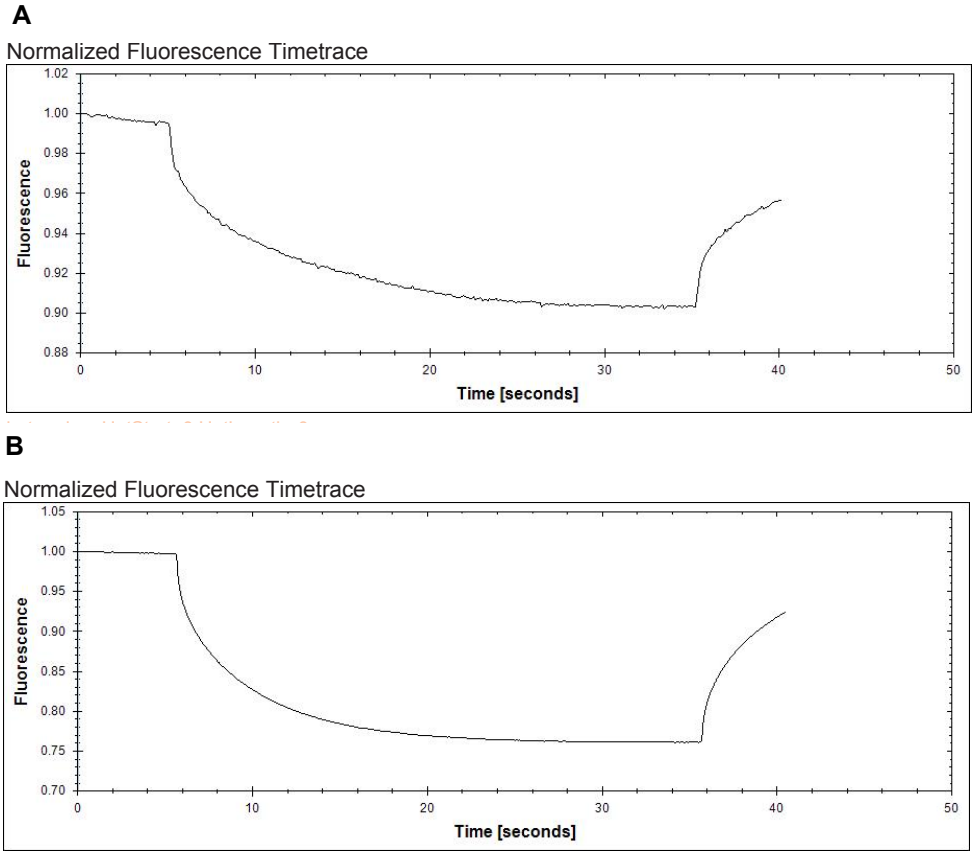

Figure 50: Comparison of BRD9 MST curve shape depending on protein freshness (5 µM compound 103). (**A**) BRD9 has been labelled, aliquoted, frozen and thawed. (**B**) BRD9 has been labelled within 24 h and kept on ice in the dark. (20 nM BRD9; 100% LED power; 20% MST power; laser-on time 30 s; laser-off time 5 s; delay 25 s; fluorescence before 5 s).

With the issue of aggregation solved, a final round of assay optimisation was required due to the fact that hydrophilic capillaries were to be discontinued by the manufacturer, NanoTemper™. With the replacement “premium-coated” capillaries, we found it was necessary to change the type of detergent from Pluronic® F127 to Tween® 20. The detergent concentration was also

increased from 0.005% to 0.05% (*v/v*). DMSO concentration was kept at 0.8% (*v/v*), while the concentration of the fluorescent molecule was increased from 20 nM to 60 nM, and the LED power was reduced to 40%.

The binding of **103** to BRD9 was then measured in triplicate. Under these conditions the normalised fluorescence was measured in the thermophoretic region, and the affinity and sensitivity was found to be relatively low (Figure 51). Shortening the time period in which fluorescence is measured, from 30 s to 4 s, resulted in a significant increase in amplitude of the bound and unbound states, such that binding could be measured (Figure 51.B). The time points in which binding is measured are reported to provide another level of detail regarding the interaction of interest.[158,209,210] For example, it is thought that 'if a molecule binds to a labeled protein in close proximity to the fluorescent dye or induces a conformational change of the protein at a position close to the dye, this binding event influences the temperature dependence of the fluorescence and will be detected in MST temperature jump'.[162,209] BRD9 has been reported to have a relatively flexible binding pocket, which may help to explain the improved results when using a smaller window around the region of temperature jump.[76,158,210]

A

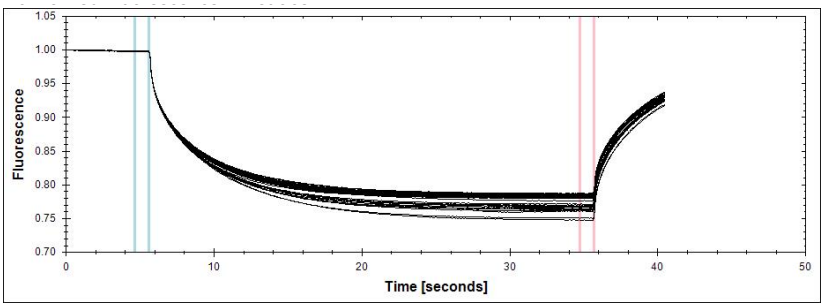

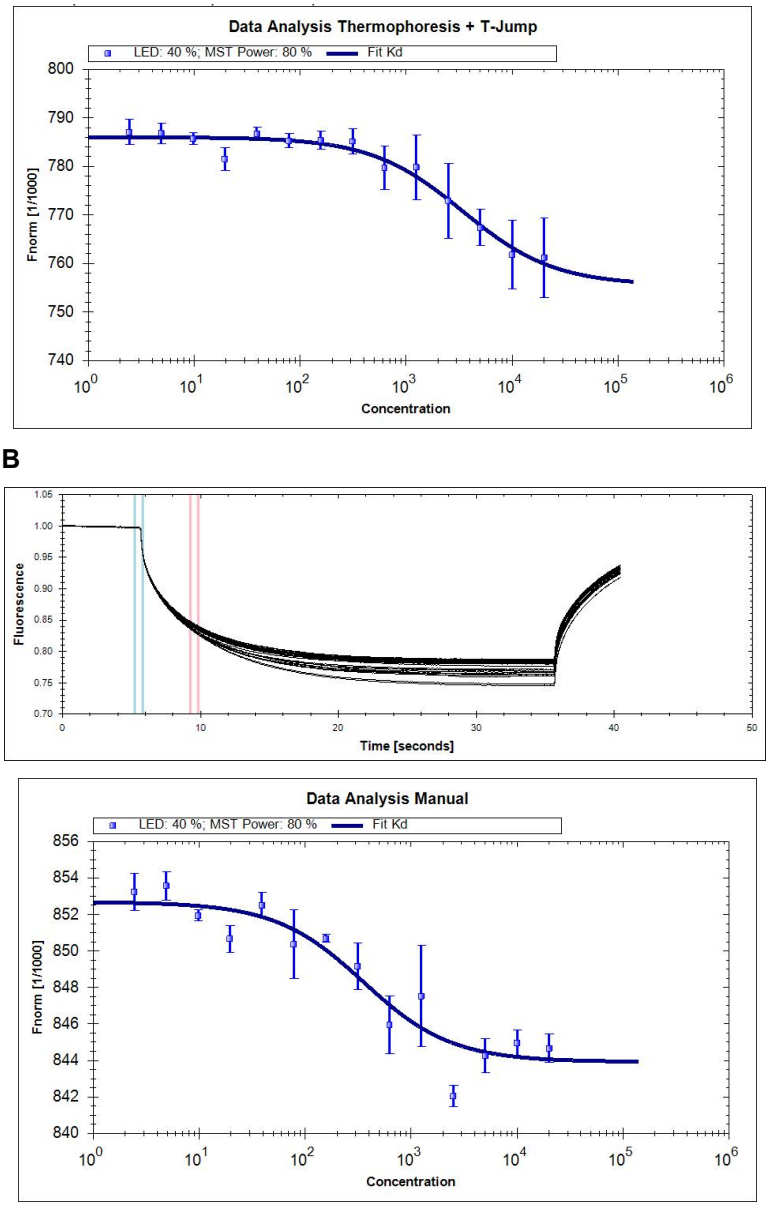

Figure 51: Examining the impact of the window over which the normalised fluorescence value is calculated, on the resulting binding curve. (**A**) Indication of where F_{norm} is calculated, over a 30 s time period (Thermophoresis + T-Jump), and binding curve of **94** to BRD9. (**B**) Indication of where F_{norm} is calculated, over a 5 s time period, and binding curve of **94** to BRD9. (In both cases: 60 nM BRD9; 40% LED power; 80% MST power; laser-on time 30 s, laser-off time 5 s, delay 25 s, fluorescence before 5 s).

In the case of the shortened analysis window, compound **103** was found to have a BRD9 K_D value of 325 ± 66 nM, in agreement with the BRD9 IC_{50} value of 104 ± 13 nM measured in a HTRF assay.

In order to validate this MST assay, the affinity of the BRD9/7 probe LP99 (**41**) was measured.[76,162] This compound was previously found to bind to BRD9 with a K_D value of 99 nM by ITC. Although the amplitude between the bound and unbound states was low (4 units), the measured K_D value by MST of 100 ± 40 nM was in good agreement with the ITC result.

3.4.6. Measurement of BRD9 K_D values by MST

With a validated assay in hand, the binding of the set of soluble triazoles was then completed (Table 16). The nitro derivative **70** had the lowest affinity (K_D = 1.32 μM) of the compounds tested, which may be due to the absence of an NH group capable of forming a hydrogen bonding interaction with Y106. The oxetane derivative **106** was the second-weakest binder, with a K_D value of 621 nM. This could be due to an electrostatic lone-pair lone-pair repulsion between the oxetane and the nearby backbone carbonyl groups of A52 and I53. The affinity of the remaining sulfonamides was relatively similar, with the morpholine derivative **108** being slightly more potent that the pyrrolidine-containing compound **107**. The oxetane **106** and morpholine **108** derivatives both contain an oxygen atom in similar positions, however **106** was found to have an approximately 3-fold lower K_D value. It is possible that **108** may be able to adopt a chair conformation that is favourable for binding to BRD9. The larger size of **108** may also have an important impact on binding.

Scaffold	Compound	Compound Number	SnapSol at pH 7.4	BRD9 K_D/nM	Error/nM
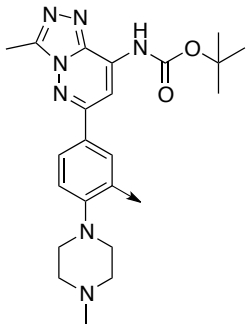		**70**	92	1320	427
		**2**	100	164	25.1
	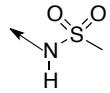	**105**	100	245	47.8
	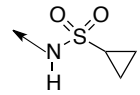	**103**	100	325	65.7
	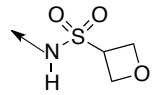	**105**	100	621	110
	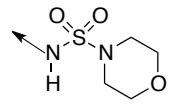	**108**	90	225	33.3
	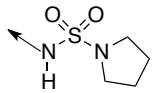	**107**	100	375	65.4
	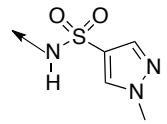	**109**	59	222	48.7
	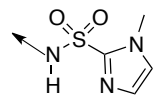	**110**	87	211	59.3

Table 16: Affinity of soluble compounds screened against BRD9 by MST. Results displayed as a heat map, with lowest IC_{50} value shown in red and the highest IC_{50} value in green. (60 nM BRD9; 40% LED power; 80% MST power; laser-on time 30 s, laser-off time 5 s, delay 25 s, fluorescence before 5 s).

The methylimidazole analogue **110** had the lowest K_D value of all sulfonamides tested, although the methyl, morpholine, and pyrazole compounds each have measured affinities that are, within error, equal to **110**. The two aryl sulfonamides **109** and **110** were found to have the highest SFI values, both of which were >5, due to the influence of the additional aryl ring.

These values are in agreement with their measured aqueous solubilities, which are among the lowest of this compound set.

Interestingly, the aniline **2** had the lowest BRD9 K_D value of 164 ± 25 nM, and its expected binding mode is discussed later in this chapter. The binding curve of **2** to BRD9 measured by MST is shown in Figure 52.

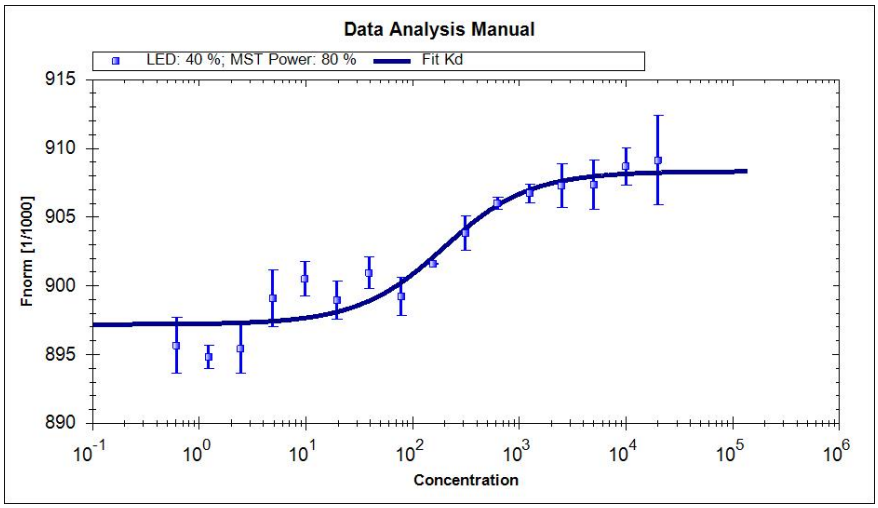

Figure 52: **Binding curve of compound 2 to BRD9.** (60 nM BRD9; 40% LED power; 80% MST power; laser-on time 30 s, laser-off time 5 s, delay 25 s, fluorescence before 5 s.)

It was then aimed to evaluate the affinity of this compound set against BRD4(1) using the same technique. This could provide us with a more detailed insight as to whether the sulfonamide analogues had improved selectivity over this bromodomain.

3.4.7. Design and optimisation of an MST assay to measure binding to BRD4(1)

To develop a small molecule assay for BRD4(1), racemic **8**, developed in our laboratory, was used as a validation tool.[76] The (*R*)- and (*S*)- enantiomers were previously found to have BRD4(1) K_D values by SPR of 360 nM, and

390 nM, respectively. Using the previously optimised MST conditions for BRD9, **8** was found to have a BRD4(1) K_D value of 347 ± 158 nM (Figure 53). The 46% error, low amplitude (7.5 units), and high noise, all required optimisation.

A **B**

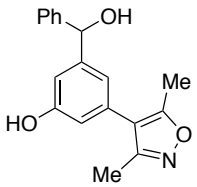

OXFBD02
8

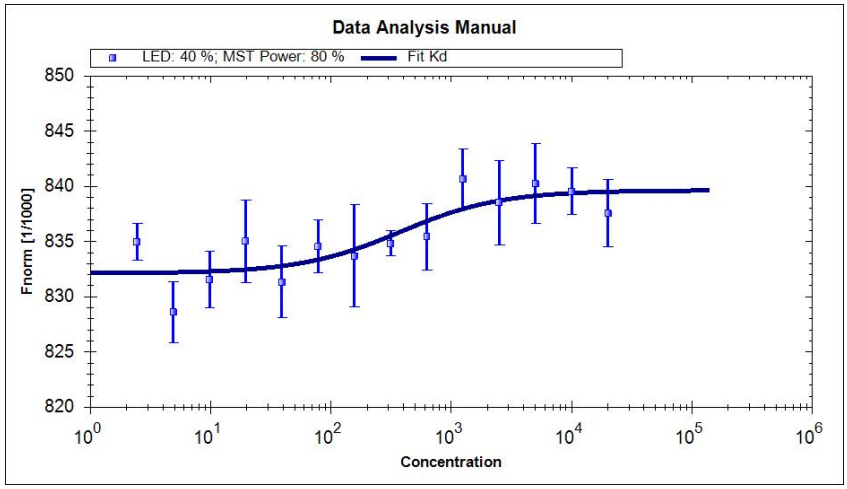

Figure 53: Binding curve of racemic 8 and BRD4(1).[76] (**A**) Structure of **8**. (**B**) Binding of 8 to BRD4(1) measured by MST. (60 nM BRD4; 40% LED power; 80% MST power; laser-on time 30 s, laser-off time 5 s, delay 25 s, fluorescence before 5 s).

The concentration of BRD4(1) was increased from 60 nM to 120 nM, as a higher protein concentration is often reported to give better sensitivity, although this gave no significant improvement. The considerable noise level at low ligand concentrations was a particular worry, suggesting that the protein was in a sub-optimal environment. By performing MST experiments in each of four capillaries in the absence of compound, the noise level in HEPES (10 units) was found to be substantially larger than that in TRIS (3 units), as shown in Figure 54.

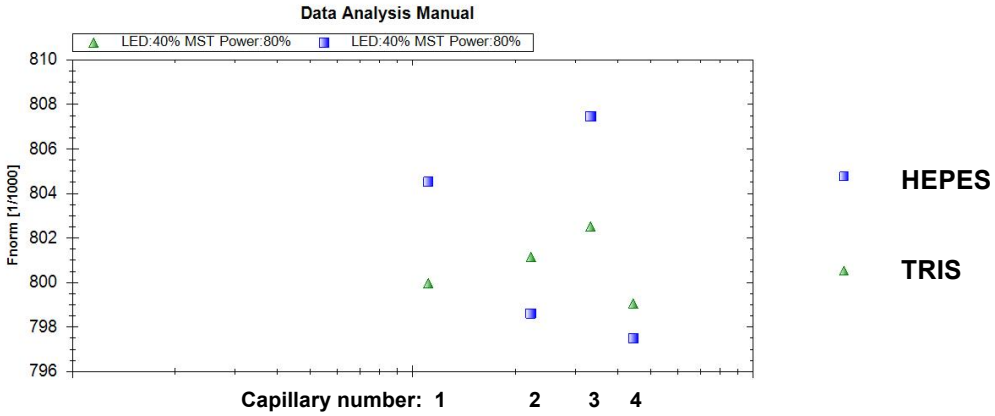

Figure 54: Comparison of noise level in HEPES and TRIS buffer. Four separate eppendorfs were filled with buffer, before addition of protein solution. (60 nM BRD4(1); 40% LED power; 80% MST power; laser-on time 30 s, laser-off time 5 s, delay 25 s, fluorescence before 5 s.)

The BRD4(1) K_D of racemic **8** was then measured in TRIS buffer, which gave a slight increase in amplitude, although the problem of high noise at both high and low ligand concentrations remained (Figure 55.A). Increasing the detergent concentration from 0.05% to 0.2% gave a slight increase in amplitude, in addition to a reduction in noise (Figure 55.B).

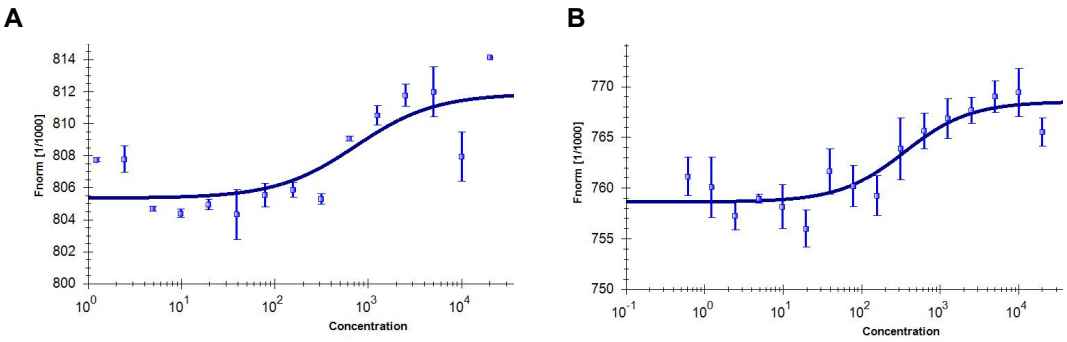

Figure 55: Comparison of binding curve of 8 to BRD4(1) with a variation in detergent concentration. (A) 0.05% Tween® 20. **(B**) 0.2% Tween® 20. (60 nM BRD4(1); 40% LED power; 80% MST power; laser-on time 30 s, laser-off time 5 s, delay 25 s, fluorescence before 5 s).

With the increase in detergent concentration giving a slightly better binding curve, the impact of a centrifugation step was then investigated. This was found to result in a 50% reduction in F_{norm} noise level on average, when a

comparison of four capillaries was made. A final optimisation step whereby the concentration of fluorescently labeled BRD4(1) was reduced from 60 nM to 20 nM, and the LED power was increased from 40% to 100%, resulted in the lowest noise level in the bound and unbound states, in addition to the highest amplitude of all conditions explored (Figure 56).

A

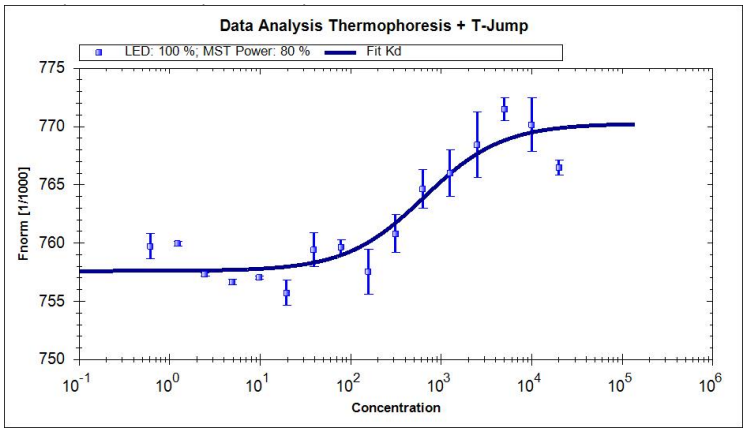

B

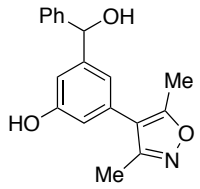

OXFBD02
8

C

Technique	Compound	BRD4(1) K_D/nM	Error/± nM
SPR	**8** *(S)*-(+)	390	30
SPR	**8** *(R)*-(−)	360	110
MST	**8** (*rac*)	641	112

Figure 56: **Summary and comparison of binding results for compound 8 to BRD4(1).**[76,191] (**A**) MST analysis of **8** binding to BRD4(1) under the optimised conditions: 0.2% DMSO; 0.2% Tween® 20; 10 nM BRD4(1); 40% LED power; 80% MST power; laser-on time 30 s, laser-off time 5 s, delay 25 s, fluorescence before 5 s.) (**B**) Structure of OXFBD02. (**C**) Comparison of K_D values found in the literature[76,211] (SPR) and during this work (MST).

The K_D value of 641 ± 112 nM for **8** is within an acceptable range of the value obtained by SPR for each of the two enantiomers (360-390 nM). As previously mentioned, SPR tends to overestimate the binding affinity of compounds, due to surface artifacts.[69,71,81,82,174,188-191,210] With the assay conditions optimised to measure binding to BRD4(1) with an extremely low

protein concentration of 10 nM, attention then turned to evaluating the set of soluble methyl triazoles.

3.4.8. Measurement of BRD4(1) K_D values by MST and evaluation of selectivity against BRD9

The BRD4(1) affinities of the nine compounds shown in Table 17 were then measured by MST, and their relative selectivity for BRD9 was calculated. As discussed earlier, each member of this compound set is hypothesised to bind to BRD4(1) in a conformation such that the sulfonamide substituent is directed to a primarily lipophilic region, known as the WPF shelf. We therefore hypothesised that polar substituents would result in a reduction in BRD4(1) affinity, and consequently an increase in selectivity for BRD9.

The nitro derivative **70** was found to have a K_D value of 756 ± 163 nM, which was lower than that measured for BRD9 (1.32 μM). A dramatic increase in selectivity for BRD9 was achieved with the aniline **2**, which was found to have 25-fold selectivity for BRD9 over BRD4(1).

Scaffold	Compound	Compound Number	SnapSol at pH 7.4	BRD9 K_D/nM	Error/nM	BRD4(1) K_D/nM	Error/nM	Fold selectivity BRD9/BRD4(1)
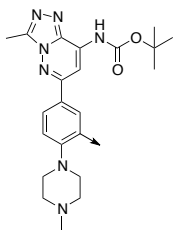		**70**	92	1320	427	756	163	0.6
		**2**	100	164	25.1	4060	289	24.8 ★
		**105**	100	245	47.8	643	108	2.6
	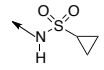	**103**	100	325	65.7	n.d.	n.d.	n.d.
	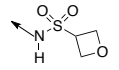	**105**	100	621	110	2030	326	3.3
	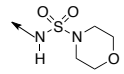	**108**	90	225	33.3	1570	128	7.0 ★
	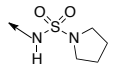	**107**	100	375	65.4	900	102	2.4
	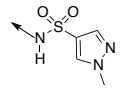	**109**	59	222	48.7	1080	228	4.9
	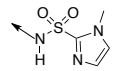	**110**	87	211	59.3	1940	200	9.2 ★

Table 17: Affinity of soluble compounds screened by MST against BRD4(1) and BRD9. Results displayed as a heat map, with lowest IC_{50} value shown in red and the highest IC_{50} value in green. (n.d. refers to no data point obtained, i.e. binding curve could not be recorded) (10 nM BRD4(1); 100% LED power; 80% MST power; laser-on time 30 s, laser-off time 5 s, delay 25 s, fluorescence before 5 s).

Both of the binding curves measured by MST, of **2** interacting with BRD9, and BRD4(1) are shown in Figure 57. The morpholine (**108**), and 1-methylimidazole (**110**) derivatives had the second and third largest selectivity, 7-fold and 9-fold, respectively, for BRD9 over BRD4(1). This is consistent with the hypothesis that the heteroatoms in the sulfonamide substituent of these compounds are poorly tolerated by the greasy WPF shelf of BRD4(1), resulting in a reduction in BRD4(1) affinity. The remaining five compounds were found to have 2-5-fold selectivity for BRD9 over BRD4(1).

A

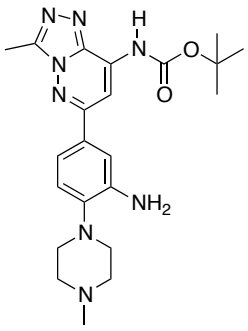

2

B

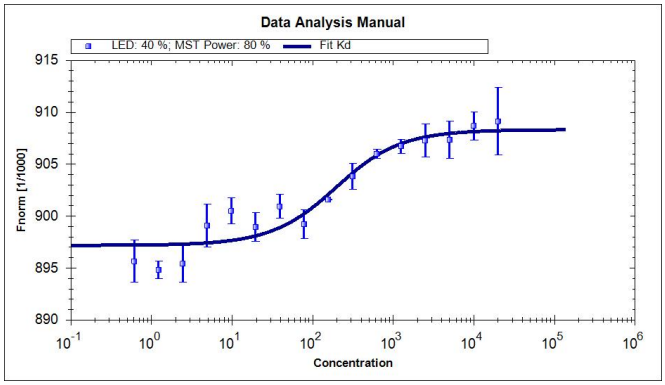

C

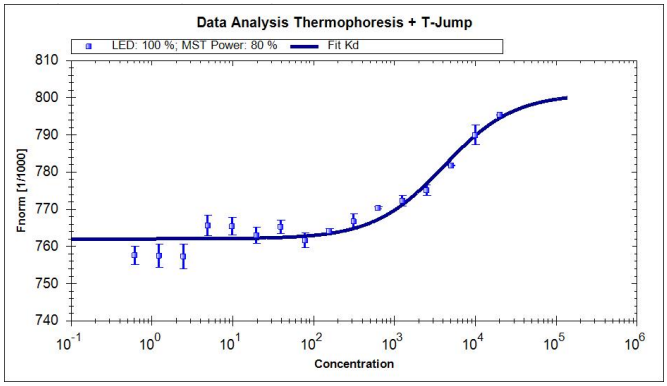

D

K_D/nM		Fold selectivity
BRD9	BRD4(1)	
164 ± 24.1	4060 ± 289	24.8

Figure 57: Summary and comparison of binding results for compound 2 to BRD9 and BRD4(1). (**A**) Structure of **2** and summary of MST results. (**B**) MST analysis of **2** binding to BRD9. (**C**) MST analysis of **2** binding to BRD4(1).

3.5. Evaluation of selective compounds 2, 108 and 110 by ITC

With these interesting results in mind, the affinities of the three most selective compounds (**2**, **108** and **110**) were evaluated by ITC. This biophysical technique provides a thermodynamic profile of ligand-receptor interactions, and although it consumes large amounts of protein and has a low throughput, it remains the "gold standard" method for evaluating small-molecule bromodomain interactions.[211,69,71,81,82,174,188-190,210,212] Compounds **110** and **108** were found to bind to BRD9 with K_D values of 658 nM, and 370 nM, respectively (Figure 58). These values are ≈ 3-fold higher than the K_D values measured by MST.

A

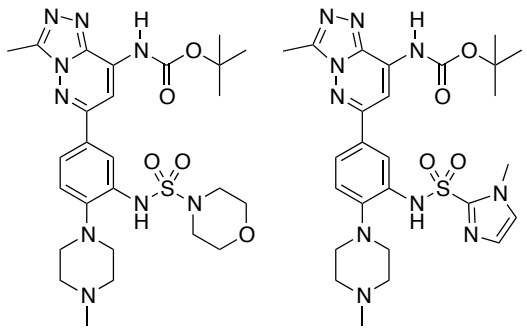

108 110

B

	BRD9	
Compound Number	**108**	**110**
N	0.94	0.88
K_A	2.70E+06	1.52E+06
K_D (nM)	370	658
ΔH (kcal/mol)	-7.22	-7.57
ΔS (cal/mol/deg)	4.80	2.44
−TΔS (kcal/mol)	-1.41	-0.72
ΔG (kcal/mol)	-8.63	-8.29

C

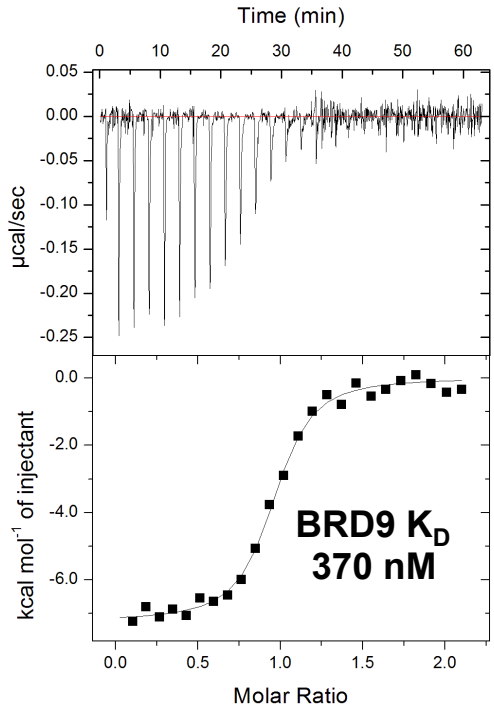

D

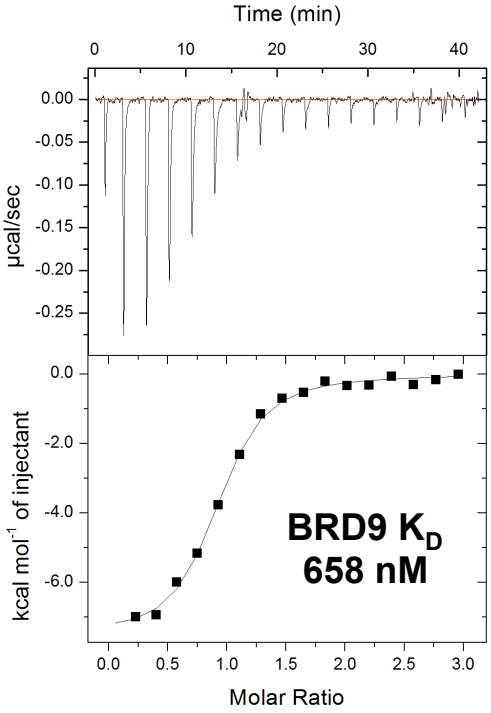

Figure 58: ITC results for 108 and 110 against BRD9. (**A**) Structure of **108** and **110**. (**B**) Summary of ITC results. (**C**) ITC trace for **108** and BRD9. (**D**) ITC trace for **110** and BRD9.

Analysis of the thermodynamic contributions to the Gibbs free energy of binding (ΔG) revealed that **108** and **110** bind to BRD9 with a major exothermic enthalpic component (ΔH) and a minor favourable entropic component (−TΔS) (Figure 58.B and Figure 59).

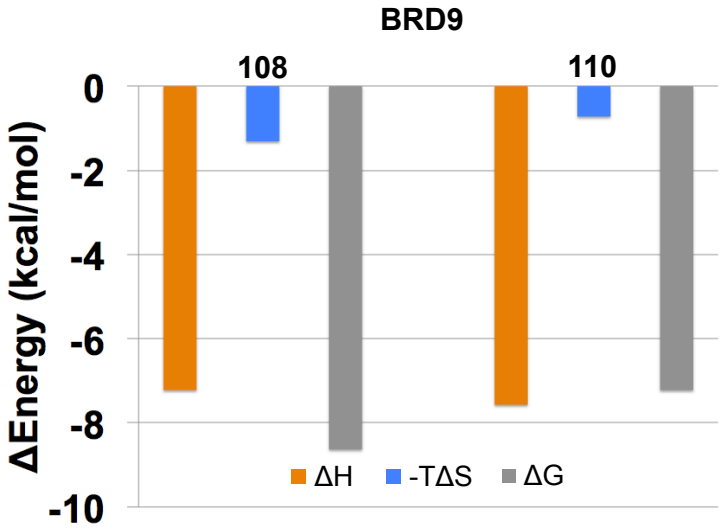

Figure 59: Comparison of relative contributions of enthalpy (ΔH) and entropy (−TΔS) to the Gibbs free energy of binding (ΔG) of compounds 108 and 110 to BRD9.

The aniline derivative **2** was also evaluated by ITC, and was found to have a BRD9 K_D value of 65.8 nM (Figure 60.A). This compound's high potency is in agreement with its K_D value measured by MST (164 nM), which was the tightest binder in this assay. Analysis of the thermodynamic contributions to the Gibbs free energy of binding (ΔG) revealed that **2** interacts with BRD9 with a major exothermic enthalpic component (ΔH), and a minor favourable entropic component (−TΔS) (Figure 60.B). As compound **2** was the tightest binder and had the highest selectivity window over BRD4(1) in the MST assay, its affinity for this bromodomain was measured by ITC, (Figure 60.D). Compound **2** was found to have a K_D value by ITC of 3.91 μM, which is close to the value found by MST (4.06 μM). Analysis of the thermodynamic contributions to the Gibbs free energy of binding (ΔG) revealed that **2** bound to BRD4(1) with a major exothermic enthalpic component (ΔH) and a large unfavourable entropic component (−TΔS) (Figure 60).

A

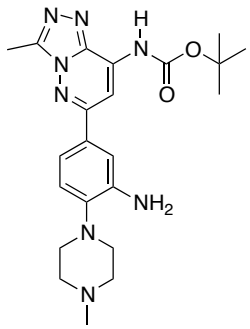

2

B

	BRD9	BRD4(1)
Compound Number	**2**	**2**
N	1.06	0.96
K_A	1.52E+07	2.56E+05
K_D (nM)	65.8	3.91E+03
ΔH (kcal/mol)	-8.33	-15.6
ΔS (cal/mol/deg)	4.46	-28.6
−TΔS (kcal/mol)	-1.31	8.38
ΔG (kcal/mol)	-9.64	-7.22

C

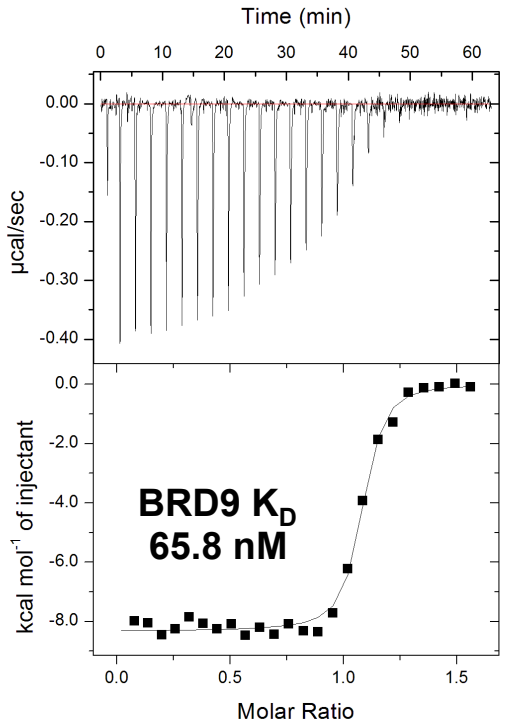

D

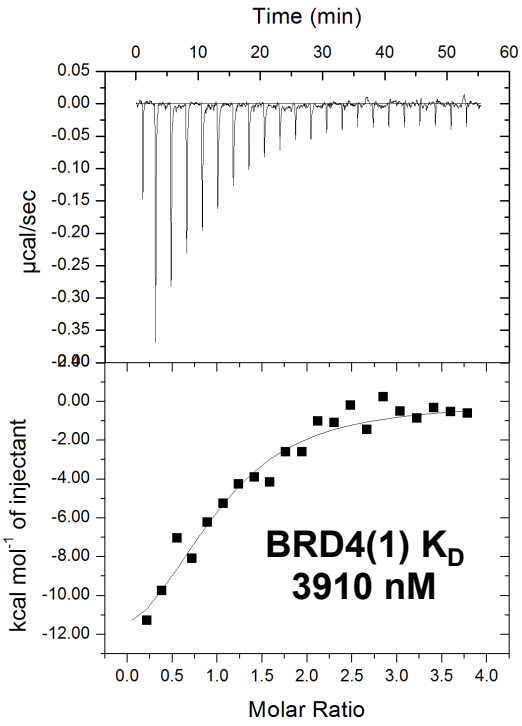

Figure 60: **ITC results for 2 interacting with BRD9 and BRD4(1).** (**A**) Structure of **2**. (**B**) Summary of ITC results. (**C**) ITC trace for **2** and BR9. (**D**) ITC trace for **2** and BRD4(1).

The selectivity for BRD9 over BRD4(1) is principally due to a difference in their entropic components, which were -1.31 kcal/mol and +8.38 kcal/mol, respectively (Figure 61).

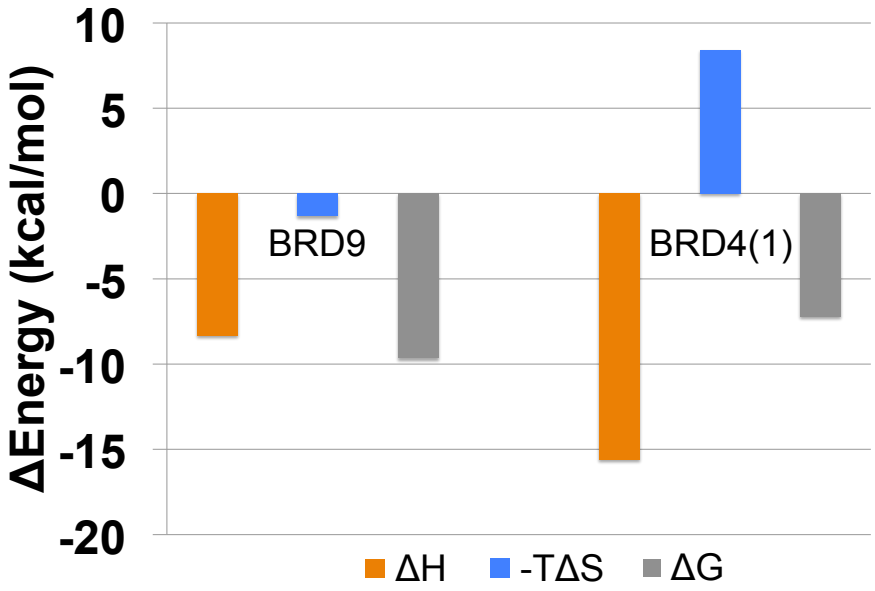

Figure 61: Comparison of relative contributions of enthalpy (ΔH) and entropy (−TΔS) to the Gibbs free energy of binding (ΔG) of compound 2 to BRD9 and BRD4(1).

It is difficult to make a prediction of the entropic component of binding to a target protein, though the large positive value of ΔS (51.3 cal/mol/deg) suggests that for binding of **2** to BRD4(1) to occur, there must be an ordering event of either the ligand **2**, or BRD4(1). This is often observed when there is a structural rearrangement of the protein.[156,211]

In comparison to the MST assay in which **2** had 25-fold selectivity for BRD9 over BRD4(1), ITC found the selectivity window to be higher, at 59-fold. The main reason for this is the discrepancy in the binding data for BRD9. ITC measured a BRD9 K_D value of 65.8 nM, whereas a value of 164 nM by MST, which is still relatively similar. One reason for this discrepancy is likely to be the relatively small difference in normalised fluoresecence in the bound and unbound states, also known as the curve's 'amplitude'. For example, with BRD4(1), the amplitude for binding of compound **2** was approximately 30 units, whereas with BRD9 it is 12 units. Communication with several MST

users and exploration of the literature revealed that this is a common problem. This is somewhat unsurprising, given the large size of a protein, and the relatively small change in charge, size or solvation shell of the interacting partners upon binding. For example, when analysing protein-protein interactions, which generally occur over larger volumes than protein-small molecule interactions, the overall change in thermophoretic characteristics of each interacting partner is large. This change in thermophoretic potential results in a large difference in the normalised fluoresecence in the bound and unbound states, making quantification of the strength of the interaction easier and more accurate.

3.6. Evaluation of selectivity of compound 2 using BROMO*scan*™

The DiscoveRx BROMO*scan*™ profiling service was used to further validate binding of compound **2** to BRD9, and quantify its affinity over suspected off-targets. This assay provides thermodynamic inhibitor K_D values over a broad range of affinities (<0.1 nM to >10 uM). The assay principle is based on binding of the bromodomain of interest to an immobilised ligand attached to a solid support (Figure 62).

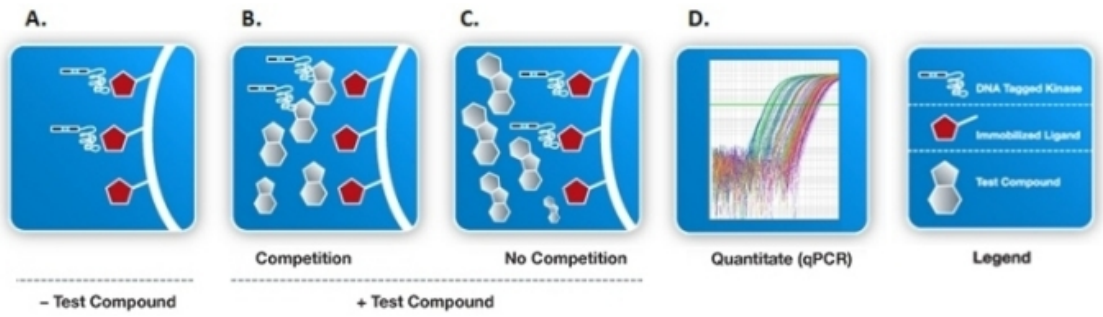

Figure 62: Priniciple of the DiscoveRx BROMO*scan*™ assay. Figure used with permission from KINOMEscan.

As outlined by DiscoveRx, “Compounds that bind the bromodomain prevent its binding to the immobilised ligand, thereby reducing the amount of protein captured on the solid support (A and B). Conversely, test molecules that do not bind the bromodomain have no effect on the amount ofprotein captured on the solid support (C). Screening "hits" are identified by measuring the amount of bromodomain captured in test versus control samples by using a quantitative, precise and ultra-sensitive qPCR method that detects the associated DNA (D).”[156,213] Further details of the assay setup can be found in the Experimental section.

Compound **2** was examined against the bromodomains of BRD9, BRD7, CECR2, and BRD4(1). The results are shown in Figure 63.

A

DiscoveRx BROMO*scan*™ K_D/nM			
BRD9	**CECR2**	**BRD7**	**BRD4(1)**
54	6.6	150	740

B

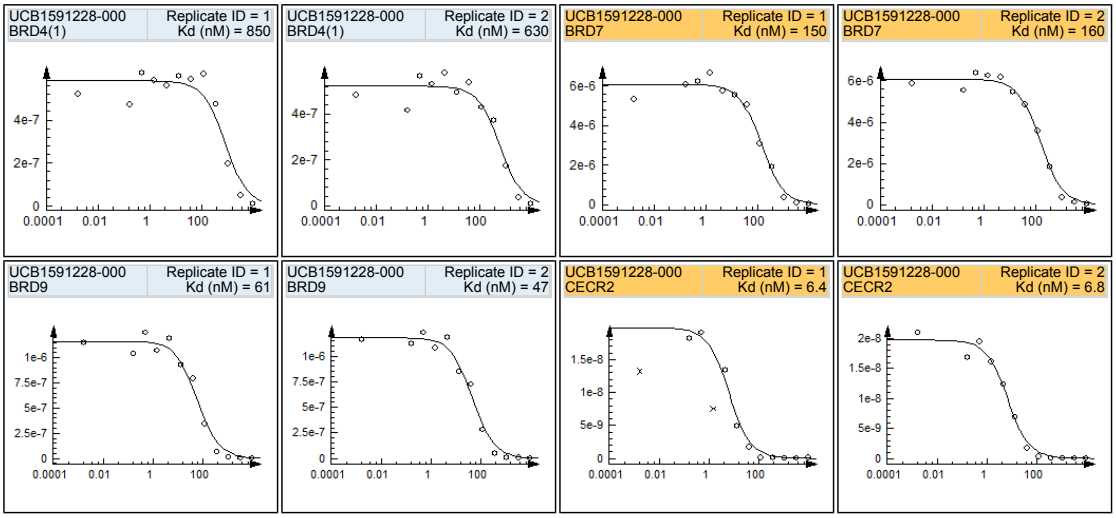

Figure 63: DiscoveRx BROMO*scan*™ profiling results for compound 2. (**A**) Summary of measured K_D values. Results are displayed as a heat map, with the lowest K_D value shown in red, and the highest K_D value in green. (**B**) Curve Images for compound **2** (UCB019-01-s-00001). The amount of bromodomain measured by qPCR (signal; y-axis) is plotted against the corresponding compound concentration in nM in $\log_{10}$ scale (x-axis). Data points marked with an "x" were not used for K_D determination.

Interestingly, compound **2** had the lowest K_D value (6.6 nM) for the CECR2 bromodomain, and a K_D value of 54 nM for BRD9. Nanomolar affinity was also observed against the bromodomains of BRD7 and BRD4(1).The BRD9 K_D value of 54 nM is in good agreement with the value of 65.8 nM measured by ITC. The high potency of **2** for CECR2 is an interesting result, suggesting that future efforts to optimise this chemotype may deliver a tool compound of this bromodomain.

3.7. Predicted binding mode of compound 2 to BRD9 and BRD4(1)

In order to understand the high potency of **2** for BRD9, and its selectivity over BRD4(1), a docking study was completed using the online docking web server of the Swiss Institute of Bioinformatics - "SwissDock".[156,212] This computational tool is reported to have a high accuracy, with a success rate of >80% is reported for ligands containing <15 free dihedral angles.

A geometry optimisation on compound **2** was completed using Gaussian 09 revision D, and the crystal structure of the tricyclic triazole **34** bound to BRD9 (PDB ID: 4NQN)[156] was used for receptor coordinates. The same procedure was repeated for **34** bound to BRD4(1) (PDB ID: 4NQM).[156] Unlike some docking techniques, SwissDock does not require an input of a suggested binding region on the protein, and instead relies on a rigorous sampling of the whole protein for a binding site of the ligand. The predicted binding mode of **2** to BRD9 is very similar to that reported by Fedorov *et al*.[156,212] for compound **34**, as shown after alignment in Figure 64.

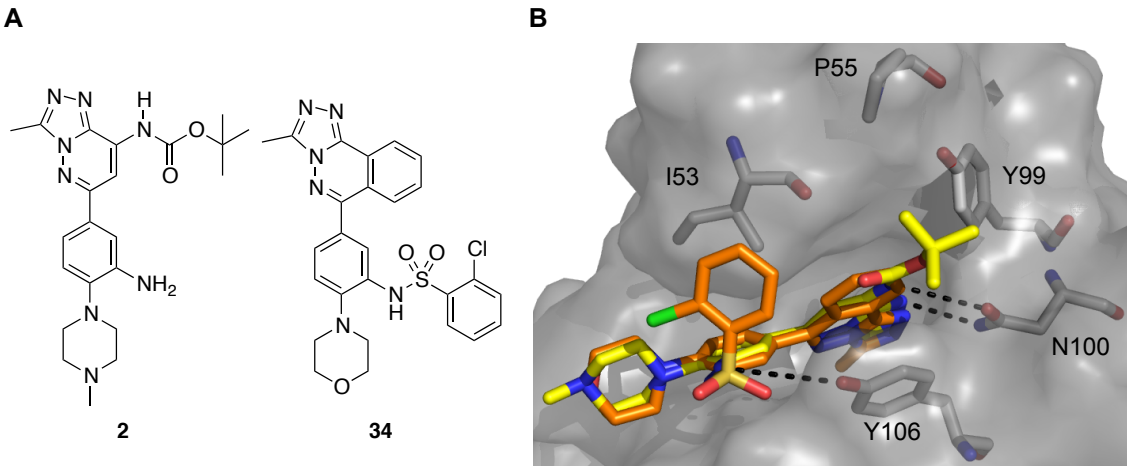

Figure 64: Predicted binding mode of compound 2 to BRD9, overlaid with reported binding mode of compound 34 obtained by Fedorov *et al.*[156,180] (**A**) Structure of docked compound **2** and reported ligand **34**. (**B**) Binding modes of **2** (yellow carbons) and **34** (orange carbons).

Compound **2** is predicted to make the expected interactions with BRD9. The triazole core sits in the KAc binding pocket, and N100 is predicted to engage in a synergistic hydrogen bonding interaction with the N1 of the triazole, and the pendant NH group, shown in a standalone representation in Figure 62. The Boc group is predicted to sit in a hydrophobic pocket formed by the residues of P55, Y99 and Y106. The NH_2 of **2** is expected to engage in a hydrogen bonding interaction with Y106, with the piperazine twisted into a conformation such that it can engage in a hydrophobic interaction with I53. These predicted interactions help to explain the large favourable exothermic component of binding measured between **2** and BRD9 by ITC.

The binding mode of **2** to BRD4(1) (Figure 65) is also predicted to be relatively similar to that of **34** bound to the same bromodomain, reported by Fedorov *et al.*[156,214] The triazole acts as the KAc mimic, forming a synergistic hydrogen bonding interaction with N140. The piperazine is predicted to engage in a hydrophobic interaction with I53 and W81.

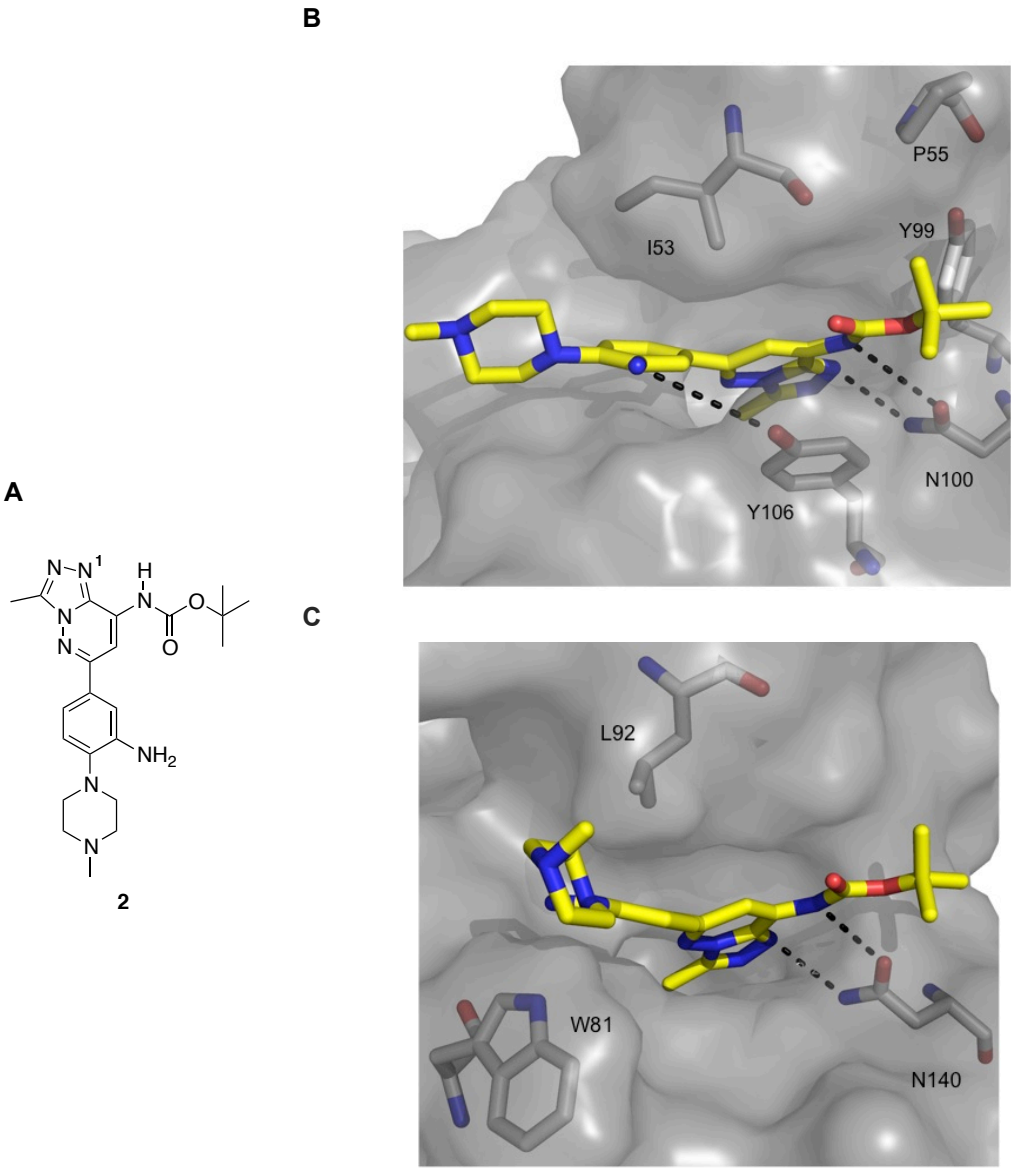

Figure 65: Predicted binding mode of compound 2 to BRD9 and BRD4(1), using SwissDock.[212,215,216] Geometry optimisation was done in the B3LYP/6-31+G(d,p) level of QM theory using Gaussian 09 revision D. Five structures with the lowest energy were analysed, with the structure shown having the lowest calculated Gibbs free energy of binding (BRD9 PDB ID: 4NQM, BRD4(1) PDB ID: 4NQN). (**A**) Structure of **2**. (**B**) Predicted binding mode of compound **2** to BRD9. (**C**) Predicted binding mode of compound **2** to BRD4(1).

Interestingly, the central phenyl ring is predicted to be twisted approximately 180° such that the amine group is directed towards the side-chain nitrogen of W81. This ligand conformation, which is different to the computed lowest energy conformation, may explain why **2** binds weakly to BRD4(1). ITC revealed that **2** binds to BRD4(1) with a large unfavourable entropic

component (−TΔS), which could be consistent with a structural rearrangement of the ligand before binding can occur.

3.8. Largescale bromodomain selectivity assessment

Compound **2** was also screened against BRD4(1), CECR2, BRD1 and BRPF1B in an AlphaScreen™ IC_{50} assay at the SGC (Figure 66). The results indicated that **2** had a CECR2 IC_{50} value of 58.2 nM. Nanomolar potency was also observed against BRPF1B (IC_{50} 208 nM), which, like BRD9, is also a member of sub-family IV.

A

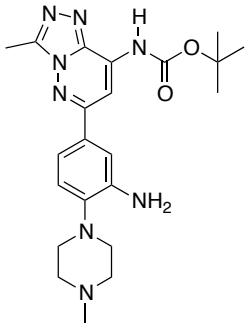

2

B

HTRF IC_{50}/nM	AlphaScreen™ IC_{50}/nM			
BRD9	CECR2	BRD4(1)	BRD1	BRPF1B
116	58.2	4082	1057	208

Figure 66: Assessment of broader selectivity of 2 *via* AlphaScreen™ and HTRF. (**A**) Structure of key compound **2**. (**B**) IC_{50} binding data recorded by the SGC. Results displayed as a heat map, with lowest IC_{50} value shown in red and the highest IC_{50} value in green.

Pleasingly, relatively low affinities were observed for the bromodomains of BRD1 and BRD4(1), which **2** was found to bind to with affinities of 1.06 μM and 4.08 μM, respectively. Binding of compound **2** to the bromodomains of BRD9 and CECR2 was also measured in a DSF assay at the SGC, where both compounds displayed ΔT_m values of 10 °C for each bromodomain.

Compound **2** was progressed for BROMO*scan* profiling against 34 bromodomains. In the single-point assay used, the concentration of compound **2** was kept at 10 μM, and results are reported as Percentage Control Compound 'POC, % Ctrl', where lower numbers indicate stronger hits. The availability of screening data from thousands of profiled compounds enables a proportional relationship between primary screening results and corresponding compound/target affinities to be made. As shown in Figure 67.B, a range of binding constants (K_D values) have been reported for the indicated ranges of POC values, with tighter binding interactions associated with lower POC values, and weaker binding associated with higher POC values. The large distribution of binding constants is characteristic of single concentration primary screens, and highlights the value of following up observed 'hits' with quantitative binding constant determinations.

Bromodomains found to bind to compound **2** are marked with red circles, where larger circles indicate higher-affinity binding (Figure 67.C). Of the 32 bromodomains compound **2** was screened against, 24 of these were found to bind to compound **2** (% Control <35%). Compound **2** bound most tightly (% Control = 0%) to the bromodomains of BRD9, CECR2, FALZ, SMARCA2, and TAF1L(2). It was of particular interest that such high affinity was observed to FALZ, TAF1L(2), and SMARCA2, members of sub-families I, VII, and VIII, respectively. It may be informative to perform a more detailed analysis of the binding of compound **2** to each of these bromodomains, perhaps through the use of ITC and crystallographic studies.

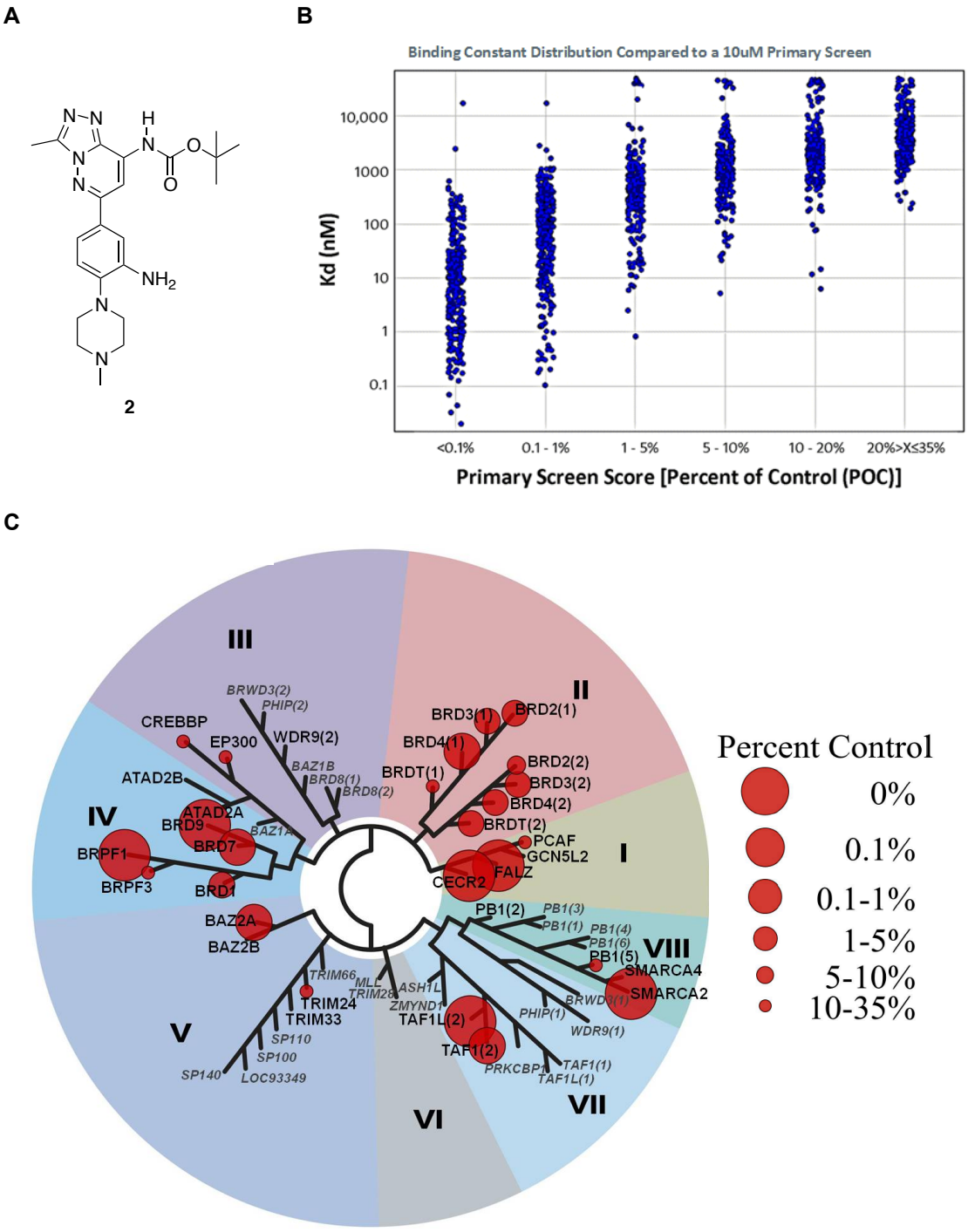

Figure 67: Bromodomain selectivity evaluation of compound 2 in the single-point BROMO*scan*™ assay. (**A**) Structure of compound **2**. (**B**) Relationship between binding constant distributions (K_D values) and single concentration primary screen values. Figure used with permission from KINOMEscan. (**C**) A representation of the single-point BROMO*scan*™ assay results obtained for compound **2** against 32 bromodomains contained in the human bromodomain phylogenetic tree (TREE*spot*™ visualisaton tool). Bromodomains found to bind are marked with red circles, where larger circles indicate higher-affinity binding.

3.9. Summary and future work

The work outlined in this Chapter has led to the development of compound **2**, which binds to BRD9 with a K_D value of 65.8 nM (ITC). This compound was found to have 25- and 59-fold selectivity over BRD4(1), by MST and ITC, respectively. This represents a large improvement in selectivity for BRD9 in comparison to the starting point for this project, **2**, which displayed approximately equal potency for BRD9 and BRD4(1) (Figure 62.C). Binding to BRD9 was confirmed in HTRF, BROMO*scan*™, and DSF assays.

There is a need for medicinal chemistry to be "balanced and multidimensional",[180,214] which is challenging but can be assisted by the use of efficiency metrics to control lipophilicity. It has been demonstrated that increasing lipophilic ligand efficiency (LLE) is associated with improved ADMET (Absorption, Distribution, Metabolism, Excretion, Toxicity) properties, likely due to a reduction of lipophilicity and increased specificity.[179,214,215-217]

Figure 68.B provides a summary of the steady improvement in LE and LLE during this work. This optimisation study led to the BRD9 inhibitor **2**, which has a respectable ligand efficiency of 0.30, and represents an improvement in comparison to the starting point **34** (LE = 0.25, Figure 62). A substantial improvement in LLE has been achieved, from 3.7 in the starting tricyclic triazole **34**, to 6.5 in aniline **2**.[156,180,214] These values compare favourably with proposed acceptable values of LE (>0.3)[179,218] and LLE (>5) [217,219] for drug candidates. This gives us greater confidence that the gain in BRD9 potency that has been made is due to an efficient optimisation of the starting scaffold,

giving a compound that engages in specific interactions with BRD9, and is more likely to succeed in future development efforts.

A

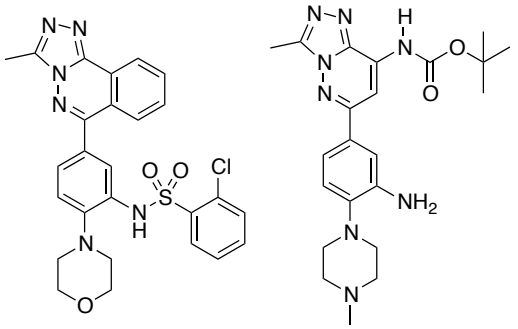

34 2

B

Compound	MW	LE	c log P	LLE
34 (tricyclic lead)*	535	0.25	3.02	3.7
71 (4-Me aryl)*	592	0.22	3.12	3.4
103 (cyclopropyl)**	543	0.26	1.40	5.6
2 (aniline)***	439	0.30	0.74	6.5

$$\mathrm{pIC_{50}} = -\log_{10} \mathrm{IC_{50}};$$

$$\mathrm{LE} = \frac{\mathrm{pIC_{50}} \times 1.4\ (\mathrm{kcal/mol})}{\text{Heavy atom count}} = \frac{(\Delta \mathrm{G})}{\mathrm{N}};$$

$$\mathrm{LLE} = \mathrm{pIC_{50}} - c\,\mathrm{logP} = \mathrm{pK_D} - c\,\mathrm{logP}$$

C

	BRD9	BRD4(1)	
Technique	**AlphaScreen™ IC_{50}/nM**	**AlphaScreen™ IC_{50}/nM**	**Fold Selectivity BRD9/BRD4(1)**
34 (tricyclic lead)	200	158	0.8
Technique	**MST K_D/nM**	**MST K_D/nM**	**Fold Selectivity BRD9/BRD4(1)**
2 (aniline)	164	4060	24.8
Technique	**ITC K_D/nM**	**ITC K_D/nM**	**Fold Selectivity BRD9/BRD4(1)**
2 (aniline)	65.8	3910	59.4
Technique	**BROMO*scan*™ K_D/nM**	**BROMO*scan*™ K_D/nM**	**Fold Selectivity BRD9/BRD4(1)**
2 (aniline)	54	150	2.8

D

DiscoveRx BROMO*scan*™ K_D/nM			
BRD9	**CECR2**	**BRD7**	**BRD4(1)**
54	6.6	150	740

Figure 68: **Selectivity and efficiency comparison of starting compound 34 and final compound 2.** (**A**) Structure of starting point **34** and compound **2**, developed in this work. (**B**) Key BRD9 efficiency parameters computed for compounds **34**, **71**, **103**, and **2**. c Log P was calculated using ACD/Labs algorithm (version 5.0.0.184). BRD9 IC_{50} assay employed: *AlphaScreen™, **HTRF, ***ITC. (**C**) Selectivity comparison of **34** and **2**.[156,161] (**D**) Summary of K_D values measured using the BROMO*scan*™ service. Results are displayed as a heat map, with the lowest K_D value shown in red, and the highest K_D value in green.

Consistent with the low lipophilicity of **2**, this compound was also found to have excellent aqueous solubility in the SnapSol solubility assay. In addition,

2 was determined to have low clearance in mouse microsomal studies, an *in vitro* model for hepatic stability (Figure 63). In order to identify the sites most liable to metabolism by cyctochrome P450 enzymes, compound **2** was inputed into the online, open access SMARTCyp (version 2.4.2) computational programme.[162,220] The three most likely metabolism sites (Figure 63.A) were predicted to reside on the piperazine ring, shown in red, in order of decreasing likelihood of metabolism from 1-3. The FAME program was also used to predict the sites of metabolism on compound **2**.[178,221] Once again, the piperazine was identified as a metabolic liability, however the methyl groups of the *tert*-butoxycarbonyl group were also predicted to be liable to metabolism.

A

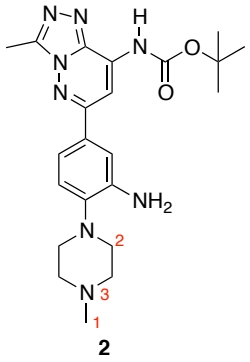

2

B

SnapSol at pH 7.4/μM	>100

C

	In vitro Cl_{int} (μL/min/mg protein)		
Species	**Low**	**Moderate**	**High**
Mouse	<9.9	9.9 - 53.6	>53.6

Mouse *In vitro* Cl_{int} (μL/min/mg protein)
2.81

Figure 63: ***In vitro* physiochemical and metabolic stability data for 2.** (**A**) Structure of optimised compound **2**, with the most likely sites of metabolism by cytochrome P450 shown in red. (**B**) SnapSol data for **2**. (**C**) *In vitro* mouse microsomal results.

An important consideration of compound **2** is that many aromatic amines have been found to give rise to safety concerns, as this moiety has been shown to be mutagenic in bacterial mutagenicity (Ames) tests.[218,222,223] This compound is likely to be a useful chemical tool, but it would be worthwhile to assess this

potential liability in future, and consider possible methods to overcome this hurdle.[219,224]

We have used the technique of MST to monitor the binding of small molecules to BRD9 and BRD4(1) for the first time. This method has proved particularly valuable due to its ease of sample preparation, speed and low consumption of protein.

Future work would be particularly informative in achieving the following objectives-

- Determine the binding mode of **2** to the bromodomains of BRD9 and BRD4(1) *via* X-ray crystallography studies. This could help explain the compound's selectivity for BRD9 and how further improvements in selectivity over BRD4(1) could be achieved. This work is ongoing at the SGC by Sarah Picaud and Panagis Filippakopoulos.
- Determine the most likely conformation of compound **2**, using X-ray crystallographic or computational studies. This may assist in interpreting the ITC results, could prove useful in developing a more potent or selective tool compound.
- Complete a more detailed analysis of the selectivity of **2** over the wider bromodomain family using the *bromo*MAX™ service, which measures K_D values against 32 bromodomains.
- It would be useful to carry out measurements of binding affinity to full-length BRD9 in its native state. FRAP assay experiments with

compound **2** and both BRD9 and BRD4(1) would be an important step to confirm cellular target engagement.

- Selectivity over a broad set of pharmacological targets, including ion channels, receptors and various kinases would be an important assessment to make.
- Assess the activity of aniline **2** in a bacterial mutagenicity (Ames) test.
- The potential therapeutic value of **2** could be evaluated by studies with a wide range of cancer cell lines. I-BRD9 has previously been shown to down-regulate four representative genes (*CLEC1*, *DUSP6*, *FES* and SAMSN1), each of which have been implicated in cancer and inflammatory indications.[161,225] LP99 has implicated BRD9 in the inflammatory response pathway.[162,225] It would be useful to confirm these results with compound **2**.
- Further optimisation of the MST assays. There was a two-fold discrepancy in K_D values measured by MST and ITC for compound **2**. This may be improved by exploring numerous factors such as the impact of alternative buffer conditions, or variation of the protein concentration.
- By carrying out MST experiments at a range of temperatures, this technique is capable of determining the binding energetics ΔG (free energy), ΔH (enthalpy) and ΔS (entropy). This could be investigated as a high throughput alternative to ITC.
- MST experiments can be carried out in cell lysate, and investigations in this area could give a more detailed insight the value of compound **2** in future biological studies.

Chapter 4: Probing the acetyl lysine binding pocket of the BRD9 bromodomain

4.1. Introduction

In the course of this work, we were intrigued by findings at Genentech that the BRD9 bromodomain could accommodate peptides longer than typical acetylated analogues. At the London EpiCongress conference in November 2013, Andrea Cochran, a Senior Scientist at Genentech, outlined preliminary results that BRD9 binds to butyrylated peptides with similar affinities as acetylated analogues. We were also interested by the findings through mass spectrometry, that a wide range of acyl modifications other than acetyl are present on histone lysine residues.[221,226] It is accepted that long-chain acylations such as myristoylation (C14) and palmitoylation (C16), cause proteins to target cellular membranes, resulting in a downstream biological outcome.[222,223,227] Alternative lysine acylations include formylation,[224,228] propionylation,[225,229] butyrylation,[225,230] crotonylation,[225,226,231-237] 2-hydroxyisobutyrylation,[225-230] succinylation,[210,228] malonylation,[229,238] and glutarylation (Figure 69).[230,239]

Propionylation and butyrylation of the ε-nitrogen atom of lysine are both catalysed by HATs. This activity has been reported for p300 and cAMP response element binding protein (CREB) binding protein CREBBP, Esa1, p300/CBP associated factor (PCAF) and bacterial general control of amino acid synthesis protein 5 (GCN5) related *N*-acetyltransferases.[225,231-237,240]

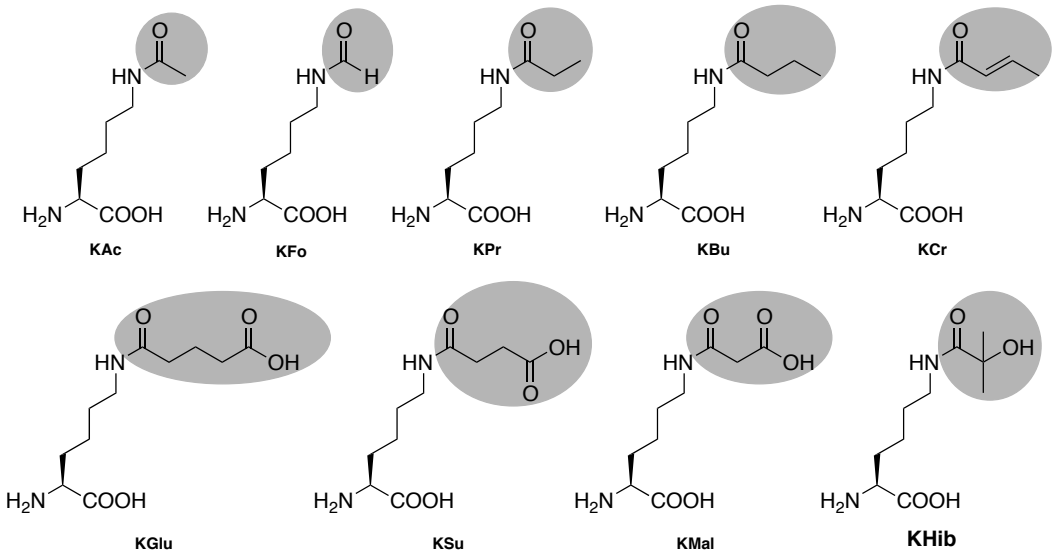

Figure 69: Short-chain acyllysine modifications reported in the literature.[225-230,241]

The function of these protein short-chain acyl-lysine modifications are unknown, but have been suggested to "represent a form of metabolic noise… from non-selective introduction by HATs or from chemical reactivity of acyl-CoA."[210,242] Yet it has recently been found that the HAT p300 introduces crotonyl histone modifications, resulting in transcriptional activation, analagous to lysine acetylation.[238,242] A specific function for these modifications is further supported by publications on the sirtuin class of HDACs, which have been found to remove selectively either acidic acyl[239,241] or fatty-acyl modifications.[240,241] It is possible that these acyl marks may be regulated in a similar manner to other epigenetic marks. A possible candidate to read these acyl-lysine modifications is the bromodomain. We therefore hypothesised that the binding information gained from ligands containing various acyl-lysine mimics could be useful in determining whether bromodomains could act as readers of a diverse set of lysine acylations.

Vollmuth and Geyer carried out a detailed study into the interaction of propionylated and butyrylated histone H3 lysine marks with BRD4

bromodomains.[241] ITC measurements showed that, in comparison to the analogous acetylated lysine peptides obtained in an earlier study,[242-244] the two propionylated sequences, H3K14prop and H3K23prop, showed approximately three-fold weaker binding affinity for BRD4(1), although the affinity of the butyrylated peptide was too weak to be quantified. X-Ray crystal structures were obtained for both H3K23prop and H3K14but bound to BRD4(1) (Figure 70).

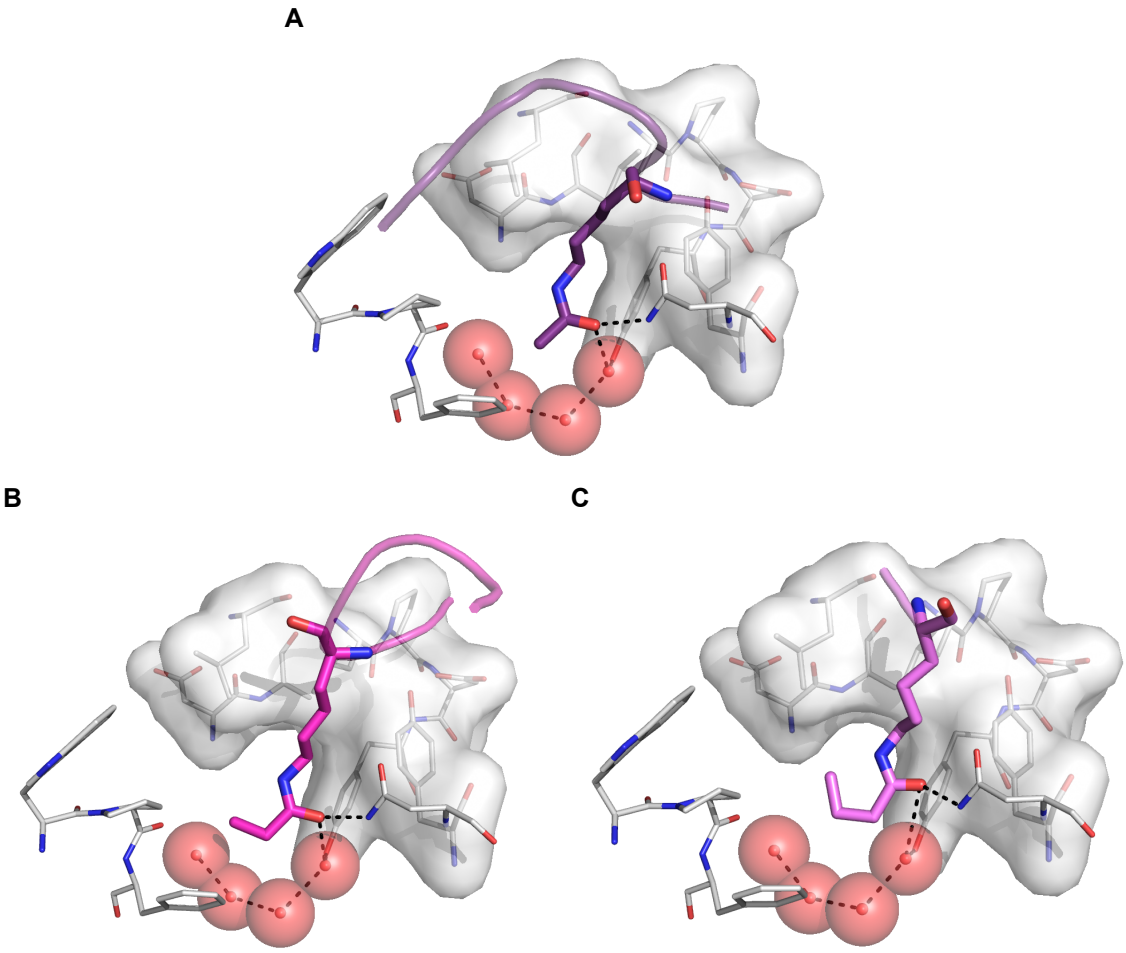

Figure 70: X-ray crystal structures of BRD4(1) in complex with (A) acetylated[156,242] **(B) propionylated**[157,241] **and (C) butyrylated histone peptides**. (PDB IDs: 3JVK, 3MUK and 3MUK respectively).[156,241] Figure produced by Prof Stuart Conway.

The structural information revealed that both peptides adopt similar binding modes in which the alkyl chain sits in a hydrophobic region formed by the ZA

and BC loops, with the shell of surrounding water molecules remaining intact.

4.1.1. Aims

The preliminary results from Genentech, a wealth of findings through mass spectrometry, and intriguing X-ray crystallography results from Vollmuth and Geyer,[156,241] led us to probe the KAc binding pocket of BRD9 in more detail. In this Chapter, we aim to do this using a small molecule SAR study, starting by molecular docking to identify novel inhibitors of the BRD9 bromodomain. Target compounds will then be synthesised and their potency and selectivity will be evaluated. An analysis of their physicochemical and *in vitro* metabolic stability will also be made, which should provide a detailed view of their potential utility *in vivo*.

4.2. Identification, synthesis and *in vitro* evaluation of compounds to probe the KAc binding pocket of BRD9

The propyl derivative **111** was docked into the BRD9 bromodomain using AutoDock Vina software[157,243,244] (Figure 71), and the position of the ligand was compared to that of the previously crystallised tricyclic triazole **34**. Four of the lowest energy binding conformations were analysed, one of which overlaid very well with **34** bound to BRD9. In both compounds, the triazole core acts as the KAc mimic, engaging in a hydrogen-bonding interaction with N100. The sulfonamide groups also occupy similar positions, directed towards Y106. Interestingly, the propyl chain is extended towards the water molecules of the KAc binding pocket, suggesting that derivatisation at this position maybe worthwhile to achieve displacement or engage in interactions with these water molecules.

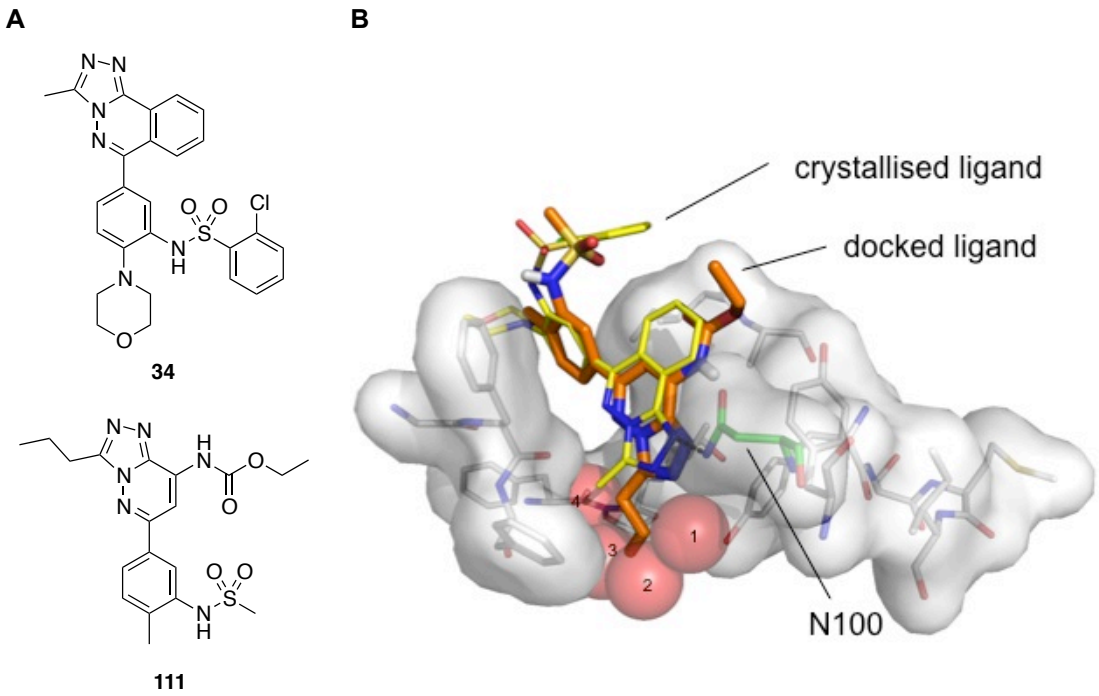

Figure 71: Propyl triazole docking study. (**A**) Structure of ligands, crystallised (**34**), and docked (**111**), with the bromodomain of BRD9. (**B**) BRD9 in complex with **34** (yellow),[156,245,246] overlaid with predicted binding mode of **111** (orange). Docking of **111** was carried out by Gregory Ross, using default settings in AutoDock Vina. The X-ray crystal structure of **34** bound to BRD9 (PDB ID: 4NQN) was used. Water molecules were removed before docking. A receptor pocket in a region close to **34** was used as a guide for the ligand docking. Figure produced by Prof. Stuart Conway.

This interesting docking result attracted further investigation into whether the KAc binding pocket of BRD9 could accommodate alkyl groups larger than methyl, and presented a possible route to gain selectivity over other bromodomains. For example, the literature published to date on the promiscuous BET family of bromodomains suggests that the water molecules in the KAc binding pocket are very tightly bound, consistent with the observation that known, potent BET ligands contain a methyl group in the KAc mimic. We therefore hypothesised that the propyl-containing compound methyl derivatisation might deliver superior selectivity for BRD9 over the BET bromodomains.

To evaluate the SAR in the KAc binding pocket of BRD9, the six compounds in Figure 72 were identified as the key targets. The linear derivatives **112**-**115**

were intended to provide a clear indication of the impact of extending the alkyl chain in the KAc binding pocket. The more sterically demanding isopropyl (**116**), and cyclopropyl (**117**), analogues were designed to provide useful SAR insights.

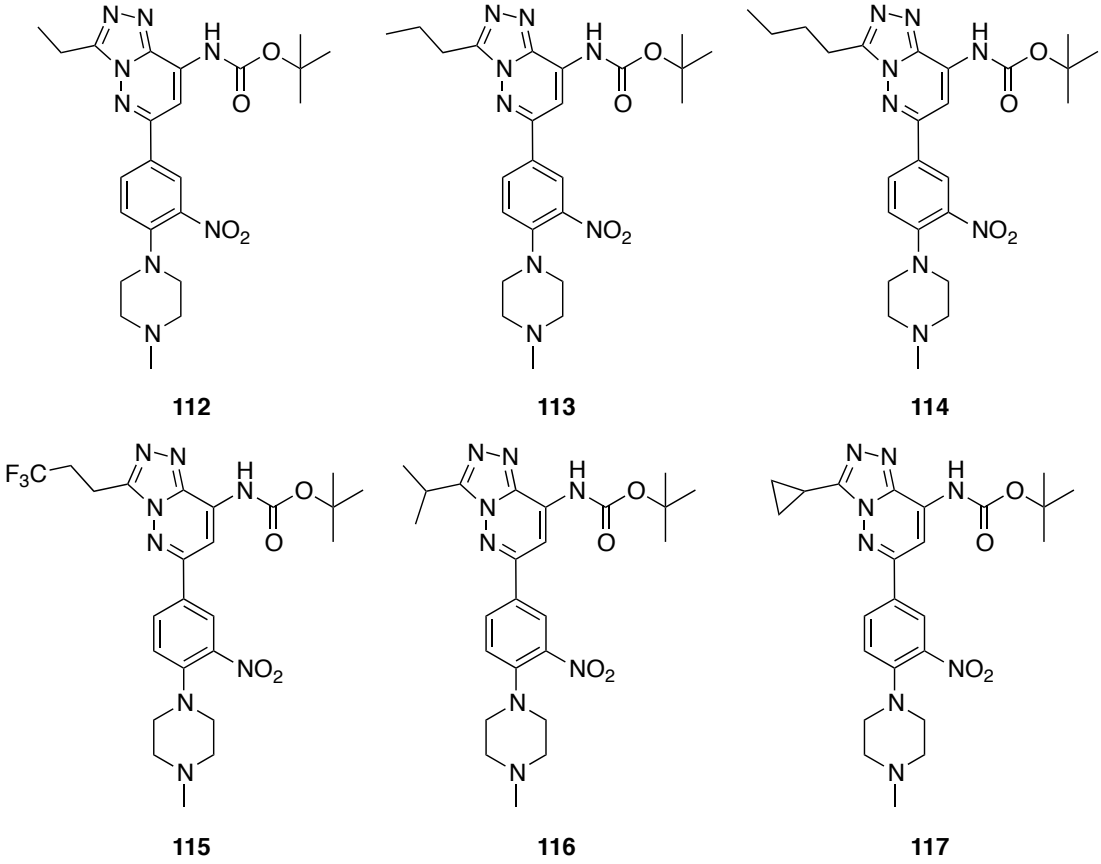

Figure 72: Target compounds 112-115, to probe the KAc-binding pocket of the BRD9 bromodomain.

Each of these compounds were successfully synthesised in three steps starting from the previously synthesised hydrazinyl compound **63**. In contrast to the methyl triazole **70**, which was generated by reaction with acetic acid under reflux for five hours, each corresponding triazole was formed under microwave irradiation for 70 min at 110 °C with the respective acids (Figure 68). Boc protection followed by Suzuki coupling gave the final compounds in

2-38% yield over three steps.

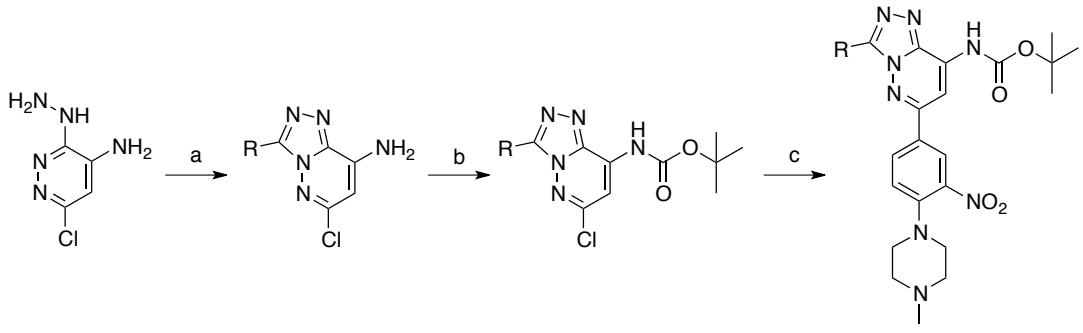

63 118 119 120

Compound Number	R	Yield over 3 steps	Compound Number	R	Yield over 3 steps
112	Et	10%	**115**	$CH_2CH_2CF_3$	2%
113	^{n}Pro	9%	**116**	^{i}Pro	6%
114	^{n}But	38%	**117**	Cyclopropyl	12%

Scheme 15 and Table 18: Synthesis of 112-117. *Reagents and* conditions: (a) RCOOH, 110 °C, Microwave (MW); (b) Boc_2O, DMAP, THF, RT; (c) **74**, K_2CO_3, $Pd(dppf)Cl_2{\cdot}CH_2Cl_2$, 1,4-dioxane/$H_2O$ (10:1), 80 °C.

Compounds were examined in a DSF assay against BRD9 and a selection of other bromodomains (Table 19). Upon extension of the alkyl chain to ethyl (**112**), there was a slight reduction in BRD9 stabilisation, and the ΔT_m value of 2 °C observed for BRD4(1) was accepted to represent binding to some extent.

Scaffold							
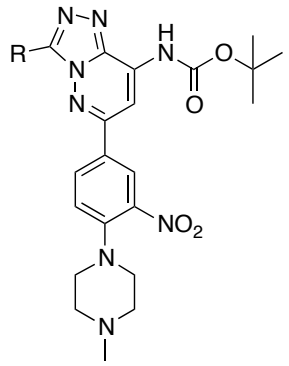							
Compound Number	**R**	**ΔT_m/°C (at 10 μM)**					
		BRD9	**CECR2**	**BRD4(1)**	**CREBBP**	**TIF1α**	**BRPF1A**
70	Me	8 (5)	10 (2)	3 (4)	0 (2)	0 (2)	4 (2)
112	Et	7 (3)	7 (2)	2 (2)	0 (2)	0 (2)	1 (2)
113	^{n}Pro	6 (5)	5 (2)	0 (10)	-1 (2)	-1 (2)	-1 (2)
114	^{n}But	5 (4)	N.D.	0 (8)	0 (2)	0 (2)	-1 (2)
116	^{i}Pro	2 (4)	2 (2)	N.D.	N.D.	N.D.	N.D.
117	Cyclopropyl	2 (4)	3 (2)	N.D.	N.D.	N.D.	N.D.

Table 19: **DSF data obtained by the SGC for the six bicyclic triazole derivatives (70 and 112-117) screened against a selection of bromodomains**. Compound concentration was 10 μM, and protein concentration was 2 μM. ΔT_m values are reported to the nearest 1 °C, with the number of measurements shown in parentheses. N.D. means no data recorded.

Further elaboration to the *n*-propyl and *n*-butyl derivatives **113** and **114**, respectively, resulted in a slight reduction of BRD9 affinity, however there was almost no binding detected to the BET family member BRD4(1). It was also noted that the *n*-propyl and *n*-butyl derivatives possessed good selectivity over the highly homologous sub-family IV member BRPF1A, which had so far proved challenging in this project. The more sterically demanding isopropyl and cyclopropyl analogues were poorly tolerated in all cases, stressing the preference for a linear chain. The *n*-butyl derivative had good selectivity,

although its BRD9 potency was slightly lower in comparison to the *n*-propyl analogue. The trifluoropropyl derivative **115** was evaluated in both a HTRF and AlphaScreen^{TM} assay against the bromodomains in Table 19, and was found to have IC_{50} values >20 μM in all cases. Clearly the nature of the substituent in the KAc binding pocket has an important impact on ligand binding. The gradual increase in lipophilicity from compounds **112**-**117** was also expected to have a detrimental impact on solubility.

An *n*-propyl chain was deemed optimal due to its high BRD9 potency in the DSF assay, good selectivity over TIF1α, CREBBP, as well as the important BET family member BRD4(1), and the highly homologous bromodomain of BRPF1A.

4.3. Synthesis and evaluation of propyl-containing triazole sulfonamides

We then decided to elaborate the *n*-propyl triazole, in order to regain the potency lost during extension of the alkyl chain. In Chapter 2, an increase in potency was observed during the introduction of 4-substituted sulfonamides. We therefore sought to gain an enhancement of potency without disrupting selectivity, by targeting the five 4-substituted sulfonamides **121**-**125** (Figure 73).

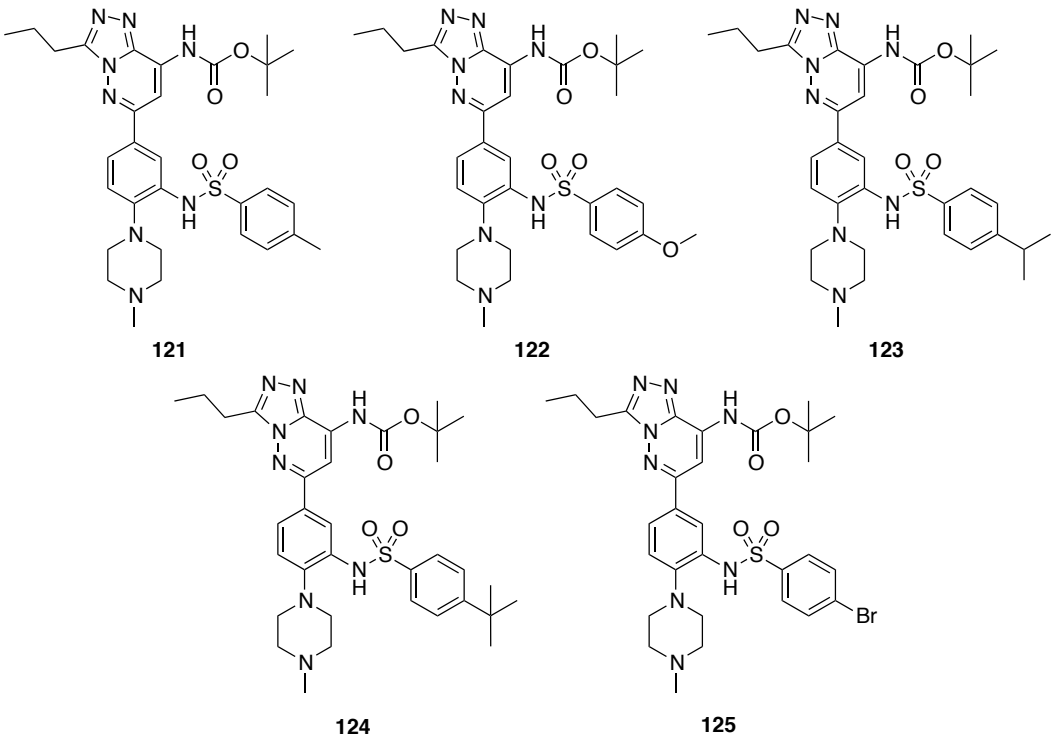

Figure 73: Propyl sulfonamide targets 121-125.

Reduction of the nitro group proceeded in high yield, employing previously optimised conditions involving an aqueous potassium fluoride work-up (Scheme 16). The resultant aniline **126** was found to be relatively unreactive in CH_2Cl_2 during reactions with sulfonyl chlorides. However, when pyridine was used as a solvent, in combination with a large excess of sulfonyl chloride, the desired final compounds were synthesised in moderate yields.

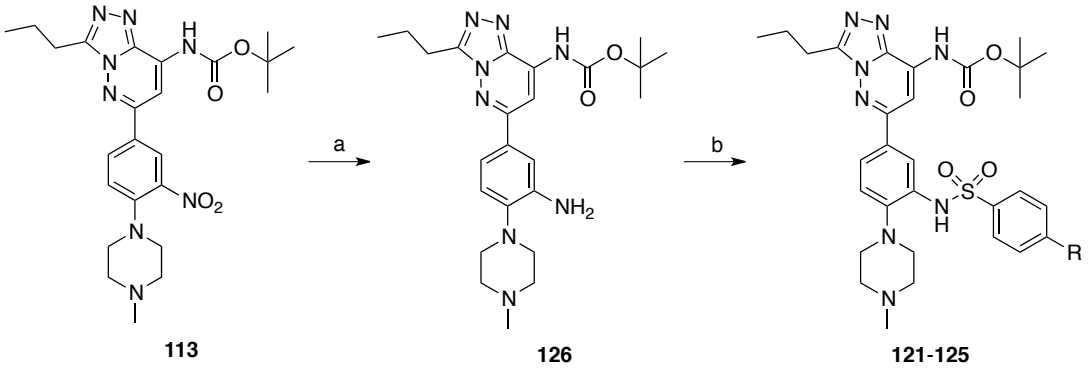

Scheme 16: *Reagents and* conditions: (a) $SnCl_2$, EtOH/Et_3N (2:1), 80 °C, 85%; (b) R, $ArSO_2Cl$, Pyridine, DMAP, 0 °C-RT: **121**, R = Me, 77%; **122**, R = OMe, 73%; **123**, R = ^{i}Pro, 50%; **124**, R = ^{t}Bu, 45%; **125**, R = Br, 45%.

These compounds were then evaluated in a DSF assay against the bromodomains of BRD9 and CECR2, and in an AlphaScreen™ assay against CECR2, BRD4(1) and FALZ (Table 20). Attempts were made to obtain BRD9 and BRPF1A AlphaScreen™ binding data, however the assay was found to be too unreliable for conclusive binding information to be gathered. Interestingly, the aniline derivative **126** displayed the highest thermal stabilisation of BRD9 and CECR2, with good selectivity over BRD4(1) and FALZ. All of the sulfonamides screened had a substantially lower ΔT_m values than anticipated. One possible reason for this could be that the *n*-propyl chain may cause the ligands to bind in an unexpected conformation in which large aryl sulfonamides cannot be accommodated.

Scaffold						
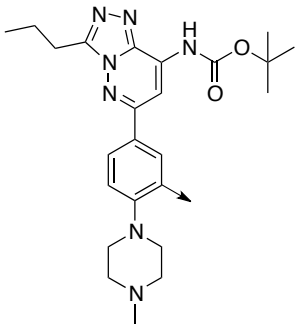						
Compound Number	**Compound**	**AlphaScreen™ % Inhibition (at 25 µM)**			**ΔT_m/°C (at 10 µM)**	
		CECR2	**BRD4(1)**	**FALZ**	**BRD9**	**CECR2**
126		99	34	37	9 (1)	5 (1)
121	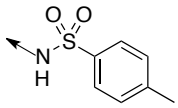	56	43	37	N.D.	N.D.
122	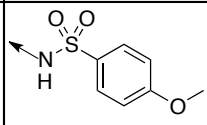	28	24	26	N.D.	N.D.
124	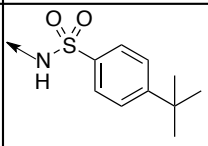	26	22	25	2 (1)	0 (1)
123	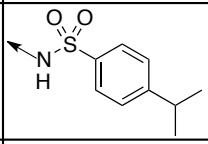	39	29	30	2 (1)	0 (1)
125	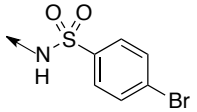	45	45	40	3 (1)	N.D.

Table 20: **DSF and AlphaScreen™ data obtained by the SGC for the seven bicyclic triazole derivatives against a selection of bromodomains**. AlphaScreen™ results are displayed as a heat map, with the tightest binder shown in red, and the weakest binder in green.

The low affinity of the *n*-propyl aryl sulfonamides may arise from the inability of the longer propyl chain to project deep into the KAc binding pocket. This could cause the triazole core to sit in an alternative position, such that its interaction with the conserved asparagine residue is slightly weaker, and the sulfonamide substituent can no longer occupy the favourable position possible

for the methyl triazole scaffold.

4.4. Development of bromosporine analogues

Given that the *n*-propyl triazoles containing an aryl sulfonamide substituent were found to have relatively low affinity for BRD9, we decided that a smaller sulfonamide substituent would be worth investigating, and may yield information concerning a potential change in binding mode with large aryl substituents. We also recognised the utility of developing analogues of bromosporine (**35**), the pan-bromodomain inhibitor. This compound was developed by the SGC and has a thermal shift of 3.9 °C against BRD9 (Table 21).[156,157] This compound has been evaluated against 19 bromodomains in a thermal shift assay and showed a $\Delta T_m \geq 3.0$ °C for 12 of these targets. Cellular potency against BRD4(1) and CREBBP was confirmed in a FRAP assay, and **35** showed moderate cytotoxicity in HeLa cells at 18 μM. The non-selectivity of this compound is likely to be useful for probing bromodomains that have yet to be interrogated with small molecule ligands. We hypothesised that by extending the methyl of the KAc mimicking triazole unit, we may be able to identify bromodomains that can accommodate longer acyl-lysine moieties. This binding information could prove to be extremely valuable in future bromodomain ligand discovery programmes. The two mesyl compounds **111** and **127** (Figure 74), were therefore identified as key propyl targets. The Boc-derivative of bromosporine (**127**) was also targeted.

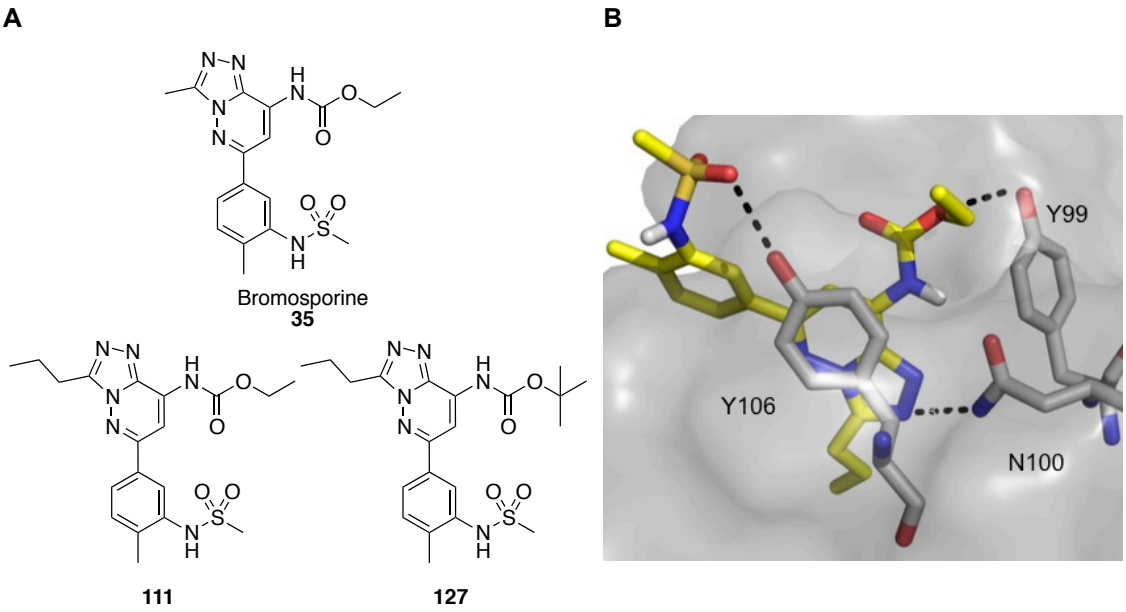

Figure 74: Target bromosporine analogues. (**A**) Bromosporine and the two target compounds **111** and **127**. (**B**) Docking result of compound **111** with BRD9 using AutoDock Vina software. Docking was performed by Gregory Ross, further details are provided in the experimental chapter. (The X-ray crystal structure of **34** bound to BRD9 (PDB ID: 4NQN)[156,247] was used.)

Computational modeling was performed by Gregory Ross, using AutoDock Vina software and the ligand-bound BRD9 crystal structure (PDB ID: 4NQN).[156,248] Docking of **111** into BRD9 predicted the expected binding mode, in which the triazole core is located in the KAc binding pocket, and Y106 engaged in a hydrogen bonding interaction with one of the sulfonamide oxygen atoms. There was also predicted to be a hydrogen bonding interaction between Y99 and the oxygen of the pendant carbamate.

The two target compounds **111** and **127** were prepared under previously optimised conditions (Scheme 17). During the synthesis of **111**, reaction of the triazole with ethylchloroformate followed by Suzuki coupling was found to be optimal in comparison with an alternative synthesis employing late stage Boc deprotection.

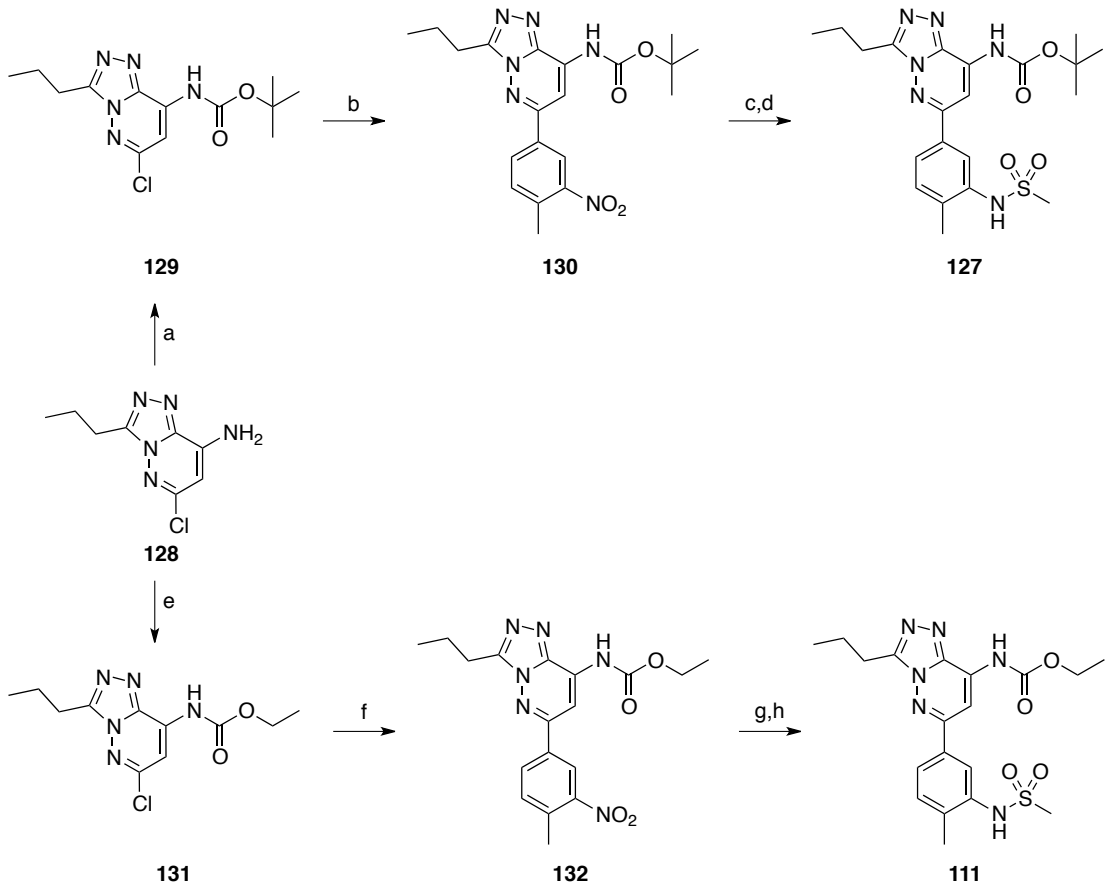

Scheme 17: *Reagents and conditions*: (a) Boc_2O, DMAP, THF, RT, 58%; (b) $ArB(OH)_2$, K_2CO_3, $Pd(dppf)Cl_2{\cdot}CH_2Cl_2$, 1,4-dioxane/$H_2O$ (10:1), 80 °C, 76%; (c) $SnCl_2$, EtOH/Et_3N (2:1), reflux; (d) $MeSO_2Cl$, DMAP, pyridine, RT, 4% (over 2 steps); (e) $ClCO_2Et$, DMAP, CH_2Cl_2, Et_3N, 93%; (f) $ArB(OH)_2$, K_2CO_3, $Pd(dppf)Cl_2{\cdot}CH_2Cl_2$, 1,4-dioxane/$H_2O$ (10:1), 80 °C, 47%; (g) $SnCl_2$, EtOH/Et_3N (2:1), reflux; (h) $MeSO_2Cl$, DMAP, pyridine, RT, 24% (over 2 steps).

Compounds **111** and **127** were screened against six bromodomains in a DSF assay (Table 21). The previously disclosed results for bromosporine (**35**)[157,249] are shown, which indicate binding to BRD9, BRD4(1) and CREBBP. Upon derivatisation of R1 to *n*-propyl, there was a substantial increase in BRD9 stabilisation, as well as a reduction in BRD4(1) stabilisation. When the larger Boc moiety was incorporated into this scaffold (compound **127**), there was a general improvement in overall selectivity, with binding detected to BRD9 only.

Scaffold								
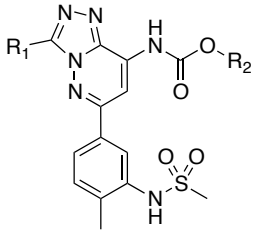								
Compound Number	**R_1**	**R_2**	**ΔT_m/°C (at 10 µM)**					
			BRD9	**BRD4(1)**	**CREBBP**	**PB1(5)**	**TIF1α**	**BRPF1A**
35	CH_3	CH_2CH_3	4 (2)	7 (2)	3 (2)	0 (2)	0 (2)	N.D.
111	$CH_2CH_2CH_3$	CH_2CH_3	7 (6)	2 (7)	0 (2)	1 (2)	-4 (2)	1 (2)
127	$CH_2CH_2CH_3$	$C(CH_3)_3$	6 (6)	0 (8)	-2 (2)	-2 (2)	-1 (2)	0 (2)

Table 21: DSF data obtained by the SGC for bromosporine and the two propyl derivatives 111 and 127, against a selection of bromodomains. Compound concentration was 10 µM, and protein concentration was 2 µM. ΔT_m values are reported to the nearest 1 °C, with the number of measurements shown in parentheses.

With these promising results in hand, the aqueous solubility of a selection of *n*-propyl triazoles was then examined in the SnapSol assay (Table 22). Upon introduction of a propyl chain, there was a dramatic reduction in aqueous solubility. Both methyl triazoles in Table 22 have high aqueous solubility (>90 µM), whereas the *n*-propyl derivatives have solubility values <20 µM, representing a major area for optimisation. This results in an inconsistent final compound concentration when the compound is diluted into aqueous buffer from the DMSO stock, such that the DSF binding information produced must be interpreted with care.

Compound Number	Compound	SnapSol pH 7.4/μM	Compound Number	Compound	SnapSol pH 7.4/μM
70	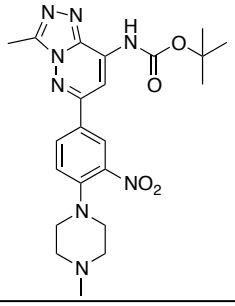	92	**113**	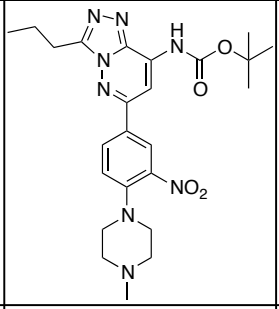	12
127	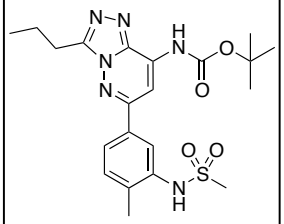	18	**111**	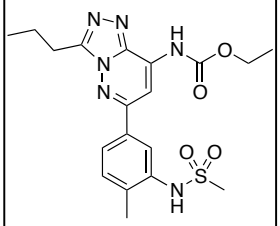	6
133	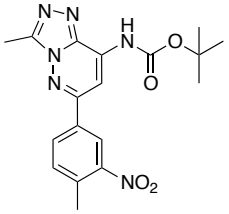	3	**134**	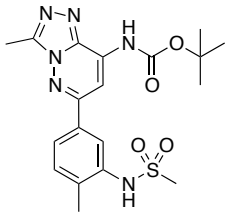	94

Table 22: SnapSol aqueous solubility results for a collection of methyl and propyl triazoles.

4.5. Improving the affinity and aqueous solubility of *n*-propyl triazole derivatives

In order to improve the aqueous solubility of this set of propyl triazoles, we first examined whether the Boc group could be altered. Solubility predictions led to identification of the three compounds **135**-**137** (Table 23), which were all found to have better physiochemical properties than **113**.

Scaffold							
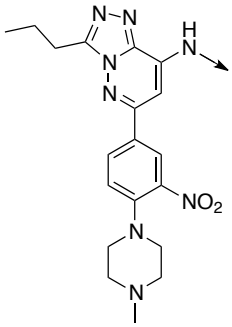							
Compound Number	**Compound**	***c* log D at pH 7.4**	**SFI**	**Compound Number**	**Compound**	***c* log D at pH 7.4**	**SFI**
113	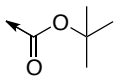	2.3	5.3	**136**	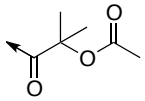	1.3	4.3
135	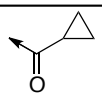	1.5	4.5	**137**	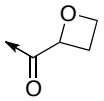	1.1	4.1

Table 23: **Predicted solubility of amide propyl triazoles.** c Log D was calculated using ACD/Labs algorithm (version 5.0.0.184).

The cyclopropyl **135** and acetate **136** derivatives were successfully synthesised from the corresponding aniline **156** and the relevant acid chloride (Scheme 18). Numerous attempts to form the oxetane derivative **137** from the corresponding carboxylic acid were unsuccessful. Compound **137** was synthesised using propylphosphonic anhydride (T3P), which has been reported in the literature to be a particularly effective coupling reagent for unreactive systems.[170,245,246,250,251] Complete consumption of **156** was achieved when *N*-methyl-2-pyrrolidone (NMP) was used as solvent, at 80 °C, however, it was not possible to isolate the desired product to a sufficient level of purity. There was evidence that **137** could be unstable, as decomposition to the aniline during handling of this compound was observed during HPLC, mass spectrometry, and NMR analysis.

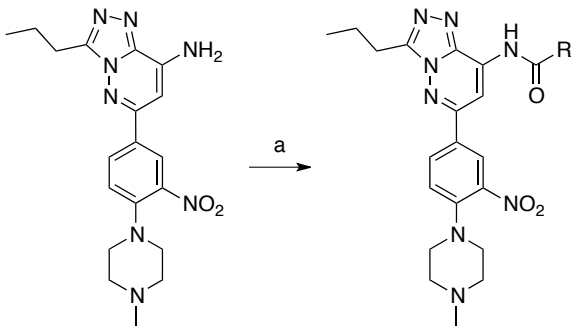

Scheme 18: *Reagents and conditions*: (a) RCOCl, CH_2Cl_2, Hünig's base, 0 °C-RT (**135**, R = cyclopropyl, 32%; **136**, R = $COC(CH_3)_2OCOCH_3$, 30%).

The aqueous solubility of the cyclopropyl **135** and acetate **136** derivatives was examined in the SnapSol assay (Table 24). Although the cyclopropyl derivative **135** was predicted to have a higher solubility than the Boc analogue **113**, its measured solubility was lower (5 μM). Upon derivatisation to the acetate **136**, there was a considerable improvement in aqueous solubility, with a measured value of 95 μM, in this assay.

Scaffold					
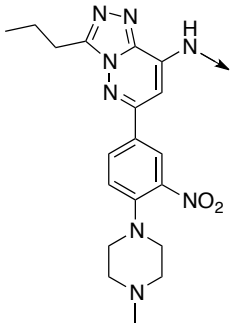					
Compound Number	**Compound**	**SnapSol at pH 7.4/μM**	**Compound Number**	**Compound**	**SnapSol at pH 7.4/μM**
113	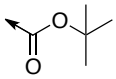	12	**135**		5
			136	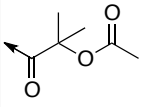	95

Table 24: Measured aqueous solubility of amide propyl triazole analogues.

With this result in mind, a range of compounds containing the acetate substituent were then designed (Figure 75). These target compounds were expected to have the desired affinity and solubility of useful tool compounds. The sulfonamide SAR was extended by synthesis of compound **139**, which introduced a hydrogen bond donating group in the form of an azetidine moiety.

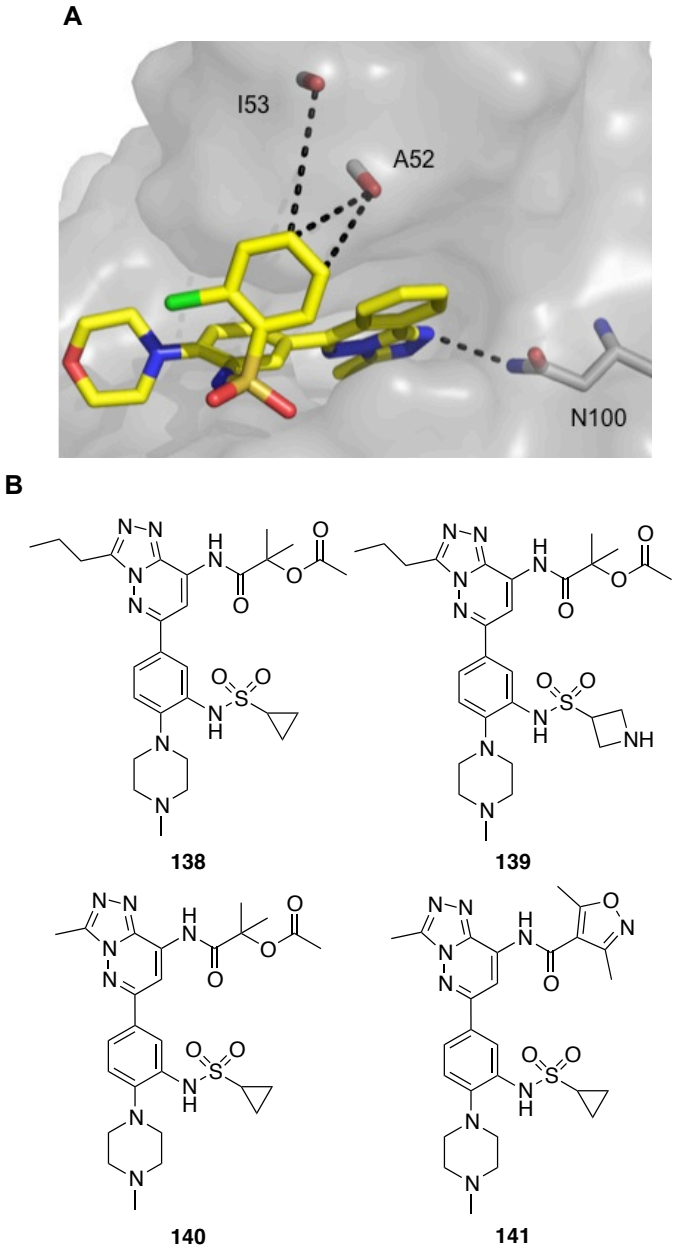

Figure 75: Exploring hydrogen bonding and π-π stacking interactions in BRD9. (**A**) Tricyclic triazole **34** bound to BRD9 (PDB ID: 4NQN), reported by Fedorov *et al*..[156,247] (**B**) Target compounds **138-141**.

The 3,5-dimethylisoxazole derivative **141** was identified as an interesting compound to explore the possibility of increasing BRD9 potency *via* a π-π stacking interaction with Y106. The cyclopropyl **138** and azetidine **139** sulfonamides were synthesised using previously optimised conditions (Scheme 19).

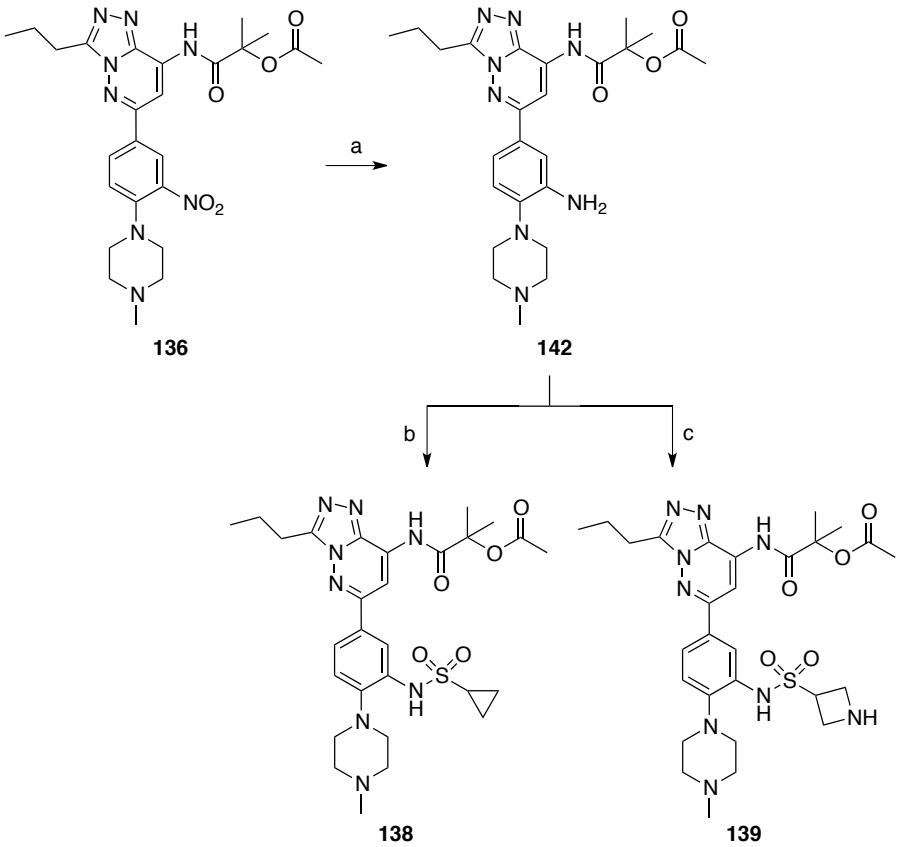

Scheme 19: *Reagents and conditions*: (a) $SnCl_2$, EtOH/Et_3N (2:1), 27%; (b) Cyclopropane sulfonylchloride, DMAP, Pyridine, 0 °C-RT, 56; (c) (i) *tert*-Butyl 3-(chlorosulfonyl)azetidine-1-carboxylate, CH_2Cl_2, Et_3N, 0 °C-RT, (ii) TFA/CH_2Cl_2 (1:1), RT, 26% (2 steps).

The acetate and isoxazole derivatives, **140** and **141** respectively, were generated in two steps from **94**, which was deprotected under acidic conditions, followed by reaction with the corresponding acid chlorides (Scheme 20).

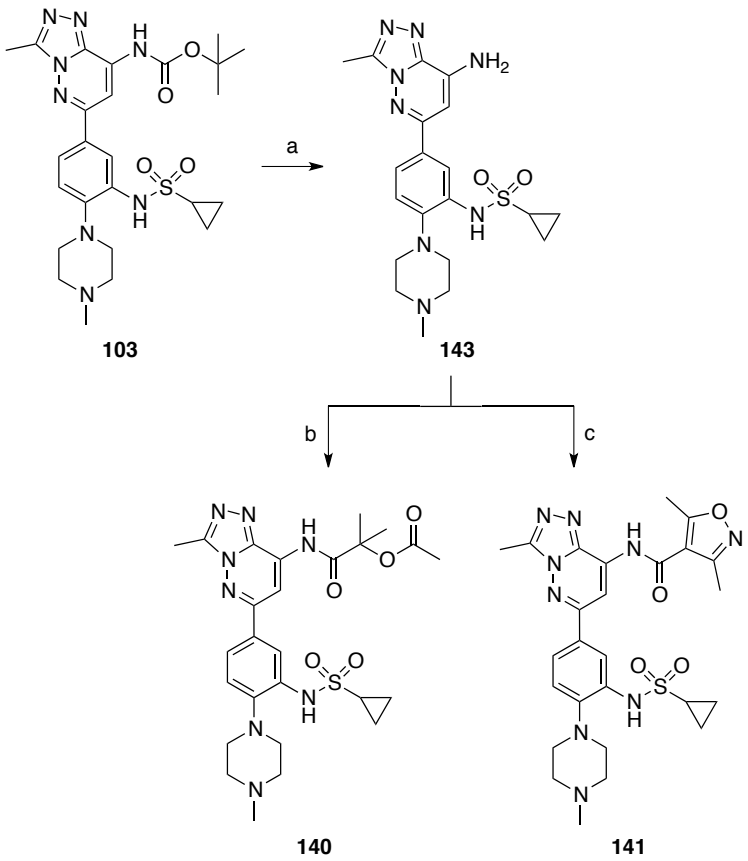

Scheme 20: *Reagents and conditions*: (a) TFA/CH_2Cl_2 (1:1), RT; (b) 1-Chloro-2-methyl-1-oxopropan-2-yl acetate, CH_2Cl_2, Hünig's base, 0 °C-RT, 35% (over 2 steps); (c) 3,5-Dimethylisoxazole-4-carbonyl chloride, CH_2Cl_2, Hünig's base, 0 °C-RT, 28% (over 2 steps).

The aqueous solubility of these compounds was evaluated in the SnapSol assay (Table 25). All acetate-containing amides were found to have solubilities >100 µM. The isoxazole derivative **141** had a lower solubility value, of 74 µM and was therefore not used in any further studies. One possible reason for the lower than expected aqueous solubility of **141** could be the relatively flat π-system of the isoxazole group, which is expected to stack extremely well in the solid phase. The BRD9 affinity of these compounds was assessed in a HTRF assay in collaboration with the SGC, using compound **103** as a standard control, which had previously been identified as a tight binder of BRD9 (Table 25).

Compound Number	Compound	SnapSol pH 7.4/µM	BRD9 IC_{50}/µM	Compound Number	Compound	SnapSol pH 7.4/µM	BRD9 IC_{50}/µM
103	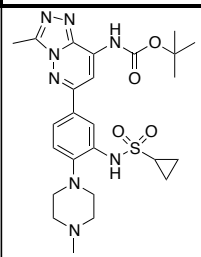	>100	0.104	**138**	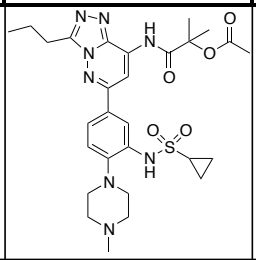	>100	>20
140	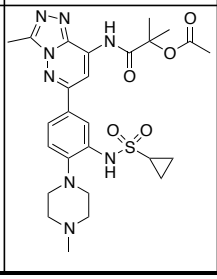	>100	>20	**139**	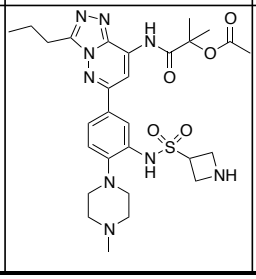	>100	>20

Table 25: **Evaluation of the BRD9 affinity of acetate derivatives in a BRD9 HTRF assay.**

The acetate derivatives were found to be inactive against BRD9, CECR2, BRD4(1) and BRPF1B in an AlphaScreen^{TM} assay, at concentrations up to 20 µM. A possible reason for the inactivity of this compound set is their ability to form an intramolecular hydrogen bonding interaction (Figure 76.A). This conformation could result in a steric clash with residues in the KAc binding pocket. This hypothesis was also supported by a ground state molecular dynamics simulation (Figure 76.B).

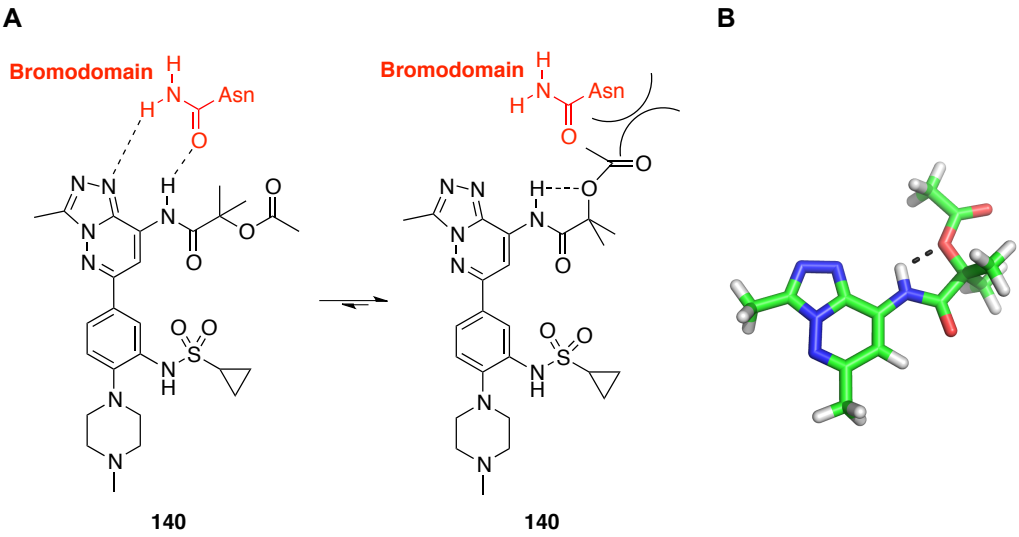

Figure 76: Hypothesised intramolecular hydrogen-bonding interaction in acetate derivatives, illustrated for 140, which disrupts the interaction with the bromodomain. (**A**) Equilibrium of the two acetate conformations. (**B**) Energy minimisation of triazole acetate. Wilian Cortopassi performed conformational searching using in-house programs written in Python with the PDDG/PM3 improved semiempirical method[247,248] and Gaussian 09 revision D software.[248,249] The lowest energy conformation was then re-optimized using 3-21G basis set and B3LYP functional and 6-31+G(d,p) basis sets. All calculations were performed with an implicit solvent model (water).[249,252]

4.6. Introduction of an *ortho*-methyl substituent to improve compound solubility

An alternative method by which to improve the solubility of the *n*-propyl triazoles was then explored. *Ortho*-substitution of biaryl rings has been shown to be a useful method to improve a compound's solubility.[170,250,251,253] This modification is thought to result in a lowest energy compound conformation in which the two aryl rings are no longer co-planar. This twisted conformation results in a disruption of crystal packing in the solid phase, lowering the stability of the crystal lattice, thereby increasing the rate of dissolution of the compound into the solvent, resulting in a higher solubility. An energy minimisation was performed on compound **144** (Figure 77), showing a conformation in which the pendant *ortho*-methyl containing ring is twisted into

a position where the $N_1C_2C_3C_4$ dihedral angle is 120°.

A **B**

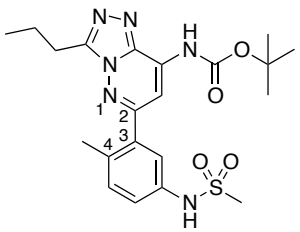

144

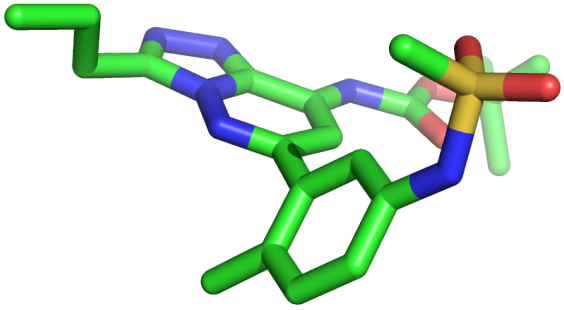

Figure 77: **Introduction of an *ortho*-methyl substituent to improve solubility.** (**A**) Structure of compound **144**. (**B**) Energy minimisation result for compound **144**. Wilian Cortopassi performed conformational searching using in-house programs written in Python with the PDDG/PM3 improved semiempirical method[158,247] and Gaussian 09 revision D software[161,248]. The lowest energy conformation was then re-optimized using 3-21G basis set for all atoms with the Hartree Fock method and an implicit solvent model (water).[148,249]

To investigate this result, the *ortho*-methyl derivative **146** was synthesised in one step *via* a Suzuki coupling reaction involving **129** and **145** (Scheme 21). The aqueous solubility of this compound was measured in the SnapSol solubility assay. Compound **146** was found to have very low aqueous solubility, as the measured SnapSol value was 3 μM, one of the lowest values for any compound in this series. Two possible reasons for the low measured aqueous solubility could be the overriding impact of this compound's high lipophilicity (*c* log D = 3.8), in addition to the three aryl rings, which result in an SFI value of 6.8, one of the highest calculated during this work.

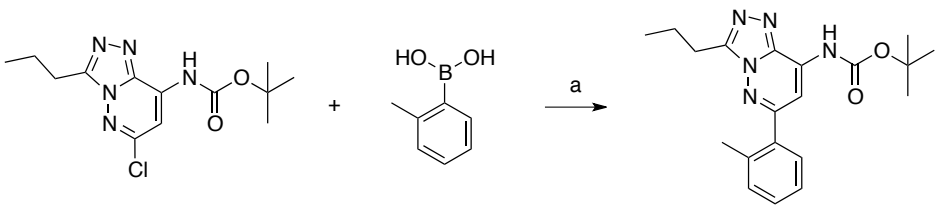

129 **145** **146**

Scheme 21: *Reagents and conditions*: (a) K_2CO_3, $Pd(dppf)Cl_2{\cdot}CH_2Cl_2$, 1,4-dioxane/$H_2O$ (10:1), 80 °C, 38%.

Extensive attempts to couple (2-methyl-5-nitrophenyl)-boronic acid *en route* to compound **144** were unsuccessful under a range of conditions.

4.7. Replacement of propyl chain by methoxy and hydroxyl sub-units

We were intrigued by a publication by Huang *et al.* in which Molecular Dynamics simulations on the bromodomains of BAZ2B and CREBBP led to the conclusion that "water molecules at the bottom of the KAc-binding pocket can be transiently displaced by ethanol or methanol".[145,148,161,252] Displacement of water molecules in the binding site of BRD9 was then thought to be an exciting route to gain potency and selectivity for this bromodomain. It has also been found that if a ligand is thought to displace the water molecules in a protein's binding site, affinity can be enhanced by introducing a group capable of engaging in interactions which mimic those between these water molecules and the protein.[210,253]

With these observations in mind, compounds **134** and **135** (Figure 78) were identified as interesting targets, with the potential of mimicking or forming interactions to water molecules in the binding site of BRD9.

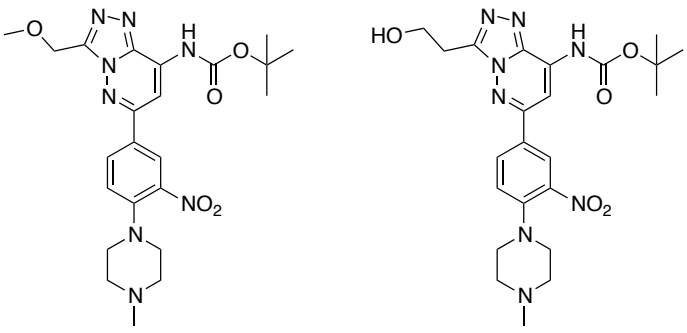

147 **148**

Figure 78: Target compounds, methoxy derivative 147, and hydroxy analogue 148.

Each of these compounds were synthesised from **63** in three steps (Scheme 22). Both **134** and **135** were found to have excellent aqueous solubilities, with SnapSol values >100 μM.

A

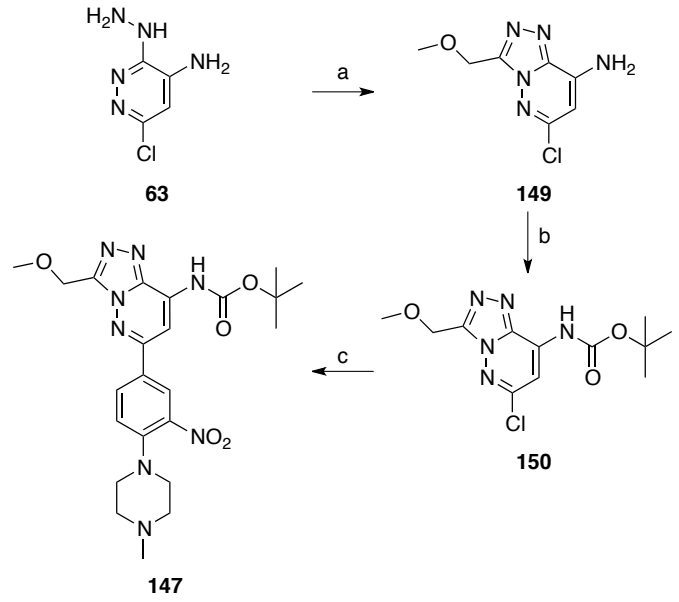

B

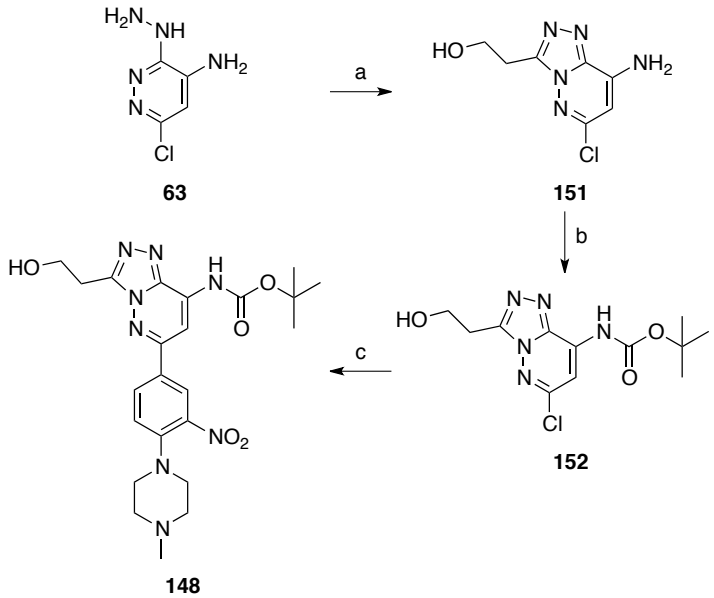

Scheme 22: *Reagents and conditions*: (**A**) (a) Methoxyacetic acid, 110 °C MW, 64%; (b) Boc_2O, 4-DMAP, THF, RT, 55%; (c) **74**, K_2CO_3, $Pd(dppf)Cl_2{\cdot}CH_2Cl_2$, 1,4-dioxane/$H_2O$ (10:1), 80 °C, 23%; (**B**) (a) 3-Hydroxypropanoic acid, 140 °C MW; (b) Boc_2O, 4-DMAP, THF, RT, 5% (over steps); (c) **74**, K_2CO_3, $Pd(dppf)Cl_2{\cdot}CH_2Cl_2$, 1,4-dioxane/$H_2O$ (10:1), 80 °C, 10% (over 2 steps).

Compounds **147** and **148** were then screened against five bromodomains, the results of which are shown in Table 26. The methoxy analogue **147** was found to bind weakly to BRD9 and CECR2, with IC_{50} values of 7.79 μM, and 4.67 μM, respectively. Negligible binding was detected to BRD4(1), BRD1, or BRPF1B, up to a compound concentration of 20 μM.

Compound Number	Compound	IC_{50}/μM				
		BRD9	CECR2	BRD4(1)	BRPF1B	BRD1
147	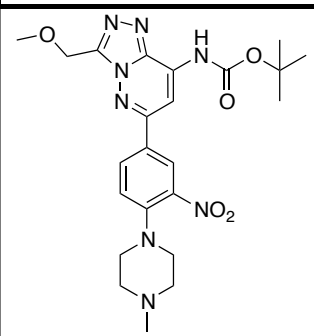	7.79	4.67	>20	>20	>20
148	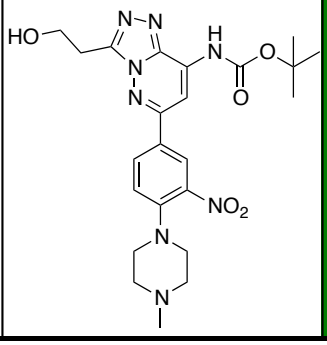	>20	3.93	>20	>20	>20

Table 26: IC_{50} results obtained by the SGC for compounds 147 and 148. BRD9 was examined in a HTRF assay. For all other bromodomains shown, an AlphaScreen™ assay was used.

The hydroxyl derivative **148** bound to CECR2 only, with an IC_{50} value of 3.93 μM. Binding of **147** to BRD9 and CECR2 was confirmed in a DSF assay, in which it displayed ΔT_m values of 3 °C, and 4 °C, against BRD9 and CECR2, respectively. Compound **148** had a ΔT_m value of 3 °C against both CECR2 and BRD9.

It is an interesting result that these atypical acyl-lysine mimetic compounds bind to bromodomains. The observation that **147** and **148** bind to

bromodomains in multiple assay formats suggests that future bromodomain ligand development programmes could benefit greatly by placing a greater emphasis on derivatisation of the substituent residing in the KAc binding pocket. However, it is difficult to make a detailed interpretation of the selectivity of these compounds, as their affinities for the bromodomains to which they bind are relatively low.

4.8. Summary and future work

The work described in this chapter has demonstrated that ligands containing a range of substituents beyond a typical methyl group can be tolerated by the bromodomains of BRD9 and CECR2. We have completed a SAR study to demonstrate that the methyl group which is proposed to occupy the KAc binding pocket in BRD9 and CECR2 can be extended to ethyl, propyl and butyl. Upon extension from C(1) to C(4) there was a reduction in affinity, and aqueous solubility. The challenge of low compound solubility was overcome by replacement of the propyl substituent with oxygen-containing methoxy, and hydroxyl chains. These compounds were shown to bind to the bromodomains of BRD9 or CECR2, with low micromolar affinity, and this binding was confirmed in a DSF assay. This modification, however, appeared to result in a loss of potency to these bromodomains, compared to the corresponding methyl derivatives.

Based on the results presented above, several strategies exist for further optimisation:

- X-Ray crystallographic studies on the methoxy and hydroxyl derivatives bound to BRD9 and CECR2 would provide a useful insight into their

binding mode and aid in future attempts to develop small molecule ligands of these bromodomains.

- Starting from a soluble fragment, it would be interesting to examine the SAR in the KAc binding pocket in more detail against a range of bromodomains. A rigorous analysis of the residues and water molecules in this region would be beneficial.
- The 'plasticity' of bromodomains is clearly emerging as an important factor to consider during the ligand design process.[158,210] Structural and computational studies on BRD9 and the wider bromodomain family would be a useful aid.

Since this work began, several ligands have been developed which contain alternatives to the typical methyl group of the KAc mimic. For example, the ethyl-containing probe I-BRD9,[158,161] the SMARCA2/4 inhibitor PFI-3, and the ATAD2 ligand **30**.[148,254]

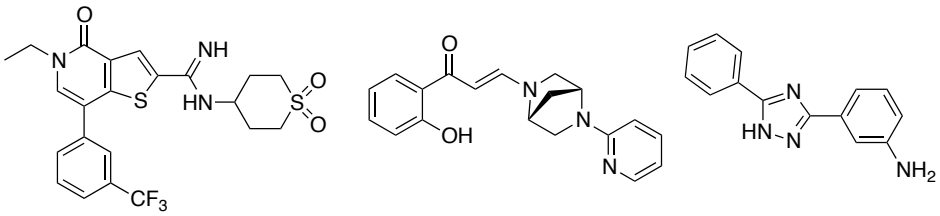

I-BRD9 **39** PFI-3 **27** **30**

Figure 79: Bromodomain ligands containing groups other than methyl as the KAc mimic.[145,148,161,255]

The work by Genentech discussed at the start of this chapter has recently been published, and demonstrates that the bromodomains of BRD9 and CECR2 are capable of reading *n*-butyryl marks on histone peptides, with similar affinities to KAc modifications.[150,210,256,257] The collaboration with Constellation Pharmaceuticals also found that the second bromodomain of

TAF1 binds to crotonyl marks on histone peptides. A broad screen of human bromodomains using peptide arrays was then followed by ITC and X-ray crystallographic studies. The ITC results are summarised in Table 27.

	H4 1-11 K5acK8ac	H4 1-11 K5prK8pr	H4 1-11 K5buK8bu	H4 1-11 K5crK8cr
	K_D, μM	**K_D, μM**	**K_D, μM**	**K_D, μM**
BRD4(2)	145 ± 8	310 ± 30	ndb	ndb
BRD9	64 ± 5	44 ± 3	60 ± 10	ndb
CECR2	26 ± 2	75 ± 5	24 ± 1	ndb

Table 27: Recognition of butyryllysine by CECR2 and BRD9, ITC results obtained by Flynn *et al.*[210,258] Results are reported as an average of at least three runs (nbd refers to no detected binding).

Upon comparison of the crystal structures of *n*-butyryl-lysine peptides in complex with BRD4(1) and BRD9, several interesting observations can be made. In BRD4(1) the *n*-butyryl chain adopts a strained, eclipsed conformation, with the terminal methyl group pointing towards the amide NH. This binding mode contrasts greatly to that in BRD9, in which the *n*-butyryl chain adopts a more favourable, staggered conformation, which allows the carbon chain to extend deeply into the binding pocket. The authors propose that the BRD9-binding pocket has "greater flexibility than is typical", a proposition which is consistent with an induced-fit binding mode previously observed for the small molecule 9*H*-purine scaffold.[158,259] It would be interesting to identify which amino acid residues are responsible for this flexibility, and whether such a feature can be predicted in other bromodomains. This area could be studied in more detail using computational methods.

Interestingly, no water molecules are displaced by the *n*-butyryl-lysine peptide in complex with BRD9. This observation, in addition to the flexibility of the

BRD9 pocket, could help to predict how the propyl and butyl analogues developed in this chapter bind to BRD9 and CECR2. Rather than dislodging the water molecules, the longer alkyl chains are likely to sit in an extended conformation, directed deep into the binding pocket. It may therefore be interesting to synthesise compounds in which a linear, extended, staggered conformation is preferred over an eclipsed pose. This could result in an improvement in potency, as the ligand would be in an energetically favourable conformation, promoting binding to BRD9 and CECR2. The discovery in this Chapter that compounds **147** and **148**, containing methoxy and hydroxyl moieties respectively, in place of the typical KAc mimetic, displayed binding to BRD9 or CECR2, is another piece of useful information which should help ligand development programmes of these bromdomains. The KAc binding pocket of bromodomains is considered to be primarily hydrophobic in nature, although the presence of a network of water molecules in this region helps to rationalise the tolerance of more polar groups, such as those present in **147** and **148**.

As it now appears that the water molecules in the binding site of BRD9 are unlikely to be displaced, it would be useful to develop more accurate tools to predict the probability that a water molecule can be displaced, and if so, which chemical groups would be most likely to achieve this. This could be investigated using more rigorous computational methods, including molecular dynamics simulations,[254,260,261] which have proved useful in supporting the discovery of new bromodomain inhibitors.[255,262] These are demanding calculations but provide more accurate predictions than typical docking experiments, by capturing important effects such as conformational flexibility

of the protein, ligand and defined water molecules.

The work in this chapter has provided evidence that BRD9 and CECR2 can bind to small molecule ligands containing a variety of acyl-lysine mimics. This information could be an important consideration during the design of future bromodomain ligands. A great amount of work remains to be done in order to assess and predict the optimal substituent in the binding pocket of this protein class.

Chapter 5: Conclusion and future work

Using a structure-based approach, the work in Chapters 2 and 3 described the optimisation of the insoluble, promiscuous bromodomain inhibitor **34**, leading to compound **2**, which has nanomolar potency for BRD9 and some selectivity over BRD4(1) (Figure 80.A). Binding to BRD9 was demonstrated using five orthogonal techniques: DSF, MST, HTRF, BROMO*scan*™, and ITC. Compound **2** has high aqueous solubility and moderate metabolic stability in an *in vitro* mouse model, and is currently undergoing a co-crystallisation study with BRD9. This will hopefully lead to a detailed understanding of its binding mode, aiding an explanation of its high potency, and how further improvements in selectivity could be made. The aniline **2** had double-digit nanomolar affinity in an AlphaScreen™ assay for the CECR2 bromodomain. Compound **2** has sub-micromolar affinity for the highly homologous sub-family IV member BRPF1A bromodomain. The high potency of **2** across multiple targets which have been linked to oncological malignancies[150,158,256,257] may be therapeutically advantageous, as "dysregulation of multiple signaling pathways is a hallmark of cancer development and progression".[74,133,258] This polypharmacology could enable multiple disease pathways to be targeted, improving the efficacy of existing cancer therapies.[156,259,260,261,263]

It would be worthwhile to initially focus on a comprehensive selectivity analysis of **2** with as many bromodomains as possible. It would be useful to confirm binding to full-length BRD9 in its native setting. This could be done by measuring the disruption of chromatin binding in a chemoproteomic study,

such a FRAP assay or nanoBRET assay. Aromatic amines such as **2** are often found to be mutagenic agents due to their susceptibility to oxidation. It would be interesting to explore this potential liability in a bacterial mutagenicity (Ames) test. The piperazine group of this scaffold may be a useful attachment point for a biotin tag, enabling the identification of binding partners of BRD9, which may help to reveal its biological role (Figure 80.B).

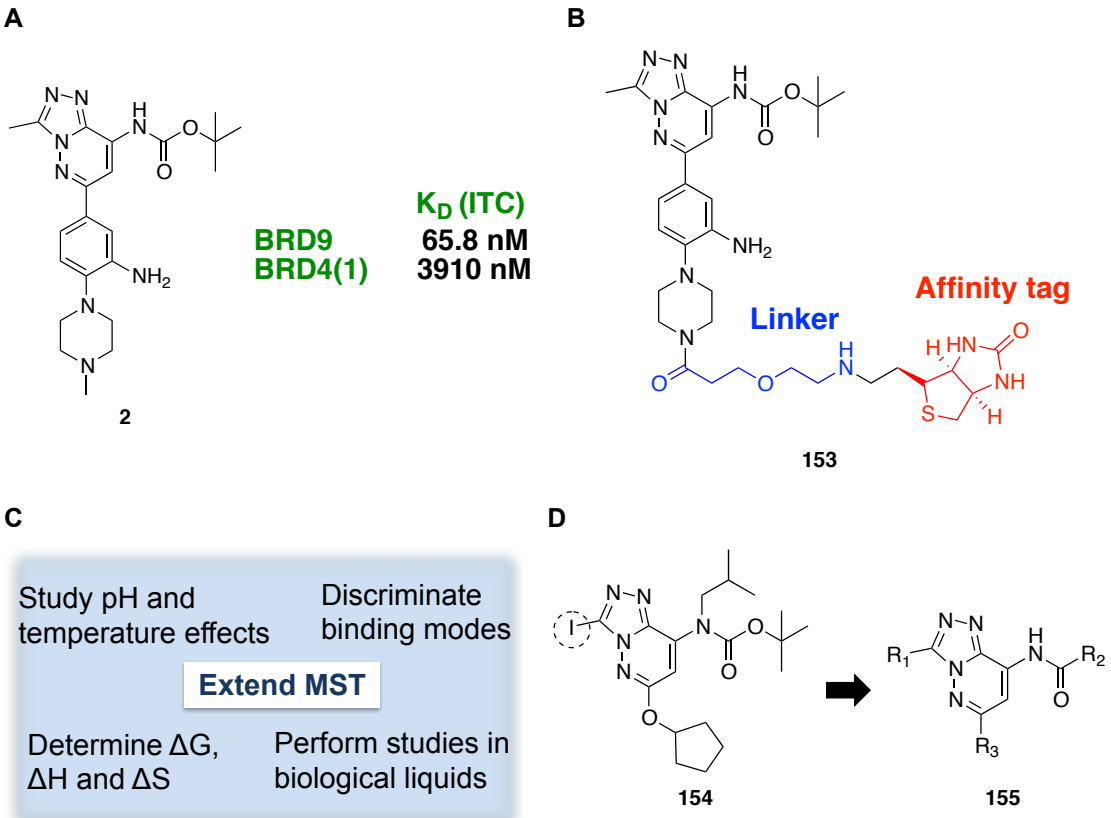

Figure 80: **Summary of areas of future work.** (**A**) Structure and key ITC results for compound **2**, which should be further evaluated for selectivity and efficacy across a wide range of bromodomain and wider pharamcoogical targets. (**B**) Possible target compound **153** for pull-down studies. (**C**) Some of the ways in which MST could be used to measure ligand binding to bromodomains. (**D**) Reported compound **154** which could enable late stage diversification for further SAR at the R1 position shown on scaffold **155**.

We have used Microscale Thermophoresis to develop an assay for bromodomain-ligand binding. This method could be extended to calculate the thermodynamic contributions of ligand binding, which currently requires the

use of SPR or ITC experiments, demanding large amounts of protein and being relatively low-throughput. This assay could be used to measure disruption of bromodomain binding to a range of histone and non-histone targets.

Chapter 4 outlined the efforts made to probe the KAc binding pocket of BRD9. The results indicated that the bromodomains of BRD9 and CECR2 might be able to accommodate larger and more chemically distinct moieties than initially anticipated. A wider range of chemical space could be examined with derivatives of the known compound **154** (Figure 80.D), which would also enable late-stage diversification.[262,264] Our SAR studies in this region were restricted due to the insolubility of the central bicyclic scaffold. Switching to an alternative monocyclic chemotype, may overcome this problem.

It would be useful to develop computational tools to assess the KAc binding pocket of the whole bromodomain family. Specifically, this could focus on exploring the displaceability of the network of water molecules with bromodomains could prove useful in future ligand development programmes. The BRD9 bromodomain has been reported to have a degree of 'plasticity'.[158,265] It may be possible to apply Molecular Dynamics simulations, which have proved useful in the development of other bromodomain inhibitors, across the whole family, to understand and predict this flexibility.[74,133,266]

Chapter 6: Experimental

6.1. Computational Methods

The docking study on 47 and similar bicyclic triazoles was carried out using ICM-Pro 3.6-1 (Molsoft LLC). The X-ray crystal structure of *apo*-BRD9 (PDB ID: 3HME) was used. The receptor was prepared from chain A of *apo*-BRD9 (PDB ID: 3HME) and water molecules numbered 2 and 165 were removed. Docking of **47** was carried out using ICM-Pro 3.6-1 (Molsoft LLC). A volume of 5 Å near the KAc binding pocket was used as a guide. The ligands were then put through a flexible-ligand docking procedure using the in-build procedure in ICM-Pro. The binding free energy between ligand and receptor was then determined for sampled conformations of the flexible ligands, with the highest scoring compounds examined in further detail.

Docking of the piperazine derivative 71 was carried out by Angelina Sekernik. The receptor was prepared from chain A of *apo*-BRD9 (PDB ID: 3HME) with a hydration state used from an analysis of the crystal structure of **34** bound to BRD9 (PDB ID: 4NQN),[125,156] i.e. water molecules numbered 2 and 165 were removed. Docking of **71** was performed using Vina. A volume of 10 $Å^3$ near the KAc binding pocket was used as a guide, with the number of accessible modes and the exhaustiveness both set to 20.

The docking study on 111 was carried out by Gregory Ross, using default settings in AutoDock Vina. The X-ray crystal structure of **34** bound to BRD9 (PDB ID: 4NQN) was used. A receptor pocket with a volume of 5 $Å^3$ close to **34** was

used as a guide for the ligand docking. All water molecules were removed before docking.

6.2. Biochemical Methods

BRD9 expression and purification by Dr Anthony Chan

Escherichia coli host, DNA plasmid, and recombinant protein expression

The *Escherichia coli* strain, BL21(DE3)[263,267] was used for expressing the N-terminal hexa-histidine-tagged BRD9 bromodomain, which is encoded in the BRD9 plasmid.[264,268] The BRD9 plasmid was a gift from Nicola Burgess-Brown (Addgene plasmid #39012). The plasmid has the pNIC28-Bsa4 vector backbone.[265,268]

E. coli transformant, i.e. *E. coli* BL21(DE3) containing the BRD9 plasmid, which was used for expressing the BRD9 bromodomain, was aerobically cultured in the 2 × TY medium (16 g L^{-1} Oxoid™ Tryptone, 10 g L^{-1} Oxoid™ Yeast Extract, 5 g L^{-1} NaCl) at 37 °C with an agitation speed of 180 rpm, in the presence of 50 μg mL^{-1} of kanamycin (Apollo Scientific Ltd.). Chemical inducer, IPTG (isopropyl β-d-1-thiogalactopyranoside), was added to a final concentration of 0.1 mM for inducing protein expression, when the bacterial culture reached an optical density of 1.0 ± 0.1 at 600 nm. After the IPTG induction, the culture temperature was lowered to 18 °C and the culture was incubated for 18-24 h of post-induction time.

Bacterial cell pellets were then collected by centrifugation after the overnight protein production, and kept at –80 °C until protein purification. IPTG was

purchased from Apollo Scientific Ltd. All other chemicals were purchased from Sigma-Aldrich unless otherwise specified. The BRD9 bromodomain protein was purified by immobilised metal affinity chromatography (IMAC) and then size-exclusion chromatography (SEC).

Protein purification by IMAC and SEC

For sample preparation, the cell pellet containing recombinant BRD9 was first suspended in Equilibration Buffer (50 mM NaH_2PO_4/Na_2HPO_4, 300 mM NaCl, pH 7.0). The pellet was suspended in 1-2% of the original culture volume in Equilibration Buffer. The serine protease inhibitor, PMSF (phenylmethylsulfonyl fluoride), was added to a final concentration of 1 mM. After complete suspension of the bacterial pellets, the cells were lysed on ice by sonication (50% amplitude, 5 s bursts interrupted by 5 s pauses for 30 cycles) to release proteins. Insoluble cell debris was removed by centrifugation at 24,000 ×g at 4 °C for 5 min. The resulting supernatant was collected, added with 1 mM PMSF, and then filtered through 0.45 μm pore size syringe filters (Merck Millipore Corp.). The clarified cell lysate filtrate was diluted fivefold with Equilibration Buffer before applying it to gravity-flow IMAC column. The empty gravity-flow IMAC column (100 mL Thompson's Single StEP Column, Generon Ltd) was packed with 5 mL bed volume of TALON metal affinity resin (Clontech Laboratories, Inc.).

For protein purification by IMAC, the packed affinity column was first rinsed with 10 bed volumes of Milli-Q water (Merck Millipore), and then equilibrated with 10 bed volumes of Equilibration Buffer. The column was subsequently

loaded with the pre-treated cell lysate. After that the column was washed by 5 and 10 bed volumes of Wash Buffer (50 mM NaH_2PO_4/Na_2HPO_4, 300 mM NaCl, 10 mM imidazole, 20% Glycerol, pH 7.0) and Equilibration Buffer, respectively. The hexa-histidine-tagged protein was eluted with 4 bed volumes of Elution Buffer (50 mM NaH_2PO_4/Na_2HPO_4, 300 mM NaCl, 150 mM imidazole, pH 7.0) in 2-mL fractions. The collected protein fractions were subjected to SDS-PAGE (sodium dodecyl sulfate polyacrylamide gel electrophoresis) and Coomassie staining and destaining for detecting the presence of target proteins before performance the next step of protein purification (Figure 81.A).

All of the buffers used in the purification procedures were pre-filtered through 0.2 μm pore size filter papers (Sartorius UK Ltd.) under vacuum to remove insoluble precipitates. The chemicals, NaH_2PO_4 and Na_2HPO_4, were purchased from Alfa Aesar and BDH Chemicals Ltd, respectively. Glycerol was bought from Thermo Fisher Scientific Inc.

After the IMAC purification steps, BRD9 was further purified by SEC. The IMAC-purified BRD9 protein was first concentrated by using Vivaspin™ sample concentrator (GE Healthcare). The concentrated protein sample was then loaded into a gel filtration column XK 16/70 (GE Healthcare) packed with 120 mL of Superdex 75 resin (GE Healthcare), which was connected to a computerized ÄKTAFPLC system (GE Healthcare). This SEC column was pre-equilibrated with 150 mL degassed SEC Buffer (50 mM HEPES (Fisher Scientific UK Ltd, 500 mM NaCl, pH 7.6). The SEC procedure (Figure 81.B)

was operated at a constant flow rate (1 mL min^{-1}; 150 mL of total flow volume) and filtrates were collected in 5-mL fractions (the sample collection was started at 20th mL of the flow). The quality of SEC-purified protein samples was checked by SDS-PAGE (Figure 81.C). The purified protein was further concentrated by Vivaspin^{TM} sample concentrator (GE Healthcare). Protein concentrations were determined by a NanoDrop 1000 spectrophotometer (Thermo Fisher Scientific Inc.), with extinction coefficient of 8.94 mM^{-1} cm^{-1} (experimentally determined) and molecular weight of 16.70 kDa as the NanoDrop inputs.

SDS-PAGE and Coomassie staining

SDS-PAGE was performed by using the Mini-PROTEAN 3 apparatus (Bio-Rad Laboratories, Inc.). The SDS-PAGE was employed the Laemmli Buffer System, according to manufacturer's specifications (Bio-Rad Laboratories, Inc). Protein samples were mixed in 1× Laemmli Sample Buffer and denatured at 95 °C for 5 min. For Coomassie staining of protein bands, hand-cast gels after SDS-PAGE were stained in Coomassie Staining Solution [0.5% (*w/v*) Brilliant Blue G, 50% (*v/v*) methanol, 10% (*v/v*) glacial acetic acid, in Milli-Q water (Merck Millipore Corp.)] for 15 min. The stained gels were then gradually destained by several washing steps with Destaining Solution [40% (*v/v*) methanol, 10% (*v/v*) glacial acetic acid, in Milli-Q water (Merck Millipore Corp.)] until protein bands on the gels become clearly visible. The images of the de-stained protein gels were captured by an image scanner. All chemicals were purchased from Sigma-Aldrich Co., except 2× Laemmli Sample Buffer (Bio-Rad Laboratories, Inc), β-mercaptoethanol (Bio-Rad Laboratories, Inc),

glacial acetic acid (Thermo Fisher Scientific Inc), and glycine (Thermo Fisher Scientific Inc).

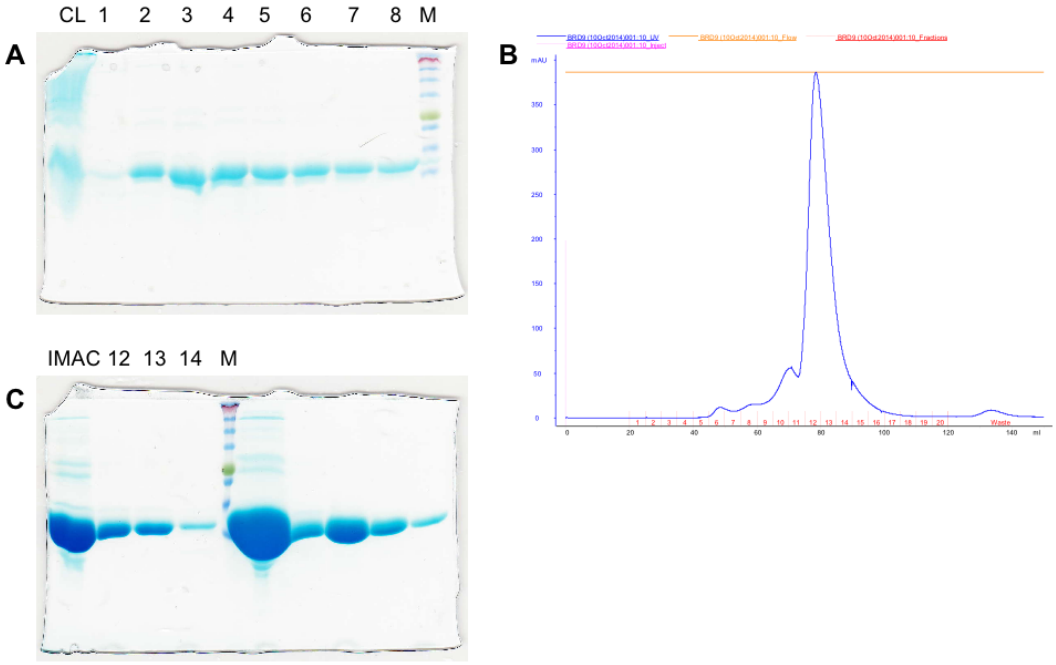

Figure 81: Purification profiles and quality of purified BRD9.
(A) SDS-PAGE analysis of BRD9 filtrate fractions purified from the IMAC. Lane 1 (Label: CL): Unpurified cell lysate released from sonication of bacterial cells. Lanes 2-9 (Labels: 1-8): Elution fractions collected from the IMAC purification. Lane 10 (Label: M): Color Prestained Protein Standard, Broad Range (New England BioLabs, Inc.). The gel was made of 16% Tris-Glycine-SDS polyacrylamide composition. **(B)** SEC purification profile of BRD9. The Blue line represents UV absorbance (mAU) trace, while the pink line indicates the point of sample injection. The linear orange line indicates constant flow rate (1 mL min^{-1}) and sample fraction numbers for collection are shown in red. **(C)** SDS-PAGE analysis of SEC-purified BRD9 fractions. Lane 1 (Label: IMAC): Concentrated IMAC-purified BRD9 protein which was used for sample injection in SEC. Lanes 2-4 (Label: 12-14): Elution fractions collected from SEC purification in B. Lane 5 (Label: M): Color Prestained Protein Standard, Broad Range (New England BioLabs, Inc.). The gel was made of 16% Tris-Glycine-SDS polyacrylamide composition. The purified protein used in this study was obtained from the non-aggregated fractions, 12-14, as shown in B and C.

BRD4(1) expression and purification by Angelina Sekirnik.

A similar protocol to that performed by Dr Anthony Chan was used.

Microbiology techniques

Standard sterile practices were followed thoroughly, using the Heracleus laminar flow hood when necessary. Media and equipment were sterilised by autoclaving at 121 °C for 20 min. Solutions of IPTG, antibiotics and other labile compounds were sterilised by filtering through 0.2 mm filters (Minisart®, Sartorius Stedim). Final concentrations of antibiotics unless indicated otherwise were: Kanamycin 30 µg/mL.

Bacterial growths

Media	**Reagent**	**Amount required per litre (g)**
2 × Typtone-Yeast (2TY) Extract	Bacto typtone	16.0
	Yeast extract	10.0
	NaCl	5.0

Table 28: Bacterial growth parameters.

All growth media were autoclaved (*Thermo Live Sciences* MAT 490 LEI) at 121 °C for 45 min before use, and left to rest overnight. Optical density readings were taken in 1.6 mL cuvettes with 5 × dilution in Milli-Q water against a reference sample of the growth media at zero time. The absorbance was measured at 600 nM using a Novaspec® II spectrophotometer.

Bacterial plate cultures were inverted and grown overnight at 37 °C in a Heraeus® TypB 6030 incubator. All agar plates were poured and streaked in a laminar flow hood (HereSafe® Model KS12 Class II Biosafety Cabinet) using sterile media and equipment. Small scale growths for starter cultures were 100 mL (in 500 mL Duran flasks) of 2-TY media containing the appropriate antibiotic, inoculated from a single colony on an agar plate and grown

overnight under foil, in a New Brunswick Scientific G25 environmental shaker at 37 °C and 250 rpm shaking.

Competent cells

E.coli strains of the following genotype was used: BL21 (DE3) Gold: F^- *ompT* *hsd*S_B ($r_B^-m_B^-$) *gal dcm* (DE3). DE3 denotes a chromosomal copy of the T7 RNA polymerase gene.
Competent cells were thawed on ice for 20 min before 1-5 µL of plasmid DNA was added to 20 µL of the competent cells in pre-chilled 50 mL Falcon tubes. The tubes were left on ice for 30 min before placement into a water bath at 42 °C ('heat shocked') for 30 sec for BL21 DE3 (Gold) cells. The tubes were returned to ice for 5 min, 300 µL 2-TY media was added gently to each tube which was then incubated at 37 °C for 1 hour before 100 µL of the transformation mixture was plated onto agar plates containing the appropriate antibiotic and incubated overnight.

Recombinant expression of bromodomains

Several bromodomain containing constructs in pNIC28-Bsa4 vector backbones were transformed into *E. coli* BL21 (DE3) Gold cells. Flasks containing 600 mL 2TY media with the appropriate antibiotic were inoculated with 1 % of the bacterial starter culture. Flasks (2000 mL PYREX® narrow-mouth graduated Erlenmeyer flasks or plastic baffled flasks) were incubated at 37 °C and 180 rpm in an Innova® 44 shaker (New Brunswick Scientific). When OD_{600} reached 0.8-1.0, the temperature was lowered to 18 °C and IPTG was added to a final concentration of 0.25 mM to induce protein expression. Cultures were incubated at 18 °C overnight, after which time cultures were harvested by centrifugation in a JA10 rotor in an Avanti J25 centrifuge (Beckman Coulter™) at 8000 rpm for 15 min at 4 °C. The resulting pellet was weighed and stored in a sealable plastic bag at –80 °C.

Purification of recombinant proteins

To purify bromodomain containing proteins, the cell pellet was dissolved in binding buffer (approximately 5-times v/w of cell pellet) and lysed by

sonication (10 s bursts at 10 s intervals for a total sonication time of 10 min). The lysate was clarified by centrifugation in an Avanti J25 centrifuge (Beckman Coulter™) using a JLA-25.50 rotor at 23,000 rpm for 20 min at 4 °C. The supernatant was decanted off, filtered through 0.45 µm filter and applied onto a 3-6 mL HisTrap™ chromatography column (GE Healthcare), which had been charged with 4 CV of 100 mM $NiSO_4$ and equilibrated with 5 CV of binding buffer prior to loading the cell lysate at 1 mL/min. The column was then washed with approximately 100 mL wash buffer. When all residual products of bacterial fermentation were eluted from the column by binding buffer, the protein of interest was batch eluted with 20 mL of elution buffer containing 500 mM imidazole. Eluted protein was collected and fractionated; fractions containing the highest levels of pure protein (as determined by SDS-PAGE gels) were loaded on a pre-equilibrated 150 mL Superdex 75 size exclusion chromatography column, and further purified by gel filtration chromatography. After elution with 150 mL of gel filtration buffer, fractions identified by UV traces as containing protein were analysed by SDS-PAGE gel electrophoresis.

Reagents	**Nickel affinity column buffers (pH 7.6 except charge buffer)**				
	Charge	Binding	Wash	Elution	Strip
HEPES	–	50 mM	50 mM	50 mM	50 mM
NaCl	–	0.5 M	0.5 M	0.5 M	0.5 M
Imidazole	–	5 mM	30 mM	500 mM	–
$NiSO_4$	100 mM	–	–	–	–
EDTA	–	–	–	–	100 mM

Table 29: Parameters for the nickel affinity column protocols.

His_6-BRD4 3 mL his column elution

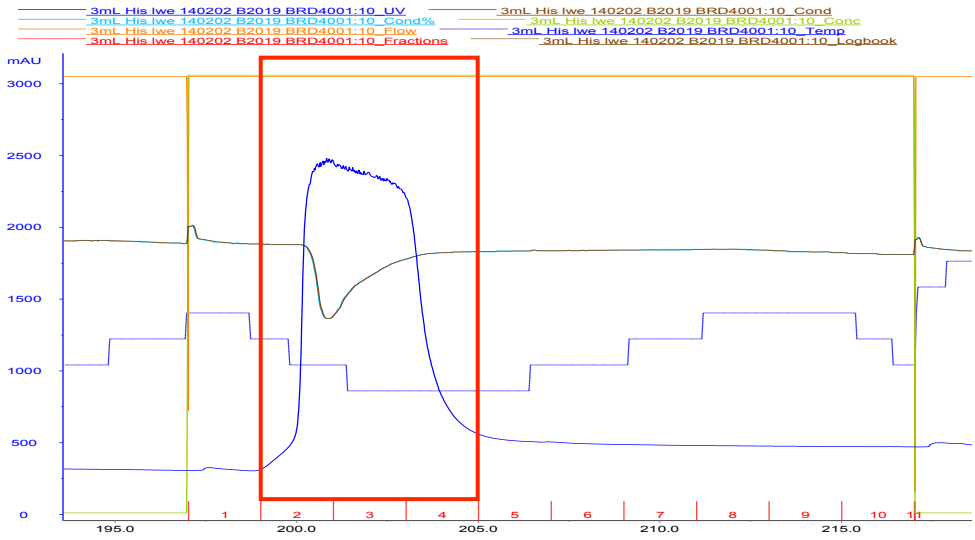

His_6-BRD4 gel filtration column elution (S75 150 mL)

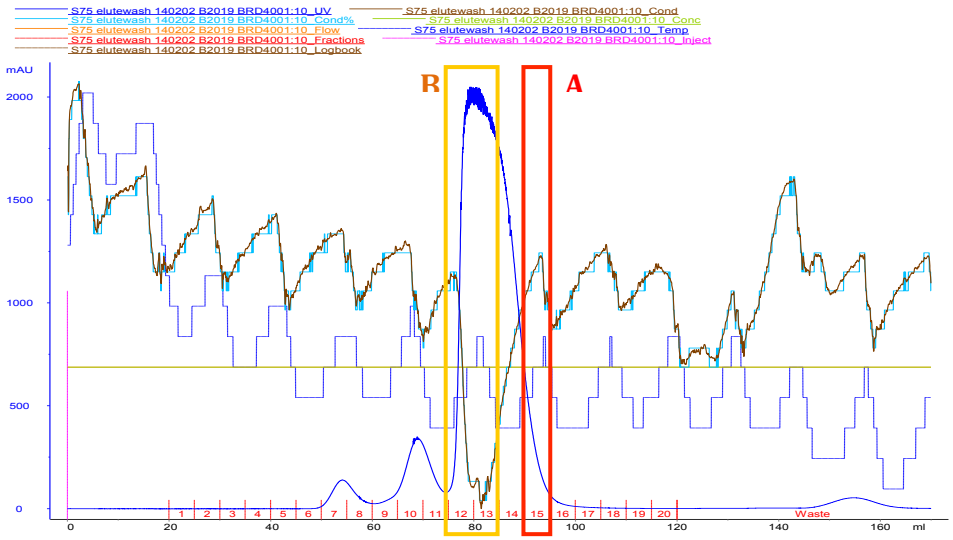

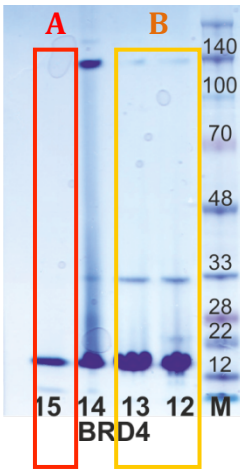

From 1.2 L growth media, 1.2 mg was concentrated at >95% purity (A), and 18 mg at ~90% purity (B), and flash frozen in liquid nitrogen (20 uL aliquots at 1.94 mg/mL [111 uM] and 30 uL aliquots at 11.88 mg/mL [677 uM], respectively). mass: 17549 Da.

6.3. Biophysical Methods

Thermal stability shift assay (SGC Oxford) measurements were carried out on a Mx3005p real-time PCR machine (Agilent). Protein concentration was 2 µM and inhibitor concentration was 100 mM. The buffer used was 10 mM HEPES, pH 7.5, 500 mM NaCl and 1:1000 dilution of SyproOrange (Invitrogen, CA). The assay and data evaluation were carried out as described previously.[266,268] Experiments were performed in duplicate; average values are reported.

Bromodomain AlphaScreen^{TM} assays (SGC Oxford) were performed as described previously[125,268] with minor modifications from the manufacturer's protocol (PerkinElmer, USA). All reagents were diluted in 25 mM HEPES, 100 mM NaCl, 0.1 % BSA, pH 7.4 supplemented with 0.05 % CHAPS and allowed to equilibrate to room temperature prior to addition to plates. An 11-point 1:2.0 serial dilution of the ligands was prepared on low-volume 384-well plates (ProxiPlateTM-384 Plus, PerkinElmer, USA), using LabCyte Eco liquid handler. Plates filled with 5 uL of the assay buffer followed by 7 uL of biotinylated peptide [H-YSGRGK$_{ac}$GGK$_{ac}$GLGK$_{ac}$GGAK$_{ac}$RHRK(Biotin)-OH and His-tagged protein to achieve final assay concentrations of 50 nM. Plates were sealed and incubated for a further 30 minutes, before the addition of 8 µL of the mixture of streptavidin-coated donor beads (12.5 µg/mL) and

nickel chelate acceptor beads (12.5 µg/mL) under low light conditions. Plates were foil-sealed to protect from light, incubated at room temperature for 60 minutes and read on a PHERAstar FS plate reader (BMG Labtech, Germany) using an AlphaScreen 680 excitation/570 emission filter set. IC_{50} values were calculated in Prism 5 (GraphPad Software, USA) after normalisation against corresponding DMSO controls and are given as the final concentration of compound in the 20 µL reaction volume.

BRD9 HTRF assay (SGC Oxford) used a GST tagged BRD9 with anti-GST antibody conjugated Eu^{3+} cyrptate (donor) and a biotinylated peptide with Streptavidin conjugated XL-665 (acceptor). When the donor and acceptor labels are in close proximity, by binding of the peptide by the bromodomain, the excitation of the donor (337 nm) triggers a Fluorescence Resonance Energy Transfer (FRET) to the acceptor which then fluoresces at specific wavelength (665 nm) (Figure 81).

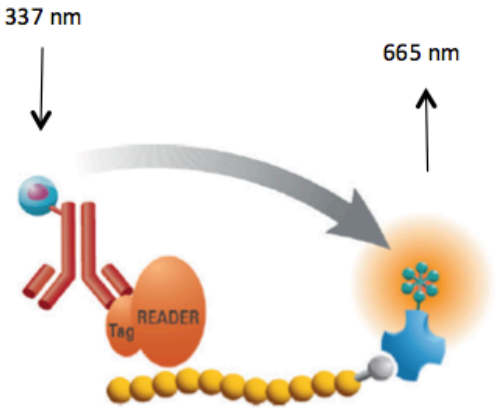

Figure 81: An illustrated representation of the BRD9 HTRF assay developed and ran by the SGC.

The optimised protocol was obtained directly from Oleg Fedorov (SGC) and is detailed below.

Materials

1.1 EPIgeneous^{TM} Binding Domain kit B, cisbio, 62BDBPEH

1.1.1 Binding domain diluent buffer

1.1.2 Binding domain detection buffer

1.1.3 Streptavidin-XL665 (15 uM)

1.1.4 Anti-GST-Eu^{3+} cryptate (50×)

1.2 GST tagged BRD9, SGC,

1.3 Peptide Histone H4 Lysine tetra acetylated-biotin (1mM)

1.4 ProxiPlate-384 Plus, Perkin Elmer, 6008289

1.5 PHERAstar microplate reader, BMG

1.6 Multidrop combi, Thermo Scientific, 5840300

1.7 DMSO, Sigma,

1.8 Echo 525 Liquid Handler, Labcyte

2.0 Methods

2.1 Peptide Titration

2.1.1 Prepare a 4× working stock of Histone H4 Lysine tetra acetylated-biotin at 1.6 mM and from this stock prepare 12 1:2 serial dilutions in diluent buffer and add 5 µl of the dilution series to 6 columns of the ProxiPlate plus.

2.1.2 Prepare a 4× working stock of SA-X665 at 0.2 mM (1/8 concentration of the peptide) and from this stock prepare 12 1:2 serial dilutions in detection buffer and add 5 µL of the dilution series to 6 columns of the ProxiPlate plus.

2.1.3 Prepare a 4× working stock of BRD9A-p038 to 20 nM in diluent buffer and add 5 µL of this solution to the first 3 columns of the proxiplate, add 5 µL diluent buffer to columns 4-6. The wells with no GST-BRD9A-p038 give the background and can be subtracted to give the specific signal.

2.1.4 Prepare a 4× working stock of anti-GST-Eu^3 cryptate at 1:50 in detection buffer and add 5 µL of the dilution series to 6 columns of the ProxiPlate plus.

2.1.5 Cover the plate and incubate at room temperature and read at 0, 3 and 24 h in the Pherastar using the HTRF module with dual emission protocol (A = ex. 320 nm em. 665 nm, B = ex. 320 nm em. 620 nm).

2.1.6 Calculate results as HTRF ratio = channel A/B *10000. Then calculate specific signal = HTRF Ratio Positive signal - HTRF Ratio Negative signal (without GST-BRD9) and plot this against peptide concentration.

2.2 Inhibition Assay

2.2.1 Dispense compounds into assay plates using the Echo liquid handler using a maximum volume of 40 nL (0.2 % DMSO). Into columns 12 and 24 dispense 40 nL DMSO into alternate wells. Column 12 will be the positive control and column 24 will be the negative control, alternate wells are used to monitor the effect of DMSO in the assay.

2.2.2 Prepare 4× working solution of BRD9-GST at 20 nM in the binding domain diluent buffer and add 5 uL to columns 1-23 of the assay

plate and add 5 uL binding domain diluent buffer to column 24 (negative control).

2.2.3 Prepare 4× working solution of peptide Histone H4 Lysine tetra acetylated-biotin at 200 nM in the binding domain diluent buffer and add 5 uL to all columns of the assay plate.

2.2.4 Prepare 4× working solution of SA-XL665 at 25 nM in the binding domain detection buffer and add 5 uL to all columns of the assay plate.

2.2.5 Prepare 4× working solution of anti-GST antibody at 1× in the binding domain detection buffer and add 5 ul to all columns of the assay plate.

2.2.6 Cover the plate and incubate at room temperature and read at 0, 3 and 24 h in the Pherastar using the HTRF module with dual emission protocol (A = ex. 320 nm em. 665 nm, B = ex. 320 nm em. 620 nm).

2.2.7 Calculate results as HTRF ratio = channel A/B *10000.

2.2.8 Calculate % inhibition as follows:

$$\%\, \boldsymbol{I} = \mathbf{100} - \frac{\boldsymbol{signal - negative\ control}}{\boldsymbol{positive\ control - negative\ control}} \times \mathbf{100}$$

2.2.9 Determine IC_{50} values by plotting % inhibition vs compound concentration and fitting the data to a non-linear sigmoidal dose response equation (4 parameter fit).

Isothermal Titraion Calorimetry (ITC) experiments were carried out with the

assistance of Cynthia Tallant on a MicroCal ITC200 calorimeter. All experiments were performed at 20 °C in 20 mM HEPES pH 7.5, 150 mM NaCl, 0.5 mM TCEP. BRD9 and BRD4(1) protein solutions were buffer exchanged overnight by dialysis into the ITC buffer. The titrations were conducted using an initial injection of 0.5 µL followed by identical injections of 1.5 µL. Injections were made over a time period of 3 seconds, with a time spacing of 150 seconds. Thermodynamic parameters were calculated using $\Delta G = \Delta H - T\Delta S = -RT\ln K_B$, where ΔG, ΔH, and ΔS are the changes in free energy, enthalpy and entropy of binding respectively. In all cases a single binding site model was employed. During the BRD9 experiments, the concentration of compounds **2**, **99**, and **101**, were 35 µM, 40 µM, and 35 µM, respectively, and the protein concentration was 240 µM, 240 µM, and 240 µM, respectively. For the BRD4(1) experiment with compound **2**, the ligand concentration was 11 µM, protein concentration was 246 µM.

BROMO*scan*™ assay protocols were performed by DiscoverRx. T7 phage strains displaying bromodomains were grown in parallel in 24-well blocks in an *E. coli* host derived from the BL21 strain. *E. coli* were grown to log-phase and infected with T7 phage from a frozen stock (multiplicity of infection = 0.4) and incubated with shaking at 32 °C until lysis (90-150 min). The lysates were centrifuged (5,000 × g) and filtered (0.2 µm) to remove cell debris. Streptavidin-coated magnetic beads were treated with biotinylated small molecule or acetylated peptide ligands for 30 min at RT to generate affinity resins for bromodomain assays. The liganded beads were blocked with excess biotin and washed with blocking buffer (SeaBlock (Pierce), 1 %

BSA, 0.05 % Tween 20, 1 mM DTT) to remove unbound ligand and to reduce non-specific phage binding. Binding reactions were assembled by combining bromodomains, liganded affinity beads, and test compounds in 1x binding buffer (17% SeaBlock, 0.33× PBS, 0.04% Tween 20, 0.02% BSA, 0.004% Sodium azide, 7.4 mM DTT). Test compounds were prepared as 1000× stocks in 100% DMSO and subsequently diluted 1:10 in monoethylene glycol (MEG) to create stocks at 100X the screening concentration (resulting stock solution is 10%DMSO/90% MEG). The compounds were then diluted directly into the assays such that the final concentration of DMSO and MEG were 0.1% and 0.9%, respectively. All reactions were performed in polystyrene 96-well plates in a final volume of 135 µL.The assay plates were incubated at room temperature with shaking for 1 h and the affinity beads were washed with wash buffer (1× PBS, 0.05% Tween 20). The beads were then re-suspended in elution buffer (1× PBS, 0.05% Tween 20, 2 µM nonbiotinylated affinity ligand) and incubated at room temperature with shaking for 30 min. The bromodomain concentration in the eluates was measured by qPCR.

Single concentration measurements

%Ctrl Calculation

$$\left[\frac{\text{test compound signal - positive control signal}}{\text{negative control signal - positive control signal}}\right] \times 100$$

test compound = compound submitted by UCB Pharma
negative control = DMSO (100%Ctrl)
positive control = control compound (0%Ctrl)

6.4. SnapSol solubility assay (UCB)

Solubility - 500 µL buffer was added to 0.5 mg solid compound in matrix tubes. Samples shaken on an orbital shaken at 37 °C for 90 minutes. 200 µL aliquots from each tube filtered through a 0.4 µm polycarbonate filter plate (Millipore MSSLBPC50) and the filtrate transferred to a 96 well plate for analysis.

Calibration - 10 mM DMSO stock solution of each compound prepared. 1000 µM, 500 µM, 100 µM and 20 µM calibration samples of each compound prepared by carrying out a serial dilution of the DMSO stock in MeCN/water.

Analysis - Solubility and calibration samples analysed on a Waters Acquity-SQD LC-MS. Compound identity confirmed using mass spectrometry. UV peak areas of the calibration samples plotted against the concentration to produce a calibration plot from which the slope can be calculated. UV peak areas of the solubility samples were used to determine the concentration of compound in solution (the solubility) from the calibration data.

6.5. *In vitro* metabolic stability assay (UCB)

Assay was designed and performed by Hayley Roy at UCB. This *in vitro* metabolic stability assay has been developed to screen research compounds to support the drug discovery process. The experimental procedure is to incubate a compound (substrate) with microsomal protein and measure its disappearance over time. The removal of parent drug is termed Clearance. Clearance mechanisms *in vivo* include hepatic and extra-hepatic (gut, lungs, kidney) metabolism, and renal and biliary elimination. This assay results in the calculation of hepatic clearance.

To determine clearance, the depletion of substrate should follow an exponential decline i.e. linear disappearance on a Natural Log (L_n) – plot, with at least 10% depletion over the time period.

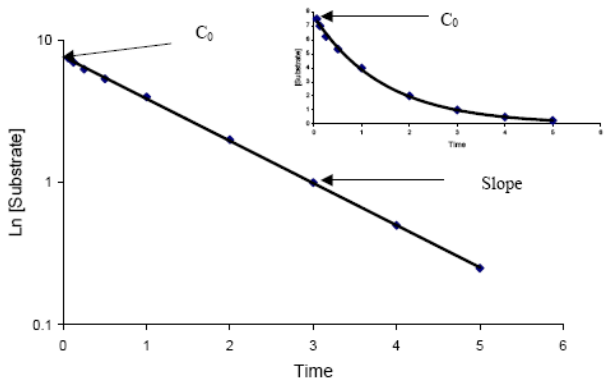

Figure 76: Substrate depletion on L_n [Substrate] v Time Plot, exponential decay in inset.

The Half-Life ($T_{1/2}$) is determined via: $T_{1/2} = L_n2/k$, where k is the elimination rate constant, calculated from the slope of the initial rate of reaction from a plot of the L_n [Substrate] *v* Time. The Intrinsic Clearance (Cl_{int}) is defined as the maximal rate of clearance that can occur in the absence of any limiting factors. Since clearance can only operate on unbound drug delivered by the blood, the limiting factors are protein binding and blood flow. Cl_{int} is determined via: $Cl_{int} = L_n\ 2 \times V/T_{1/2,}$ where V = Incubation Volume (µL)/Microsomal protein incubated (mg). This is scaled to Hepatic Clearance and an Extraction Ratio is calculated to classify the clearance as low, moderate or high, but is a guide for phase I metabolism only. This is an automated assay with 6 time points. All incubations were performed in singlet. NADPH was used. Ketoconazole was the internal standard.

Calculation of results

Result output is described in Table 30.

RESULT CALCULATIONS	
k (elimination constant)	This is the gradient of the plot multiplied by –1. Units are µL/min
In vitro Cl_{int}	= k*(1000/protein concentration mg/mL). Units are µl/min/mg microsomal protein
In vivo Cl_{int}	=(in vitro Cl_{int}/1000)*mg microsomal protein/g liver per kg animal Units are ml/min/kg animal
E_h (extraction ratio)	=in vivo Cl_{int}/(hepatic blood flow + in vivo Cl_{int}) No units, results on a scale of 0-1

Table 30: Calculation of *in vitro* clearance.

The natural log of the Peak Area Ratio (or Peak Area) is plotted against time. The gradient of this line is multiplied by -1 to obtain the elimination rate constant (k). The protein concentration used in the incubation is incorporated to obtain *in vitro* Cl_{int}. *In vitro* Cl_{int} is scaled to *in vivo* Cl_{int} t using the physiological scaling factors presented in Table 31.

Species	Hepatic Blood Flow mL/min/kg	Liver Weight (g) /Body Weight (kg)	mg microsomal protein/g liver
Human	20.2	24.5	40
Mouse	120	55	47

Table 31: Scaling of *in vitro* Cl_{int}.

The extraction ratio (E_h) is calculated as the ratio of *in vivo* Cl_{int} and hepatic blood flow. Compounds are classified based on their E_h. E_h < 0.3 is classified as low clearance and > 0.7 is high. Cl_{int} values can also be characterised as follows:

Species	*In Vitro* Cl_{int} (µl/min/mg) (Extraction Ratio)		
	Low	Moderate	High
Human	<8.5 (0.3)	8.5 - 47 (0.3-0.7)	>47 (0.7)
Mouse	<8 (0.3)	8-43 (0.3-0.7)	>43 (0.7)

Table 32: Classification of Cl_{int} values.

6.6. Synthetic Methods

Reagents and solvents used, unless otherwise stated, were of commercially available reagent grade quality and were used without further purification. Where appropriate and if not stated otherwise, all non-aqueous reactions were carried out in a flame dried flask under an inert atmosphere of nitrogen or argon. Anhydrous solvent was purchased from Sigma-Aldrich UK in SureSeal™ bottles, and used without purification, or dried according to the procedure outlined by Pangborn *et al.*[267] Solvents for use in organometallic reactions were degassed by at least three freeze-thaw cycles under vacuum and were stored under an argon atmosphere over 3 Å molecular sieves. Triethylamine for use in organometallic reactions was dried with KOH and distilled onto KOH pellets. *In vacuo* refers to solvent removal under reduced pressure using a Buchi™ rotary evaporator. Brine refers to a saturated aqueous solution of sodium chloride. Petroleum ether refers to the fraction of light petroleum ether boiling in the range 40-60 °C.

Reactions with microwave irradiation were carried out in a Biotage Initiator microwave synthesiser or a Discover CEM microwave synthesiser.

Analytical thin layer chromatography (TLC) was carried out on Merck silica gel 60 F_{254} aluminium-supported thin layer chromatography sheets. For TLC on aluminium oxide, Polygram^{TM} ALOX N/UV_{254} plastic sheets were used. Visualisation was by absorption of UV light (λ_{max} 254 or 365 nm), or thermal development after dipping in one of: **a** ethanolic solution of phosphomolybdic

acid; **b** aqueous solution of potassium permanganate, potassium carbonate and sodium hydroxide; **c** ethanolic solution of ninhydrin.

Silica gel flash Column chromatography was carried out either on Merck silica gel 60 (240-400 mesh), eluting with solvents as supplied under a positive pressure of compressed air, or on a Biotage® SP1 system using KP-Sil™ cartridges.

Melting points were determined using a Kofler hot stage microscope and are uncorrected. The solvent of crystallisation is shown in parentheses.

Specific optical rotations were measured using a Perkin-Elmer 341 polarimeter with a water-jacketed 1 dm path-length cell maintained at 20 °C. The light source was maintained at 589 nm. The concentration (*c*) is expressed in g/100 mL and specific rotations are denoted $[\alpha]_D^T$ with implied units of 10^{-1} deg cm^2 g^{-1} (where T = ambient temperature in °C).

Microanalyses were obtained at the Elemental Analysis Service, London Metropolitan University, London. Elemental analysis was carried out in duplicate; average values are reported.

Infrared spectra were obtained as a thin film on sodium chloride discs or from neat samples mounted directly using a diamond ATR module. The spectra were recorded on a Bruker Tensor 27 spectrometer and a

representative number of absorption maxima are reported in wavenumbers (cm^{-1}) and assigned as s (strong), m (medium), w (weak) or br (broad).

^{1}H NMR spectra were recorded on Bruker AV400 (400 MHz), AVIII400 (400 MHz) or Bruker AVII 500 (500 MHz) using $CDCl_3$ (unless indicated otherwise) as a reference for internal deuterium lock. The chemical shift data for each signal are given as δ_H in units of parts per million (ppm) relative to tetramethylsilane (TMS) where δ_H (TMS) = 0.00 ppm. The multiplicity of each signal is indicated by: s (singlet); br s (broad singlet); d (doublet); t (triplet); q (quartet); dd (doublet of doublets); ddd (doublet of doublet of doublets) etc.; or m (multiplet). The number of protons (n) for a given resonance signal is indicated by nH. Coupling constants (*J*) are quoted in Hz and are recorded to the nearest 0.1 Hz. Identical proton coupling constants (*J*) are averaged in each spectrum and reported to the nearest 0.1 Hz. The coupling constants are determined by analysis using Bruker TopSpin software.

^{13}C NMR spectra were recorded on Bruker AV400 (100 MHz), Bruker AVII 500 (126 MHz) or AVIIIHD 600 MHz (151 MHz) spectrometers with broadband proton decoupling and internal deuterium lock. The chemical shift data for each signal are given as δ_C in units of parts per million (ppm) relative to tetramethylsilane (TMS) where δ_C (TMS) = 0.00 ppm. Coupling constants (*J*) are quoted in Hz and are recorded to the nearest 0.1 Hz. Identical proton coupling constants (*J*) are averaged in each spectrum and reported to the nearest 0.1 Hz. The coupling constants are determined by analysis using

Bruker TopSpin software. ^{1}H and ^{13}C spectra were assigned using 2D NMR experiments including COSY, HSQC and HMBC.

^{19}F NMR spectra were recorded on a Bruker AVII 500 (470 MHz) using a broadband proton decoupling pulse sequence and deuterium internal lock. The chemical shift data for each signal are given as δ_F in units of parts per million (ppm).

^{11}B NMR spectra were recorded on a Bruker DRX500 (160 MHz). The chemical shift data for each signal are given as δ_B in units of parts per million (ppm).

High-resolution mass spectra were acquired on a Bruker MicroTOF spectrometer or a Waters G2 Xevo QToF-MS coupled to a H Class Acquity LC system from solutions of methanol or water (ESI). A Waters GCT TOF spectrometer with a temperature-programmed solids probe inlet operating in positive or negative mode was used for the EI/FI method.

Low-resolution mass spectra were recorded on a Waters LCT Premier spectrometer or Agilent 6120 Quadrupole LC/MS spectrometer (ESI). *m/z* values are reported in Daltons and followed by their percentage abundance in parentheses.

Analytical HPLC was carried out using two methods:

Method 1; A PerkinElmer Flexar system with a Binary LC Pump and UV/VIS LC Detector was used. For determination of compound purity, a Dionex Acclaim® 120 column (C18, 5 µm, 120 Å, 4.6 × 150 mm) was employed, with a 10-minute gradient of 95% water/5% MeCN + 0.1% TFA (Solvent A) to 95% MeCN/5% water + 0.1% TFA (Solvent B), flow rate 1 mL/min and detection at 254 nm. Samples were injected in DMSO. The method was as described below:

Step length (min)	**Elapsed time (min)**	**%A**	**%B**
1	1	100	0
15	16	0	100
3	19	0	100
1	20	100	0

Method 2; The reverse phase separation was carried out on a Waters X-Bridge, C18, 2.1 x 20 mm, 2.5 µm silica particle column at pH 3 and pH 10. Samples were injected in DMSO. Parameter details are described below;

Injection volume	1-5 µL
UV data	230 to 400 nm, Peak Width 0.1 sec
Column temperature	40 °C
Flow rate	1.0 mL/min
Split to MS	~0.05 mL/min
Split to DAD and ELSD	~0.05 mL/min

pH 3 Method: A 4-minute gradient of water + 0.1% formic acid (Solvent A) to 95% MeCN + 5% + 0.1% formic acid (Solvent B) was used.

pH 10 Method: A 4-minute gradient of water + 0.1% NH_3 solution (Solvent A) to MeCN + 5% Solvent A + 0.1% NH_3 solution (Solvent B) was used.

The gradient program at both pH settings is as described below:

Step length (min)	**Elapsed time (min)**	**%A**	**%B**
0	0	95.0	5.0
4	4	5.0	95.0
1	5	5.0	95.0
0.1	5.1	95.0	5.0

Chiral HPLC was carried out on an Agilent 1100 LC System at a flow rate of 1 mL/min. An isocratic method of 100% methanol at a run time of 10 min was used, with visualisation using a DAD method from 190-400 nm. The column was a LUX Cellulose-4, 150 x 4.6 mm 3 µM particle size, and the run temperature was 40 °C.

Preparative HPLC was carried out at UCB Slough by Justin Staniforth using a Waters Fractionlynx system, with 2525 pump, 2996 PDA, 2767 fraction collector and a ZQ2000 MS setup. Crude samples were injected in DMSO, and the column was run at ambient temperature through a Waters XBridge Prep C18 5 µM OBD column, using the programme setting 'pH10_35_30 focused gradient.' Flow rate was 19 mL/min (+ 1 mL/min MeCN column dilution) and detection was carried out using a Diode Array Detection (DAD) method from 230-400 nm. The solvent systems and gradient programmes are described below;

Solvent A: 10 mM ammonium bicarbonate + 0.1 % ammonium hydroxide
Solvent B : MeCN + 0.1% ammonium hydroxide

Step length (min)	Elapsed time (min)	%A	%B
0	0	65	35
2.3	2.3	65	35
8.7	11	50	50
0.4	11.5	5	95
1.5	13	5	95
0.2	13.2	65	35

6.7. Synthetic Procedures

Chapter 2 Procedures

4-Bromo-1,2-dihydropyridazine-3,6-dione (**60**)

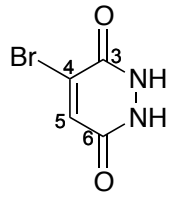

Bromomaleic anhydride **59** (50.0 g, 282 mmol, 1.0 eq) was added to a solution of sulfuric acid (98%, 15 mL) in water (125 mL). Hydrazine monohydrate (20.0 mL, 412 mmol, 1.5 eq) was added and the reaction mixture was heated under reflux for 6 h, resulting in the formation of a colourless solid. TLC analysis indicated complete consumption of **59**. The reaction mixture was cooled to RT, the solid was collected by filtration, washed with ice-cold acetone (70 mL) and dried *in vacuo* to give 4-bromo-1,2-dihydropyridazine-3,6-dione **60** (53.3 g, 99%) as a colourless powder: R_f 0.10 (CH_2Cl_2/methanol, 80:20); mp 251-252 °C (from methanol) [Lit.[268] 260-263 °C, dec.]; ν_{max} (thin film)/cm^{-1} 3314 (br, w), 2970 (m), 2361 (m), 2304 (m), 1739 (m), 1639 (m), 1554 (s), 1380 (s), 1264 (m), 1041 (m); ^{1}H NMR (500 MHz; D_6-DMSO) δ 12.35 (1H, br s, N*H*), 11.16 (1H, br s, N*H*), 7.58 (1H, s, C(5)*H*); ^{13}C NMR (126 MHz; D_6-DMSO) δ 156.3 (*C*(3)=O), 152.5 (*C*(6)=O), 130.3 (*C*(5)H), 129.4 (*C*(4)Br); *m/z* (ES$^+$) 191 ([^{79}M+H]$^+$, 71%), 193 ([^{81}M+H]$^+$, 100%). These data are in accordance with the literature values.[268]

3,4,6-Trichloropyridazine (**61**)

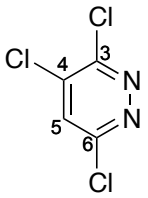

Phosphorus oxychloride (414 mL, 679 g, 2.22 mol, 8.0 eq) was added to 4-bromo-1,2-dihydropyridazine-3,6-dione **60** (53.3 g, 279 mmol, 1.0 eq), and the reaction mixture was heated under reflux for 4 h, after which time TLC analysis indicated complete consumption of **60**. After cooling, volatile components were removed *in vacuo*, and the resultant mixture was cooled and poured on to ice (350 g). The orange precipitate was collected by filtration, dissolved in diethyl ether (250 mL), and the organic layer was dried over magnesium sulfate. After filtration, the solvent was removed *in vacuo* to give 3,4,6-trichloropyridazine **61** (33.0 g, 65%) as a pale orange solid; R_f 0.27 (CH_2Cl_2/petroleum ether, 30:70); mp 52-54 °C (from $CHCl_3$) [Lit.[268] 51-52 °C (CH_2Cl_2/hexane)]; ν_{max} (thin film)/cm^{-1} 3090 (m), 3031 (m), 1534 (s), 1343 (s); ^{1}H NMR (400 MHz; $CDCl_3$) δ 7.68 (1H, s, C(5)*H*); ^{13}C NMR (126 MHz; $CDCl_3$) δ 155.2 (*C*(6)), 154.8 (*C*(3)), 138.9 (*C*(4)), 129.4 (*C*(5)H); *m/z* (EI/FI$^+$) 182 ([^{35}M-e]$^+$, 100%), 184 ([^{37}M–e]$^+$, 96%); HRMS *m/z* (EI/FI$^+$) [Found, (M–e)$^+$ 181.9208. $C_4H^{35}Cl^{35}Cl^{35}ClN_2$ requires M$^+$, 181.9205]; Anal. calcd for $C_4HCl_3N_2$: C, 26.2; H, 0.6; N, 15.3. Found: C, 26.1; H, 0.5; N 15.2. These data are in accordance with the literature values.[268]

4-Amino-3,6-dichloropyridazine (**62**)

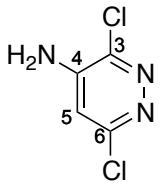

To a 10-20 mL MW vial were added 3,4,6-trichloropyridazine **61** (2.50 g, 13.7 mmol, 1.0 eq), followed by a 2 M solution of NH_3 in isopropanol (20.5 mL, 41.0 mmol, 3.0 eq) *via* syringe, and the reaction mixture was heated at 130 °C under microwave conditions for 4 h. (This procedure was repeated for the remaining 30.5 g (166 mmol) of 3,4,6-trichloropyridazine, then cooled to RT). The solvent was removed *in vacuo* and the residues were combined. The resulting light brown solid was purified by crystallisation from water to give *4-amino-3,6-dichloropyridazine* **62** (18.5 g, 63%) as a colourless crystalline solid: R_f 0.20 (ethyl acetate/petroleum ether, 20:80); mp 204-205 °C (from water); ν_{max} (solid)/cm^{-1} 3460 (m), 3293 (br), 3049 (m), 2963 (w), 1635 (m), 1562 (s), 1382 (s), 1124 (s), 1052 (s); ^{1}H NMR (400 MHz; D_6-DMSO) δ 7.18 (2H, br s, N*H*$_2$), 6.83 (1H, s, C(5)*H*); ^{13}C NMR (126 MHz; D_6-DMSO) δ 154.1 (*C*(6)), 145.8 (*C*(4)), 143.3 (*C*(3)), 108.0 (*C*(5)); *m/z* (ES^-) 162 ([M−H]$^-$, 100%); HRMS *m/z* (ES^-) [Found, $(M-H)^-$ 161.9628. $C_4H_2Cl_2N_3$ requires $(M-H)^-$, 161.9631]; Anal. calcd for $C_4H_3Cl_2N_3$: C, 29.4; H, 1.8; N, 25.6. Found: C, 29.4; H, 1.8; N 25.5.

6-Chloro-3-hydrazinylpyridazin-4-amine (**63**)

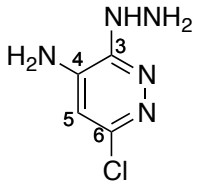

To 4-amino-3,6-dichloropyridazine **62** (18.5 g, 113 mmol, 1.0 eq) was added hydrazine monohydrate (340 mL, 347 g, 10.8 mol, 95.6 eq), and the reaction mixture was heated under reflux for 3 h, at which point TLC analysis indicated complete consumption of **62**. After cooling to RT, addition of water (170 mL) aided precipitation. The resultant crystalline solid was collected by filtration, washed with cold water and dried under reduced pressure to give *6-chloro-3-hydrazinylpyridazin-4-amine* **63** as a colourless crystalline solid (7.70 g, 43%): R_f 0.34 (reverse phase, water/methanol, 50:50); 189-190 °C (from ethanol); ν_{max} (solid)/cm^{-1} 3319 (br), 3101 (m), 3052 (m), 1576 (s), 1454 (s), 1275 (m), 1100 (m); ^{1}H NMR (400 MHz; D_6-DMSO) δ 7.30 (1H, br s, N*H*NH$_2$), 6.38 (1H, s, C(5)*H*), 6.28 (2H, br s, Ar-N*H*$_2$), 4.26 (2H, br s, NHN*H*$_2$); ^{13}C NMR (126 MHz; D_6-DMSO) δ 150.7 (*C*(6)), 146.7 (*C*(3)), 137.5 (*C*(4)), 103.9 (*C*(5)H); *m/z* (ES$^+$) 160 ([M+H]$^+$, 100%), 182 ([M+Na]$^+$, 21%); HRMS *m/z* (ES$^+$) [Found, (M+H)$^+$ 160.0379. $C_4H_7ClN_5$ requires M$^+$, 160.0384]; Anal. calcd for $C_4H_6ClN_5$: C, 30.1; H, 3.8; N, 43.9. Found: C, 30.2; H, 3.7; N, 43.8.

6-Chloro-3-methyl[1,2,4]triazolo[4,3-*b*]pyridazin-8-amine (**64**)

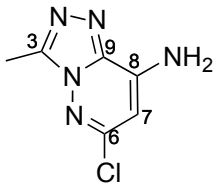

To 6-chloro-3-hydrazinylpyridazin-4-amine **63** (7.6 g, 47.6 mmol) was added AcOH (109 mL, 114 g, 1.91 mol, 40.1 eq), and the reaction mixture was heated under reflux for 5 h. At 100 °C a solution formed, and upon reaching reflux a colourless precipitate was observed. After 5 h the reaction suspension was cooled to RT and quenched with ice-cold water (150 mL) and the colourless precipitate was collected by filtration. The solid was purified by crystallisation from methanol (200 mL). Excess AcOH was removed by azeotropic distillation with toluene (1 L) to give *6-chloro-3-methyl[1,2,4]triazolo[4,3-b]pyridazin-8-amine* **64** (5.6 g, 64%) as a colourless solid: R_f 0.47 (methanol/CH_2Cl_2, 10:90); mp 203-205 °C (from methanol); ν_{max} (solid)/cm^{-1} 3370-3306 (br), 3147 (m), 1648 (m), 1600 (s), 1470 (m), 1423 (m), 1124 (m), 1056 (m); ^{1}H NMR (400 MHz; D_6-DMSO) 7.90 (2H, br s, N*H*$_2$), 6.11 (1H, s, C(7)*H*), 2.59 (3H, s, C*H*$_3$); ^{13}C NMR (126 MHz; D_6-DMSO) δ 149.3 (*C*(6)), 146.7 (*C*(3)), 143.9 (*C*(9)), 139.4 (*C*(8)), 93.6 (*C*(7)H), 9.46 (*C*H$_3$); *m/z* (ES^-) 182 ([M–H]$^-$, 100%), 218 ([M+Cl]$^-$, 10%); HRMS *m/z* (ES^-) [Found, (M–H)$^-$ 182.0236. $C_6H_5ClN_5$ requires M$^-$, 182.0239]; Anal. calcd for $C_6H_6ClN_5$: C, 39.3; H, 3.3; N, 38.1. Found: C, 39.4; H, 3.1; N, 38.0.

***tert*-Butyl-(6-chloro-3-methyl[1,2,4]triazolo[4,3-*b*]pyridazin-8-yl) carbamate** (**55**)

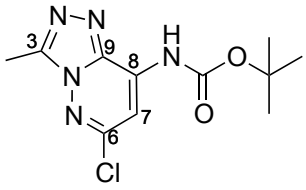

A solution of 6-chloro-3-methyl[1,2,4]triazolo[4,3-b]pyridazin-8-amine **64** (186 mg, 1.02 mmol, 1.0 eq), di-*tert*-butyl dicarbonate (334 mg, 1.53 mmol, 1.5 eq), and 4-DMAP (6.2 mg, 0.05 mmol, 0.05 eq) in THF (3.8 mL) was stirred at RT for 24 h. The solvent was removed *in vacuo* and the resulting solid was redissolved in ethyl acetate (30 mL), then washed with saturated aqueous NH_4Cl (2 × 30 mL), water (2 × 30 mL) and brine (30 mL). The organic layer was dried over magnesium sulfate, filtered, and concentrated *in vacuo*. The resultant solid (268 mg) was suspended in methanol (8 mL) and 2 M aqueous NaOH (2 mL). A colourless suspension formed, which was stirred at RT for 14 h. The mixture was neutralised with saturated aqueous NH_4Cl and extracted with ethyl acetate (3 × 50 mL). The organic extracts were combined, washed with water (2 × 150 mL), brine (100 mL), dried over magnesium sulfate, filtered, and concentrated *in vacuo* to give *tert-butyl-(6-chloro-3-methyl[1,2,4]triazolo[4,3-b]pyridazin-8-yl) carbamate* **55** (208 mg, 72%) as a colourless solid: R_f 0.32 (ethyl acetate/petroleum ether, 50:50); mp 129-131 °C (from ethyl acetate); ν_{max} (thin film)/cm^{-1} 3400 (m), 2981 (m), 2935 (m), 1737 (s), 1555 (s), 1244 (s), 1154 (s); ^{1}H NMR (400 MHz; $CDCl_3$) δ 8.12 (1H, br s, N*H*), 7.71 (1H, s, C(7)*H*), 2.79 (3H, s, CH_3), 1.57 (9H, s, (CH_3)$_3$); ^{13}C NMR (126 MHz; $CDCl_3$) δ 151.13 (*C*=O), 151.11 (*C*(6)), 148.2 (*C*(3)), 138.5 (*C*(8)), 134.8 (*C*(9)), 103.0 (*C*(7)H), 83.7 (*C*(CH_3)$_3$), 28.0 ((*C*H_3)$_3$), 9.8

(C(3)*C*H$_3$); *m/z* (ES$^+$) 284 ([M+H]$^+$, 91%), 306 ([M+H]$^+$, 100%), 589 ([2M+Na]$^+$, 68%), 872 ([3M+Na]$^+$, 24%); HRMS *m/z* (ES$^+$) [Found (M+Na)$^+$ 306.0728. $C_{11}H_{14}ClN_5NaO_2^+$ requires M$^+$, 306.0728]; Anal. calcd for $C_{11}H_{14}ClN_5O_2$: C, 46.6; H, 5.0; N, 24.7. Found: C 46.6; H, 5.1; N, 24.6.

***tert*-Butyl-(3-methyl-6-(3'-nitrophenyl)[1,2,4]triazolo[4,3-*b*]pyridazin-8-yl)carbamate** (**54**)

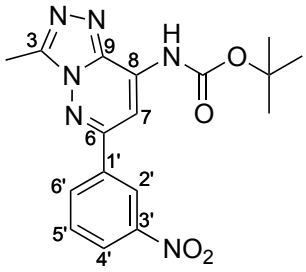

To each of six 10-20 mL MW vials were added *tert*-butyl-(6-chloro-3-methyl[1,2,4]triazolo[4,3-b]pyridazin-8-yl) carbamate **55** (300 mg, 1.06 mmol, 1 eq), K_2CO_3 (366 mg, 2.65 mmol, 2.5 eq), 3-nitrophenylboronic acid (443 mg, 2.65 mmol, 2.5 eq), and Pd(dppf)Cl_2·CH_2Cl_2 (87 mg, 106 µmol, 0.1 eq). 1,4-Dioxane and water (10:1, 20 mL), was added *via* syringe, and the reaction mixture was heated at 80 °C for 20 h. After cooling to RT the six reaction mixtures were combined, filtered through Celite® (eluent CH_2Cl_2), and concentrated *in vacuo*. The residue was redissolved in CH_2Cl_2 (200 mL), washed with water (200 mL), brine (200 mL), dried over sodium sulfate, filtered, and concentrated *in vacuo*. The residue was purified by silica gel column chromatography, eluting with petroleum ether, ethyl acetate and triethylamine (70:29:1, 40:59:1), to give *tert*-butyl-(3-methyl-6-(3'-nitrophenyl)[1,2,4]triazolo[4,3-*b*]pyridazin-8-yl)carbamate **54** (2.04 g, 86%) as a colourless solid: R_f 0.18 (petrol/ethyl acetate, 65:35); mp >250°C (from

$CHCl_3$); ν_{max} (thin film)/cm^{-1} 3401 (br), 2981 (m), 2935 (m), 1735 (s), 1566 (s), 1534 (s), 1348 (s), 1244 (s), 1150 (s); ^1H NMR (500 MHz; $CDCl_3$) δ 8.90 (1H, dd, *J* 2.2, 1.5, C(2')*H*), 8.43 (1H, br s, N*H*), 8.39 (1H, ddd, *J* 8.2, 2.2, 1.0, C(4')*H*), 8.34 (1H, ddd, *J* 7.9, 1.5, 1.0, C(6')*H*), 8.23 (1H, s, C(7)*H*), 7.73 (1H, dd, *J* 8.2, 7.9, C(5')*H*), 2.90 (3H, s, CH_3), 1.60 (9H, s, (CH_3)$_3$); ^{13}C NMR (126 MHz; $CDCl_3$) δ 153.5 (*C*(6)), 151.6 (*C*=O), 148.8 (*C*(3)), 148.6 (*C*(3')H), 138.8 (*C*(9)), 137.0 *C*(1'), 134.8 *C*(8), 133.2 (*C*(6')H), 130.1 (*C*(5')H), 125.1 (*C*(4')H), 122.4 (*C*(2')H), 99.9 (*C*(7)H), 83.5 (*C*(CH_3)$_3$), 28.1 ((*C*H_3)$_3$), 10.0 (C(3)*C*H_3); *m/z* (ES^+) 371 ([M+H]$^+$, 100%), 393 ([M+Na]$^+$, 84%); HRMS *m/z* (ES^+) [Found (M+Na)$^+$ 393.1268. $C_{17}H_{18}N_6NaO_4^+$ requires M^+, 393.1282]; Anal. calcd for $C_{17}H_{18}N_6O_4$: C, 55.1; H, 4.9; N, 22.7. Found: C, 54.8; H, 5.0; N, 22.8.

3-Methyl-6-(3'-nitrophenyl)[1,2,4]triazolo[4,3-*b*]pyridazin-8-amine (**53**)

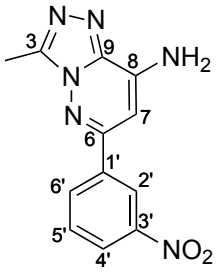

To a solution of **54** (778 mg, 2.10 mmol, 1.0 eq) in CH_2Cl_2 (40 mL) was added TFA (40 mL, 60 g, 520 mmol, 248 eq). The pale green solution was stirred at RT for 2.5 h, at which point TLC analysis indicated complete consumption of **54**. Excess TFA was removed by azeotropic distillation with toluene (50 mL). The crude material was redissolved in ethyl acetate (600 mL), washed with saturated aqueous $NaHCO_3$ (400 mL), water (500 mL), brine (400 mL), dried over sodium sulfate, filtered, and concentrated *in vacuo*, to afford *3-methyl-6-(3'-nitrophenyl)[1,2,4]triazolo[4,3-b]pyridazin-8-amine* **53** (431 mg, 76%) as a

yellow solid: R_f 0.20 (ethyl acetate/petrol/triethylamine, 70:29:1); mp >250 °C (from methanol); ν_{max} (thin film)/cm^{-1} 3470 (m), 3065 (m), 1648 (s), 1603 (w), 1566 (s), 1346 (s), 1243 (m); ^{1}H NMR (500 MHz; D$_6$-DMSO) δ 8.68 (1H, dd, *J* 1.0, 0.9, C(2')*H*), 8.38 (1H, ddd, *J* 6.7, 2.3, 1.0, C(6')*H*), 8.36 (1H, ddd, *J* , 6.9, 2.3, 0.9, C(4')*H*), 7.84 (1H, dd, *J* 6.9, 6.7, C(5')*H*), 7.67 (2H, br s, N*H*$_2$), 6.68 (1H, s, C(7)*H*), 2.90 (s, 3H, C*H*$_3$); ^{13}C NMR (126 MHz; D$_6$-DMSO) δ 152.1 (*C*(6)), 148.2 (*C*(3')), 147.1 (*C*(3)), 143.3 (*C*(8)), 139.8 (*C*(9)), 137.6 (*C*(1')), 133.1 (*C*(6')H), 130.6 (*C*(5')H), 124.5 (*C*(4')H), 121.2 (*C*(2')H), 91.7 (*C*(7)H), 9.6 (*C*H$_3$); *m/z* (ES$^-$) 269 ([M–H]$^-$, 100%), 305 ([M+Cl]$^-$, 28%); HRMS *m/z* (ES$^+$) [Found (M+H)$^+$ 271.0935. $C_{12}H_{11}N_6O_2^+$ requires M$^+$, 271.0938]; Anal. calcd for $C_{12}H_{10}N_6O_2$: 53.3; H, 3.7; N, 31.1. Found: C, 53.1; H, 3.7; N, 30.8.

_N_-(3-Methyl-6-(3'-nitrophenyl)[1,2,4]triazolo[4,3-*b*]pyridazin-8-yl)acetamide (**58**)

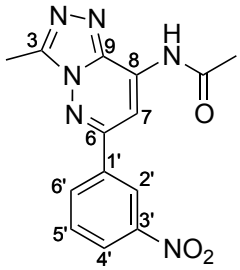

A suspension of 3-methyl-6-(3'-nitrophenyl)[1,2,4]triazolo[4,3-b]pyridazin-8-amine **53** (50 mg, 185 µmol, 1.0 eq) and 4-DMAP (23 mg, 185 µmol, 1 eq) in pyridine (5 mL) was stirred at RT for 10 min, before acetic anhydride (500 µL, 540 mg, 5.3 mmol, 29 eq) was added dropwise *via* syringe. The reaction mixture was stirred at RT for 24 h, then concentrated *in vacuo*. The residue was redissolved in ethyl acetate (10 mL), extracted with aqueous citric acid

(10% *w/v*), washed with brine, dried over sodium sulfate, filtered, and concentrated *in vacuo*. The resulting residue was purified by silica gel column chromatography, eluting with petroleum ether, ethyl acetate and triethylamine (50:49:1, 0:99:1). The resulting solid was purified by crystallisation from chloroform to furnish *N-(3-methyl-6-(3'-nitrophenyl)[1,2,4]triazolo[4,3-b]pyridazin-8-yl)acetamide* **58** (37 mg, 53%) as a colourless crystalline solid; R_f 0.27 (ethyl acetate/petrol/triethylamine, 50:49:1): mp >250 °C (from $CHCl_3$); ν_{max} (thin film)/cm^{-1} 3237 (m), 3200 (m), 3145 (m), 2924 (s), 2853 (m), 1710 (s), 1615 (m), 1529 (s), 1350 (s), 1229 (s); ^{1}H NMR (500 MHz; $CDCl_3$) δ 9.62 (1H, br s, N*H*), 8.90 (1H, dd, *J* 1.2, 0.8, C(2')*H*), 8.58 (1H, s, C(7)*H*), 8.40 (1H, ddd, *J* 8.8, 2.2, 0.8, C(4')*H*), 8.33 (1H, ddd, *J* 8.2, 2.2, 1.2, C(6')*H*), 7.75 (1H, dd, *J* 8.8, 8.2, C(5')*H*), 2.90 (3H, s, C(3)CH_3), 2.42 (3H, s, COCH_3); ^{13}C NMR (126 MHz; $CDCl_3$) 170.7 (*C*=O), 153.7 (*C*(6)), 148.8 (*C*(3)), 148.7 (*C*(3')), 139.0 (*C*(9)), 136.9 (*C*(1')), 134.0 (*C*(8)), 133.2 (*C*(6')), 130.1 (*C*(5')H), 125.2 (*C*(4')H), 122.4 (*C*(2')H), 102.3 (*C*(7)H), 24.9 (CO*C*H_3), 10.0 (C(3)*C*H_3); *m/z* (ES^-) 311 ($[M–H]^-$, 100%); HRMS *m/z* (ES^+) [Found $(M+Na)^+$ 335.0848. $C_{14}H_{12}N_6NaO_3^+$ requires M^+, 335.0863; Anal. calcd for $C_{14}H_{12}N_6O_3$: 53.9; H, 3.9; N, 26.9. Found: C, 53.7; H, 4.0; N, 26.8.

Ethyl (3-methyl-6-(3'-nitrophenyl)[1,2,4]triazolo[4,3-*b*]pyridazin-8-yl)carbamate (**57**)

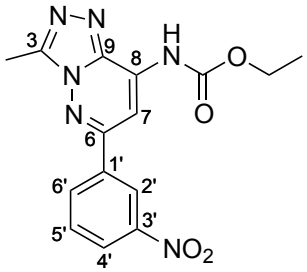

DMF (4 mL) was added to 3-methyl-6-(3'-nitrophenyl)[1,2,4]triazolo[4,3-b]pyridazin-8-amine **53** (100 mg, 370 μmol, 1 eq) and sodium hydride (60% dispersion in mineral oil) (31 mg, 780 μmol, 2.1 eq) at 4 °C. Ethylchloroformate (71 μL, 84 mg, 780 μmol, 2.1 eq) was added dropwise to the mixture *via* syringe. The reaction mixture was stirred for 2 h at 4 °C, then warmed to RT and stirred for 48 h, at which time saturated aqueous NH_4Cl (4 mL) was added, followed by ethyl acetate (4 mL). The resulting mixture was diluted with ethyl acetate (20 mL), and extracted with water (20 mL). The organic layer was washed with brine (20 mL), dried over sodium sulfate, filtered, and concentrated *in vacuo*. The resulting residue was purified by silica gel column chromatography, eluting with hexane, ethyl acetate and triethylamine (69:30:1, 59:40:1). Crystallisation of the chromatographed solid, from acetone, furnished *ethyl (3-methyl-6-(3'-nitrophenyl)[1,2,4]triazolo[4,3-b]pyridazin-8-yl)carbamate* **57** (12 mg, 10%) as a colourless crystalline solid: R_f 0.42 (hexane/ethyl acetate/triethylamine, 49:50:1); mp 240 °C dec. (from acetone); ν_{max} (solid)/cm^{-1} 3296 (br), 2988 (w), 1742 (s), 1568 (s), 1531 (s), 1378 (s), 1025 (m); ^{1}H NMR (500 MHz; $(CD_3)_2CO$) δ 9.42 (1H, N*H*), 8.88 (1H, dd, *J* 2.2, 1.6, C(2')*H*,), 8.47 (1H, ddd, *J* 7.9, 4.2, 1.6, C(6')*H*), 8.52 (1H, ddd, *J* 8.1, 4.2, 2.2, C(4')*H*), 8.30 (1H, s, C(7)*H*), 7.95 (1H, dd, 8.1, 7.9, C(5')*H*),

4.37 (2H, q, *J* 7.0, C*H*$_2$), 2.82 (3H, s, C(3)C*H*$_3$), 1.38 (3H, t, *J* 7.0 CH$_2$C*H*$_3$); ^{13}C NMR (126 MHz; (CD$_3$)$_2$CO) δ 154.2 (*C*=O), 153.7 (*C*(6)), 149.8 (*C*(3')), 148.8 (*C*(3)), 139.7 (*C*(8)), 138.3 (*C*(1')), 136.2 (*C*(9)), 134.2 (*C*(4')H), 131.6 (*C*(5')H), 125.8 (*C*(6')H), 122.7 (*C*(2')H), 100.6 (*C*(7)H), 63.1 (O*C*H$_2$), 14.6 (OCH$_2$*C*H$_3$), 9.8 (C(3)*C*H$_3$); *m/z* (ES$^+$) 341 ([M+H]$^+$, 100%); HRMS *m/z* (ES$^+$) [Found, 365.0960 (M+Na)$^+$. $C_{15}H_{14}N_6NaO_4^+$ requires M$^+$, 365.0969]; Anal. calcd for $C_{15}H_{14}N_6O_4$: C, 52.6; H, 4.1; N, 24.6. Found: C, 52.6; H, 4.1; N, 24.4.

***tert*-Butyl-(3-methyl-6-(phenylamino)[1,2,4]triazolo[4,3-*b*]pyridazin-8-yl)carbamate** (**44**)

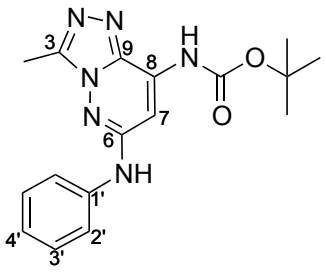

To each of three flame dried 10-20 mL MW vials were added *tert*-butyl-(6-chloro-3-methyl[1,2,4]triazolo[4,3-*b*]pyridazin-8-yl) carbamate **55** (500 mg, 1.76 mmol, 1.0 eq), (2-biphenyl)di-*tert*-butylphosphine (210 mg, 704 μmol, 0.4 eq), sodium *tert*-butoxide (237 mg, 2.46 mmol, 1.4 eq), and tris(dibenzylideneacetone)dipalladium(0) (161 mg, 176 μmol, 0.1 eq). Aniline **65** (650 μL, 660 mg, 7.1 mmol, 4.1 eq) was added *via* syringe, and the reaction mixture was heated at 80 °C for 21 h. After this time the reaction mixture was cooled to RT, diluted with CH_2Cl_2 (15 mL), and filtered through Celite® (eluent CH_2Cl_2). The solvent was removed *in vacuo*. The crude material from three batches were combined and purified by silica gel column chromatography, eluting with petroleum ether, ethyl acetate and triethylamine

(70:29:1, 50:49:1), to afford *tert-butyl-(3-methyl-6-(phenylamino)[1,2,4]triazolo[4,3-b]pyridazin-8-yl)carbamate* **44** (1.19 g, 66%) as a colourless solid: R_f 0.30 (ethyl acetate/petroleum ether, 60:40); mp 224-225 °C (from $CHCl_3$); ν_{max} (thin film)/cm^{-1} 3388 (m), 3287 (w), 3099 (m), 1736 (s), 1580 (m), 1496 (m), 1442 (m) 1176 (m); ^{1}H NMR (400 MHz; $CDCl_3$) δ 8.01 (1H, br s, N*H*), 7.66 (2H, d, *J* 7.8, C(2')*H*), 7.36 (2H, dd, *J* 7.8, 7.4, C(3')*H*), 7.31 (1H, s, C(7)*H*), 7.30 (1H, br s, N*H*), 7.08 (1H, t, *J* 7.4, C(4')*H*), 2.74 (3H, s, CH_3), 1.49 (9H, s, (CH_3)$_3$); ^{13}C NMR (126 MHz; $CDCl_3$) 153.1 (*C*(6)), 151.8 (C=O), 147.9 (*C*(3)), 139.6 (*C*(1')), 138.7 (*C*(9)), 133.4 (*C*(8)), 129.1 (*C*(3')H), 122.9 (*C*(4')H), 119.3 (*C*(2')H), 96.7 (*C*(7)H), 82.7 (*C*(CH$_3$)$_3$), 28.0 ((*C*H$_3$)$_3$), 9.9 (*C*H$_3$); *m/z* (ES$^+$) 341 ([M+H]$^+$, 72%), 363 ([M+Na]$^+$, 100%); HRMS *m/z* (ES$^+$) [Found, (M+Na)$^+$ 363.1534. $C_{17}H_{20}N_6NaO_2^+$ requires M$^+$, 363.1540]; Anal. calcd for $C_{17}H_{20}N_6O_2$: C, 60.0; H, 5.9; N, 24.7. Found: C, 59.9; H, 5.8; N, 24.6.

3-Methyl-*N*^{6}-phenyl[1,2,4]triazolo[4,3-*b*]pyridazine-6,8-diamine (**66**)

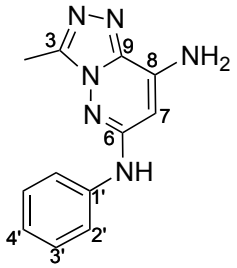

To a solution of *tert*-butyl-(3-methyl-6-(phenylamino)[1,2,4]triazolo[4,3-b]pyridazin-8-yl)carbamate **44** (850 mg, 2.50 mmol, 1 eq) in CH_2Cl_2 (40 mL) was added TFA (40 mL, 60 g, 520 mmol, 210 eq). The pale green solution was stirred at RT for 2 h, at which time TLC analysis indicated complete consumption of **44**. Excess TFA was removed by azeotropic distillation with

toluene (2 × 30 mL). The residue was redissolved in isopropanol/$CHCl_3$ (5:1, 600 mL), washed with saturated aqueous $NaHCO_3$ (400 mL), water (500 mL), brine (400 mL), dried over sodium sulfate, filtered, and concentrated *in vacuo*, to afford **66** (562 mg, 94%) as a colourless solid: R_f 0.30 (ethyl acetate/petrol/triethylamine, 60:39:1); mp 171-172 °C (from methanol); ν_{max} (solid)/cm^{-1} 3438 (m), 3378 (m), 3311 (m), 3145 (m) C-H, 1598 (m), 1578 (m), 1499 (s), 1309 (m), 1238 (m); ^{1}H NMR (500 MHz; D_6-DMSO) δ 9.03 (1H, br s, N*H*), 7.71 (2H, d, *J* 8.4, C(2')*H*), 7.30 (2H, dd, *J* 8.4, 7.5, C(3')*H*), 7.02 (2H, br s, NH_2), 6.93 (1H, t, *J* 7.5 C(4')*H*), 5.87 (1H, s, C(7)*H*), 2.57 (3H, s, CH_3); ^{13}C NMR (126 MHz; D_6-DMSO) δ 153.8 (*C*(6)), 146.0 (*C*(3)), 141.7 (*C*(8)), 141.2 (*C*(1')), 139.4 (*C*(9)), 128.7 (*C*(3')H), 120.8 (*C*(4')H), 118.2 (*C*(2')H), 86.7 (*C*(7)H), 9.5 (*C*H_3); *m/z* (ES^+) 241 ($[M+H]^+$, 100%), 263 ($[M+Na]^+$, 46%); HRMS *m/z* (ES^+) [Found, $(M+H)^+$ 241.1196. $C_{12}H_{13}N_6^+$ requires M^+, 241.1196]; HPLC (method 1) retention time 11.20 min, purity 100%.

***tert*-Butyl-(3-methyl-6-(1-methyl-1*H*-indazol-4-yl)[1,2,4]triazolo[4,3-*b*]pyridazin-8-yl)carbamate** (**67**)

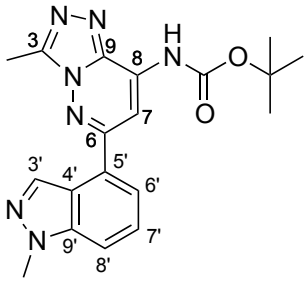

To a 2-5 mL MW vial containing *tert*-butyl-(6-chloro-3-methyl[1,2,4]triazolo[4,3-*b*]pyridazin-8-yl)carbamate **55** (50 mg, 180 μmol, 1.0 eq) was added 1-methyl-1*H*-indazole-4-boronic acid pinacol ester (91 mg, 350 μmol, 2.0 eq), K_2CO_3 (49 mg, 350 μmol, 2.0 eq) and Pd(dppf)Cl_2·CH_2Cl_2

(14 mg, 18 μmol, 0.1 eq). A solution of 1,4-dioxane/water (10:1, 2 mL) was added *via* syringe and the reaction mixture was heated at 80 °C for 20 h. After cooling to RT the reaction mixture was filtered through Celite® (eluent CH_2Cl_2) and concentrated *in vacuo*. The residue was redissolved in CH_2Cl_2 (20 mL), washed with water (20 mL), then brine (20 mL), dried over sodium sulfate, filtered, and concentrated *in vacuo*. The crude material was purified by silica gel column chromatography, eluting with ethyl acetate and isohexane (20:80, 30:70, 40:60, 50:50, 60:40, 70:30, 80:20, 90:10, 100:0) to afford *tert-butyl-(3-methyl-6-(1-methyl-*1*H-indazol-4-yl)[1,2,4]triazolo[4,3-b]pyridazin-8-yl)carbamate* **67** (10 mg, 15%) as a colourless solid: R_f 0.79 (methanol/ethyl acetate/triethylamine, 20:79:1); mp 191-193 °C (from ethyl acetate); ν_{max} (thin film)/cm^{-1} 3452 (m), 3369 (w), 2981 (w), 2938 (w), 1734 (m), 1724 (m), 1566 (s), 1546 (s), 1478 (m), 1398 (m), 1372 (m), 1311 (s), 1155 (s); ^{1}H NMR (400 MHz; $CDCl_3$) δ 8.63 (1H, s, C(3')*H*), 8.34 (1H, s, C(7)*H*), 8.29 (1H, br s, N*H*), 7.73 (1H, d, *J* 6.9, C(6')*H*), 7.52 (1H, d, *J* 8.4, C(8')*H*), 7.50 (1H, dd, *J* 8.4, 6.9, C(8')*H*), 4.16 (3H, s, NCH_3), 2.92 (3H, s, C(3)CH_3), 1.59 (9H, s, (CH_3)$_3$); ^{13}C NMR (101 MHz; $CDCl_3$) δ 155.4 (*C*(6)), 151.8 (*C*=O), 148.6 (*C*(3)), 140.7 (*C*(9')), 139.1 (*C*(9)), 134.1 (*C*(8)), 133.9 (*C*(3')H), 128.6 (*C*(5')), 126.2 (*C*(7')H), 121.5 (*C*(6')H), 121.4 (*C*(4')), 111.8 (*C*(8')H), 101.3 (*C*(7)H), 83.2 (*C*(CH$_3$)$_3$), 28.2 (C(*C*H$_3$)$_3$, 10.1 (C(3)*C*H$_3$); *m/z* (ES$^+$) 324 [100%], 380 [(M+H)$^+$, 85%]; HRMS *m/z* (ES$^+$) [Found (M+H)$^+$ 380.1823. $C_{19}H_{22}N_7O_2^+$ requires M$^+$, 380.1829]; HPLC (method 2) pH 10 retention time 2.23 min, purity 100%, pH 3 retention time 2.22 min, purity 100%.

***tert*-Butyl-(6-(isoquinolin-5-yl)-3-methyl-[1,2,4]triazolo[4,3-*b*]pyridazin-8-yl)carbamate** (**68**)

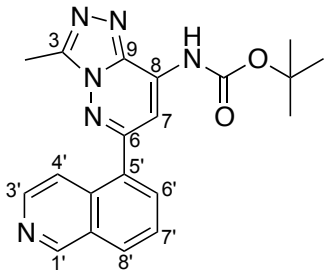

To a 2-5 mL MW vial were added *tert*-butyl-(6-chloro-3-methyl-[1,2,4]triazolo[4,3-*b*]pyridazin-8-yl)carbamate **55** (50 mg, 176 μmol, 1.0 eq), K_2CO_3 (36 mg, 264 μmol, 1.5 eq), 4-isoquinolineboronic acid (76 mg, 440 μmol, 2.5 eq) and Pd(dppf)Cl_2·CH_2Cl_2 (14 mg, 18 μmol, 0.1 eq). 1,4-Dioxane and water (10:1, 1.5 mL) was added *via* syringe and the reaction mixture was heated at 80 °C for 20 h. After cooling to RT the reaction mixture was filtered through Celite® (eluent CH_2Cl_2) and concentrated *in vacuo*. The residue was redissolved in CH_2Cl_2 (100 mL), washed with water (2 × 100 mL) and brine (100 mL), dried over sodium sulfate, filtered, and concentrated *in vacuo*. The crude material was purified by preparative HPLC to give *tert-butyl-(6-(isoquinolin-5-yl)-3-methyl-[1,2,4]triazolo[4,3-b]pyridazin-8-yl)carbamate* **68** (7 mg, 11%) as a colourless solid: R_f 0.52 (methanol/ethyl acetate/triethylamine, 4:95:1); mp 139-141 °C (from $CHCl_3$); ν_{max} (thin film)/cm^{-1} 3388 (br, w), 3139 (br, w), 2976 (w), 2932 (w), 2188 (w), 2166 (m), 2100 (m), 2050 (m), 1992 (m), 1973 (m), 1737 (s), 1623 (w), 1377 (m), 1265 (m), 1244 (s), 1155 (s), 1128 (m); ^{1}H NMR (500 MHz; $CDCl_3$) δ 9.36 (1H, s, C(1')*H*), 8.60 (1H, d, *J* 6.1, C(3')*H*), 8.26 (1H, br s, N*H*), 8.14 (1H, d, *J* 8.1, C(8')*H*), 7.97 (1H, s, C(7)*H*), 7.96 (1H, d, *J* 6.1, C(4')*H*), 7.95 (1H, d, *J* 7.3, C(6')*H*), 7.74 (1H, dd, *J* 8.1, 7.3, C(7')*H*), 2.85 (3H, s, C(3)CH_3), 1.55 (9H, s,

C(CH_3)$_3$); ^{13}C NMR (126 MHz; $CDCl_3$) δ 155.8 (*C*(6)), 153.2 (*C*(1')H), 151.5 (*C*=O), 148.6 (*C*(3)), 144.4 (*C*(3')H), 139.0 (*C*(9)), 134.2 (*C*(8)), 133.5 (C(1)*C*C(8)), 133.0 (*C*(5')), 132.1 (*C*(6')H), 130.0 (*C*(8)H), 128.9 (C(4)*C*C(5)), 126.7 (*C*(7')H), 117.8 (*C*(4')H), 103.6 (*C*(7)H), 83.3 (*C*(CH_3)$_3$), 28.1 ((*C*H_3)$_3$), 10.0 (C(3)*C*H_3); *m/z* (ES^+) 377 [$(M+H)^+$, 100%], 399 [$(M+Na)^+$, 10%]; HRMS *m/z* (ES^+) [Found $(M+H)^+$ 377.1711. $C_{20}H_{21}N_6O_2^+$ requires M^+, 377.1721]; HPLC (method 2) pH 10 retention time 2.20 min, purity 93.8%; pH 3 retention time 1.98 min, purity 93.6%.

tert-Butyl-(3-methyl-6-(quinolin-5-yl)-[1,2,4]triazolo[4,3-*b*]pyridazin-8-yl)carbamate (**69**)

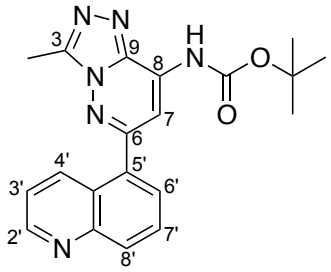

To a 2-5 mL MW vial was added *tert*-butyl-(6-chloro-3-methyl-[1,2,4]triazolo[4,3-*b*]pyridazin-8-yl)carbamate **55** (50 mg, 0.176 mmol, 1.0 eq), K_2CO_3 (36 mg, 0.264 mmol, 1.5 eq), 5-quinolineboronic acid (76 mg, 0.440 mmol, 2.5 eq) and Pd(dppf)Cl_2·CH_2Cl_2 (14 mg, 0.018 mmol, 0.1 eq). Dioxane and water (10:1, 1.5 mL) was added *via* syringe and the reaction mixture was heated at 80 °C for 20 h. After cooling to RT the reaction mixture was filtered through Celite® (eluent CH_2Cl_2) and concentrated *in vacuo*. The residue was redissolved in CH_2Cl_2 (100 mL), washed with water (2 × 100 mL) and brine (100 mL), dried over sodium sulfate, filtered, and concentrated *in vacuo*. The crude material was purified by preparative HPLC to give **69** (8 mg,

12%) as a colourless solid: R_f 0.42 (methanol/ethyl acetate/triethylamine, 4:95:1); mp >250 °C (from $CHCl_3$); ν_{max} (thin film)/cm^{-1} 3364 (br, w), 3088 (br, w), 2976 (w), 2963 (w), 2932 (w), 1733 (m), 1601 (w), 1534 (m), 1504 (m), 1479 (m), 1466 (m), 1456 (m), 1409 (m), 1391 (m), 1370 (m), 1346 (m), 1317 (m), 1303 (m), 1242 (s), 1158 (m), 1119 (s); ^{1}H NMR (500 MHz; $CDCl_3$) δ 9.00 (1H, dd, *J* 4.1, 1.6, C(2')*H*), 8.49 (1H, dd, *J* 8.6, 1.6, C(4')*H*), 8.27 (1H, dd, *J* 8.2, 1.4, C(8')*H*), 8.22 (1H, br s, N*H*), 7.93 (1H, s, C(7)*H*), 7.83 (1H, dd, *J* 8.2, 7.2, C(7')*H*), 7.80 (1H, dd, *J* 7.2, 1.4, C(6')*H*), 7.47 (1H, dd, *J* 8.6, 4.1, C(3')*H*), 2.84 (3H, s, C(3)CH_3), 1.55 (9H, s, C(CH_3)$_3$); ^{13}C NMR (126 MHz; $CDCl_3$) δ 156.1 (*C*(6)), 151.5 (*C*=O), 150.8 (*C*(2')H), 148.5 (N*C*C(8)), 148.4 (*C*(3)), 139.0 (*C*(9)), 134.16 (*C*(8)), 134.12 (*C*(5')), 133.5 (*C*(4)H), 131.8 (*C*(8)H), 128.8 (*C*(7)H), 128.4 (*C*(6)H), 126.1 (C(4')*C*C(5')), 122.0 (*C*(3)H), 103.8 (*C*(7)H), 83.3 (*C*(CH_3)$_3$), 28.1 ((*C*H_3)$_3$), 10.0 (C(3)*C*H_3); *m/z* (ES^+) 377 [$(M+H)^+$, 100%], 399 [$(M+Na)^+$, 10%]; HRMS *m/z* (ES^+) [Found $(M+H)^+$ 377.1714. $C_{20}H_{21}N_6O_2^+$ requires M^+, 377.1721.]; HPLC: (method 2) pH 10 retention time 2.17 min, purity 93.7%; pH 3 retention time 2.10 min, purity 93.8%.

1'-Methyl-4'-(2-nitro-4-bromophenyl)piperazine (**73**)

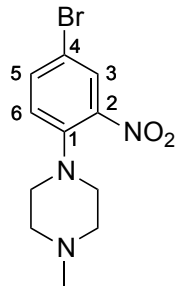

To a solution of 2,5-dibromonitrobenzene **72** (3.00 g, 10.7 mmol, 1.0 eq) in isopropanol (12 mL), was added 1-methylpiperazine (2.40 mL, 2.17 g, 21.7 mmol, 2.0 eq) and triethylamine (1.80 mL, 1.31 g, 12.9 mmol, 1.2 eq). The reaction mixture was heated under reflux for 11 h, after which time TLC analysis indicated complete consumption of **72**. The solvents were removed *in vacuo*, and the residue was redissolved in CH_2Cl_2 (100 mL) and washed with water (2 × 100 mL). The organic layer was washed with brine, dried over sodium sulfate, filtered, and concentrated *in vacuo*, furnishing *1'-methyl-4'-(2-nitro-4-bromophenyl)piperazine* **73** as an orange oil (3.11 g, 97%): R_f 0.44 (methanol/CH_2Cl_2, 10:90); ν_{max} (thin film)/cm^{-1} 2939 (m), 1600 (m), 1522 (s), 1344 (s), 1234 (m), 1142 (m); ^{1}H NMR (400 MHz; $CDCl_3$) δ 7.89 (1H, d, *J* 2.3, C(3)*H*), 7.56 (1H, dd, *J* 8.9, 2.3, C(5)*H*), 7.02 (1H, d, *J* 8.9, C(6)*H*), 3.07 (4H, t, *J* 4.5, ArNCH_2), 2.57 (4H, t, *J* 4.5, ArNCH$_2$CH_2), 2.35 (3H, s, CH_3); ^{13}C NMR (500 MHz; $CDCl_3$) δ 145.0 (*C*(1)), 143.3 (*C*(2)), 136.3 (*C*(5)), 128.6 (*C*(3)), 122.5 (*C*(6)), 113.2 (*C*(4)), 54.8 (ArNCH$_2$*C*H$_2$), 51.5 (ArN*C*H$_2$), 46.0 (*C*H$_3$); *m/z* (ES$^+$) 300 ([^{79}M+H]$^+$, 98%), 302 ([^{81}M+H]$^+$, 100%), 322 ([^{79}M+Na]$^+$, 8%), 324 ([^{81}M+Na]$^+$, 8%); HRMS *m/z* (ES$^+$) [Found, (M+H)$^+$ 300.0346, 302.0325; $C_{11}H_{15}{}^{79}BrN_3O_2$ requires M$^+$, 300.0342; $C_{11}H_{15}{}^{81}BrN_3O_2$ requires M$^+$, 302.0322]; Anal. calcd for $C_{11}H_{14}BrN_3O_2$: C 44.0; H, 4.7; N, 14.0; Found C 44.1; H, 4.8; N, 14.0.

1'-Methyl-4'-(2-nitro-4-(4'',4'',5'',5''-tetramethyl-1'',3'',2''-dioxaborolan-2''-yl)phenyl)piperazine (**74**)

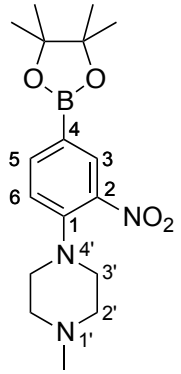

A solution of 1'-methyl-4'-(2-nitro-4-bromophenyl)piperazine **73** (10.4 g, 34.6 mmol, 1.0 eq) in 1,4-dioxane and DMSO (30:1, 200 mL) was added to bispinacolato diboron (8.8 g, 35 mmol, 1.0 eq), potassium acetate (8.48 g, 86.5 mmol, 2.5 eq), and Pd(dppf)Cl_2·CH_2Cl_2 (1.42 g, 1.73 mmol, 0.05 eq). The reaction mixture was heated at 109 °C for 13 h then cooled to RT, filtered, through Celite® (eluent CH_2Cl_2), and concentrated *in vacuo*. The residue was redissolved in CH_2Cl_2 (1 L) and washed with brine (2 × 1 L), dried over sodium sulfate, filtered, and concentrated *in vacuo*. The crude material was passed through a plug of neutral activated aluminum oxide (Brockmann I), eluting with ethyl acetate, to afford *1'-methyl-4'-(2-nitro-4-(4'',4'',5'',5''-tetramethyl-1'',3'',2''-dioxaborolan-2''-yl)phenyl)piperazine* **74** (5.38 g, 45%) as a dark yellow oil: R_f 0.43 (methanol/ethyl acetate/triethylamine, 30:69:1); ν_{max} (thin film)/cm^{-1} 2978 (w), 2938 (w), 2842 (w), 2699 (w), 1610 (s), 1530 (m), 1504 (m), 1356 (s), 1293 (m), 1268 (m), 1237 (m), 1141 (s); ^{1}H NMR (500 MHz; ($CDCl_3$) δ 8.17 (1H, d, *J* 1.5, C(3)*H*), 7.83 (1H, dd, *J* 8.3, 1.5, C(5)*H*), 7.05 (1H, d, *J* 8.3, C(6)*H*), 3.14 (4H, t, *J* 4.9, $CH_3NCH_2CH_2$), 2.57 (4H, t, *J* 4.9, $CH_3NCH_2CH_2$), 2.35 (3H, s, NCH_3); ^{13}C NMR (126 MHz; $CDCl_3$) δ

147.6 (*C*(1)), 141.8 (*C*(2)), 139.6 (*C*(5)H), 132.7 (*C*(3)H), 121.1 (*C*(4)), 119.3 (*C*(6)H), 84.1 (*C*CH_3), 54.7 (ArNCH$_2$*C*H$_2$), 50.9 (ArNCH$_2$), 46.0 (N*C*H$_3$), 24.8 (C*C*H$_3$); ^{11}B NMR (160 MHz; $CDCl_3$) δ 30.2 (br s); *m/z* (ES^+) 348 ($[M+H]^+$, 100%); HRMS *m/z* (ES^+) [Found, 348.2090 $(M+H)^+$. $C_{17}H_{27}BN_3O_4^+$ requires M^+, 348.2092]; Anal. calcd for $C_{17}H_{26}BN_3O_4$: C, 58.8; H, 7.6; N, 12.1. Found: C, 58.7; H, 7.7; N, 12.0.

1'-Methyl-4'-(2-nitro-4-(tributylstannyl)phenyl)piperazine (**75**)

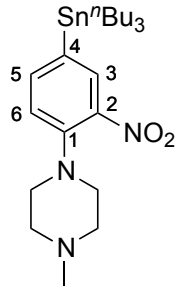

To each of two 10-20 mL MW vials was added $Pd(PPh_3)_4$ (300 mg, 260 μmol, 0.05 eq) followed by a solution of 1'-methyl-4'-(2-nitro-4-bromophenyl)piperazine **73** (1.57 g, 5.20 mmol, 1 eq) in toluene (12 mL). Bis(tributyltin) (4.0 mL, 4.6 g, 7.9 mmol, 1.5 eq) was added *via* syringe, and each reaction vessel was heated at 114 °C for 44 h, then cooled to RT. The reaction mixtures were combined, filtered through Celite® (eluent CH_2Cl_2) and stirred vigorously in saturated aqueous KF solution (30 mL) for 2 h. The mixture was then diluted with CH_2Cl_2 (600 mL), washed with water (2 × 400 mL), brine (400 mL), dried over sodium sulfate, filtered, and concentrated *in vacuo* to give a dark green oil. This oil was purified by silica gel column chromatography, eluting with ethyl acetate, petroleum ether and triethylamine (5:94:1, 20:79:1) to afford *1'-methyl-4'-(2-nitro-4-(tributylstannyl)phenyl)piperazine* **75** (1.34 g, 25%) as a yellow oil: R_f 0.23

(ethyl acetate/petrol/triethylamine, 20:79:1); ν_{max} (thin film)/cm^{-1} 2957 (s), 2927 (s), 2850 (s), 1593 (s), 1520 (s), 1456 (m), 1375 (s), 1344 (m), 1264 (m), 1236 (m); ^{1}H NMR (500 MHz; $CDCl_3$) δ 7.76 (1H, d, *J* 1.2, C(3)*H*), 7.53 (1H, dd, *J* 7.5, 1.2, C(5)*H*), 7.11 (1H, d, *J* 7.5, C(6)*H*), 3.12 (4H, t, *J* 4.5, ArNCH_2), 2.62 (4H, t, *J* 4.5, ArNCH$_2$CH_2), 2.38 (3H, s, NCH_3), 1.54-1.51 (6H, m, SnCH$_2$CH_2), 1.36-1.31 (6H, m, CH_2CH$_3$), 1.08-1.05 (6H, m, SnCH_2), 0.90 (9H, t, *J* 7.3, CH$_2$CH_3); ^{13}C NMR (126 MHz; $CDCl_3$) δ 145.3 (*C*(2)), 143.5 (*C*(1)), 141.3 (*C*(5)H), 135.2 (*C*(4)), 132.8 (*C*(3)H), 120.3 (*C*(6)H), 54.9 (ArNCH$_2$*C*H$_2$), 51.3 (ArN*C*H$_2$), 45.8 (*C*(1')), 28.9 (SnCH$_2$*C*H$_2$), 27.3 (CH_2CH$_3$), 13.6 (CH$_2$*C*H$_3$), 9.8 (SnCH_2); ^{19}Sn NMR (187 MHz; $CDCl_3$) δ −35.0; *m/z* (ES$^+$) 512 ([^{120}M+H]$^+$, 100%), 510 ([^{118}M+H]$^+$, 71%); HRMS *m/z* (ES$^+$) [Found (^{120}M+H)$^+$ 512.2294. $C_{23}H_{42}N_3O_2{}^{120}Sn^+$ requires M$^+$, 512.2298]; Anal. calcd for $C_{23}H_{41}N_3O_2Sn$: C, 54.1; H, 8.1; N, 8.2. Found: C, 54.2; H, 8.2; N 8.3.

***tert*-Butyl-(3-methyl-6-(4'-(4''-methylpiperazin-1-yl)-3'-nitrophenyl)[1,-2,4]triazolo[4,3-*b*]pyridazin-8-yl)carbamate** (**70**)

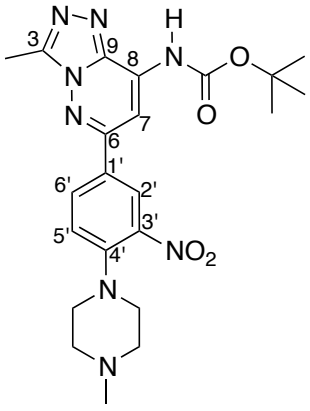

To a 10-20 mL MW vial containing 1'-methyl-4'-(2-nitro-4-(4'',4'',5'',5''-tetramethyl-1'',3'',2''-dioxaborolan-2''-yl)phenyl)piperazine **74** (920 mg,

2.65 mmol, 2.5 eq) were added 3-methyl-6-(3'-nitrophenyl)[1,2,4]triazolo[4,3-b]pyridazin-8-amine **55** (300 mg, 1.06 mmol, 1 eq), $Pd(dppf)Cl_2 \cdot CH_2Cl_2$ (90 mg, 110 μmol, 0.1 eq), and K_2CO_3 (220 mg, 1.59 mmol, 1.5 eq). The reaction mixture was heated at 80 °C for 21 h then cooled to RT, filtered through Celite® (eluent CH_2Cl_2), and concentrated *in vacuo*. The residue was redissolved in CH_2Cl_2 (50 mL), washed with brine (50 mL), dried over sodium sulfate, filtered, and concentrated *in vacuo*. The crude material was purified by silica gel column chromatography, eluting with ethyl acetate, petroleum ether and triethylamine (10:89:1, 30:69:1, 40:59:1, 50:49:1, 60:39:1, 70:29:1, 80:19:1, 90:9:1, 99:0:1), to afford *tert-butyl-(3-methyl-6-(4'-(4''-methylpiperazin-1-yl)-3'-nitrophenyl)[1,2,4]triazolo[4,3-b]pyridazin-8-yl)carbamate* **70** (405 mg, 65%) as an orange solid: R_f 0.64 (methanol/CH_2Cl_2/triethylamine, 10:89:1); mp 192-194 °C (from $CHCl_3$); ν_{max} (thin film)/ cm^{-1} 3400-3500 (w), 2963 (m), 2929 (br), 2850 (m), 2799 (m), 1809 (s), 1614 (m), 1568 (m), 1531 (s), 1371 (m), 1260 (m), 1241 (m) 1150 (s), 1091 (s), 1010 (s); ^{1}H NMR (500 MHz; $CDCl_3$) δ 8.47 (1H, d, *J* 2.2, C(2')*H*), 8.15 (1H, br s, N*H*), 8.11 (1H, dd, *J* 8.6, 2.2, C(6')*H*), 8.10 (1H, s, C(7)*H*), 7.22 (1H, d, *J* 8.6, C(5')*H*), 3.25 (4H, t, *J* 2.2, ArNCH_2), 2.68 (4H, t, *J* 2.2, $ArNCH_2CH_2$), 1.58 (9H, s, $(CH_3)_3$); ^{13}C NMR (126 MHz; $CDCl_3$) δ 153.1 (*C*(6)), 151.6 (*C*=O), 148.5 (*C*(3)), 146.9 (*C*(3')), 142.1 (*C*(4')), 139.0 (*C*(1')), 134.4 (*C*(8)), 127.9 (*C*(9)), 125.3 (*C*(2')H), 120.6 (*C*(5')H), 99.3 (*C*(7)H), 83.2 ($C(CH_3)_3$), 54.6 ($ArNCH_2CH_2$), 50.8 ($ArNCH_2$), 45.8 (NCH_3), 28.1 ($(CH_3)_3$), 9.9 (C(3)CH_3); *m/z* (ES^+) 469 ($[M+H]^+$, 100%); HRMS m/z (ES^+) found $(M+H)^+$ 469.2309. $C_{22}H_{29}N_8O_4^+$ requires 469.2306; Anal. calcd for $C_{22}H_{28}N_8O_4$: C, 56.4; H, 6.0; N, 23.9. Found: C, 56.3; H, 5.9; N, 23.8.

5-Bromo-2-hydrazinyl-3-nitropyridine (**78**)

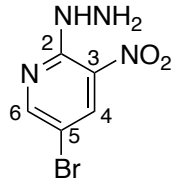

Ethanol (12 mL) was added to 5-bromo-2-chloro-3-nitropyridine **77** (1.00 g, 4.22 mmol, 1.0 eq) and the mixture was sonicated for 2 min to give a pale yellow solution. Hydrazine monohydrate (1.2 mL, 1.24 g, 24.8 mmol, 5.9 eq) was added and immediately an orange precipitate began to form. The mixture was stirred for 1 h at RT, then filtered. The orange solid was washed with ethanol (8 mL), water (5 mL) and diethyl ether (10 mL), then dried *in vacuo* to give *5-bromo-2-hydrazinyl-3-nitropyridine* **78** (868 mg, 88%) as an orange crystalline solid: R_f 0.55 (hexane/ethyl acetate, 80:20); mp 143-144 °C (from $CHCl_3$); ν_{max} (thin film)/cm^{-1} 3321-3290 (m), 3074 (m), 1603 (s), 1551 (s), 1508 (m), 1485 (m), 1412 (m), 1366 (m), 1321 (m), 1229 (s), 1148 (w), 1111 (w); ^{1}H NMR (400 MHz; $CDCl_3$) 8.97 (br s, N*H*), 8.56 (1H, d, *J* 1.9, C(4)*H*), 8.51 (1H, d, *J* 1.9, C(6)*H*), 4.26 (2H, br s, NH_2); ^{13}C NMR (126 MHz; $CDCl_3$) δ 156.1 (*C*(6)H), 152.2 *C*(2), 137.0 (*C*(4)H), 127.9 (*C*(3)), 105.4 (*C*(5)); *m/z* (EI/FI$^+$) 232.0 (^{79}[M−e]$^+$, 100%), 234.0 ([^{81}M−e]$^+$, 98%); HRMS *m/z* (EI/FI$^+$) [Found, (M−e)$^+$ 231.9607, 233.9601. $C_5H_5{}^{79}BrN_4O_2{}^+$ requires M$^+$, 231.9596; $C_5H_5{}^{81}BrN_4O_2{}^+$ requires M$^+$, 233.9601]; Anal. calcd for $C_5H_5BrN_4O_2$: C, 25.8; H, 2.2; N, 24.0. Found: C, 25.7; H, 2.2; N, 23.9.

***N'*-(5-Bromo-3-nitropyridin-2-yl)acetohydrazide** (**79**)

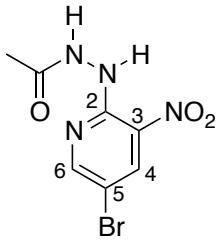

To a suspension of 5-bromo-2-hydrazinyl-3-nitropyridine **78** (500 mg, 2.15 mmol, 1 eq) in CH_2Cl_2 (2.5 mL) at 0 °C was added a solution of CH_2Cl_2 (2.5 mL), triethylamine (299 µL, 217 mg, 2.15 mmol, 1.0 eq), and acetic anhydride (405 µL, 437 mg, 4.29 mmol, 2.0 eq) dropwise over 30 min, after which time a yellow precipitate had formed. The reaction mixture was warmed to RT, filtered, and the solid washed with CH_2Cl_2 (4 mL) to give *N'-(5-bromo-3-nitropyridin-2-yl)acetohydrazide* **79** (375 mg, 64%) as a yellow solid: R_f 0.33 (hexane/ethyl acetate, 80:20); mp 170-172 °C (from $CHCl_3$); ν_{max} (thin film)/cm^{-1} 3321-3250 (m), 3075 (m), 1675 (s), 1603 (s), 1557 (m), 1539 (m), 1475 (s), 1364 (m), 1349 (m), 1315 (w), 1241 (s), 1216 (s); ^{1}H NMR (500 MHz; $CDCl_3$) δ 9.70 (1H, br s, N*H*), 8.60 (1H, d, *J* 2.2, C(4)*H*), 8.47 (1H, d, *J* 2.2, C(6)*H*), 8.05 (1H, br s, N*H*), 2.17 (3H, s, CH_3); ^{13}C NMR (126 MHz; $CDCl_3$) 167.8 (*C*=O), 155.6 (*C*(6)H), 149.0 (*C*(2)), 137.1 (*C*(4)H), 128.7 (*C*(3)), 107.7 (*C*(5), 20.9 (*C*H_3); *m/z* (ES^-) 273 ([^{79}M–H]$^-$, 100%), 275 ([^{81}M–H]$^-$, 95%); HRMS *m/z* (ES^+) [Found, $(M+Na)^+$ 296.9596, 298.9580. $C_7H_7{}^{79}BrN_4NaO_3^+$ requires M^+ 296.9594; $C_7H_7{}^{81}BrN_4NaO_3^+$ requires 298.9574]; Anal. calcd for $C_7H_7BrN_4O_3$: C, 30.6; H, 2.6; N, 20.4. Found: C, 30.4; H, 2.6; N, 20.2.

6-Bromo-3-methyl-8-nitro[1,2,4]triazolo[4,3-*a*]pyridine (**80**)

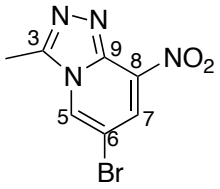

To a 2-5 mL MW vial containing *N*'-(5-bromo-3-nitropyridin-2-yl)acetohydrazide **79** (372 mg, 1.35 mmol, 1 eq), was added AcOH (3.70 mL, 3.89 g, 3.89 mmol, 48.0 eq). The reaction mixture was heated at 180 °C under microwave conditions for 1.5 h then concentrated *in vacuo.* Excess AcOH was removed by azeotropic distillation with toluene (5 × 30 mL) to give *6-bromo-3-methyl-8-nitro[1,2,4]triazolo[4,3-a]pyridine* **80** (330 mg, 95%) as a brown powdery solid: R_f 0.81 (ethyl acetate); mp 181-184 °C (from $CHCl_3$); ν_{max} (thin film)/cm^{-1} 3086 (w), 3067 (m), 1624 (m), 1536 (s), 1492 (m), 1477 (s), 1437 (m), 1348 (s), 1301 (s), 1273 (s), 1195 (w), 1101 (m), 1028 (m); ^{1}H NMR (500 MHz; $CDCl_3$) δ 9.77 (1H, d, *J* 1.7, C(5)*H*), 8.77 (1H, d, *J* 1.7, C(7)H), 2.57 (3H, s, CH_3); ^{13}C NMR (126 MHz; $CDCl_3$) δ 165.6 (*C*(3)), 144.1 (*C*(9)), 135.5 (*C*(5)H), 135.0 (*C*(8)), 131.2 (*C*(7)H), 104.2 (*C*(6)), 13.5 (*C*H_3); *m/z* (ES^+) 257 ([^{79}M+H]$^+$, 100%), 259 ([^{81}M+H]$^+$, 97%); HRMS *m/z* (ES^+) [Found, $(M+H)^+$ 256.9670. $C_7H_6{}^{79}BrN_4O_2^+$ requires M^+, 256.9669]; Anal. calcd for $C_7H_5BrN_4O_2$: C, 32.7; H, 2.0; N, 21.8. Found: C, 32.9; H, 1.9; N, 21.7.

6-Bromo-3-methyl[1,2,4]triazolo[4,3-*a*]pyridin-8-amine (**81**)

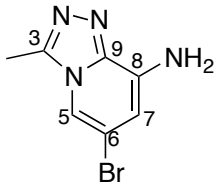

To a 1-2 mL MW vial containing 6-bromo-3-methyl-8-nitro[1,2,4]triazolo[4,3-*a*]pyridine **80** (50 mg, 200 µmol, 1.0 eq) was added AcOH and water (4:1, 800 µL) *via* syringe, and the mixture was sonicated for 1 min. Iron powder (76 mg, 1.4 mmol, 7.0 eq) was added, and the reaction mixture was heated at 80 °C for 70 min, at which time TLC analysis indicated complete consumption of **81**. The reaction mixture was cooled to RT, filtered through Celite® (eluent CH_2Cl_2) and concentrated *in vacuo*. The residue was redissolved in ethyl acetate (30 mL), and washed with saturated aqueous $NaHCO_3$ (30 mL). The organic layer was washed with brine (30 mL), dried over sodium sulfate, filtered, and concentrated *in vacuo* to give *6-bromo-3-methyl[1,2,4]triazolo[4,3-a]pyridin-8-amine* **81** (36 mg, 82%): R_f 0.65 (ethyl acetate/petroleum ether, 70:30); mp >250 °C (from $CHCl_3$); ν_{max} (thin film)/cm^{-1} 3453 (m), 3308 (m), 3210 (m), 3076 (m), 1634 (s), 1618 (m), 1563 (s), 1502 (m), 1454 (m) 1312 (s), 1142 (m); ^{1}H NMR (500 MHz; D_6-DMSO) 8.30 (1H, d, *J* 1.7, C(5)*H*), 6.63 (1H, d, *J* 1.7, C(7)*H*), 6.24 (2H, br s, NH_2), 2.43 (3H, s, CH_3); ^{13}C NMR (126 MHz; D_6-DMSO) 161.1 (*C*(3)), 143.1 (*C*(9)), 137.0 (*C*(8)), 115.6 (*C*(5)H), 107.6 (*C*(7)H), 104.2 (*C*(6)), 13.9 (*C*H_3); *m/z* (ES$^+$) 227 ([^{79}M+H]$^+$, 100%), 229 ([^{81}M+H]$^+$, 97%); HRMS *m/z* (ES$^+$) [Found, (M+H)$^+$ 226.9920; $C_7H_8{}^{79}BrN_4{}^+$ requires M$^+$, 226.9927]; Anal. calcd for $C_7H_7BrN_4$: C, 37.0; H, 3.1; N, 24.7. Found: C, 37.1; H, 3.2; N, 24.6.

***tert*-Butyl (3-methyl-6-(4'-(4-methylpiperazin-1-yl)-3'-nitrophenyl)-[1,2,4]triazolo[4,3-*a*]pyridin-8-yl)carbamate** (**83**)

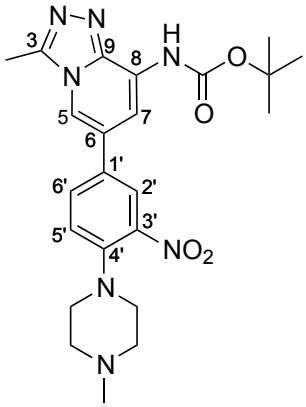

To a suspension of **81** (100 mg, 441 µmol, 1.0 eq) in DMF 2 mL was added di-*tert*-butyl dicarbonate (158 mg, 722 µmol, 1.6 eq) and 4-DMAP (3 mg, 20 µmol, 0.05 eq), and the solution was stirred at RT for 48 h. The solution was concentrated *in vacuo*, redissolved in CH_2Cl_2 (20 mL), washed with water (20 mL), brine (20 mL), dried over sodium sulfate, filtered, and concentrated *in vacuo*. The crude material was purified by silica gel column chromatography, (petroleum ether/ethyl acetate/triethylamine, 79:20:1 to 0:99:1) to give a crude sample of **82** (110 mg) that was used without further purification. To a 10-20 mL MW vial under argon was added **82** (100 mg, 310 µmol, 1.0 eq), 1'-methyl-4'-(2-nitro-4-(4'',4'',5'',5''-tetramethyl-1'',3'',2''-dioxaborolan-2''-yl)phen-yl)-piperazine **74** (270 mg, 770 µmol, 2.5 eq), K_2CO_3 (63 mg, 460 µmol, 1.5 eq) and Pd(dppf)Cl_2·CH_2Cl_2 (60 mg, 30 µmol, 0.01 eq). 1,4-Dioxane and water (10:1, 4 mL) was added *via* syringe and the reaction mixture was heated at 80 °C for 26 h. After cooling to RT, the reaction mixture was concentrated *in vacuo*, redissolved in CH_2Cl_2 (20 mL), washed with water (20 mL), brine (20 mL), dried over sodium sulfate, filtered, and concentrated *in vacuo*. The crude material was purified by silica gel column chromatography,

(petroleum ether/ethyl acetate/triethylamine, 79:20:1 to 0:99:1), to afford *tert-butyl (3-methyl-6-(4'-(4-methylpiperazin-1-yl)-3'-nitrophenyl)-[1,2,4]triazolo[4,3-a]pyridin-8-yl)carbamate* **83** (81 mg, 39% over two steps) as a yellow solid: R_f 0.17 (methanol/CH_2Cl_2/triethylamine, 4:95:1); mp 229-230 °C ($CHCl_3$); ν_{max} (thin film)/cm^{-1} 3329 (w), 3093 (w), 2962 (w), 2932 (w), 2847 (w), 2801 (w), 2768 (w), 1734 (w), 1704 (m), 1632 (w), 1565 (m), 1529 (s), 1504 (s), 1485 (s), 1457 (m), 1432 (w), 1377 (m), 1356 (m), 1340 (m), 1293 (m), 1260 (m), 1239 (s), 1205 (s), 1153 (s), 1090 (s), 1021 (m), 1005 (s); ^{1}H NMR (500 MHz; $CDCl_3$) δ 8.32 (1H, m, C(5)*H*), 8.31 (1H, m, C(7)*H*), 8.01 (1H, d, *J* 2.8, C(2')*H*), 7.72 (1H, dd, *J* 10.7, 2.8, C(6')*H*), 7.65 (1H, br s, N*H*), 7.24 (1H, d, *J* 10.7, C(5)*H*), 3.16-3.19 (4H, m, ArNCH_2), 2.60-2.70 (4H, m, ArNCH$_2$CH_2), 2.61 (3H, s, C(3)CH_3), 2.40 (3H, s, NCH_3), 1.56 (9H, s, (CH_3)$_3$); ^{13}C NMR (500 MHz; $CDCl_3$) δ 163.2 (*C*(3)), 152.3 (*C*=O), 145.4 (*C*(8)), 144.0 (*C*(9)), 143.22 (*C*(4')), 143.18 (*C*(3')), 132.0 (*C*(6')H), 127.1 (*C*(1')), 126.3 (*C*(6)), 124.5 (*C*(2')H), 121.7 (*C*(5')H), 118.3 (*C*(5)H), 112.5 (*C*(7)H), 81.8 (*C*(CH$_3$)$_3$), 54.7 (ArNCH$_2$*C*H$_2$), 51.1 (ArN*C*H$_2$), 45.7 (N*C*H$_3$), 28.2 ((*C*H$_3$)$_3$), 14.3 (C(3)*C*H$_3$); *m/z* (ES$^+$) 468 [(M+H)$^+$, 100%]; HRMS *m/z* (ES$^+$) [Found (M+H)$^+$ 468.2336. $C_{23}H_{30}N_7O_4^+$ requires M$^+$, 468.2354]; HPLC (method 1) retention time 13.15 min, purity 98.8%

5'-(2'-(4-Bromo-2-nitrophenyl)piperazin-1-yl)ethanone (**88**)

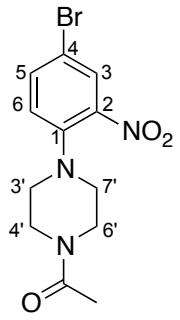

To a 1-2 mL MW vial containing 2,5-dibromonitrobenzene **72** (60 mg, 210 µmol, 1.0 eq) and 1-(piperazin-1-yl)ethanone **87** (40 mg, 310 µmol, 1.5 eq) were added isopropanol (300 µL) and triethylamine (36 µL, 23 mg, 230 µmol, 1.1 eq). The reaction mixture was heated under reflux for 3 days then cooled to 40 °C and concentrated *in vacuo*, redissolved in ethyl acetate (15 mL), washed with 2 M aqueous HCl (2 × 15 mL), brine (15 mL), and dried over sodium sulfate to give *5'-(2'-(4-bromo-2-nitrophenyl)piperazin-1-yl)ethanone* **88** (59 mg, 84%) as an orange oil: R_f 0.75 (methanol/ethyl acetate/triethylamine, 20:79:1); ν_{max} (thin film)/cm^{-1} 3079 (w), 3010 (w), 2915 (w), 2824 (w), 1648 (s), 1627 (m), 1599 (m), 1553 (m), 1521 (s), 1485 (m), 1443 (s), 1424 (m), 1385 (m), 1356 (m), 1331 (m), 1281 (m), 1252 (m), 1230 (s), 1207 (m), 1166 (m), 1140 (m), 1098 (m), 1037 (m); ^{1}H NMR (500 MHz; $CDCl_3$) δ 7.87 (1H, d, *J* 2.6, C(3)*H*), 7.96 (1H, d, *J* 8.8, C(6)*H*), 7.54 (1H, dd, *J* 8.8, 2.6 C(5)*H*), 3.70 (2H, m), 3.55 (2H, m), 2.96 (4H, m), 2.06 (3H, s, CH_3); ^{13}C NMR (126 MHz; $CDCl_3$) δ 169.1 (*C*=O), 144.7 (*C*(2)), 144.1 (*C*(1)), 136.5 (*C*(5)H), 128.7 (*C*(6)H), 123.1 (*C*(3)H), 114.8 (*C*(4)), 52.3 (*C*(4')H) or (*C*(6')H), 51.3 (*C*(4')H) or (*C*(6')H), 46.3 (*C*(3'')H) or (*C*(7')H), 41.3 (*C*(3')H) or (*C*(7')H), 21.4 (*C*H$_3$); *m/z* (ES$^+$) 300 ([^{79}M+H]$^+$, 98%), 302 ([^{81}M+H]$^+$, 100%), 322 ([^{79}M+Na]$^+$, 8%), 324

([^{81}M+Na]$^+$, 8%); HRMS *m/z* (ES$^+$) [Found, (M+H)$^+$ 300.0346, 302.0325; $C_{12}H_{14}{}^{79}BrN_3NaO_3^+$ requires M$^+$, 300.0342; $C_{12}H_{14}{}^{81}BrN_3NaO_3^+$ requires M$^+$, 302.0322.].

1-(4-(2-Nitro-4-(4,4,5,5-tetramethyl-1,3,2-dioxaborolan-2-yl)phenyl)piperazin-1-yl)ethanone (**89**)

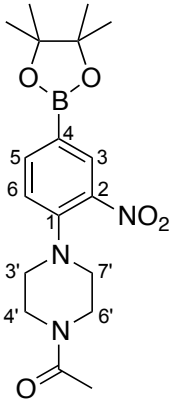

To a 2-5 mL MW vial containing 5'-(2'-(4-bromo-2-nitrophenyl)piperazin-1-yl)ethanone **88** (100 mg, 305 µmol, 1.0 eq) was added bispinacolato diboron (85 mg, 336 µmol, 1.1 eq), potassium acetate (75 mg, 760 µmol, 2.5 eq) and Pd(dppf)Cl_2·CH_2Cl_2 (12 mg, 15 µmol, 0.05 eq). 1,4-Dioxane and DMSO (30:1, 1.5 mL) were added *via* syringe and the reaction mixture was heated at 109 °C for 13 h then cooled to RT, filtered through Celite® (eluent CH_2Cl_2), and concentrated *in vacuo*. The residue was redissolved in CH_2Cl_2 (20 mL), washed with brine (2 × 20 mL), dried over sodium sulfate, filtered, and concentrated *in vacuo*. The residue was passed through a plug of neutral activated aluminum oxide (Brockmann I), eluting with ethyl acetate, to afford *1-(4-(2-nitro-4-(4,4,5,5-tetramethyl-1,3,2-dioxaborolan-2-yl)phenyl)piperazin-1-yl)ethanone* **89** (37 mg, 32%) as a yellow oil: R_f 0.75 (methanol/ethyl acetate/triethylamine, 20:79:1); ν_{max} (thin film)/cm^{-1} 2978 (w), 2930 (w), 1650 (s), 1610 (s), 1544 (s), 1529 (m), 1502 (m), 1469 (m), 1443 (m),

1392 (m), 1357 (s), 1322 (s), 1287 (m), 1232 (m), 1143 (s), 1106 (m); ^{1}H NMR (500 MHz; $CDCl_3$) δ 8.14 (1H, d, *J* 1.3, C(3)*H*), 7.80 (1H, d, *J* 8.3, C(6)*H*), 7.80 (1H, dd, *J* 8.3, 1.3 C(5)*H*), 3.72-3.70 (2H, m), 3.56-3.54 (2H, m), 3.04-3.01 (4H, m), 2.06 (3H, s, CH_3) 1.26 (12H, s, OC(CH_3)$_2$); ^{13}C NMR (126 MHz; $CDCl_3$) δ 169.2 (*C*=O), 147.4 (*C*(1)), 142.5 (*C*(2)), 139.8 (*C*(5)H), 132.6 (*C*(3)H), 119.8 (*C*(6)H), 84.3 (*C*(4)), 51.7 (*C*(4')H) or (*C*(6')H), 50.8 (*C*(4')H) or (*C*(6')H), 46.2 (*C*(3')H) or (*C*(7')H), 41.3 (*C*(3')H) or (*C*(7')H), 21.4 CO*C*H$_3$ BO*C*; *m/z* (ES$^+$) 376 ([M+H]$^+$, 100%), 398 ([M+Na]$^+$, 90%); HRMS *m/z* (ES$^+$) [Found, (M+H)$^+$ 398.1865; $C_{18}H_{26}BN_3NaO_5^+$ requires M$^+$, 398.1861].

tert-Butyl-(6-(4'-(4''-acetylpiperazin-1-yl)-3'-nitrophenyl)-3-methyl[1,2,4]-triazolo[4,3-*b*]pyridazin-8-yl)carbamate (84)

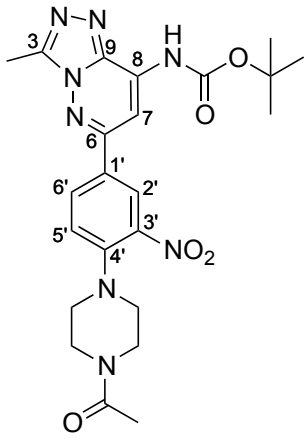

To a 10-20 mL MW vial containing *tert*-butyl(6-chloro-3-methyl-[1,2,4]triazolo[4,3-b]pyridazin-8-yl) carbamate **55** (79 mg, 280 μmol, 1.0 eq), 1-(4-(2-nitro-4-(4,4,5,5-tetramethyl-1,3,2-dioxaborolan-2-yl)phenyl)piperazin-1-yl)ethanone **89** (209 mg, 557 μmol, 2.0 eq), Pd(dppf)Cl_2·CH_2Cl_2 (23 mg, 28 μmol, 0.1 eq) and K_2CO_3 (58 mg, 420 mmol, 1.5 eq), was added 1,4-dioxane/water (10:1, 3 mL) *via* syringe. The reaction mixture was heated at

80 °C for 22.5 h then cooled to RT, filtered through Celite® (eluent CH_2Cl_2) and concentrated *in vacuo*. The residue was redissolved in CH_2Cl_2 (50 mL) and washed with brine (50 mL), dried over sodium sulfate, filtered, and concentrated *in vacuo*. The crude material was purified by silica gel chromatography, eluting with ethyl acetate, petrol and triethylamine (20:79:1, 40:59:1, 60:39:1, 80:19:1, 99:0:1), then crystallised from isopropanol to afford *tert-butyl (6-(4'-(4''-acetylpiperazin-1-yl)-3'-nitrophenyl)-3-methyl-[1,2,4]triazolo[4,3-b]pyridazin-8-yl)carbamate* **84** (61 mg, 44%) as a yellow solid: R_f 0.53 (methanol/ethyl acetate/triethylamine, 10:89:1); mp 142-143 °C (from isopropanol); ν_{max} (thin film)/cm^{-1} 3405 (w), 2981 (w), 2935 (w), 1736 (m), 1614 (s), 1569 (m), 1533 (s), 1504 (m), 1469 (m), 1446 (m), 1419 (m), 1393 (m), 1370 (m), 1348 (m), 1242 (s), 1205 (m), 1153 (m), 1153 (s), 1092 (w); ^{1}H NMR (400 MHz; $CDCl_3$) δ 8.50 (1H, d, *J* 2.2, C(2')*H*), 8.14 (1H, dd, *J* 8.8, 2.2, C(6')*H*), 8.13 (1H, br s, N*H*), 8.10 (1H, s, C(7)*H*), 7.21 (1H, d, *J* 8.8, C(5')*H*), 3.83 (2H, t, *J* 5.1, C(3'')H_2 or C(5'')H_2), 3.67 (2H, t, *J* 5.1, C(3'')H_2 or C(5'')H_2), 3.18 (4H, t, *J* 5.1, C(2'')H_2, C(6'')H_2), 2.85 (3H, s, C(3)CH_3), 2.15 (3H, s, NCOCH_3), 1.58 (9H, s, C(CH_3)$_3$); ^{13}C NMR (126 MHz; $CDCl_3$) δ 169.2 (N*C*=OCH_3), 152.9 (*C*(6)), 151.6 (NH*C*=O), 148.6 (*C*(3)), 146.8 (*C*(4')), 142.7 (*C*(3')), 139.0 (*C*(9)), 134.5 (*C*(8)), 132.1 (*C*(6')H), 128.9 (*C*(1')), 125.3 (*C*(2')H), 121.0 (*C*(5')H), 99.3 (*C*(7)H), 83.4 (*C*$(CH_3)_3$), 51.0 (*C*(2'')H_2 and *C*(6'')H_2), 46.1 (*C*(5'')H), 41.2 (*C*(3'')H_2), 28.1 ((*C*H_3)$_3$), 21.4 (NCO*C*H_3), 10.0 (C(3)*C*H_3); *m/z* (ES^+) 497 [$(M+H)^+$, 100%]; HRMS *m/z* (ES^+) [Found $(M+H)^+$ 497.2255. $C_{23}H_{29}N_8O_5^+$ requires M^+, 497.2255.]; HPLC (method 2) retention time 14.53 min, purity 95.9%.

(*S*)-*tert*-Butyl-4-(4-bromo-2-nitrophenyl)-4'-methylpiperazine-5'-carboxylate (**91**)

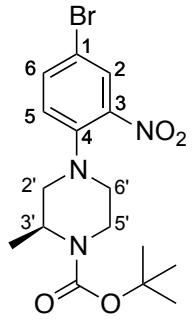

To a 10-20 mL MW vial containing 2,5-dibromonitrobenzene **72** (551 mg, 1.96 mmol, 1.0 eq) and (*S*)-*tert*-butyl-2-methylpiperazine-1-carboxylate (784 mg, 3.92 mmol, 2.0 eq) were added isopropanol (5.5 mL) and triethylamine (330 µL, 240 mg, 2.35 mmol, 1.1 eq). The reaction mixture was heated at 90 °C for 3 days, at which time TLC analysis indicated complete consumption of **72**. The reaction solution was cooled to 40 °C and concentrated *in vacuo*. The residue was redissolved in CH_2Cl_2 (40 mL), washed with water (2 × 40 mL), brine (40 mL), dried over sodium sulfate, filtered, and concentrated *in vacuo*. The crude material was purified by silica gel column chromatography eluting with ethyl acetate and petroleum ether (10:90), to afford *(S)-tert-butyl-4-(4-bromo-2-nitrophenyl)-4'-methylpiperazine-5'-carboxylate* **91** (774 mg, 99%) as an orange oil: R_f 0.30 (ethyl acetate/petroleum ether, 10:90); $[\alpha]_D^{25}$ −13.1 (*c* 1.0 in $CHCl_3$); ν_{max} (thin film)/cm^{-1} 3077 (w), 2975 (w), 2930 (w), 2874 (w), 2830 (w), 1693 (s), 1600 (m), 1528 (m), 1482 (m), 1456 (m), 1408 (m), 1387 (m), 1365 (m), 1345 (m), 1332 (m), 1281 (m), 1221 (m), 1169 (s), 1126 (m), 1089 (m), 1043 (m), 1007 (m); ^{1}H NMR (500 MHz; $CDCl_3$) δ 7.86 (1H, d, *J* 2.4, C(3)*H*), 7.58 (1H, d, *J* 8.6, 2.4, C(5)*H*), 7.02 (1H, d, *J* 8.6, C(6)*H*), 4.33-4.31 (1H, m,

C(3')*H*), 3.89-3.87 (1H, m, C(5')*H*), 3.33-3.28 (1H, m, C(5')*H*), 3.13-3.11 (1H, m, C(6')*H*), 3.08-3.07 (1H, m, C(2')*H*), 3.00-2.97 (1H, m, C(2')*H*), 2.83 (1H, ddd, *J* 11.8, 11.7, 3.4, C(6')*H*), 1.48 (9H, s, C(CH_3)$_3$); ^{13}C NMR (126 MHz; $CDCl_3$) δ 154.5 (*C*=O), 145.1 (*C*(1)), 144.2 (*C*(2)), 136.1 (*C*(5)H), 128.2 (*C*(3)H), 122.9 (*C*(6)H), 114.1 (*C*(4)), 79.9 (*C*(CH_3)$_3$), 55.8 (*C*(2')H), 52.0 (*C*(6')H), 47.0 (*C*(3')H), 38.7 (*C*(5')H), 28.4 ((*C*H_3)$_3$), 15.6 (C(3')*C*H_3); ***m/z*** (ES$^+$) 422 [(^{79}M+Na)$^+$, 98%], 424 ([^{81}M+Na]$^+$, 100%); HRMS ***m/z*** (ES$^+$) [Found, (M+Na)$^+$ 422.0692, 424.0677; $C_{16}H_{22}{}^{79}BrN_3NaO_4^+$ requires M$^+$, 422.0686; $C_{16}H_{22}{}^{81}BrN_3NaO_4^+$ requires M$^+$, 424.0666]; HPLC (method 2) pH 10 retention time 3.26 min, purity 99.3%, pH 3 retention time 3.42 min, purity 99.0%.

(*S*)-4-(1-Bromo-3-nitrophenyl)-4'-methylpiperazine (**92**)

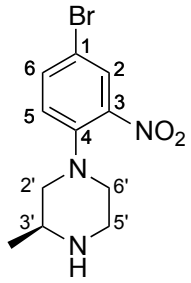

To a solution of (S)-*tert*-butyl-4-(4-bromo-2-nitrophenyl)-4'-methylpiperazine-5'-carboxylate **91** (785 mg, 1.96 mmol, 1.0 eq) in CH_2Cl_2 (3 mL), was added TFA (3.0 mL, 4.5 g, 39 mmol, 20 eq) and the reaction solution was stirred at RT for 2.5 h, after which time TLC analysis indicated complete consumption of starting material. The reaction mixture was concentrated *in vacuo*, redissolved in CH_2Cl_2 (40 mL), washed with saturated aqueous $NaHCO_3$ (3 × 40 mL), dried over sodium sulfate, filtered, and concentrated *in vacuo* to give *(S)-4-(1-bromo-3-nitrophenyl)-4'-methylpiperazine* **92** (589 mg, 76%) as an orange oil: R_f 0.28 (methanol/ethyl acetate/triethylamine, 30:69:1); $[\alpha]_D^{25}$ −24.6 (*c* 1.0 in

$CHCl_3$) ν_{max} (thin film)/cm^{-1} 3300-3200 (w), 3079 (w), 2961 (w), 2833 (w), 1599 (m), 1550 (m), 1518 (s), 1484 (s), 1451 (m), 1375 (m), 1329 (s), 1276 (m), 1232 (s), 1178 (m), 1159 (m), 1139 (m), 1109 (m), 1089 (m), 1071 (m), 1034 (m), 998 (m); ^{1}H NMR (500 MHz; $CDCl_3$) δ 7.88 (1H, d, *J* 2.4, C(3)*H*), 7.54 (1H, d, *J* 8.8, 2.4, C(5)*H*), 6.70 (1H, d, *J* 8.8, C(6)*H*), 3.12-3.08 (2H, m, C(6')*H*), 3.08-3.05 (1H, m, C(2')*H*), 3.07-3.04 (1H, m, C(3')*H*), 2.89-2.84 (1H, m, C(5')*H*), 3.04-3.00 (1H, m, C(5')*H*), 2.89-2.84 (1H, m, C(2')*H*), 2.52 (1H, dd, *J* 11.6, 9.7, C(2')*H*), 2.05 (1H, br s, N*H*), 1.08 (3H, d, *J* 6.3, CH_3); ^{13}C NMR (126 MHz; $CDCl_3$) δ 145.2 (*C*(1)), 143.2 (*C*(2)), 136.3 (*C*(5)H), 128.6 (*C*(3)H), 122.7 (*C*(6)H), 113.1 (*C*(4)), 59.0 (*C*(2')H), 51.9 (*C*(6')H), 50.5 (*C*(3')H), 45.7 (*C*(5')H), 19.4 (*C*H_3); *m/z* (ES^+) 300 [(^{79}M+Na)$^+$, 99%], 302 ([^{81}M+Na]$^+$, 100%); HRMS *m/z* (ES^+) [Found, $(M+H)^+$ 300.0349, 302.0334; $C_{11}H_{15}{}^{79}BrN_3O_2{}^+$ requires M^+, 300.0342; $C_{16}H_{22}{}^{81}BrN_3NaO_4{}^+$ requires M^+, 302.0322]; HPLC (method 2) pH 10 retention time 2.09 min, purity 99.0%, pH 3 retention time 1.32 min, purity 99.8%.

(*S*)-4-(1-Bromo-3-nitrophenyl)-3',4'-dimethylpiperazine (**93**)

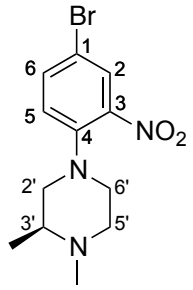

To a 10-20 mL MW vial containing **92** (424 mg, 1.41 mmol, 1.0 eq) was added formaldehyde (40% aqueous solution, 1.50 mL, 20.0 mmol, 14.2 eq) and formic acid (9.2 mL, 11 g, 240 mmol, 170 eq) *via* syringe. The reaction solution was heated at 150 °C for 30 min under MW irradiation, after which

time TLC analysis indicated complete consumption of bromide. The solution was cooled to RT, concentrated *in vacuo*, suspended in CH_2Cl_2 (120 mL) and washed with saturated aqueous $NaHCO_3$ (3 × 120 mL), brine (120 mL), dried over sodium sulfate, filtered, and concentrated *in vacuo* to *give (S)-4-(1-bromo-3-nitrophenyl)-3',4'-dimethylpiperazine* **93** (438 mg, 99%) as an orange oil: R_f 0.16 (methanol/ethyl acetate/triethylamine, 10:89:1); $[\alpha]_D^{25}$ +4.8 (*c* 1.0 in $CHCl_3$); ν_{max} (thin film)/cm^{-1} 3080 (w), 2953 (w), 2880 (w), 2841 (w), 2795 (m), 2132 (w), 1725 (s), 1600 (m), 1551 (m), 1522 (s), 1485 (s), 1454 (s), 1373 (m), 1341 (s), 1277 (m), 1234 (s), 1178 (m), 1164 (m), 1143 (m), 1122 (m), 1054 (m); ^{1}H NMR (500 MHz; $CDCl_3$) δ 7.90 (1H, d, *J* 2.4, C(2')*H*), 7.55 (1H, dd, *J* 8.8, 2.4, C(5)*H*), 7.00 (1H, d, *J* 8.8, C(6)*H*), 3.11-3.10 (1H, m, C(6')*H*), 3.07-3.04 (1H, m, C(6')*H*), 3.04-3.02 (1H, m, C(2')*H*), 2.84-2.82 (1H, m, C(5')*H*), 2.69-2.64 (1H, m, C(2')*H*), 2.48 (1H, ddd, *J* 11.2, 11.2, 3.2, C(5')*H*), 2.35-2.25 (1H, m, C(3')*H*), 1.08 (3H, d, *J* 6.3, C(3')CH_3); ^{13}C NMR (126 MHz; $CDCl_3$) δ 144.8 *C*(1), 143.2 *C*(2), 136.3 *C*(5)*H*, 128.6 *C*(3)*H*, 122.5 *C*(6)*H*, 113.2 *C*(4), 58.3 *C*(2')H, 57.4 *C*(3')H, 55.1 *C*(5')H, 51.7 *C*(6')H, 42.4 N*C*H_3, 16.7 C(4)*C*H_3; *m/z* (ES^+) [$(M+H)^+$, 100%]; *m/z* (ES^+) 314 [(^{79}M+H)$^+$, 97%], 316 ([^{81}M+H]$^+$, 100%); HRMS *m/z* (ES^+) [Found, $(M+H)^+$ 314.0502, 316.0484; $C_{12}H_{17}{}^{79}BrN_3O_2^+$ requires M^+, 314.0499; $C_{12}H_{17}{}^{81}BrN_3O_2^+$ requires M^+, 316.0479]; HPLC (method 2) pH 10 retention time 2.42 min, purity 98.2%, pH 3 retention time 1.47 min, purity 99.3%.

(*S*)-*tert*-Butyl-(6-(4'-(3'',4''-dimethylpiperazin-1-yl)-3'-nitrophenyl)-3-methyl[1,2,4]triazolo[4,3-*b*]pyridazin-8-yl)carbamate (**85**)

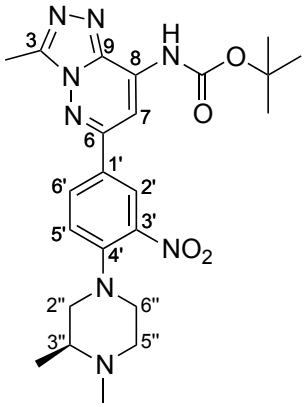

To a 2-5 mL MW vial containing (*S*)-4-(4-bromo-2-nitrophenyl)-1,2-dimethylpiperazine **93** (500 mg, 1.59 mmol, 1.0 eq) was added bispinacolato diboron (445 mg, 1.75 mmol, 1.1 eq), potassium acetate (392 mg, 4.0 mmol, 2.5 eq) and Pd(dppf)Cl_2·CH_2Cl_2 (13 mg, 16 µmol, 0.05 eq). 1,4-Dioxane and DMSO (30:1, 4 mL) were added *via* syringe and the reaction mixture was heated at 109 °C for 13 h then cooled to RT, filtered through Celite® (eluent CH_2Cl_2), and concentrated *in vacuo*. The residue was redissolved in CH_2Cl_2 (30 mL), washed with brine (2 × 30 mL), dried over sodium sulfate, filtered, and concentrated *in vacuo*. The residue was passed through a plug of neutral activated aluminum oxide (Brockmann I), eluting with ethyl acetate, to afford a crude sample of *(S)-1,2-dimethyl-4-(2-nitro-4-(4,4,5,5-tetramethyl-1,3,2-dioxaborolan-2-yl)phenyl)piperazine* (300 mg, 32%) as a yellow oil. To a 5 mL MW vial containing *(S)-1,2-dimethyl-4-(2-nitro-4-(4,4,5,5-tetramethyl-1,3,2-dioxaborolan-2-yl)phenyl)piperazine* (159 mg, 440 µmol, 2.5 eq) was added *tert*-butyl-(6-chloro-3-methyl[1,2,4]triazolo[4,3-*b*]pyridazin-8-yl)carbamate **55** (50 mg, 176 µmol, 1.0 eq), K_2CO_3 (36 mg, 0.261 mmol, 1.5 eq), and Pd(dppf)Cl_2·CH_2Cl_2 (14 mg, 17 µmol, 0.1 eq). 1,4-Dioxane and water (10:1,

2.0 mL) was added *via* syringe and the reaction mixture was heated at 80 °C for 20 h. After cooling to RT the reaction mixture was filtered through Celite® (eluent CH_2Cl_2) and concentrated *in vacuo*. The residue was redissolved in CH_2Cl_2 (80 mL) and washed with brine (80 mL), dried over sodium sulfate, filtered, and concentrated *in vacuo*. The crude material was purified by silica gel column chromatography, eluting with petroleum ether, ethyl acetate and triethylamine (79:20:1, 59:40:1, 39:60:1, 19:80:1, 0:99:1). Crystallisation of the chromatographed solid from ethyl acetate afforded *(S)-tert-butyl-(6-(4'-(3'',4''-dimethylpiperazin-1-yl)-3'-nitrophenyl)-3-methyl[1,2,4]triazolo[4,3-b]pyridazin-8-yl)carbamate* **85** (16 mg, 19%) as a yellow solid: R_f 0.21 (methanol/ethyl acetate/triethylamine, 10:89:1); mp 182-183 °C (from ethyl acetate); $[\alpha]_D^{25}$ −31.0 (*c* 1.0 in $CHCl_3$); ν_{max} (thin film)/cm^{-1} 3408 (w), 2942 (m), 2849 (w), 2798 (w), 1737 (s), 1614 (m), 1569 (s), 1532 (m), 1456 (m), 1370 (m), 1243 (s), 1152 (s); ^{1}H NMR (500 MHz; $CDCl_3$) δ 8.45 (1H, d, *J* 2.3, C(2')*H*), 8.14 (1H, br s, N*H*), 8.09 (1H, dd, *J* 8.8, 2.3, C(6')*H*), 8.08 (1H, s, C(7)*H*), 7.18 (1H, d, *J* 8.8, C(5')*H*), 3.27-3.24 (1H, m, C(6'')*H*), 3.18-3.16 (1H, m, C(6'')*H*), 3.16-3.14 (1H, m, C(2'')*H*), 2.86-2.85 (1H, m, C(5'')*H*), 2.84 (3H, s, C(3)CH_3), 2.79 (1H, dd, *J* 12.0, 10.0, C(2'')*H*), 2.51 (1H, ddd, *J* 11.3, 11.2, 3.2, C(5'')*H*)), 2.38-2.36 (1H, m, C(3'')*H*), 2.36 (3H, s, NCH_3), 1.58 (9H, s, C(CH_3)$_3$), 1.12 (3H, d, *J* 6.3, C(3'')CH_3); ^{13}C NMR (126 MHz; $CDCl_3$) δ 153.1 (*C*(6)), 151.6 (*C*=O), 148.5 (*C*(3)), 146.8 (*C*(4')), 141.7 (*C*(3')), 139.1 (*C*(9)), 134.4 (*C*(8)), 132.0 (*C*(6')H), 127.4 (*C*(1')), 125.4 (*C*(2')H), 120.4 (*C*(5')H), 99.4 (*C*(7)H), 83.3 (*C*(CH_3)$_3$), 57.7 (*C*(2'')H), 57.4 (*C*(3'')H), 55.0 (*C*(5'')H), 51.2 (*C*(6'')H), 28.1 ((*C*H_3)$_3$), 16.8 (C(3'')*C*H_3), 10.0 (C(3)*C*H_3); *m/z* (ES^+) 483 [$(M+H)^+$, 100%]; HRMS *m/z* (ES^+) [Found $(M+H)^+$ 483.2456.

$C_{23}H_{31}N_8O_4^+$ requires M^+, 483.2463]; HPLC (method 1) retention time 12.35 min, purity 98.0%; Chiral HPLC, retention time 5.05 min, ee >99%.

(*R*)-*tert*-Butyl-(6-(4-(3,4-dimethylpiperazin-1-yl)-3-nitrophenyl)-3-methyl[1,2,4]triazolo[4,3-*b*]pyridazin-8-yl)carbamate (**78**)

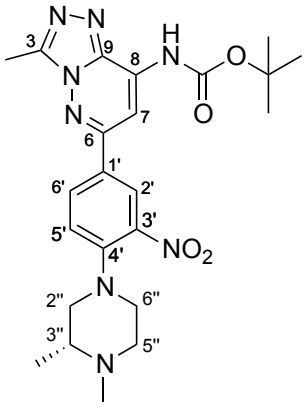

To a 25 mL round-bottom flask containing 2,5-dibromonitrobenzene **72** (617 mg, 2.20 mmol, 1.0 eq) and (*R*)-*tert*-butyl-2-methylpiperazine-1-carboxylate **94** (500 mg, 3.92 mmol, 2.0 eq) were added isopropanol (5.0 mL) and triethylamine (918 µL, 667 mg, 6.60 mmol, 3.0 eq). The reaction mixture was heated under reflux for 4 days, at which point TLC analysis indicated complete consumption of **72**. The reaction solution was cooled to 40 °C and concentrated *in vacuo*. The residue was redissolved in CH_2Cl_2 (30 mL), washed with water (2 × 30 mL), brine (30 mL), dried over sodium sulfate, filtered, and concentrated *in vacuo* to afford *(R)-4-(4-bromo-2-nitrophenyl)-1,2-dimethylpiperazine* **95** (601 mg) as a volatile orange oil which was used without further purification. To a 2-5 mL MW vial containing (*R*)-4-(4-bromo-2-nitrophenyl)-1,2-dimethylpiperazine (594 mg, 1.89 mmol, 1.0 eq), bispinacolato diboron (85 mg, 336 µmol, 1.1 eq), potassium acetate (75 mg, 760 µmol, 2.5 eq) and $Pd(dppf)Cl_2 \cdot CH_2Cl_2$ (12 mg, 15 µmol, 0.05 eq) were

added. 1,4-Dioxane and DMSO (30:1, 4.0 mL) was added *via* syringe and the reaction mixture was heated at 109 °C for 13 h then cooled to RT, filtered through Celite® (eluent CH_2Cl_2) and concentrated *in vacuo*. The residue was redissolved in CH_2Cl_2 (40 mL) and washed with brine (2 × 20 mL), dried over sodium sulfate, filtered, and concentrated *in vacuo*. The residue was passed through a plug of neutral activated aluminum oxide (Brockmann I), eluting with ethyl acetate, to afford *(R)-1,2-dimethyl-4-(2-nitro-4-(4,4,5,5-tetramethyl-1,3,2-dioxaborolan-2-yl)phenyl)piperazine* **96** (127 mg) as a yellow oil. (Complete removal of pinacol could not be achieved, so this material was used in the next step.) To a 2-5 mL MW vial containing the crude (*R*)-1,2-dimethyl-4-(2-nitro-4-(4,4,5,5-tetramethyl-1,3,2-dioxaborolan-2-yl)phenyl)piperazine **86** (127 mg, 352 μmol, 2.0 eq) was added **55** (50 mg, 180 μmol, 1.0 eq), K_2CO_3 (36 mg, 260 μmol, 1.5 eq), and $Pd(dppf)Cl_2 \cdot CH_2Cl_2$ (15 mg, 32 μmol, 0.1 eq). 1,4-Dioxane and water (10:1, 1.0 mL) was added *via* syringe and the reaction mixture was heated at 80 °C for 20 h. The reaction mixture was then cooled to RT, filtered through Celite® (eluent CH_2Cl_2) and concentrated *in vacuo*. The residue was redissolved in CH_2Cl_2 (30 mL) and washed with brine (30 mL), dried over sodium sulfate, filtered, and concentrated *in vacuo*. The crude material was purified by silica gel column chromatography, eluting with ethyl acetate, petroleum ether, triethylamine (79:20:1, 69:30:1, 59:40:1, 29:70:1, 9:90:1, 0:99:1) and then by preparative HPLC to afford *(R)-tert-butyl-(6-(4-(3,4-dimethylpiperazin-1-yl)-3-nitrophenyl)-3-methyl[1,2,4]triazolo[4,3-b]pyridazin-8-yl)carbamate* **78** (7 mg, 1% over 3 steps) as a yellow solid: R_f 0.31 (methanol/ethyl acetate, 20:80); mp 113-114 °C (from ethyl acetate); $[\alpha]_D^{21}$ +25.1 (*c* 1.0 in $CHCl_3$); ν_{max} (thin film)/cm^{-1} 3401 (w), 2982 (w),

2842 (w), 1739 (m), 1611 (w), 1571 (m), 1499 (m), 1456 (m), 1419 (m), 1371 (m), 1341 (m), 1287 (m), 1207 (m), 1150 (s); ^{1}H NMR (500 MHz; $CDCl_3$) δ 8.45 (1H, d, *J* 2.3, C(2')*H*), 8.16 (1H, br s, N*H*), 8.09 (1H, dd, *J* 8.8, 2.3, C(6')*H*), 8.09 (1H, s, C(7)*H*), 7.19 (1H, d, *J* 8.8, C(5')*H*), 3.30-3.27 (1H, m, C(6'')*H*)), 3.20-3.17 (1H, m, C(6'')*H*), 3.19-3.17 (1H, m, C(5''*H*)), 2.91-2.85 (1H, m, C(2'')*H*), 2.81-2.78 (1H, m, C(5'')*H*)), 2.53-2.49 (1H, m, C(2'')*H*)), 2.39-2.36 (1H, m, C(3'')*H*), 2.84 (3H, s, C(3)CH_3), 2.36 (3H, s, NCH_3), 1.58 (9H, s, (CH_3)$_3$), 1.11 (3H, s, ArNCH$_2$CCH_3); ^{13}C NMR (126 MHz; $CDCl_3$) δ 153.2 (*C*(6)), 151.6 (*C*=O), 148.5 (*C*(3)), 146.8 (*C*(4')), 141.7 (*C*(3')), 139.1 (*C*(9)), 134.4 (*C*(8)), 132.0 (*C*(6')H), 127.4 (*C*(1')), 125.4 (*C*(2')H), 120.4 (*C*(5')H), 99.4 (*C*(7)H), 83.3 (*C*(CH$_3$)$_3$), 57.7 (*C*(3'')H), 57.4 (*C*(5'')H), 55.0 (*C*(2'')H$_2$), 51.2 (*C*(6)H$_2$), 42.5 (N*C*H$_3$), 28.1 ((*C*H$_3$)$_3$), 16.8 (ArNCH$_2$C*C*H$_3$), 10.0 (C(3)*C*H$_3$); *m/z* (ES$^+$) 483 [(M+H)$^+$, 100%]; HRMS *m/z* (ES$^+$) [Found (M+H)$^+$ 483.2458. $C_{23}H_{31}N_8O_4^+$ requires M$^+$, 483.2463]; HPLC (method 2) pH 10 retention time 2.55 min, purity 99.4%, pH 3 retention time 1.78 min, purity 98.8%; Chiral HPLC, retention time 4.09 min, ee >99%.

***tert*-Butyl-(6-(3'-amino-4-(4'-methylpiperazin-1''-yl)phenyl)-3-methyl[1,2,4]triazolo[4,3-*b*]pyridazin-8-yl)carbamate** (**2**)

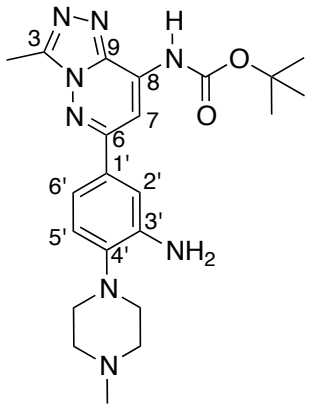

To a 25 mL round-bottomed flask containing *tert-butyl-(3-methyl-6-(4'-(4''-methylpiperazin-1-yl)-3'-nitrophenyl)[1,2,4]triazolo[4,3-b]pyridazin-8-yl)carbamate* **70** (300 mg, 640 µmol, 1.0 eq), was added tin(II) chloride (304 mg, 1.60 mmol, 2.5 eq) followed by ethanol and triethylamine (2:1, 8 mL) *via* syringe. The solution was heated at 70 °C for 3 h, after which time TLC analysis indicated complete consumption of **70**. The reaction was cooled to RT and the residue was suspended in ethyl acetate (20 mL). The residue was removed by filtration, and the filtrate was concentrated *in vacuo*. The residue was stirred vigorously in saturated aqueous KF (60 mL), then extracted with ethyl acetate (60 mL), and washed with water (2 × 60 mL), brine (60 mL), dried over sodium sulfate, filtered, and concentrated *in vacuo*. This dark orange solid was further purified by preparative HPLC by Justin Staniforth at UCB, to give **2** (100 mg, 36%) as a pale yellow solid: R_f 0.45 (methanol/CH_2Cl_2/triethylamine, 10:89:1); mp 143-144 °C (from ethyl acetate); ν_{max} (thin film)/cm^{-1} 3458 (w), 3332 (w), 2934 (w), 1739 (m), 1612 (w), 1558 (m), 1539 (m), 1516 (m), 1466 (m), 1454 (m), 1394 (m), 1370 (m), 1289 (m), 1267 (m), 1244 (m), 1195 (m), 1156 (s), 1089 (m); ^{1}H NMR

(500 MHz; $CDCl_3$) δ 8.11 (1H, br s, N*H*), 8.08 (1H, s, C(7)*H*), 7.38 (1H, d, *J* 1.8, C(2')*H*), 7.37 (1H, dd, *J* 8.8, 1.8, C(6')*H*), 7.08 (1H, d, *J* 8.8, C(5')*H*), 4.08 (2H, br s, NH_2), 3.01 (4H, br s, ArNCH_2), 2.61 (4H, br s, ArNCH$_2$CH_2), 2.83 (3H, s, C(3)CH_3), 2.38 (3H, s, NCH_3), 1.57 (9H, s, (CH_3)$_3$); ^{13}C NMR (126 MHz; $CDCl_3$) δ 155.6 (*C*(6)), 151.7 (*C*=O), 148.4 (*C*(3)), 141.7 (*C*(4')), 141.6 (*C*(3')), 139.3 (*C*(9)), 133.7 (*C*(8)), 131.3 (*C*(1')), 119.9 (*C*(5')H), 118.1 (*C*(6')H), 113.6 (*C*(2')H), 100.6 (*C*(7)H), 82.9 (*C*(CH$_3$)$_3$), 55.8 (ArNCH$_2$*C*H$_2$), 50.6 (ArN*C*H$_2$), 46.2 (N*C*H$_3$), 28.1 ((*C*H$_3$)$_3$), 10.0 (C(3)*C*H$_3$); *m/z* (ES$^+$) 439 [(M+H)$^+$, 100%]; HRMS *m/z* (ES$^+$) [Found (M+H)$^+$ 439.2553. $C_{22}H_{31}N_8O_2^+$ requires M$^+$, 439.2564]; HPLC (method 2) pH 10 retention time 2.15 min, purity 100%, pH 3 retention time 1.50 min, purity 100%.

***tert*-Butyl-(6-(3'-(2'',5''-dichlorophenylsulfonamido)-4'-(4-methylpiperazin-1-yl)phenyl)-3-methyl[1,2,4]triazolo[4,3-*b*]pyridazin-8-yl)carbamate** (**97**)

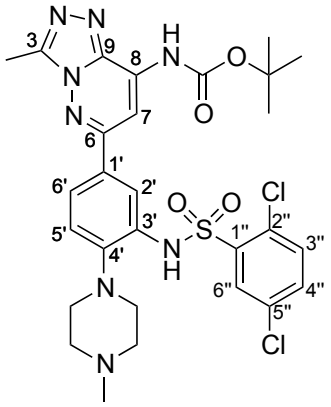

To a solution of *tert*-butyl-(6-(3'-amino-4'-(4-methylpiperazin-1-yl)phenyl)-3-methyl[1,2,4]triazolo[4,3-*b*]pyridazin-8-yl)carbamate **2** (100 mg, 228 μmol, 1.0 eq) in CH_2Cl_2 (1.0 mL) was added triethylamine (34 μL, 25 mg, 250 μmol, 1.1 eq), then cooled to 0 °C. A solution of 4-DMAP (1 mg, 0.008 mmol,

0.04 eq) and 2,5-dichlorobenzenesulfonyl chloride (85 mg, 340 μmol, 1.5 eq) in pyridine (1.5 mL) was added dropwise *via* syringe at 0 °C, over a period of 30 min. The reaction mixture was stirred at RT for 24 h, then concentrated *in vacuo*, redissolved in CH_2Cl_2 (50 mL), washed with brine (3 × 50 mL), dried over sodium sulfate, filtered, and concentrated *in vacuo*. The crude material was purified by silica gel column chromatography, eluting with petroleum ether, ethyl acetate and triethylamine (79:20:1, 69:30:1 49:50:1), then crystallised from ethanol to afford *tert-butyl-(6-(3-(2,5-dichlorophenylsulfonamido)-4-(4-methylpiperazin-1-yl)phenyl)-3-methyl[1,2,4]triazolo[4,3-b]pyridazin-8-yl)carbamate* **97** (16 mg, 11%) as a colourless crystalline solid: R_f 0.35 (methanol/EtOAc/triethylamine, 30:69:1); mp 175-180 °C (from ethanol); ν_{max} (thin film)/cm^{-1} 3520 (w), 3250 (w), 3415 (w), 3089 (w), 3006 (w), 2843 (w), 2795 (w), 1739 (s), 1571 (m), 1453 (m), 1396 (m), 1242 (s), 1151 (s); ^{1}H NMR (500 MHz; $CDCl_3$) δ 8.71 (1H, br s, N*H*), 8.30 (1H, d, *J* 1.7, C(6'')*H*), 8.12 (1H, d, *J* 2.0, C(2')*H*), 8.10 (1H, br s, N*H*) 8.04 (1H, s C(7)*H*), 7.60 (1H, dd, 8.3, 2.0, C(6')*H*), 7.45 (1H, dd, *J* 8.5, 1.7, C(4'')*H*), 7.40 (1H, d, *J* 8.5, C(3'')*H*), 7.31 (1H, d, *J* 8.3, C(5')*H*), 3.00 (4H, br s, ArNCH_2), 2.88 C(3)CH_3, 2.75 (4H, br s, ArNCH_2CH_2), 2.48 (3H, s, NCH_3), 1.58 (9H, s, (CH_3)$_3$); ^{13}C NMR (126 MHz; $CDCl_3$) δ 155.5 (*C*(6)), 151.5 (*C*=O), 148.5 (*C*(3)), 139.1 (*C*(9)), 137.7 (*C*(1'')), 134.3 (*C*(4'')H), 134.2 (*C*(4')), 133.5 (*C*(8)), 133.3 (*C*(2'')), 132.9 (*C*(3'')H), 131.8 (*C*(6'')H), 129.7 (*C*(5'')), 123.4 (*C*(6')H), 122.5 (*C*(2')H), 114.6 (*C*(5')H), 100.5 (*C*(7)H), 83.1 (*C*(CH$_3$)$_3$), 55.3 (ArNCH$_2$*C*H$_2$), 52.1 (ArN*C*H$_2$), 45.8 (N*C*H$_3$), 28.1 ((*C*H$_3$)$_3$), 9.9 (C(3)*C*H$_3$); *m/z* (ES$^+$) 647 [(M+H)$^+$, 100%]; HRMS *m/z* (ES$^+$) [Found (M+H)$^+$ 647.1725. $C_{28}H_{33}Cl_2N_8O_4S^+$ requires M$^+$, 647.1717]; HPLC (method 1) retention time

13.83 min, purity 99.5%.

***tert*-Butyl-(6-(3-(2,4-dichlorophenylsulfonamido)-4-(4-methylpiperazin-1-yl)phenyl)-3-methyl[1,2,4]triazolo[4,3-*b*]pyridazin-8-yl)carbamate** (**98**)

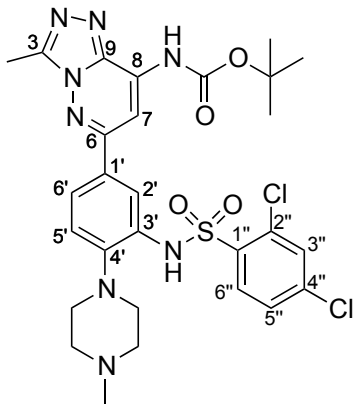

To a solution of *tert*-butyl-(6-(3'-amino-4'-(4-methylpiperazin-1-yl)phenyl)-3-methyl[1,2,4]triazolo[4,3-*b*]pyridazin-8-yl)carbamate **2** (100 mg, 228 μmol, 1.0 eq) in CH_2Cl_2 (1.0 mL) was added triethylamine (34 μL, 25 mg, 250 μmol), then cooled to 0 °C. A solution of 4-DMAP (1 mg, 8 μmol, 0.04 eq) and 2,4-dichlorobenzenesulfonyl chloride (85 mg, 340 μmol, 1.5 eq) in pyridine (1.5 mL) was added dropwise at 0 °C over a period of 25 min. The reaction mixture was stirred at RT for 24 h then concentrated *in vacuo*, redissolved in CH_2Cl_2 (50 mL), washed with brine (3 × 50 mL), dried over sodium sulfate, filtered, and concentrated *in vacuo*. Crystallisation from ethanol afforded *tert-butyl-(6-(3-(2,4-dichlorophenylsulfonamido)-4-(4-methylpiperazin-1-yl)phenyl)-3-methyl[1,2,4]triazolo[4,3-b]pyridazin-8-yl)carbamate* **98** (18 mg, 12%) as a colourless crystalline solid: R_f 0.35 (methanol/EtOAc/triethylamine, 30:69:1); mp 231-232 °C (from ethanol); ν_{max} (thin film)/cm^{-1} 3410 (w), 3396 (w), 2980 (w), 2939 (w), 2842 (w), 2794 (w), 1736 (s), 1572 (s), 1432 (s), 1397 (s), 1368 (m), 1244 (s), 1152 (s); ^{1}H NMR (500 MHz; $CDCl_3$) δ 8.69 (1H, br s, N*H*), 8.35 (1H, d, *J* 8.6, C(6'')*H*), 8.11 (1H, br s, N*H*), 7.94 (1H, d, *J* 2.0, C(2')*H*), 7.94 (1H, s C(7)*H*), 7.63 (1H, dd, 8.3,

2.0, C(6')*H*), 7.51 (1H, dd, *J* 8.6, 2.0, C(5'')*H*), 7.48 (1H, d, *J* 2.0, C(3'')*H*), 7.30 (1H, d, *J* 8.3, C(5')*H*), 2.95-3.05 (4H, m, ArNCH_2), 2.84 (3H, s, C(3)CH_3), 2.71-2.60 (4H, m, ArNCH$_2$CH_2), 2.43 (3H, s, NCH_3), 1.61 (9H, s, (CH_3)$_3$); ^{13}C NMR (126 MHz; $CDCl_3$) δ 154.8 (*C*(6)), 151.6 (C=O), 148.3 (*C*(3)), 142.8 (*C*(1')), 140.2 (*C*(1'')), 139.0 (*C*(9)), 134.6 (*C*(8)), 134.1 (*C*(4'')), 133.6 (*C*(6'')H), 133.2 (*C*(4')), 132.8 (*C*(3'')), 132.4 (*C*(2'')H), 131.7 (*C*(3'')H), 128.0 (*C*(5'')H), 123.0 (*C*(6')H), 122.5 (*C*(5')H), 114.4 (*C*(2')H), 100.3 (*C*(7)H), 83.1 (*C*(CH$_3$)$_3$), 55.5 (ArNCH$_2$*C*H$_2$), 52.3 (ArN*C*H$_2$), 46.0 (N*C*H$_3$), 28.1 ((*C*H$_3$)$_3$), 9.9 (C(3)*C*H$_3$); *m/z* (ES$^+$) 647 [(M+H)$^+$, 100%]; HRMS *m/z* (ES$^+$) [Found (M+H)$^+$ 647.1703. $C_{28}H_{33}Cl_2N_8O_4S^+$ requires M$^+$, 647.1717]; Anal. calcd for $C_{28}H_{32}Cl_2N_8O_4S$: C, 51.9; H, 5.0; N, 17.3. Found: C, 52.1; H, 5.0; N, 17.2; HPLC (method 1) retention time 14.14 min, purity 97.2%.

tert-Butyl-(6-(3-(4''-bromo-2-chlorophenylsulfonamido)-4'-(4-methylpiperazin-1-yl)phenyl)-3-methyl[1,2,4]triazolo[4,3-*b*]pyridazin-8-yl)carbamate (**99**)

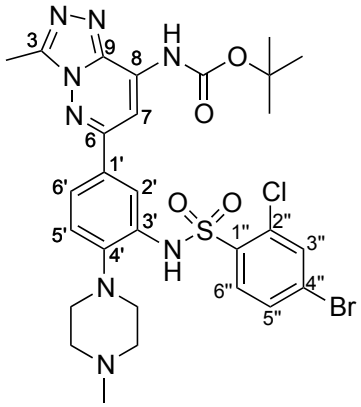

To a solution of *tert*-butyl-(6-(3'-amino-4'-(4-methylpiperazin-1-yl)phenyl)-3-methyl[1,2,4]triazolo[4,3-*b*]pyridazin-8-yl)carbamate **2** (50 mg, 110 μmol, 1.0 eq) in CH_2Cl_2 (0.75 mL) was added triethylamine (17 μL, 13 mg, 130 μmol, 1.1 eq), then cooled to 0 °C. A solution of 4-DMAP (1 mg, 8 μmol, 0.07 eq)

and 4-bromo-2-chlorobenzenesulfonyl chloride (66 mg, 230 μmol, 2.0 eq) in pyridine (0.75 mL) was added dropwise at 0 °C over a period of 25 min. The reaction mixture was stirred at RT for 24 h then concentrated *in vacuo*, and the residue was redissolved in CH_2Cl_2 (25 mL), washed with brine (3 × 25 mL), dried over sodium sulfate, filtered, and concentrated *in vacuo*. Crystallisation from ethanol afforded *tert-butyl-(6-(3-(4''-bromo-2-chlorophenylsulfonamido)-4'-(4-methylpiperazin-1-yl)phenyl)-3-methyl[1,2,4]triazolo[4,3-b]pyridazin-8-yl)carbamate* **99** (35 mg, 50%) as a colourless crystalline solid: R_f 0.40 (EtOAc/petrol/triethylamine, 70:29:1); mp 170-174 °C (from ethanol); ν_{max} (thin film)/cm^{-1} 3379 (w), 3089 (w), 2977 (w), 2936 (w), 2840 (w), 2797 (w), 1735 (s), 1565 (m), 1478 (m), 1384 (m), 1335 (m), 1220 (s), 1150 (s); ^{1}H NMR (500 MHz; $CDCl_3$) δ 8.68 (1H, br s, N*H*), 8.27 (1H, d, *J* 8.3, C(5)*H*), 8.10 (1H, br s, C(8)N*H*), 8.27 (1H, d, *J* 8.5, C(6'')*H*), 7.94 (1H, d, *J* 1.9, C(2')*H*), 7.64 (1H, d, *J* 2.0, C(3'')*H*), 7.63 (1H, dd, *J* 8.3, 1.9, C(6')*H*), 7.31 (1H, *J* 8.3, C(5')*H*), 2.96 (4H, br s, ArNCH_2), 2.84 (3H, s, C(3)CH_3), 2.64 (4H, br s, ArNCH$_2$CH_2), 2.44 (3H, s, NCH_3), 1.61 (9H, s, (CH_3)$_3$); ^{13}C NMR (500 MHz; $CDCl_3$) δ 154.8 (*C*(6)), 151.6 (*C*=O), 148.4 (*C*(3)), 142.7 (*C*(4')), 139.0 (*C*(9)), 135.1 (*C*(1'')), 134.5 (*C*(3'')H), 134.1 (*C*(8)), 133.6 (C(6'')H), 133.3 (*C*(2'')), 132.4 (*C*(3')), 131.0 (*C*(5'')H), 128.5 (*C*(4'')), 123.1 (*C*(6')H), 122.6 (*C*(5')H), 114.5 (*C*(2')H), 100.3 (*C*(7)H), 83.1 (*C*(CH$_3$)$_3$), 55.5 (ArNCH$_2$*C*H$_2$), 52.2 (ArN*C*H$_2$), 46.0 (N*C*H$_3$), 28.1 ((*C*H$_3$)$_3$), 9.9 (C(3)*C*H$_3$); *m/z* (ES$^+$) 693 [(^{81}M+H)$^+$, 100%], 691 [(^{79}M+H)$^+$, 100%]; HRMS m/z (ES$^+$) [Found (M+H)$^+$ 691.1229, 693.1167. $C_{28}H_{33}{}^{79}BrClN_8O_4S^+$ requires M$^+$, 691.1212; $C_{28}H_{33}{}^{81}BrClN_8O_4S^+$ requires M$^+$, 693.1192]; HPLC (method 1) retention time 14.29 min, purity 96.8%.

***tert*-Butyl-(3-methyl-6-(3'-(4''-methylphenylsulfonamido)-4'-(4-methylpiperazin-1-yl)phenyl)[1,2,4]triazolo[4,3-*b*]pyridazin-8-yl)carbamate** (**71**)

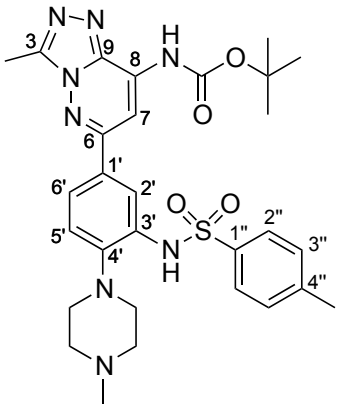

To a solution of *tert*-butyl-(6-(3'-amino-4'-(4-methylpiperazin-1-yl)phenyl)-3-methyl[1,2,4]triazolo[4,3-*b*]pyridazin-8-yl)carbamate **2** (50 mg, 110 µmol, 1.0 eq) in CH_2Cl_2 (400 µL) was added triethylamine (17 µL, 13 mg, 250 µmol, 1.1 eq), then cooled to 0 °C. A solution of 4-DMAP (1 mg, 6 µmol, 0.05 eq) and 4-toluenesulfonyl chloride (109 mg, 571 µmol, 5.0 eq) in pyridine (800 µL) was added dropwise at 0 °C over a period of 30 min. The reaction mixture was stirred at RT for 24 h, at which point TLC analysis indicated complete consumption of **2**. The reaction mixture was concentrated *in vacuo*, redissolved in CH_2Cl_2 (50 mL), washed with brine (2 × 30 mL), dried over sodium sulfate, filtered, and concentrated *in vacuo*. The crude material was purified by silica gel column chromatography, eluting with ethyl acetate, petroleum ether and triethylamine (50:49:1, 75:25:1, 99:0:1) followed by elution with ethyl acetate, methanol and triethylamine (98:1:1). Crystallisation from ethanol afforded *tert-butyl-(3-methyl-6-(3'-(4''-methylphenylsulfonamido)-4'-(4-methylpiperazin-1-yl)phenyl)[1,2,4]triazolo[4,3-b]pyridazin-8-yl)carbamate* **71** (54 mg, 44%) as a colourless crystalline solid: R_f 0.26

(methanol/ethyl acetate/triethylamine, 20:79:1); mp 165-169 °C (from ethanol); ν_{max} (thin film)/cm^{-1} 3300-3250 (br), 2978 (w), 2938 (w), 2842 (w), 2798 (w), 1735 (s), 1609 (s), 1569 (m), 1538 (m), 1510 (m), 1473 (s), 1371 (m), 1242 (s), 1154 (s); ^{1}H NMR (400 MHz; $CDCl_3$) δ 8.17 (1H, d, *J* 2.1, C(2')*H*), 8.14 (1H, br s, N*H*), 8.07 (1H, s, C(7)*H*), 7.92 (1H, br s, N*H*), 7.84 (2H, d, *J* 8.2, C(2'')*H*), 7.62 (1H, dd, *J* 8.3, 2.1, C(6')*H*), 7.29 (1H, d, *J* 8.2, C(3'')*H*), 7.22 (1H, d, *J* 8.3, C(5')*H*), 2.86 (3H, s, C(3)CH_3), 2.75 (4H, br s, ArNCH_2), 2.60 (4H, br s, ArNCH$_2$CH_2), 2.38 (3H, C(4'')CH_3), 2.40 (3H, s, NCH_3), 1.60 (9H, s, (CH_3)$_3$); ^{13}C NMR (126 MHz; $CDCl_3$) δ 154.9 (*C*(6)), 151.6 (*C*=O), 148.4 (*C*(3)), 144.1 (*C*(4'')), 143.7 (*C*(4')), 139.1 (*C*(9)), 136.4 (*C*(1'')), 134.1 (*C*(8)), 133.6 (*C*(1')), 133.0 (*C*(3')), 129.8 (C(3'')H), 127.3 (*C*(2'')H), 123.3 (*C*(6)H), 122.0 (*C*(5')H), 116.8 (*C*(2')H), 100.3 (*C*(7)H), 83.0 (*C*(CH$_3$)$_3$), 55.4 (ArNCH$_2$*C*H$_2$), 52.2 (ArN*C*H$_2$**),** 46.0 (N*C*H$_3$), 28.1 ((*C*H$_3$)$_3$), 21.6 (C(4'')*C*H$_3$), 9.9 (C(3)*C*H$_3$); *m/z* (ES$^+$) 593 [(M+H)$^+$, 100%]; HRMS *m/z* (ES$^+$) [Found (M+H)$^+$ 593.2647. $C_{29}H_{37}N_8O_4S^+$ requires M$^+$, 593.2653]; HPLC: retention time 13.24 min, purity 95.5%.

***tert*-Butyl-(6-(3'-(4''-chlorophenylsulfonamido)-4'-(4-methylpiperazin-1-yl)phenyl)-3-methyl[1,2,4]triazolo[4,3-*b*]pyridazin-8-yl)carbamate** (**100**)

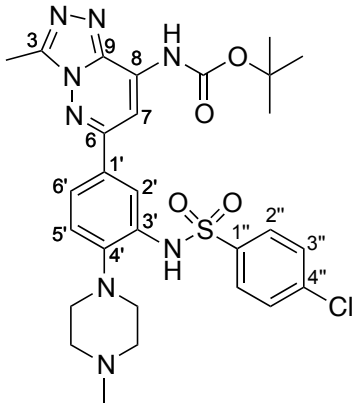

To a solution of *tert*-butyl-(6-(3'-amino-4'-(4-methylpiperazin-1-yl)phenyl)-3-methyl[1,2,4]triazolo[4,3-*b*]pyridazin-8-yl)carbamate **2** (50 mg, 110 µmol, 1.0 eq) in pyridine (300 µL), was added triethylamine (32 µL, 23 mg, 230 µmol, 2.0 eq). A solution of 4-DMAP (14 mg, 110 µmol, 1.0 eq) and 4-chlorobenzene-1-sulfonyl chloride (120 mg, 571 µmol, 5.0 eq) in pyridine (700 µL) was added dropwise at RT over a time period of 10 min. The reaction mixture was stirred at RT for 24 h, at which point TLC analysis indicated complete consumption of **2**. The reaction mixture was concentrated *in vacuo*, redissolved in CH_2Cl_2 (30 mL), washed with brine (2 × 30 mL), dried over sodium sulfate, filtered, and concentrated *in vacuo*. The crude material was purified by silica gel column chromatography, eluting with ethyl acetate, petroleum ether and triethylamine (50:49:1, 75:25:1, 99:0:1), followed by further elution with ethyl acetate, methanol and triethylamine (98:1:1) to afford *tert-butyl-(6-(3'-(4''-chlorophenylsulfonamido)-4'-(4-methylpiperazin-1-yl)phenyl)-3-methyl[1,2,4]triazolo[4,3-b]pyridazin-8-yl)carbamate* **100** (46 mg, 66%) as a colourless crystalline solid: R_f 0.48 (methanol/ethyl acetate/triethylamine, 20:79:1); mp 136-137 °C (from ethanol); ν_{max} (thin

film)/cm^{-1} 3400-3200 (br, w), 2976 (w), 2939 (w), 1745 (m), 1609 (m), 1569 (m), 1532 (m), 1509 (m), 1473 (m), 1455 (m), 1433 (m), 1370 (m), 1338 (m), 1241 (m), 1152 (s), 1091 (m); ^{1}H NMR (400 MHz; $CDCl_3$) δ 8.13 (1H, br s, N*H*), 8.10 (1H, d, *J* 2.0, C(2')*H*), 8.05 (1H, s, C(7)*H*), 7.92 (2H, d, *J* 8.6, C(2'')*H*), 7.66 (1H, dd, *J* 8.3, 2.0, C(6'')*H*), 7.50 (2H, d, *J* 8.3, C(3'')*H*), 7.25 (1H, d, *J* 8.3, C(5')*H*), 2.86 (3H, s, C(3)CH_3), 2.71 (4H, br s, ArNCH_2), 2.46 (4H, br s, $ArNCH_2CH_2$), 2.18 (3H, s, NCH_3), 1.80 (1H, br, N*H*), 1.60 (9H, s, $(CH_3)_3$); ^{13}C NMR (126 MHz; $CDCl_3$) δ 154.7 (*C*(6)H), 151.6 (*C*=O), 148.4 (*C*(3)CH_3), 143.6 (*C*(4')), 139.8 (*C*(4'')), 139.1 (*C*(9)), 137.8 (*C*(1'')), 134.1 (*C*(8)), 133.11 (*C*(1')), 133.09 (*C*(3')), 129.6 (*C*(3'')H), 128.8 (*C*(2'')H), 123.6 (*C*(6')H), 122.2 (*C*(5')H), 116.5 (*C*(2')H), 100.2 (*C*(7)H), 83.1 (*C*$(CH_3)_3$), 55.4 ($ArNCH_2CH_2$), 52.2 ($ArNCH_2$**),** 46.0 (NCH_3), 28.1 ($(CH_3)_3$), 9.9 (C(3)CH_3); *m/z* (ES^+) 613 [$(M+H)^+$, 100%]; HRMS *m/z* (ES^+) [Found $(M+H)^+$ 613.2100. $C_{28}H_{34}ClN_8O_4S^+$ requires M^+, 613.2107]; HPLC (method 1) retention time 13.57 min, purity 98.8%.

***tert*-Butyl-(3-methyl-6-(4'-(4-methylpiperazin-1-yl)-3'-(phenylsulf-onamido)phenyl)[1,2,4]triazolo[4,3-*b*]pyridazin-8-yl)carbamate** (**101**)

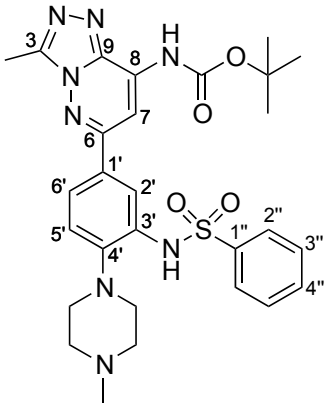

To a solution of *tert*-butyl-(6-(3'-amino-4'-(4-methylpiperazin-1-yl)phenyl)-3-methyl[1,2,4]triazolo[4,3-*b*]pyridazin-8-yl)carbamate **2** (50 mg, 110 µmol, 1.0 eq) in CH_2Cl_2 (800 µL) was addded triethylamine (32 µL, 23 mg, 230 µmol, 2.0 eq). A solution of benzenenesulfonyl chloride (15 µL, 20 mg, 110 µmol, 1.0 eq) in CH_2Cl_2 (800 µL) was added dropwise to the solution of **2**, at 0°C over a time period of 10 min. The reaction mixture was stirred at RT for 24 h then concentrated *in vacuo*, redissolved in CH_2Cl_2 (15 mL), washed with brine (2 × 15 mL), dried over sodium sulfate, filtered, and concentrated *in vacuo*. The crude material was crystallised from ethanol to afford *tert-butyl-(3-methyl-6-(4'-(4-methylpiperazin-1-yl)-3'-(phenylsulfonamido)phenyl)[1,2,4]triazolo[4,3-b]pyridazin-8-yl)carbamate* **101** (24 mg, 66%) as a colourless crystalline solid: R_f 0.27 (methanol/ethyl acetate/triethylamine, 20:79:1); mp 121-124 °C (dec.) (from ethanol); ν_{max} (thin film)/cm^{-1} 3473-3270 (br, w), 3230 (w), 2978 (m), 2939 (m), 2842 (m), 2798 (m), 1735 (s), 1609 (m), 1569 (s), 1538 (m), 1510 (m), 1473 (m), 1449 (m), 1432 (m), 1395 (s), 1370 (m), 1337 (m), 1290 (m), 1265 (m), 1242 (s), 1152 (s), 1091 (m); ^{1}H NMR (500 MHz; $CDCl_3$) δ 8.18 (1H, d, *J* 2.1, C(2')*H*), 8.15 (1H, br s, N*H*), 8.07 (1H, s, C(7)*H*), 7.97-

7.84 (2H, m, C(2'')*H*), 7.94 (1H, br s, N*H*), 7.64 (1H, dd, *J* 8.6, 2.1, C(6')*H*), 7.62-7.51 (1H, m, C(4'')*H*), 7.50 (2H, m, C(3'')*H*), 7.22 (1H, d, *J* 8.6 C(5')*H*), 2.86 (3H, s, C(3)CH_3), 2.66 (4H, br s, ArNCH_2), 2.57 (4H, br s, ArNCH$_2$CH_2), 2.39 (3H, s, NCH_3), 1.59 (9H, s, (CH_3)$_3$); ^{13}C NMR (126 MHz; $CDCl_3$) δ 154.8 (*C*(6)), 151.6 (*C*=O), 148.4 (*C*(3)), 143.8 (*C*(4')), 139.4 (*C*(3')), 139.1 (*C*(9')), 134.1 (*C*(8')), 133.5 (*C*(1')), 133.2 (*C*(1'')), 133.1 (*C*(4'')), 129.2 (*C*(3'')H), 127.2 (*C*(2'')H), 123.5 (*C*(6')H), 122.1 (*C*(5')H), 117.1 (*C*(2')H), 100.3 (*C*(7')H), 83.0 (*C*(CH$_3$)$_3$), 55.4 (ArNCH$_2$*C*H$_2$), 52.2 (ArN*C*H$_2$), 46.0 (N*C*H$_3$), 28.1 ((*C*H$_3$)$_3$), 9.9 (C(3)*C*H$_3$); *m/z* (ES$^+$) 579 [(M+H)$^+$, 100%]; HRMS *m/z* (ES$^+$) [Found (M+H)$^+$ 579.2492. $C_{28}H_{35}N_8O_4S^+$ requires M$^+$, 579.2496]; HPLC (method 2); pH 10 retention time 2.20 min, purity 100%; pH 3 retention time 2.18 min, purity 100%.

***tert*-Butyl-(3-methyl-6-(4'-(4-methylpiperazin-1-yl)-3'-(quinoline-8-sulfonamido)phenyl)[1,2,4]triazolo[4,3-*b*]pyridazin-8-yl)carbamate** (**102**)

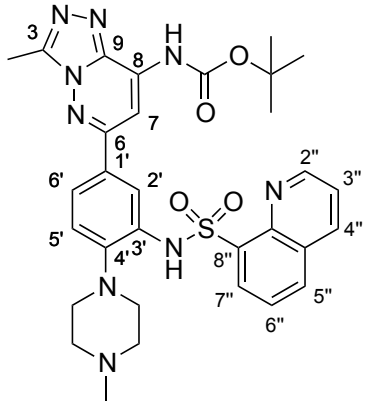

To a solution of *tert*-butyl-(6-(3'-amino-4'-(4-methylpiperazin-1-yl)phenyl)-3-methyl[1,2,4]triazolo[4,3-*b*]pyridazin-8-yl)carbamate **2** (50 mg, 110 µmol, 1.0 eq) in pyridine (500 µL), was added triethylamine (32 µL, 23 mg, 230 µmol, 2.0 eq). A solution of 4-DMAP (14 mg, 110 µmol, 1.0 eq) and 8-

quinolinesulfonyl chloride (130 mg, 571 μmol, 5.0 eq) in pyridine (2.0 mL) was added dropwise to the solution of **2**, at RT over a time period of 10 min. The reaction mixture was stirred at RT for 72 h then concentrated *in vacuo*, redissolved in CH_2Cl_2 (30 mL), washed with brine (2 × 30 mL), dried over sodium sulfate, filtered, and concentrated *in vacuo*. The crude material was purified by silica gel column chromatography, eluting with ethyl acetate, petroleum ether, and triethylamine (50:49:1, 75:25:1, 99:0:1, followed by ethyl acetate/methanol/triethylamine, 98:1:1), then crystallised from ethanol to afford *tert-butyl-(3-methyl-6-(4'-(4-methylpiperazin-1-yl)-3'-(quinoline-8-sulfonamido)phenyl)[1,2,4]triazolo[4,3-b]pyridazin-8-yl)carbamate* **102** (24 mg, 33%) as a pale brown crystalline solid: R_f 0.43 (methanol/ethyl acetate/triethylamine, 20:79:1); mp 239-240 °C (from ethanol); ν_{max} (thin film)/cm^{-1} 3400-3200 (br, w), 2976 (w), 2940 (w), 1741 (m), 1509 (m), 1495 (m), 1455 (m), 1434 (m), 1394 (m), 1371 (m), 1238 (m), 1142 (m), 1044 (m); ^{1}H NMR (500 MHz; $CDCl_3$) δ 9.16 (1H, br s, N*H*SO_2), 9.08 (1H, s, C(2'')*H*), 8.75 (1H, dd, *J* 7.3, 1.2, C(7'')*H*), 8.21 (1H, dd, *J* 4.3, 1.7, C(4'')*H*), 8.20 (1H, d, *J* 2.0, C(2')*H*), 8.11 (1H, br s, C(8)N*H*), 8.02 (1H, dd, 8.3, 1.2, C(5'')*H*), 7.94 (1H, s, C(7)*H*), 7.71 (1H, dd, 8.3, 7.3, C(6'')*H*), 7.47 (1H, dd, J 8.3, 2.0, C(6')*H*), 7.52 (1H, dd, 4.3, 4.1, C(3'')*H*), 7.12 (1H, d, *J* 8.3, C(5')*H*), 2.84 (3H, s, C(3)CH_3), 2.86 (4H, br s, ArNCH_2), 2.68 (4H, br s, ArNCH_2CH_2), 2.46 (3H, s, NCH_3), 1.61 (9H, s, (CH_3)$_3$); ^{13}C NMR (126 MHz; $CDCl_3$) δ 155.1 (*C*(6)), 151.5 (*C*=O), 151.1 (*C*(2'')), 148.3 (*C*(3)), 143.5 (C(8'')), 143.3 (*C*(4')), 139.1 (*C*(9)), 136.8 (*C*(4'')H), 135.2 (*C*(8)), 133.94 (*C*(5'')H), 133.93 (*C*(8'')), 133.8 (*C*(1')), 133.1 (*C*(3'')), 132.5 (*C*(7'')H), 128.9 (C(4'')*C*C(6'')), 125.7 (C(6'')), 122.4 (*C*(6)H), 122.1 (*C*(3'')H),

121.5 (*C*(5')H), 115.2 (*C*(2')H), 100.5 (*C*(7)H), 82.9 (*C*$(CH_3)_3$), 55.5 (ArNCH$_2$*C*H$_2$), 51.9 (ArN*C*H$_2$), 46.2 (N*C*H$_3$), 28.1 ((*C*H$_3$)$_3$), 9.9 (C(3)*C*H$_3$); *m/z* (ES^+) 630 [$(M+H)^+$, 100%]; HRMS *m/z* (ES^+) [Found $(M+H)^+$ 630.2607. $C_{31}H_{36}N_9O_4S^+$ requires M^+, 630.2605]; HPLC (method 1) retention time 12.92 min, purity 96.7%.

***tert*-Butyl-(6-(3'-(cyclopropanesulfonamido)-4'-(4-methylpiperazin-1-yl)phenyl)-3-methyl[1,2,4]triazolo[4,3-*b*]pyridazin-8-yl)carbamate** (**103**)

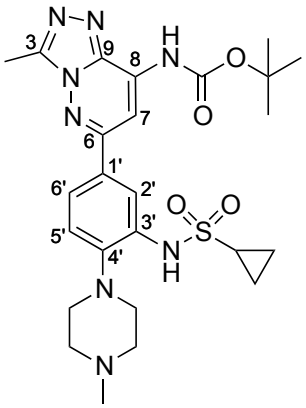

A solution of *tert*-butyl-(6-(3'-amino-4'-(4-methylpiperazin-1-yl)phenyl)-3-methyl[1,2,4]triazolo[4,3-*b*]pyridazin-8-yl)carbamate **2** (50 mg, 110 µmol, 1.0 eq) in pyridine (300 µL) was stirred at 0 °C for a period of 10 min. To this, a solution of 4-DMAP (14 mg, 110 µmol, 1.0 eq) and cyclopropanesulfonyl chloride (88 µL, 80 mg 570 µmol, 5.0 eq) in pyridine (300 µL) was added dropwise at 0 °C over a period of 15 min. The reaction mixture was warmed to RT and stirred for 20 h, at which point TLC analysis indicated complete consumption of **2**. The reaction solution was concentrated *in vacuo*, redissolved in CH_2Cl_2 (30 mL), washed with brine (30 mL), dried over sodium sulfate, filtered, and concentrated *in vacuo*. The crude material was purified by silica gel column chromatography, eluting with ethyl acetate, petroleum ether and triethylamine (50:49:1, 75:25:1, 99:0:1) followed by ethyl acetate, methanol and triethylamine (98:1:1, 97:2:1), to afford *tert-butyl-(6-(3'-(cyclopropanesulfonamido)-4'-(4-methylpiperazin-1-yl)phenyl)-3-methyl[1,2,4]triazolo[4,3-b]pyridazin-8-yl)carbamate* **103** (42 mg, 44%) as a colourless crystalline solid; R_f 0.27 (methanol/ethyl acetate/triethylamine,

20:79:1); mp 202-205 °C (dec.) (from ethanol); ν_{max} (thin film)/cm^{-1} 3473-3270 (br, w), 3111 (w), 2979 (w), 2937 (w), 2886 (w), 2844 (w), 2795 (w), 2744 (w), 2686 (w), 1736 (m), 1609 (m), 1571 (s), 1538 (m), 1511 (m), 1474 (m), 1454 (m), 1432 (m), 1396 (m), 1370 (m), 1335 (m), 1292 (m), 1267 (m), 1242 (s), 1152 (s), 1115 (m), 1089 (m), 1074 (m), 1044 (m), 1009 (m); ^{1}H NMR (500 MHz; $CDCl_3$) δ 8.25 (1H, d, *J* 2.0, C(2')*H*), 8.15 (1H, br s, N*H*), 8.10 (1H, br s, N*H*), 7.72 (1H, br s, N*H*), 7.68 (1H, dd, *J* 8.3, 2.0, C(6')*H*), 7.34 (1H, d, *J* 8.3, C(5')*H*), 2.98 (4H, br s, ArNCH_2), 2.85 (3H, s, C(3)CH_3), 2.70 (4H, br s, ArNCH$_2$CH_2), 2.65-2.50 (1H, m, SC*H*), 2.41 (3H, s, NCH_3), 1.58 (9H, s, (CH_3)$_3$) 1.39-1.37 (2H, m, SCHCH_A), 1.08-1.06 (2H, m, SCHCH_B); ^{13}C NMR (126 MHz; $CDCl_3$) δ 154.9 (*C*(6)), 151.6 (*C*=O), 148.4 (*C*(3)), 143.7 (*C*(4')), 139.1 (*C*(9)), 134.1 (*C*(8)), 133.8 (*C*(3')), 123.3 (*C*(6')H), 122.0 (*C*(5')H), 116.7 (*C*(2')H), 100.3 (*C*(7)H), 83.0 (*C*(CH$_3$)$_3$), 55.4 (ArNCH$_2$*C*H$_2$), 52.2 (ArN*C*H$_2$), 46.0 (N*C*H$_3$), 30.6 (NS*C*), 28.1 ((*C*H$_3$)$_3$), 9.9 (C(3)*C*H$_3$), 6.1 (SC*C*); *m/z* (ES$^+$) 543 [(M+H)$^+$, 100%]; HRMS *m/z* (ES$^+$) [Found (M+H)$^+$ 543.2497. $C_{25}H_{35}N_8O_4S^+$ requires M$^+$, 543.2496]; HPLC (method 1) retention time 12.00 min, purity 95.3%.

Chapter 3 Procedures

***tert*-Butyl-(3-methyl-6-(4-(4-methylpiperazin-1-yl)-3-(methylsulfonamido)phenyl)[1,2,4]triazolo[4,3-*b*]pyridazin-8-yl)carbamate** (**105**)

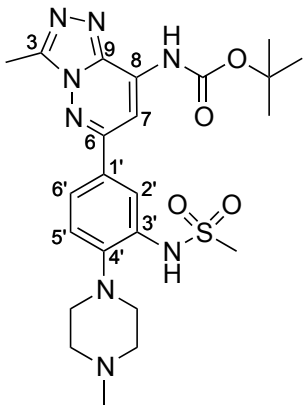

To a solution of *tert*-butyl-(6-(3-amino-4-(4-methylpiperazin-1-yl)phenyl)-3-methyl[1,2,4]triazolo[4,3-*b*]pyridazin-8-yl)carbamate **2** (50 mg, 110 µmol, 1.0 eq) in CH_2Cl_2 (1.0 mL) was added triethylamine (32 µL, 23 mg, 230 µmol, 2.0 eq). The reaction solution was cooled to 0 °C and stirred for 10 min, at which point methanesulfonyl chloride (9 µL, 13 mg, 110 µmol, 1.0 eq) was added *via* syringe and the reaction solution was warmed to RT and stirred for 21 h after which time TLC analysis indicated complete consumption of **2**. The reaction solution was concentrated *in vacuo* and the residue was redissolved methanol (1.5 mL) and aqueous 2 M aqueous NaOH (2.0 mL) and stirred for 1 h at RT. This suspension was diluted with CH_2Cl_2 (50 mL) and washed with water (3 × 50 mL), brine (50 mL), dried over sodium sulfate, filtered, and concentrated *in vacuo*. The crude material was purified by preparative HPLC to give *tert-butyl-(3-methyl-6-(4-(4-methylpiperazin-1-yl)-3-(methylsulfonamido)phenyl)[1,2,4]triazolo[4,3-b]pyridazin-8-yl)carbamate* **105** (15 mg, 25%) as a colourless solid: R_f 0.13 (methanol/ethyl acetate/triethylamine, 10:89:1); mp 160 °C (from ethyl acetate); ν_{max} (thin

film)/cm^{-1} 2917 (m), 2849 (m), 1737 (m), 1570 (m), 1532 (m), 1472 (m), 1393 (m), 1368 (m), 1242 (s), 1368 (s); ^{1}H NMR (600 MHz; $CDCl_3$) δ 8.15 (1H, d, *J* 1.9, C(2')*H*), 8.12 (1H, br s, N*H*), 8.08 (1H, br s, N*H*), 7.69 (1H, dd, *J* 8.1, 1.9, C(6')*H*), 7.41 (1H, d, *J* 8.1, C(5')*H*), 3.20 (4H, br s, ArNCH_2), 3.18 (3H, s, SO_2CH_3), 3.06 (4H, br s, $ArNCH_2CH_2$), 2.84 (3H, s, C(3)CH_3), 2.67 (3H, s, NCH_3), 1.57 (9H, s, $(CH_3)_3$); ^{13}C NMR (151 MHz; $CDCl_3$) δ 154.7 (*C*(6)), 151.6 (*C*=O), 148.5 (*C*(3)), 142.3 (*C*(4')), 139.1 (*C*(9)), 134.3 (*C*(8)), 134.1 (*C*(1')), 133.5 (*C*(3')), 123.8 (*C*(5')H), 122.5 (*C*(2')H), 116.0 (*C*(6')H), 100.3 (*C*(7)H), 83.2 ($C(CH_3)_3$), 54.6 ($ArNCH_2CH_2$), 50.6 (ArNCH_2), 44.7 (NCH_3), 40.4 (SO_2CH_3), 28.1 ($(CH_3)_3$), 9.9 (C(3)CH_3); *m/z* (ES^+) 517 [$(M+H)^+$, 100%]; HRMS *m/z* (ES^+) [Found $(M+H)^+$ 517.2350. $C_{23}H_{33}N_8O_4S^+$ requires M^+, 517.2340]; HPLC (method 2) pH 10 retention time 1.48 min, purity 100%, pH 3 retention time 1.52 min, purity 100%.

***tert*-Butyl-(3-methyl-6-(4-(4-methylpiperazin-1-yl)-3-(oxetane-3-sulfonamido)phenyl)[1,2,4]triazolo[4,3-*b*]pyridazin-8-yl)carbamate** (**106**)

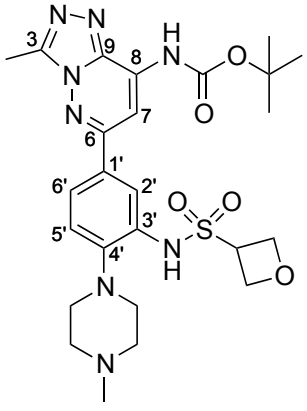

To a solution of *tert*-butyl-(6-(3-amino-4-(4-methylpiperazin-1-yl)phenyl)-3-methyl[1,2,4]triazolo[4,3-*b*]pyridazin-8-yl)carbamate **2** (50 mg, 110 μmol, 1.0 eq) in CH_2Cl_2 (1.0 mL) was added triethylamine (32 μL, 23 mg, 230 μmol,

2.0 eq). The reaction solution was cooled to 0 °C and stirred for 10 min, at which point oxetane-3-sulfonyl chloride (36 mg, 230 μmol, 2.0 eq) was added *via* syringe and the reaction solution was warmed to RT and stirred for 21 h after which time TLC analysis indicated complete consumption of **2**. The reaction solution was concentrated *in vacuo* and the residue was redissolved in CH_2Cl_2 (15 mL) and washed with water (2 × 15 mL), brine (15 mL), dried over sodium sulfate, filtered, and concentrated *in vacuo*. The crude material was purified by preparative HPLC to give *tert-butyl-(3-methyl-6-(4-(4-methylpiperazin-1-yl)-3-(oxetane-3-sulfonamido)phenyl)[1,2,4]triazolo[4,3-b]pyridazin-8-yl)carbamate* **106** (9 mg, 14%) as a colourless solid: R_f 0.09 (methanol/ethyl acetate/ triethylamine, 10:89:1); mp 143-144 °C (from ethyl acetate); ν_{max} (thin film)/cm^{-1} 3224 (w), 2971 (w), 2887 (w), 1736 (m), 1608 (m), 1570 (m), 1536 (m), 1510 (m), 1472 (m), 1456 (m), 1371 (s), 1334 (m), 1368 (s), 1242 (s), 1152 (s); ^{1}H NMR (400 MHz; $CDCl_3$) δ 8.15 (1H, d, *J* 2.0, C(2')*H*), 8.13 (1H, br s, N*H*), 8.07 (1H, s, C(7)*H*), 7.83 (1H, br s, N*H*), 7.69 (1H, dd, *J* 8.3, 2.0, C(6')*H*), 7.41 (1H, d, *J* 8.3, C(5')*H*), 5.00 (2H, dd, *J* 6.8, 6.3, SO_2CCH_a), 4.87 (2H, dd, *J* 6.8, 6.3 SO_2CCH_b), 4.68-4.63 (1H, m, SO_2CH), 2.97 (4H, br s, $ArNCH_2$), 2.84 (3H, s, $C(3)CH_3$), 2.69 (4H, br s, $ArNCH_2CH_2$), 2.44 (3H, s, NCH_3), 1.57 (9H, s, $(CH_3)_3$); ^{13}C NMR (151 MHz; $CDCl_3$) δ 154.7 (*C*(6)), 151.6 (*C*=O), 148.5 (*C*(3)), 143.4 (*C*(4')), 139.1 (*C*(9)), 134.3 (*C*(8)), 133.6 (*C*(1')), 133.2 (*C*(3')), 124.0 (*C*(6')H), 122.4 (*C*(5')H), 116.3 (*C*(2')H), 100.3 (*C*(7)H), 83.2 ($C(CH_3)_3$), 71.2 ($SCCH_aH_b$), 55.4 (S*C*H), 55.3 ($ArNCH_2CH_2$), 52.2 ($ArNCH_2$), 45.9 (NCH_3), 28.1 ($(CH_3)_3$), 9.9 ($C(3)CH_3$); *m/z* (ES^+) 559 [$(M+H)^+$, 100%]; HRMS *m/z* (ES^+) [Found $(M+H)^+$ 559.2449. $C_{25}H_{35}N_8O_5S^+$ requires M^+, 559.2446]; HPLC (method 2)

pH 10 retention time 1.46 min, purity 100%, pH 3 retention time 1.50 min, purity 96.3%.

***tert*-Butyl-(3-methyl-6-(4-(4-methylpiperazin-1-yl)-3-(pyrrolidine-1-sulfonamido)phenyl)[1,2,4]triazolo[4,3-*b*]pyridazin-8-yl)carbamate** (**107**)

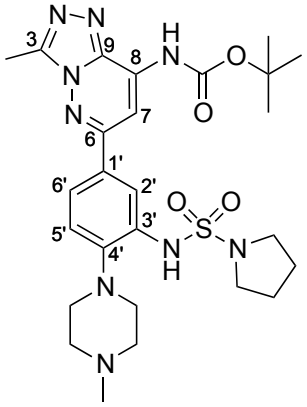

To a solution of *tert*-butyl-(6-(3-amino-4-(4-methylpiperazin-1-yl)phenyl)-3-methyl[1,2,4]triazolo[4,3-*b*]pyridazin-8-yl)carbamate **2** (50 mg, 110 µmol, 1.0 eq) and 4-DMAP (14 mg, 110 µmol, 1.0 eq) in 1,4-dioxane (1.0 mL) was added pyrrolidine-1-sulfonyl chloride (65 µL, 97 mg, 570 µmol, 5.0 eq) dropwise *via* syringe. The solution was heated for 17 h at 80 °C, at which point TLC analysis indicated complete consumption of **2**. After cooling to RT the solution was concentrated *in vacuo* and the residue was redissolved in CH_2Cl_2 (40 mL) and washed with brine (40 mL), dried over sodium sulfate, filtered, and concentrated *in vacuo*. The crude material was purified by silica gel column chromatography, eluting with ethyl acetate, petroleum ether, triethylamine (50:49:1, 75:24:1, 99:0:1) to give an oil which was further purified by preparative HPLC to give *tert-butyl-(3-methyl-6-(4-(4-methylpiperazin-1-yl)-3-(pyrrolidine-1-sulfonamido)phenyl)[1,2,4]triazolo[4,3-b]pyridazin-8-yl)carbamate* **107** (9 mg, 14%) as a colourless solid: R_f 0.51 (methanol/ethyl acetate, 20:80); mp 125-129 °C (from ethyl acetate); ν_{max}

(thin film)/cm^{-1} 3253 (w), 2938 (w), 2845 (w), 2795 (w), 1731 (m), 1534 (m), 1511 (m), 1454 (m), 1368 (m), 1292 (m), 1077 (s), 1048 (m), 1154 (s); ^{1}H NMR (500 MHz; $CDCl_3$) δ 8.12 (1H, d, *J* 2.0, C(7)*H*), 8.11 (1H, br s, N*H*), 8.02 (1H, d, *J* 2.0, C(2')*H*), 7.69 (1H, dd, *J* 8.4, 2.0, C(6')*H*), 7.60 (1H, br s, N*H*), 7.31 (1H, d, *J* 8.4, C(5')*H*), 3.51-3.49 (4H, m, $NSO_2C\mathit{H}_2$), 3.02 (4H, br s, $ArNC\mathit{H}_2$), 2.82 (3H, s, $C(3)C\mathit{H}_3$), 2.72 (4H, br s, $ArNCH_2C\mathit{H}_2$), 2.45 (3H, s, $NC\mathit{H}_3$), 1.99-1.96 (4H, m, $NSO_2CH_2C\mathit{H}_2$), 1.56 (9H, s, $(C\mathit{H}_3)_3$); ^{13}C NMR (126 MHz; $CDCl_3$) δ 154.9 (*C*(6)), 151.6 (*C*=O), 148.4 (*C*(3)), 142.7 (*C*(4')), 139.2 (*C*(9)), 134.1 (*C*(8)), 134.0 (*C*(1')), 132.7 (*C*(3')), 122.5 (*C*(6')H), 121.6 (*C*(5')H), 115.6 (*C*(2')H), 100.3 (*C*(7)H), 83.0 ($\mathit{C}(CH_3)_3$), 55.4 ($ArNCH_2\mathit{C}H_2$), 51.8 ($ArN\mathit{C}H_2$), 48.2 ($SO_2N\mathit{C}H_2$), 45.8 ($N\mathit{C}H_3$), 28.1 ($(\mathit{C}H_3)_3$), 25.9 ($SO_2NCH_2\mathit{C}H_2$), 9.9 ($C(3)\mathit{C}H_3$); *m/z* (ES^+) 574 [100%], 572 [$(M+H)^+$, 90%]; HRMS *m/z* (ES^+) [Found $(M+H)^+$ 572.2755. $C_{26}H_{38}N_9O_4S^+$ requires M^+, 572.2762]; HPLC (method 2) pH 10 retention time 2.29 min, purity 100%, pH 3 retention time 1.73 min, purity 100%.

***tert*-Butyl-(3-methyl-6-(4-(4-methylpiperazin-1-yl)-3-(morpholine-4-sulfonamido)phenyl)[1,2,4]triazolo[4,3-*b*]pyridazin-8-yl)carbamate** (**108**)

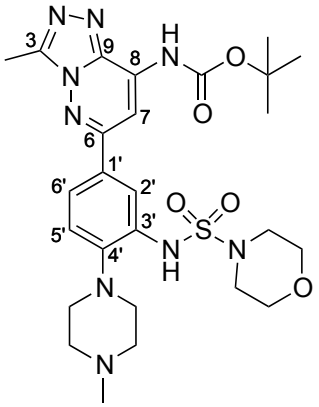

To a solution of *tert*-butyl-(6-(3-amino-4-(4-methylpiperazin-1-yl)phenyl)-3-methyl[1,2,4]triazolo[4,3-*b*]pyridazin-8-yl)carbamate **2** (50 mg, 114 µmol, 1.0 eq) and 4-DMAP (14 mg, 110 µmol, 1.0 eq) in 1,4-dioxane (1 mL) was added morpholine-4-sulfonyl chloride (69 µL, 110 mg, 570 µmol, 5.0 eq) dropwise *via* syringe. The solution was heated for 17 h at 80 °C, at which point TLC analysis indicated complete consumption of **2**. After cooling to RT the solution was concentrated *in vacuo* and the residue was redissolved in CH_2Cl_2 (40 mL) and washed with brine (40 mL), dried over sodium sulfate, filtered, and concentrated *in vacuo*. The crude material was purified by silica gel silica gel column chromatography, eluting with ethyl acetate, petroleum ether and triethylamine (50:49:1, 75:24:1, 99:0:1) to give an oil which was further purified by preparative HPLC to give *tert-butyl-(6-(3-amino-4-(4-methylpiperazin-1-yl)phenyl)-3-methyl[1,2,4]triazolo[4,3-b]pyridazin-8-yl)carbamate* **108** (8 mg, 12%) as a colourless solid: R_f 0.46 (methanol/ethyl acetate, 20:80); mp 130-134 °C (from ethyl acetate); ν_{max} (thin film)/cm^{-1} 3242 (w), 2934 (w), 2854 (w), 1734 (m), 1609 (m), 1395 (w), 1370 (m), 1340 (m), 1293 (m), 1262 (m), 1241 (s), 1151 (s); ^{1}H NMR

(500 MHz; $CDCl_3$) δ 8.13 (1H, br s, N*H*), 8.13 (1H, d, *J* 2.0, C(7)*H*), 8.08 (1H, d, *J* 2.0, C(2')*H*), 7.75 (1H, dd, *J* 8.3, 2.0, C(6')*H*), 7.60 (1H, br s, N*H*), 7.34 (1H, d, *J* 8.3, C(5')*H*), 3.81-3.79 (4H, m, OCH_2), 3.42-3.40 (4H, m, SO_2NCH_2), 3.05 (4H, br s, $ArNCH_2$), 2.83 (3H, s, $C(3)CH_3$), 2.79 (4H, br s, $ArNCH_2CH_2$), 2.49 (3H, s, NCH_3), 1.56 (9H, s, $(CH_3)_3$); ^{13}C NMR (126 MHz; $CDCl_3$) δ 154.7 (*C*(6)), 151.6 (*C*=O), 148.4 (*C*(3)), 142.8 (*C*(4')), 139.2 (*C*(9)), 134.2 (*C*(8)), 133.6 (*C*(1')), 133.0 (*C*(2')H), 133.0 (*C*(3')), 123.0 (*C*(6')H), 121.9 (*C*(5')H), 100.2 (*C*(7)H), 83.1 ($C(CH_3)_3$), 66.3 (OCH_2), 55.3 ($ArNCH_2CH_2$), 51.7 ($ArNCH_2$), 45.7 (NCH_3), 36.3 (SO_2NCH_2), 28.1 ($(CH_3)_3$), 9.9 ($C(3)CH_3$); *m/z* (ES^+) 589 [100%], 588 [$(M+H)^+$, 90%]; HRMS *m/z* (ES^+) [Found $(M+H)^+$ 588.2710. $C_{26}H_{38}N_9O_5S^+$ requires M^+, 588.2711]; HPLC (method 2) pH 3 retention time 1.76 min, purity 95.4%, pH 10 retention time 2.16 min, purity 95.5%.

***tert*-Butyl-(3-methyl-6-(3-(1-methyl-1*H*-pyrazole-4-sulfonamido)-4-(4-methylpiperazin-1-yl)phenyl)[1,2,4]triazolo[4,3-*b*]pyridazin-8-yl)carbamate** (**109**)

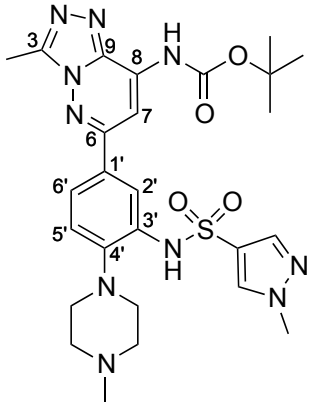

To a solution of *tert*-butyl-(6-(3-amino-4-(4-methylpiperazin-1-yl)phenyl)-3-methyl[1,2,4]triazolo[4,3-*b*]pyridazin-8-yl)carbamate **2** (50 mg, 110 μmol,

1.0 eq) and 4-DMAP (0.7 mg, 6 μmol, 0.05 eq) in pyridine (500 μL) was added 1-methyl-1*H*-pyrazole-4-sulfonyl chloride (103 mg, 570 μmol, 5.0 eq) dropwise *via* syringe. The solution was heated for 17 h at 70 °C, at which point TLC analysis indicated complete consumption of **2**. The solution was cooled to RT, concentrated *in vacuo* and the residue was redissolved in CH_2Cl_2 (40 mL), washed with brine (40 mL), dried over sodium sulfate, filtered, and concentrated *in vacuo*. The crude material was purified by preparative HPLC to give *tert-butyl-(3-methyl-6-(3-(1-methyl-*1*H-pyrazole-4-sulfonamido)-4-(4-methylpiperazin-1-yl)phenyl)[1,2,4]triazolo[4,3-b]pyridazin-8-yl)carbamate* **109** (8 mg, 12%) as a colourless solid: R_f 0.31 (methanol/ethyl acetate, 20:80); mp 153-155 °C (from ethyl acetate); ν_{max} (thin film)/cm^{-1} 3319 (w), 2942 (w), 2802 (w), 1735 (m), 1609 (w), 1569 (m), 1531 (m), 1510 (m), 1456 (m), 1370 (m), 1337 (m), 1289 (m), 1241 (m), 1153 (s); ^{1}H NMR (400 MHz; $CDCl_3$) δ 8.19 (1H, br s, N*H*), 8.12 (1H, d, *J* 2.1, C(2')*H*), 8.06 (1H, d, *J* 2.0, C(7)*H*), 8.00 (1H, s, CH_3NC*H*), 7.95 (1H, br s, N*H*), 7.82 (1H, s, CH_3NNC*H*), 7.67 (1H, dd, *J* 8.2, 2.1, C(6')*H*), 7.27 (1H, d, *J* 8.2, C(5')*H*), 3.91 (3H, s, CH_3NN), 2.86 (3H, s, C(3)CH_3), 2.83 (4H, br s, ArNCH_2), 2.61 (4H, br s, $ArNCH_2CH_2$), 2.39 (3H, s, NCH_3), 1.59 (9H, s, $(CH_3)_3$); ^{13}C NMR (126 MHz; $CDCl_3$) δ 155.0 (*C*(6)), 151.8 (*C*=O), 148.5 (*C*(3)), 143.3 (*C*(4')), 139.1 (*C*(9)), 138.6 (CH_3NNCH), 134.1 (*C*(8)), 133.4 (*C*(1')), 132.9 (*C*(3')), 132.6 ($CH_3NCHCSO_2$), 123.1 (*C*(5')H), 122.0 (*C*(6')H), 121.4 (SO_2C), 115.7 (*C*(2')H), 100.4 (*C*(7)H), 83.1 ($C(CH_3)_3$), 55.4 ($ArNCH_2CH_2$), 52.2 ($ArNCH_2$), 46.1 (NCH_3), 39.6 (CH_3NN), 28.1 ($(CH_3)_3$), 10.0 (C(3)CH_3); *m/z* (ES^+) 583 [$(M+H)^+$, 100%]; HRMS *m/z* (ES^+) [Found $(M+H)^+$ 583.2557.

$C_{26}H_{35}N_{10}O_4S^+$ requires M^+, 583.2558]; HPLC (method 2) pH 10 retention time 1.94 min, purity 100%, pH 3 retention time 1.56 min, purity 100%.

***tert*-Butyl-(3-methyl-6-(3-(1-methyl-1*H*-imidazole-2-sulfonamido)-4-(4-methylpiperazin-1-yl)phenyl)[1,2,4]triazolo[4,3-*b*]pyridazin-8-yl)carbamate** (**110**)

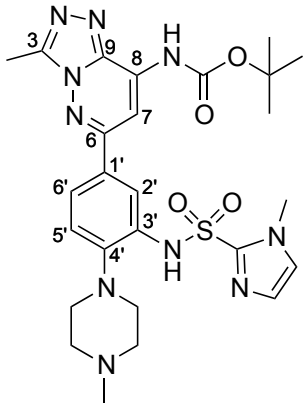

To a solution of *tert*-butyl-(6-(3-amino-4-(4-methylpiperazin-1-yl)phenyl)-3-methyl[1,2,4]triazolo[4,3-*b*]pyridazin-8-yl)carbamate **2** (50 mg, 110 µmol, 1.0 eq) and 4-DMAP (1 mg, 8 µmol, 0.07 eq) in pyridine (1.0 mL) was added 1-methyl-1*H*-imidazole-2-sulfonyl chloride (103 mg, 570 µmol, 5.0 eq) dropwise *via* syringe. The solution was heated for 17 h at 70 °C then cooled to RT and concentrated *in vacuo*. The residue was redissolved in CH_2Cl_2 (40 mL), washed with brine (40 mL), dried over sodium sulfate, filtered, and concentrated *in vacuo*. The crude material was purified by preparative HPLC to give *tert-butyl-3-methyl-6-(3-(1-methyl-*1*H-imidazole-2-sulfonamido)-4-(4-methylpiperazin-1-yl)phenyl)[1,2,4]triazolo[4,3-b]pyridazin-8-yl)carbamate* **110** (10 mg, 15%) as a colourless solid: R_f 0.05 (methanol/ethyl acetate, 20:80); mp 127-130 °C (from ethyl acetate); ν_{max} (thin film)/cm^{-1} 3401 (m), 2981 (m), 1735 (m), 1570 (m), 1539 (m), 1505 (m), 1470 (m), 1418 (m), 1396 (s),

1371 (m), 1371 (m), 1345 (s), 1152 (s), 1116 (s); ^{1}H NMR (500 MHz; $CDCl_3$) δ 8.15 (1H, d, *J* 1.9, C(2')*H*), 8.12 (1H, br s, N*H*), 8.01 (1H, s, C(7)*H*), 7.67 (1H, dd, *J* 8.1, 1.9, C(6')*H*), 7.29 (1H, d, *J* 8.1, C(5')*H*), 7.07 (1H, d, *J* 0.8, SO_2CNCH_3CCH), 6.93 (1H, d, *J* 0.8, SO_2CNCH_3CH), 4.01 (3H, s, SO_2CNCH_3) 2.93 (4H, t, *J* 4.7, $ArNCH_2$), 2.65 (4H, br s, $ArNCH_2CH_2$), 2.82 (3H, s, $C(3)CH_3$), 2.39 (3H, s, NCH_3), 1.57 (9H, s, $(CH_3)_3$); ^{13}C NMR (126 MHz; $CDCl_3$) δ 154.9 *C*(6), 151.6 (*C*=O), 148.4 (*C*(3)), 144.1 (*C*(4')), 139.1 (*C*(9)), 134.1 (*C*(8)), 133.3 (C(1')), 133.0 (*C*(3')), 122.2 (*C*(5')H), 123.9 (*C*(6')H), 116.6 (*C*(2')H), 100.4 (*C*(7)H), 83.0 ($C(CH_3)_3$), 55.5 ($ArNCH_2CH_2$), 52.3 ($ArNCH_2$), 46.1 (NCH_3), 28.1 ($(CH_3)_3$), 9.9 ($C(3)CH_3$); *m/z* (ES^+) 583 [$(M+H)^+$, 100%]; HRMS *m/z* (ES^+) [Found $(M+H)^+$ 583.2550. $C_{26}H_{35}N_{10}O_4S^+$ requires M^+, 583.2558]; HPLC (method 2) pH 10 retention time 1.55 min, purity 99.5%, pH 3 retention time 1.63 min, purity 99.3%.

Chapter 4 Procedures

6-Chloro-3-ethyl[1,2,4]triazolo[4,3-*b*]pyridazin-8-amine (**112i**)

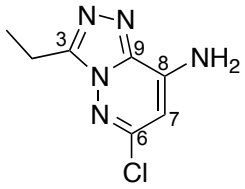

Propionoic acid (4.0 mL, 4.0 g, 25 mmol, 9.9 eq) was added *via* syringe to a 2-5 mL MW vial containing **63** (400 mg, 2.50 mmol, 1 eq) and the reaction mixture was heated at 110 °C with microwave irradiation for 70 min. After cooling to RT, addition of water (1 mL) aided precipitation. The residue was washed with cold water (5 mL), redissolved in ethyl acetate (100 mL) and washed with 2 M K_2CO_3 (3 × 100 mL), brine (100 mL), dried over sodium sulfate, filtered, and concentrated *in vacuo* to give **112i** (264 mg, 54%) as a colourless solid: R_f 0.46 (methanol/CH_2Cl_2, 10:90); mp 171-174 °C (from acetone); ν_{max} (thin film)/cm^{-1} 3320-3300 (br, w), 3156 (m), 2963 (w), 1657 (s), 1567 (s), 1469 (s), 1431 (m), 1369 (w), 1341 (w), 1260 (w), 1101 (s), 1020 (s); ^{1}H NMR (700 MHz; D_6-acetone) δ 7.18 (2H, br s, N*H*$_2$), 6.26 (1H, s, C(7)*H*), 3.04 (2H, q, *J* 7.6, C*H*$_2$), 1.40 (3H, t, *J* 7.6, C*H*$_3$); ^{13}C NMR (126 MHz; D_6-acetone) δ 151.1 (*C*(3)), 149.7 (*C*(6)), 143.8 (*C*(8)), 139.6 (*C*(9)), 94.3 (*C*(7)H), 17.5 (*C*H$_2$), 10.3 (*C*H$_3$); *m/z* (ES^+) 198 [$(M+H)^+$, 100%]; *m/z* (ES^+) 198.0546 [$(M+H)^+$, 100%]; HRMS *m/z* (ES^+) [Found, 198.0546 $(M+H)^+$; $C_7H_9ClN_5^+$ requires M^+, 198.0541].

***tert*-Butyl-(6-chloro-3-ethyl[1,2,4]triazolo[4,3-*b*]pyridazin-8-yl)carbamate** (**112ii**)

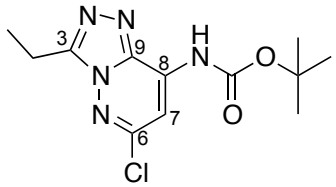

To a solution of 6-chloro-3-ethyl[1,2,4]triazolo[4,3-*b*]pyridazin-8-amine **112i** (261 mg, 1.32 mmol, 1.0 eq) in THF (15 mL), was added a solution of di-*tert*-butyl dicarbonate (316 mg, 1.45 mmol, 1.1 eq) and 4-DMAP (8 mg, 70 µmol, 0.05 eq) in THF (2.0 mL), dropwise at RT. The reaction solution was stirred at RT for 24 h, then concentrated *in vacuo*, redissolved in ethyl acetate (60 mL), washed with saturated aqueous NH_4Cl (2 × 50 mL), water (50 mL) and brine (50 mL). The organic layer was dried over magnesium sulfate, filtered, and concentrated *in vacuo*, then purified by silica gel column chromatography, eluting with diethyl ether and petroleum ether (40:60) to afford *tert-butyl-(6-chloro-3-ethyl[1,2,4]triazolo[4,3-b]pyridazin-8-yl)carbamate* **112ii** (160 mg, 41%) as a colourless solid: R_f 0.19 (diethyl ether/petroleum ether, 50:50); mp 143-144 °C (from methanol); ν_{max} (solid)/cm^{-1} 3169 (w), 3127 (w), 2976 (w), 2931 (w), 1737 (s), 1612 (w), 1539 (m), 1466 (m), 1416 (m), 1393 (m), 1367 (m), 1336 (m), 1292 (m), 1264 (m), 1241 (s), 1157 (s), 1110 (s), 1045 (m); ^{1}H NMR (400 MHz; $CDCl_3$) δ 8.18 (1H, br s, N*H*), 7.69 (1H, s, C(7)*H*), 3.17 (2H, q, *J* 7.6, C(3)CH_2), 1.56 (9H, s, C(CH_3)$_3$)), 1.49 (3H, t, *J* 7.6, C(3)CH_2CH_3); ^{13}C NMR (126 MHz; $CDCl_3$) δ 152.5 (*C*(3)), 151.2 (*C*(6)), 150.9 (C=O), 139.4 (*C*(8)), 138.6 (*C*(9)), 103.1 (*C*(7)H), 83.7 (*C*(CH_3)$_3$), 28.0 ((*C*H_3)$_3$), 17.9 (C(3)*C*H_2), 11.0 (C(3)CH_2CH_3); *m/z* (ES$^+$) 298 [(M+H)$^+$, 100%], 320 [(M+Na)$^+$, 30%); HRMS *m/z* (ES$^+$) [Found (M+H)$^+$,

320.0888; $C_{12}H_{16}ClN_5NaO_2^+$ requires M^+, 320.0885]; HPLC (method 1) retention time 16.14 min, purity 97.7%.

tert-Butyl-(6-chloro-3-propyl[1,2,4]triazolo[4,3-*b*]pyridazin-8-yl)carbamate (129)

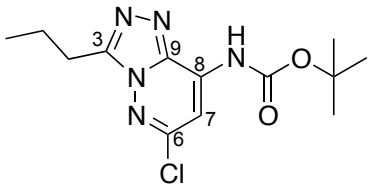

Butyric acid (2.0 mL, 1.9 g, 22 mmol, 22.2 eq) was added *via* syringe to a 2-5 mL MW vial containing **63** (200 mg, 1.25 mmol, 1.0 eq) and the reaction mixture was heated at 110 °C with microwave irradiation for 70 min. After cooling to RT, the reaction mixture was concentrated *in vacuo*. The residue was redissolved in ethyl acetate (100 mL) and washed with 2 M aqueous K_2CO_3 (3 × 100 mL), brine (100 mL), dried over sodium sulfate, filtered, and concentrated *in vacuo* to give *6-chloro-3-propyl-[1,2,4]triazolo[4,3-b]pyridazin-8-amine* **128** (172 mg, 65%) as a colourless solid, which was used without further purification. 6-Chloro-3-propyl[1,2,4]triazolo[4,3-*b*]pyridazin-8-amine (170 mg, 802 µmol, 1.0 eq) was dissolved in THF (15 mL). To this, a solution of di-*tert*-butyl dicarbonate (192 mg, 882 µmol, 1.1 eq) and 4-DMAP (5 mg, 40 µmol, 0.05 eq) in THF (3.0 mL) was added dropwise at RT. The reaction solution was stirred at RT for 24 h, after which time TLC analysis indicated complete consumption of amine. The reaction solution was concentrated *in vacuo*, redissolved in ethyl acetate (50 mL), washed with saturated aqueous NH_4Cl (2 × 50 mL), water (50 mL), and brine (50 mL). The organic layer was dried over magnesium sulfate, filtered, and concentrated *in vacuo*, then

purified by silica gel column chromatography, eluting with diethyl ether, petroleum ether and triethylamine (30:69:1, 40:69:1), to afford **129** (78 mg, 20% over two steps) as a colourless solid: R_f 0.18 (diethyl ether/petrol/triethylamine, 49.5:49.5:1); mp 122-123 °C (from methanol); ν_{max} (solid)/cm^{-1} 3174 (w), 3131 (w), 2961 (w), 2930 (w), 2873 (w), 1735 (s), 1610 (m), 1558 (s), 1465 (s), 1413 (m), 1393 (m), 1367 (m), 1335 (m), 1298 (m), 1280 (w), 1264 (m), 1241 (s), 1156 (s), 1076 (m), 1047 (s); ^{1}H NMR (500 MHz; $CDCl_3$) δ 8.17 (1H, br s, N*H*), 7.69 (1H, s C(7)*H*), 3.13 (2H, t, *J* 7.5, C(3)CH_2), 1.95-1.91 (2H, m, C(3)CH$_2$CH_2), 1.56 (9H, s, C(CH_3)$_3$), 1.05 (3H, t, *J* 7.4, C(3)CH$_2$CH$_2$CH_3); ^{13}C NMR (126 MHz; $CDCl_3$) δ 151.9 (*C*(3)), 151.5 (*C*(6)), 150.9 (C=O), 138.5 (C(9)), 134.9 (*C*(8)), 103.1 (*C*(7)H), 83.7 (*C*(CH$_3$)$_3$), 28.0 (C(*C*H$_3$)$_3$), 26.0 (C(3)*C*H$_2$), 20.1 (C(3)CH$_2$*C*H$_2$), 13.8 (C(3)CH$_2$*C*H$_2$*C*H$_3$); *m/z* (ES$^+$) 312 [(M+H)$^+$, 100%], 334 [(M+Na)$^+$, 20%); HRMS *m/z* (ES$^+$) [Found (M+Na)$^+$, 334.1050; $C_{13}H_{18}ClN_5NaO_2^+$ requires M$^+$, 334.1041]; HPLC (method 1) retention time 13.06 min, purity 95.0%.

tert-Butyl-(6-chloro-3-isopropyl[1,2,4]triazolo[4,3-*b*]pyridazin-8-yl)carbamate (**116i**)

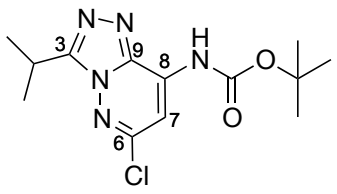

Isobutyric acid (2.0 mL, 1.94 g, 22.0 mmol, 17.6 eq) was added *via* syringe to a 2-5 mL MW vial containing 6-chloro-3-hydrazinylpyridazin-4-amine **63** (200 mg, 1.25 mmol, 1 eq) and the mixture was heated at 110 °C under

microwave irradiation for 70 min. After cooling to RT the mixture was concentrated *in vacuo*. The residue was partially redissolved in ethyl acetate (40 mL) and washed with 2 M aqueous K_2CO_3 (3 × 40 mL), brine (40 mL), dried over sodium sulfate, filtered, and concentrated *in vacuo* to give a pale brown solid (224 mg). This solid was redissolved in THF (25 mL) and stirred at RT for 10 min. A solution of di-*tert*-butyl dicarbonate (204 mg, 936 μmol, 0.75 eq) and 4-DMAP (5 mg, 41 μmol, 0.03 eq) in THF (5.0 mL) was added dropwise to the amine solution *via* syringe and stirred for 24 h at RT. After this time the reaction mixture was concentrated *in vacuo* then redissolved in ethyl acetate (100 mL), washed with saturated aqueous NH_4Cl (100 mL), water (2 × 100 mL) and brine (100 mL). The organic layer was dried over magnesium sulfate, filtered, and concentrated *in vacuo*, then purified by silica gel column chromatography, eluting with diethyl ether, petroleum ether and triethylamine (30:69:1), to afford *tert-butyl-(6-chloro-3-isopropyl[1,2,4]triazolo[4,3-b]pyridazin-8-yl)carbamate* **116i** (62 mg, 16%) as a colourless solid: R_f 0.64 (diethyl ether/petroleum ether, 50:50); mp 166-167 °C (from $CHCl_3$); ν_{max} (thin film)/cm^{-1} 3396 (w), 3176 (m), 2360 (w), 2341 (w), 1737 (s), 1611 (m), 1556 (m), 1465 (m), 1416 (m), 1393 (m), 1368 (m), 1335 (m), 1288 (m), 1264 (m), 1243 (s), 1153 (s), 1109 (s); ^{1}H NMR (500 MHz; $CDCl_3$) δ 8.19 (1H, br s, N*H*), 7.69 (1H, s, C(7)*H*), 3.60 (1H, sp, *J* 7.0, C(3)C*H*), 1.57 (9H, s, (CH_3)$_3$), 1.52 (6H, d, *J* 7.0, C(3)CH(CH_3)$_2$); ^{13}C NMR (126 MHz; $CDCl_3$) δ 155.6 (*C*(3)), 151.2 (*C*=O), 150.7 (*C*(6)), 138.5 (*C*(9)), 134.9 (*C*(8)), 103.0 (*C*(7)H), 83.7 (*C*(CH$_3$)$_3$), 28.1 ((*C*H$_3$)$_3$), 25.2 (C(3)*C*H), 19.9 (C(3)CH(*C*H$_3$)$_2$); *m/z* (ES$^+$) 312 [(M+H)$^+$, 100%], 334 [(M+Na)$^+$, 35%];

HRMS *m/z* (ES^+) [Found $(M+H)^+$ 312.1219. $C_{13}H_{19}N_5O_2Cl^+$ requires M^+, 312.1222]; HPLC (method 1) retention time 17.08 min, purity 98.1%.

tert-Butyl-(6-chloro-3-cyclopropyl[1,2,4]triazolo[4,3-*b*]pyridazin-8-yl)carbamate (**117i**)

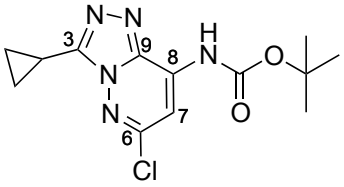

Cyclopropanecarboxylic acid (2.0 mL, 2.2 g, 22.0 mmol, 25 eq) was added *via* syringe to a 2-5 mL MW vial containing 6-chloro-3-hydrazinylpyridazin-4-amine **63** (200 mg, 1.25 mmol, 20.1 eq) and the reaction mixture was heated at 110 °C with microwave irradiation for 70 min. After cooling to RT, the reaction mixture was concentrated *in vacuo*. The residue was washed partially redissolved in ethyl acetate (40 mL) and washed with 2 M aqueous K_2CO_3 (3 × 40 mL), brine (40 mL), dried over sodium sulfate, filtered, and concentrated *in vacuo* to give a pale brown solid (183 mg). This solid was redissolved in THF (20 mL) and stirred at RT for 10 min. A solution of di-*tert*-butyl dicarbonate (148 mg, 679 µmol, 0.54 eq) and 4-DMAP (3 mg, 30 µmol, 0.024 eq) in THF (4.0 mL) was added dropwise to the amine solution *via* syringe and stirred for 24 h at RT. After this time the reaction mixture was concentrated *in vacuo* then redissolved in ethyl acetate (70 mL), washed with saturated aqueous NH_4Cl (70 mL), water (2 × 70 mL) and brine (70 mL). The organic layer was dried over magnesium sulfate, filtered, and concentrated *in vacuo*, then purified by silica gel column chromatography, eluting with diethyl ether, petroleum ether and triethylamine (20:79:1), to afford *tert-butyl-(6-*

chloro-3-cyclopropyl[1,2,4]triazolo[4,3-b]pyridazin-8-yl)carbamate **117i** (117 mg, 30%) as a colourless solid: R_f 0.28 (diethyl ether/petroleum ether, 1:1); mp 173-175 °C (from $CHCl_3$); ν_{max} (thin film)/cm^{-1} 3400 (w), 2980 (w), 3950 (w), 1737 (s), 1611 (w), 1556 (s), 1465 (m), 1416 (m), 1369 (m), 1289 (m), 1242 (s), 1152 (s), 1109 (m), 1025 (w); *m/z* (ES^+) 310 [$(M+H)^+$, 100%], 332 [$(M+Na)^+$, 55%]; ^1H NMR (400 MHz; $CDCl_3$) δ 8.13 (1H, br s, N*H*), 7.69 (1H, s, C(7)*H*), 2.45-2.40 (1H, m, C(3)C*H*), 1.55 (9H, s, $C(CH_3)_3$), 1.36-1.33 (2H, m, C(3)CHCH_A), 1.23-1.20 (2H, m, C(3)CHCH_B); HRMS *m/z* (ES^+) [Found $(M+H)^+$ 310.1059. $C_{13}H_{17}O_2N_5Cl$ requires M^+, 310.1065]; HPLC: retention time 16.47 min, purity 98.1%.

***tert*-Butyl-(3-butyl-6-chloro[1,2,4]triazolo[4,3-*b*]pyridazin-8-yl)carbamate** (**114i**)

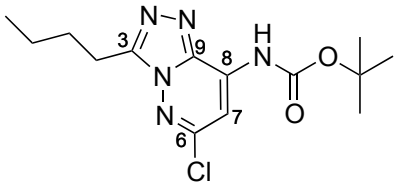

To a 2-5 mL MW vial containing 6-chloro-3-hydrazinylpyridazin-4-amine **63** (200 mg, 1.25 mmol, 1.0 eq) was added valeric acid (2.0 mL, 1.9 g, 15 mmol, 18 eq) *via* syringe and the reaction mixture was heated at 110 °C with microwave irradiation for 70 min after which time TLC analysis indicated complete consumption of **63**. After cooling to RT the reaction mixture was concentrated *in vacuo*. The residue was partially redissolved in ethyl acetate (125 mL) and washed with 2 M aqueous K_2CO_3 (3 × 125 mL), brine (125 mL), dried over sodium sulfate, filtered, and concentrated *in vacuo* to give a pale brown solid (250 mg, 0.904 mmol). This solid was redissolved in THF (25 mL)

and stirred at RT for 10 min. A solution of di-*tert*-butyl dicarbonate (250 mg, 1.15 mmol, 1.27 eq) and 4-DMAP (8 mg, 70 μmol, 0.07 eq) in THF (5.0 mL) was added dropwise to the amine solution *via* syringe and stirred for 20 h at RT. After this time the reaction mixture was concentrated *in vacuo* then redissolved in ethyl acetate (120 mL), washed with saturated aqueous NH_4Cl (3 × 120 mL), water (120 mL) and brine (120 mL). The organic layer was dried over magnesium sulfate, filtered, and concentrated *in vacuo*, then purified by silica gel column chromatography, eluting with diethyl ether, petroleum ether and triethylamine (30:69:1) to afford *tert-butyl-(3-butyl-6-chloro[1,2,4]triazolo[4,3-b]pyridazin-8-yl)carbamate* **114i** (328 mg, 80%) as a colourless solid: R_f 0.80 (ethyl acetate/petroleum ether, 80:20); mp 120-121 °C (from diethyl ether); ν_{max} (thin film)/cm^{-1} 3404 (w), 3175 (w), 3133 (w), 2961 (w), 2932 (w), 1738 (s), 1610 (m), 1556 (s), 1464 (m), 1292 (m), 1265 (m), 1244 (s), 1154 (s), 1110 (w); ^{1}H NMR (500 MHz; $CDCl_3$) δ 8.22 (1H, br s, N*H*), 7.69 (1H, C(7)*H*), 3.14 (2H, t, *J* 7.7, C(3)CH_2), 1.88 (2H, qt, *J* 7.7, 7.6, C(3)$CH_2C\mathit{H}_2$), 1.56 (9H, s, C($C\mathit{H}_3$)$_3$), 1.46 (2H, qt, *J* 7.6, 7.4, C(3)$CH_2CH_2C\mathit{H}_2$), 0.97 (3H, t, *J* 7.4, C(3)$CH_2CH_2C\mathit{H}_2C\mathit{H}_3$); ^{13}C NMR (126 MHz; $CDCl_3$) δ 151.7 (*C*(3)), 151.2 (*C*=O), 150.9 (*C*(6)), 138.6 (*C*(9)), 134.9 (*C*(8)), 103.1 (*C*(7)H), 83.7 (*C*(CH_3)$_3$), 28.4 (C(3)$CH_2C\mathit{H}_2$), 28.1 (C($C\mathit{H}_3$)$_3$), 23.9 (C(3)$C\mathit{H}_2$), 22.4 (C(3)$CH_2CH_2C\mathit{H}_3$) 13.7 (C(3)$CH_2CH_2CH_2C\mathit{H}_3$); *m/z* ($ES^+$) 326 [$(M+H)^+$, 100%]; HRMS *m/z* ($ES^+$) [Found $(M+Na)^+$ 348.1190. $C_{14}H_{20}N_5ClO_2Na^+$ requires M^+, 348.1198]; HPLC (method 1) retention time 18.18 min, purity 98.9%.

***tert*-Butyl-(3-ethyl-6-(4-(4-methylpiperazin-1-yl)-3-nitrophenyl)[1,2,4]-triazolo[4,3-*b*]pyridazin-8-yl)carbamate** (**112**)

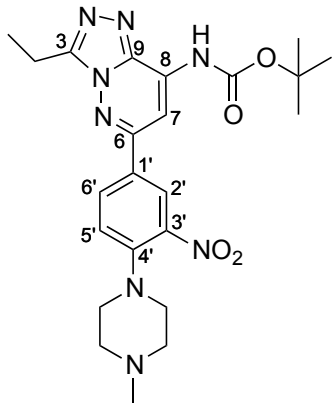

To a 5 mL MW vial containing 1-methyl-4-(2-nitro-4-(4,4,5,5-tetramethyl-1,3,2-dioxaborolan-2-yl)phenyl)piperazine **74** (225 mg, 648 µmol, 2.0 eq) was added *tert*-butyl-(6-chloro-3-ethyl[1,2,4]triazolo[4,3-b]pyridazin-8-yl)carbamate **112ii** (97 mg, 0.324 µmol, 1.0 eq), K_2CO_3 (67 mg, 490 µmol, 1.5 eq), and Pd(dppf)Cl_2·CH_2Cl_2 (26 mg, 32 µmol, 0.1 eq). 1,4-Dioxane and water (10:1, 3 mL) was added *via* syringe and the reaction mixture was heated at 80 °C for 20 h. After cooling to RT the reaction mixture was filtered through Celite® (eluent CH_2Cl_2) and concentrated *in vacuo*. The residue was redissolved in CH_2Cl_2 (50 mL) and partitioned between brine (50 mL), dried over sodium sulfate, filtered, and concentrated *in vacuo*. The crude material was purified by silica gel column chromatography, eluting with petroleum ether, ethyl acetate and triethylamine (79:20:1, 69:30:1, 59:40:1, 29:70:1, 9:90:1, 0:99:1), to afford *tert-butyl-(3-ethyl-6-(4-(4-methylpiperazin-1-yl)-3-nitrophenyl)[1,2,4]triazolo[4,3-b]pyridazin-8-yl)carbamate* **112** (68 mg, 43%) as an orange-yellow oil: R_f 0.10 (methanol/ethyl acetate/triethylamine, 3:96:1); ν_{max} (solid)/cm^{-1} 3406 (w), 3173 (w), 2979 (w), 2939 (w), 2882 (w), 2844 (w), 2801 (w), 1735 (m), 1614 (m), 1569 (m), 1532 (s), 1506 (m), 1466 (m),

1420 (m), 1394 (m), 1367 (m), 1292 (m), 1239 (m), 1202 (m), 1152 (s), 1094 (m), 1045 (m); ^{1}H NMR (500 MHz; $CDCl_3$) δ 8.43 (1H, d, *J* 2.2, C(2')*H*), 8.16 (1H, br s, N*H*), 8.08 (1H, dd, *J* 8.7, 2.2, C(6')*H*), 8.08 (1H, s, C(7)*H*), 7.42 (1H, d, *J* 8.7, C(5')*H*), 3.25 (2H, q, *J* 7.5, C(3)CH_2), 3.20 (4H, t, *J* 4.8, ArNCH_2), 2.60 (4H, t, *J* 4.8, ArNCH$_2$CH_2), 2.37 (3H, s, NCH_3), 1.57 (9H, s, C(CH_3)$_3$), 1.52 (3H, t, *J* 7.5, C(3)CH$_2$CH_3); ^{13}C NMR (126 MHz; $CDCl_3$) δ 152.9 (*C*(6)), 152.8 (*C*(3)), 151.6 (*C*=O), 147.0 (*C*(4')), 142.0 (*C*(3')), 139.1 (*C*(9)), 134.5 (*C*(8)), 131.9 (*C*(6')H), 127.9 (*C*(1')), 125.3 (*C*(2')H), 120.5 (*C*(5')H), 99.4 (*C*(7)H), 83.2 (*C*(CH$_3$)$_3$), 54.7 (ArNCH$_2$*C*H$_2$), 51.0 (ArN*C*H$_2$), 46.0 (N*C*H$_3$) 28.1 (C(*C*H$_3$)$_3$), 18.1 (C(3)*C*H$_2$), 11.1 (C(3)CH$_2$*C*H$_3$); *m/z* (ES$^+$) 483 [(M+H)$^+$, 100%]; HRMS *m/z* (ES$^+$) [Found (M+Na)$^+$, 483.2461; $C_{23}H_{31}N_8O_4^+$ requires M$^+$, 483.2463]; HPLC (method 1) retention time 12.52 min, purity 95.8%.

***tert*-Butyl-(6-(4-(4-methylpiperazin-1-yl)-3-nitrophenyl)-3-propyl[1,2,4]triazolo[4,3-*b*]pyridazin-8-yl)carbamate** (**113**)

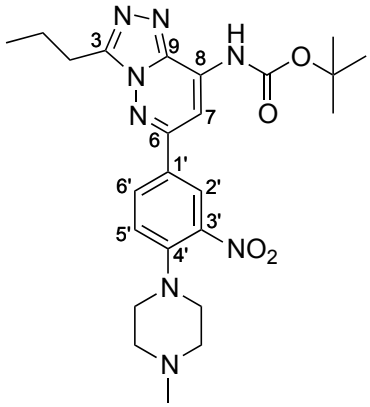

To a 2-5 mL MW vial containing 1-methyl-4-(2-nitro-4-(4,4,5,5-tetramethyl-1,3,2-dioxaborolan-2-yl)phenyl)piperazine **74** (200 mg, 578 µmol, 2.5 eq) was added *tert*-butyl-(6-chloro-3-propyl[1,2,4]triazolo[4,3-*b*]pyridazin-8-yl)carbamate **129** (72 mg, 230 µmol, 1.0 eq), K_2CO_3 (48 mg, 350 µmol, 1.5 eq), and Pd(dppf)Cl_2·CH_2Cl_2 (19 mg, 23 µmol, 0.1 eq). 1,4-Dioxane and water (10:1, 3 mL) was added *via* syringe and the reaction mixture was heated at 80 °C for 20 h. After cooling to RT the reaction mixture was filtered through Celite® (eluent CH_2Cl_2) and concentrated *in vacuo*. The residue was redissolved in CH_2Cl_2 (120 mL) and partitioned between brine (120 mL), dried over sodium sulfate, filtered, and concentrated *in vacuo*. The crude material was purified by silica gel column chromatography, eluting with petroleum ether, ethyl acetate and triethylamine (79:20:1, 69:30:1, 59:40:1, 49:50:1, 29:70:1, 19:80:1) to afford *tert-butyl-(6-(4-(4-methylpiperazin-1-yl)-3-nitrophenyl)-3-propyl[1,2,4]triazolo[4,3-b]pyridazin-8-yl)carbamate* **113** (68 mg, 43%) as an orange-yellow oil: R_f 0.08 (methanol/ethyl acetate/triethylamine, 3:96:1); ν_{max} (thin film)/cm^{-1} 3407 (w), 2968 (w), 2876 (w), 2842 (w), 2800 (w), 1736 (m), 1614 (m), 1569 (s), 1532 (s), 1464 (m), 1419 (m), 1394 (m),

1367 (m), 1293 (m), 1242 (s), 1201 (m), 1152 (m), 1092 (m); ^{1}H NMR (500 MHz; $CDCl_3$) δ 8.42 (1H, d, *J* 2.2, C(2')*H*), 8.16 (1H, br s, N*H*), 8.08 (1H, dd, *J* 8.7, 2.2, C(6')*H*), 8.07 (1H, s, C(7)*H*), 7.20 (1H, d, *J* 8.7, C(5')*H*), 3.22 (2H, t, *J* 7.5, C(3)CH_2), 3.21 (4H, t, *J* 4.8, ArNCH_2), 2.60 (4H, t, *J* 4.8, ArN CH_2CH_2), 2.37 (3H, s, NCH_3), 1.99-1.96 (2H, m, C(3)CH_2CH_2), 1.57 (9H, s, C(CH_3)$_3$), 1.08 (3H, t, *J* 7.5, C(3)$CH_2CH_2CH_3$); ^{13}C NMR (126 MHz; $CDCl_3$) δ 152.9 (*C*(6)), 151.8 (*C*=O), 151.7 (*C*(3)), 147.0 (*C*(3')), 142.0 (*C*(4')), 139.1 (*C*(9), 134.5 (*C*(8)), 132.0 (*C*(6')H), 127.7 (*C*(1')), 125.3 (C(2')H), 120.6 (*C*(5')H), 99.4 (*C*(7)H), 83.2 (*C*$(CH_3)_3$), 54.7 (ArNCH$_2$*C*H$_2$), 51.0 (ArN*C*H$_2$), 46.0 (N*C*H$_3$), 28.1 (C(*C*H$_3$)$_3$), 26.2 (C(3)*C*H$_2$), 20.2 (C(3)CH$_2$*C*H$_2$), 13.9 (C(3)CH$_2$*C*H$_2$*C*H$_3$); *m/z* (ES$^+$) 497 [(M+H)$^+$, 100%]; HRMS *m/z* (ES$^+$) [Found (M+Na)$^+$, 497.2621; $C_{24}H_{33}N_8O_4^+$ requires M$^+$, 497.2619]; HPLC: retention time 13.06 min, purity 95.0%.

***tert*-Butyl-(3-butyl-6-(4-(4-methylpiperazin-1-yl)-3-nitrophenyl)[1,2,4]triazolo[4,3-*b*]pyridazin-8-yl)carbamate** (**114**)

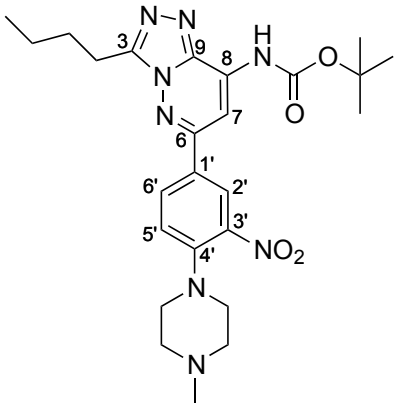

To a 10-20 mL MW vial containing *tert*-butyl-(3-butyl-6-chloro[1,2,4]triazolo[4,3-*b*]pyridazin-8-yl)carbamate **114i** (93 mg, 290 μmol, 1.0 eq), 1-methyl-4-(2-nitro-4-(4,4,5,5-tetramethyl-1,3,2-dioxaborolan-2-

yl)phenyl)piperazine **74** (247 mg, 712 μmol, 2.5 eq), Pd(dppf)Cl_2·CH_2Cl_2 (23 mg, 29 μmol, 0.1 eq) and K_2CO_3 (60 mg, 428 μmol, 1.5 eq), was added 1,4-dioxane/water (10:1, 2.5 mL) *via* syringe. This mixture was stirred at RT with sonication for 5 min to dissolve, then heated at 80 °C for 21 h, at which point it was cooled to RT, filtered through Celite® (eluent CH_2Cl_2) and concentrated *in vacuo*. The residue was redissolved in CH_2Cl_2 (40 mL) and washed with water (40 mL), brine (40 mL), dried over sodium sulfate, filtered, and concentrated *in vacuo*. The crude material was purified by silica gel column chromatography, eluting with ethyl acetate, petroleum ether and triethylamine (20:79:1, 30:69:1, 40:59:1, 50:49:1, 66:33:1, 80:19:1, 99:0:1). Excess pinacol was removed by azeotroping with acetonitrile and water (50:50, 4 mL) then the residue was redissolved in $CHCl_3$ (4 mL), dried over sodium sulfate, filtered, and concentrated *in vacuo* to afford *tert-butyl-(3-butyl-6-(4-(4-methylpiperazin-1-yl)-3-nitrophenyl)[1,2,4]triazolo[4,3-b]pyridazin-8-yl)carbamate* **114** (69 mg, 47%) as a viscous orange oil: R_f 0.61 (methanol/ethyl acetate, 10:90); ν_{max} (thin film)/cm^{-1} 3407 (w), 2960 (w), 2935 (w), 2873 (w), 1736 (s), 1614 (m), 1568 (m), 1553 (s), 1531 (m), 1465 (m), 1202 (s), 1151 (s); ^{1}H NMR (500 MHz; $CDCl_3$) δ 8.43 (1H, d, *J* 2.3, C(2')*H*), 8.15 (1H, br s, N*H*), 8.09 (1H, dd, *J* 8.8, 2.3, C(6')*H*), 8.07 (1H, s, C(7)*H*), 7.20 (1H, d, *J* 8.8, C(5')*H*), 3.23 (2H, t, *J* 4.7, C(3)CH_2), 3.21 (4H, t, *J* 4.7, ArNCH_2), 2.61 (4H, t, *J* 4.7, ArNCH_2CH_2), 2.38 (3H, s, NCH_3), 1.93 (2H, tt, *J* 7.6, 4.7, C(3)CH_2CH_2), 1.57 (9H, s, C(CH_3)$_3$), 1.48 (2H, qt, *J* 7.6, 7.4, C(3)CH_2CH_2CH_2), 1.08 (3H, t, *J* 7.5, C(3)CH_2CH_2CH_3), 0.99 (3H, t, *J* 7.4, C(3)CH_2CH_2CH_2CH_3); ^{13}C NMR (126 MHz; $CDCl_3$) δ 152.9 (*C*(6)), 152.0 (*C*(3)), 151.7 (*C*=O), 147.0 (*C*(4')),

142.0 (*C*(3')), 134.5 (*C*(8)), 139.0 (*C*(9)), 134.5 (*C*(3')), 132.0 (*C*(6')H), 127.7 (*C*(1')), 125.3 (C(2')H), 120.6 (*C*(5')H), 99.4 (*C*(7)H), 83.2 ($C(CH_3)_3$), 54.7 ($ArNCH_2CH_2$), 51.0 ($ArNCH_2$), 46.0 (NCH_3), 28.8 ($C(3)CH_2$), 28.1 ($C(CH_3)_3$), 22.4 ($C(3)CH_2CH_2CH_2CH_3$), 20.4 ($C(3)CH_2CH_2$), 13.8 ($C(3)CH_2CH_2CH_2CH_3$); *m/z* (ES^+) 511 [$(M+H)^+$, 100%]; HRMS *m/z* (ES^+) [Found $(M+H)^+$ 511.2758. $C_{25}H_{35}N_8O_4^+$ requires M^+, 511.2776]; HPLC (method 1) retention time 13.71 min, purity 95.9%.

***tert*-Butyl-(6-(4-(4-methylpiperazin-1-yl)-3-nitrophenyl)-3-(3,3,3-trifluoropropyl)[1,2,4]triazolo[4,3-*b*]pyridazin-8-yl)carbamate** (**115**)

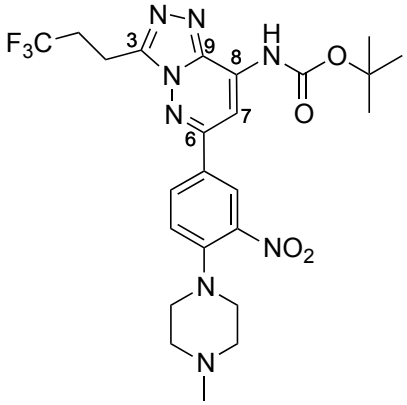

To a 2-5 mL MW vial containing 4,4,4-trifluorobutanoic acid (440 mg, 3.10 mmol, 2.5 eq), in 1,4-dioxane (2.0 mL) was added 6-chloro-3-hydrazinylpyridazin-4-amine **63** (200 mg, 1.25 mmol, 1.0 eq). The reaction solution was heated at 110 °C with microwave irradiation for 3 h, after which time TLC analysis indicated complete consumption of **63**. The solution was cooled to RT overnight, filtered, and washed with water (3.0 mL) to give a pale yellow solid (70 mg). This solid was redissolved in THF (8.0 mL) and a solution of di-*tert*-butyl dicarbonate (55 µL, 52 mg, 237 µmol, 0.9 eq) and 4-DMAP (1.6 mg, 13 µmol, 0.05 eq) in THF (2.0 mL) was added dropwise *via*

syringe. The reaction solution was stirred for 22 h at RT, after which time TLC analysis indicated complete consumption of the aniline. The reaction mixture was concentrated *in vacuo* and redissolved in ethyl acetate (20 mL), washed with saturated aqueous NH_4Cl (2 × 20 mL), water (20 mL) and brine (20 mL). The organic layer was dried over magnesium sulfate, filtered, and concentrated *in vacuo*, then purified by silica gel column chromatography, eluting with diethyl ether and petroleum ether (30:70, 40:60, 50:50, 75:25), to afford *tert*-butyl-(6-chloro-3-(3,3,3-trifluoropropyl)-[1,2,4]triazolo[4,3-*b*]pyridazin-8-yl)carbamate (49 mg) as a colourless solid. To this solid (49 mg, 130 μmol, 1.0 eq), in a 2-5 mL MW vial were added 1-methyl-4-(2-nitro-4-(4,4,5,5-tetramethyl-1,3,2-dioxaborolan-2-yl)phenyl)piperazine **74** (116 mg, 335 μmol, 2.5 eq), $Pd(dppf)Cl_2 \cdot CH_2Cl_2$ (11 mg, 13 μmol, 0.1 eq) and K_2CO_3 (28 mg, 200 μmol, 1.5 eq). 1,4-Dioxane and water (10:1, 3 mL) was added *via* syringe. The reaction solution was heated at 80 °C for 23 h then cooled to RT, filtered through Celite® (eluent CH_2Cl_2) and concentrated *in vacuo*. The residue was redissolved in CH_2Cl_2 (20 mL) and washed with water (20 mL), brine (20 mL), dried over sodium sulfate, filtered, and concentrated *in vacuo*. The crude material was purified by silica gel column chromatography, eluting with ethyl acetate, petroleum ether and triethylamine (10:89:1, 25:74:1, 40:59:1, 60:39:1, 80:19:1), to afford *tert-butyl-(6-(4-(4-methylpiperazin-1-yl)-3-nitrophenyl)-3-(3,3,3-trifluoropropyl)[1,2,4]triazolo[4,3-b]pyridazin-8-yl)carbamate* **115** (14 mg, 2% over 3 steps) as a yellow solid: R_f 0.26 (methanol/ethyl acetate, 10:90); mp 95-98 °C (from ethyl acetate); ν_{max} (thin film)/cm^{-1} 2937 (w), 1737 (m), 1614 (s), 1570 (m), 1533 (s), 1446 (m), 14423 (m), 1369 (m), 1294 (m), 1149 (s); ^1H NMR (500 MHz; $CDCl_3$) 8.42 (1H, d, *J* 2.3,

C(2')*H*), 8.14 (1H, br s, N*H*), 8.10 (1H, dd, *J* 8.9, 2.3, C(6')*H*), 8.13 (1H, s, C(7)*H*), 7.21 (1H, d, *J* 8.9, C(5')*H*), 3.51-3.48 (2H, m, C(3)CH_2), 3.21 (4H, t, *J* 4.9, ArNCH_2), 2.91-2.81 (2H, m, C(3)$CH_2C H_2$), 2.60 (4H, t, *J* 4.9, ArN$CH_2C H_2$), 2.38 (3H, s, NCH_3), 1.58 (9H, s, C(CH_3)$_3$); ^{13}C NMR (126 MHz; $CDCl_3$) δ 153.6 (*C*(6)), 151.5 (*C*=O), 148.7 (*C*(3)), 147.2 (*C*(4')), 141.7 (*C*(3')), 139.5 (*C*(9)), 134.6 (*C*(8)), 131.9 (*C*(6')H), 127.0 (*C*(1')), 125.4 (*C*(2')H), 120.8 (*C*(5')H), 99.8 (*C*(7)H), 83.5 (*C*$(CH_3)_3$), 54.7 (ArN$CH_2C H_2$), 51.0 (ArNCH_2), 30.8 (q, J_{C-F} 29.5, *C*F_3), 29.7 (C(3)CH_2), 28.1 ((*C*H_3)$_3$), 17.8 (q, J_{C-F} = 3.8, (C(3)CH_2CH_2))); ^{19}F NMR (377 MHz; $CDCl_3$) δ −66.9 (t, *J* 10.3, C*F*$_3$); *m/z* (ES$^+$) 551 [(M+H)$^+$, 100%]; HRMS *m/z* (ES$^+$) [Found (M+H)$^+$ 551.2322. $C_{24}H_{30}N_8O_4F_3^+$ requires M$^+$, 551.2337]; HPLC (method 2) pH 10 retention time 1.92 min, purity 98.4%; pH 3 retention time 1.99 min, purity 98.4%.

***tert*-Butyl-(3-isopropyl-6-(4'-(4''-methylpiperazin-1-yl)-3'-nitrophenyl)[1,-2,4]triazolo[4,3-*b*]pyridazin-8-yl)carbamate** (**116**)

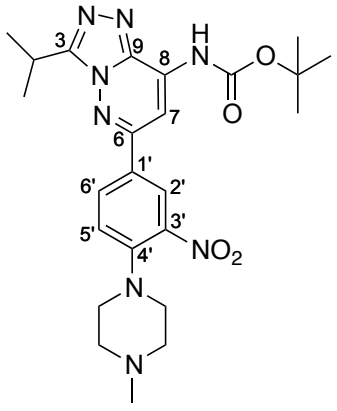

To a 5 mL MW vial containing 1-methyl-4-(2-nitro-4-(4,4,5,5-tetramethyl-1,3,2-dioxaborolan-2-yl)phenyl)piperazine **74** (129 mg, 375 μmol, 2.0 eq) were added *tert*-butyl-(6-chloro-3-isopropyl[1,2,4]triazolo[4,3-*b*]pyridazin-8-

yl)carbamate **116i** (58 mg, 190 μmol, 1.0 eq), K_2CO_3 (39 mg, 280 μmol, 1.5 eq), and Pd(dppf)Cl_2·CH_2Cl_2 (15 mg, 18 μmol, 0.1 eq). 1,4-Dioxane and water (10:1, 2 mL) was added *via* syringe and the reaction mixture was heated at 80 °C for 20 h. After cooling to RT the reaction mixture was filtered through Celite® (eluent CH_2Cl_2) and concentrated *in vacuo*. The residue was redissolved in CH_2Cl_2 (50 mL) and partitioned between brine (50 mL), dried over sodium sulfate, filtered, and concentrated *in vacuo*. The crude material was purified by silica gel column chromatography, eluting with petroleum ether, ethyl acetate and triethylamine (79:20:1, 59:40:1, 39:60:1, 19:80:1) to afford *tert-butyl-(3-isopropyl-6-(4'-(4''-methylpiperazin-1-yl)-3'-nitrophenyl)[1,2,4]triazolo[4,3-b]pyridazin-8-yl)carbamate* **116** (37 mg, 40%) as a pale yellow solid: R_f 0.17 (methanol:ethyl acetate:triethylamine, 8:91:1); mp 191-196 °C (from ethyl acetate); ν_{max} (thin film)/cm^{-1} 3400 (w), 2975 (w), 2934 (w), 2849 (w), 2801 (w), 1735 (m), 1614 (m), 1569 (s), 1532 (s), 1466 (m), 1421 (m), 1367 (m), 1238 (s), 1152 (s), 1008 (w); ^{1}H NMR (400 MHz; $CDCl_3$) δ 8.42 (1H, d, *J* 2.3, C(2')*H*), 8.14 (1H, dd, *J* 8.7, 2.3, C(6')*H*), 8.07 (1H, s, C(7)*H*), 8.06 (1H, br s, N*H*), 7.20 (1H, d, *J* 8.7, C(5')*H*), 3.70 (1H, sp, *J* 7.0, C(3)C*H*), 3.20 (4H, t, *J* 4.8, ArNCH_2), 2.60 (4H, t, *J* 4.8, ArNCH_2CH_2), 2.37 (3H, s, NCH_3), 1.58 (9H, s, C(CH_3)$_3$), 1.56 (6H, d, *J* 7.0 C(3)CH(CH_3)$_2$); ^{13}C NMR (126 MHz; $CDCl_3$) δ 155.9 (*C*(3)), 152.7 (*C*(6)), 151.7 (*C*=O), 147.0 (*C*(4')), 142.0 (*C*(3')), 139.3 (*C*(9)), 134.5 (*C*(8)), 131.9 (*C*(6')H), 127.7 (*C*(1')), 125.3 (*C*(2')H), 120.5 (*C*(5')H), 99.3 (*C*(7)H), 83.1 (*C*(CH_3)$_3$), 54.7 (ArNCH_2*C*H_2), 51.0 (ArN*C*H_2**),** 46.1 (N*C*H_3), 28.1 ((*C*H_3)$_3$), 25.4 (C(3)*C*H), 20.0 (C(3)CH(*C*H_3)$_2$); *m/z* (ES^+) 497 [$(M+H)^+$, 100%]; HRMS

m/z (ES^+) [Found $(M+H)^+$ 497.2613. $C_{24}H_{33}N_8O_4$ requires M^+, 497.2619]; HPLC: retention time 12.97 min, purity 96.2%.

***tert*-Butyl-(6-(3-(cyclopropanesulfonamido)-4'-(4''-methylpiperazin-1-yl)phenyl)-3-methyl[1,2,4]triazolo[4,3-*b*]pyridazin-8-yl)carbamate** (**117**)

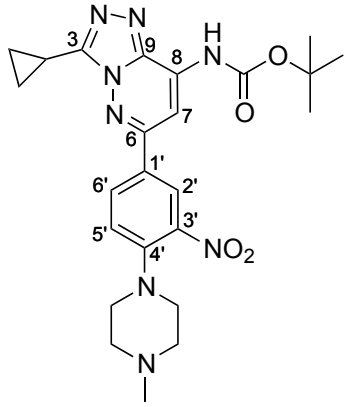

To a 2-5 mL MW vial containing 1-methyl-4-(2-nitro-4-(4,4,5,5-tetramethyl-1,3,2-dioxaborolan-2-yl)phenyl)piperazine **74** (130 mg, 375 µmol, 2.0 eq) were added *tert*-butyl-(6-chloro-3-cyclopropyl[1,2,4]triazolo[4,3-*b*]pyridazin-8-yl)carbamate **117i** (58 mg, 190 µmol, 1.0 eq), K_2CO_3 (39 mg, 280 µmol, 1.5 eq), and $Pd(dppf)Cl_2 \cdot CH_2Cl_2$ (15 mg, 180 µmol, 0.1 eq). 1,4-Dioxane and water (10:1, 1.5 mL) was added *via* syringe and the reaction mixture was heated at 80 °C for 20 h. After cooling to RT the reaction mixture was filtered through Celite® (eluent CH_2Cl_2) and concentrated *in vacuo*. The residue was redissolved in CH_2Cl_2 (80 mL) and washed with brine (80 mL), dried over sodium sulfate, filtered, and concentrated *in vacuo*. The crude material was purified by silica gel column chromatography, eluting with petroleum ether, ethyl acetate and triethylamine (79:20:1, 59:40:1, 39:60:1, 19:80:1), to afford *tert-butyl-(6-(3-(cyclopropanesulfonamido)-4'-(4''-methylpiperazin-1-yl)phenyl)-3-methyl[1,2,4]triazolo[4,3-b]pyridazin-8-yl)carbamate* **117** (37 mg, 40%) as

an orange-yellow oil: R_f 0.14 (methanol/ethyl acetate/triethylamine, 8:91:1); ν_{max} (thin film)/cm^{-1} 3390 (w), 2973 (w), 2934 (w), 2850 (w), 2801 (w), 1736 (m), 1614 (m), 1569 (s), 1532 (s), 1466 (m), 1421 (m), 1367 (m), 1238 (s), 1152 (s), 1008 (w); ^{1}H NMR (400 MHz; $CDCl_3$) δ 8.45 (1H, d, *J* 2.3, C(2')*H*), 8.14 (1H, br s, N*H*), 8.09 (1H, dd, *J* 8.8, 2.3, C(6')*H*), 8.06 (1H, s, C(7)*H*), 7.19 (1H, d, *J* 8.8, C(5')*H*), 3.20 (4H, t, *J* 4.8, ArNCH_2), 2.60 (4H, t, *J* 4.8, ArNCH$_2$CH_2), 2.58-2.54 (1H, m, C(3)C*H*), 2.37 (3H, s, NCH_3), 1.57 (9H, s, C(CH_3)$_3$), 1.42-1.38 (2H, m, C(3)CHCH_A), 1.26-1.21 (2H, m, C(3)CHCH_B); ^{13}C NMR (126 MHz; $CDCl_3$) δ 155.9 (*C*(3)), 152.9 (*C*(6)), 151.7 (*C*=O), 147.0 (*C*(4')), 142.0 (*C*(3')), 139.1 (*C*(9)), 134.4 (*C*(8)), 132.0 (*C*(6')H), 127.7 (*C*(1')), 125.3 (*C*(2')H), 120.5 (*C*(5')H), 99.3 (*C*(7)H), 83.2 (*C*(CH$_3$)$_3$), 54.7 (ArNCH$_2$*C*H$_2$), 51.0 (ArN*C*H$_2$), 46.1 (N*C*H$_3$), 28.1 ((*C*H$_3$)$_3$), 7.9 (C(3)C(*C*H$_2$)$_2$), 5.4 (C(3)*C*H); *m/z* (ES$^+$) 536 [(M+MeCN+H)$^+$, 100%], 495 [(M+H)$^+$, 99%], 989 [(2M+H)$^+$, 75%]; HRMS *m/z* (ES$^+$) [Found (M+H)$^+$ 495.2448. $C_{24}H_{31}N_8O_4^+$ requires M$^+$, 495.2463]; HPLC (method 1) retention time 12.81 min, purity 95.5%.

***tert*-Butyl-(6-(3-amino-4-(4-methylpiperazin-1-yl)phenyl)-3-propyl[1,2,4]triazolo[4,3-*b*]pyridazin-8-yl)carbamate** (**126**)

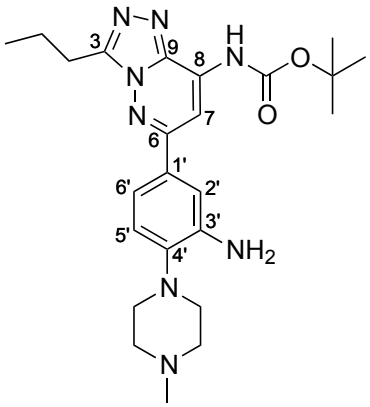

To a suspension of *tert*-butyl-(3-methyl-6-(4-(4-methylpiperazin-1-yl)-3-nitrophenyl)[1,2,4]triazolo[4,3-*b*]pyridazin-8-yl)carbamate **113** (249 mg, 501 µmol, 1.0 eq) in ethanol/triethylamine (2:1, 7.5 mL) was added tin(II) chloride (392 mg, 1.50 mmol, 3.0 eq) and the reaction solution was heated at 70 °C for 1 h after which time TLC analysis indicated complete consumption of **113**. The reaction was cooled to RT and the colourless precipitate was removed *via* filtration and washed with ethyl acetate (17 mL). The filtrate was concentrated *in vacuo*, then saturated aqueous potassium fluoride (15 mL) was added. The suspension was stirred for 24 h at RT, diluted with water (250 mL) and extracted with ethyl acetate (250 mL). The organic layer was washed with water (3 × 250 mL), brine (250 mL), dried over sodium sulfate, filtered, and concentrated *in vacuo* to give *tert-butyl-(6-(3-amino-4-(4-methylpiperazin-1-yl)phenyl)-3-propyl[1,2,4]triazolo[4,3-b]pyridazin-8-yl)carbamate* **126** (233 mg, 85%) as an orange solid: R_f 0.05 (methanol/ethyl acetate/triethylamine, 10:89:1); ν_{max} (thin film)/cm^{-1} 3401 (w), 3335 (w), 3176 (w), 2966 (w), 2936 (w), 2798 (w), 1734 (m), 1613 (s), 1566 (m), 1394 (m), 1437 (m), 1369 (m), 1290 (m), 1241 (s), 1152 (s); ^{1}H NMR

(500 MHz; $CDCl_3$) δ 8.07 (1H, br s, C(8)N*H*), 8.06 (1H, s, C(7)*H*), 7.37 (1H, dd, *J* 8.3, 2.1, C(6')*H*), 7.36 (1H, d, *J* 2.1, C(2')*H*), 7.09 (1H, d, *J* 8.3, C(5')*H*), 4.08 (2H, br s, NH_2), 3.21 (2H, t, *J* 7.6, C(3)CH_2), 3.08-2.91 (4H, br s, ArNCH_2), 2.83-2.44 (4H, br s, ArNCH$_2$CH_2), 2.39 (3H, s, NCH_3), 1.98 (2H, qt, *J* 7.6, 7.4, C(3)CH$_2$CH_2), 1.57 (9H, s, C(CH_3)$_3$), 1.06 (3H, t, *J* 7.4, C(3)CH$_2$CH$_2$CH_3); ^{13}C NMR (126 MHz; $CDCl_3$) δ 155.4 (*C*(6)), 151.74 (*C*=O), 151.67 (*C*(3)), 141.7 (*C*(4')), 144.5 (*C*(3')), 139.3 (*C*(9)), 133.7 (*C*(8)), 131.4 (*C*(1')), 119.9 (*C*(5')H), 118.2 (*C*(6')H), 113.6 (*C*(2')H), 100.6 (*C*(7)H), 82.8 (*C*(CH$_3$)$_3$), 55.7 (ArNCH$_2$*C*H$_2$), 50.6 (ArN*C*H$_2$), 46.2 (N*C*H$_3$), 28.1 (C(*C*H$_3$)$_3$), 26.3 (C(3)*C*H$_2$), 20.2 (C(3)CH$_2$*C*H$_2$), 14.0 (C(3)CH$_2$CH$_2$*C*H$_3$); *m/z* (ES^+) 467 [$(M+H)^+$, 100%]; HRMS *m/z* (ES^+) [Found $(M+H)^+$ 467.2869. $C_{24}H_{35}N_8O_2$ requires M^+, 467.2878]; HPLC (method 1) retention time 13.63 min, purity 96.8%.

***tert*-Butyl-(6-(3-(4-methylphenylsulfonamido)-4-(4-methylpiperazin-1-yl)phenyl)-3-propyl[1,2,4]triazolo[4,3-*b*]pyridazin-8-yl)carbamate** (**121**)

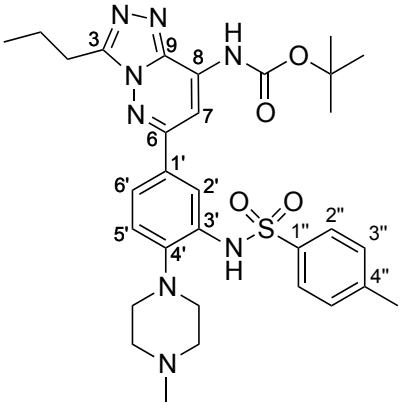

To a solution of *tert*-butyl-(6-(3-amino-4-(4-methylpiperazin-1-yl)phenyl)-3-propyl[1,2,4]triazolo[4,3-*b*]pyridazin-8-yl)carbamate **126** (50 mg, 107 μmol, 1.0 eq) in pyridine (700 μL) was added a solution of 4-toluenesulfonyl chloride

(102 mg, 536 μmol, 5.0 eq) and 4-DMAP (1 mg, 8 μmol, 0.1 eq) in pyridine (300 μL) at 0 °C dropwise *via* syringe. The reaction solution was warmed to RT and stirred for 24 h after which time TLC analysis indicated complete consumption of **126**. The reaction solution was concentrated *in vacuo* then redissolved in CH_2Cl_2 (25 mL) and washed with water (25 mL), brine (25 mL), dried over sodium sulfate, filtered, and concentrated *in vacuo*. The crude material was purified by silica gel column chromatography, eluting with ethyl acetate, petroleum ether and triethylamine (50:49:1, 75:24:1, 99:0:1), to afford *tert-butyl-(6-(3-(4-methylphenylsulfonamido)-4-(4-methylpiperazin-1-yl)phenyl)-3-propyl[1,2,4]triazolo[4,3-b]pyridazin-8-yl)carbamate* **121** (51 mg, 77%) as a colourless oil: R_f 0.10 (methanol/ethyl acetate/triethylamine, 10:89:1); ν_{max} (thin film)/cm^{-1} 3192 (w), 2967 (m), 2937 (m), 2875 (m), 2843 (m), 2798 (m), 1735 (m), 1608 (s), 1534 (m), 1513 (m), 1437 (m), 1396 (m), 1290 (m), 1265 (m), 1242 (s), 1154 (s); ^{1}H NMR (500 MHz; $CDCl_3$) δ 8.17 (1H, d, *J* 2.1, C(2')*H*), 8.05 (1H, s, C(7)*H*), 7.92 (1H, br s, C(8)N*H*), 7.82 (2H, d, *J* 8.3, C(2'')*H*, C(6'')*H*), 7.60 (1H, dd, *J* 8.3, 2.1, C(6')*H*), 7.27 (2H, d, *J* 8.3, C(3'')*H*, C(5'')*H*), 7.26 (1H, br s, C(8)N*H*), 7.20 (1H, d, *J* 8.3, C(5')*H*), 3.22 (2H, t, *J* 7.5, C(3)CH_2), 2.70 (4H, br s, ArNCH$_2$CH_2), 2.54 (4H, br s, ArNCH_2), 2.38 (3H, s C(4'')CH_3), 2.36 (3H, s, NCH_3), 2.01 (2H, qt, *J* 7.5, 7.4, C(3)CH$_2$CH_2), 1.58 (9H, s, C(CH_3)$_3$), 1.08 (3H, t, *J* 7.4, C(3)CH$_2$CH$_2$CH_3); ^{13}C NMR (126 MHz; $CDCl_3$) δ 154.7 (*C*(6)), 151.7 (*C*=O), 151.6 (*C*(3)), 143.6 (*C*(4')), 144.1 (*C*(4'')), 139.2 (*C*(9)), 136.4 (*C*(1'')), 134.2 (*C*(8)), 133.6 (*C*(1')), 133.1 (*C*(3')), 123.3 (*C*(6')H), 122.0 (*C*(5')H), 129.8 (*C*(3'')H), 127.3 (*C*(2'')H), 116.7 (*C*(2')H), 100.4 (*C*(7)H), 83.0 (*C*(CH$_3$)$_3$), 55.5 (ArNCH$_2$*C*H$_2$), 52.3 (ArNCH$_2$),

46.1 (N*C*H_3), 28.1 (C(*C*H_3)$_3$), 26.3 (C(3)*C*H_2), 21.6 (*C*(4'')CH_3), 20.2 (C(3)CH_2*C*H_2), 14.0 (C(3)CH_2CH_2*C*H_3); *m/z* (ES^+) 621 [$(M+H)^+$, 100%]; HRMS *m/z* (ES^+) [Found $(M+H)^+$ 621.2943. $C_{31}H_{41}N_8O_4S^+$ requires M^+, 621.2966]; HPLC (method 1) retention time 14.09 min, purity 96.4%.

***tert*-Butyl-(6-(3-(4-methoxyphenylsulfonamido)-4-(4-methylpiperazin-1-yl)phenyl)-3-propyl[1,2,4]triazolo[4,3-*b*]pyridazin-8-yl)carbamate** (**122**)

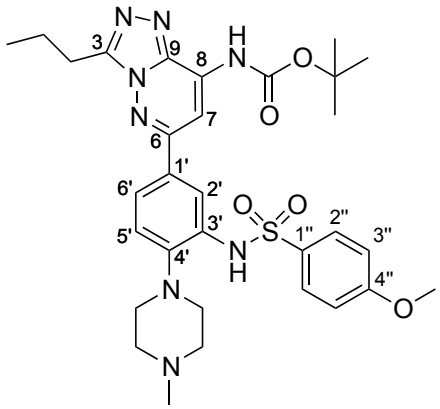

To a solution of *tert*-butyl-(6-(3-amino-4-(4-methylpiperazin-1-yl)phenyl)-3-propyl[1,2,4]triazolo[4,3-*b*]pyridazin-8-yl)carbamate **126** (50 mg, 107 µmol, 1.0 eq) in pyridine (700 µL) was added a solution of 4-methoxybenzenenesulfonyl chloride (111 mg, 536 µmol, 5.0 eq) and 4-DMAP (1 mg, 8 µmol, 0.1 eq) in pyridine (300 µL) at 0 °C dropwise *via* syringe. The reaction solution was warmed to RT and stirred for 24 h after which time TLC analysis indicated complete consumption of **126**. The reaction solution was concentrated *in vacuo* then redissolved in CH_2Cl_2 (25 mL) and washed with water (25 mL), brine (25 mL), dried over sodium sulfate, filtered, and concentrated *in vacuo*. The crude material was purified by silica gel column chromatography, eluting with ethyl acetate, petroleum ether and triethylamine (50:49:1, 75:24:1, 99:0:1), to afford *tert-butyl-(6-(3-(4-*

methoxyphenylsulfonamido)-4-(4-methylpiperazin-1-yl)phenyl)-3-propyl[1,2,4]triazolo[4,3-b]pyridazin-8-yl)carbamate **122** (50 mg, 73%) as a colourless oil: R_f 0.10 (methanol/ethyl acetate/triethylamine, 10:89:1); ν_{max} (thin film)/cm^{-1} 3215 (w), 2969 (w), 2937 (w), 2844 (w), 2806 (w), 1736 (m), 1596 (m), 1571 (m), 1499 (m), 1470 (m), 1440 (m), 1395 (m), 1369 (m), 1290 (m), 1338 (m), 1290 (m), 1241 (s), 1155 (s), 1114 (m), 1093 (m); ^{1}H NMR (500 MHz; $CDCl_3$) δ 8.16 (1H, br s, C(8)N*H*), 8.15 (1H, d, *J* 2.1, C(2')*H*), 8.05 (1H, s, C(7)*H*), 7.91 (1H, br s, C(8)N*H*), 7.88 (2H, d, *J* 9.0, C(2'')*H*, C(6'')*H*), 7.61 (1H, dd, *J* 8.3, 2.1, C(6')*H*), 7.21 (1H, d, *J* 8.3, C(5')*H*), 6.94 (2H, d, *J* 9.0, C(3'')*H*, C(5'')*H*), 3.80 (3H, s, OCH_3), 3.22 (2H, t, *J* 7.6, C(3)CH_2), 2.76 (4H, br s, ArNCH_2CH_2), 2.54 (4H, br s, ArNCH_2), 2.39 (3H, s, NCH_3), 2.01 (2H, qt, *J* 7.6, 7.4, C(3)CH_2CH_2), 1.58 (9H, s, C(CH_3)$_3$), 1.08 (3H, t, *J* 7.4, C(3)CH_2CH_2CH_3); ^{13}C NMR (126 MHz; $CDCl_3$) δ 163.6 (*C*(4'')), 154.7 (*C*(6)), 151.74 (*C*=O), 151.66 (*C*(3)), 143.6 (*C*(4')), 139.2 (*C*(9)), 130.1 (*C*(1'')), 134.2 (*C*(8)), 133.6 (*C*(1')), 133.1 (*C*(3')), 130.1 (*C*(1'')), 123.3 (*C*(6')H), 122.0 (*C*(5')H), 129.5 (*C*(2'')H), 116.6 (*C*(2')H), 114.4 (*C*(3'')H), 100.4 (*C*(7)H), 83.0 (*C*(CH$_3$)$_3$), 55.6 (O*C*H$_3$), 55.4 (ArNCH$_2$*C*H$_2$), 52.2 (ArN*C*H$_2$), 46.1 (N*C*H$_3$), 28.1 (C(*C*H$_3$)$_3$), 26.3 (C(3)*C*H$_2$), 20.2 (C(3)CH$_2$*C*H$_2$), 13.9 (C(3)CH$_2$CH$_2$*C*H$_3$); *m/z* (ES^+) 637 [$(M+H)^+$, 100%]; HRMS *m/z* (ES^+) [Found $(M+H)^+$ 637.29031. $C_{31}H_{41}N_8O_5S^+$ requires M^+, 637.2915]; HPLC (method 1) retention time 13.76 min, purity 95.5%.

***tert*-Butyl-(6-(3-(4-(*tert*-butyl)phenylsulfonamido)-4-(4-methylpiperazin-1-yl)phenyl)-3-propyl[1,2,4]triazolo[4,3-*b*]pyridazin-8-yl)carbamate** (**124**)

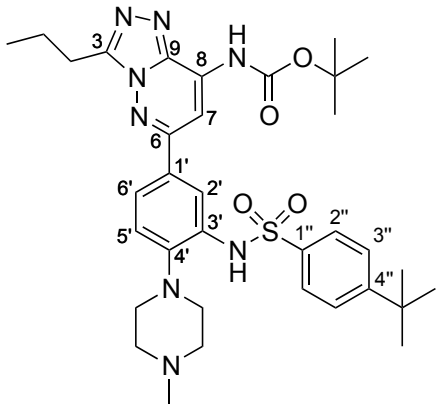

To a solution of *tert*-butyl-(6-(3-amino-4-(4-methylpiperazin-1-yl)phenyl)-3-propyl[1,2,4]triazolo[4,3-*b*]pyridazin-8-yl)carbamate **126** (30 mg, 65 µmol, 1.0 eq) in pyridine (300 µL) was added a solution of 4-*tert*-butylbenzenenesulfonyl chloride (75 mg, 322 µmol, 5.0 eq) and 4-DMAP (1 mg, 8 µmol, 0.1 eq) in pyridine (700 µL) at 0 °C dropwise *via* syringe. The reaction solution was warmed to RT and stirred for 24 h after which time TLC analysis indicated complete consumption of **126**. The reaction solution was concentrated *in vacuo* then redissolved in CH_2Cl_2 (25 mL) and washed with water (25 mL), brine (25 mL), dried over sodium sulfate, filtered, and concentrated *in vacuo*. The crude material was purified by silica gel column chromatography, eluting with ethyl acetate, petroleum ether and triethylamine (50:49:1, 75:24:1, 99:0:1), to afford *tert-butyl-(6-(3-(4-(tert-butyl)phenylsulfonamido)-4-(4-methylpiperazin-1-yl)phenyl)-3-propyl[1,2,4]triazolo[4,3-b]pyridazin-8-yl)carbamate* **124** (32 mg, 45%) as a colourless oil: R_f 0.17 (methanol/ethyl acetate/triethylamine, 10:89:1); ν_{max} (thin film)/cm^{-1} 3406 (w), 3186 (w), 2965 (w), 2874 (w), 2844 (w), 2799 (w), 2177 (w), 2049 (w), 2036 (m), 2009 (m), 1993 (m), 1735 (m), 1608 (m),

1569 (s), 1534 (m), 1470 (m), 1397 (m), 1339 (m), 1290 (m), 1266 (m), 1242 (s), 1198 (m), 1154 (s), 1113 (m); ^{1}H NMR (500 MHz; $CDCl_3$) δ 8.23 (1H, d, *J* 2.1, C(2')*H*), 8.17 (1H, br s, N*H*), 8.08 (1H, s, C(7)*H*), 7.88 (1H, br s, N*H*), 7.84 (2H, d, *J* 8.6, C(2'')*H*), 7.63 (1H, dd, *J* 8.3, 2.1, C(6')*H*), 7.48 (2H, d, *J* 8.6, C(3'')*H*), 7.21 (1H, d, *J* 8.3, C(5')*H*), 3.23 (2H, t, *J* 7.5, C(3)CH_2), 2.64 (4H, br s, ArNCH_2), 2.51 (4H, br s, ArNCH_2CH_2), 2.37 (3H, s, NCH_3), 2.01 (2H, qt, *J* 7.5, 7.4, C(3)CH_2CH_2), 1.59 (9H, s, C(CH_3)$_3$), 1.27 (9H, s, C(4'')C(CH_3)$_3$), 1.08 (3H, t, *J* 7.4, C(3)CH_2CH_2CH_3); ^{13}C NMR (126 MHz; $CDCl_3$) δ 157.1 (*C*(4'')), 154.7 (*C*(6)), 151.8 (*C*=O), 151.7 (*C*(3)), 143.8 (*C*(4')), 139.2 (*C*(9)), 136.4 (*C*(1'')), 134.2 (*C*(8)), 133.7 (*C*(1')), 133.2 (*C*(3')), 127.0 (*C*(2'')H)), 126.2 (*C*(3'')H), 123.4 (*C*(6')H), 122.1 (*C*(5')H), 117.2 (*C*(2')H), 100.5 (*C*(7)H), 83.0 (*C*(CH_3)$_3$), 55.5 (ArCH_2*C*H_2), 52.2 (ArN*C*H_2), 46.1 (N*C*H_3), 28.1 (C(*C*H_3)$_3$), 35.2 (C(4'')*C*(CH_3)$_3$), 31.0 (C(4'')C(*C*H_3)$_3$), 26.3 (C(3)*C*H_2), 20.2 (C(3)CH_2*C*H_2), 14.0 (C(3)CH_2CH_2*C*H_3); *m/z* (ES$^+$) 663 [(M+H)$^+$, 100%]; HRMS *m/z* (ES$^+$) [Found (M+H)$^+$ 663.3415. $C_{34}H_{47}N_8O_4S^+$ requires M$^+$, 663.3436]; HPLC (method 1) retention time 15.40 min, purity 99.1%.

***tert*-Butyl-(6-(3-(4-isopropylphenylsulfonamido)-4-(4-methylpiperazin-1-yl)phenyl)-3-propyl[1,2,4]triazolo[4,3-*b*]pyridazin-8-yl)carbamate** (**123**)

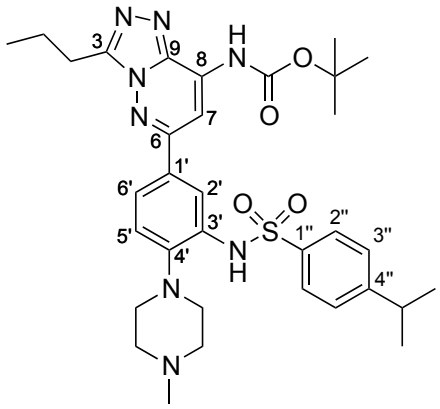

To a solution of *tert*-butyl-(6-(3-amino-4-(4-methylpiperazin-1-yl)phenyl)-3-propyl[1,2,4]triazolo[4,3-*b*]pyridazin-8-yl)carbamate **126** (30 mg, 65 µmol, 1.0 eq) in pyridine (300 µL) was added a solution of 4-isopropylbenzenenesulfonyl chloride (57 µL, 70 mg, 322 µmol, 5.0 eq) and 4-DMAP (1 mg, 8 µmol, 0.1 eq) in pyridine (700 µL) at 0 °C dropwise *via* syringe. The reaction solution was warmed to RT and stirred for 24 h after which time TLC analysis indicated complete consumption of **126**. The reaction solution was concentrated *in vacuo* then redissolved in CH_2Cl_2 (25 mL) and washed with water (25 mL), brine (25 mL), dried over sodium sulfate, filtered, and concentrated *in vacuo*. The crude material was purified by silica gel column chromatography, eluting with ethyl acetate, petroleum ether and triethylamine (50:49:1, 75:24:1, 99:0:1). The residue was then redissolved in MeCN (2 mL) and washed with hexane (3 × 2 mL) to afford *tert-butyl-(6-(3-(4-isopropylphenylsulfonamido)-4-(4-methylpiperazin-1-yl)phenyl)-3-propyl[1,2,4]triazolo[4,3-b]pyridazin-8-yl)carbamate* **123** (21 mg, 50%) as a colourless oil: R_f 0.17 (methanol/ethyl acetate/triethylamine, 10:89:1); ν_{max} (thin film)/cm^{-1} 3195 (w), 2960 (w), 2928 (w), 2871 (w), 1737 (m), 1609 (m),

1598 (m), 1568 (m), 1467 (m), 1394 (m), 1368 (m), 1337 (m), 1239 (s), 1152 (s), 1092 (m); ^{1}H NMR (500 MHz; $CDCl_3$) δ 8.22 (1H, d, *J* 2.1, C(2')*H*), 8.19 (1H, br s, C(8)N*H*), 8.07 (1H, s, C(7)*H*), 7.88 (1H, br s, C(8)N*H*), 7.83 (2H, d, *J* 8.4, C(2'')*H*), 7.63 (1H, dd, *J* 8.3, 2.1, C(6')*H*), 7.22 (1H, d, *J* 8.3, C(5')*H*), 6.94 (2H, d, *J* 8.4, C(3'')*H*), 3.23 (2H, t, *J* 7.5, C(3)CH_2), 2.91 (1H, sep, *J* 6.9, C(4'')C*H*), 2.68 (4H, br s, ArNCH_2), 2.53 (4H, br s, ArNCH$_2$CH_2), 2.39 (3H, s, NCH_3), 2.01 (2H, qt, *J* 7.5, 7.4, C(3)CH$_2$CH_2), 1.58 (9H, s, C(CH_3)$_3$), 1.20 (6H, d, *J* 6.9, C(4'')(CH_3)$_2$), 1.08 (3H, t, *J* 7.4, C(3)CH$_2$CH$_2$CH_3); ^{13}C NMR (126 MHz; $CDCl_3$) δ 154.9 (*C*(4'')), 154.7 (*C*(6)), 151.8 (*C*=O), 151.7 (*C*(3)), 143.8 (*C*(4')), 139.2 (*C*(9)), 134.2 (*C*(8)), 136.7 (*C*(1'')), 133.6 (*C*(1')), 133.2 (*C*(3')), 127.33 (*C*(2'')H), 127.31 (*C*(3'')H), 123.4 (*C*(6')H), 122.1 (*C*(5')H), 117.2 (*C*(2')H), 100.5 (*C*(7)H), 83.0 (*C*(CH$_3$)$_3$), 55.4 (ArNCH$_2$CH_2), 52.1 (ArNCH_2), 46.0 (NCH$_3$), 34.2 (C(4'')*C*H), 28.1 (C(*C*H$_3$)$_3$), 26.3 (C(3)*C*H$_2$), 23.6 (C(4'')C*C*H$_3$), 20.2 (C(3)CH$_2$*C*H$_2$), 14.0 (C(3)CH$_2$CH$_2$*C*H$_3$); *m/z* (ES$^+$) 649 [(M+H)$^+$, 100%]; HRMS *m/z* (ES$^+$) [Found (M+H)$^+$ 649.3257. $C_{33}H_{45}N_8O_4S^+$ requires M$^+$, 649.3279]; HPLC (method 1) retention time 15.03 min, purity 95.1%.

***tert*-Butyl-(6-(3-(4-bromophenylsulfonamido)-4-(4-methylpiperazin-1-yl)phenyl)-3-propyl[1,2,4]triazolo[4,3-*b*]pyridazin-8-yl)carbamate** (**125**)

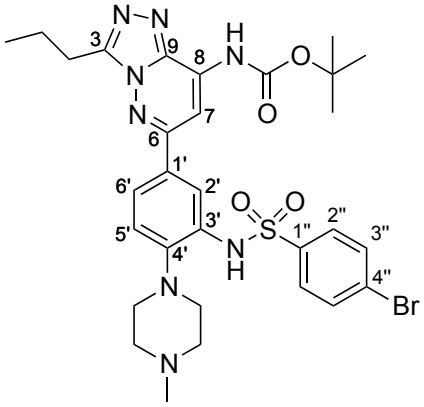

To a solution of *tert*-butyl-(6-(3-amino-4-(4-methylpiperazin-1-yl)phenyl)-3-propyl[1,2,4]triazolo[4,3-*b*]pyridazin-8-yl)carbamate **126** (26 mg, 56 µmol, 1.0 eq) in pyridine (500 µL) was added a solution of 4-bromobenzenenesulfonyl chloride (71 mg, 279 µmol, 5.0 eq) and 4-DMAP (1 mg, 8 µmol, 0.1 eq) in pyridine (700 µL) at 0 °C dropwise *via* syringe. The reaction solution was warmed to RT and stirred for 24 h after which time TLC analysis indicated complete consumption of **126**. The reaction solution was concentrated *in vacuo* then redissolved in CH_2Cl_2 (25 mL) and washed with water (25 mL), brine (25 mL), dried over sodium sulfate, filtered, and concentrated *in vacuo*. The crude material was purified by silica gel column chromatography, eluting with ethyl acetate, petroleum ether and triethylamine (50:49:1, 75:24:1, 99:0:1), to afford *tert-butyl-(6-(3-(4-bromophenylsulfonamido)-4-(4-methylpiperazin-1-yl)phenyl)-3-propyl[1,2,4]triazolo[4,3-b]pyridazin-8-yl)carbamate* **253** (32 mg, 45%) as a colourless oil: R_f 0.17 (methanol/ethyl acetate/triethylamine, 10:89:1); ν_{max} (thin film)/cm^{-1} 3186 (w), 2966 (w), 2935 (w), 2875 (w), 2875 (w), 2844 (w), 1735 (m), 1572 (s), 1513 (m), 1470 (m), 1369 (m), 1340 (m), 1290 (m),

1242 (s), 1153 (s), 1090 (m); ^{1}H NMR (500 MHz; $CDCl_3$) δ 8.16 (1H, br s, N*H*), 8.10 (1H, d, *J* 2.2, C(2')*H*), 7.83 (2H, d, *J* 8.4, C(2'')*H*), 7.65 (2H, d, *J* 8.4, C(3'')*H*), 7.64 (1H, dd, *J* 8.3, 2.1, C(6')*H*), 7.24 (1H, d, *J* 8.3, C(5')*H*), 3.22 (2H, t, *J* 7.6, C(3)CH_2), *2*.76 (4H, br s, ArNCH_2), 2.68-2.47 (4H, br s, ArNCH$_2$CH_2), 2.39 (3H, s, NCH_3), 2.01 (2H, qt, *J* 7.6, 7.4, C(3)CH$_2$CH_2), 1.59 (9H, s, C(CH_3)$_3$), 1.08 (3H, t, *J* 7.4, C(3)CH$_2$CH$_2$CH_3); ^{13}C NMR (126 MHz; $CDCl_3$) δ 154.5 (*C*(6)), 151.73 (*C*(3)), 151.68 (*C*=O), 143.6 (*C*(4')), 139.1 (*C*(9)), 138.4 (*C*(1'')), 134.3 (*C*(8)), 133.2 (*C*(1')), 133.1 (*C*(3')), 132.6 (*C*(3'')H), 128.9 (*C*(2'')H), 128.4 (*C*(4'')), 123.6 (*C*(6')H), 122.2 (*C*(5')H), 116.5 (*C*(2')H), 100.3 (*C*(7)H), 83.1 (*C*(CH$_3$)$_3$), 55.4 (ArNCH$_2$*C*H$_2$), 52.3 (ArN*C*H$_2$), 46.1 (N*C*H$_3$), 28.1 (C(*C*H$_3$)$_3$), 26.3 (C(3)*C*H$_2$), 20.2 (C(3)CH$_2$*C*H$_2$), 14.0 (C(3)CH$_2$CH$_2$*C*H$_3$); *m/z* (ES$^+$) 687 [(^{81}M+H)$^+$, 100%], 685 [(^{79}M+H)$^+$, 93%]; HRMS *m/z* (ES$^+$) [Found (M+H)$^+$ 685.1897, 687.1877. $C_{30}H_{38}N_8O_4{}^{79}BrS^+$ requires M$^+$, 685.1915; $C_{30}H_{38}N_8O_4{}^{81}BrS^+$ requires M$^+$, 687.1894]; HPLC (method 1) retention time 14.60 min, purity 95.4%.

***tert*-Butyl-(6-(4-methyl-3-nitrophenyl)-3-propyl[1,2,4]triazolo[4,3-*b*]pyridazin-8-yl)carbamate-*tert*-butyl-(6-(4-methyl-3-nitrophenyl)-3-propyl[1,2,4]triazolo[4,3-*b*]pyridazin-8-yl)carbamate** (**130**)

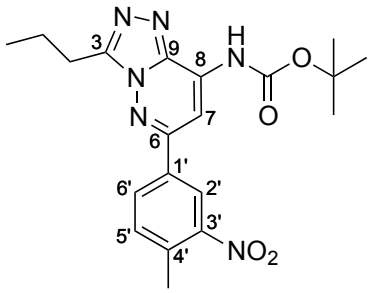

To a 10-20 mL MW vial containing *tert-butyl-(6-chloro-3-propyl[1,2,4]triazolo[4,3-b]pyridazin-8-yl)carbamate* **129** (444 mg, 1.42 mmol, 1.0 eq), 4-methyl-3-nitrobenzeneboronic acid (644 mg, 3.56 mmol, 2.5 eq), $Pd(dppf)Cl_2 \cdot CH_2Cl_2$ (116 mg, 14 μmol, 0.1 eq) and K_2CO_3 (294 mg, 2.13 mmol, 1.5 eq), was added 1,4-dioxane and water (10:1, 15 mL) *via* syringe. This mixture was stirred at RT with sonication for 5 min to dissolve. The reaction solution was heated at 80 °C for 23 h then cooled to RT, filtered through Celite® (eluent CH_2Cl_2) and concentrated *in vacuo*. The residue was redissolved in CH_2Cl_2 (100 mL) and washed with water (100 mL), brine (100 mL), dried over sodium sulfate, filtered, and concentrated *in vacuo*. The crude material was purified by silica gel column chromatography, eluting with diethyl ether, petroleum ether and triethylamine (15:84:1, 20:79:1, 30:69:1, 40:19:1, 50:59:1, 60:39:1, 75:24:1) to afford *tert-butyl-(6-(4-methyl-3-nitrophenyl)-3-propyl[1,2,4]triazolo[4,3-b]pyridazin-8-yl)carbamatetert-butyl-(6-(4-methyl-3-nitrophenyl)-3-propyl[1,2,4]triazolo[4,3-b]pyridazin-8-yl)carbamate* **130** (444 mg, 76%) as a colourless solid: R_f 0.64 (diethyl ether); mp 168-170 °C (from diethyl ether); ν_{max} (thin film)/cm^{-1} 3404 (w), 2970 (w), 2934 (w), 2876 (w), 1734 (m), 1614 (m), 1562 (m), 1532 (s), 1500 (m), 1469 (m),

1394 (m), 1309 (m), 1266 (m), 1243 (s), 1150 (s), 1095 (w); ^{1}H NMR (500 MHz; $CDCl_3$) δ 8.60 (1H, d, *J* 1.9, C(2')*H*), 8.19 (1H, br s, N*H*), 8.12 (1H, s, C(7)*H*), 8.11 (1H, dd, *J* 8.1, 1.9, C(6')*H*), 7.49 (1H, d, *J* 8.1, C(5')*H*), 3.23 (2H, t, *J* 7.6, C(3)CH_2), 2.68 (3H, s, C(4')CH_3), 2.00 (2H, qt, *J* 7.6, 7.4, C(3)CH_2CH_2), 1.58 (9H, s, C(CH_3)$_3$), 1.08 (3H, t, *J* 7.4, C(3)CH_2CH_2CH_3); ^{13}C NMR (126 MHz; $CDCl_3$) δ 153.0 (*C*(6)), 151.9 (*C*=O), 151.6 (*C*(3)), 149.8 (*C*(4')), 139.1 (*C*(9)), 135.7 (C(1')), 134.8 (*C*(3')), 134.7 (*C*(8)), 133.4 (*C*(5')H), 131.3 (C(6')H), 123.4 (C(2')H), 99.5 (*C*(7)H), 83.3 (*C*$(CH_3)_3$), 20.4 (C(4')*C*H_3), 28.1 (C(*C*H_3)$_3$), 26.2 (C(3)*C*H_2), 20.2 (C(3)CH_2*C*H_2), 13.9 (C(3)CH_2*C*H_2*C*H_3); *m/z* (ES^+) 413 [$(M+H)^+$, 100%]; HRMS *m/z* (ES^+) [Found $(M+H)^+$ 413.1922. $C_{20}H_{25}N_6O_4^+$ requires M^+, 413.1932]; HPLC (method 1) retention time 18.71 min, purity 95.5 %.

***tert*-Butyl-(6-(4-methyl-3-(methylsulfonamido)phenyl)-3-propyl[1,2,4]triazolo[4,3-*b*]pyridazin-8-yl)carbamate** (**127**)

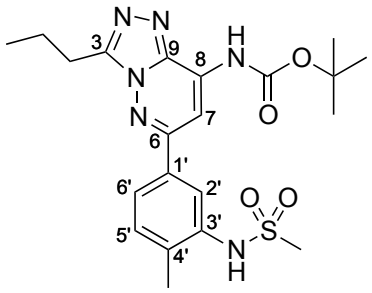

To a suspension of *tert*-butyl-(6-(4-methyl-3-nitrophenyl)-3-propyl[1,2,4]triazolo[4,3-*b*]pyridazin-8-yl)carbamate **130** (200 mg, 485 μmol, 1.0 eq) in ethanol/triethylamine (2:1, 6.0 mL) was added tin(II) chloride (634 mg, 2.43 mmol, 5.0 eq) and the reaction mixture was heated under reflux for 5 h after which time TLC analysis indicated complete consumption of **130**. The reaction was cooled to RT and the colourless precipitate was removed

via filtration and washed with ethyl acetate (17 mL). The filtrate was concentrated *in vacuo*, then saturated aqueous potassium fluoride (20 mL) was added and the suspension was stirred for 24 h at RT then diluted with water (100 mL) and extracted with ethyl acetate (100 mL). The organic layer was washed with water (3 × 100 mL), brine (100 mL), dried over sodium sulfate, filtered, and concentrated *in vacuo* to give a colourless oil (104 mg) which was used in the next step without further purification. To a solution of this oil (71 mg, 190 µmol, 1.0 eq) in pyridine (1.5 mL) was added methanesulfonyl chloride (57 µL, 85 mg, 740 µmol, 4.0 eq) at 0 °C dropwise *via* syringe. The reaction solution was warmed to RT and stirred for 24 h after which time TLC analysis indicated complete consumption of starting material amine. The reaction solution was concentrated *in vacuo* then redissolved in CH_2Cl_2 (20 mL) and washed with water (20 mL), brine (20 mL), dried over sodium sulfate, filtered, and concentrated *in vacuo*. The crude material was purified by silica gel column chromatography, eluting with diethyl ether, petroleum ether and triethylamine (40:59:1, 50:49:1, 60:39:1, 70:29:1, 80:19:1, 99:0:1), to give **127** as a colourless solid containing product, a grease impurity detected by ^{1}H-NMR, and 2,6-bis(1,1-dimethylethyl)-4-methylphenol (BHT). The colourless solid was redissolved in ethyl acetate (15 mL) and washed with 2 M aqueous K_2CO_3 (3 × 15 mL), brine (15 mL), dried over sodium sulfate, filtered, and concentrated *in vacuo*. The residue was redissolved in MeCN (2 mL) and precipitated by addition of hexane (1 mL). This solid was collected and concentrated *in vacuo* to afford *tert-butyl-(6-(4-methyl-3-(methylsulfonamido)phenyl)-3-propyl[1,2,4]triazolo[4,3-b]pyridazin-8-yl)carbamate* **127** (8 mg, 4%) as a colourless solid: R_f 0.30 (diethyl ether);

mp 135-137 °C (from diethyl ether); ν_{max} (thin film)/cm^{-1} 3103 (w), 2971 (w), 2933 (w), 2875 (w), 1737 (m), 1614 (w), 1568 (s), 1533 (m), 1473 (m), 1420 (m), 1395 (m), 1329 (m), 1243 (s), 1153 (s); ^{1}H NMR (500 MHz; $CDCl_3$) δ 8.12 (1H, d, *J* 1.8, C(2')*H*), 8.18 (1H, br s, N*H*), 8.09 (1H, s, C(7)*H*), 7.74 (1H, dd, *J* 8.0, 1.8, C(6')*H*), 7.36 (1H, d, *J* 8.0, C(5')*H*), 6.46 (1H, br s, N*H*), 3.22 (2H, t, *J* 7.5, C(3)CH_2), 3.10 (3H, s, SO_2CH_3), 2.42 (3H, s, C(4')CH_3), 1.99 (2H, qt, *J* 7.5, 7.4, C(3)CH_2CH_2), 1.57 (9H, s, C(CH_3)$_3$), 1.07 (3H, t, *J* 7.4, C(3)$CH_2CH_2CH_3$); ^{13}C NMR (126 MHz; $CDCl_3$) δ 154.4 (*C*(6)), 151.8 (*C*(3)), 151.7 (*C*=O), 135.2 (*C*(4')), 139.2 (*C*(9)), 134.9 (*C*(8)), 134.3 (C(1')), 133.3 (*C*(3')), 131.7 (*C*(5')H), 125.2 (*C*(6')H), 121.8 (*C*(2')H), 100.2 (*C*(7)H), 83.1 (*C*(CH_3)$_3$), 40.2 (SO_2CH_3), 18.1 (C(4')CH_3), 28.1 (C(CH_3)$_3$), 26.3 (C(3)CH_2), 20.2 (C(3)CH_2CH_2), 13.9 (C(3)$CH_2CH_2CH_3$); *m/z* (ES$^+$) 461 [(M+H)$^+$, 98%], 462 [100%]; HRMS *m/z* (ES$^+$) [Found (M+H)$^+$ 461.1958. $C_{21}H_{29}N_6O_4^+$ requires M$^+$, 461.1966]; HPLC (method 1) retention time 15.56 min, purity 95.3%.

Ethyl-(6-chloro-3-propyl[1,2,4]triazolo[4,3-*b*]pyridazin-8-yl)carbamate (**131**)

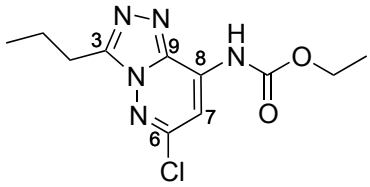

To a solution of ethyl-(6-chloro-3-propyl[1,2,4]triazolo[4,3-*b*]pyridazin-8-yl)carbamate **128** (400 mg, 1.89 mmol, 1.0 eq) and triethylamine (789 µL, 573 mg, 3.0 eq) in CH_2Cl_2 (60 mL) at 0 °C was added a solution of ethylchloroformate (361 µL, 412 mg, 3.78 mmol, 2.0 eq) in CH_2Cl_2 (8 mL) dropwise *via* syringe. The reaction solution was warmed to RT with stirring for 24 h after which time TLC analysis indicated complete consumption of **128**. The reaction solution was concentrated *in vacuo* then redissolved in CH_2Cl_2 (160 mL) and washed with 2 M aqueous K_2CO_3 (3 × 160 mL), brine (200 mL), dried over sodium sulfate, filtered, and concentrated *in vacuo*. The crude material was purified by silica gel column chromatography, eluting with diethyl ether, petroleum ether and triethylamine (25:74:1, 40:59:1, 60:39:1, 80:19:1), to give *ethyl-(6-chloro-3-propyl[1,2,4]triazolo[4,3-b]pyridazin-8-yl)carbamate* **131** (499 mg, 93%): R_f 0.60 (diethyl ether); mp 131-133 °C (from diethyl ether); ν_{max} (thin film)/cm^{-1} 3179 (w), 3131 (w), 2966 (w), 2935 (w), 1741 (s), 1611 (m), 1553 (s), 1463 (s), 1412 (m), 1265 (m), 12214 (s), 1113 (m); ^{1}H NMR (500 MHz; $CDCl_3$) 8.90 (1H, br s, N*H*), 7.72 (1H, s, C(7)*H*), 4.30 (2H, q, *J* 7.1, $CO_2CH_2CH_3$), 3.11 (2H, t, *J* 7.6, C(3)CH_2), 1.91 (2H, qt, *J* 7.6, 7.4, C(3)CH_2CH_2), 1.33 (3H, t, *J* 7.1, $CO_2CH_2CH_3$), 1.03 (3H, t, *J* 7.4, C(3)$CH_2CH_2CH_3$); ^{13}C NMR (126 MHz; $CDCl_3$) δ 152.6 (C=O), 151.4 (C(3)), 150.9 (C(6)), 138.5 (C(9)), 134.9 (C(8)), 103.6 (C(7)H), 63.0 (CO_2CH_2),

26.0 (C(3)*C*H_2), 20.1 (C(3)CH_2*C*H_2), 14.2 (CO_2*C*H_2*C*H_3), 13.8 (C(3)CH_2*C*H_2*C*H_3); *m/z* (ES^+) 284 [$(M+H)^+$, 100%]; HRMS *m/z* (ES^+) [Found $(M+Na)^+$ 306.0724. $C_{11}H_{14}N_5ClO_2Na^+$ requires M^+, 306.0728]; HPLC: retention time 15.02 min, purity 98.8%.

Ethyl-(6-(4-methyl-3-nitrophenyl)-3-propyl[1,2,4]triazolo[4,3-*b*]pyridazin-8-yl)carbamate (**132**)

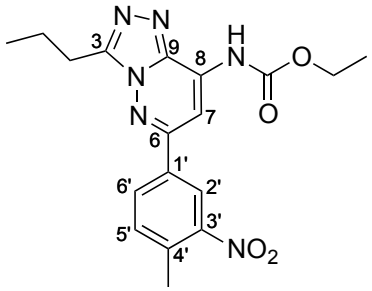

To a 10-20 mL MW vial containing ethyl-(6-chloro-3-propyl[1,2,4]triazolo[4,3-b]pyridazin-8-yl)carbamate **131** (400 mg, 1.42 mmol, 1.0 eq), 4-methyl-3-nitrobenzeneboronic acid (580 mg, 3.20 mmol, 2.3 eq), Pd(dppf)Cl_2·CH_2Cl_2 (100 mg, 90 µmol, 0.1 eq) and K_2CO_3 (294 mg, 2.13 mmol, 1.4 eq), was added 1,4-dioxane and water (10:1, 12 mL) *via* syringe. This mixture was stirred at RT with sonication for 5 min to dissolve all components. The reaction solution was heated at 80 °C for 21 h then cooled to RT, filtered through Celite® (eluent CH_2Cl_2) and concentrated *in vacuo*. The residue was redissolved in CH_2Cl_2 (110 mL) and washed with water (100 mL), brine (100 mL), dried over sodium sulfate, filtered, and concentrated *in vacuo*. The crude material was purified by silica gel column chromatography, eluting with diethyl ether, petroleum ether and triethylamine (30:69:1, 40:59:1, 50:49:1, 60:39:1, 65:34:1, 70:29:1, 75:24:1, 80:19:1) to afford *ethyl-(6-(4-methyl-3-nitrophenyl)-3-propyl[1,2,4]triazolo[4,3-b]pyridazin-8-yl)carbamate*

132 (257 mg, 47%) as a colourless solid: R_f 0.48 (ethyl acetate/petroleum ether, 50:50); mp 171-172 °C (from diethyl ether); ν_{max} (thin film)/cm^{-1} 3100 (w), 2967 (w), 2935 (w), 2875 (w), 1738 (s), 1562 (s), 1532 (s), 1503 (m), 1469 (m), 1414 (m), 1395 (m), 1304 (m), 1279 (m), 1227 (s), 1101 (m); ^{1}H NMR (500 MHz; $CDCl_3$); ^{1}H NMR (500 MHz; $CDCl_3$) δ 8.60 (1H, d, *J* 1.9, C(2')H), 8.41 (1H, br s, N*H*), 8.17 (1H, s, C(7)*H*), 8.11 (1H, dd, *J* 8.1, 1.9, C(6)*H*), 7.51 (1H, d, *J* 8.1, C(5')*H*), 4.36 (2H, q, *J* 7.2, CO_2CH_2), 3.24 (2H, t, *J* 7.6, C(3)CH_2), 2.69 (3H, s, C(4')CH_3), 2.00 (2H, qt, *J* 7.6, 7.4, C(3)CH_2CH_2), 1.39 (3H, q, *J* 7.2, $CO_2CH_2CH_3$), 1.09 (3H, t, *J* 7.4, C(3)CH_2 CH_2CH_3); ^{13}C NMR (126 MHz; $CDCl_3$) δ 153.0 (*C*(6)), 152.8 (*C*=O), 152.6 (*C*(3)), 149.8 (*C*(4')), 139.0 (*C*(9)), 135.8 (*C*(3')), 134.6 (C(1')), 134.5 (*C*(8)), 133.5 (*C*(5')H), 131.3 (C(6')H), 123.4 (*C*(2')H), 99.9 (*C*(7)H), 62.9 (CO_2CH_2), 26.2 (C(3)CH_2), 20.4 (C(4')CH_3), 20.2 (C(3)CH_2CH_2), 14.3 ($CO_2CH_2CH_3$), 13.9 C(3)$CH_2CH_2CH_3$; *m/z* (ES$^+$) 385 [(M+H)$^+$, 100%]; HRMS *m/z* (ES$^+$) [Found (M+Na)$^+$ 407.1429. $C_{18}H_{20}N_6O_4Na^+$ requires M$^+$, 407.1438]; HPLC (method 1) retention time 17.19 min, purity 98.1%.

Ethyl-(6-(4-methyl-3-(methylsulfonamido)phenyl)-3-propyl[1,2,4]triazolo-[4,3-*b*]pyridazin-8-yl)carbamate (**111**)

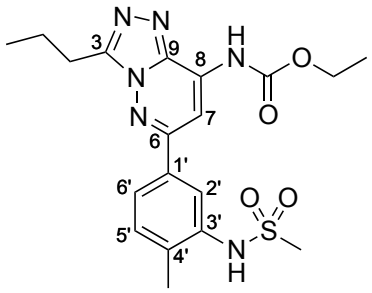

To a suspension of ethyl-(6-(4-methyl-3-nitrophenyl)-3-propyl[1,2,4]triazolo[4,3-b]pyridazin-8-yl)carbamate **132** (230 mg, 599 μmol,

1.0 eq) in ethanol and triethylamine (2:1, 9.0 mL) was added tin(II) chloride (782 mg, 2.43 mmol, 5.0 eq) and the reaction solution was heated under reflux for 5 h after which time TLC analysis indicated complete consumption of **132**. The reaction was cooled to RT and the colourless precipitate was removed *via* filtration and washed with ethyl acetate (30 mL). The filtrate was concentrated *in vacuo*, then saturated aqueous potassium fluoride (25 mL) was added and the suspension was stirred for 24 h at RT then diluted with water (200 mL) and extracted with ethyl acetate (200 mL). The organic layer was washed with water (3 × 200 mL), brine (200 mL), dried over sodium sulfate, filtered, and concentrated *in vacuo* to give a pale yellow solid (193 mg) which was used in the next step without further purification. To a solution of this solid (165 mg, 466 µmol, 1.0 eq) in pyridine (1.9 mL) was added methanesulfonyl chloride (144 µL, 214 mg, 1.86 mmol, 4.0 eq) at 0 °C dropwise *via* syringe. The reaction solution was warmed to RT and stirred for 24 h after which time TLC analysis indicated complete consumption of starting material amine. The reaction solution was concentrated *in vacuo* then the residue was redissolved in CH_2Cl_2 (130 mL) and washed with water (130 mL), brine (130 mL), dried over sodium sulfate, filtered, and concentrated *in vacuo*. The crude material was purified by silica gel column chromatography, eluting with diethyl ether, petroleum ether and triethylamine (40:59:1, 50:49:1, 60:39:1, 70:29:1, 80:19:1, 95:4:1, 99:0:1), to give a colourless solid. In order to remove grease impurities detected by ^{1}H-NMR, and 2,6-bis(1,1-dimethylethyl)-4-methylphenol (BHT), the compound was further purified using a silica plug, eluting with ethyl acetate and petroleum ether (1:1, 3:1, 1:0) to give *ethyl-(6-(4-methyl-3-(methylsulfonamido)phenyl)-3-*

propyl[1,2,4]triazolo[4,3-b]pyridazin-8-yl)carbamate **111** (63 mg, 24% over two steps) as a fluffy colourless solid: R_f 0.16 (ethyl acetate/petroleum ether, 50:50); mp 171-175 °C (from diethyl ether); ν_{max} (thin film)/cm^{-1} 3103 (w), 2971 (w), 2933 (w), 2875 (w), 1737 (m), 1614 (m), 1568 (m), 1533 (m), 1473 (m), 1420 (m), 1395 (m), 1369 (m), 1329 (m), 1153 (s); ^{1}H NMR (500 MHz; $CDCl_3$) δ 8.45 (1H, br s, C(8)N*H*), 8.16 (1H, s, C(7)*H*), 8.13 (1H, d, *J* 1.4, C(2')*H*), 7.74 (1H, dd, *J* 7.9, 1.4, C(6)*H*), 7.39 (1H, d, *J* 7.9, C(5')*H*), 6.45 (1H, br s, C(3')N*H*), 4.35 (2H, q, *J* 7.1, CO_2CH_2), 3.22 (2H, t, *J* 7.6, C(3)CH_2), 3.10 (3H, s, SO_2CH_3), 2.42 (3H, s, C(4')CH_3), 2.00 (2H, qt, *J* 7.6, 7.4, C(3)CH_2CH_2), 1.38 (3H, q, *J* 7.2, $CO_2CH_2CH_3$), 1.07 (3H, t, *J* 7.4, C(3)CH_2 CH_2CH_3); ^{13}C NMR (126 MHz; $CDCl_3$) δ 154.6 (*C*(6)), 152.8 (*C*(3)), 152.9 (*C*=O), 138.9 (*C*(9)), 135.6 (*C*(8)), 134.7 (C(1')), 134.0 (*C*(4')), 133.3 (*C*(3')), 131.8 (*C*(5')H), 125.0 (C(6')H), 121.7 (*C*(2')H), 100.9 (*C*(7)H), 62.8 (CO_2CH_2), 26.3 (C(3)CH_2), 20.1 (C(3)CH_2CH_2), 14.3 ($CO_2CH_2CH_3$), 18.1 (C(4')CH_3), 13.9 (C(3)$CH_2CH_2CH_3$); *m/z* (ES$^+$) 433 [(M+H)$^+$, 100%]; HRMS *m/z* (ES$^+$) [Found (M+H)$^+$ 433.1642. $C_{19}H_{25}N_6O_4^+$ requires M$^+$, 433.1653]; HPLC (method 1) retention time 14.24 min, purity 99.7%.

***tert*-Butyl (3-methyl-6-(4-methyl-3-(methylsulfonamido)phenyl)-[1,2,4]triazolo[4,3-*b*]pyridazin-8-yl)carbamate** (**134**)

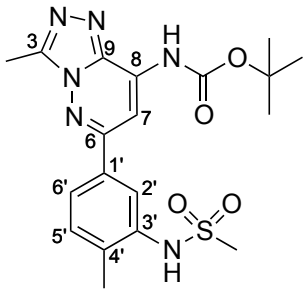

To a solution of *tert*-butyl-(6-(3-amino-4-methylphenyl)-3-methyl[1,2,4]triazolo[4,3-*b*]pyridazin-8-yl)carbamate (60 mg, 160 μmol, 1.0 eq) in pyridine (700 μL) was added methanesulfonyl chloride (48 μL, 72 mg, 630 μmol, 4.0 eq) at 0 °C dropwise *via* syringe. The reaction solution was warmed to RT and stirred for 24 h after which time TLC analysis indicated complete consumption of starting material. The reaction solution was concentrated *in vacuo* then redissolved in CH_2Cl_2 (15 mL) and washed with water (15 mL), brine (15 mL), dried over sodium sulfate, filtered, and concentrated *in vacuo*. The crude material was purified by silica gel column chromatography, eluting with diethyl ether, petroleum ether and triethylamine (99:0:1, 10:89:1, 20:79:1, 30:69:1, 40:59:1, 50:49:1, 60:39:1, 70:29:1, 80:19:1, 90:9:1), to *give tert-butyl-(3-methyl-6-(4-methyl-3-(methylsulfonamido)phenyl)[1,2,4]triazolo[4,3-b]pyridazin-8-yl)carbamate* **134** (23 mg, 34%) as a colourless solid: R_f 0.16 (ethyl acetate/petroleum ether, 50:50); mp 228-230 °C (from ethanol); ν_{max} (thin film)/cm^{-1} 3011 (w), 1737 (m), 1571 (m), 1538 (m), 1475 (w), 1370 (m), 1153 (s); ^{1}H NMR (600 MHz; $CDCl_3$) δ 8.17 (1H, br s, N*H*), 8.13 (1H, d, *J* 1.9, C(2')*H*), 8.10 (1H, s, C(7)*H*), 7.75 (1H, dd, *J* 7.9, 1.9, C(6')*H*), 7.38 (1H, d, *J* 7.9, C(5')*H*), 6.55 (1H, br s, N*H*), 3.09 (3H, s, SO_2CH_3), 2.84 (3H, s, C(3)CH_3), 2.43 (3H, s, C(4')CH_3),

1.57 (9H, s, (CH_3)$_3$); ^{13}C NMR (151 MHz; $CDCl_3$) δ 154.7 (*C*(6)H), 151.7 (*C*=O), 148.5 (*C*(3)CH_3), 139.2 (*C*(9)), 135.5 (*C*(3')), 134.9 (*C*(1')), 134.3 (*C*(8)), 133.5 (*C*(4)), 131.7 (*C*(5)H), 125.3 (*C*(6')H), 122.1 (*C*(2')H), 100.3 (*C*(7)H), 83.1 (*C*(CH_3)$_3$), 40.3 (SO_2CH_3), 28.1 ((*C*H_3)$_3$), 18.1 (C(4)*C*H_3), 9.9 (C(3)*C*H_3); *m/z* (ES^+) 433 [$(M+H)^+$, 100%]; HRMS *m/z* (ES^+) [Found $(M+H)^+$ 433.1635. $C_{19}H_{25}N_6O_4S^+$ requires M^+, 433.1653]; HPLC (method 2) pH 10 retention time 1.95 min, purity 100.0%, pH 3 retention time 2.01 min, purity 100.0%.

_N_-(6-(4-(4-Methylpiperazin-1-yl)-3-nitrophenyl)-3-propyl[1,2,4]triazolo[4,3-*b*]pyridazin-8-yl)cyclopropanecarboxamide (**135**)

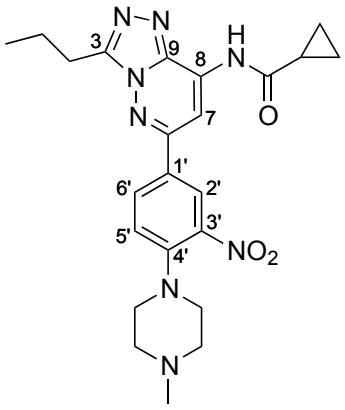

A solution of **113** (100 mg, 172 μmol, 1.0 eq) in TFA and CH_2Cl_2 (1:1, 2 mL) was stirred at RT for 3 h, after which time TLC analysis indicated complete consumption of **113**. The solution was concentrated *in vacuo* and the residue was redissolved in CH_2Cl_2 (30 mL), washed with saturated aqueous $NaHCO_3$ (30 mL), brine (30 mL), dried over sodium sulfate, filtered, and concentrated *in vacuo* to give a sample of *6-(4-(4-methylpiperazin-1-yl)-3-nitrophenyl)-3-propyl[1,2,4]triazolo[4,3-b]pyridazin-8-amine* **156** (80 mg),

which was used without further purification. To a suspension of 6-(4-(4-methylpiperazin-1-yl)-3-nitrophenyl)-3-propyl[1,2,4]triazolo[4,3-*b*]pyridazin-8-amine **156** (80 mg, 202 μmol, 1.0 eq) and Hünig's base (70 μL, 52 mg, 400 μmol, 2.0 eq) in CH_2Cl_2 (1 mL) was added cyclopropanecarbonyl chloride (18 μL, 21 mg, 200 μmol, 1.0 eq) at 0 °C dropwise *via* syringe. The reaction solution was stirred for 2 h at 0 °C, after which time TLC analysis indicated complete consumption of **156**. The solution was warmed to RT, diluted with CH_2Cl_2 (25 mL) and washed with a solution of 2 M aqueous K_2CO_3 (25 mL), water (2 × 25 mL), brine (25 mL), dried over sodium sulfate, filtered, and concentrated *in vacuo*. The crude material was purified by preparative HPLC to afford *N-(6-(4-(4-methylpiperazin-1-yl)-3-nitrophenyl)-3-propyl[1,2,4]triazolo[4,3-b]pyridazin-8-yl)cyclopropanecarboxamide* **136** (30 mg, 32%) as a yellow solid: R_f 0.29 (methanol/CH_2Cl_2, 4:96); mp 234-238 °C (from ethyl acetate); ν_{max} (thin film)/cm^{-1} 3176 (w), 3088 (w), 2964 (w), 2846 (w), 2157 (w), 1694 (m), 1615 (m), 1526 (s), 1453 (m), 1403 (m), 1341 (m), 1194 (m), 1159 (m), 1008 (m); ^{1}H NMR (600 MHz; D_6-DMSO) δ 11.56 (1H, br s, N*H*), 8.42 (1H, s, C(7)*H*), 8.33 (1H, d, *J* 2.3, C(2')*H*), 8.09 (1H, dd, *J* 8.9, 2.3, C(6')*H*), 7.44 (1H, d, *J* 8.9, C(5')*H*), 3.14 (2H, t, *J* 7.4, C(3)CH_2), 3.12 (4H, t, *J* 4.9, ArNCH_2), 2.45 (4H, t, *J* 4.9, ArNCH$_2$CH_2), 2.23 (3H, s, NCH_3), 1.91 (2H, qt, *J* 7.4, 7.4, C(3)CH$_2$CH_2), 1.01 (3H, t, *J* 7.4, C(3)CH$_2$CH$_2$CH_3), 1.00-0.94 (2H, m, C=OCHCH_A), 0.98-0.90 (2H, m, SCHCH_B); ^{13}C NMR (151 MHz; D_6-DMSO) δ 175.3 (*C*=O), 152.4 (*C*(6)), 150.5 (*C*(3)), 146.4 (*C*(4')), 140.7 (C(1')), 138.7 (*C*(9)), 134.2 (*C*(8)), 131.8 (*C*(6')H), 126.4 (*C*(3')), 124.6 (*C*(2')H), 121.3 (*C*(5')H), 101.5 (*C*(7)H), 54.3 (ArNCH$_2$*C*H$_2$), 50.3 (ArN*C*H$_2$), 45.7 (N*C*H$_3$), 25.6 (C(3)*C*H$_2$),

19.5 (C(3)CH_2CH_2), 14.4 (*C*C=O), 13.7 (C(3)$CH_2CH_2CH_3$), 9.00 (H_2*C*CC=O); *m/z* (ES^+) 465 [$(M+H)^+$, 100%]; HRMS *m/z* (ES^+) [Found $(M+H)^+$ 465.2346. $C_{23}H_{29}N_8O_3^+$ requires M^+, 465.2357]; HPLC (method 2) pH 10 retention time 1.64 min, purity 100%; pH 3 retention time 2.93 min, purity 100%.

2-Methyl-1-((6-(4-(4-methylpiperazin-1-yl)-3-nitrophenyl)-3-propyl[1,2,4]triazolo[4,3-*b*]pyridazin-8-yl)amino)-1-oxopropan-2-yl acetate (**136**)

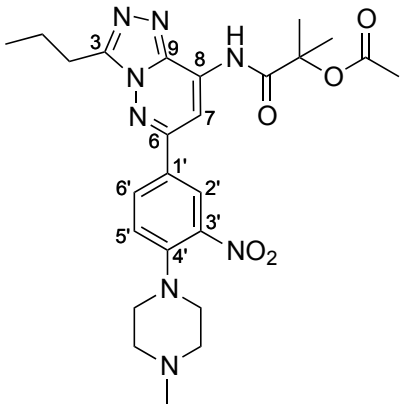

A solution of **113** (532 mg, 1.07 mol, 1.0 eq) in TFA and CH_2Cl_2 (1:1, 3 mL) was stirred at RT for 3 h, after which time TLC analysis indicated complete consumption of **113**. The solution was concentrated *in vacuo* and the residue was redissolved in CH_2Cl_2 (30 mL), washed with saturated aqueous $NaHCO_3$ (30 mL), brine (30 mL), dried over sodium sulfate, filtered, and concentrated *in vacuo* to give a sample of *6-(4-(4-methylpiperazin-1-yl)-3-nitrophenyl)-3-propyl[1,2,4]triazolo[4,3-b]pyridazin-8-amine* **156** (425 mg), which was used without further purification. To a suspension of 6-(4-(4-methylpiperazin-1-yl)-3-nitrophenyl)-3-propyl[1,2,4]triazolo[4,3-*b*]pyridazin-8-amine **156** (425 mg, 1.07 mmol, 1.0 eq) and Hünig's base (372 µL, 276 mg, 2.14 mmol, 2.0 eq) in CH_2Cl_2 (10 mL) was added chlorocarbonyl-1-

methylethyl acetate (169 μL, 195 mg, 1.18 mmol, 1.1 eq) at RT dropwise *via* syringe. A solution formed after 30 min which was stirred for 20 h, at which point an additional chlorocarbonyl-1-methylethyl acetate (20 μL, 23 mg, 140 μmol, 0.1 eq) was added and the solution was stirred for a further 2 h. After this time, the solution was diluted with CH_2Cl_2 (70 mL) and washed with saturated aqueous $NaHCO_3$ (75 mL), brine (75 mL), dried over sodium sulfate, filtered, and concentrated *in vacuo*. This material was purified by silica gel column chromatography, eluting with methanol and CH_2Cl_2 (0:100, 5:95, 10:90,15:85, 20:80) to afford *2-methyl-1-((6-(4-(4-methylpiperazin-1-yl)-3-nitrophenyl)-3-propyl[1,2,4]triazolo[4,3-b]pyridazin-8-yl)amino)-1-oxopropan-2-yl acetate* **136** (20 mg, 30%) as a yellow solid: R_f 0.09 (methanol/ethyl acetate/triethylamine, 10:89:1); mp 182-184 °C (from ethyl acetate); ν_{max} (thin film)/cm^{-1} 3341 (w), 2966 (w), 2899 (w), 1719 (m), 1614 (s), 1565 (s), 1553 (s), 1526 (m), 1292 (m), 1239 (m), 1217 (m), 1201 (m), 1201 (m); ^{1}H NMR (600 MHz; CD_3CN) δ 9.13 (1H, br s, N*H*C=O), 8.36 (1H, d, *J* 2.3, C(2')*H*), 8.31 (1H, s, C(7)*H*), 8.12 (1H, dd, *J* 8.8, 2.3, C(6')*H*), 7.32 (1H, d, *J* 8.8, C(5')*H*), 3.16 (4H, t, *J* 4.7, ArNCH$_2$C*H*$_2$), 3.15 (2H, t, *J* 7.5, C(3)C*H*$_2$), 2.48 (4H, t, *J* 4.7, ArNC*H*$_2$), 2.27 (3H, s, NC*H*$_3$), 2.15 (3H, s, OC=OC*H*$_3$), 1.95 (2H, qt, *J* 7.5, 7.4, C(3)CH$_2$C*H*$_2$), 1.72 (6H, s, NC=OC(C*H*$_3$)$_2$), 1.04 (3H, t, *J* 7.4, C(3)CH$_2$CH$_2$C*H*$_3$); ^{13}C NMR (151 MHz; CD_3CN) δ 174.1 (N*C*=O), 170.9 (O*C*=O), 153.7 (*C*(6)), 152.4 (*C*(3)), 147.9 (*C*(4')), 142.5 (*C*(3')), 140.0 (*C*(9)), 134.1 (*C*(8)), 132.7 (*C*(6')H), 127.8 (*C*(1')), 125.9 (*C*(2')H), 122.0 (*C*(5')H), 102.4 (*C*(7)H), 81.6 (NC=O*C*), 55.4 (ArNCH$_2$*C*H$_2$), 51.6 (ArN*C*H$_2$), 46.2 (N*C*H$_3$), 26.7 (C(3)*C*H$_2$), 24.4 (NC=OC(*C*H$_3$)$_2$), 21.8 (OC=O*C*H$_3$), 20.7 (C(3)CH$_2$*C*H$_2$), 13.7 (C(3)CH$_2$CH$_2$*C*H$_3$); *m/z* (ES$^-$)

523 [(M−H)$^-$, 100%]; HRMS *m/z* (ES$^+$) [Found (M+H)$^+$ 525.2581. $C_{25}H_{33}N_8O_5^+$ requires M$^+$, 525.2568]; HPLC (method 2) pH 10 retention time 2.31 min, purity 96.5%, pH 3 retention time 1.70 min, purity 96.4%.

1-((6-(3-Amino-4-(4-methylpiperazin-1-yl)phenyl)-3-propyl[1,2,4]triazolo[4,3-*b*]pyridazin-8-yl)amino)-2-methyl-1-oxopropan-2-yl acetate (**142**)

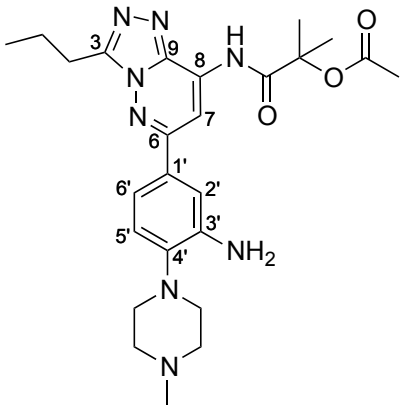

To a 100 mL round-bottomed flask containing 2-methyl-1-((6-(4-(4-methylpiperazin-1-yl)-3-nitrophenyl)-3-propyl[1,2,4]triazolo[4,3-*b*]pyridazin-8-yl)amino)-1-oxopropan-2-yl acetate **136** (674 mg, 1.28 mmol, 1.0 eq), was added tin(II) chloride (732 mg, 3.85 mmol, 3.0 eq) followed by a solution of ethanol and triethylamine (2:1, 15 mL) *via* syringe. The solution was heated at 70 °C for 1.5 h after which time TLC analysis indicated complete consumption of **136**. The reaction was cooled to RT and the residue was suspended in ethyl acetate (20 mL). The colourless residue was filtered off and the filtrate was concentrated *in vacuo* then stirred vigorously in saturated aqueous KF (60 mL), extracted with ethyl acetate (60 mL) and washed with water (2 × 60 mL), brine (60 mL), dried over sodium sulfate, filtered, and concentrated *in vacuo* to give *1-((6-(3-amino-4-(4-methylpiperazin-1-*

yl)phenyl)-3-propyl[1,2,4]triazolo[4,3-b]pyridazin-8-yl)amino)-2-methyl-1-oxopropan-2-yl acetate **142** (171 mg, 27%) as a yellow solid: R_f 0.14 (methanol/ethyl acetate/triethylamine, 15:84:1); mp 90-91 °C (from ethyl acetate); ν_{max} (thin film)/cm^{-1} 3394 (w), 2964 (w), 2936 (w), 1743 (m), 1717 (m), 1614 (s), 1558 (s), 1521 (s), 1469 (m), 1371 (m), 1237 (m), 1142 (s), 1135 (s); ^{1}H NMR (400 MHz; $CDCl_3$) δ 9.08 (1H, br s, N*H*C=O), 8.40 (1H, s, C(7)*H*), 7.38 (1H, dd, *J* 8.0, 2.0, C(6')*H*), 7.36 (1H, d, *J* 2.0, C(2')*H*), 7.09 (1H, d, *J* 8.8, C(5')*H*), 4.06 (2H, br s, NH_2), 3.07 (4H, br s, ArNCH_2), 3.21 (2H, t, *J* 7.5, C(3)CH_2), 2.70 (4H, br s, ArNCH$_2$CH_2), 2.44 (3H, s, NCH_3), 2.20 (3H, s, OC=OCH_3), 1.98 (2H, qt, *J* 7.5, 7.4, C(3)CH$_2$CH_2), 1.76 (6H, s, NC=OC(CH_3)$_2$), 1.07 (3H, t, *J* 7.4, C(3)CH$_2$CH$_2$CH_3); ^{13}C NMR (151 MHz; $CDCl_3$) δ 173.2 (N*C*=O), 169.9 (O*C*=O), 155.6 (*C*(6)), 152.0 (*C*(3)), 141.8 (*C*(3')), 141.5 (*C*(4')), 139.3 (*C*(9)), 132.5 (*C*(1')), 131.3 (*C*(8)), 120.1 (*C*(5')H), 118.3 (*C*(6')H), 113.8 (*C*(2')H), 103.1 (*C*(7)H), 81.2 (NC=O*C*), 55.7 (ArNCH$_2$*C*H$_2$), 50.4 (ArN*C*H$_2$), 46.1 (N*C*H$_3$), 26.3 (C(3)*C*H$_2$), 24.3 (NC=OC(*C*H$_3$)$_2$), 21.9 (OC=O*C*H$_3$), 20.3 (C(3)CH$_2$*C*H$_2$), 14.0 (C(3)CH$_2$CH$_2$*C*H$_3$); *m/z* (ES^+) 495 [$(M+H)^+$, 100%]; HRMS *m/z* (ES^+) [Found $(M+H)^+$ 495.2827. $C_{25}H_{35}N_8O_3^+$ requires M^+, 495.2811]; HPLC (method 2) pH 10 retention time 2.08 min, purity 97.4%, pH 3 retention time 1.36 min, purity 97.4%.

1-((6-(3-(Cyclopropanesulfonamido)-4-(4-methylpiperazin-1-yl)phenyl)-3-propyl[1,2,4]triazolo[4,3-*b*]pyridazin-8-yl)amino)-2-methyl-1-oxopropan-2-yl acetate (**138**)

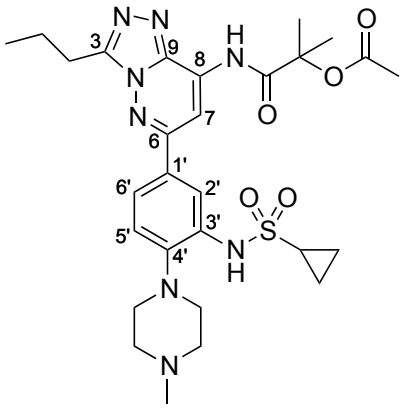

A solution of 1-((6-(3-amino-4-(4-methylpiperazin-1-yl)phenyl)-3-propyl[1,2,4]triazolo[4,3-*b*]pyridazin-8-yl)amino)-2-methyl-1-oxopropan-2-yl acetate **142** (40 mg, 81 µmol, 1.0 eq) in pyridine (500 µL) was stirred at 0 °C for 15 min. After this time, a solution of cyclopropanesulfonyl chloride (41 µL, 57 mg, 400 µmol) and 4-DMAP (10 mg, 81 µmol, 1.0 eq) in pyridine (300 µL) was added dropwise *via* syringe to the solution of **142**, and the reaction solution was stirred for 19 h at RT. The reaction solution was then concentrated *in vacuo* and the residue was redissolved in CH_2Cl_2 (100 mL) and washed with brine (100 mL), dried over sodium sulfate, filtered, and concentrated *in vacuo*. The resultant oil was purified by preparative HPLC to give **138** (27 mg, 56%) as a colourless solid: R_f 0.52 (methanol/CH_2Cl_2/triethylamine, 10:89:1); mp 71-73 °C (from ethyl acetate); ν_{max} (thin film)/cm^{-1} 3390 (w), 3272 (w), 2965 (w), 1743 (m), 1724 (m), 1558 (s), 1522 (s), 1468 (m), 1398 (m), 1336 (m), 1238 (s), 1142 (s); ^{1}H NMR (500 MHz; $CDCl_3$) δ 9.13 (1H, br s, N*H*C=O), 8.43 (1H, s, C(7)*H*), 8.25 (1H, d, *J* 2.1, C(2')*H*), 7.70 (1H, br s, N*H*SO_2), 7.66 (1H, dd, *J* 8.1, 2.1, C(6')*H*), 7.33 (1H, d, *J* 8.1, C(5')*H*), 3.22 (2H, t, *J* 7.6, C(3)CH_2), 2.98 (4H,

t, *J* 7.7, ArNC*H*$_2$), 2.65 (4H, br s, ArNCH$_2$C*H*$_2$), 2.63-2.57 (1H, m, SC*H*), 2.40 (3H, s, NC*H*$_3$), 2.20 (3H, s, OC=OC*H*$_3$), 1.99 (2H, tq, *J* 7.6, 7.4, C(3)CH$_2$C*H*$_2$), 1.76 (6H, s, NC=OC(C*H*$_3$)$_2$), 1.39-1.36 (2H, m, SO$_2$CC*H*$_a$), 1.09-1.05 (2H, m, SO$_2$CC*H*$_b$), 1.07 (3H, t, *J* 7.4, C(3)CH$_2$CH$_2$C*H*$_3$); ^{13}C NMR (126 MHz; CDCl$_3$) δ 173.2 (N*C*=O), 169.9 (O*C*=O), 154.9 (*C*(6)), 152.1 (*C*(3)), 143.9 (*C*(4')), 139.2 (*C*(9)), 134.0 (*C*(8)), 133.1 (*C*(3')), 132.9 (*C*(1')), 123.4 (*C*(6')H), 122.1 (*C*(5')H), 116.7 (*C*(2')H), 102.8 (*C*(7)H), 81.2 (NC=O*C*), 55.6 (ArNCH$_2$*C*H$_2$), 52.4 (ArN*C*H$_2$), 46.2 (N*C*H$_3$), 30.8 (S*C*H), 26.4 (C(3)*C*H$_2$), 24.3 (NC=OC(*C*H$_3$)$_2$), 21.9 (OC=O*C*H$_3$), 20.3 (C(3)CH$_2$*C*H$_2$), 14.0 (C(3)CH$_2$CH$_2$*C*H$_3$), 6.2 (SC*C*); *m/z* (ES$^+$) 599 [(M+H)$^+$, 100%]; HRMS *m/z* (ES$^+$) [Found (M+H)$^+$ 599.2755. $C_{28}H_{39}N_8O_5S^+$ requires M$^+$, 599.2759]; HPLC (method 2) pH 10 retention time 2.15 min, purity 97.9%, pH 3 retention time 1.60 min, purity 97.8%.

1-((6-(3-(Azetidine-3-sulfonamido)-4-(4-methylpiperazin-1-yl)phenyl)-3-propyl[1,2,4]triazolo[4,3-*b*]pyridazin-8-yl)amino)-2-methyl-1-oxopropan-2-yl acetate (**139**)

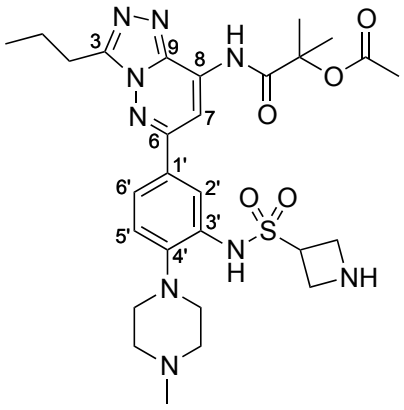

A solution of 1-((6-(3-amino-4-(4-methylpiperazin-1-yl)phenyl)-3-propyl[1,2,4]triazolo[4,3-*b*]pyridazin-8-yl)amino)-2-methyl-1-oxopropan-2-yl acetate **142** (50 mg, 100 μmol, 1.0 eq) in CH_2Cl_2 (900 μL) was stirred at 0 °C

for 15 min. After this time, a solution of *tert*-butyl 3-(chlorosulfonyl)azetidine-1-carboxylate (39 mg, 150 μmol, 1.5 eq) and 4-DMAP (1 mg, 8 μmol, 0.08 eq) in CH_2Cl_2 (400 μL) was added dropwise *via* syringe and the reaction solution was stirred for 19 h at RT. After this time the reaction solution was concentrated *in vacuo* and the residue was redissolved in CH_2Cl_2 (100 mL) and washed with brine (100 mL), dried over sodium sulfate, filtered, and concentrated *in vacuo*. The residue was purified by silica gel column chromatography, eluting with methanol and CH_2Cl_2 (0:100, 5:95, 10:90,15:85, 20:80) to give a crude sample (41 mg) as a pale yellow oil. This oil was redissolved in CH_2Cl_2 (1.6 mL) and TFA (400 μL, 600 mg, 5.3 mmol, 92 eq) was added dropwise *via* syringe. After 3 h TLC analysis indicated complete consumption of starting material. The solution was concentrated *in vacuo* and the residue was redissolved in CH_2Cl_2 (30 mL) and washed with saturated aqueous $NaHCO_3$ (30 mL), brine (30 mL), dried over sodium sulfate, filtered, and concentrated *in vacuo*. The resultant oil was purified by preparative HPLC to give *1-((6-(3-(azetidine-3-sulfonamido)-4-(4-methylpiperazin-1-yl)phenyl)-3-propyl[1,2,4]triazolo[4,3-b]pyridazin-8-yl)amino)-2-methyl-1-oxopropan-2-yl acetate* **139** (16 mg, 26%) as a yellow solid: R_f 0.11 (methanol/CH_2Cl_2/triethylamine, 20:79:1); mp 93-95 °C (from ethyl acetate); ν_{max} (thin film)/cm^{-1} 3390 (w), 2965 (w), 2942 (w), 1743 (m), 1558 (m), 1522 (s), 1468 (s), 1371 (s), 1425 (m), 1371 (m), 1200 (m), 1155 (m), 1141 (s); ^{1}H NMR (500 MHz; $CDCl_3$) δ 9.13 (1H, br s, N*H*C=O), 8.41 (1H, s, C(7)*H*), 8.16 (1H, d, *J* 2.1, C(2')*H*), 7.66 (1H, dd, *J* 8.6, 2.1, C(6')*H*), 7.32 (1H, d, *J* 8.6, C(5')*H*), 4.42-4.30 (1H, m, SC*H*), 4.16 (2H, dd, *J* 9.1, 6.8 SCCH_a), 3.82-3.78 (2H, m, SCCH_b), 3.22 (2H, t, *J* 7.5, C(3)CH_2),

2.94 (4H, t, *J* 4.3, $CH_3NCH_2CH_2$), 2.64 (4H, br s, CH_3NCH_2), 2.40 (3H, s, NCH_3), 2.20 (3H, s, $OC{=}OCH_3$), 1.99 (2H, tq, *J* 7.5, 7.4, $C(3)CH_2CH_2$), 1.87 (1H, br s, $NHSO_2$), 1.76 (6H, s, $NC{=}OC(CH_3)_2$), 1.63 (1H, br s, SCCN*H*), 1.07 (3H, t, *J* 7.4, $C(3)CH_2CH_2CH_3$); ^{13}C NMR (126 MHz; $CDCl_3$) δ 173.2 (N*C*=O), 170.0 (O*C*=O), 154.8 (*C*(6)), 152.1 (*C*(3)), 143.8 (*C*(4')), 139.2 (*C*(9)), 133.6 (*C*(8)), 133.0 (*C*(3')), 133.2 (*C*(1')), 123.7 (*C*(6')H), 122.3 (*C*(5')H), 116.4 (*C*(2')H), 102.8 (*C*(7)H), 81.2 (NC=O*C*), 55.6 ($ArNCH_2CH_2$), 54.7 (S*C*H), 52.5 ($ArNCH_2$), 48.6 ($SCCH_aH_b$), 46.2 (NCH_3), 26.4 ($C(3)CH_2$), 24.3 ($NC{=}OC(CH_3)_2$), 21.9 ($OC{=}OCH_3$), 20.3 ($C(3)CH_2CH_2$), 14.1 ($C(3)CH_2CH_2CH_3$; *m/z* (ES^+) 614 [$(M+H)^+$, 100%]; HRMS *m/z* (ES^+) [Found $(M+H)^+$ 614.2865. $C_{28}H_{40}N_9O_5S^+$ requires M^+, 614.2868]; HPLC (method 2) pH 10 retention time 1.57 min, purity 100%.

1-((6-(3-(Cyclopropanesulfonamido)-4-(4-methylpiperazin-1-yl)phenyl)-3-methyl[1,2,4]triazolo[4,3-*b*]pyridazin-8-yl)amino)-2-methyl-1-oxopropan-2-yl acetate (**140**)

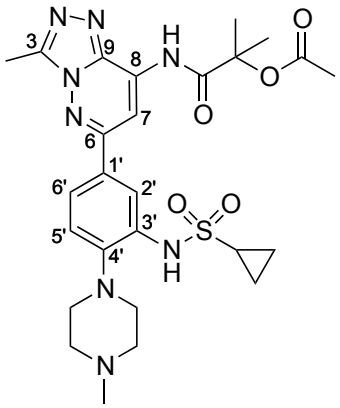

A solution of **103** (120 mg, 221 µmol, 1.0 eq) in TFA and CH_2Cl_2 (1:1, 2 mL) was stirred at RT for 3 h, after which time TLC analysis indicated complete consumption of **103**. The solution was concentrated *in vacuo* and the residue was redissolved in CH_2Cl_2 (30 mL), washed with saturated aqueous $NaHCO_3$ (30 mL), brine (30 mL), dried over sodium sulfate, filtered, and concentrated *in vacuo* to give a sample of *1-((6-(3-amino-4-(4-methylpiperazin-1-yl)phenyl)-3-propyl[1,2,4]triazolo[4,3-b]pyridazin-8-yl)amino)-2-methyl-1-oxopropan-2-yl acetate* **143** (90 mg), which was used without further purification. To a suspension of 1-((6-(3-amino-4-(4-methylpiperazin-1-yl)phenyl)-3-propyl[1,2,4]triazolo[4,3-b]pyridazin-8-yl)amino)-2-methyl-1-oxopropan-2-yl acetate **143** (37 mg, 84 µmol, 1.0 eq) and Hünig's base (44 µL, 32 mg, 92 µmol, 1.1 eq) in CH_2Cl_2 (5.0 mL) was added chlorocarbonyl-1-methylethyl acetate (13 µL, 15 mg, 92 µmol, 1.1 eq) at 0 °C dropwise *via* syringe. A solution formed after 30 min which was stirred for 2 h at 0 °C after which time TLC analysis indicated complete consumption of starting material. The solution was warmed to RT, diluted with CH_2Cl_2 (25 mL)

and washed with saturated aqueous $NaHCO_3$ (3 × 25 mL), brine (25 mL), dried over sodium sulfate, filtered, and concentrated *in vacuo*. This material was purified by silica gel column chromatography, eluting with methanol and CH_2Cl_2 (0:100, 5:95, 10:90,15:85, 20:80) and further purified by preparative HPLC to afford *1-((6-(3-(cyclopropanesulfonamido)-4-(4-methylpiperazin-1-yl)phenyl)-3-methyl[1,2-,4]triazolo[4,3-b]pyridazin-8-yl)amino)-2-methyl-1-oxopropan-2-yl acetate* **140** (18 mg, 35% over 2 steps) as a colourless solid: R_f 0.13 (methanol/ethyl acetate/triethylamine, 20:79:1); mp 114-117 °C (from ethyl acetate); ν_{max} (thin film)/cm^{-1} 3392 (w), 2925 (w), 2852 (w), 1741 (m), 1562 (m), 1531 (s), 1509 (m), 1470 (s), 1371 (m), 1153 (s), 1143 (s); ^{1}H NMR (400 MHz; $CDCl_3$) δ 9.08 (1H, br s, N*H*C=O), 8.43 (1H, s, C(7)*H*), 8.24 (1H, d, *J* 2.0, C(2')*H*), 7.68 (1H, dd, *J* 8.3, 2.0, C(6')*H*), 7.64 (1H, br s, N*H*SO_2), 7.35 (1H, d, *J* 8.3, C(5')*H*), 2.85 (3H, s, C(3)CH_3), 3.07 (4H, br s, ArNCH_2), 2.65-2.61 (1H, m, SC*H*), 2.79 (4H, br s, ArNCH$_2$CH_2), 2.50 (3H, s, NCH_3), 2.20 (3H, s, OC=OCH_3), 1.76 (6H, s, NC=OC(CH_3)$_2$), 1.42-1.38 (2H, m, SO_2CCH_a), 1.12-1.07 (2H, m, SO_2CCH_b); ^{13}C NMR (101 MHz; $CDCl_3$) δ 173.1 (N*C*=O), 169.9 (O*C*=O), 155.1 (*C*(6)), 148.8 (*C*(3)), 143.7 (*C*(3')), 139.2 (*C*(9)), 133.9 (*C*(8)), 133.1 (*C*(4')), 133.0 (*C*(1')), 123.6 (*C*(6')H), 122.3 (*C*(5')H), 117.1 (*C*(2')H), 102.7 (*C*(7)H), 81.2 (NC=O*C*), 55.4 (ArNCH$_2$*C*H$_2$), 51.8 (ArN*C*H$_2$), 45.8 (N*C*H$_3$), 30.9 (S*C*H), 24.3 (NC=OC(*C*H$_3$)$_2$), 21.8 (OC=O*C*H$_3$), 10.1 (C(3)*C*H$_3$), 6.3 (SC*C*); *m/z* (ES^+) 571 [$(M-H)^-$, 100%]; HRMS *m/z* (ES^+) [Found $(M+H)^+$ 571.2418. $C_{26}H_{35}N_8O_5S^+$ requires M^+, 571.2446]; HPLC (method 2) pH 10 retention time 1.92 min, purity 97.1%, pH 3 retention time 1.37 min, purity 98.1%.

***N*-(6-(3-(Cyclopropanesulfonamido)-4-(4-methylpiperazin-1-yl)phenyl)-3-methyl[1,2,4]triazolo[4,3-*b*]pyridazin-8-yl)-3,5-dimethylisoxazole-4-carboxamide** (**141**)

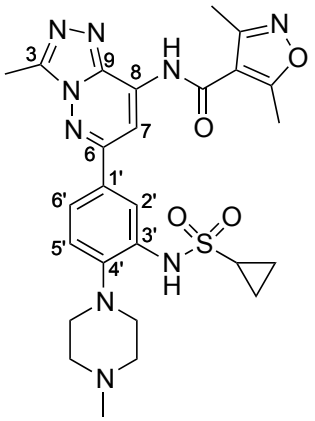

A solution of **103** (120 mg, 221 µmol, 1.0 eq) in TFA and CH_2Cl_2 (1:1, 2 mL) was stirred at RT for 3 h, after which time TLC analysis indicated complete consumption of **103**. The solution was concentrated *in vacuo* and the residue was redissolved in CH_2Cl_2 (30 mL), washed with saturated aqueous $NaHCO_3$ (30 mL), brine (30 mL), dried over sodium sulfate, filtered, and concentrated *in vacuo* to give a sample of *N-(5-(8-amino-3-methyl[1,2,4]triazolo[4,3-b]pyridazin-6-yl)-2-(4-methylpiperazin-1-yl)phenyl)cyclopropanesulfonamide* **143** (90 mg), which was used without further purification. To a suspension of *N*-(5-(8-amino-3-methyl[1,2,4]triazolo[4,3-*b*]pyridazin-6-yl)-2-(4-methylpiperazin-1-yl)phenyl)cyclopropanesulfonamide **143** (37 mg, 84 µmol, 1.0 eq) and Hünig's base (44 µL, 32 mg, 92 mmol, 1.1 eq) in CH_2Cl_2 (5 mL) was added 3,5-dimethylisoxazole-4-carbonylchloride (12 µL, 15 mg, 92 mmol, 1.1 eq) at 0 °C dropwise *via* syringe. A solution formed after 30 min which was stirred for a further 2 h at 0 °C after which time TLC analysis indicated complete consumption of **143**. The solution was diluted with CH_2Cl_2 (25 mL) and washed with saturated aqueous $NaHCO_3$ (2 × 25 mL), brine (25 mL), dried

over sodium sulfate, filtered, and concentrated *in vacuo*. The crude material was purified by silica gel column chromatography, eluting with methanol, CH_2Cl_2 (0:100, 5:95, 10:90, 15:85) and then by preparative HPLC, to afford *N-(6-(3-(yclopropanesulfonamido)-4-(4-methylpiperazin-1-yl)phenyl)-3-methyl[1,2,4]triazolo[4,3-b]pyridazin-8-yl)-3,5-dimethylisoxazole-4-carboxamide* **141** (14 mg, 28% over 2 steps) as a colourless solid: R_f 0.13 (methanol/ethyl acetate/triethylamine, 20:79:1); mp 139-140 °C (from ethyl acetate); ν_{max} (thin film)/cm^{-1} 3407 (w), 3244 (w), 2926 (w), 2849 (w), 1695 (m), 1606 (m), 1560 (s), 1531 (s), 1509 (s), 1425 (m), 1393 (m), 1335 (m), 1209 (m), 1142 (s); ^{1}H NMR (600 MHz; $CDCl_3$) δ 8.92 (1H, br s, N*H*C=O), 8.48 (1H, s, C(7)*H*), 8.27 (1H, d, *J* 2.0, C(2')*H*), 7.71 (1H, dd, *J* 8.3, 2.0, C(6')*H*), 7.69 (1H, br s, N*H*SO_2), 7.37 (1H, d, *J* 8.3, C(5')*H*), 3.03 (4H, br s, ArNCH_2), 2.87 (3H, s, C(3)CH_3), 2.82 (3H, s, OCCH_3), 2.73 (4H, br s, ArNCH$_2$CH_2), 2.66 (3H, s, NCCH_3), 2.65-2.59 (1H, m, SC*H*), 2.45 (3H, s, NCH_3), 2.20 (3H, s, OC=OCH_3), 1.76 (6H, s, NC=OC(CH_3)$_2$), 1.41-1.37 (2H, m, SO_2CCH_a) 1.11-1.07 (2H, m, SO_2CCH_b); ^{13}C NMR (151 MHz; $CDCl_3$) δ 168.7 (O*C*CH_3), 159.9 (*C*(6)), 155.8 (*C*=O), 152.5 (N*C*CH_3), 143.5 (*C*(3)), 138.5 (*C*(9)), 133.8 (*C*(8)), 128.7 (*C*(4')), 127.60 (*C*(3')), 127.59 (*C*(1')), 118.2 (*C*(6')H), 116.9 (*C*(5')H), 111.6 (*C*(2')H), 106.2 (C=O*C*), 97.4 (*C*(7)H), 50.1(ArNCH$_2$*C*H$_2$), 46.7 (ArN*C*H$_2$), 40.6 (N*C*H$_3$), 25.5 (S*C*H), 8.3 (OC*C*H$_3$), 6.7 (NC*C*H$_3$), 4.7 (C(3)*C*H$_3$), 0.9 (SC*C*H$_a$H$_b$); *m/z* (ES$^+$) 566 [(M+H)$^+$, 100%]; HRMS *m/z* (ES$^+$) [Found (M+H)$^+$ 566.2299. $C_{26}H_{32}N_9O_4S^+$ requires M$^+$, 566.2298]; HPLC (method 2) pH 10 retention time 1.40 min, purity 99.4%, pH 3 retention time 1.33 min, purity 100%.

***tert*-Butyl-(3-methyl-6-(*o*-tolyl)[1,2,4]triazolo[4,3-*b*]pyridazin-8-yl)carbamate** (**146**)

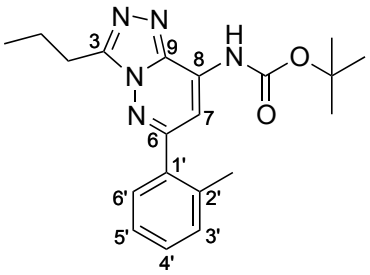

To a 2-5 mL MW vial containing *tert*-butyl-(6-chloro-3-propyl[1,2,4]triazolo[4,3-*b*]pyridazin-8-yl)carbamate **129** (50 mg, 160 µmol, 1.0 eq) were added *o*-tolylboronic acid **145** (55 mg, 300 µmol, 1.9 eq), K_2CO_3 (33 mg, 240 µmol, 1.5 eq), and Pd(dppf)Cl_2·CH_2Cl_2 (13 mg, 16 µmol, 0.1 eq). A solution of 1,4-dioxane and water (10:1, 3 mL) was added *via* syringe and the reaction mixture was heated at 80 °C for 20 h. After cooling to RT the reaction mixture was filtered through Celite® (eluent CH_2Cl_2) and concentrated *in vacuo*. The residue was redissolved in CH_2Cl_2 (20 mL), washed with water (20 mL), then brine (20 mL), dried over sodium sulfate, filtered, and concentrated *in vacuo*. The crude material was purified by silica gel column chromatography, eluting with isohexane, ethyl acetate and triethylamine (29:70:1, 9:90:1, 0:99:1) to afford *tert-butyl-(3-methyl-6-(o-tolyl)[1,2,4]triazolo[4,3-b]pyridazin-8-yl)carbamate* **146** (25 mg, 38%) as a colourless solid: R_f 0.31 (isohexane/ethyl acetate, 50:50); mp 183-187 °C (from ethanol); ν_{max} (thin film)/cm^{-1} 2968 (w), 2929 (w), 1733 (s), 1558 (m), 1534 (m), 1473 (m), 1366 (m) 1242 (m), 1150 (s), 1045 (m); ^{1}H NMR (600 MHz; $CDCl_3$) δ 8.42 (1H, br s, N*H*), 7.84 (1H, s, C(7)*H*), 7.48−7.44 (1H, m, C(4')*H*), 7.39-7.36 (1H, m, C(6')*H*), 7.35-7.33 (1H, m, C(3')*H*), 7.33-7.31 (1H, m, C(5')*H*),

3.18 (2H, t, *J* 7.6, C(3)CH_2), 2.42 (3H, s, C(2')CH_3), 1.96 (2H, qt, *J* 7.6, 7.5, C(3)CH_2CH_2), 1.55 (9H, s, (CH_3)$_3$), 1.05 (3H, t, *J* 7.5, C(3)CH_2CH_2CH_3); ^{13}C NMR (126 MHz; $CDCl_3$) δ 157.9 (*C*(6)), 151.64 (*C*(3)), 151.57 (*C*=O), 138.7 (*C*(9)), 136.3 (*C*(2')), 136.0 (*C*(1')), 133.5 (*C*(8)), 131.1 (*C*(3')H), 129.7 (*C*(6)H), 129.6 (*C*(4)H), 126.2 (*C*(5')H), 104.2 (*C*(7')H), 83.1 (*C*(CH_3)$_3$), 28.1 (C(*C*H_3)$_3$), 26.2 (C(3)*C*H_2), 20.5 (C(2')*C*H_3), 20.2 (C(3)CH_2*C*H_2), 13.9 (C(3)CH_2CH_2*C*H_3); ***m/z*** (ES$^-$) 366 [(M−H)$^-$, 100%]; HRMS ***m/z*** (ES$^+$) [Found (M+H)$^+$ 368.2064. $C_{18}H_{22}N_5O_2^+$ requires M$^+$, 368.2087]; HPLC (method 2) pH 10 retention time 2.87 min, purity 100%, pH 3 retention time 2.93 min, purity 100%.

6-Chloro-3-(methoxymethyl)[1,2,4]triazolo[4,3-*b*]pyridazin-8-amine (**149**)

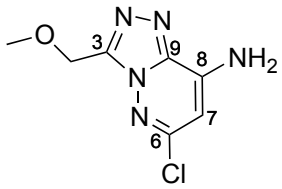

To a 2-5 mL MW vial containing 6-chloro-3-hydrazinylpyridazin-4-amine **63** (300 mg, 1.90 mmol, 1.0 eq) was added methoxyacetic acid (3.0 mL, 3.5 g, 39 mmol, 21 eq) and the mixture was heated at 110 °C with microwave irradiation for 70 min. After cooling to RT, the residue was redissolved in ethyl acetate (100 mL) and washed with 2 M aqueous K_2CO_3 (3 × 100 mL), water (100 mL), brine (100 mL), dried over sodium sulfate, filtered, and concentrated *in vacuo* to give *6-chloro-3-(methoxymethyl)[1,2,4]triazolo[4,3-b]pyridazin-8-amine* **149** (261 mg, 64%) as a colourless solid: R_f 0.19 (methanol/ethyl acetate, 20:80); mp 182-183 °C (from ethanol); ν_{max} (solid)/cm^{-1} 3402 (w), 3296 (w), 3134 (w), 2963 (m), 1645 (s), 1564 (s),

1471 (m), 1429 (m), 1243 (m), 1155 (m), 1091 (m), 1060 (m); ^{1}H NMR (600 MHz; D_6-DMSO) δ 7.98 (2H, br s, NH_2), 6.17 (1H, s, C(7)*H*), 4.79 (2H, s, C(3)CH_2), 3.32 (3H, s, OCH_3); ^{13}C NMR (126 MHz; $CDCl_3$) δ 150.3 (*C*(6)), 147.2 (*C*(3)), 144.3 (*C*(8)), 140.4 (*C*(9)), 94.8 (*C*(7)H), 62.5 (C(3)*C*H_2), 58.4 (O*C*H_3); *m/z* (ES^-) 212 [$(M-H)^-$, 100%]; HRMS *m/z* (ES^+) [Found $(M+H)^+$ 214.0493. $C_7H_9ClN_5O^+$ requires M^+, 214.0490]; HPLC (method 2) pH 10 retention time 0.86 min, purity 98.2%, pH 3 retention time 0.85 min, purity 98.3%.

tert-Butyl-(6-chloro-3-(methoxymethyl)[1,2,4]triazolo[4,3-*b*]pyridazin-8-yl)carbamate (**150**)

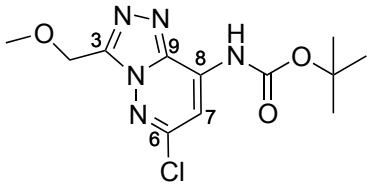

To a solution of 6-chloro-3-(methoxymethyl)[1,2,4]triazolo[4,3-b]pyridazin-8-amine **149** (251 mg, 1.17 mmol, 1.0 eq) and 4-DMAP (7 mg, 60 μmmol, 0.05 eq) in THF (50 mL) was added di-*tert*-butyl dicarbonate (1.0 M in THF, 1.2 mL, 1.2 mmol, 1.0 eq) dropwise at RT and the reaction solution was stirred for 24 h after which time TLC analysis indicated complete consumption of **149**. The reaction solution was concentrated *in vacuo* and the residue was redissolved in ethyl acetate (60 mL) and washed with saturated aqueous NH_4Cl (2 × 60 mL), water (60 mL) and brine (60 mL), dried over magnesium sulfate, filtered, and concentrated *in vacuo*. The resultant oil was purified by silica gel column chromatography, eluting with ethyl acetate and isohexane (3:97, 25:75) to give *tert-butyl-(6-chloro-3-(methoxymethyl)[1,2,4]triazolo[4,3-*

b]pyridazin-8-yl)carbamate **150** (202 mg, 55%) as a colourless solid: R_f 0.31 (isohexane/ethyl acetate, 50:50); mp 107-108 °C (from ethyl acetate); ν_{max} (thin film)/cm^{-1} 3175 (w), 3134 (w), 2980 (w), 2932 (w), 1737 (s), 1554 (s), 1460 (m), 1415 (m), 1368 (m), 1239 (m), 1148 (m); ^{1}H NMR (400 MHz; $CDCl_3$) δ 8.17 (1H, br s, N*H*), 7.75 (1H, s, C(7)*H*), 4.97 (2H, s, C(3)CH_2), 3.50 (3H, s, OCH_3), 1.56 (9H, s, (CH_3)$_3$); ^{13}C NMR (126 MHz; $CDCl_3$) δ 151.8 (*C*=O), 151.0 (*C*(6)), 147.8 (*C*(3)), 139.1 (*C*(9)), 134.9 (*C*(8)), 103.8 (*C*(7)H), 83.9 (*C*(CH_3)$_3$), 62.6 (C(3)*C*H_2), 59.0 (O*C*H_3), 28.0 (C(*C*H_3)$_3$); *m/z* (ES$^-$) 312 [(M−H)$^-$, 100%]; HRMS *m/z* (ES$^+$) [Found (M+H)$^+$ 314.1002. $C_{12}H_{17}ClN_5O_3^+$ requires M$^+$, 314.1014]; HPLC (method 2) pH 10 retention time 2.03 min, purity 100%, pH 3 retention time 2.06 min, purity 100%.

tert-Butyl-(3-(methoxymethyl)-6-(4-(4-methylpiperazin-1-yl)-3-nitrophenyl)[1,2,4]triazolo[4,3-*b*]pyridazin-8-yl)carbamate (**147**)

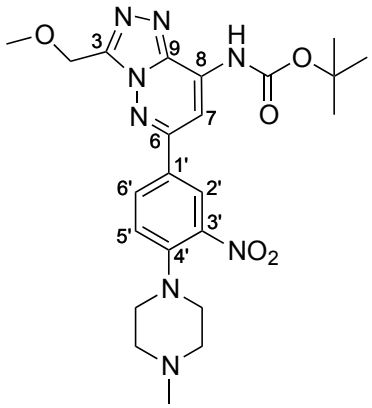

To a 2-5 mL MW vial containing 1-methyl-4-(2-nitro-4-(4,4,5,5-tetramethyl-1,3,2-dioxaborolan-2-yl)phenyl)piperazine **74** (276 mg, 796 µmol, 2.5 eq) were added *tert*-butyl-(6-chloro-3-(methoxymethyl)[1,2,4]triazolo[4,3-b]pyridazin-8-yl)carbamate **150** (100 mg, 318 µmol, 1.0 eq), K_2CO_3 (66 mg, 480 µmol, 1.5 eq), and Pd(dppf)Cl_2·CH_2Cl_2 (26 mg, 32 µmol, 0.1 eq).

A solution of 1,4-dioxane and water (10:1, 3 mL) was added *via* syringe and the reaction mixture was heated at 80 °C for 20 h. After cooling to RT the reaction mixture was filtered through Celite® (eluent CH_2Cl_2) and concentrated *in vacuo*. The residue was redissolved in CH_2Cl_2 (20 mL), washed with water (20 mL), then brine (20 mL), dried over sodium sulfate, filtered, and concentrated *in vacuo*. The crude material was purified firstly by silica gel column chromatography, eluting with methanol and CH_2Cl_2 (0.5:99.5) and secondly by preparative HPLC to afford *tert-butyl-(3-(methoxymethyl)-6-(4-(4-methylpiperazin-1-yl)-3-nitrophenyl)[1,2,4]triazolo[4,3-b]pyridazin-8-yl)carbamate* **147** (36 mg, 23%) as a yellow solid: R_f 0.20 (methanol/ethyl acetate/triethylamine, 20:79:1); mp 100-101 °C (from ethyl acetate); ν_{max} (thin film)/cm^{-1} 3403 (w), 2979 (w), 2937 (w), 2844 (w), 1737 (m), 1614 (m), 1569 (s), 1532 (s), 1464 (m), 1394 (m), 1369 (m), 1242 (s), 1203 (s), 1152 (s); ^{1}H NMR (600 MHz; $CDCl_3$) $CDCl_3$) δ 8.44 (1H, d, *J* 2.2, C(2')*H*), 8.16 (1H, br s, N*H*), 8.14 (1H, s, C(7)*H*), 8.11 (1H, dd, *J* 8.7, 2.2, C(6')*H*), 7.20 (1H, d, *J* 8.7, C(5')*H*), 5.06 (2H, s, C(3)CH_2), 3.53 (3H, s, 2H, C(3)CH_2OCH_3), 3.22 (4H, br s, ArNCH_2), 2.63 (4H, br s, ArNCH_2CH_2), 2.40 (3H, s, NCH_3), 1.58 (9H, s, C(CH_3)$_3$); ^{13}C NMR (151 MHz; $CDCl_3$) δ 153.7 (*C*(6)), 151.5 (*C*(3)), 148.1 (*C*=O), 147.1 (*C*(3')), 141.9 (*C*(4')), 139.6 (*C*(9)), 134.5 (*C*(8)), 132.1 (*C*(6')H), 127.4 (*C*(1')), 125.5 (*C*(2')H), 120.6 (*C*(5')H), 100.0 (*C*(7)H), 83.4 (*C*(CH_3)$_3$), 62.7 (C(3)*C*H_2), 59.0 (C(3)CH_2O*C*H_3), 54.6 (ArNCH_2*C*H_2), 50.9 (ArNCH_2), 45.9 (N*C*H_3) 28.1 (C(*C*H_3)$_3$); *m/z* (ES^+) 499 [$(M+H)^+$, 100%]; HRMS *m/z* (ES^+) [Found $(M+H)^+$ 499.2401. $C_{23}H_{31}N_8O_5^+$ requires M^+, 499.2412]; HPLC (method 2) pH 10 retention time 1.55 min, purity 99.5%, pH 3 retention time 1.65 min, purity 99.5%.

***tert*-Butyl-(6-chloro-3-(2-hydroxyethyl)[1,2,4]triazolo[4,3-*b*]pyridazin-8-yl)carbamate** (**152**)

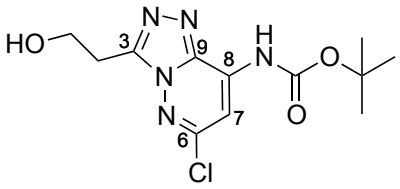

To a 10-20 mL MW vial containing 6-chloro-3-hydrazinylpyridazin-4-amine **63** (481 mg, 3.01 mmol, 1.0 eq) was added 30% aqueous solution 3-hydroxypropanoic acid (8.0 mL, 2.4 g, 27 mmol, 8.9 eq) and the suspension was stirred at RT for 10 min. The reaction mixture was then heated at 140 °C for 3 h under microwave irradiation. The solution was cooled to RT and added to 2 M aqueous K_2CO_3 (100 mL). The aqueous phase was extracted with ethyl acetate (3 × 100 mL) and the organic extracts were combined and washed with water (300 mL), brine (300 mL), dried over magnesium sulfate, filtered, and concentrated *in vacuo* to give a pale brown solid (900 mg). To a suspension of this solid and 4-DMAP (18 mg, 15 µmol, 0.05 eq) in THF (30 mL) was added di-*tert*-butyl dicarbonate (1.0 M in THF, 3.3 mL, 3.3 mmol, 1.1 eq) dropwise *via* syringe and the reaction solution was stirred at RT for 24 h then concentrated *in vacuo*. The residue was redissolved in ethyl acetate (100 mL) and washed with saturated aqueous NH_4Cl (2 × 100 mL), water (100 mL) and brine (100 mL), dried over magnesium sulfate, filtered, and concentrated *in vacuo*. The resultant oil was suspended in 2 M aqueous LiOH (10 mL) and stirred for 2 h at RT then diluted with water (100 mL) and extracted with ethyl acetate (2 × 100 mL). The organic extracts were combined, washed with brine (100 mL), dried over magnesium sulfate, filtered, and concentrated *in vacuo* to give a pale brown oil which was purified by silica

gel column chromatography, eluting with ethyl acetate and isohexane (50:50, 60:40, 70:30, 80:20, 90:10, 100:0) to give *tert-butyl-(6-chloro-3-(2-hydroxyethyl)[1,2,4]triazolo[4,3-b]pyridazin-8-yl)carbamate* **152** (44 mg, 5% over 2 steps) as a colourless solid: R_f 0.76 (methanol/ethyl acetate/triethylamine, 10:89:1); mp 181-182 °C (from ethyl acetate); ν_{max} (thin film)/cm^{-1} 3307 (w), 2980 (w), 2933 (w), 1741 (m), 1557 (s), 1466 (m), 1370 (m), 1243 (s), 1153 (s), 1110 (m); ^{1}H NMR (400 MHz; $CDCl_3$) δ 8.21 (1H, br s, N*H*), 7.74 (1H, s, C(7)*H*), 4.28 (2H, t, *J* 5.8, C(3)CH_2), 3.38 (2H, t, *J* 5.8, C(3) CH_2CH_2), 1.57 (9H, s, C(CH_3)$_3$); ^{13}C NMR (126 MHz; $CDCl_3$) δ 151.5 (*C*(6)), 151.1 (*C*=O), 149.7 (*C*(3)), 138.6 (*C*(9)), 134.9 (*C*(8)), 83.9 (*C*(CH_3)$_3$), 28.0 (C(*C*H_3)$_3$); *m/z* (ES^-) 312 [$(M-H)^-$, 100%]; HRMS *m/z* (ES^+) [Found $(M+H)^+$ 314.1009. $C_{12}H_{17}ClN_5O_3^+$ requires M^+, 314.1014]; HPLC (method 2) pH 10 retention time 1.78 min, purity 97.1%, pH 3 retention time 1.80 min, purity 96.6%.

***tert*-Butyl-(3-(2-hydroxyethyl)-6-(4-(4-methylpiperazin-1-yl)-3-nitrophenyl)[1,2,4]triazolo[4,3-*b*]pyridazin-8-yl)carbamate** (**148**)

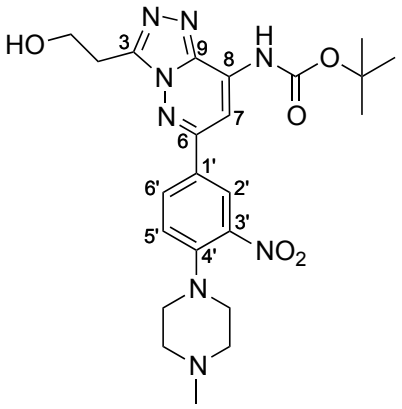

To a 2-5 mL MW vial containing *tert*-butyl-(6-chloro-3-(2-hydroxyethyl)[1,2,4]triazolo[4,3-b]pyridazin-8-yl)carbamate **152** (46 mg, 150 µmol, 1.0 eq) and 1-methyl-4-(2-nitro-4-(4,4,5,5-tetramethyl-1,3,2-dioxaborolan-2-yl)phenyl)piperazine **74** (102 mg, 292 µmol, 2.0 eq), K_2CO_3 (30 mg, 220 µmol, 1.5 eq) and Pd(dppf)Cl_2·CH_2Cl_2 (12 mg, 15 µmol, 0.1 eq). A solution of 1,4-dioxane/water (10:1, 2 mL) was added *via* syringe and the reaction mixture was heated at 80 °C for 20 h. After cooling to RT the reaction mixture was filtered through Celite® (eluent CH_2Cl_2) and concentrated *in vacuo*. The residue was redissolved in CH_2Cl_2 (20 mL), washed with water (20 mL), then brine (20 mL), dried over sodium sulfate, filtered, and concentrated *in vacuo*. The crude material was purified by silica gel column chromatography, (methanol/CH_2Cl_2, 0:100, 5:95, 10:90, 15:85) to afford *tert-butyl-(3-(2-hydroxyethyl)-6-(4-(4-methylpiperazin-1-yl)-3-nitrophenyl)[1,2,4]triazolo[4,3-b]pyridazin-8-yl)carbamate* **148** (7 mg, 10%) as a colourless solid: R_f 0.06 (methanol/ethyl acetate/triethylamine, 10:89:1); mp 171-174 °C (from ethyl acetate); ν_{max} (thin film)/cm^{-1} 3349 (w), 2923 (w), 2583 (w), 1737 (m), 1613 (m), 1570 (s), 1466 (m), 1394 (m), 1369 (m),

1203 (s); ^{1}H NMR (400 MHz; $CDCl_3$) δ 8.42 (1H, d, *J* 2.2, C(2')*H*), 8.15 (1H, br s, N*H*), 8.11 (1H, s, C(7)*H*), 8.08 (1H, dd, *J* 8.8, 2.2, C(6')*H*), 7.21 (1H, d, *J* 8.8, C(5')*H*), 4.24 (2H, t, *J* 5.7, C(3)CH_2), 3.47 (2H, t, *J* 5.7, C(3)CH_2CH_2), 3.26 (4H, br s, ArNCH_2), 2.70 (4H, br s, ArNCH_2CH_2), 2.44 (3H, s, NCH_3), 1.58 (9H, s, C(CH_3)$_3$), 1.20 (1H, br s, C(3)CH_2CH_2O*H*); ^{13}C NMR (126 MHz; $CDCl_3$) δ 153.7 (*C*(6)), 151.6 (*C*=O), 150.2 (*C*(3)), 147.1 (*C*(3')), 142.3 (*C*(4')), 139.2 (*C*(9)), 134.7 (*C*(8)), 132.1 (*C*(6')H), 128.9 (*C*(1')), 125.4 (C(2')H), 120.9 (*C*(5')H), 99.8 (*C*(7)H), 83.5 (*C*$(CH_3)_3$), 59.5 (C(3)*C*H_2), 54.6 (ArNCH_2*C*H_2), 50.8 (ArN*C*H_2), 45.8 (N*C*H_3), 28.2 (C(*C*H_3)$_3$), 27.9 (C(3)CH_2*C*H_2); *m/z* (ES^+) 499 [$(M+H)^+$, 100%]; HRMS *m/z* (ES^+) [Found $(M+H)^+$ 499.2411. $C_{23}H_{31}N_8O_5^+$ requires M^+, 499.2412]; HPLC (method 2) pH 10 retention time 1.49 min, purity 100%, pH 3 retention time 1.48 min, purity 100%.

References

(1) International Human Genome Sequencing Consortium. (2004) Finishing the euchromatic sequence of the human genome. *Nature 431*, 931–945.
(2) Jensen, O. N. (2004) Modification-specific proteomics: characterization of post-translational modifications by mass spectrometry. *Current Opinion in Chemical Biology 8*, 33–41.
(3) Lynch, M., and Conery, J. S. (2003) The origins of genome complexity. *Science 302*, 1401–1404.
(4) Wang, E. T., Sandberg, R., Luo, S., Khrebtukova, I., Zhang, L., Mayr, C., Kingsmore, S. F., Schroth, G. P., and Burge, C. B. (2008) Alternative isoform regulation in human tissue transcriptomes. *Nature 456*, 470–476.
(5) Wang, Y.-C., Peterson, S. E., and Loring, J. F. (2014) Protein post-translational modifications and regulation of pluripotency in human stem cells. *Cell Research 24*, 143–160.
(6) Seo, J., and Lee, K.-J. (2004) Post-translational modifications and their biological functions: proteomic analysis and systematic approaches. *J. Biochem. Mol. Biol. 37*, 35–44.
(7) Mann, M., and Jensen, O. N. (2003) Proteomic analysis of post-translational modifications. *Nature Biotechnology 21*, 255–261.
(8) Cohen, P. (2000) The regulation of protein function by multisite phosphorylation – a 25 year update. *Trends in Biochemical Sciences 25*, 596–601.
(9) Zhang, J., Yang, P. L., and Gray, N. S. (2009) Targeting cancer with small molecule kinase inhibitors. *Nat. Rev. Cancer 9*, 28–39.
(10) Turner, B. M. (1993) Decoding the nucleosome. *Cell 75*, 5–8.
(11) Bowman, G. D., and Poirier, M. G. (2015) Post-translational modifications of histones that influence nucleosome dynamics. *Chem. Rev. 115*, 2274–2295.
(12) Allfrey, V. G., Faulkner, R., and Mirsky, A. E. (1964) Acetylation and methylation of histones and their possible role in the regulation of RNA synthesis. *Proc. Natl. Acad. Sci. U.S.A. 51*, 786–794.
(13) Gershey, E. L., Vidali, G., and Allfrey, V. G. (1968) Chemical studies of histone acetylation. The occurrence of epsilon-N-acetyllysine in the f2a1 histone. *J. Biol. Chem. 243*, 5018–5022.
(14) Racey, L. A., and Byvoet, P. (1970) Histone acetyltransferase in chromatin: Evidence for in vitro enzymatic transfer of acetate from acetyl-coenzyme A to histones. *Experimental Cell Research* 366–370.
(15) Inoue, A., and Fujimoto, D. (1969) Enzymatic deacetylation of histone. *Biochemical and Biophysical Research Communications 36*, 146–150.
(16) Vidali, G., Boffa, L. C., and Allfrey, V. G. (1972) Properties of an Acidic Histone-binding Protein Fraction from Cell Nuclei *247*, 7365–7373.
(17) Taunton, J., Hassig, C. A., and Schreiber, S. L. (1996) A Mammalian Histone Deacetylase Related to the Yeast Transcriptional Regulator Rpd3p. *Science 272*, 408–411.
(18) Strahl, B. D., and Allis, C. D. (2000) The language of covalent histone modifications. *Nature 403*, 41–45.
(19) Mizzen, C., Kuo, M. H., Smith, E., Brownell, J., Zhou, J., Ohba, R., Wei, Y., Monaco, L., Sassone-Corsi, P., and Allis, C. D. (1998) Signaling to

chromatin through histone modifications: how clear is the signal? *Cold Spring Harb. Symp. Quant. Biol. 63*, 469–481.
(20) NIGMS. (2010) The New Genetics. *National Institute of General Medical Sciences* 1–98.
(21) Wang, Z., Zang, C., Cui, K., Schones, D. E., Barski, A., Peng, W., and Zhao, K. (2009) Genome-wide Mapping of HATs and HDACs Reveals Distinct Functions in Active and Inactive Genes. *Cell 138*, 1019–1031.
(22) Jaenisch, R., and Bird, A. (2003) Epigenetic regulation of gene expression: how the genome integrates intrinsic and environmental signals. *Nat Genet 33*, 245–254.
(23) Egger, G., Liang, G., Aparicio, A., and Jones, P. A. (2004) Epigenetics in human disease and prospects for epigenetic therapy. *Nature 429*, 457–463.
(24) Yang, X.-J., and Seto, E. (2008) Lysine Acetylation: Codified Crosstalk with Other Posttranslational Modifications. *Mol Cell 31*, 449–461.
(25) Choudhary, C., Kumar, C., Gnad, F., Nielsen, M. L., Rehman, M., Walther, T. C., Olsen, J. V., and Mann, M. (2009) Lysine Acetylation Targets Protein Complexes and Co-Regulates Major Cellular Functions. *Science 325*, 834–840.
(26) Kouzarides, T. (2000) Acetylation: a regulatory modification to rival phosphorylation? *EMBO J. 19*, 1176–1179.
(27) Lee, B. M., and Mahadevan, L. C. (2009) Stability of histone modifications across mammalian genomes: implications for “epigenetic” marking. *J. Cell. Biochem. 108*, 22–34.
(28) Martin, C., and Zhang, Y. (2005) The diverse functions of histone lysine methylation. *Nat. Rev. Mol. Cell Biol. 6*, 838–849.
(29) Kim, S. C., Sprung, R., Chen, Y., Xu, Y., Ball, H., Pei, J., Cheng, T., Kho, Y., Xiao, H., Xiao, L., Grishin, N. V., White, M., Yang, X.-J., and Zhao, Y. (2006) Substrate and functional diversity of lysine acetylation revealed by a proteomics survey. *Mol Cell 23*, 607–618.
(30) Zhao, S., Xu, W., Jiang, W., Yu, W., Lin, Y., Zhang, T., Yao, J., Zhou, L., Zeng, Y., Li, H., Li, Y., Shi, J., An, W., Hancock, S. M., He, F., Qin, L., Chin, J., Yang, P., Chen, X., Lei, Q., Xiong, Y., and Guan, K.-L. (2010) Regulation of Cellular Metabolism by Protein Lysine Acetylation. *Science 327*, 1000–1004.
(31) Mujtaba, S., He, Y., Zeng, L., Farooq, A., Carlson, J. E., Ott, M., Verdin, E., and Zhou, M.-M. (2002) Structural Basis of Lysine-Acetylated HIV-1 Tat Recognition by PCAF Bromodomain. *Mol Cell 9*, 575–586.
(32) L'Hernault, S. W., and Rosenbaum, J. L. (1985) Chlamydomonas .alpha.-tubulin is posttranslationally modified by acetylation on the .epsilon.-amino group of a lysine. *Biochemistry 24*, 473–478.
(33) Gu, W., and Roeder, R. G. Activation of p53 Sequence-Specific DNA Binding by Acetylation of the p53 C-Terminal Domain. *Cell 90*, 595–606.
(34) Ott, M., Schnölzer, M., Garnica, J., Fischle, W., Emiliani, S., Rackwitz, H.-R., and Verdin, E. Acetylation of the HIV-1 Tat protein by p300 is important for its transcriptional activity. *Current Biology 9*, 1489–1493.
(35) Choudhary, C., Weinert, B. T., Nishida, Y., Verdin, E., and Mann, M. (2014) The growing landscape of lysine acetylation links metabolism and cell signalling. *Nature Publishing Group 15*, 536–550.
(36) Ivanov, G. S., Ivanova, T., Kurash, J., Ivanov, A., Chuikov, S., Gizatullin, F., Herrera-Medina, E. M., Rauscher, F., Reinberg, D., and Barlev, N. A.

Methylation-Acetylation Interplay Activates p53 in Response to DNA Damage. *Molecular and Cellular Biology 27*, 6756–6769.
(37) Macek, B., Gnad, F., Soufi, B., Kumar, C., Olsen, J. V., Mijakovic, I., and Mann, M. (2008) Phosphoproteome Analysis of E. coli Reveals Evolutionary Conservation of Bacterial Ser/Thr/Tyr Phosphorylation. *Molecular & Cellular Proteomics 7*, 299–307.
(38) Weinert, B. T., Wagner, S. A., Horn, H., Henriksen, P., Liu, W. R., Olsen, J. V., Jensen, L. J., and Choudhary, C. (2011) Proteome-Wide Mapping of the Drosophila Acetylome Demonstrates a High Degree of Conservation of Lysine Acetylation. *Science Signaling 4*, 48–48.
(39) Gnad, F., Forner, F., Zielinska, D. F., Birney, E., Gunawardena, J., and Mann, M. Evolutionary Constraints of Phosphorylation in Eukaryotes, Prokaryotes, and Mitochondria. *Mol. Cell Proteomics 9*, 2642–2653.
(40) Olsen, J. V., Blagoev, B., Gnad, F., Macek, B., and Kumar, C. (2006) Global, in vivo, and site-specific phosphorylation dynamics in signaling networks. *Cell* 635–648.
(41) Smith, K. T., and Workman, J. L. (2009) Introducing the acetylome. *Nature Biotechnology 27*, 917–919.
(42) Tamkun, J. W., Deuring, R., Scott, M. P., Kissinger, M., Pattatucci, A. M., Kaufman, T. C., and Kennison, J. A. (1992) brahma: A regulator of Drosophila homeotic genes structurally related to the yeast transcriptional activator SNF2SWI2. *Cell 68*, 561–572.
(43) Jeanmougin, F., Wurtz, J.-M., Le Douarin, B., Chambon, P., and Losson, R. The bromodomain revisited. *Trends in Biochemical Sciences 22*, 151–153.
(44) Kanno, T., Kanno, Y., Siegel, R. M., Jang, M. K., Lenardo, M. J., and Ozato, K. Selective Recognition of Acetylated Histones by Bromodomain Proteins Visualized in Living Cells. *Mol Cell 13*, 33–43.
(45) Crowley, T. E., Kaine, E. M., Yoshida, M., Nandi, A., and Wolgemuth, D. J. (2002) Reproductive cycle regulation of nuclear import, euchromatic localization, and association with components of Pol II mediator of a mammalian double-bromodomain protein. *Mol Endocrinol 16*, 1727–1737.
(46) Denis, G. V., McComb, M. E., Faller, D. V., Sinha, A., Romesser, P. B., and Costello, C. E. (2006) Identification of transcription complexes that contain the double bromodomain protein Brd2 and chromatin remodeling machines. *J. Proteome Res. 5*, 502–511.
(47) Sinha, A., Faller, D. V., and Denis, G. V. (2005) Bromodomain analysis of Brd2-dependent transcriptional activation of cyclin A. *Biochem J 387*, 257–269.
(48) LeRoy, G., Rickards, B., and Flint, S. J. (2008) The double bromodomain proteins Brd2 and Brd3 couple histone acetylation to transcription. *Mol Cell 30*, 51–60.
(49) Jennings, L. E., Measures, A. R., Wilson, B. G., and Conway, S. J. (2014) Phenotypic screening and fragment-based approaches to the discovery of small-molecule bromodomain ligands. *Future Medicinal Chemistry 6*, 179–204.
(50) Mujtaba, S., Zeng, L., and Zhou, M. M. Structure and acetyl-lysine recognition of the bromodomain. *Oncogene 26*, 5521–5527.
(51) Filippakopoulos, P. P., Picaud, S. S., Mangos, M. M., Keates, T. T., Lambert, J.-P. J., Barsyte-Lovejoy, D. D., Felletar, I. I., Volkmer, R. R., Müller, S. S., Pawson, T. T., Gingras, A.-C. A., Arrowsmith, C. H. C., and Knapp, S.

S. (2012) Histone recognition and large-scale structural analysis of the human bromodomain family. *Cell 149*, 214–231.
(52) Hewings, D. S., Rooney, T. P. C., Jennings, L. E., Hay, D. A., Michaels, D., Brennan, P. E., Knapp, S., and Conway, S. J. (2012) Progress in the Development and Application of Small Molecule Inhibitors of Bromodomain–Acetyl-lysine Interactions. *J. Med. Chem. 55*, 9393–9413.
(53) Zuber, J., Shi, J., Wang, E., Rappaport, A. R., Herrmann, H., Sison, E. A., Magoon, D., Qi, J., Blatt, K., Wunderlich, M., Taylor, M. J., Johns, C., Chicas, A., Mulloy, J. C., Kogan, S. C., Brown, P., Valent, P., Bradner, J. E., Lowe, S. W., and Vakoc, C. R. (2011) RNAi screen identifies Brd4 as a therapeutic target in acute myeloid leukaemia. *Nature 478*, 524–528.
(54) Jang, M. K., Mochizuki, K., Zhou, M., Jeong, H.-S., Brady, J. N., and Ozato, K. The Bromodomain Protein Brd4 Is a Positive Regulatory Component of P-TEFb and Stimulates RNA Polymerase II-Dependent Transcription. *Mol Cell 19*, 523–534.
(55) (2013) The bromodomain protein Brd4 insulates chromatin from DNA damage signalling 1–7.
(56) Zhang, G., Liu, R., Zhong, Y., Plotnikov, A. N., Zhang, W., Zeng, L., Rusinova, E., Gerona-Nevarro, G., Moshkina, N., Joshua, J., Chuang, P. Y., Ohlmeyer, M., He, J. C., and Zhou, M. M. (2012) Down-regulation of NF- B Transcriptional Activity in HIV-associated Kidney Disease by BRD4 Inhibition. *Journal of Biological Chemistry 287*, 28840–28851.
(57) Chiang, C.-M. (2009) Brd4 engagement from chromatin targeting to transcriptional regulation: selective contact with acetylated histone H3 and H4. *F1000 Biology Reports 1*, 98.
(58) Lee, A.-Y., and Chiang, C.-M. (2009) Chromatin Adaptor Brd4 Modulates E2 Transcription Activity and Protein Stability. *Journal of Biological Chemistry 284*, 2778–2786.
(59) Zippo, A., Serafini, R., Rocchigiani, M., Pennacchini, S., Krepelova, A., and Oliviero, S. (2009) Histone crosstalk between H3S10ph and H4K16ac generates a histone code that mediates transcription elongation. *Cell 138*, 1122–1136.
(60) Prinjha, R. K., Witherington, J., and Lee, K. (2012) Place your BETs: the therapeutic potential of bromodomains. *Trends in Pharmacological Sciences 33*, 146–153.
(61) French, C. A., Miyoshi, I., Kubonishi, I., Grier, H. E., Perez-Atayde, A. R., and Fletcher, J. A. (2003) BRD4-NUT Fusion Oncogene: A Novel Mechanism in Aggressive Carcinoma. *Cancer Res 63*, 304–307.
(62) Houzelstein, D., Bullock, S. L., Lynch, D. E., Grigorieva, E. F., Wilson, V. A., and Beddington, R. S. P. (2002) Growth and Early Postimplantation Defects in Mice Deficient for the Bromodomain-Containing Protein Brd4†. *Molecular and Cellular Biology 22*, 3794–3802.
(63) Wu, S.-Y., Lee, A.-Y., Hou, S. Y., Kemper, J. K., Erdjument-Bromage, H., Tempst, P., and Chiang, C.-M. (2006) Brd4 links chromatin targeting to HPV transcriptional silencing. *Genes & Development 20*, 2383–2396.
(64) Stockwell, B. R. (2004) Exploring biology with small organic molecules. *Nature 432*, 846–854.
(65) Wu, S.-Y., and Chiang, C.-M. (2007) The Double Bromodomain-containing Chromatin Adaptor Brd4 and Transcriptional Regulation. *Journal of Biological Chemistry 282*, 13141–13145.

(66) Filippakopoulos, P., and Knapp, S. (2014) Targeting bromodomains: epigenetic readers of lysine acetylation. *Nat Rev Drug Discov 13*, 337–356.
(67) Gaucher, J., Boussouar, F., Montellier, E., Curtet, S., Buchou, T., Bertrand, S., Hery, P., Jounier, S., Depaux, A., Vitte, A.-L., Guardiola, P., Pernet, K., Debernardi, A., Lopez, F., Holota, H., Imbert, J., Wolgemuth, D. J., Gérard, M., Rousseaux, S., and Khochbin, S. (2012) Bromodomain-dependent stage-specific male genome programming by Brdt. *EMBO J. 31*, 3809–3820.
(68) Filippakopoulos, P., Qi, J., Picaud, S., Shen, Y., Smith, W. B., Fedorov, O., Morse, E. M., Keates, T., Hickman, T. T., Felletar, I., Philpott, M., Munro, S., McKeown, M. R., Wang, Y., Christie, A. L., West, N., Cameron, M. J., Schwartz, B., Heightman, T. D., La Thangue, N., French, C. A., Wiest, O., Kung, A. L., Knapp, S., and Bradner, J. E. (2010) Selective inhibition of BET bromodomains. *Nature 468*, 1067–1073.
(69) Nicodeme, E., Jeffrey, K. L., Schaefer, U., Beinke, S., Dewell, S., Chung, C.-W., Chandwani, R., Marazzi, I., Wilson, P., Coste, H., White, J., Kirilovsky, J., Rice, C. M., Lora, J. M., Prinjha, R. K., Lee, K., and Tarakhovsky, A. (2011) Suppression of inflammation by a synthetic histone mimic. *Nature 468*, 1119–1123.
(70) Dawson, M. A., Prinjha, R. K., Dittmann, A., Giotopoulos, G., Bantscheff, M., Chan, W.-I., Robson, S. C., Chung, C.-W., Hopf, C., Savitski, M. M., Huthmacher, C., Gudgin, E., Lugo, D., Beinke, S., Chapman, T. D., Roberts, E. J., Soden, P. E., Auger, K. R., Mirguet, O., Doehner, K., Delwel, R., Burnett, A. K., Jeffrey, P., Drewes, G., Lee, K., Huntly, B. J. P., and Kouzarides, T. (2011) Inhibition of BET recruitment to chromatin as an effective treatment for MLL-fusion leukaemia. *Nature 478*, 529–533.
(71) Chung, C.-W., Coste, H., White, J. H., Mirguet, O., Wilde, J., Gosmini, R. L., Delves, C., Magny, S. M., Woodward, R., Hughes, S. A., Boursier, E. V., Flynn, H., Bouillot, A. M., Bamborough, P., Brusq, J.-M. G., Gellibert, F. J., Jones, E. J., Riou, A. M., Homes, P., Martin, S. L., Uings, I. J., Toum, J., Clément, C. A., Boullay, A.-B., Grimley, R. L., Blandel, F. M., Prinjha, R. K., Lee, K., Kirilovsky, J., and Nicodeme, E. (2011) Discovery and Characterization of Small Molecule Inhibitors of the BET Family Bromodomains. *J. Med. Chem. 54*, 3827–3838.
(72) Zhao, Y., Yang, C.-Y., and Wang, S. (2013) The making of I-BET762, a BET bromodomain inhibitor now in clinical development. *J. Med. Chem. 56*, 7498–7500.
(73) Clinical trial identifer: NCT01587703. https://clinicaltrials.gov/ct2/show/NCT01587703?term=gsk525762A&rank=1.
(74) Filippakopoulos, P., Qi, J., Picaud, S., Shen, Y., Smith, W. B., Fedorov, O., Morse, E. M., Keates, T., Hickman, T. T., Felletar, I., Philpott, M., Munro, S., McKeown, M. R., Wang, Y., Christie, A. L., West, N., Cameron, M. J., Schwartz, B., Heightman, T. D., La Thangue, N., French, C. A., Wiest, O., Kung, A. L., Knapp, S., and Bradner, J. E. (2011) Selective inhibition of BET bromodomains. *Nature 468*, 1067–1073.
(75) Bamborough, P., Diallo, H., Goodacre, J. D., Gordon, L., Lewis, A., Seal, J. T., Wilson, D. M., Woodrow, M. D., and Chung, C.-W. (2012) Fragment-Based Discovery of Bromodomain Inhibitors Part 2: Optimization of Phenylisoxazole Sulfonamides. *J. Med. Chem. 55*, 587–596.
(76) Hewings, D. S., Fedorov, O., Filippakopoulos, P., Martin, S., Picaud, S.,

Tumber, A., Wells, C., Olcina, M. M., Freeman, K., Gill, A., Ritchie, A. J., Sheppard, D. W., Russell, A. J., Hammond, E. M., Knapp, S., Brennan, P. E., and Conway, S. J. (2013) Optimization of 3,5-dimethylisoxazole derivatives as potent BET bromodomain ligands. *J. Med. Chem. 56*, 3217–3227.
(77) Bailey, D., Jahagirdar, R., Gordon, A., Hafiane, A., Campbell, S., Chatur, S., Wagner, G. S., Hansen, H. C., Chiacchia, F. S., Johansson, J., Krimbou, L., Wong, N. C. W., and Genest, J. RVX-208: A Small Molecule That Increases Apolipoprotein A-I and High-Density Lipoprotein Cholesterol In Vitro and In Vivo. *Journal of the American College of Cardiology 55*, 2580–2589.
(78) Oncoethix | Site. *OncoEthix*. http://www.oncoethix.com
(79) OncoEthix. http://www.oncoethix.com/wp-content/uploads/2015/06/Merck-News-Release_OncoEthix-Aquisition.pdf.
(80) Nicholls, S. J., Gordon, A., Johansson, J., Wolski, K., Ballantyne, C. M., Kastelein, J. J. P., Taylor, A., Borgman, M., and Nissen, S. E. (2011) Efficacy and Safety of a Novel Oral Inducer of Apolipoprotein A-I Synthesis in Statin-Treated Patients With Stable Coronary Artery Disease: A Randomized Controlled Trial. *Journal of the American College of Cardiology 57*, 1111–1119.
(81) Picaud, S., Wells, C., Felletar, I., Brotherton, D., Martin, S., Savitsky, P., Diez-Dacal, B., Philpott, M., Bountra, C., Lingard, H., Fedorov, O., Müller, S., Brennan, P. E., Knapp, S., and Filippakopoulos, P. (2013) RVX-208, an inhibitor of BET transcriptional regulators with selectivity for the second bromodomain. *Proc. Natl. Acad. Sci. U.S.A. 110*, 19754–19759.
(82) McLure, K. G., Gesner, E. M., Tsujikawa, L., Kharenko, O. A., Attwell, S., Campeau, E., Wasiak, S., Stein, A., White, A., Fontano, E., Suto, R. K., Wong, N. C. W., Wagner, G. S., Hansen, H. C., and Young, P. R. (2013) RVX-208, an inducer of ApoA-I in humans, is a BET bromodomain antagonist. *PLoS ONE 8*, 1–12 (e83190).
(83) Noel, J. K., Iwata, K., Ooike, S., Sugahara, K., Nakamura, H., and Daibata, M. (2014) Abstract C244: Development of the BET bromodomain inhibitor OTX015. *Molecular Cancer Therapeutics 12*, C244–C244.
(84) Boi, M., Gaudio, E., Bonetti, P., Kwee, I., Bernasconi, E., Tarantelli, C., Rinaldi, A., Testoni, M., Cascione, L., Ponzoni, M., Mensah, A. A., Stathis, A., Stussi, G., Riveiro, M. E., Herait, P., Inghirami, G., Cvitkovic, E., Zucca, E., and Bertoni, F. (2015) The BET Bromodomain Inhibitor OTX015 Affects Pathogenetic Pathways in Preclinical B-cell Tumor Models and Synergizes with Targeted Drugs. *Clinical Cancer Research 21*, 1628–1638.
(85) Clinical trial identifier: NCT01058018.
https://clinicaltrials.gov/ct2/show/NCT01058018?term=RVX208&rank=3.
(86) Clinical trial identifier: NCT01728467.
https://clinicaltrials.gov/ct2/show/NCT01728467?term=rvx208&rank=2.
(87) Clinical trial identifier: NCT02296476.
https://clinicaltrials.gov/ct2/show/NCT02296476?term=OTX015&rank=1.
(88) Clinical trial identifier: NCT02259114.
https://clinicaltrials.gov/ct2/show/NCT02259114?term=OTX015&rank=3.
(89) Clinical trial identifier: NCT01713582.
https://clinicaltrials.gov/ct2/show/NCT01713582?term=OTX015&rank=2.
(90) Clinical trial identifier: NCT01949883.
https://clinicaltrials.gov/ct2/show/NCT01949883?term=bet+inhibitor&rank=1.
(91) Clinical trial identifier: NCT02158858.

https://clinicaltrials.gov/ct2/show/NCT02158858?term=CPI-0610&rank=3.
(92) Clinical trial identifier: NCT02157636.
https://clinicaltrials.gov/ct2/show/NCT02157636?term=CPI-0610&rank=2.
(93) Clinical trial identifier: NCT02308761.
https://clinicaltrials.gov/ct2/show/NCT02308761?term=TEN-010&rank=1.
(94) Clinical trial identifier: NCT01987362.
https://clinicaltrials.gov/ct2/show/NCT01987362?term=TEN-010&rank=2.
(95) Constellation Pharmaceuticals.
http://www.constellationpharma.com/2013/09/constellation-pharmaceuticals-initiates-clinical-development-of-cpi-0610-a-novel-bet-protein-bromodomain-inhibitor-in-patients-with-lymphoma/.
(96) Constellation Pharmaceuticals.
http://www.constellationpharma.com/2014/08/constellation-expands-clinical-studies-of-cpi-0610/.
(97) Tensha Pharmaceuticals. http://www.tenshatherapeutics.com/program-clinical.php.
(98) Mirguet, O., Lamotte, Y., Donche, F., Toum, J., Gellibert, F., Bouillot, A., Gosmini, R., Nguyen, V.-L., Delannée, D., Seal, J., Blandel, F., Boullay, A.-B., Boursier, E., Martin, S., Brusq, J.-M., Krysa, G., Riou, A., Tellier, R., Costaz, A., Huet, P., Dudit, Y., Trottet, L., Kirilovsky, J., and Nicodeme, E. (2012) From ApoA1 upregulation to BET family bromodomain inhibition: discovery of I-BET151. *Bioorganic & Medicinal Chemistry Letters 22*, 2963–2967.
(99) Brand, M., Measures, A. M., Wilson, B. G., Cortopassi, W. A., Alexander, R., Höss, M., Hewings, D. S., Rooney, T. P. C., Paton, R. S., and Conway, S. J. (2015) Small Molecule Inhibitors of Bromodomain–Acetyl-lysine Interactions. *ACS Chem. Biol. 10*, 22–39.
(100) Filippakopoulos, P., and Knapp, S. (2014) Targeting bromodomains: epigenetic readers of lysine acetylation. *Nat Rev Drug Discov* 1–20.
(101) Garnier, J.-M., Sharp, P. P., and Burns, C. J. (2013) BET bromodomain inhibitors: a patent review. *Expert Opin. Ther. Patents* 1–15.
(102) Bowser, R., Giambrone, A., and Davies, P. (1995) FAC1, a novel gene identified with the monoclonal antibody Alz50, is developmentally regulated in human brain. *Developmental Neuroscience 17*, 20–37.
(103) Burrows, A. E., Smogorzewska, A., and Elledge, S. J. (2010) Polybromo-associated BRG1-associated factor components BRD7 and BAF180 are critical regulators of p53 required for induction of replicative senescence. *Proc. Natl. Acad. Sci. U.S.A. 107*, 14280–14285.
(104) Pons, D., Trompet, S., de Craen, A. J. M., Thijssen, P. E., Quax, P. H. A., de Vries, M. R., Wierda, R. J., van den Elsen, P. J., Monraats, P. S., Ewing, M. M., Heijmans, B. T., Slagboom, P. E., Zwinderman, A. H., Doevendans, P. A. F. M., Tio, R. A., de Winter, R. J., de Maat, M. P. M., Iakoubova, O. A., Sattar, N., Shepherd, J., Westendorp, R. G. J., Jukema, J. W., PROSPER study group, WOSCOPS study group, GENDER study group. (2011) Genetic variation in PCAF, a key mediator in epigenetics, is associated with reduced vascular morbidity and mortality: evidence for a new concept from three independent prospective studies. *Heart 97*, 143–150.
(105) Arking, D. E., Junttila, M. J., Goyette, P., Huertas-Vazquez, A., Eijgelsheim, M., Blom, M. T., Newton-Cheh, C., Reinier, K., Teodorescu, C., Uy-Evanado, A., Carter-Monroe, N., Kaikkonen, K. S., Kortelainen, M.-L., Boucher, G., Lagacé, C., Moes, A., Zhao, X., Kolodgie, F., Rivadeneira, F.,

Hofman, A., Witteman, J. C. M., Uitterlinden, A. G., Marsman, R. F., Pazoki, R., Bardai, A., Koster, R. W., Dehghan, A., Hwang, S.-J., Bhatnagar, P., Post, W., Hilton, G., Prineas, R. J., Li, M., Köttgen, A., Ehret, G., Boerwinkle, E., Coresh, J., Kao, W. H. L., Psaty, B. M., Tomaselli, G. F., Sotoodehnia, N., Siscovick, D. S., Burke, G. L., Marbán, E., Spooner, P. M., Cupples, L. A., Jui, J., Gunson, K., Kesäniemi, Y. A., Wilde, A. A. M., Tardif, J.-C., O'Donnell, C. J., Bezzina, C. R., Virmani, R., Stricker, B. H. C. H., Tan, H. L., Albert, C. M., Chakravarti, A., Rioux, J. D., Huikuri, H. V., and Chugh, S. S. (2011) Identification of a sudden cardiac death susceptibility locus at 2q24.2 through genome-wide association in European ancestry individuals. *PLoS Genet. 7*, e1002158.
(106) Fusco, C., Micale, L., Augello, B., Teresa Pellico, M., Menghini, D., Alfieri, P., Cristina Digilio, M., Mandriani, B., Carella, M., Palumbo, O., Vicari, S., and Merla, G. (2014) Smaller and larger deletions of the Williams Beuren syndrome region implicate genes involved in mild facial phenotype, epilepsy and autistic traits. *Eur. J. Hum. Genet. 22*, 64–70.
(107) Knijnenburg, J., van Bever, Y., Hulsman, L. O. M., van Kempen, C. A. P., Bolman, G. M., van Loon, R. L. E., Beverloo, H. B., and van Zutven, L. J. C. M. (2012) A 600 kb triplication in the cat eye syndrome critical region causes anorectal, renal and preauricular anomalies in a three-generation family. *Eur. J. Hum. Genet. 20*, 986–989.
(108) Fairbridge, N. A., Dawe, C. E., Niri, F. H., Kooistra, M. K., King-Jones, K., and McDermid, H. E. (2010) Cecr2 mutations causing exencephaly trigger misregulation of mesenchymal/ectodermal transcription factors. *Birth Defects Research Part A: Clinical and Molecular Teratology* (Greene, N. D. E., and Carmichael, S. L., Eds.) *88*, 619–625.
(109) Dawe, C. E., Kooistra, M. K., Fairbridge, N. A., Pisio, A. C., and McDermid, H. E. (2011) Role of chromatin remodeling gene Cecr2 in neurulation and inner ear development. *Dev. Dyn. 240*, 372–383.
(110) Marzuillo, P., Grandone, A., Coppola, R., Cozzolino, D., Festa, A., Messa, F., Luongo, C., Del Giudice, E. M., and Perrone, L. (2013) Novel cAMP binding protein-BP (CREBBP) mutation in a girl with Rubinstein-Taybi syndrome, GH deficiency, Arnold Chiari malformation and pituitary hypoplasia. *BMC Med. Genet. 14*, 28.
(111) Kosho, T., Okamoto, N., Ohashi, H., Tsurusaki, Y., Imai, Y., Hibi-Ko, Y., Kawame, H., Homma, T., Tanabe, S., Kato, M., Hiraki, Y., Yamagata, T., Yano, S., Sakazume, S., Ishii, T., Nagai, T., Ohta, T., Niikawa, N., Mizuno, S., Kaname, T., Naritomi, K., Narumi, Y., Wakui, K., Fukushima, Y., Miyatake, S., Mizuguchi, T., Saitsu, H., Miyake, N., and Matsumoto, N. (2013) Clinical correlations of mutations affecting six components of the SWI/SNF complex: detailed description of 21 patients and a review of the literature. *Am. J. Med. Genet. A 161A*, 1221–1237.
(112) Allouch, A., Di Primio, C., Alpi, E., Lusic, M., Arosio, D., Giacca, M., and Cereseto, A. (2011) The TRIM family protein KAP1 inhibits HIV-1 integration. *Cell Host Microbe 9*, 484–495.
(113) Chikuma, S., Suita, N., Okazaki, I.-M., Shibayama, S., and Honjo, T. (2012) TRIM28 prevents autoinflammatory T cell development in vivo. *Nature Immunology 13*, 596–603.
(114) Matsuura, E., Ishiguro, N., Katsumata, Y., Urano, W., Yamanaka, H., Kondo, M., Kuwana, M., Kaji, K., Hamaguchi, Y., Fujimoto, M., and

Kawashima, M. (2012) Two young-adult female cases of dermatomyositis with antibodies for transcriptional intermediary factor 1-γ. *Eur J Dermatol 22*, 668–671.
(115) Malvaez, M., Mhillaj, E., Matheos, D. P., Palmery, M., and Wood, M. A. (2011) CBP in the nucleus accumbens regulates cocaine-induced histone acetylation and is critical for cocaine-associated behaviors. *J. Neurosci. 31*, 16941–16948.
(116) Nyegaard, M., Severinsen, J. E., Als, T. D., Hedemand, A., Straarup, S., Nordentoft, M., McQuillin, A., Bass, N., Lawrence, J., Thirumalai, S., Pereira, A. C. P., Kandaswamy, R., Lydall, G. J., Sklar, P., Scolnick, E., Purcell, S., Curtis, D., Gurling, H. M. D., Mortensen, P. B., Mors, O., and Børglum, A. D. (2010) Support of association between BRD1 and both schizophrenia and bipolar affective disorder. *Am. J. Med. Genet. B Neuropsychiatr. Genet. 153B*, 582–591.
(117) Williams, H. J., Craddock, N., Russo, G., Hamshere, M. L., Moskvina, V., Dwyer, S., Smith, R. L., Green, E., Grozeva, D., Holmans, P., Owen, M. J., and O'Donovan, M. C. (2011) Most genome-wide significant susceptibility loci for schizophrenia and bipolar disorder reported to date cross-traditional diagnostic boundaries. *Human Molecular Genetics 20*, 387–391.
(118) Koga, M., Ishiguro, H., Yazaki, S., Horiuchi, Y., Arai, M., Niizato, K., Iritani, S., Itokawa, M., Inada, T., Iwata, N., Ozaki, N., Ujike, H., Kunugi, H., Sasaki, T., Takahashi, M., Watanabe, Y., Someya, T., Kakita, A., Takahashi, H., Nawa, H., Muchardt, C., Yaniv, M., and Arinami, T. (2009) Involvement of SMARCA2/BRM in the SWI/SNF chromatin-remodeling complex in schizophrenia. *Human Molecular Genetics 18*, 2483–2494.
(119) Dhalluin, C., Carlson, J. E., Zeng, L., He, C., Aggarwal, A. K., and Zhou, M. M. (1999) Structure and ligand of a histone acetyltransferase bromodomain. *Nature 399*, 491–496.
(120) Zeng, L., Li, J., Muller, M., Yan, S., Mujtaba, S., Pan, C., Wang, Z., and Zhou, M.-M. (2005) Selective Small Molecules Blocking HIV-1 Tat and Coactivator PCAF Association. *J. Am. Chem. Soc. 127*, 2376–2377.
(121) Mujtaba, S. S., He, Y. Y., Zeng, L. L., Yan, S. S., Plotnikova, O. O., Sachchidanand, Sanchez, R. R., Zeleznik-Le, N. J. N., Ronai, Z. Z., and Zhou, M.-M. M. (2004) Structural Mechanism of the Bromodomain of the Coactivator CBP in p53 Transcriptional Activation. *Mol Cell 13*, 251–263.
(122) Sachchidanand, Resnick-Silverman, L., Yan, S., Mutjaba, S., Liu, W.-J., Zeng, L., Manfredi, J. J., and Zhou, M.-M. (2006) Target Structure-Based Discovery of Small Molecules that Block Human p53 and CREB Binding Protein Association. *Chemistry & Biology 13*, 81–90.
(123) Gosmini, R., Nguyen, V.-L., Toum, J., Simon, C., Brusq, J.-M. G., Krysa, G., Mirguet, O., Riou-Eymard, A. M., Boursier, E. V., Trottet, L., Bamborough, P., Clark, H., Chung, C.-W., Cutler, L., Demont, E. H., Kaur, R., Lewis, A. J., Schilling, M. B., Soden, P. E., Taylor, S., Walker, A. L., Walker, M. D., Prinjha, R. K., and Nicodeme, E. (2014) The discovery of I-BET726 (GSK1324726A), a potent tetrahydroquinoline ApoA1 up-regulator and selective BET bromodomain inhibitor. *J. Med. Chem. 57*, 8111–8131.
(124) Borah, J. C., Mujtaba, S., Karakikes, I., Zeng, L., Muller, M., Patel, J., Moshkina, N., Morohashi, K., Zhang, W., Gerona-Navarro, G., Hajjar, R. J., and Zhou, M.-M. (2011) A Small Molecule Binding to the Coactivator CREB-Binding Protein Blocks Apoptosis in Cardiomyocytes. *Chemistry & Biology 18*,

531–541.
(125) Philpott, M. M., Yang, J. J., Tumber, T. T., Fedorov, O. O., Uttarkar, S. S., Filippakopoulos, P. P., Picaud, S. S., Keates, T. T., Felletar, I. I., Ciulli, A. A., Knapp, S. S., and Heightman, T. D. T. (2011) Bromodomain-peptide displacement assays for interactome mapping and inhibitor discovery. *Mol Biosyst 7*, 2899–2908.
(126) Hewings, D. S., Wang, M., Philpott, M., Fedorov, O., Uttarkar, S., Filippakopoulos, P., Picaud, S., Vuppusetty, C., Marsden, B., Knapp, S., Conway, S. J., and Heightman, T. D. (2011) 3,5-Dimethylisoxazoles Act As Acetyl-lysine-mimetic Bromodomain Ligands. *J. Med. Chem. 54*, 6761–6770.
(127) Rooney, T. P. C., Filippakopoulos, P., Fedorov, O., Picaud, S., Cortopassi, W. A., Hay, D. A., Martin, S., Tumber, A., Rogers, C. M., Philpott, M., Wang, M., Thompson, A. L., Heightman, T. D., Pryde, D. C., Cook, A., Paton, R. S., Müller, S., Knapp, S., Brennan, P. E., and Conway, S. J. (2014) A Series of Potent CREBBP Bromodomain Ligands Reveals an Induced-Fit Pocket Stabilized by a Cation-π Interaction. *Angew. Chem. Int. Ed. 53*, 6126–6130.
(128) Philpott, M., Rogers, C. M., Yapp, C., Wells, C., Lambert, J.-P., Strain-Damerell, C., Burgess-Brown, N. A., Gingras, A.-C., Knapp, S., and Müller, S. (2014) Assessing cellular efficacy of bromodomain inhibitors using fluorescence recovery after photobleaching. *Epigenetics & Chromatin 7*, 1–12.
(129) Hay, D., Fedorov, O., Filippakopoulos, P., Martin, S., Philpott, M., Picaud, S., Hewings, D. S., Uttakar, S., Heightman, T. D., Conway, S. J., Knapp, S., and Brennan, P. E. (2012) The design and synthesis of 5- and 6-isoxazolylbenzimidazoles as selective inhibitors of the BET bromodomains. *Med. Chem. Commun. 4*, 140–144.
(130) Hay, D. A., Fedorov, O., Martin, S., Singleton, D. C., Tallant, C., Wells, C., Picaud, S., Philpott, M., Monteiro, O. P., Rogers, C. M., Conway, S. J., Rooney, T. P. C., Tumber, A., Yapp, C., Filippakopoulos, P., Bunnage, M. E., Müller, S., Knapp, S., Michaels, D., and Brennan, P. E. (2014) Discovery and Optimization of Small-Molecule Ligands for the CBP/p300 Bromodomains. *J. Am. Chem. Soc. 136*, 9308–9319.
(131) Hammitzsch, A., Tallant, C., Fedorov, O., O'Mahony, A., Brennan, P. E., Hay, D. A., Martinez, F. O., Al-Mossawi, M. H., de Wit, J., Vecellio, M., Wells, C., Wordsworth, P., Müller, S., Knapp, S., and Bowness, P. (2015) CBP30, a selective CBP/p300 bromodomain inhibitor, suppresses human Th17 responses. *Proc. Natl. Acad. Sci. U.S.A. 112*, 10768–10773.
(132) Unzue, A., Xu, M., Dong, J., Wiedmer, L., Spiliotopoulos, D., Caflisch, A., and Nevado, C. (2015) Fragment-based Design of Selective Nanomolar Ligands of the CREBBP Bromodomain. *J. Med. Chem.*
(133) Xu, M., Unzue, A., Dong, J., Spiliotopoulos, D., Nevado, C., and Caflisch, A. (2015) Discovery of CREBBP Bromodomain Inhibitors by High-Throughput Docking and Hit Optimization Guided by Molecular Dynamics. *J Med Chem DOI: 10.1021-acs.jmedchem.5b00171*.
(134) Structural Genomics Consortium. http://www.thesgc.org/chemical-probes/I-CBP112/teaser.
(135) Vidler, L. R., Brown, N., Knapp, S., and Hoelder, S. (2012) Druggability Analysis and Structural Classification of Bromodomain Acetyl-lysine Binding Sites. *J. Med. Chem. 55*, 7346–7359.
(136) Ferguson, F. M., Fedorov, O., Chaikuad, A., Philpott, M., Muniz, J. R.

C., Felletar, I., Delft, von, F., Heightman, T., Knapp, S., Abell, C., and Ciulli, A. (2013) Targeting low-druggability bromodomains: fragment based screening and inhibitor design against the BAZ2B bromodomain. *J. Med. Chem. 56*, 10183–10187.
(137) Drouin, L., McGrath, S., Vidler, L. R., Chaikuad, A., Monteiro, O., Tallant, C., Philpott, M., Rogers, C., Fedorov, O., Liu, M., Akhtar, W., Hayes, A., Raynaud, F., Müller, S., Knapp, S., and Hoelder, S. (2015) Structure Enabled Design of BAZ2-ICR, A Chemical Probe Targeting the Bromodomains of BAZ2A and BAZ2B. *J. Med. Chem. 58*, 2553–2559.
(138) Vidler, L. R., Filippakopoulos, P., Fedorov, O., Picaud, S., Martin, S., Tomsett, M., Woodward, H., Brown, N., Knapp, S., and Hoelder, S. (2013) Discovery of Novel Small-Molecule Inhibitors of BRD4 Using Structure-Based Virtual Screening. *J. Med. Chem. 56*, 8073–8088.
(139) Chen, P., Chaikuad, A., Bamborough, P., Bantscheff, M., Bountra, C., Chung, C.-W., Fedorov, O., Grandi, P., Jung, D., Lesniak, R., Lindon, M., Müller, S., Philpott, M., Prinjha, R., Rogers, C., Selenski, C., Tallant, C., Werner, T., Willson, T. M., Knapp, S., and Drewry, D. H. (2015) Discovery and Characterization of GSK2801, a Selective Chemical Probe for the Bromodomains BAZ2A and BAZ2B. *J Med Chem DOI: 10.1021/acs.jmedchem.5b00209*.
(140) Demont, E. H., Bamborough, P., Chung, C.-W., Craggs, P. D., Fallon, D., Gordon, L. J., Grandi, P., Hobbs, C. I., Hussain, J., Jones, E. J., Le Gall, A., Michon, A.-M., Mitchell, D. J., Prinjha, R. K., Roberts, A. D., Sheppard, R. J., and Watson, R. J. (2014) 1,3-Dimethyl Benzimidazolones Are Potent, Selective Inhibitors of the BRPF1 Bromodomain. *ACS Med. Chem. Lett. 5*, 1190–1195.
(141) Tsai, W.-W., Wang, Z., Yiu, T. T., Akdemir, K. C., Xia, W., Winter, S., Tsai, C.-Y., Shi, X., Schwarzer, D., Plunkett, W., Aronow, B., Gozani, O., Fischle, W., Hung, M.-C., Patel, D. J., and Barton, M. C. (2010) TRIM24 links a non-canonical histone signature to breast cancer. *Nature 468*, 927–932.
(142) Palmer, W. S., Poncet-Montange, G., Liu, G., Petrocchi, A., Reyna, N., Subramanian, G., Theroff, J., Yau, A., Kost-Alimova, M., Bardenhagen, J. P., Leo, E., Shepard, H. E., Tieu, T. N., Shi, X., Zhan, Y., Zhao, S., Barton, M. C., Draetta, G., Toniatti, C., Jones, P., Geck Do, M., and Andersen, J. N. (2015) Structure-Guided Design of IACS-9571, a Selective High-Affinity Dual TRIM24-BRPF1 Bromodomain Inhibitor. *J. Med. Chem.*
(143) Bennett, J., Fedorov, O., Tallant, C., Monteiro, O., Meier, J., Gamble, V., Savitsky, P., Nunez-Alonso, G. A., Haendler, B., Rogers, C., Brennan, P. E., Müller, S., and Knapp, S. (2015) Discovery of a Chemical Tool Inhibitor Targeting the Bromodomains of TRIM24 and BRPF. *J Med Chem DOI: 10.1021/acs.jmedchem.5b0045810.1021-acs.jmedchem.5b00171*.
(144) Beaudet, L., Rodriguez-Suarez, R., Venne, M. H., and Caron, M. (2008) AlphaLISA immunoassays: the no-wash alternative to ELISAs for research and drug discovery. *Nature*.
(145) Structural Genomics Consortium. http://www.thesgc.org/chemical-probes/PFI-3/teaser.
(146) Vangamudi, B., Paul, T. A., Shah, P. K., Kost-Alimova, M., Nottebaum, L., Shi, X., Zhan, Y., Leo, E., Mahadeshwar, H. S., Protopopov, A., Futreal, A., Tieu, T. N., Peoples, M., Heffernan, T. P., Marszalek, J. R., Toniatti, C., Petrocchi, A., Verhelle, D., Owen, D. R., Draetta, G. F., Jones, P., Palmer, W.

S., Sharma, S., and Andersen, J. N. (2015) The SMARCA2/4 ATPase domain surpasses the bromodomain as a drug target in SWI/SNF mutant cancers: Insights from cDNA rescue and PFI-3 inhibitor studies. *Cancer Res*.
(147) Chaikuad, A., Petros, A. M., Fedorov, O., Xu, J., and Knapp, S. (2014) Structure-based approaches towards identification of fragments for the low-druggability ATAD2 bromodomain. *Med. Chem. Commun. 5*, 1843–1848.
(148) Harner, M. J., Chauder, B. A., Phan, J., and Fesik, S. W. (2014) Fragment-based screening of the bromodomain of ATAD2. *J. Med. Chem. 57*, 9687–9692.
(149) Demont, E. H., Chung, C.-W., Furze, R. C., Grandi, P., Michon, A.-M., Wellaway, C., Barrett, N., Bridges, A. M., Craggs, P. D., Diallo, H., Dixon, D. P., Douault, C., Emmons, A. J., Jones, E. J., Karamshi, B. V., Locke, K., Mitchell, D. J., Mouzon, B. H., Prinjha, R. K., Roberts, A. D., Sheppard, R. J., Watson, R. J., and Bamborough, P. (2015) Fragment-Based Discovery of Low-Micromolar ATAD2 Bromodomain Inhibitors. *J Med Chem DOI: 10.1021/acs.jmedchem.5b00772*.
(150) Scotto, L., Narayan, G., Nandula, S. V., Subramaniyam, S., Kaufmann, A. M., Wright, J. D., Pothuri, B., Mansukhani, M., Schneider, A., Arias-Pulido, H., and Murty, V. V. (2008) Integrative genomics analysis of chromosome 5p gain in cervical cancer reveals target over-expressed genes, including Drosha. *Mol. Cancer 7*, 58.
(151) Kang, J. U., Koo, S. H., Kwon, K. C., Park, J. W., and Kim, J. M. (2008) Gain at chromosomal region 5p15.33, containing TERT, is the most frequent genetic event in early stages of non-small cell lung cancer. *Cancer Genetics and Cytogenetics 182*, 1–11.
(152) Kadoch, C., Hargreaves, D. C., Hodges, C., Elias, L., Ho, L., Ranish, J., and Crabtree, G. R. (2013) Proteomic and bioinformatic analysis of mammalian SWI/SNF complexes identifies extensive roles in human malignancy. *Nature Publishing Group 45*, 592–601.
(153) Middeljans, E., Wan, X., Jansen, P. W., Sharma, V., Stunnenberg, H. G., and Logie, C. (2012) SS18 together with animal-specific factors defines human BAF-type SWI/SNF complexes. *PLoS ONE 7*, e33834.
(154) Bandyopadhyay, D., Okan, N. A., Bales, E., Nascimento, L., Cole, P. A., and Medrano, E. E. (2002) Down-Regulation of p300/CBP Histone Acetyltransferase Activates a Senescence Checkpoint in Human Melanocytes. *Cancer Res 62*, 6231–6239.
(155) Albrecht, B. K., Harmange, J. C., Cote, A., and Taylor, A. M. (2014) Bromodomain inhibitors and uses thereof. Google Patents.
(156) Fedorov, O., Lingard, H., Wells, C., Monteiro, O. P., Picaud, S., Keates, T., Yapp, C., Philpott, M., Martin, S. J., Felletar, I., Marsden, B. D., Filippakopoulos, P., Müller, S., Knapp, S., and Brennan, P. E. (2014) [1,2,4]Triazolo[4,3- a]phthalazines: Inhibitors of Diverse Bromodomains. *J. Med. Chem. 57*, 462–476.
(157) Structural Genomics Consortium. http://www.thesgc.org/chemical-probes/Bromosporine/teaser.
(158) Picaud, S., Strocchia, M., Terracciano, S., Lauro, G., Méndez, J., Daniels, D. L., Riccio, R., Bifulco, G., Bruno, I., and Filippakopoulos, P. (2015) 9H-purine scaffold reveals induced-fit pocket plasticity of the BRD9 bromodomain. *J. Med. Chem. 58*, 2718–2736.
(159) Duarte, C., Barreiro, E., and Fraga, C. (2007) Privileged Structures: A

Useful Concept for the Rational Design of New Lead Drug Candidates. *Mini-Reviews in Medicinal Chemistry 7*, 1108–1119.
(160) Rosemeyer, H. (2004) The chemodiversity of purine as a constituent of natural products. *Chemistry & Biodiversity* 361–401.
(161) Theodoulou, N. H., Bamborough, P., Bannister, A. J., Becher, I., Bit, R. A., Che, K. H., Chung, C.-W., Dittmann, A., Drewes, G., Drewry, D. H., Gordon, L., Grandi, P., Leveridge, M., Lindon, M., Michon, A.-M., Molnar, J., Robson, S. C., Tomkinson, N. C. O., Kouzarides, T., Prinjha, R. K., and Humphreys, P. G. (2015) Discovery of I-BRD9, a Selective Cell Active Chemical Probe for Bromodomain Containing Protein 9 Inhibition. *J Med Chem DOI: 10.1021-acs.jmedchem.5b0017110.1021/acs.jmedchem.5b00256*.
(162) Clark, P. G. K., Vieira, L. C. C., Tallant, C., Fedorov, O., Singleton, D. C., Rogers, C. M., Monteiro, O. P., Bennett, J. M., Baronio, R., Müller, S., Daniels, D. L., Méndez, J., Knapp, S., Brennan, P. E., and Dixon, D. J. (2015) LP99: Discovery and Synthesis of the First Selective BRD7/9 Bromodomain Inhibitor. *Angew. Chem. Int. Ed. Engl. 54*, 6217–6221.
(163) Hay, D. A., Rogers, C. M., Fedorov, O., Tallant, C., Martin, S., Monteiro, O. P., Müller, S., Knapp, S., Michaels, D., and Brennan, P. E. (2015) Design and synthesis of potent and selective inhibitors of BRD7 and BRD9 bromodomains. *Med. Chem. Commun. 6*, 1381–1386.
(164) Ritchie, T. J., and Macdonald, S. J. F. (2009) The impact of aromatic ring count on compound developability – are too many aromatic rings a liability in drug design? *Drug discovery today 14*, 1011–1020.
(165) Hill, A. P., and Young, R. J. (2010) Getting physical in drug discovery: a contemporary perspective on solubility and hydrophobicity. *Drug discovery today 15*, 648–655.
(166) (2002) be selective 1–12.
(167) Niesen, F. H., Berglund, H., and Vedadi, M. (2007) The use of differential scanning fluorimetry to detect ligand interactions that promote protein stability. *Nat Protoc 2*, 2212–2221.
(168) Barder, T. E., and Buchwald, S. L. (2004) Efficient Catalyst for the Suzuki−Miyaura Coupling of Potassium Aryl Trifluoroborates with Aryl Chlorides. *Org. Lett. 6*, 2649–2652.
(169) EMBOSS Matcher. http://www.ebi.ac.uk/Tools/psa/emboss_matcher/.
(170) Ishikawa, M., and Hashimoto, Y. (2011) Improvement in Aqueous Solubility in Small Molecule Drug Discovery Programs by Disruption of Molecular Planarity and Symmetry. *J. Med. Chem. 54*, 1539–1554.
(171) Dumas, J. M., Peurichard, H., and Gomel, M. (1978) CX4···base interactions as models of weak charge-transfer interactions: comparison with strong charge-transfer and hydrogen-bond interactions. *J. Chem. Res.* 54–55.
(172) Wilcken, R., Zimmermann, M. O., Lange, A., Joerger, A. C., and Boeckler, F. M. (2013) Principles and Applications of Halogen Bonding in Medicinal Chemistry and Chemical Biology. *J. Med. Chem. 56*, 1363–1388.
(173) Clark, T., Hennemann, M., Murray, J., and Politzer, P. (2007) Halogen bonding: the σ-hole. *J Mol Model 13*, 291–296.
(174) Filippakopoulos, P., Qi, J., Picaud, S., Shen, Y., Smith, W. B., Fedorov, O., Morse, E. M., Keates, T., Hickman, T. T., Felletar, I., Philpott, M., Munro, S., McKeown, M. R., Wang, Y., Christie, A. L., West, N., Cameron, M. J., Schwartz, B., Heightman, T. D., La Thangue, N., French, C. A., Wiest, O.,

Kung, A. L., Knapp, S., and Bradner, J. E. (2011) Selective inhibition of BET bromodomains. *Nature 468*, 1067–1073.
(175) Holdgate, G. A., and Ward, W. H. J. Measurements of binding thermodynamics in drug discovery. *Drug discovery today 10*, 1543–1550.
(176) Degorce, F., Card, A., Soh, S., Trinquet, E., Knapik, G. P., and Xie, B. (2009, October 28) HTRF: A Technology Tailored for Drug Discovery –A Review of Theoretical Aspects and Recent Applications. *Current Chemical Genomics*.
(177) Obach, R. S. (1999) Prediction of human clearance of twenty-nine drugs from hepatic microsomal intrinsic clearance data: An examination of in vitro half-life approach and nonspecific binding to microsomes. *Drug Metab. Dispos. 27*, 1350–1359.
(178) Kirchmair, J., Williamson, M. J., Afzal, A. M., Tyzack, J. D., Choy, A. P. K., Howlett, A., Rydberg, P., and Glen, R. C. (2013) FAst MEtabolizer (FAME): A Rapid and Accurate Predictor of Sites of Metabolism in Multiple Species by Endogenous Enzymes. *J. Chem. Inf. Model. 53*, 2896–2907.
(179) Leeson, P. D., and Springthorpe, B. (2007) The influence of drug-like concepts on decision-making in medicinal chemistry. *Nat Rev Drug Discov 6*, 881–890.
(180) Hopkins, A. L., Keserü, G. M., Leeson, P. D., Rees, D. C., and Reynolds, C. H. (2014) The role of ligand efficiency metrics in drug discovery. *Nat Rev Drug Discov 13*, 105–121.
(181) Ito, T., Umehara, T., Sasaki, K., Nakamura, Y., Nishino, N., Terada, T., Shirouzu, M., Padmanabhan, B., Yokoyama, S., Ito, A., and Yoshida, M. (2011) Real-time imaging of histone H4K12-specific acetylation determines the modes of action of histone deacetylase and bromodomain inhibitors. *Chemistry & Biology 18*, 495–507.
(182) Fish, P. V., Filippakopoulos, P., Bish, G., Brennan, P. E., Bunnage, M. E., Cook, A. S., Federov, O., Gerstenberger, B. S., Jones, H., Knapp, S., Marsden, B., Nocka, K., Owen, D. R., Philpott, M., Picaud, S., Primiano, M. J., Ralph, M. J., Sciammetta, N., and Trzupek, J. D. (2012) Identification of a Chemical Probe for Bromo and Extra C-Terminal Bromodomain Inhibition through Optimization of a Fragment-Derived Hit. *J. Med. Chem. 55*, 9831–9837.
(183) Schuck, P. (1997) Use of surface plasmon resonance to probe the equilibrium and dynamic aspects of interactions between biological macromolecules. *Annu. Rev. Biophys. Biomol. Struct. 26*, 541–566.
(184) Pattaik, P. (2005) Surface Plasmon Resonance. *Applied Biochemistry and Biotechnology 126*, 79–92.
(185) Seal, J., Lamotte, Y., Donche, F., Bouillot, A., Mirguet, O., Gellibert, F., Nicodeme, E., Krysa, G., Kirilovsky, J., Beinke, S., McCleary, S., Rioja, I., Bamborough, P., Chung, C.-W., Gordon, L., Lewis, T., Walker, A. L., Cutler, L., Lugo, D., Wilson, D. M., Witherington, J., Lee, K., and Prinjha, R. K. (2012) Identification of a novel series of BET family bromodomain inhibitors: Binding mode and profile of I-BET151 (GSK1210151A). *Bioorganic & Medicinal Chemistry Letters 22*, 2968–2972.
(186) (2013) Targeting low-druggability bromodomains: Fragment basedscreening and inhibitor design against the BAZ2B bromodomain 1–7.
(187) Gehling, V. S., Hewitt, M. C., Vaswani, R. G., Leblanc, Y., Côté, A., Nasveschuk, C. G., Taylor, A. M., Harmange, J.-C., Audia, J. E., Pardo, E.,

Joshi, S., Sandy, P., Mertz, J. A., Sims, R. J., III, Bergeron, L., Bryant, B. M., Bellon, S., Poy, F., Jayaram, H., Sankaranarayanan, R., Yellapantula, S., Bangalore Srinivasamurthy, N., Birudukota, S., and Albrecht, B. K. (2013) Discovery, Design, and Optimization of Isoxazole Azepine BET Inhibitors. *ACS Med. Chem. Lett. 4*, 835–840.
(188) Filippakopoulos, P., Picaud, S., Fedorov, O., Keller, M., Wrobel, M., Morgenstern, O., Bracher, F., and Knapp, S. (2012) Benzodiazepines and benzotriazepines as protein interaction inhibitors targeting bromodomains of the BET family. *Bioorganic & Medicinal Chemistry 20*, 1878–1886.
(189) Picaud, S., Da Costa, D., Thanasopoulou, A., Filippakopoulos, P., Fish, P. V., Philpott, M., Fedorov, O., Brennan, P., Bunnage, M. E., Owen, D. R., Bradner, J. E., Taniere, P., O'Sullivan, B., Muller, S., Schwaller, J., Stankovic, T., and Knapp, S. (2013) PFI-1, a Highly Selective Protein Interaction Inhibitor, Targeting BET Bromodomains. *Cancer Res 73*, 3336–3346.
(190) Lucas, X., Wohlwend, D., Hügle, M., Schmidtkunz, K., Gerhardt, S., Schüle, R., Jung, M., Einsle, O., and Günther, S. (2013) 4-Acyl Pyrroles: Mimicking Acetylated Lysines in Histone Code Reading. *Angew. Chem. Int. Ed. Engl. 52*, 14055–14059.
(191) Jecklin, M. C., Schauer, S., Dumelin, C. E., and Zenobi, R. (2009) Label-free determination of protein-ligand binding constants using mass spectrometry and validation using surface plasmon resonance and isothermal titration calorimetry. *J. Mol. Recognit. 22*, 319–329.
(192) Myszka, D. G. (1997) Kinetic analysis of macromolecular interactions using surface plasmon resonance biosensors. *Current opinion in biotechnology*.
(193) Chung, C.-W., Dean, A. W., Woolven, J. M., and Bamborough, P. (2012) Fragment-Based Discovery of Bromodomain Inhibitors Part 1: Inhibitor Binding Modes and Implications for Lead Discovery. *J. Med. Chem. 55*, 576–586.
(194) DiscoverRX. https://www.discoverx.com/technologies-platforms/competitive-binding-technology/bromoscan-technology-platform.
(195) Jerabek-Willemsen, M., André, T., Wanner, R., Roth, H. M., Duhr, S., Baaske, P., and Breitsprecher, D. (2014) MicroScale Thermophoresis: Interaction analysis and beyond. *Journal of Molecular Structure 1077*, 101–113.
(196) Ludwig, C., and Staatsdruckerei, K. (1856) Diffusion zwischen ungleich erwärmten Orten gleich zusammengesetzter Lösung.
(197) Rauch, J., and Köhler, W. (2002) Diffusion and thermal diffusion of semidilute to concentrated solutions of polystyrene in toluene in the vicinity of the glass transition. *Phys. Rev. Lett. 88*, 185901.
(198) Köhler, W., and Wiegand, S. (2002) Thermal Nonequilibrium Phenomena in Fluid Mixtures.
(199) Masi, A., Cicchi, R., Carloni, A., Pavone, F., and Arcangeli, A. (2010) Optical Methods in the Study of Protein-Protein Interactions, in *Advances in Experimental Medicine and Biology* (Becchetti, A., and Arcangeli, A., Eds.), pp 33–42. Springer New York.
(200) Wienken, C. J., Baaske, P., Rothbauer, U., Braun, D., and Duhr, S. (2010) Protein-binding assays in biological liquids using microscale thermophoresis. *Nat Commun 1*, 1–7.
(201) Razinkov, V. I., Treuheit, M. J., and Becker, G. W. (2013) Methods of

high throughput biophysical characterization in biopharmaceutical development. *Curr Drug Discov Technol 10*, 59–70.
(202) Stumpfe, D., Bill, A., Novak, N., and Loch, G. (2010) Targeting multifunctional proteins by virtual screening: structurally diverse cytohesin inhibitors with differentiated biological functions. *ACS chemical …*.
(203) Baaske, P., Duhr, S., and Braun, D. (2007) Melting curve analysis in a snapshot. *Applied Physics Letters*.
(204) Reineck, P., Wienken, C. J., and Braun, D. (2010) Thermophoresis of single stranded DNA. *Electrophoresis 31*, 279–286.
(205) Baaske, P., Weinert, F. M., Duhr, S., Lemke, K. H., Russell, M. J., and Braun, D. (2007) Extreme accumulation of nucleotides in simulated hydrothermal pore systems. *Proc. Natl. Acad. Sci. U.S.A. 104*, 9346–9351.
(206) Hiruma, Y., Sacristan, C., Pachis, S. T., Adamopoulos, A., Kuijt, T., Ubbink, M., Castelmur, von, E., Perrakis, A., and Kops, G. J. P. L. (2015) CELL DIVISION CYCLE. Competition between MPS1 and microtubules at kinetochores regulates spindle checkpoint signaling. *Science 348*, 1264–1267.
(207) Ji, Z., Gao, H., and Yu, H. (2015) CELL DIVISION CYCLE. Kinetochore attachment sensed by competitive Mps1 and microtubule binding to Ndc80C. *Science 348*, 1260–1264.
(208) Seidel, S. A. I., Dijkman, P. M., Lea, W. A., van den Bogaart, G., Jerabek-Willemsen, M., Lazic, A., Joseph, J. S., Srinivasan, P., Baaske, P., Simeonov, A., Katritch, I., Melo, F. A., Ladbury, J. E., Schreiber, G., Watts, A., Braun, D., and Duhr, S. (2013) Microscale thermophoresis quantifies biomolecular interactions under previously challenging conditions. *Methods 59*, 301–315.
(209) Jerabek-Willemsen, M., Wienken, C. J., Braun, D., Baaske, P., and Duhr, S. (2011) Molecular Interaction Studies Using Microscale Thermophoresis. *ASSAY and Drug Development Technologies 9*, 342–353.
(210) Flynn, E. M., Huang, O. W., Poy, F., Oppikofer, M., Bellon, S. F., Tang, Y., and Cochran, A. G. (2015) A Subset of Human Bromodomains Recognizes Butyryllysine and Crotonyllysine Histone Peptide Modifications. *Structure/Folding and Design* 1–15.
(211) Klebe, G. (2015) PERSPECTIVES. *Nat Rev Drug Discov 14*, 95–110.
(212) Swissdock.ch. http://www.swissdock.ch/docking.
(213) Fabian, M. A., Biggs, W. H., Treiber, D. K., Atteridge, C. E., Azimioara, M. D., Benedetti, M. G., Carter, T. A., Ciceri, P., Edeen, P. T., Floyd, M., Ford, J. M., Galvin, M., Gerlach, J. L., Grotzfeld, R. M., Herrgard, S., Insko, D. E., Insko, M. A., Lai, A. G., Lélias, J.-M., Mehta, S. A., Milanov, Z. V., Velasco, A. M., Wodicka, L. M., Patel, H. K., Zarrinkar, P. P., and Lockhart, D. J. (2005) A small molecule-kinase interaction map for clinical kinase inhibitors. *Nature Biotechnology 23*, 329–336.
(214) Tarcsay, Á., Nyíri, K., and Keserü, G. M. (2012) Impact of Lipophilic Efficiency on Compound Quality. *J. Med. Chem. 55*, 1252–1260.
(215) Hann, M. M., Leach, A. R., and Harper, G. (2001) Molecular Complexity and Its Impact on the Probability of Finding Leads for Drug Discovery. *J. Chem. Inf. Model. 41*, 856–864.
(216) Oprea, T. I., Davis, A. M., Teague, S. J., and Leeson, P. D. (2001) Is There a Difference between Leads and Drugs? A Historical Perspective. *J. Chem. Inf. Model. 41*, 1308–1315.

(217) Kuntz, I. D., Chen, K., Sharp, K. A., and Kollman, P. A. (1999) The maximal affinity of ligands. *Proc. Natl. Acad. Sci. U.S.A. 96*, 9997–10002.
(218) (2011) IARC Monographs on the Evaluation of Carcinogenic Risks to Humans. *International Agency For Research on Cancer: Lyon 99*, 1–706.
(219) Birch, A. M., Groombridge, S., Law, R., Leach, A. G., Mee, C. D., and Schramm, C. (2012) Rationally designing safer anilines: the challenging case of 4-aminobiphenyls. *J. Med. Chem. 55*, 3923–3933.
(220) SmartCYP. http://www.farma.ku.dk/smartcyp/smartcyp.php.
(221) Arnaudo, A. M., and Garcia, B. A. (2013) Proteomic characterization of novel histone post-translational modifications. *Epigenetics & Chromatin 6*, 1–7.
(222) Resh, M. D. (2006) Trafficking and signaling by fatty-acylated and prenylated proteins. *Nat. Chem. Biol. 2*, 584–590.
(223) Gerlach, H., Laumann, V., Martens, S., Becker, C. F. W., Goody, R. S., and Geyer, M. (2010) HIV-1 Nef membrane association depends on charge, curvature, composition and sequence. *Nat. Chem. Biol. 6*, 46–53.
(224) Jiang, T., Zhou, X., Taghizadeh, K., Dong, M., and Dedon, P. C. (2007) N-formylation of lysine in histone proteins as a secondary modification arising from oxidative DNA damage. *Proc. Natl. Acad. Sci. U.S.A. 104*, 60–65.
(225) Chen, Y., Sprung, R., Tang, Y., Ball, H., Sangras, B., Kim, S. C., Falck, J. R., Peng, J., Gu, W., and Zhao, Y. (2007) Lysine propionylation and butyrylation are novel post-translational modifications in histones. *Mol. Cell Proteomics 6*, 812–819.
(226) Tan, M., Luo, H., Lee, S., Jin, F., Yang, J. S., Montellier, E., Buchou, T., Cheng, Z., Rousseaux, S., Rajagopal, N., Lu, Z., Ye, Z., Zhu, Q., Wysocka, J., Ye, Y., Khochbin, S., Ren, B., and Zhao, Y. (2011) Identification of 67 histone marks and histone lysine crotonylation as a new type of histone modification. *Cell 146*, 1016–1028.
(227) Dai, L., Peng, C., Montellier, E., Lu, Z., Chen, Y., Ishii, H., Debernardi, A., Buchou, T., Rousseaux, S., Jin, F., Sabari, B. R., Deng, Z., Allis, C. D., Ren, B., Khochbin, S., and Zhao, Y. (2014) Lysine 2-hydroxyisobutyrylation is a widely distributed active histone mark. *Nat. Chem. Biol. 10*, 365–370.
(228) Xie, Z., Dai, J., Dai, L., Tan, M., Cheng, Z., Wu, Y., Boeke, J. D., and Zhao, Y. (2012) Lysine succinylation and lysine malonylation in histones. *Mol. Cell Proteomics 11*, 100–107.
(229) Peng, C., Lu, Z., Xie, Z., Cheng, Z., Chen, Y., Tan, M., Luo, H., Zhang, Y., He, W., Yang, K., Zwaans, B. M. M., Tishkoff, D., Ho, L., Lombard, D., He, T.-C., Dai, J., Verdin, E., Ye, Y., and Zhao, Y. (2011) The First Identification of Lysine Malonylation Substrates and Its Regulatory Enzyme. *Molecular & Cellular Proteomics 10*.
(230) Tan, M., Peng, C., Anderson, K. A., Chhoy, P., Xie, Z., Dai, L., Park, J., Chen, Y., Huang, H., Zhang, Y., Ro, J., Wagner, G. R., Green, M. F., Madsen, A. S., Schmiesing, J., Peterson, B. S., Xu, G., Ilkayeva, O. R., Muehlbauer, M. J., Braulke, T., Mühlhausen, C., Backos, D. S., Olsen, C. A., McGuire, P. J., Pletcher, S. D., Lombard, D. B., Hirschey, M. D., and Zhao, Y. (2014) Lysine glutarylation is a protein posttranslational modification regulated by SIRT5. *Cell Metabolism 19*, 605–617.
(231) Garrity, J., Gardner, J. G., Hawse, W., Wolberger, C., and Escalante-Semerena, J. C. (2007) N-lysine propionylation controls the activity of propionyl-CoA synthetase. *J. Biol. Chem. 282*, 30239–30245.

(232) Berndsen, C. E., Albaugh, B. N., Tan, S., and Denu, J. M. (2007) Catalytic mechanism of a MYST family histone acetyltransferase. *Biochemistry 46*, 623–629.
(233) Leemhuis, H., Packman, L. C., Nightingale, K. P., and Hollfelder, F. (2008) The human histone acetyltransferase P/CAF is a promiscuous histone propionyltransferase. *Chembiochem 9*, 499–503.
(234) Liu, B., Lin, Y., Darwanto, A., Song, X., Xu, G., and Zhang, K. (2009) Identification and Characterization of Propionylation at Histone H3 Lysine 23 in Mammalian Cells. *Journal of Biological Chemistry 284*, 32288–32295.
(235) Zhang, K., Chen, Y., Zhang, Z., and Zhao, Y. (2009) Identification and Verification of Lysine Propionylation and Butyrylation in Yeast Core Histones Using PTMap Software. *J. Proteome Res. 8*, 900–906.
(236) Cheng, Z., Tang, Y., Chen, Y., Kim, S., Liu, H., Li, S. S. C., Gu, W., and Zhao, Y. (2009) Molecular characterization of propionyllysines in non-histone proteins. *Mol. Cell Proteomics 8*, 45–52.
(237) Okanishi, H., Kim, K., Masui, R., and Kuramitsu, S. (2014) Lysine propionylation is a prevalent post-translational modification in Thermus thermophilus. *Mol. Cell Proteomics 13*, 2382–2398.
(238) Sabari, B. R., Tang, Z., Huang, H., Yong-Gonzalez, V., Molina, H., Kong, H. E., Dai, L., Shimada, M., Cross, J. R., Zhao, Y., Roeder, R. G., and Allis, C. D. (2015) Intracellular crotonyl-CoA stimulates transcription through p300-catalyzed histone crotonylation. *Mol Cell 58*, 203–215.
(239) Du, J., Zhou, Y., Su, X., Yu, J. J., Khan, S., Jiang, H., Kim, J., Woo, J., Kim, J. H., Choi, B. H., He, B., Chen, W., Zhang, S., Cerione, R. A., Auwerx, J., Hao, Q., and Lin, H. (2011) Sirt5 is a NAD-dependent protein lysine demalonylase and desuccinylase. *Science 334*, 806–809.
(240) Feldman, J. L., Baeza, J., and Denu, J. M. (2013) Activation of the protein deacetylase SIRT6 by long-chain fatty acids and widespread deacylation by mammalian sirtuins. *Journal of Biological Chemistry 288*, 31350–31356.
(241) Vollmuth, F., and Geyer, M. (2010) Interaction of propionylated and butyrylated histone H3 lysine marks with Brd4 bromodomains. *Angew. Chem. Int. Ed. Engl. 49*, 6768–6772.
(242) Vollmuth, F., Blankenfeldt, W., and Geyer, M. (2009) Structures of the Dual Bromodomains of the P-TEFb-activating Protein Brd4 at Atomic Resolution. *Journal of Biological Chemistry 284*, 36547–36556.
(243) Trott, O., and Olson, A. J. (2010) AutoDock Vina: Improving the speed and accuracy of docking with a new scoring function, efficient optimization, and multithreading. *J. Comput. Chem. 31*, 455–461.
(244) Rauf, M. A., Zubair, S., and Azhar, A. (2015) Ligand docking and binding site analysis with pymol and autodock/vina. *International Journal of Basic and Applied Sciences 4*, 168–177.
(245) Klose, J., Bienert, M., Mollenkopf, C., Wehle, D., Zhang, C.-W., Carpino, L. A., and Henklein, P. (1999) 2-Propanephosphonic acid anhydride (T3P)-mediated segment coupling and head-to-tail cyclization of sterically hindered peptides. *Chem. Commun.* 1847–1848.
(246) Dunetz, J. R., Xiang, Y., Baldwin, A., and Ringling, J. (2011) General and Scalable Amide Bond Formation with Epimerization-Prone Substrates Using T3P and Pyridine. *Org. Lett. 13*, 5048–5051.
(247) Repasky, M. P., Chandrasekhar, J., and Jorgensen, W. L. (2002)

PDDG/PM3 and PDDG/MNDO: Improved semiempirical methods. *J. Comput. Chem. 23*, 1601–1622.
(248) Frisch, M. J., Trucks, G. W., Schlegel, H. B., Scuseria, G. E., Robb, M. A., Cheeseman, J. R., Scalmani, G., Barone, V., Mennucci, B., Petersson, G. A., Nakatsuji, H., Caricato, M., Li, X., Hratchian, H. P., Izmaylov, A. F., Bloino, J., Zheng, G., Sonnenberg, J. L., Hada, M., Ehara, M., Toyota, K., Fukuda, R., Hasegawa, J., Ishida, M., Nakajima, T., Honda, Y., Kitao, O., Nakai, H., Vreven, T., Montgomery, J. A., Jr, Peralta, J. E., Ogliaro, F., Bearpark, M. J., Heyd, J., Brothers, E. N., Kudin, K. N., Staroverov, V. N., Kobayashi, R., Normand, J., Raghavachari, K., Rendell, A. P., Burant, J. C., Iyengar, S. S., Tomasi, J., Cossi, M., Rega, N., Millam, N. J., Klene, M., Knox, J. E., Cross, J. B., Bakken, V., Adamo, C., Jaramillo, J., Gomperts, R., Stratmann, R. E., Yazyev, O., Austin, A. J., Cammi, R., Pomelli, C., Ochterski, J. W., Martin, R. L., Morokuma, K., Zakrzewski, V. G., Voth, G. A., Salvador, P., Dannenberg, J. J., Dapprich, S., Daniels, A. D., Farkas, Ö., Foresman, J. B., Ortiz, J. V., Cioslowski, J., and Fox, D. J. (2009) Gaussian 09.
(249) Marenich, A. V., Cramer, C. J., and Truhlar, D. G. (2009) Universal Solvation Model Based on Solute Electron Density and on a Continuum Model of the Solvent Defined by the Bulk Dielectric Constant and Atomic Surface Tensions. *J. Phys. Chem. B 113*, 6378–6396.
(250) Lee, M. C., Chian, E., and Griffin, R. A. (1979) Solubility of polychlorinated biphenyls and capacitor fluid in water. *Water Research* 1249–1258.
(251) Gavezzotti, A. (1995) Molecular symmetry, melting temperatures and melting enthalpies of substituted benzenes and naphthalenes. *J. Chem. Soc., Perkin Trans. 2* 1399–1404.
(252) Huang, D., Rossini, E., Steiner, S., and Caflisch, A. (2013) Structured Water Molecules in the Binding Site of Bromodomains Can Be Displaced by Cosolvent. *ChemMedChem 9*, 573–579.
(253) Michel, J., Tirado-Rives, J., and Jorgensen, W. L. (2009) Energetics of Displacing Water Molecules from Protein Binding Sites: Consequences for Ligand Optimization. *J. Am. Chem. Soc. 131*, 15403–15411.
(254) MacKerell, A. D., Bashford, D., Bellott, M., Dunbrack, R. L., Evanseck, J. D., Field, M. J., Fischer, S., Gao, J., Guo, H., Ha, S., Joseph-McCarthy, D., Kuchnir, L., Kuczera, K., Lau, F. T., Mattos, C., Michnick, S., Ngo, T., Nguyen, D. T., Prodhom, B., Reiher, W. E., Roux, B., Schlenkrich, M., Smith, J. C., Stote, R., Straub, J., Watanabe, M., Wiórkiewicz-Kuczera, J., Yin, D., and Karplus, M. (1998) All-atom empirical potential for molecular modeling and dynamics studies of proteins. *J. Phys. Chem. B 102*, 3586–3616.
(255) Pantano, S., Marcello, A., and Ferrari, A. (2006) Insights on HIV‐1 Tat: P/CAF bromodomain molecular recognition from in vivo experiments and molecular dynamics simulations. *Proteins: Structure*.
(256) Toyoshima, M., Howie, H. L., Imakura, M., Walsh, R. M., Annis, J. E., Chang, A. N., Frazier, J., Chau, B. N., Loboda, A., Linsley, P. S., Cleary, M. A., Park, J. R., and Grandori, C. (2012) Functional genomics identifies therapeutic targets for MYC-driven cancer. *Proc. Natl. Acad. Sci. U.S.A. 109*, 9545–9550.
(257) Banting, G. S., Barak, O., Ames, T. M., Burnham, A. C., Kardel, M. D., Cooch, N. S., Davidson, C. E., Godbout, R., McDermid, H. E., and Shiekhattar, R. (2005) CECR2, a protein involved in neurulation, forms a

novel chromatin remodeling complex with SNF2L. *Human Molecular Genetics 14*, 513–524.
(258) Hanahan, D., and Weinberg, R. A. (2011) Hallmarks of Cancer: The Next Generation. *Cell 144*, 646–674.
(259) Ciceri, P., Müller, S., O'Mahony, A., Fedorov, O., Filippakopoulos, P., Hunt, J. P., Lasater, E. A., Pallares, G., Picaud, S., Wells, C., Martin, S., Wodicka, L. M., Shah, N. P., Treiber, D. K., and Knapp, S. (2014) Dual kinase-bromodomain inhibitors for rationally designed polypharmacology. *Nat. Chem. Biol. 10*, 305–312.
(260) Boran, A. D., and Iyengar, R. (2010) Systems approaches to polypharmacology and drug discovery. *Current opinion in drug discovery & development 13*, 297–309.
(261) Haber, D. A., Gray, N. S., and Baselga, J. (2011) The Evolving War on Cancer. *Cell 145*, 19–24.
(262) Hashizume, K., Tadano, H., Sato, G., Tamura, J., and Mitsuoka, Y. Preparation of aminoimidazolpyrazinylbenzamide derivatives and analogs for use as TTK inhibitors
. *U.S. Pat. Appl. Publ. (2012), US 20120059162 A1*.
(263) Jeong, H., Barbe, V., Lee, C. H., Vallenet, D., Yu, D. S., Choi, S.-H., Couloux, A., Lee, S.-W., Yoon, S. H., Cattolico, L., Hur, C.-G., Park, H.-S., Ségurens, B., Kim, S. C., Oh, T. K., Lenski, R. E., Studier, F. W., Daegelen, P., and Kim, J. F. Genome Sequences of Escherichia coli B strains REL606 and BL21(DE3). *Journal of Molecular Biology 394*, 644–652.
(264) AddGene. https://www.addgene.org/39012/.
(265) Savitsky, P., Bray, J., Cooper, C. D. O., Marsden, B. D., Mahajan, P., Burgess-Brown, N. A., and Gileadi, O. (2010) High-throughput production of human proteins for crystallization: The SGC experience. *New Trends in Protein Expression 172*, 3–13.
(266) Bullock, A. N., Debreczeni, J. É., Fedorov, O. Y., Nelson, A., Marsden, B. D., and Knapp, S. (2005) Structural Basis of Inhibitor Specificity of the Human Protooncogene Proviral Insertion Site in Moloney Murine Leukemia Virus (PIM-1) Kinase. *J. Med. Chem. 48*, 7604–7614.
(267) Pangborn, A. B., Giardello, M. A., Grubbs, R. H., Rosen, R. K., and Timmers, F. J. (1996) Safe and Convenient Procedure for Solvent Purification. *Organometallics 15*, 1518–1520.
(268) Kasnar, B., Wise, D. S., Kucera, L. S., Drach, J. C., and Townsend, L. B. (1994) Synthesis of 2′,3′-Dideoxy- and 3′-Azido-2′,3′-dideoxy-pyridazine Nucleosides as Potential Antiviral Agents. *Nucleosides and Nucleotides 13*, 459–479.

Appendix

Appendix- ^{1}H and ^{13}C NMR Spectra